19 August 2005

Science

Vol. 309 No. 5738
Pages 1137–1284 $10

125 YEARS OF GLOBAL Science

AAAS

Now The Right Side Knows What The Left Side Is Doing.

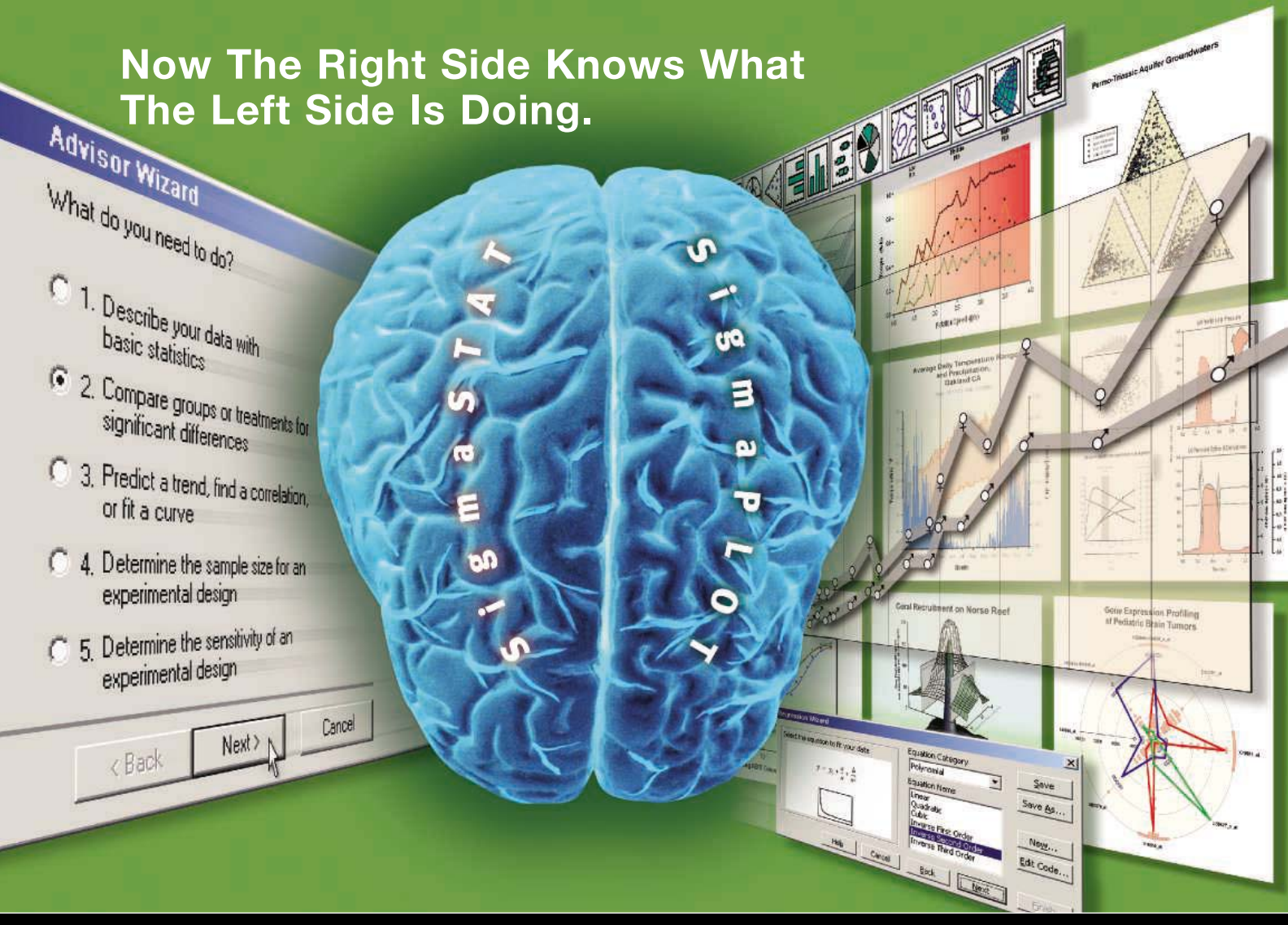

Combine the Powerful Statistical Output of SigmaStat with the Publication-quality Graph Creation of SigmaPlot

SigmaPlot is the award-winning technical graphing and data analysis software package used by more than 100,000 researchers worldwide who need to produce defensible research and create compelling graphs that clearly present their results for technical publications, presentations or the web. SigmaStat 3.1 now seamlessly integrates with SigmaPlot 9.0 for deeper statistical analysis within SigmaPlot's statistics menu.

SigmaPlot allows you to:

> Create graphs easily and publish your work anywhere
> Analyze and manage your data quickly and easily
> Choose over 80 different 2-D and 3-D graph types
> Customize every element of your graphs
> Instantly access SigmaPlot from Microsoft® Excel
> Streamline your work by automating repetitive tasks

SIGMAPLOT
Exact Graphs for Exact Science

Add SigmaStat 3.1 to get easy-to-use, expert statistical analysis within SigmaPlot!

SigmaStat guides you through your analysis:

> Suggests the appropriate statistical test
> Checks assumptions in the data to avoid statistical error
> If your data violates any of those assumptions, the Advisor Wizard suggests another test
> Generates an intelligent report that explains your results in plain English – not statistical jargon
> Even handles messy data with missing values

SIGMASTAT
Advisory Statistics for Scientists

With SigmaStat you'll have the expertise of a professional statistical consultant at your fingertips!

FREE ONLINE TUTORIALS & 30-DAY TRIAL SOFTWARE AVAILABLE AT WWW.SYSTAT.COM

SigmaScan®
Automated Image Analysis

TABLECurve 2D
Automated Curve Fitting Analysis

TABLECurve 3D
Automated Surface Fitting Analysis

PeakFit
Automated Peak Separation Analysis

SYSTAT
Comprehensive Statistical Analysis

adsci

High-performance features come standard.

The best real-time PCR system just got better.

Stratagene's Mx3005P™ Real-Time PCR System sets the next benchmark in real-time PCR with new high-performance features, increased flexibility to support more applications and chemistries, and affordable pricing for the individual researcher (€29,900 list price*).Real-time PCR systems starting at €24,950 list price*.

- **The *only* instrument with five (5) color multiplex capability and user-selected filters**
- **Novel custom filter path selection for FRET probe chemistries**
- **Includes Beacon Designer™ oligo design software**

Need More Information? Give Us A Call:

Stratagene USA and Canada
Order: (800) 424-5444 x3
Technical Services: (800) 894-1304

Stratagene Europe
Order: 00800-7000-7000
Technical Services: 00800-7400-7400

Stratagene Japan K.K.
Order: 03-5159-2060
Technical Services: 03-5159-2070

www.stratagene.com

*Pricing only available in Benelux, France, Germany, Austria, and Switzerland.

STRATAGENE®

GE Healthcare

Ni Sepharose™

4x greater binding capacity in histidine-tagged protein purification

Ni Sepharose™ products from GE Healthcare give you the highest binding capacity available for histidine-tagged protein purification. With up to four times the binding capacity, it's no longer pure imagination to dramatically increase your yield, while saving time and costs. Maximum target protein activity is assured, thanks to tolerance of a wide range of additives and negligible nickel ion leakage. The flexibility to use a variety of protocols ensures the highest possible purity. Ni Sepharose 6 FF is excellent for manual procedures such as gravity/batch and easy scale-up, while the HP version is designed for high-performance in automated purification systems – both are available in different formats, including prepacked columns. Outstanding performance has never been easier to achieve.

www.amershambiosciences.com/his

imagination at work

GE10-05

Science

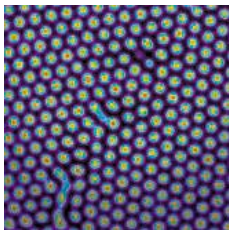

COVER A crystal of colloidal particles far below its melting temperature. A grain boundary rises diagonally from left to right, separating sections of the crystal with different orientations. Circles denote the time-averaged position of each particle, with red indicating a lower degree and blue a higher degree of positional fluctuation about its equilibrium position. See page 1207. [Image: A. M. Alsayed *et al.*]

Volume 309
19 August 2005
Number 5738

DEPARTMENTS

NEWS OF THE WEEK

NEWS FOCUS

RETHINKING NUCLEAR POWER

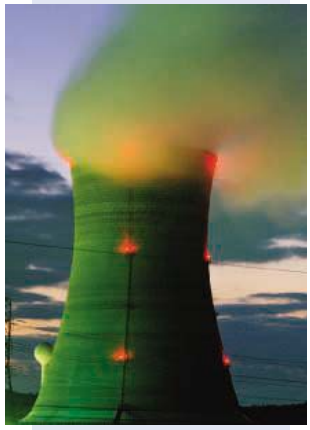

1168

1188

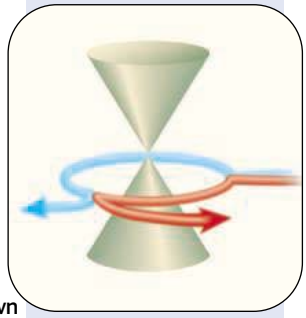

1195 & 1227

LETTERS

BOOKS *ET AL.*

POLICY FORUM

PERSPECTIVES

REVIEW

Contents continued

Systems Biology — Cell-Free Protein Synthesis

EasyXpress — the fast and easy way to produce proteins

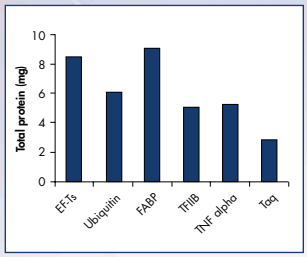

Typical yields from a single large-scale kit

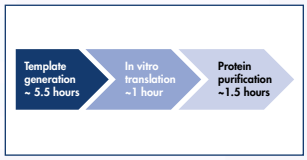

Fast procedures — from gene to protein in a single day

Producing proteins used to be difficult and time-consuming. Not any more. QIAGEN's EasyXpress is the fast and easy way to produce proteins.

By using EasyXpress™ Kits you get:

- **Efficient in vitro synthesis** — of native and posttranslationally modified eukaryotic proteins
- **Application-specific labeling** — for screening, protein interaction, and structural studies
- **Scalable, high yields** — a range of kits offering 3 µg to 5 mg of protein per reaction
- **Fast procedures and easy handling** — pure protein in hours, compared to weeks using conventional methods

To find out how fast and easy producing protein can be, visit www.qiagen.com/EasyXpress !

QIAGEN

Science

SCIENCE EXPRESS www.sciencexpress.org

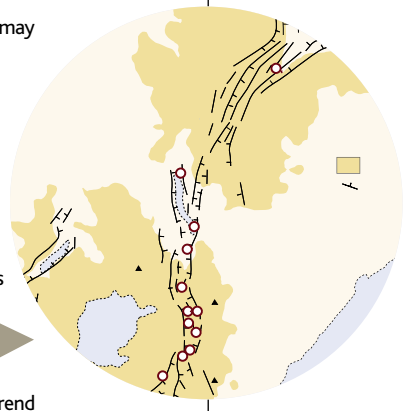

TECHNICAL COMMENT ABSTRACTS

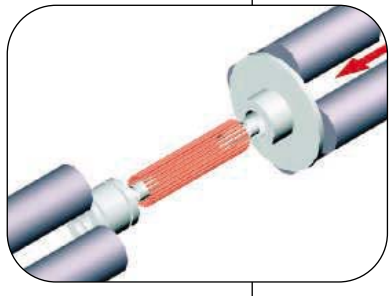

1219

BREVIA

RESEARCH ARTICLES

REPORTS

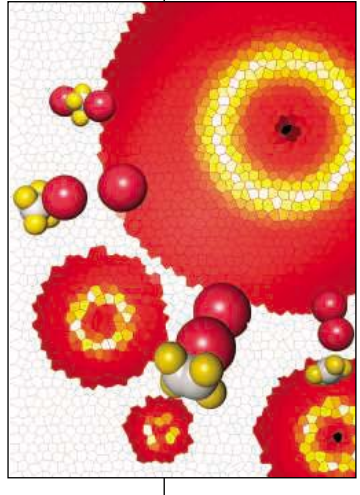

1192 & 1223

Contents continued

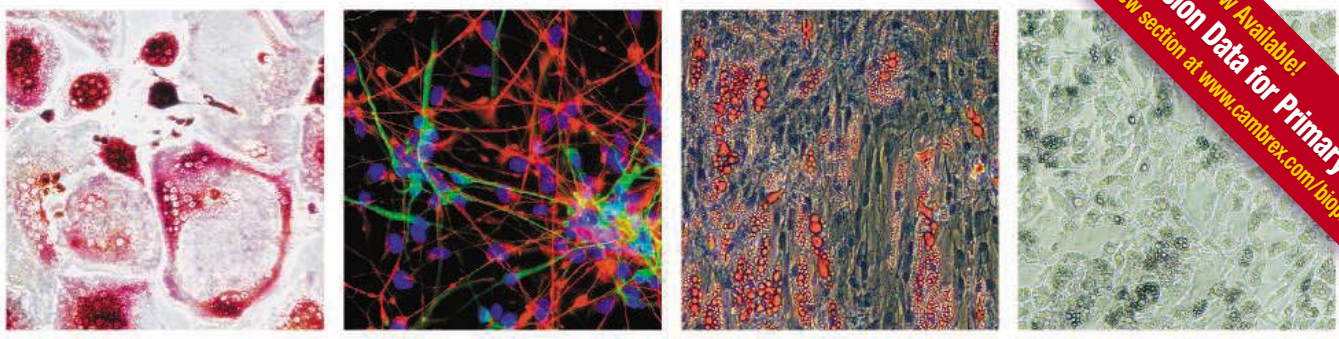

Primary. Human. Ready to Use.

Poietics™ Differentiating Cell Systems

Bone, Adipose, Neural Cells and Media Kits

- Osteoclast precursors that stain positive for TRAP and resorb bone upon differentiation.
- Preadipocytes isolated from subcutaneous and visceral fat.
- Neural progenitors stained positive for β-tubulin III and GFAP.

Hematopoietic Progenitor Cells

- Fresh unprocessed bone marrow from a wide donor selection.
- Progenitors include $CD34^+$, $CD133^+$, mononuclear cells, and erythroid progenitors.
- Sources include mobilized and normal peripheral blood, bone marrow, and cord blood.

Mesenchymal Stem Cells

- Highly homogeneous MSC population tested and guaranteed in 3 different lineages.
- Media kits available for the expansion of MSCs, and the differentiation of osteoblasts, chondrocytes, and adipocytes.

Immune Cells

- $CD14^+$ Monocytes.
- Dendritic cells and precursors.
- $CD4^+$ T cells and $CD19^+$ B cells from cord blood.

Cambrex, the source for Clonetics® and Poietics™ Cell Systems, BioWhittaker™ Classical Media, SeaPlaque® and NuSieve® Agarose, and PAGEr® *Precast Gels.*

For more information contact us at:
www.cambrex.com
U.S. **800-638-8174** | Europe **32 (0) 87 32 16 09**

Cambrex Bio Science Walkersville, Inc.
8830 Biggs Ford Road | Walkersville, MD 21793

CAMBREX
Innovation. Experience. Performance.

REPORTS CONTINUED

MICHAEL KULWIEC/DIVERSA CORPORATION

1242

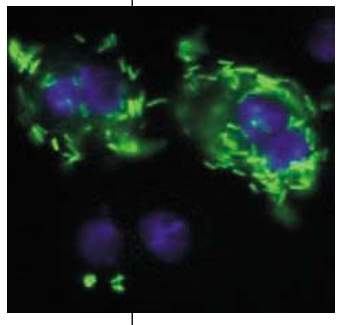

1248 & 1251

AAAS
ADVANCING SCIENCE, SERVING SOCIETY

SCIENCE (ISSN 0036-8075) is published weekly on Friday, except the last week in December, by the American Association for the Advancement of Science, 1200 New York Avenue, NW, Washington, DC 20005. Periodicals Mail postage (publication No. 484460) paid at Washington, DC, and additional mailing offices. Domestic individual membership and subscription (51 issues): $135 ($74 allocated to subscription). Domestic institutional subscription (51 issues): $550; Foreign postage extra: Mexico, Caribbean (surface mail) $55; other countries (air assist delivery) $85. First class, airmail, student, and emeritus rates on request. Canadian rates with GST available upon request, GST #1254 88122. Publications Mail Agreement Number 1069624. **Printed in the U.S.A.**

Change of address: allow 4 weeks, giving old and new addresses and 8-digit account number. **Postmaster:** Send change of address to *Science*, P.O. Box 1811, Danbury, CT 06813–1811. **Single copy sales:** $10.00 per issue prepaid includes surface postage; bulk rates on request. **Authorization to photocopy** material for internal or personal use under circumstances not falling within the fair use provisions of the Copyright Act is granted by AAAS to libraries and other users registered with the Copyright Clearance Center (CCC) Transactional Reporting Service, provided that $15.00 per article is paid directly to CCC, 222 Rosewood Drive, Danvers, MA 01923. The identification code for *Science* is 0036-8075/83 $15.00. *Science* is indexed in the *Reader's Guide to Periodical Literature* and in several specialized indexes.

Contents continued ▶

sciencenow www.sciencenow.org Daily News Coverage

How Babies Find Their Groove
Infants appreciate nuances of foreign music—until they get older.

Buying Happiness
Money brings pleasure, but only if you're richer than your neighbors are.

Your Career in a Number
Researcher proposes "h index" to measure impact of scientists' work.

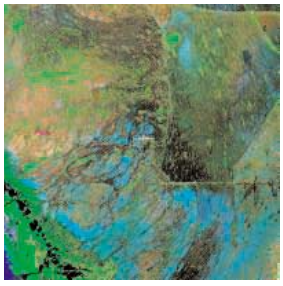

Careers in geospatial information.

science's next wave www.nextwave.org Career Resources for Young Scientists

US: Careers in Geoscience and Remote Sensing *A. Fazekas*
Next Wave talks to geospatial information industry leaders about this rapidly growing field.

US: The Etiquette of the Job Search—Mr. Manners Hits the Interviewing Trail *D. Jensen*
Your manners say something about you and they can affect your job search.

UK: Your Real Alternative to a Career in Science *P. Dee*
Phil Dee contemplates his departure from scientific research and reflects on alternative career options.

MiSciNet: Russell Stands-Over-Bull—Building Community and Developing Natural Resources *A. Sasso*
A Native American geoscientist helps develop tribally owned natural resources in Montana.

GrantsNet: International Grants and Fellowships Index *Next Wave Staff*
Here is the latest listing of funding opportunities and competitions happening outside the United States.

science's sage ke www.sageke.org Science of Aging Knowledge Environment

Perspective: Making Young Tumors Old—A New Weapon Against Cancer? *J. Sage*
Oncogene-induced senescence acts as a tumor suppressor mechanism.

News Focus: Beta Testing *M. Leslie*
Lethargic pancreas gene might unleash diabetes.

News Focus: Hairy Breakup *M. Beckman*
Alone, protein that replenishes chromosome ends finds capacity to fire up hair stem cells.

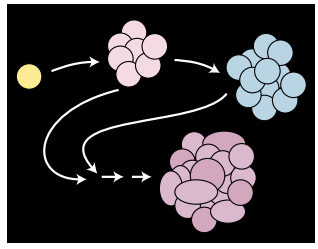

Senescence fights back.

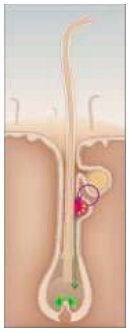

Hair stem cell choices.

science's stke www.stke.org Signal Transduction Knowledge Environment

Perspective: Checkpoints of Melanocyte Stem Cell Development *L. Sommer*
Intrinsic and extrinsic factors interact to regulate melanocyte stem cell self-renewal and differentiation.

Protocol: Robust Enrichment of Phosphorylated Species in Complex Mixtures by Sequential Protein and Peptide Metal-Affinity Chromatography and Analysis by Tandem Mass Spectrometry *M. O. Collins, L. Yu, H. Husi, W. P. Blackstock, J. S. Choudhary, S. G. N. Grant*
These methods describe effective detection of the phosphoproteome.

Separate individual or institutional subscriptions to these products may be required for full-text access.

Visit us in Booth 412 at CHIPS TO HITS in Boston

Roche Applied Science

LightCycler® 480 Real-Time PCR System

Rapid by nature, *accurate by design*

▲ LightCycler® 480 Thermoblock for 96 or 384 wells, easily exchanged by users within minutes.

For years, Roche has provided real-time automated PCR solutions you can count on. Now, you can obtain the proven performance and benefits of the original LightCycler® System in a 96- or 384-well instrument platform for high-throughput applications – the new **LightCycler® 480 Real-Time PCR System**.

Speed – Save time without sacrificing the quality of your results – precise, high-speed temperature changes maximize specificity and yield.

Accuracy – Benefit from our novel thermal block and data-capture technologies to eliminate edge-effects for outstanding accuracy and precision.

Versatility – Combine 5 excitation and 6 detection channels, multiple probe formats, proven analysis software, and true master mix reagents to meet your specific application needs.

Compatibility – Take advantage of the instrument's automation and LIMS capabilities to interface with your current systems and future workflows.

Visit ***www.roche-applied-science.com/lightcycler480*** for more information.

In Development. Planned introduction: September, 2005.

For general laboratory use.
Not for use in diagnostic procedures.

Roche Diagnostics

Roche Diagnostics GmbH
Roche Applied Science
68298 Mannheim
Germany

Polymer Production

Organic chemists have developed a wide range of techniques for linking and functionalizing small molecules that polymer chemists have exploited for creating larger molecules with controlled architectures and chain lengths. A rich toolbox is now available for making macromolecules that could not be made using standard polymerization techniques. **Hawker and Wooley** (p. 1200) review a number of key advances, and show how these new polymeric systems are showing promise for applications including encapsulation, drug delivery, and thin-film patterning, as well as for the study of fundamental polymer properties.

Tracking a Proton Propeller

Discovery of superacids revealed that, with a weak enough counterion, even a molecule as inert as methane could bind an extra proton. The product when methane is acidified, the CH_5^+ ion, has long puzzled theorists and spectroscopists alike. The hydrogen atoms seem to change places with one another too rapidly to assign the geometry and bonding mode reliably. **Asvany *et al.*** (p. 1219, published online 30 June 2005) have now measured the vibrational spectrum of CH_5^+ by detecting its infrared-induced reaction with CO_2. Comparison with simulations supports a structure in which a CH_3 tripod binds an H_2 fragment through a three-centered, two-electron bond, with a barrier for exchange between these different sites of 0.3 kilocalorie per mole.

Melting and Freezing

Melting and crystallization are often easier to study in colloids, where the particles are readily visualized (see the Perspective by **Pusey**). Premelting can occur at the crystal surfaces below the bulk melting temperature, but this phenomenon has not been observed in the bulk itself. **Alsayed *et al.*** (p. 1207, published online 30 June 2005) studied the melting of colloidal crystals composed of microgel particles that undergo large volume changes with small changes in temperature. Premelting can occur in the bulk at grain boundaries and dislocations and depends on the interfacial free energy associated with each type of defect. The addition of impurities to a melt can stop, slow down, or accelerate the crystallization of the bulk material. The interactions between impurity and bulk are complex, because one needs to consider differences in shape and size, as well as the nature of the chemical interactions between the two materials. **De Villeneuve *et al.*** (p. 1231) examine the role of curvature in which the impurities were large colloidal particles embedded in a sea of smaller ones. The presence of impurities did not necessarily slow down crystallization, but the relative curvature did play a role in pinning grain boundaries that formed. Each impurity was surrounded by a mobile layer of small particles.

Resolving Resolvase Structure and Function

The site-specific serine recombinase, resolvase, catalyzes recombination between two sites on negatively supercoiled DNA. This process requires double-strand cleavage at each site, strand exchange between the two sites, and religation. **Li *et al.*** (p. 1210, published online 30 June 2005) provide insight into how this occurs by reporting a 3.4 angstrom resolution crystal structure of a synaptic intermediate of resolvase linked to two cleaved duplex DNAs. The DNA duplexes lie on opposite sides of a tetramer of resolvase. The tetramer structure differs from a presynaptic complex between dimeric resolvase and DNA and places the catalytic serine close to the scissile phosphate. The structure supports a subunit rotation hypothesis that posits a 180° rotation of two resolvase subunits to accomplish strand exchange. A flat interface in the tetramer makes such a rotation feasible.

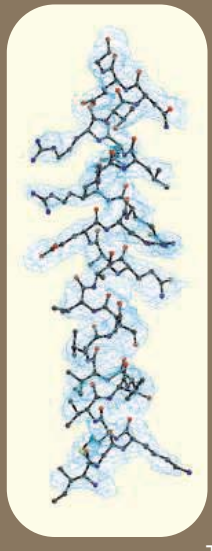

Snapshots in Solution

X-ray diffraction has long permitted chemists to map out the molecular structure of solids. Recently, short and intense x-ray pulses from synchrotrons have produced time-resolved pictures of structural rearrangements, but the samples, such as proteins, first had to be immobilized. **Ihee *et al.*** (p. 1223, published online 14 July 2005; see the Perspective by **Anfinrud and Schotte**) used intense 100-picosecond x-ray pulses to probe a reaction in solution. The sensitivity of x-rays for heavy atoms allowed them to follow an iodine atom in the photoinduced decomposition of diiodoethane to I_2 and C_2H_4. Over a large solvent background, the data offer direct structural evidence for a long-hypothesized I-bridged C_2H_4I intermediate.

Grainy Signatures

Grains from other stars were incorporated into our solar nebula when it formed. **Brandon *et al.*** (p. 1233) obtained osmium isotope data from such grains in primitive meteorites which indicate that elements as rhenium and osmium were derived from small stars with a higher neutron density than that which formed our solar system. Furthermore, the data require that these and other grains produced in our solar system were extremely well mixed in our solar nebula when solids started forming.

Strong Thin Sheets

Exploiting the strength of carbon nanotubes in most applications will require their assembly into macroscopic films and fibers. **Zhang *et al.*** (p. 1215) show that by attaching a sticky sheet of paper to a forest of vertically oriented nanotubes, they can draw them into sheets that are centimeters wide and meters in length. The sheets initially take the form of a highly anisotropic electrically conducting aerogel, and can be compressed into dense, strong sheets that are only tens of nanometers thick.

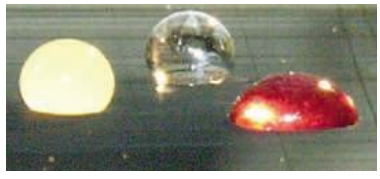

CONTINUED ON PAGE 1151

CREDITS (TOP TO BOTTOM): LI *ET AL.*; ZHANG *ET AL.*

Get remarkably robust DNA amplification. Again and again and again.

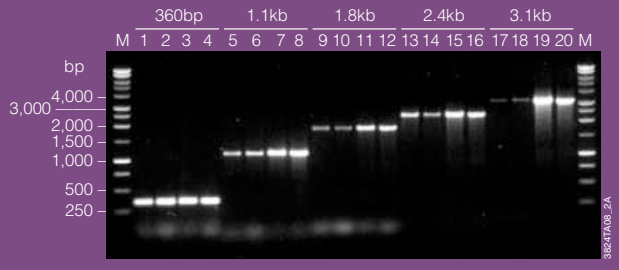

Regular *Taq* vs. GoTaq DNA Polymerase over a wide range of target sizes. In each set the left two lanes are *Taq* DNA Polymerase and the right two lanes are GoTaq DNA Polymerase.

Reap the benefits of consistent, robust performance every time you amplify with GoTaq® Polymerases.

- Harvest spectacular yields with optimal enzyme and buffer
- See faster results with the all-in-one reaction buffer that doubles as a gel loading buffer
- Perform perfect gel tracking with the GoTaq Green buffer – tracks small fragments and bumper products
- Enjoy the Promega PCR Performance Guarantee

Prove it to yourself...again and again and again.

To learn more, visit **www.promega.com/gotaq**

PROMEGA CORPORATION • www.promega.com

Promega

Why Large Size Increases Extinction Risk

A statistical analysis of extinction risk patterns for about 4000 mammal species by **Cardillo *et al.*** (p. 1239, published online 21 July 2005; see the 22 July news story by **Stokstad**) has provided an explanation for why species of large body size suffer the highest risk of extinction. Sensitivity to a variety of risk-promoting factors, such as low reproductive rate and low population density, increases sharply above a threshold of around 3 kilograms. For species below this threshold, extinction risk reflects simply where species live; above it, extinction risk also reflects biological traits, so that larger species are more likely to be predisposed to decline. The disproportionate disadvantages of large size might accelerate the loss of large-mammal biodiversity in the face of environmental threats.

Controlled Mobilization

Tissue stem cells have the capacity to self-renew and generate differentiated cells that replace lost cells as an organism ages. Quiescent stem cells typically reside in specific microenvironments or "niches." When needed, they begin proliferating and exit the niche, a process thought to be controlled by extracellular cues from the niche and by intrinsic genetic programs. Studying mouse models, **Flores *et al.*** (p. 1253, published online 21 July 2005) now show that epidermal stem cell mobilization is regulated by telomeres, the nucleoprotein structures at the ends of chromosomes. Short telomeres impaired mobilization, whereas overexpression of telomerase, the enzyme that synthesizes telomeres, promoted mobilization. The effect of telomeres on stem cell function could potentially explain, at least in part, their role in aging and cancer.

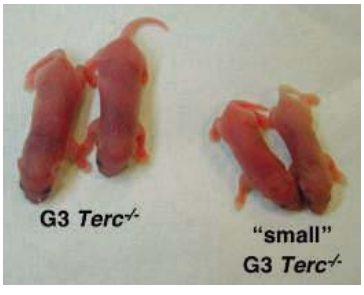

CREDIT: FLORES *ET AL.*

The Smaller the Better

Small α-proteobacteria account for about a quarter of all bacteria in the oceans. **Giovannoni *et al.*** (p. 1242) reveal that *Pelagibacter*, the first isolate from this clade, has the smallest genome yet observed in a free-living organism. Unlike many parasites and symbionts, *Pelagibacter* retains a nearly full suite of biosynthetic genes, but it shows no trace of "junk" DNA. Because of the extremely large population size, it seems that selection can act on the very small fitness costs of replicating functionless DNA. In contrast to *Pelagibacter*, other heterotrophic marine bacteria for which genome sequences are available have relatively large genomes.

Host Factors Required for Microbial Residence

The host cells characteristics that allow for microbial invasion and residence are less well defined than the virulence factors that allow microbe entry. Using a genome-wide screening approach, **Philips *et al.*** (p. 1251, published online 14 July 2005) identified host factors required for infection by *Mycobacterium fortuitum*, which divides within vacuoles. Factors fell into two main categories: those that generally affect phagocytosis (the process by which cells engulf extracellular particles) and those that cause a specific defect in mycobacterial uptake or growth. A *Drosophila* member of the CD36 family of scavenger receptors was specifically required for the uptake of mycobacteria. Using a similar approach, **Agaisse *et al.*** (p. 1248, published online 14 July 2005) identified host factors that affect intracellular infection by *Listeria monocytogenes*, a bacterial pathogen that escapes from phagocytic vacuoles and replicates within the cytosol of host cells. Several phenotypes were observed, including decreases in the percentage of host cells infected, alterations of intracellular growth rates, and changes in subcellular location of bacteria. The identified host factors spanned a wide range of cellular functions. Comparing the two studies revealed host factors that specifically affect access to the cytosol by *L. monocytogenes* and host pathways that are differentially required for intracellular infection by a cytosolic versus a vacuolar intracellular bacterial pathogen.

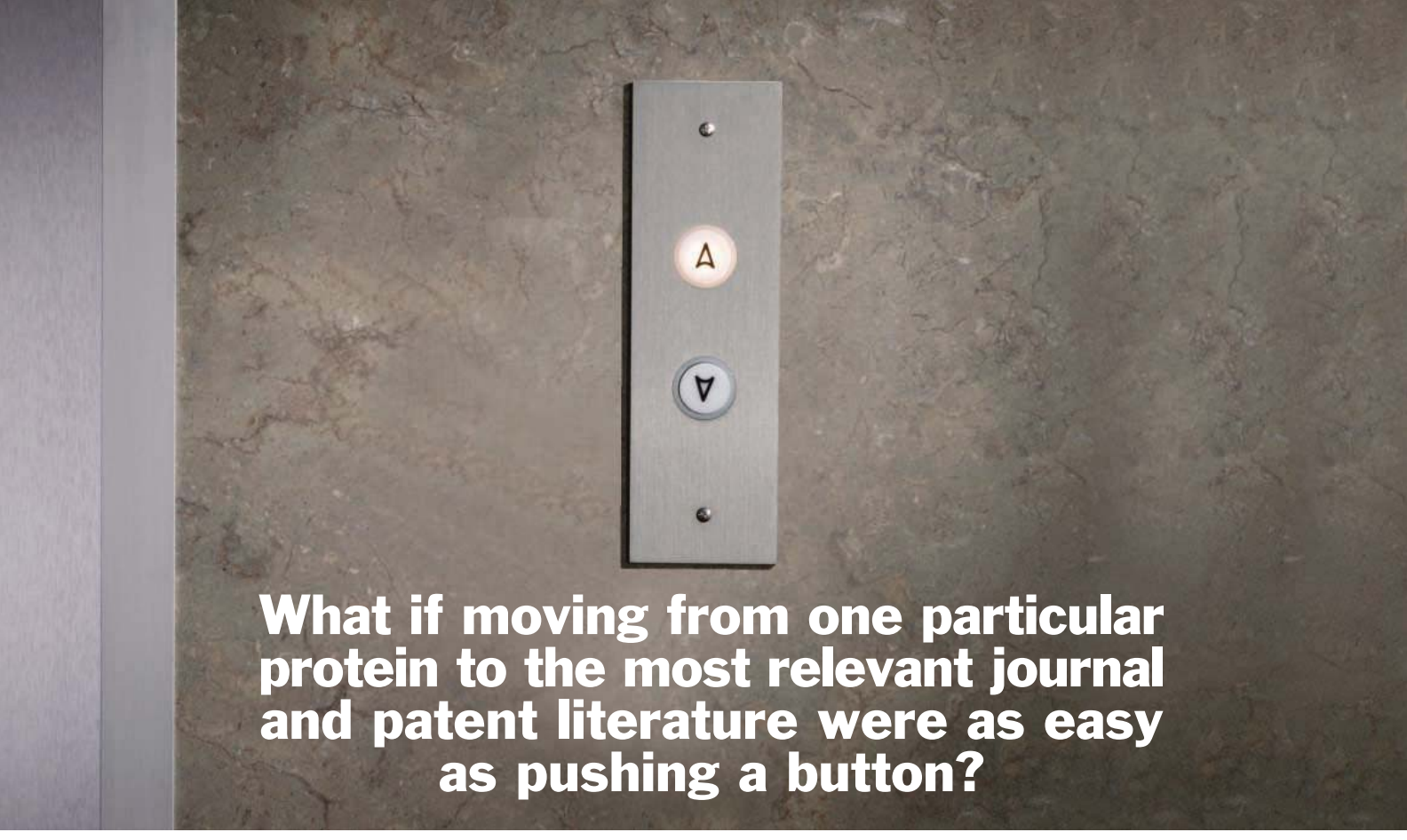

What if moving from one particular protein to the most relevant journal and patent literature were as easy as pushing a button?

It is.

Not only does SciFinder provide access to more proteins and nucleic acids than any publicly available source, but they're a single click away from their referencing patents and original research.

Coverage includes everything from the U.S. National Library of Medicine's (NLM) MEDLINE® and much more. In fact, SciFinder is the only single source of patents and journals worldwide.

Once you've found relevant literature, you can use SciFinder's powerful refinement tools to focus on a specific research area, for example: biological studies such as target organisms or diseases; expression microarrays; or analytical studies such as immunoassays, fluorescence, or PCR analysis. From each reference, you can link to the electronic full text of the original paper or patent, plus use citation tools to track how the research has evolved and been applied.

Visualization tools help you understand results at a glance. You can categorize topics and substances, identify relationships between areas of study, and see areas that haven't been explored at all.

Comprehensive, intuitive, seamless—SciFinder directs you. It's part of the process. To find out more, call us at 1-800-753-4227 (North America) or 1-614-447-3700 (worldwide) or visit www.cas.org/SCIFINDER.

SciFinder®

Part of the process.℠

Anniversary Reflections

Last month, we marked *Science*'s 125th birthday with an issue that celebrated the great open questions that advance science. We have pondered with interest the various responses to our anniversary edition, and here we offer some reflections, as some of the comments get to the heart of larger issues. A quick review of what we did: The top 25 "Big Questions" facing science were selected by a long and sometimes exhausting conversation among our News and Editorial staffs, with input from our Board of Reviewing Editors. To arrive at the anniversary number of 125, we added 100 slightly less central ones and also used the EurekAlert! Kids' Portal to find out what questions youngsters were asking.*

There were welcome compliments on our choice to emphasize questions rather than answers, and some thoughtful speculations on how long getting the answers would take. The children, in particular, produced some fascinating responses: Can black holes suck up stars? Can artificial life-support systems sustain human life on hostile terrains? How is nature better than technology? There was also praise for the opening essay by Tom Siegfried that reflected on the major questions in physics and biology that were influenced by what was happening in 1880, when our first issue was published.

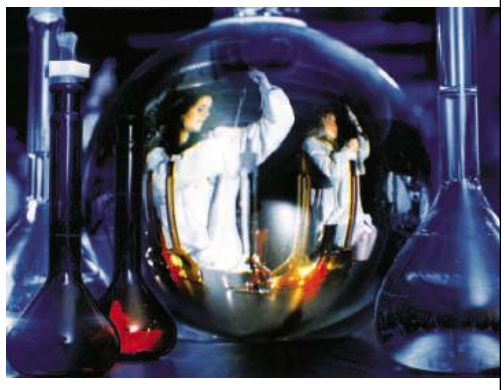

There were some complaints about the Milestone Poster produced by the American Association for the Advancement of Science (AAAS) business office, one pointing out that it failed to pay adequate attention to non-Western achievements. The most troubling comments for me, however, were objections from two female scientists to the absence of women among the photographs associated with the Siegfried essay—concerns surfacing just when the issue of women in science has become a topic of intense and sometimes corrosive discussion in the academic community.

Where do we stand now in representing our enterprise to the children, women, and minority scientists who seek entry? The practice of science in 2005 is very different from what it was in 1980, our last anniversary. More research is being done by more people, working in increasingly larger teams, with tools that were undreamed of two decades ago. To illustrate: The average number of authors per paper in this anniversary issue was 12, with a range from 2 to 50. Exactly 5 years earlier in the issue of the corresponding date, the average number was only 4, and no author list was in double figures.

Thus, more people are working, and working together, in a tight job market when funding is harder to get. And young scholars entering universities—especially women—are not choosing science as frequently as we would wish. Our 25 Big Questions emphasize that this is a time of great intellectual opportunity in science. These are the best of times; so good, indeed, that we must act now to brighten the prospects for future scientists. In this work, there is surely a role for governments in making more support available and making good science an important political priority. But there is also a role for the community itself. We need to inspire kids—those who wrote to us and beyond. We simply can't afford to leave out any fraction of the eligibility pool.

That means that we must make special efforts to make science more attractive to women by strengthening incentives for undergraduate women to undertake doctoral work, and by ensuring that there are highly visible women in science leadership positions to demonstrate what is possible. On p. 1190 of this issue, Jo Handelsman and a distinguished group of senior academic women scientists provide exactly that sort of demonstration. They step around the minefield of largely discredited intellectual differences and provide a rich assessment of the cultural issues that may discourage women.

Finally, I refer back to the comments of the two distinguished women scientists mentioned above, one of whom is a close colleague who was civil but unsparing in her candor. They are right in that we missed some opportunities in our anniversary issue; for example, we should have used a picture or description of Marie Curie as one of those pathbreaking 19th-century scientists. Handlesman *et al*. point out that people "who are committed to egalitarian principles and believe that they are not biased may nevertheless unconsciously or inadvertently behave in discriminatory ways." A good reminder for all of us, your editors included.

Donald Kennedy
Editor-in-Chief

*www.eurekalert.org/scienceforkids/125th. EurekAlert! is a service of AAAS.

10.1126/science.1118183

Spend less time looking for antibodies and more time doing research...

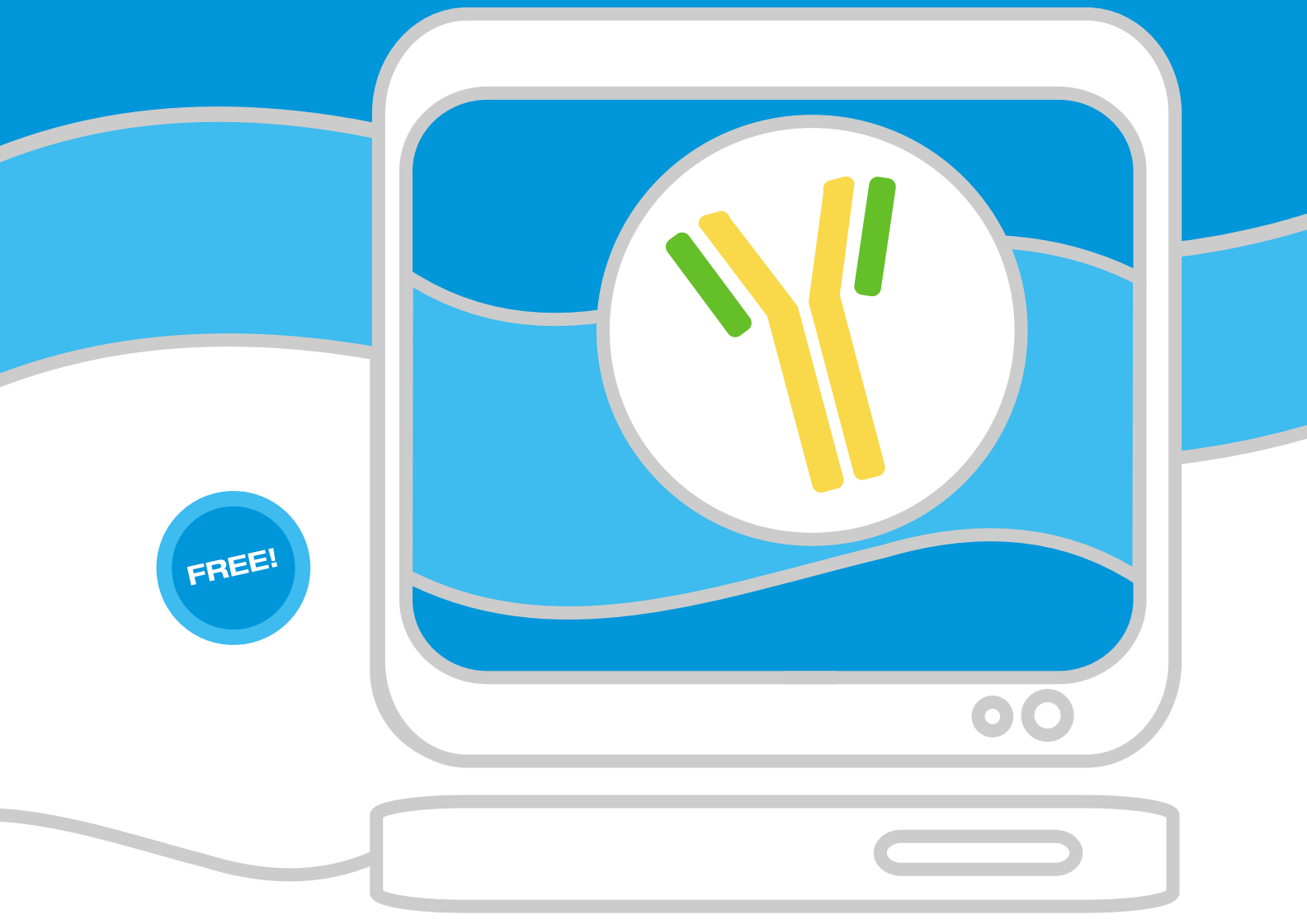

FREE!

Find Antibodies Online

Search over 130,000 antibodies from over 100 companies by antigen, species reactivity, and application... free and online.

- Over 130,000 Antibodies
- Over 100 Antibody Companies
- No Registration Required
- Full Product Specifications
- Over 225,000 Research Products and Instruments
- Direct Access to Product Pages on Company Websites

biocompare®

The Buyer's Guide for Life Scientists™

www.biocompare.com

EDITORS' CHOICE

edited by Gilbert Chin

EARTH SCIENCE

An Impending Cloud of Death

On 12 August 1986, a deadly cloud of CO_2 and water mist was released from Lake Nyos, Cameroon, and killed more than 1700 people by asphyxiation as it spilled into adjacent valleys. The dense cloud of gas, which was 50 m thick and traveled farther than 20 km at speeds of 20 to 50 km/hour, was produced by the dissolution of CO_2 in the deep part of the lake; a convective overturn displaced the lower layer of the stratified lake, causing the CO_2-rich water that had been at the bottom to degas like a bottle of fizzy water being opened. Such events have happened before in this region, and may happen again if steps are not taken to prevent them.

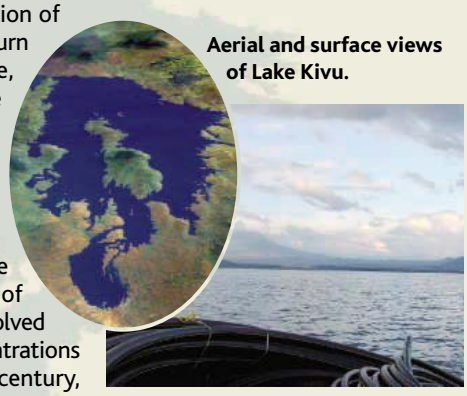

Aerial and surface views of Lake Kivu.

Schmid *et al.* report that a similar situation is developing at Lake Kivu, an East African rift lake between Rwanda and the Democratic Republic of Congo. The depths of Lake Kivu are amassing dissolved CO_2 and CH_4 at a rate fast enough that CH_4 concentrations will approach saturation toward the end of this century, making it likely that a magmatic eruption in the volcanically active lake basin, or some other disturbance, could trigger overturn and the release of another lethal CO_2 cloud. Without human intervention to reduce the concentration of CH_4, the 2 million people along the Lake Kivu shoreline may suffer a catastrophic gas release. — HJS

Geochem. Geophys. Geosyst. 10.1029/2004GC000892 (2005).

CHEMISTRY

Designing Carbenes

In the past 10 years, *N*-heterocyclic carbenes (NHCs) have grown from being regarded as chemical curiosities to become versatile ligands for a wide range of homogeneously catalyzed reactions. Most carbenes (molecules bearing a two-coordinate divalent carbon) are unstable at room temperature, but in an NHC, the unsaturated carbon is stabilized by electron-donating nitrogen atoms on either side.

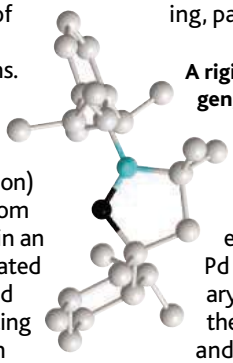

A rigid and bulky CAAC (nitrogen, blue; carbene, black).

Lavallo *et al.* have designed a different type of carbene, termed a cyclic alkyl(amino) carbene (CAAC), in which one of the nitrogens is replaced by a quaternary alkyl center. By appending bulky groups such as cyclohexane to this center, the authors can prepare compounds with stabilities comparable to those of NHCs, but sporting distinct steric and electronic properties. As a ligand, the CAAC is a strong σ-electron donor, and crystallography of a CAAC-coordinated palladium complex reveals steric crowding, particularly close to the metal center. One practical result of these properties is the efficient catalysis by this Pd complex of unactivated aryl chloride couplings to the α-position of aldehydes and ketones. — JSY

Angew. Chem. Int. Ed. 10.1002/anie.200501841 (2005).

CELL BIOLOGY

Minimalist Machinery

The fusion of two biological membranes requires the concerted action of integral membrane proteins (either endogenous ones or those carried by enveloped viruses) that rearrange the lipid bilayers in such a way as to facilitate membrane merger. Top *et al.* describe a recently characterized family of reovirus proteins that lack a well-defined hydrophobic fusion peptide and hence appear to promote fusion via a somewhat different trigger than that utilized by the archetypal influenza virus hemagglutinin. These fusion-associated small transmembrane (FAST) proteins mediate efficient cell-cell fusion when transfected into a variety of cells. Furthermore, when reconstituted into proteo-liposomes, a reptilian reovirus FAST protein promoted time- and temperature-dependent liposome-cell and liposome-liposome fusion as assessed by the mixing of lipids and of liposome contents. The precise mechanism by which this simple machine can initiate membrane fusion remains to be elucidated, but may involve the combined action of chaotropic modules in the extramembraneous portions of the FAST protein. — SMH

EMBO J. 10.1038/sj.emboj.7600767 (2005).

BIOMEDICINE

Insig(ht)s into Metabolic Control

Cholesterol has received a lot of bad press, but it is essential for human health. When we don't get enough cholesterol from our diet, our bodies—specifically our liver—begin to synthesize it. Conversely, when we eat lots of high-cholesterol foods, this biosynthetic machinery shuts down. How this feedback regulation works has fascinated scientists for over 70 years, and in the past decade, considerable progress has been made toward answering that question at the molecular level.

Among the potentially important metabolic regulators identified in studies of cultured cells are the membrane proteins Insigs-1 and -2, so named because they are encoded by insulin-induced genes. The Insigs reside in the endoplasmic reticulum, and they appear to act in part by trapping within this compartment a transcription factor that is required in the nucleus to turn on the expression of genes involved in cholesterol biosynthesis. Engelking *et al.* show that mice with liver-specific deletions of the Insig genes display a severely blunted feedback response; that is, they continue making cholesterol even when fed a high-cholesterol diet. These results establish the physiological significance of the Insigs in a whole-animal setting and highlight the importance of the liver as the site where the cholesterol feedback system operates. — PAK

J. Clin. Invest. 10.1172/JCI25614 (2005).

CONTINUED ON PAGE 1157

Launch Your Discovery with MISSION™ RNAi

Introducing the MISSION shRNA Library of The RNAi Consortium

The RNAi Consortium (TRC), based at the Broad Institute of MIT and Harvard, is developing pre-cloned MISSION shRNA libraries targeting the human and mouse genomes. As a member of TRC, Sigma-Aldrich is a principle collaborator and global supplier of the lentiviral based shRNA vector collections for use in transient or stable transfection, as well as viral particle generation. The complete libraries will target 15,000 human and 15,000 mouse genes.

You'll Discover:

- *~35,000 clones available targeting diverse gene families*
- *Renewable resource compared to siRNA*
- *Long term knockdown and phenotypic studies*
- *Lentiviral particles facilitate silencing in difficult cell lines*
- *Sequence-verified clones*

*Experience the **MISSION shRNA** libraries for yourself.*
*Search our target gene database at: **sigma-aldrich.com/mission_px4***

Plus, register to receive our latest literature and updates on upcoming product formats and gene family sets.

MISSION RNAi

Member of *The RNAi Consortium*

DEVELOPMENTAL BIOLOGY

Beams and Hangers

The fully grown oocyte of the frog *Xenopus laevis* contains considerable internal architecture—in particular, an extensive cytokeratin network—even though it is only a single cell. One of the features of this network is that it compartmentalizes maternally encoded RNA molecules, which are important for development of the embryo after fertilization; disruption of the network results in release of these RNAs.

Kloc *et al.* show that the cytokeratin network is also necessary for formation of the germinal granules during oogenesis. A class of maternal RNA molecules forms

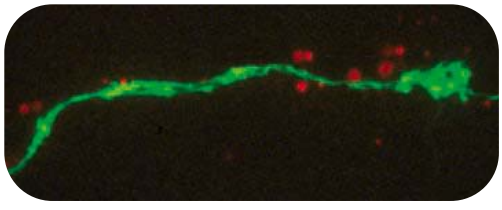

Association of Xlsirts RNA (red) with cytokeratin filament (green).

part of the germinal granules, which accumulate in the oocyte and are passed into a small but important lineage of cells: the primordial germ cells that will eventually give rise to eggs and sperm. The cytokeratin network depends for its own structural integrity on two molecules, VegT and Xlsirts, and both of these function in this setting as RNAs, not as translated proteins. The structural components of this cellular network thus seem to include RNA molecules as well as cytokeratin filaments. — PJH

Development **132**, 3445 (2005).

CHEMISTRY

Not So Inert

Sulfur hexafluoride (SF_6) is so unreactive that it can be used, among other applications, as a protective blanket for processing highly reactive magnesium metal, yet its long lifetime in the atmosphere (>3000 years) has caused concern because it has the strongest greenhouse effect known for any gas. Despite the reputation of SF_6 for inertness, Basta *et al.* report a reaction in which it proves to be a faster fluorinating agent than normally more reactive compounds such as XeF_2 or CoF_3. The low-valent Ti compound, Ti[1,3-C_5H_3(*tert*-C_4H_9)$_2$](6,6-dimethylcyclohexadienyl)($P(CH_3)_3$), which can be regarded as a half-open titanocene, reacted readily with SF_6 to produce the tetrameric product {Ti[1,3-C_5H_3(*tert*-C_4H_9)$_2$]F_2}$_4$ and the byproduct $(CH_3)_3PS$. The authors propose that SF_6 can coordinate an F atom to the metal center and drive the reaction through an oxidative inner-sphere electron transfer. — PDS

J. Am. Chem. Soc. 10.1021/ja052214s (2005).

HIGHLIGHTED IN *SCIENCE*'S SIGNAL TRANSDUCTION KNOWLEDGE ENVIRONMENT

Science's STKE www.stke.org

The Ligand Is a Gas

Nuclear receptors function as ligand-regulated transcription factors, but for many members of this family, the ligands are not known. In fact, before the fine piece of detective work described by Reinking *et al.*, only 1 of the 18 nuclear receptor proteins in *Drosophila* had an identified ligand. The clue that led to the unexpected partner for the receptor known as E75 was the blood-red color of the purified protein. Electron absorption and mass spectrometry analysis revealed that the receptor has a tightly associated heme group. Further analysis led the authors to propose three possible functions of the receptor complex. First, heme was required for stability of the E75 protein, and thus E75 could serve as a sensor of cellular heme concentration. Second, heme-containing proteins are known to bind diatomic gases, and E75 is no exception. Binding of CO and NO to E75 was detected spectrophotometrically. E75 interacts with another nuclear receptor, HR3, and inhibits activation of target genes by HR3. CO binding inhibited interaction of a peptide from HR3 with E75. Treatment of cells with NO donors relieved the inhibitory effects of E75 on HR3-induced transcription. Thus, E75 may sense CO and NO as intracellular signaling molecules. Finally, E75 might function as a redox sensor because only the reduced form of E75 was stabilized by interaction with the HR3 peptide. — LBR

Cell **122**, 195 (2005).

CREDITS: KLOC *ET AL.*, *DEVELOPMENT* **132**, 3445 (2005)

GENETIC IMAGINE SOLVING

YOUNG SCIENTIST AWARD

ABOUT THE SPONSORS:

GE Healthcare
GE Healthcare helps predict, diagnose, inform and treat so that every individual can live life to the fullest. GE Healthcare employs more than 42,500 people in more than 100 countries and is one of the world's leading suppliers of transformational medical technologies.

AAAS/*Science*
As well as publishing the journal *Science*, AAAS is an international non-profit organization dedicated to advancing science around the world by serving as an educator, leader, spokesperson and professional association.

DISEASE:
A 20-YEAR RIDDLE

Well that's just what one young scientist did when she unlocked the secrets of the spliceosome, a crucial molecular machine within the cell. Dr. Saba Valadkhan's breakthrough discovery won her the 2004 Young Scientist Award.

The spliceosome plays a key role in human health. Errors in its function are thought to cause up to 50% of all genetic disease – the tiniest mistake can result in retinal degeneration or neurological disease. A clear understanding of how this large and complex structure works had evaded scientists despite two decades of research. But Dr. Valadkhan has changed that with the successful development of a novel, minimal spliceosome stripped down to the core elements. This is now shedding light on how spliceosome errors translate into mistakes in gene expression.

Dr. Valadkhan won the grand prize in the 2004 Young Scientist Award competition with an essay based on her research in this area. She is now an assistant professor at the Center for RNA Molecular Biology at Case Western Reserve University in Cleveland, Ohio (USA). She says: "The prize has been very beneficial to my career. It has given me valuable new connections, and a great deal of recognition in the scientific community. It has also helped me see my work in a wider context, and understand what science is really all about."

YOUR OPPORTUNITY TO WIN IS NOW

The Young Scientist Award was established in 1995, and is presented by *Science*/AAAS and GE Healthcare. The aim of the prize is to recognize outstanding most recent Ph.D.s from around the world and reward their research in the field of molecular biology.

This is your chance to gain international acclaim and recognition for yourself and your faculty. If you were awarded your Ph.D. in molecular biology* during 2004, describe your work in a 1,000-word essay. Then submit it for the 2005 Young Scientist Award. Your essay will be reviewed by a panel of distinguished scientists who will select one grand prize winner and up to seven regional winners. The grand prize winner will get his or her essay published in *Science*, receive US$25,000, and be flown to the awards ceremony in St. Louis, Missouri (USA). Entries should be received by **September 30, 2005**.

Go to **www.aaas.org/youngscientistaward** to find the entry form. We wish continued success to Dr. Valadkhan. And to you.

Read Dr. Saba Valadkhan's latest findings in *RNA*. 2003 Jul, **9** (7): 892-904.

Established and presented by:

Science AAAS

GE imagination at work

* For the purpose of this prize, molecular biology is defined as "that part of biology which attempts to interpret biological events in terms of the physico-chemical properties of molecules in a cell" (*McGraw-Hill Dictionary of Scientific and Technical Terms*, 4th Edition).

www.sciencemag.org

Science

1200 New York Avenue, NW
Washington, DC 20005
Editorial: 202-326-6550, FAX 202-289-7562
News: 202-326-6500, FAX 202-371-9227

Bateman House, 82-88 Hills Road
Cambridge, UK CB2 1LQ
+44 (0) 1223 326500, FAX +44 (0) 1223 326501

Subscription Services For change of address, missing issues, new orders and renewals, and payment questions: 800-731-4939 or 202-326-6417, FAX 202-842-1065. Mailing addresses: AAAS, P.O. Box 1811, Danbury, CT 06813 or AAAS Member Services, 1200 New York Avenue, NW, Washington, DC 20005

Institutional Site Licences please call 202-326-6755 for any questions or information

Reprints: Author Inquiries 800-635-7181
Commercial Inquiries 803-359-4578
Corrections 202-326-6501

Permissions 202-326-7074, FAX 202-682-0816

Member Benefits Bookstore: AAAS/BarnesandNoble.com bookstore www.aaas.org/bn; Car purchase discount: Subaru VIP Program 202-326-6417; Credit Card: MBNA 800-847-7378; Car Rentals: Hertz 800-654-2200 CDP#343457, Dollar 800-800-4000 #AA1115; AAAS Travels: Betchart Expeditions 800-252-4910; Life Insurance: Seabury & Smith 800-424-9883; Other Benefits: AAAS Member Services 202-326-6417 or www.aaasmember.org.

science_editors@aaas.org (for general editorial queries)
science_letters@aaas.org (for queries about letters)
science_reviews@aaas.org (for returning manuscript reviews)
science_bookrevs@aaas.org (for book review queries)

Published by the **American Association for the Advancement of Science (AAAS)**, *Science* serves its readers as a forum for the presentation and discussion of important issues related to the advancement of science, including the presentation of minority or conflicting points of view, rather than by publishing only material on which a consensus has been reached. Accordingly, all articles published in *Science*—including editorials, news and comment, and book reviews—are signed and reflect the individual views of the authors and not official points of view adopted by the AAAS or the institutions with which the authors are affiliated.

AAAS was founded in 1848 and incorporated in 1874. Its mission is to advance science and innovation throughout the world for the benefit of all people. The goals of the association are to: foster communication among scientists, engineers and the public; enhance international cooperation in science and its applications; promote the responsible conduct and use of science and technology; foster education in science and technology for everyone; enhance the science and technology workforce and infrastructure; increase public understanding and appreciation of science and technology; and strengthen support for the science and technology enterprise.

Information for Contributors

See pages 135 and 136 of the 7 January 2005 issue or access www.sciencemag.org/feature/contribinfo/home.shtml

EDITOR-IN-CHIEF **Donald Kennedy**
EXECUTIVE EDITOR **Monica M. Bradford**
DEPUTY EDITORS **R. Brooks Hanson, Katrina L. Kelner**
NEWS EDITOR **Colin Norman**

Editorial SUPERVISORY SENIOR EDITORS Barbara Jasny, Phillip D. Szuromi; SENIOR EDITOR/PERSPECTIVES Lisa D. Chong; SENIOR EDITORS Gilbert J. Chin, Pamela J. Hines, Paula A. Kiberstis (Boston), Beverly A. Purnell, L. Bryan Ray, Guy Riddihough (Manila), H. Jesse Smith, Valda Vinson, David Voss; ASSOCIATE EDITORS Marc S. Lavine, Jake S. Yeston; ONLINE EDITOR Stewart Wills; CONTRIBUTING EDITOR Ivan Amato; ASSOCIATE ONLINE EDITOR Tara S. Marathe; BOOK REVIEW EDITOR Sherman J. Suter; ASSOCIATE LETTERS EDITOR Etta Kavanagh; INFORMATION SPECIALIST Janet Kegg; EDITORIAL MANAGER Cara Tate; SENIOR COPY EDITORS Jeffrey E. Cook, Harry Jach, Barbara P. Ordway; COPY EDITORS Cynthia Howe, Alexis Wynne Mogul, Sabrah M. n'haRaven, Jennifer Sills, Trista Wagoner; EDITORIAL COORDINATORS Carolyn Kyle, Beverly Shields; PUBLICATION ASSISTANTS Chris Filiatreau, Joi S. Granger, Jeffrey Hearn, Lisa Johnson, Scott Miller, Jerry Richardson, Brian White, Anita Wynn; EDITORIAL ASSISTANTS Ramatoulaye Diop, E. Annie Hall, Patricia M. Moore, Brendan Nardozzi, Michael Rodewald; EXECUTIVE ASSISTANT Sylvia S. Kihara; ADMINISTRATIVE SUPPORT Patricia F. Fisher

News SENIOR CORRESPONDENT Jean Marx; DEPUTY NEWS EDITORS Robert Coontz, Jeffrey Mervis, Leslie Roberts, John Travis; CONTRIBUTING EDITORS Elizabeth Culotta, Polly Shulman; NEWS WRITERS Yudhijit Bhattacharjee, Adrian Cho, Jennifer Couzin, David Grimm, Constance Holden, Jocelyn Kaiser, Richard A. Kerr, Eli Kintisch, Andrew Lawler (New England), Greg Miller, Elizabeth Pennisi, Robert F. Service (Pacific NW), Erik Stokstad; Carolyn Gramling, Genevra Ornelas, Cathy Tran (interns); CONTRIBUTING CORRESPONDENTS Marcia Barinaga (Berkeley, CA), Barry A. Cipra, Jon Cohen (San Diego, CA), Daniel Ferber, Ann Gibbons, Robert Irion, Mitch Leslie (NetWatch), Charles C. Mann, Evelyn Strauss, Gary Taubes, Ingrid Wickelgren; COPY EDITORS Linda B. Felaco, Rachel Curran, Sean Richardson; ADMINISTRATIVE SUPPORT Scherraine Mack, Fannie Groom BUREAUS: Berkeley, CA: 510-652-0302, FAX 510-652-1867, New England: 207-549-7755, San Diego, CA: 760-942-3252, FAX 760-942-4979, Pacific Northwest: 503-963-1940

Production DIRECTOR James Landry; SENIOR MANAGER Wendy K. Shank; ASSISTANT MANAGER Rebecca Doshi; SENIOR SPECIALISTS Vicki J. Jorgensen, Jessica K. Moshell; SPECIALISTS Jay R. Covert, Stacey Ferebee; **Preflight** DIRECTOR David M. Tompkins; MANAGER Marcus Spiegler; SPECIALIST Jessie Mudjitaba;

Art DIRECTOR Joshua Moglia; ASSOCIATE ART DIRECTOR Kelly Buckheit; ILLUSTRATOR Katharine Sutliff; SENIOR ART ASSOCIATES Holly Bishop, Laura Creveling, Preston Huey, Julie White; ASSOCIATE Nayomi Kevitiyagala; PHOTO RESEARCHER Leslie Blizard

***Science* International**

Europe (science@science-int.co.uk) EDITORIAL: INTERNATIONAL MANAGING EDITOR Andrew M. Sugden; SENIOR EDITOR/PERSPECTIVES Julia Fahrenkamp-Uppenbrink; SENIOR EDITORS Caroline Ash (Geneva: +41 (0) 222 346 3106), Stella M. Hurtley, Ian S. Osborne, Stephen J. Simpson, Peter Stern; EDITORIAL SUPPORT Emma Westgate; Deborah Dennison ADMINISTRATIVE SUPPORT Janet Clements, Phil Marlow, Jill White; NEWS: INTERNATIONAL NEWS EDITOR Eliot Marshall DEPUTY NEWS EDITOR Daniel Clery; CORRESPONDENT Gretchen Vogel (Berlin: +49 (0) 30 2809 3902, FAX +49 (0) 30 2809 8365); CONTRIBUTING CORRESPONDENTS Michael Balter (Paris), Martin Enserink (Amsterdam and Paris); INTERN Mason Inman

Asia Japan Office: Asca Corporation, Eiko Ishioka, Fusako Tamura, 1-8-13, Hirano-cho, Chuo-ku, Osaka-shi, Osaka, 541-0046 Japan; +81 (0) 6 6202 6272, FAX +81 (0) 6 6202 6271; asca@os.gulf.or.jp JAPAN NEWS BUREAU: Dennis Normile (contributing correspondent, +81 (0) 3 3391 0630, FAX 81 (0) 3 5936 3531; dnormile@gol.com); CHINA REPRESENTATIVE Hao Xin, + 86 (0) 10 6307 4439 or 6307 3676, FAX +86 (0) 10 6307 4358; haoxin@earthlink.net; SOUTH ASIA Pallava Bagla (contributing correspondent +91 (0) 11 2271 2896; pbagla@vsnl.com); ASIA Richard Stone (rstone@aaas.org)

EXECUTIVE PUBLISHER **Alan I. Leshner**
PUBLISHER **Beth Rosner**

Fulfillment & Membership Services (membership@aaas.org) DIRECTOR Marlene Zendell; MANAGER Waylon Butler; SYSTEMS SPECIALIST Andrew Vargo SPECIALISTS Pat Butler; Laurie Baker, Tamara Alfson, Karena Smith, Vicki Linton

Business Operations and Administration DIRECTOR Deborah Rivera-Wienhold; BUSINESS MANAGER Randy Yi; SENIOR BUSINESS ANALYST Lisa Donovan; BUSINESS ANALYST Jessica Tierney; FINANCIAL ANALYST Michael LoBue, Farida Yeasmin; RIGHTS AND PERMISSIONS: ADMINISTRATOR Emilie David; ASSOCIATE Elizabeth Sandler; MARKETING: DIRECTOR John Meyers; MARKETING MANAGERS Darryl Walter, Allison Pritchard; MARKETING ASSOCIATES Julianne Wielga, Mary Ellen Crowley, Amanda Donathen, Catherine Featherston; DIRECTOR OF INTERNATIONAL MARKETING AND RECRUITMENT ADVERTISING Deborah Harris; INTERNATIONAL MARKETING MANAGER Wendy Sturley; MARKETING/MEMBER SERVICES EXECUTIVE: Linda Rusk; JAPAN SALES AND MARKETING MANAGER Jason Hannaford; SITE LICENSE SALES: DIRECTOR Tom Ryan; SALES AND CUSTOMER SERVICE Mehan Dossani, Catherine Holland, Wendy Wise; ELECTRONIC MEDIA: PRODUCTION MANAGER Lizabeth Harman; ASSISTANT PRODUCTION MANAGER Wendy Stengel; PRODUCTION ASSOCIATES Sheila Mackall, Amanda K. Skelton, Lisa Stanford, Nichele Johnston; APPLICATIONS DEVELOPER Carl Saffell

Advertising DIRECTOR WORLDWIDE AD SALES Bill Moran
Product (science_advertising@aaas.org); MIDWEST Rick Bongiovanni: 330-405-7080, FAX 330-405-7081 • WEST COAST/W. CANADA B. Neil Boylan (Associate Director): 650-964-2266, FAX 650-964-2267 • EAST COAST/E. CANADA Christopher Breslin: 443-512-0330, FAX 443-512-0331 • UK/SCANDINAVIA/FRANCE/ITALY/BELGIUM/NETHERLANDS Andrew Davies (Associate Director): +44 (0)1782 750111, FAX +44 (0) 1782 751999 • GERMANY/SWITZERLAND/AUSTRIA Tracey Peers (Associate Director): +44 (0) 1782 752530, FAX +44 (0) 1782 752531 JAPAN Mashy Yoshikawa: +81 (0) 33235 5961, FAX +81 (0) 33235 5852 ISRAEL Jessica Nachlas +9723 5449123 • TRAFFIC MANAGER Carol Maddox; SALES COORDINATOR Deiandra Simms
Classified (advertise@sciencecareers.org); U.S.: SALES DIRECTOR Gabrielle Boguslawski: 718-491-1607, FAX 202-289-6742; INTERNET SALES MANAGER Beth Dwyer: 202-326-6534; INSIDE SALES MANAGER Daryl Anderson: 202-326-6543; WEST COAST/MIDWEST Kristine von Zedlitz: 415-956-2531; EAST COAST Jill Downing: 631-580-2445; CANADA, MEETINGS AND ANNOUNCEMENTS Kathleen Clark: 510-271-8349; LINE AD SALES Emnet Tesfaye: 202-326-6740; SALES COORDINATORS Erika Bryant; Rohan Edmonson Christopher Normile, Joyce Scott, Shirley Young; INTERNATIONAL: SALES MANAGER Tracy Holmes: +44 (0) 1223 326525, FAX +44 (0) 1223 326532; SALES Christina Harrison, Svitlana Barnes; SALES ASSISTANT Helen Moroney; JAPAN: Jason Hannaford: +81 (0) 52 789 1860, FAX +81 (0) 52 789 1861; PRODUCTION: MANAGER Jennifer Rankin; ASSISTANT MANAGER Deborah Tompkins; ASSOCIATES Christine Hall; Amy Hardcastle; PUBLICATIONS ASSISTANTS Robert Buck; Natasha Pinol

AAAS Board of Directors RETIRING PRESIDENT, CHAIR Shirley Ann Jackson; PRESIDENT Gilbert S. Omenn; PRESIDENT-ELECT John P. Holdren; TREASURER David E. Shaw; CHIEF EXECUTIVE OFFICER Alan I. Leshner; BOARD Rosina M. Bierbaum; John E. Burris; John E. Dowling; Lynn W. Enquist; Susan M. Fitzpatrick; Richard A. Meserve; Norine E. Noonan; Peter J. Stang; Kathryn D. Sullivan

AAAS
ADVANCING SCIENCE, SERVING SOCIETY

NetWatch

edited by Mitch Leslie

DATABASE

Unveiling the Deep Sky

To weed out distractions during his search for comets, French astronomer Charles Messier (1730–1817) tallied other fuzzy heavenly bodies that could be mistaken for the periodic visitors. His Messier Catalog, which you can browse at this site from Students for the Exploration and Development of Space, was more than a mere collection of interstellar smudges. Messier penned the first systematic listing of "deep-sky" objects that include star clusters, galaxies, and nebulae where new suns are born. Among the 110 Messier objects is the Whirlpool Galaxy M51 (above), spotted in 1773. Each object's entry offers basic data such as its position and apparent brightness, describes its discovery and study, and features plenty of images.

www.seds.org/messier

DATABASE

Follow the Money

The U.S. government pumped more than $111 billion into research and development (R&D) in 2003 and an estimated $121 billion in 2004. Find out how much money each agency doles out, who gets it, and what they're spending it on at RaDiUS from the RAND Corp. Users previously had to pay to see the database, but RAND made it free earlier this year.

RaDiUS compiles all nonclassified federal R&D spending dating back to 1993. You can sift through more than 600,000 individual awards or organize them by agency, program, or project. At $59 billion, the Department of Defense was the largest funder in 2003, followed by the Department of Health and Human Services and NASA. Although access is free, you'll still have to apply for a "site license" and wait for a RAND employee to call with a username and password. Also note that the URL must include "https."

https://radius.rand.org

LINKS

The Social Scene

The social sciences span disciplines as diverse as anthropology, economics, and linguistics. To find resources in this sprawling area, check out the Social Science Information Gateway from Bristol University in the U.K. This vast collection of annotated links includes an anthropological study of India's Andaman Islanders, a dictionary of phobias, and a statistical primer for social scientists. You can also page through a calendar of upcoming conferences or find potential collaborators using the "Likeminds" listing.

sosig.esrc.bris.ac.uk

PODCASTS

Audio Infection

Microbe buffs can get an earful of information from their iPods every day, thanks to the American Society for Microbiology. The society has begun podcasting its MicrobeWorld Radio, a 90-second daily program of microbiology news. Pod people can automatically download new episodes as soon as they go online, then listen to the files on the computer or a digital audio player. Recent MicrobeWorld Radio shows have explored subjects such as methane on Mars, a possible indicator of life, and antimicrobial foods such as garlic and dried plum extract.

www.microbeworld.org

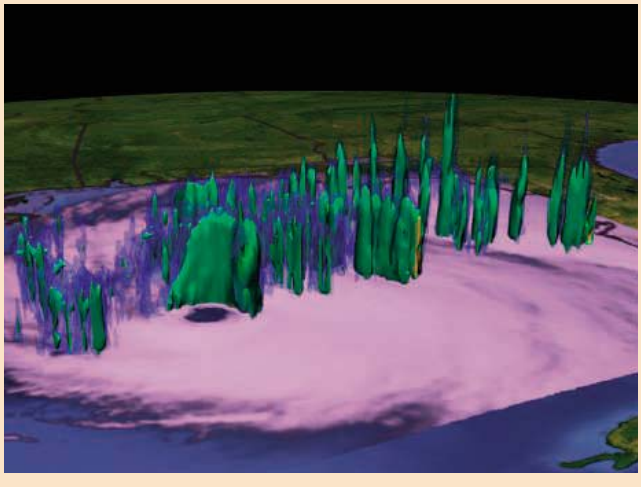

IMAGES

A Hard Rain's A-Gonna Fall

This year's Atlantic hurricane season opened with a roar. A record five tropical storms and two hurricanes hit the radar screens by the end of July. As we enter the most active part of the season, you can get updates on current storms and learn about incipient ones at this site, part of NASA's Life on Earth home page.

Bulletins post fresh satellite shots and let you call up storm-tracking maps. The site also offers plenty of data on past events and background information on hurricanes. For example, a short video traces the storms' birthplace to the highlands of Ethiopia, where winds bouncing over the rough terrain spawn air eddies. You can also step into galleries packed with satellite photos, movies, and diagrams such as this illustration (left) of precipitation from Hurricane Ivan, which swept ashore in Alabama last September. Green areas received 1.25 cm of rain or more per hour.

www.nasa.gov/vision/earth/lookingatearth/hurricane_2005.html

Send site suggestions to netwatch@aaas.org. Archive: www.sciencemag.org/netwatch

CREDITS (TOP TO BOTTOM): NASA AND THE HUBBLE HERITAGE TEAM; CDC; NASA

This Week

PAGE 1164
Crunch time in the Antarctic

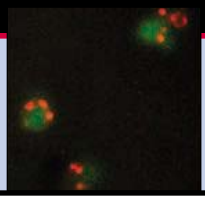

1166
Immune surprise

WILDLIFE BIOLOGY

'Genetic Rescue' Helps Panthers But Puts Researchers on the Spot

Ten years ago, the Florida panther seemed on the brink of extinction. Now, a new analysis concludes that a risky experiment to reinvigorate the panther population has paid off. But both the conclusions and the methodology of the analysis are proving controversial.

In 1995, wildlife biologists transplanted eight female panthers from Texas to south Florida in a last-ditch attempt to reverse the worrisome effects of inbreeding, including heart murmurs and defective sperm. A team of biologists led by ecologist Stuart Pimm of Duke University in Durham, North Carolina, has now analyzed a decade's worth of panther data and concluded that hybrid cats with Texas ancestry are surviving better than purebred Florida panthers and increasing the species' ranges of habitat. "This will be the strongest demonstration that a genetic introduction program can have a major positive impact on an endangered species," says conservation biologist Paul Beier of Northern Arizona University in Flagstaff.

The work, which is being released this week by *Animal Conservation*, is not without critics. Some doubt the introduction of Texas panthers deserves full credit for the population rebound. The group officially compiling the data analyzed by Pimm's team is also crying foul.

The decision to transplant endangered animals, especially large, charismatic predators such as panthers, is a political and scientific hot potato. Most efforts, such as the return of wolves to Yellowstone National Park, have been reintroductions into areas with no survivors. One exception is an effort with the prairie chicken, which was deemed a success (*Science*, 27 November 1998, p. 1695). Pimm had doubts that a population as inbred as the Florida panthers would benefit, arguing that conservation efforts ought instead to focus on land conservation and restoration.

After lengthy consultations with scientists and stakeholders, state and federal agencies permitted the taking of eight females from Texas and releasing them in south Florida. Biologists with the Florida Fish and Wildlife Conservation Commission (FFWCC) joined contractors in tracking the Texas panthers using radio collars and studying 54 offspring from the five Texas females that reproduced.

FFWCC publishes an annual report on the panthers, but it has not yet published a peer-reviewed study of the introduction. This delay frustrated Pimm, a conservation biologist. Working with Oron "Sonny" Bass Jr., an experienced panther biologist at Florida's Everglades National Park, and Duke doctoral student Luke Dollar, Pimm combed through the demographic data and movements of panthers contained in the annual reports.

Pimm's group calculates that the survival rate of the hybrid kittens was three times higher than that for the 118 purebred Florida kittens. Once adults, hybrid females also survived "considerably better" than purebreds did, Pimm says. Hybrid males, however, had shorter life spans than purebreds.

Still, the team concluded that hybrid males are expanding into new habitats, such as grasslands. That finding is controversial because it contradicts the long-standing policy of FFWCC and the U.S. Fish and Wildlife Service, which have determined that forests are the key for panther survival, a view that was contested by a scientific review team appointed by the agencies in 2002. "You certainly don't want to give up areas to developers by assuming that panthers cannot occupy them," says Pimm.

However, David Maehr of the University of Kentucky in Lexington, who led the FFWCC panther team from 1985 to 1994, maintains that panthers depend on forests and says he has a paper in press that will bolster this view. Any expansion by panthers into Everglades National Park may not last, he says: "It is dangerous to suggest that these often-flooded and low-prey-density areas will be a long-term benefit to panther recovery."

Maehr and other critics have additional bones to pick with Pimm's analysis. Pimm compared purebreds to all hybrids, irrespective of how much Texas ancestry they had, for example, to compare kitten survival rates. "I would have much more confidence if the people who had collected the data had made this conclusion," says Phil Hedrick, a population geneticist at Arizona State University in Tempe. "I think they're being much more cautious than Pimm is."

Hybrid vigor. Introduction of panthers from Texas has helped inbred Florida panthers (*above*) and increased survival of kittens.

CREDITS: FLORIDA FISH AND WILDLIFE CONSERVATION COMMISSION

Darrell Land, FFWCC's current panther team leader, says that Pimm's team may have acted unethically. "We feel they are seeking to publish other people's data. They never talked to us," says Land, noting that he and others have been working on a publication. But John Gittleman of the University of Virginia in Charlottesville, an editor of *Animal Conservation*, disagrees because the data are public: "I think that independent assessment is perfectly within their rights." —ERIK STOKSTAD

1167
Stone-cold reality

1168
The nuclear option, again

EVOLUTION

Kansas Prepares New Standards

The Kansas Board of Education last week endorsed science standards that would allow for the teaching of alternatives to evolutionary theory. Scientists say the new draft standards are a thinly disguised attempt to slip intelligent design (ID) into the curriculum by highlighting uncertainty and gaps in current scientific thinking. But it's an open question whether they will translate into changes in the classroom.

The 6–4 vote by the deeply divided board represents the latest skirmish in a long-running battle that has attracted national attention. The new standards follow May hearings that were boycotted by national scientific organizations, which saw them as a way to confer scientific legitimacy upon ID. The hearings were scheduled after an advisory panel set up by the board to revise the standards voted against including alternatives to evolution. The board is expected to adopt the standards this fall after an external review.

The 123-page draft document* calls on students "to learn about the best evidence for modern evolutionary theory, but also to learn about areas where scientists are raising scientific criticisms of the theory." Board member Kathy Martin, who voted with the majority, says that "these standards will ensure that our students learn to analyze scientific evidence critically. … They are the best thing to have happened to education in Kansas."

That's not what most scientists think, however. Although the standards do not mention ID—the idea that some features of living systems are best explained by an intelligent cause—the draft "is littered with language that is routinely used by intelligent design advocates," says Steven Case, committee chair and a biologist at the University of Kansas (KU) in Lawrence. The Kansas draft standards, he and others say, contain distorted definitions of evolutionary concepts and misstatements about biology. Biological evolution, for example, is described as "postulat[ing] an unguided natural process that has no discernable (*sic*) direction or goal"—a statement that Case says introduces the false idea that science addresses the purpose and meaning of natural phenomena. And Case says the statement that "the sequence of the nucleotide bases within genes is not dictated by any known chemical or physical law" deliberately ignores the fact that scientists are still exploring the organization of nucleotide bases. "If you say the sequences are not dictated by any known chemical or physical law, which is itself untrue, you could go one step further and ask if the sequences are dictated by a divine law," says Case.

The new standards may not represent anything more than a moral victory for ID proponents, however. None of the controversial items in the standards has been marked for assessment, which means they won't show up in state assessment tests, says John Poggio, co-director of KU's Center for Educational Testing and Evaluation, which designs and coordinates those examinations. And because most school districts tailor their curriculums to the tests, he adds, the revisions may have little impact on the classroom.

Even so, Poggio says test designers might drop some evolution-related questions from the tests. Martin sees that as an ideal solution, arguing that "some students have deeply held convictions about this topic, which puts them at a disadvantage while answering questions on a test."

Apart from battling the standards, many scientists have also targeted a statewide election in November 2006 involving the seats of five board members, including four conservatives. Sue Gamble, one of the four board members who opposed the standards, says that a wholesale reshuffling is the only way to stop "this assault" on science education. But she worries that a debate over evolution might "polarize the state further" and overshadow the bigger issue of how best to train Kansas students for the workplace.

–YUDHIJIT BHATTACHARJEE

Paper threat? Board member Kathy Martin calls draft standards "the best thing to have happened to education in Kansas."

CREDIT: ANTHONY S. BUSH/*TOPEKA CAPITAL-JOURNAL*/AP PHOTO

* www.ksde.org/outcomes/scstdworkingdoc7122005.pdf

HIGH-ENERGY PHYSICS

Costs Force NSF to Cancel Brookhaven Project

The National Science Foundation (NSF) has withdrawn its support for a high-energy physics project planned for the Department of Energy's Brookhaven National Laboratory in Upton, New York, after deciding that its budget couldn't handle the soaring costs. The decision, unusual for NSF, effectively kills the Rare Symmetry Violating Processes (RSVP) project just before construction was to begin on its two massive detectors.

"These are compelling experiments, and the scientific rationale for doing them is still strong," says Michael Turner, head of NSF's math and physical sciences directorate. "It was a very difficult decision, but the increased costs were too much to bear."

RSVP consisted of twin experiments. One, MECO, would have examined whether a subatomic particle called the muon could transform into an electron, an interaction not allowed by the prevailing theory of particles, the Standard Model. The other, KOPIO, would have looked for unexpected differences in the behavior of matter and antimatter by studying a specific decay of a particle called a K^0 meson to another called a π^0 meson, a neutrino, and an antineutrino. The rare decay is allowed by the Standard Model, but researchers hoped to see a deviation from the predicted rate, which would be a sign of undetected particles or interactions.

Originally approved in 2000 as a $145 million project at Brookhaven, RSVP last fall received its first $15 million in construction funds from Congress. That triggered a fresh review of the project that bumped its ▶

construction costs to $282 million. Its lifetime operating costs tripled, from $80 million over 5 years to $250 million over 8 years.

The main culprit in the increase was a required upgrade of the lab's aging Alternating Gradient Synchrotron (AGS), the accelerator that would provide a beam of protons for the experiments. Since 2002, AGS has been used primarily to feed particles into the much larger Relativistic Heavy Ion Collider (RHIC), which studies nuclear physics. Not only did AGS need to be tweaked to meet the more exacting requirements of RSVP but also its entire operating budget would have fallen on RSVP if RSVP outlasted RHIC.

Turner says these added costs had to be weighed against the potential scientific gains from several large physical science projects on the drawing board, including an underground laboratory to house experiments in physics, geology, and biology; a giant segmented mirror telescope; and an energy-recovery linear accelerator that would power an x-ray source for materials science research. In addition, he says RSVP's higher operating costs would have eaten into the directorate's existing budget for investigator grants.

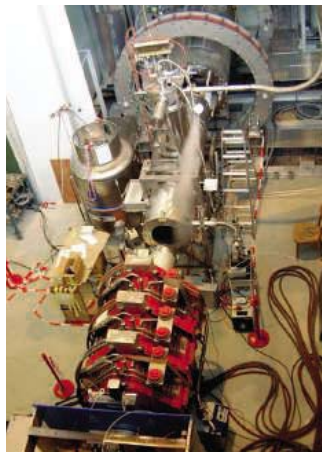

European reply. An experiment in Switzerland will explore some of the ground that RSVP hoped to cover.

Scientists involved in RSVP say that they anticipated the foundation's decision after both House and Senate spending panels this spring yanked the project from NSF's 2006 budget request. "Given Congress's position, I didn't see what else the National Science Board could do," says Michael Zeller of Yale University, co-spokesperson for KOPIO, RSVP's matter-antimatter experiment.

RSVP's demise opens the field to non-U.S.-led efforts, notably the MEG experiment to begin next year at the Paul Scherrer Institute in Villigen, Switzerland, and a pair of proposed experiments at the Japanese Proton Accelerator Research Complex in Tokai. Meanwhile, with the exception of neutrino experiments, all accelerator-based particle physics experiments in the United States will likely shut down within a few years. "To see the accelerators coming to an end in the U.S.—if they are—is amazing to me," says William Willis, a physicist at Columbia University and project manager for RSVP. "Things looked a lot different a few years ago."

—JEFFREY MERVIS AND ADRIAN CHO

U.S. POLAR SCIENCE

NSF Taps Russian Vessel for Antarctic Icebreaking

With one eye on its wallet and the other on Congress, the National Science Foundation (NSF) has decided to charter a Russian icebreaking vessel this winter to clear a path to its major research station in Antarctica. The cost-saving move appears to be at odds with pending Senate language that NSF should continue its historic reliance on U.S. government ships (*Science*, 1 July, p. 31). But the decision dovetails with a new report from an NSF advisory panel recommending less costly and more reliable ways to resupply McMurdo Station, the hub of NSF's Antarctic operations.

Breaking the ice. U.S. officials visited the *Krasin* last year when the Russian icebreaker was working in the Antarctic.

McMurdo, the largest of NSF's three Antarctic stations, sits at the end of a sound that must be cleared of ice every austral summer. The workhorses of that effort have been two 30-year-old icebreakers owned and operated by the U.S. Coast Guard. But the NSF panel calls this resupply system "inherently risky." The Coast Guard ships are increasingly frail, it notes, a condition exacerbated by the calving of a massive iceberg in 2000 that produced unusually thick and persistent sea ice in the sound. The system is also expensive and inefficient: In addition to growing maintenance and repair costs, the ships themselves consume about a quarter of the nine million gallons of fuel delivered each year to operate McMurdo and the inland South Pole station.

Earlier this year, NSF hired the *Krasin*, a Russian-owned and -operated icebreaker, to help the U.S. *Polar Star* crunch through the ice (*Science*, 21 January, p. 338). This winter, says NSF polar chief Karl Erb, the agency wants to use the *Krasin* as the lead dog and hold the *Polar Star* in reserve. "The Coast Guard thinks we should have two icebreakers," he says, "but we think that one will do it because storms have pushed the icebergs away."

It's a win-win situation, he says. "The *Krasin* is cheaper to operate and more fuel-efficient," he notes. "The $5 million we'll save by keeping *Polar Star* in reserve could be put toward fixing the *Polar Sea*. And the *Polar Star* will be available next year [when it's otherwise scheduled for major repairs] if we don't use it this year." Last week, the plan was endorsed by the National Science Board, NSF's oversight body.

Deferring to a foreign vessel isn't what Senator Patty Murray (D–WA), who represents the state where the icebreakers are berthed, was thinking when she slipped restrictive language into NSF's pending 2006 budget. "The NSF director shall procure polar ice breaking services from the Coast Guard," says the Senate report accompanying the spending bill. NSF is allowed to shop elsewhere "if the Coast Guard is unable to provide" such services, it notes, before adding that NSF and the White House should "work jointly to ensure that the Coast Guard fleet is capable of meeting NSF's future ice breaking needs."

That language could be altered or dropped in an upcoming conference to reconcile differences with the House, which told NSF in its report to use "the most cost-effective means of obtaining icebreaking services." NSF Director Arden Bement says he hopes that legislators will see the benefits of leasing the *Krasin*, which he says is consistent with existing U.S. policy to ensure access to Antarctica and promote polar science. NSF is responsible for carrying out that policy in a fiscally and environmentally prudent manner, he notes. The ▶

CREDITS (TOP TO BOTTOM): TOSHINORI MORI/THE UNIVERSITY OF TOKYO; FESCO 2005

Coast Guard says the decision rests with NSF; Murray's office declined comment.

Meanwhile, the advisory panel to NSF's polar programs presented Erb with 68 pages of innovative options to reduce NSF's dependence on icebreakers and, at the same time, improve operations throughout the Antarctic continent. Their proposals include building a runway that would allow the South Pole station to be resupplied by planes from New Zealand, improving NSF's ability to move supplies over land to the pole and various remote field sites, and running a leaner operation at McMurdo. They also suggest that NSF explore using heavy-lift blimps and contracting with commercial operators to reduce its dependence on military transportation. Even so, the report notes that NSF may someday need access to a new icebreaker capable of resupplying McMurdo. –JEFFREY MERVIS

SPACE AND EARTH SCIENCES

Budget Woes Greet NASA Science Chief

An engineer and former astronaut with a background in biology is taking the helm of NASA's $6 billion science program. Mary Cleave, who has been briefly in charge of the space agency's beleaguered earth science effort, now faces the tough task of reining in spiraling costs on several major science projects and ensuring the repair of the Hubble Space Telescope. At the same time, she'll try to protect the overall research budget from cuts to feed the space shuttle, station, and a new space flight vehicle that is central to the exploration vision of President George W. Bush.

Cleave is one of several senior appointments made last week by NASA chief Michael Griffin, who has known her for years. But despite her current job, she is not a familiar face to space and earth scientists. "She doesn't have experience doing science, and she doesn't have long experience working with the scientific community," says one researcher who has worked with Cleave. He adds, however, that she is "very focused" on abiding by the research goals laid out by recent reports on long-term planning for astronomy, solar system exploration, and earth sciences from the National Academies in Washington, D.C.

NASA chief scientist James Garvin, who has known Cleave for a decade, predicts she will be "a strong, pro-science" manager and that her experience with human space flight will help her make the case for research. Charles Kennel, director of the Scripps Institution of Oceanography in San Diego, California, and chair of the NASA Advisory Council, adds that "during the next few years, science will be the engine of NASA's public relations success. [Cleave's] job needs someone who understands the science and can create the strong support to carry out its science mission."

Cleave studied microbial ecology and civil and environmental engineering and flew twice on the space shuttle in the 1980s. She was NASA project manager for an ocean color sensor spacecraft before joining headquarters in 2000 and only became chief of earth sciences last year after the office was merged with the space science office. Her new deputy, Colleen Hartman, is a physicist who ran NASA's solar system program before working in the White House Office of Science and Technology Policy and the National Oceanic and Atmospheric Administration.

Right stuff? Ex-astronaut Mary Cleave now heads NASA's science programs.

One of Cleave's first challenges will be to manage the $1 billion cost overrun on the James Webb Space Telescope now under development. An internal report due next month is expected to consider alternatives that include drastically scaling back the instrument's capabilities. Another challenge, the fate of the Hubble, won't be resolved until after the shuttle flies again, an event that could be pushed back until as late as next spring. Both the Webb overrun and the Hubble mission could force Cleave to cut back in other areas.

Despite Cleave's background, oversight of biological sciences will fall not to her but to the space operations office led by engineer William Gerstenmaier, until now chief of the space station effort. This month, NASA began to cancel contracts to build long-planned facilities related to biological research on the space station, including work on the advanced animal habitat and the plant research units. –ANDREW LAWLER

CREDITS (TOP TO BOTTOM): NASA; RENEE BROUCHARD/NASA

ScienceScope

Mars Bound

NASA's $720 million Mars Reconnaissance Orbiter (MRO) roared into space 12 August, beginning a 7-month journey to the Red Planet. If all goes well, 6 months after arriving it should settle into its orbit and start to beam back data on the atmosphere, ground conditions, and geology beneath the rocks and ice on the surface. The successful launch of MRO came shortly after NASA canceled the Mars Telecommunications Orbiter (MTO), designed to handle large amounts of data from Mars missions early in the next decade. That mission succumbed to budget pressures being faced by NASA's science program (see p. 1165). NASA still plans to launch a rover in 2007, followed by a sophisticated Mars Science Laboratory in 2009. NASA chief scientist James Garvin, who called the launch "utterly stupendous," said that the 2009 mission could use other spacecraft to help transmit its data upon arrival, which made MTO expendable. But a more ambitious effort to return a Mars sample to Earth is still only a dream, say NASA officials.

–ANDREW LAWLER

EPA Issues Yucca Limits

Opponents of the Yucca Mountain nuclear waste repository are gearing up to fight new radiation limits proposed last week by the Environmental Protection Agency (EPA).

Under the new standard, the Department of Energy (DOE) would have to show that, for 10,000 years, a hypothetical resident of the area would receive only 15 millirems of radiation per year above the background exposure of 350 millirems per year. For the next 990,000 years, the limit would be 350 millirems per year above the background level. EPA says that residents of Denver, Colorado, currently receive that yearly level of background—whose sources include radon, cosmic rays, and medical components—and that setting acceptable limits given the vast unknowns is arbitrary. But the Minneapolis-based Institute for Energy and Environmental Research said the 350-millirem limit would be the "worst in the Western world." The public has 60 days to comment; once finalized, DOE must prove it can meet the limits. –ELI KINTISCH

IMMUNOLOGY

Versatile Development Gene Aids Insect Immune Response

Just like people, insects get infected by a multitude of microbes. But unlike people, they don't produce millions of distinct antibodies that can bind to and thwart pathogens with great specificity. Instead, insects were thought to depend on just a small number of molecules that recognize features common to many microbes.

But new results published online this week in *Science* (www.sciencemag.org/cgi/content/abstract/1116887) from a group at Harvard Medical School in Boston, Massachusetts, point to a more complex insect immune system. *Drosophila melanogaster* can muster its own army of proteins against microbial invaders, says Harvard's Dietmar Schmucker, a developmental neurobiologist.

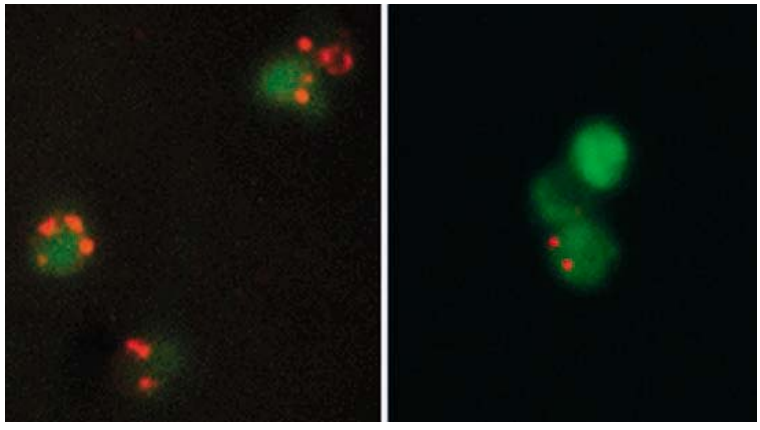

Seek and destroy. Fly immune cells (green) readily spread out to gobble up bacteria (red), but not if they are lacking Dscam proteins (*right*).

To fight infection, the fruit fly has harnessed a complex gene previously known for its role in differentiating nerve cells and guiding their extensions, called axons, Schmucker and his colleagues report. The gene, called *Dscam* for Down syndrome cell adhesion molecule, stands out among genes because it has 116 coding regions, most of which can mix to encode up to 38,000 subtly different proteins in neurons. "We had thought that *Dscam* has a role exclusively in axon patterning," says James Clemens, a neuroscientist at the University of California, Los Angeles. That the gene works in the immune system, too, "is a very intriguing discovery."

Although much more work needs to be done to establish *Dscam*'s immune function, the findings hint that the gene's molecules function like primitive antibodies, guiding scavenging cells to particular pathogens. "It could be an early step" in the evolution of adaptive immunity, the ability of an immune system to remember and respond ever more effectively against infection, suggests Brian Lazzaro, an evolutionary geneticist at Cornell University.

Over the past 5 years, researchers have established that the proteins made by *Dscam* in insects vary from nerve cell to nerve cell, helping define neuronal identities (*Science*, 6 February 2004, p. 744). This reminded Schmucker of the specificity seen in vertebrate immune cells and prompted him to look beyond the nervous system for Dscam proteins.

Using antibodies that recognize such proteins, Schmucker's postdoc Fiona Watson found the molecules in fruit fly hemolymph—the insect equivalent of blood serum—and on the surfaces of fat body cells and immune cells called hemocytes. Graduate student Roland Püttmann-Holgado also showed through microarray studies that the insect's immune system used a wide variety of Dscam proteins.

When Watson inhibited *Dscam* expression in hemocytes using the RNA interference technique, she found that they gobbled up 30% fewer bacteria. In other tests, the researchers demonstrated that the versions of Dscam made by fruit flies bound with different affinities to the bacterium *Escherichia coli*, possibly indicating that ▶

CREDIT: FIONA WATSON

ENVIRONMENTAL SCIENCE

Sperm Whales Bear Testimony to Worldwide Pollution

Early results are in from the first-ever global survey of toxic contaminants in marine mammals—and they're not pretty. Sperm whales across the Pacific, even in midocean areas thought to be pristine, are accumulating humanmade chemicals called persistent organic pollutants (POPs). DDT was the most common pollutant, followed by polychlorinated biphenyls. The survey's sponsor now plans to take a similar worldwide look at contaminants in people.

"It doesn't matter where you are, these animals are polluted," says biologist Roger Payne, president and chief scientist of the Ocean Alliance, a Lincoln, Massachusetts–based conservation group that funded the whale work. Data from the survey were slated to be announced this week after the research vessel *Odyssey* sailed into Boston Harbor, completing its 5-year investigation of pollution across the world's marine food webs (*Science*, 11 June 2004, p. 1584). The *Odyssey*'s 12-person crew surveyed sperm whales, which range the globe and eat fish and giant squid. These massive mammals were thought to accumulate POPs in their tissues, making them a likely indicator of the health of the world's oceans.

Researchers shot nearby sperm whales with an arrow that removes a small core of skin and blubber without harming the whale. Samples from 424 whales were then analyzed by toxicologist Celine Godard of the University of Southern Maine in Portland. Her preliminary findings showed that whales in the Sea of Cortez, between the west coast of Mexico and Baja California, had nearly twice the levels of CYP1A1, an enzyme that detoxifies pollutants, as whales in an area of the mid-Pacific thousands of kilometers from land. One suspected cause for the disparity is agricultural runoff. (Whales near the Galápagos Islands have even higher CYP1A1 levels, but Payne is not sure why.) To make sure regional variations are real, the team is measuring contamination in tissue samples from prey species that never leave the region, says toxicologist John Wise of the University of Southern Maine.

Preliminary tests by ecotoxicologist David Evers and colleagues at the BioDiversity Research Institute in Gorham, Maine, show that mercury levels were higher in skin samples from sperm whales near the Galápagos and in the Sea of Cortez compared with whales elsewhere in the Pacific. Sperm whales may provide a much-needed global standard to compare mercury pollution in different regions, Evers says.

Peter Ross of the Canadian Department of Fisheries and Oceans predicts that the results, once published, will "build a case that these chemicals move around the planet with relative impunity." Payne's team is planning to circumnavigate the globe in 2006 and 2007 to test for pollutants in people who live near especially contaminated areas.

–DAN FERBER

variants are tuned to specific pathogens. "Maybe these [Dscam proteins] allow fruit flies a sophistication that we haven't seen before," says Schmucker.

Vertebrate immune and nervous systems are also known to share genes. In 2003, for example, researchers discovered that a key vertebrate immune system gene complex that forms the unique MHC molecules on the surface of T and B cells is also active in the nervous system. "I think we will find other examples of this," says Clemens.

Whereas the human version of *Dscam* encodes only a few proteins and has no obvious immune role, Schmucker notes that flour beetles—which are separated from fruit flies by about 250 million years of evolution from their common ancestor—use Dscam proteins in the same way as fruit flies do. It "is clearly a very ancient process" in insects, says Brenton Graveley, a molecular biologist at the University of Connecticut, Farmington.

–ELIZABETH PENNISI

ASTRONOMY

Second Failure Cripples Suzaku Satellite

TOKYO—Astronomers trying to answer questions about the evolution of galaxies and the mechanics of black holes cheered mightily last month when Suzaku, a joint U.S.-Japanese satellite, settled into its orbit around Earth. Launched on 10 July, Suzaku was a replacement for a 2000 mission lost due to a rocket failure. For 19 days, its main instrument, the x-ray spectrometer (XRS), worked perfectly during calibration tests, measuring the energy of individual x-ray photons to an unprecedented level of accuracy. "We thought we were on our way," says Richard Kelley, XRS principal investigator for NASA, which jointly developed the mission with the Japan Aerospace Exploration Agency (JAXA).

Dewar die. The inability to maintain a vacuum doomed the lead instrument on Suzaku.

CREDIT: GSFC/NASA

Then they started noticing a glitch. To achieve its unprecedented resolution, XRS uses liquid helium and frozen neon packed around the instrument in a cryogenic container called a Dewar to maintain a supercooled temperature of 0.06 kelvin. On 29 July, anomalous temperature readings led controllers to conclude that helium was leaking into the Dewar's vacuum space. The leaks were sporadic. But in one climactic incident last week, enough helium entered the vacuum space to degrade its insulating capabilities. The remaining helium evaporated into space, rendering XRS useless.

"Now there is a lot of frontier science we just won't be able to do," says Hajime Inoue, an astrophysicist and project manager for Suzaku at JAXA's Institute for Space and Astronautical Science. Timothy Heckman, an astronomer at Johns Hopkins University in Baltimore, Maryland, planned to use Suzaku to study winds of hot gas ejected from galaxies rich with newborn stars. XRS would have gauged the wind speeds and the specific gas ingredients for the first time. "This was a revolutionary capability to help us understand how galaxies evolve and propel heavy elements into space," Heckman says.

Kelley says that the spectrometer's brief performance validated its design and engineering. The failure of its cryogenic system is expected to spur a search for alternative mechanical cooling schemes on future missions, such as NASA's proposed Constellation-X mission, which would use similar ultracooled instruments on four satellites to measure x-rays with exquisite sensitivity.

Suzaku carries two instruments that are unaffected by the loss of the cryogenics and are still functioning. One is the hard x-ray detector, and the other is a collection of four x-ray charge-coupled-device cameras. Together, the instruments cover a wide energy range that Inoue says should provide new data on violent astrophysical phenomena occurring near black holes and within active galaxies, which are centered on supermassive black holes. The original observation program was based on using XRS. Mission managers will now select other observational targets to make best use of the surviving instruments.

–DENNIS NORMILE

With reporting by Robert Irion.

ScienceScope

Bandazhevsky Freed

Belarusian pathologist Yuri Bandazhevsky was released halfway through an 8-year sentence earlier this month under a general declaration of amnesty by Belarus President Aleksandr Lukashenko. Bandazhevsky, former rector of the Gomel State Medical Institute, had criticized the government's response to thousands affected by nuclear fallout that drifted into the Gomel region after the Chornobyl accident (*Science*, 20 April 2001, p. 424). He had been convicted in 2001 of taking bribes, but Amnesty International and other groups called him a political prisoner. Bandazhevsky plans to stay in Belarus to build a biomedical lab with French research nonprofit CRIIAD.

–BRYON MACWILLIAMS

Blue-Ribbon Blues

Does the United States need a blue-ribbon commission to consider the perilous state of its science education? Yes. No. Maybe. When members of the National Science Board floated the idea at last week's meeting, opinions were all over the map. The board, which oversees the National Science Foundation, discussed a proposed commission to reexamine training for the next generation of scientists and engineers. But board president Warren Washington failed miserably to bring its 24 members anywhere near consensus. Reactions ranged from "Let's start a revolution" to "Let's stay on the sidelines." Some questioned whether there was anything left to say, whereas others argued that important messages need to be repeated. In the end, Washington gave up on reaching an agreement by next month's board meeting but pledged to continue the dialogue. –JEFFREY MERVIS

Grad Student Ranks Swell

A surge in the number of U.S. students pursuing graduate degrees in science and engineering has helped raise overall graduate enrollment in technical fields at U.S. universities to a record high of 474,203 in 2003, according to a report released last week by the National Science Foundation. The number, representing a 4% increase over 2002, was reached in spite of an 8% decrease in first-time foreign student enrollment. That decline followed a similar drop in 2002, confirming a trend that many attribute to the toughening of U.S. visa policies. But a 6% increase in domestic students' enrollments more than compensated for the decline.

–YUDHIJIT BHATTACHARJEE

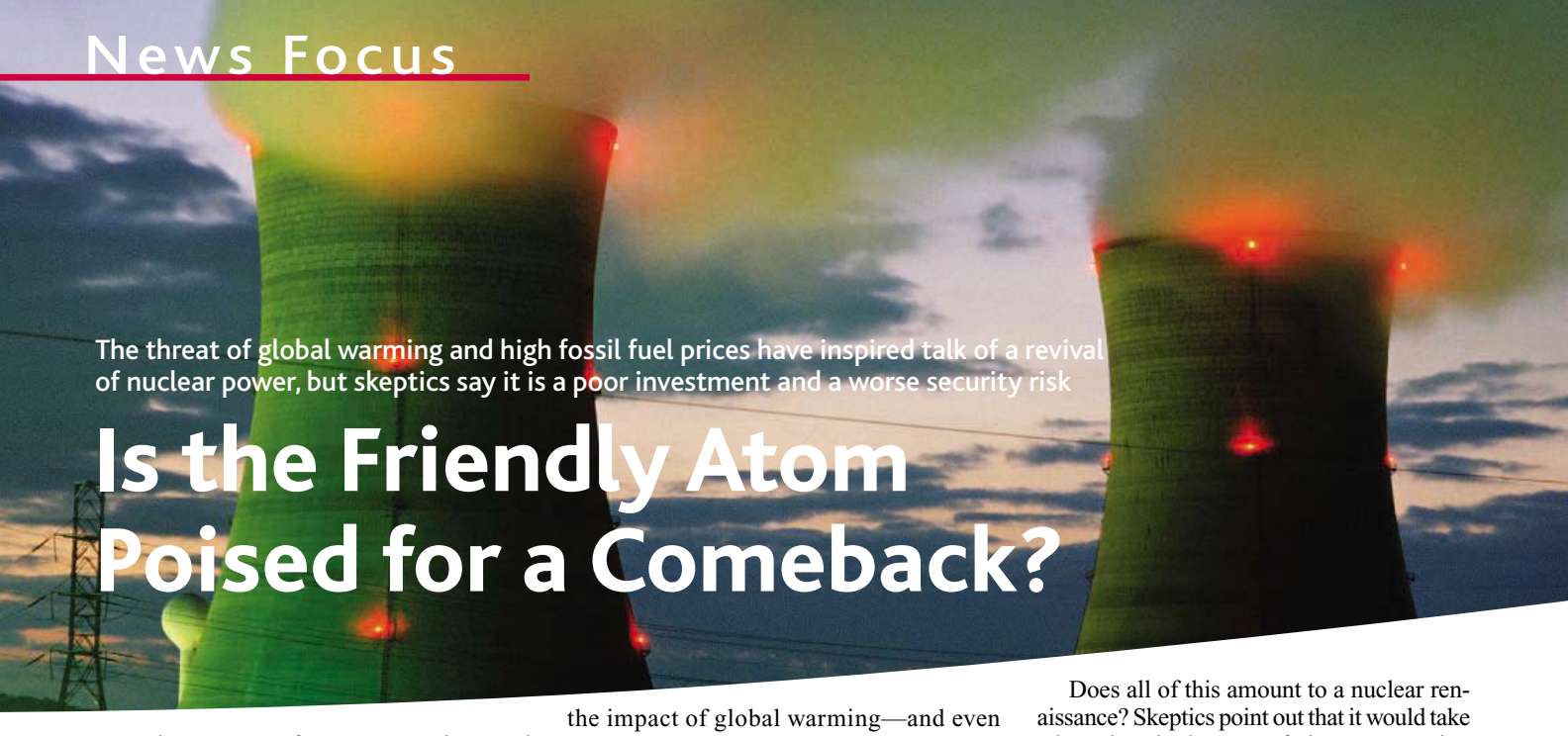

The threat of global warming and high fossil fuel prices have inspired talk of a revival of nuclear power, but skeptics say it is a poor investment and a worse security risk

Is the Friendly Atom Poised for a Comeback?

"Nuclear power faces stagnation and decline." So warned a group of scientists in a sweeping review published 2 years ago by the Massachusetts Institute of Technology (MIT) in Cambridge.* Led by chemist John Deutch and physicist Ernest Moniz, both of MIT, the study concluded that nuclear power was in trouble and deserved a helping hand from government. Despite high construction costs, the authors argued that the United States should triple the number of nuclear power plants by midcentury because they can deliver electricity without emitting greenhouse gases such as CO_2. The MIT group proposed a hefty tax on carbon emissions to help get this cleaner energy source moving.

The political and economic environment has changed dramatically since that report came out. On 8 August, President George W. Bush signed into law the first major U.S. energy bill in a decade. Although it does not tax carbon, it promises subsidies across the board for new investments in renewable energy, such as wind and solar power, and a grab bag of more than $6 billion in benefits narrowly tailored for builders of new nuclear reactors (*Science*, 5 August, p. 863). The bill was a plum for the nuclear power industry—one of several events that have got people talking about a "nuclear renaissance." Indeed, that's the title of a book published earlier this year by physicist and energy policy analyst William Nuttall of the University of Cambridge, U.K. One reason for optimism, Nuttall points out, is that oil and natural gas prices have shot up since 2003, making non–fossil fuel energy more attractive. Meanwhile, some public leaders have cited nuclear power as a way to reduce the impact of global warming—and even some environmental advocates seem to agree.

Although a few Asian countries never got off the nuclear bandwagon, new ones are now climbing aboard to meet rapidly growing electricity demand. India, with the most reactors under construction in the world, is planning a unique system that relies mainly on thorium rather than uranium fuel (see p. 1174). Japan continues work on fast neutron reactors that can "breed" plutonium (see p. 1177). And China announced in April that it will more than quadruple its nuclear electric capacity by 2020, buying among other designs a new "pebble bed" reactor that shuts down if it overheats. Nuclear advocates in the West also hope that advanced reactor designs can help overcome the lingering memories of Three Mile Island and Chornobyl (see p. 1172).

Does all of this amount to a nuclear renaissance? Skeptics point out that it would take a huge leap in the pace of plant construction simply to maintain nuclear power's current global share of electric output—about 17%—let alone increase it. Many aging U.S. and European reactors will have to be dismantled in the next couple of decades. Even new ones remain more expensive than coal- or gas-fired systems. And governments are not imposing stiff taxes on carbon emissions, the one strategy the MIT report said would tip investment decisions toward nuclear. Moreover, even if the economics were to favor nuclear power, two issues will continue to dog the industry: fears of nuclear weapons proliferation and disputes about how to dispose of high-level wastes (see p. 1179).

Optimists still think that the problems can be fixed. Reiterating his view of 2 years ago,

Praise. U.S. President George W. Bush advocated subsidies for nuclear power as an "environmentally friendly" source of electricity while visiting a reactor in Maryland in June.

CREDITS (TOP TO BOTTOM): GETTY IMAGES; DENNIS BRACK-POOL/GETTY IMAGES

* "The Future of Nuclear Power," funded by MIT and the Alfred P. Sloan Foundation, MIT, Cambridge, Massachusetts, 2003.

Deutch says: "If nuclear power can get its costs down and address the important issues of waste management and proliferation, its future will be very bright." The next few years may reveal just how bright.

Apocalypse pending

The threat of global warming is perhaps the key factor in the rethinking of nuclear power. The nuclear industry, in particular, has seized on it as a reason to switch from fossil fuel to the atom. For example, John Ritch, executive director of the London-based World Nuclear Association (WNA), an advocacy group backed by power supply companies, told an audience in Idaho last month that unless the world cuts greenhouse gases, it will "face catastrophic climate change, with the severest consequences for sea levels, species extinction, epidemic disease, drought, and extreme weather events that could combine to disrupt all civilization."

WNA suggests that the best solution would be to raise the number of nuclear electric plants in the world from 441 today to 5000 by the end of the century. That is the most ambitious scheme anyone has proposed, but so far, it has few takers. A more modest proposal—to maintain the nuclear share of electricity at the current level as a "bridge" to future clean energy technologies—has struck a chord, however.

David King, science adviser to the U.K. government, has spoken publicly about the need to keep nuclear power as a clean energy option. Britain, the world's most visible campaigner for action on global warming, faces a common dilemma, as King explained to the *Independent* newspaper in May. He described a looming "gap" in clean energy production. About 27% of U.K. electricity now comes from nuclear power, he noted, but without a "new build," only one reactor unit (Sizewell B) will still be running in 2025, producing an estimated 4% of the needed electricity. King said he was "not a great fan of nuclear" but was willing to consider it because "the climate change issue is so important."

A recent U.K. government forecast lends weight to King's analysis: Solar panels, windmills, and wave-driven generators cannot pick up the slack anytime soon. An electricity strategy issued in May by the U.K. Council of Science and Technology, which reports to King, notes that "the existing policy to reduce CO_2 will not be sufficient … since the nuclear stations are likely to be replaced by carbon-based technology (e.g., gas) in the short term."

And even the United Kingdom, which has championed the international effort to curb CO_2 emissions, is failing to meet its self-imposed CO_2 reduction goals. Physicist David Wallace, vice president of the Royal Society in London, warned in May that "our emissions are clearly going in the wrong direction," and that U.K. government forecasts of achievable CO_2 reductions have been "frankly unrealistic." Royal Society president Robert May has written that "it is difficult to see how we can reduce our dependence on fossil fuels without the help of nuclear power."

CREDIT: ASSOCIATED PRESS

Condemnation. Iran resumed work at a uranium enrichment plant this month—an "unacceptable" action, according to the White House.

A few leaders in the green movement have endorsed the idea of using nuclear power as a bridge to cleaner systems in the future—including U.K. ecologist James Lovelock. Creator of the "Gaia" metaphor that describes Earth as a living organism, Lovelock published a broad appeal last year. "Only one immediately available source [of energy] does not cause global warming, and that is nuclear energy," he wrote. "I entreat my friends in the movement to drop their wrong-headed opposition [to it]." A few others, such as Greenpeace co-founder Patrick Moore, have made similar statements. But environmental advocacy groups are not following.

> "It is difficult to see how we can reduce our dependence on fossil fuels without the help of nuclear power." —ROBERT MAY, PRESIDENT OF THE ROYAL SOCIETY, U.K.

Stephen Tindale, executive director of Greenpeace International in London, says it's "misleading" to suggest that "the green movement is suddenly embracing nuclear power on the back of Lovelock's statement." He sees nuclear revival talk as "a big distraction" from the need to invest in moderate-scale, renewable energy systems. He adds that Moore is "vehemently opposed to everything that Greenpeace stands for" and now makes his living "by being anti-Greenpeace."

Likewise, the head of Friends of the Earth in London, Tony Juniper, says, "we have reviewed our position on nuclear power," in part because of the urgency of the climate change issue, and concluded that it is a "false solution" pushed as part of "a clever public relations campaign" by "nuclear industrial interests."

The Natural Resources Defense Council has also reviewed its policy recently, says NRDC physicist Thomas Cochran in the Washington, D.C., office, and concluded that nuclear couldn't survive without massive subsidies. As a June NRDC issue paper says, nuclear "suffers from too many security, safety, and environmental exposure problems and excessive costs to qualify as a leading means to combat global warming pollution."

Cochran offers a scenario to illustrate why he doesn't see nuclear as a good option. He begins with a modest goal: avoiding a small amount (0.2°C) of global warming at the end of this century. He calculates that relying on nuclear electricity for this benefit would require increasing the number of reactors in the world from the current 441 to at least 700 by mid-century and holding that number steady for 50 years. Allowing for retirement of obsolete equipment, he suggests, this will require building 1200 new plants in all, at a rate of about 17 per year. The support requirements, he argues, would be staggering: a dozen new fuel-enrichment plants for reprocessing, the same number of Yucca Mountain–sized waste repositories if there were no reprocessing—or hundreds of thousands of tons of material to guard during reprocessing. Because just 8 kilograms of diverted plutonium would be enough to "take out lower Manhattan," a nuclear renaissance isn't worth the risk, Cochran says.

The MIT review 2 years ago acknowledged that "shortcomings" in the international safeguards on nuclear materials "raise significant questions about the wisdom of a global growth scenario" for nuclear power. It did offer a fix: Tighten up the management of nuclear materials by the International Atomic Energy Agency (IAEA) and persuade France, Japan, Russia, and the United Kingdom to cut down the traffic in plutonium by shutting their reprocessing factories. But those changes have not occurred.

The threat of global warming may not have sparked a nuclear renaissance yet, but it is breathing new life into a debate over nuclear power that, in many countries, had been quiescent for the past few years. **–ELIOT MARSHALL**

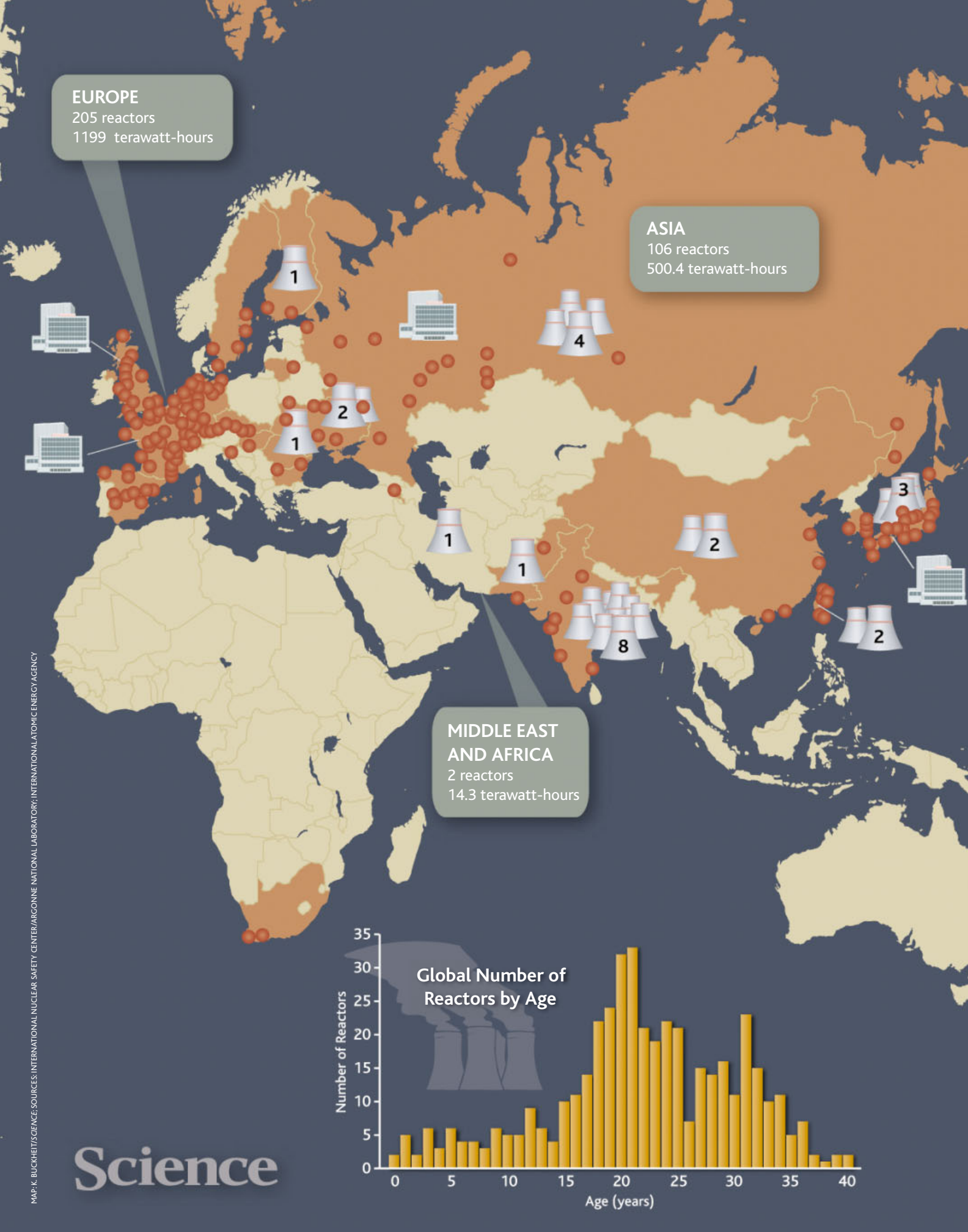

Science

MAP: K. BUCKHEIT/*SCIENCE*; SOURCES: INTERNATIONAL NUCLEAR SAFETY CENTER/ARGONNE NATIONAL LABORATORY; INTERNATIONAL ATOMIC ENERGY AGENCY

Nuclear Power's Expanding Territory

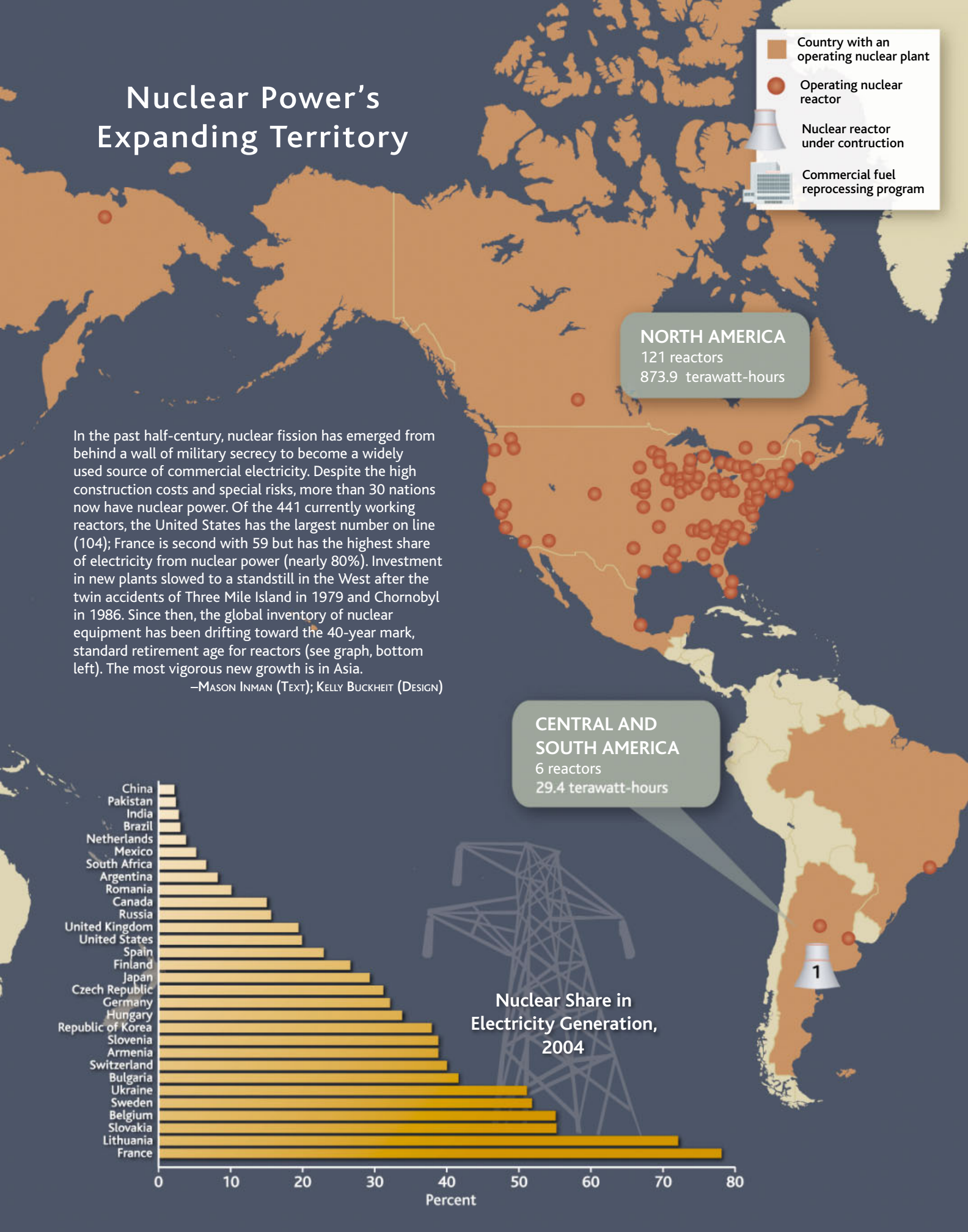

In the past half-century, nuclear fission has emerged from behind a wall of military secrecy to become a widely used source of commercial electricity. Despite the high construction costs and special risks, more than 30 nations now have nuclear power. Of the 441 currently working reactors, the United States has the largest number on line (104); France is second with 59 but has the highest share of electricity from nuclear power (nearly 80%). Investment in new plants slowed to a standstill in the West after the twin accidents of Three Mile Island in 1979 and Chornobyl in 1986. Since then, the global inventory of nuclear equipment has been drifting toward the 40-year mark, standard retirement age for reactors (see graph, bottom left). The most vigorous new growth is in Asia.

–Mason Inman (Text); Kelly Buckheit (Design)

Nuclear Share in Electricity Generation, 2004

Nuclear Industry Dares to Dream of a New Dawn

Reactor builders think that fossil fuel prices and climate fears will revive nuclear power. But will new reactor designs overcome the concerns of utilities and the public?

The nuclear industry is biding its time. Amid all the hullabaloo about climate change, rising prices of natural gas, dwindling oil stocks, and the environmental impact of wind farms, the makers of nuclear power plants feel that their time is about to come. Sometime soon, they believe, people will realize that the only carbon-free way to keep our society humming along—and fuel the rapidly growing economies of China and the developing world—is to use nuclear reactors. "The signposts are there for a renaissance" of nuclear power, says Peter Wells, marketing manager for GE Energy's nuclear business.

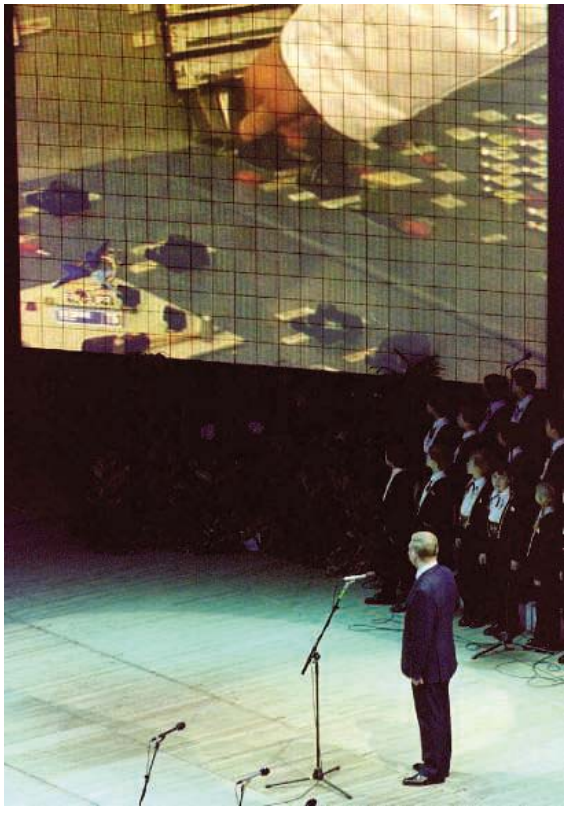

End of a nightmare. Ukraine's President Leonid Kuchma speaks at the Chornobyl closure ceremony in Kiev in 2000.

CREDIT: MIKHAIL CHERNICHKIN/REUTERS

The industry has not been idle during the 2 decades since the Chornobyl accident brought reactor building to a virtual standstill. Designs for light water reactors (LWRs), the main type in use today, have been thoroughly reworked. They are now simpler and incorporate so-called passive safety measures—simple systems that automatically kick in when something goes wrong. A trickle of orders from countries such as Japan, Korea, and China has kept companies afloat, and the energy bill signed by President George W. Bush this month contains generous measures to coax U.S. power utilities to start building nuclear again.

But many nuclear experts think that the coming boom will not be a simple rerun of nuclear power's heyday in the 1960s and '70s. For a start, many more countries want nuclear power, but not all want the 1000-plus-megawatt-sized plants favored by large industrialized nations. They want reactors to be quick to build and safe and easy to run, whereas the leading nuclear nations want to ensure that spent fuel can't be diverted to other purposes. In some cases, the plants may not even generate electricity. Alternative uses include powering desalination plants in arid areas, providing heat for petrochemical processes, and even generating hydrogen for the much-touted hydrogen economy.

In such situations, some experts say, large monolithic LWRs do not fit. Instead, they point to the high-temperature gas-cooled reactor. Plants cooled with air or carbon dioxide have been around for decades, but a few companies are in the process of reinventing them for the 21st century. New-generation plants are cooled with inert helium, which directly drives a gas turbine to generate electricity. They work best at smaller sizes—a few hundred megawatts—and run at much higher temperatures than conventional reactors, between 500° and 1000°C. High temperature makes energy conversion more efficient and suits applications such as hydrogen production.

But perhaps their best trick is that they go one better than passive safety: Their cores are designed so that a runaway nuclear reaction simply can't happen. You can fire up such a reactor to full power, vent away its coolant, pull the control rods right out, and nothing bad will result. "It's a walkaway reactor," says Dave Nicholls, chief technology officer of South African reactor builder PBMR (named after its Pebble Bed Modular Reactor). "You can come back in a few days and sort things out."

Enthusiasts say gas-cooled reactors will eventually displace LWRs. Although they don't achieve the economies of scale possible with big plants, reactor builders can make a virtue of their small size by mass-producing components and shipping them to construction sites by road or rail. And if utilities want big megawatts, they can install a battery of small reactors at the same site, sharing facilities. Twenty years from now, "gas-cooled reactors will begin to dominate. Every new reactor ordered will be gas-cooled," says Mike Campbell, senior vice president at U.S. nuclear company General Atomics.

Not everyone agrees that the nuclear industry is poised for revolution. "All big utilities look at the costs and want the cheapest possible electricity," says Philippe Garderet, vice president for research and innovation at French reactor company AREVA. "There just isn't a market" for small reactors.

The Bush Administration, however, is prepared to take a gamble. The new energy bill authorizes $1.3 billion for the Department of Energy (DOE) to construct a new experimental nuclear reactor at the Idaho National Engineering and Environmental Laboratory. Industry watchers expect this Next Generation Nuclear Plant (NGNP) to be a high-temperature gas-cooled reactor for producing electricity and hydrogen. "We need to show that gas will work. That's why the NGNP is so vital for the next step into gas," says nuclear engineer Andrew Kadak of the Massachusetts Institute of Technology in Cambridge.

Liquid vs. gas

Although nuclear power generation has long been dominated by water-cooled reactors, there have been frequent attempts to establish gas-cooled designs. The first—Britain's Dragon reactor, which began operating in 1965—led to a number of carbon dioxide–cooled plants in the U.K., some of which are still in use today. General Atomics pioneered their use in the United States, and in the early 1970s it had orders for 10 machines. All were canceled when the 1973 oil crisis led to a collapse in energy demand. Meanwhile, water-cooled reactors were getting larger and larger and increasingly complex. Then the twin shocks of Three Mile Island in 1979 and Chornobyl in 1986 caused a major rethink of reactor design.

Most of the plants being built today in Asia and elsewhere are "evolutionary" improvements on the water-cooled designs from the boom years. Westinghouse's current offering, the AP1000, uses gravity, natural circulation, and compressed gas to cool its core in an emergency. As a result, the reactor

has 50% fewer valves, 83% less piping, 87% less control cable, and 35% fewer pumps than a conventional plant. With less equipment, there is less to go wrong. Similarly, GE's latest design, the Economic Simplified Boiling Water Reactor, holds emergency cooling water high up in the reactor vessel. If anything gets too hot, a release valve is automatically triggered and water flows down under gravity. "The reactor then remains below water level, and you don't get the core exposed," says GE's Wells.

But, according to Kadak, "these evolutionary designs are still too expensive. No one is buying." At the vanguard of the movement to sweep aside such leviathans are two efforts to build small gas-cooled demonstrator reactors, one in South Africa and one in China, by around 2010. Both use a reactor design that has its origins in the postwar scramble to find new uses for atomic power.

New ground. Pebble bed pioneer Dave Nicholls plans a new reactor here at Koeberg, South Africa.

A rocky road

Just after World War II, researchers at what was soon to become the Oak Ridge National Laboratory in Tennessee investigated a reactor for generating electricity designed by physical chemist Farrington Daniels of the University of Wisconsin, Madison. He proposed encapsulating enriched fuel in small graphite balls, placing a large number of them in a reactor vessel, and cooling them with helium. The design, known as a pebble bed reactor, was considered too complicated and was abandoned in 1948.

In the 1950s, German physicist Rudolf Schulten resurrected the idea and built a small demonstrator reactor which operated from 1968 for 22 years. In 1985, a firm in Germany also built a commercial-scale reactor, but both machines were closed down soon after the Chornobyl accident.

There the pebble bed story might have ended, except that in the 1990s, South African utility company Eskom began looking for new power plants. South Africa has abundant coal, so power is cheap. But the coalfields are all in the high interior of the country; Eskom wanted a new type of plant to power coastal cities. Pebble bed seemed to fit the bill, so Eskom licensed the German technology. Today the company PBMR is poised to start building a demonstrator plant at Koeberg near Cape Town, which it hopes to connect to the grid in 2010. "Nuclear must change technology to meet the needs of society," says PBMR's Nicholls.

The pebble bed design is simple. Tiny flecks of low-enriched uranium are coated in layers of silicon carbide and carbon to make particles 1 millimeter across. Some 15,000 such particles are then mixed with graphite powder and pressed into a sphere the size of a tennis ball, which is again coated and hardened. Each "pebble" is only 4% uranium. When the reactor is ready for commissioning, engineers load 456,000 pebbles into the ring-shaped core. Control rods run through cavities in the graphite reflector material around the edge. The helium coolant simply flows through the pile of balls, is heated, and drives a turbine directly connected to a generator.

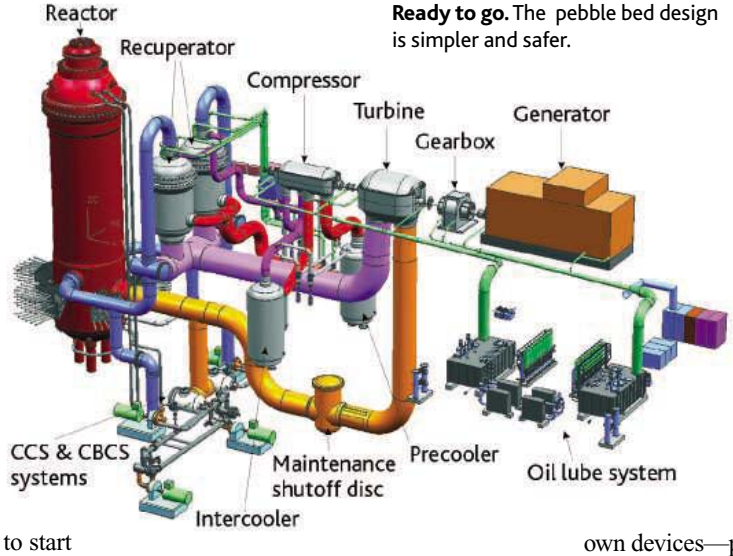

Ready to go. The pebble bed design is simpler and safer.

One great benefit of the pebble bed design is that it does not need to be shut down to rearrange or renew the fuel. Instead, every day some pebbles are taken from the bottom of the reactor and weighed to see if they still have usable fuel inside; those that do are fed back onto the top of the pile. In this way the fuel is continually moved around to achieve an even burn and full utilization. Each pebble passes through the reactor six times over the course of 3 years. Much of the equipment is straight off the shelf, Nicholls says. "We're not trying to push the state of the art at the component level," he says. "We just put it together better."

Meanwhile, researchers at the Institute of Nuclear and New Energy Technology (INET) at Tsinghua University near Beijing, China, also took a leaf out of Schulten's book during the 1990s and in 2003 fired up their 10-megawatt High-Temperature Reactor. According to INET director Zhang Zuoyi, this experiment-sized pebble bed has been steadily churning out power ever since. On three occasions, he says, the team has tested the reactor's safety by pulling out its control rods and leaving it to its own devices—producing a short-lived rise in temperature but no danger to the reactor.

Pebble beds are considered inherently safe because their cores are only sparsely loaded with nuclear material; they also exploit a natural ability of uranium-238, the nonfissile isotope that makes up the bulk of uranium fuel. As the temperature of the reactor rises

CREDITS (TOP TO BOTTOM): LOUISE GUBB/CORBIS; PBMR

India's Homegrown Thorium Reactor

KALPAKKAM, INDIA—For more than 5 decades, India has followed its own path on nuclear power. After refusing to join the Nuclear Nonproliferation Treaty and detonating a nuclear device in 1974, it was excluded from the international group that shares fission technology. In isolation, it launched an ambitious nuclear electric program that relies heavily on homegrown technology.

What makes India's strategy unique is its plan to build commercial reactors that run not on uranium but on a lighter element, thorium-232. India has one of the world's largest reserves of thorium—about 225,000 metric tons—but little uranium ore. Thorium does not fission; when irradiated with neutrons from a source material such as uranium-235, however, some of the thorium becomes uranium-233 (U-233), which does fission and can sustain a nuclear reaction.

In 1958, India announced that it was embarking on an ambitious, three-stage plan to exploit its thorium reserves. The first stage required building pressurized heavy-water reactors powered by natural uranium; they yield plutonium as a byproduct. Twelve are now operational. The plan called for stage two to kick in after sufficient plutonium had been extracted from spent cores; it would be used as a fuel in future fast-neutron reactors, which can irradiate thorium and produce U-233 as a byproduct. In the third stage, Advanced Heavy Water Reactors will burn a mixture of U-233 and thorium, generating about two-thirds of their power from thorium. Other nations—including the United States, Russia, Germany, and Israel—have studied the route but have not attempted to use it to generate electricity.

Stage two of this grand strategy began officially last October. In the sleepy south-

First of a kind. Project director Prabhat Kumar at the site of a new thorium-uranium reactor in Kalpakkam.

CREDIT: PALLAVA BAGLA

above its normal operating level, uranium-238 starts to become better at absorbing neutrons, the particles that spark the nuclear chain reaction. So when the coolant or the reaction-damping control rods are removed, the reactor temperature begins to rise, but as uranium-238 starts to make the core less reactive, it cools naturally by radiation and conduction. "We can calculate the peak temperature the fuel will reach," says Nicholls.

With this experience in its pocket, the INET team and the company Chinergy are planning to build a commercial prototype in Shandong province in the east of China by 2011. INET also signed an agreement last month to join a consortium with Westinghouse to put in a bid to build the NGNP in Idaho. Westinghouse is one of the backers of the PBMR, and the South African company is part of the consortium. Pebble bed enthusiasts hope that their design will be chosen for this $1.3 billion test reactor.

The pebble bed approach is not the only way to make a high-temperature gas-cooled reactor. General Atomics, for example, has developed the Gas Turbine Modular Helium Reactor (GT-MHR). As in pebble beds, the uranium fuel starts out as tiny coated particles, but instead of pebbles, the fuel for the GT-MHR is formed into hexagonal prisms about the size of two large paint cans stacked up. The prisms are arranged in an array in the reactor core and stacked 10 high. Japanese researchers have built an experimental "prismatic" gas-cooled reactor, the High Temperature Test Reactor, which has been operating successfully since 1998.

Arkal Shenoy, director of the GT-MHR project at General Atomics, says the design is pretty well worked out now. "We're waiting for someone to say 'Do you want to build this thing?' " Shenoy says that in a conventional reactor, one-third of all systems are safety-related, and you hope you will never have to use them: "We've eliminated the need for safety systems. The physics is such that the worst case of accident can never happen."

Idaho or bust

Despite all the advantages of the new generation of gas-cooled reactors, proponents concede that utilities are going to be wary of unproven technology. "Without a full demo reactor, utilities won't buy. They're used to 90% availability. No amount of analysis will get you this," says Shenoy. The South African and Chinese demo reactors are being heavily subsidized by their governments, and U.S. researchers hope their government will follow that example. "Until the NGNP is finished, you won't see a gas reactor being built in the U.S. We need to reduce the risk [for utilities]," says General Atomics' Campbell. "It must be an Administration priority. Otherwise it won't be real."

Researchers are also confident that DOE will want a high-temperature gas-cooled reactor because of its interest in hydrogen production. "All the buzz about the hydrogen economy really comes from gas-cooled reactors," says Nicholls. There are various ways of extracting hydrogen from water, including electrolysis and thermochemical splitting, and they are all much more efficient at high temperature. "Nuclear is the only really practical source of hydrogen, and the only nuclear technology that gets you there is the high-temperature gas-cooled reactor," Nicholls says.

One thing these reactors do not do is resolve the issue of waste. The highly encapsulated fuel in gas-cooled reactors is very effective at containing nasty fission products, and it would be extremely difficult for any potential terrorist to extract any usable bomb-grade material from it. But the downside is bulk. All that graphite and multiple coatings make for large volumes of waste. The nuclear industry in the United States has never reprocessed its spent fuel, nor has the government come up with an accepted solution for long-term waste storage.

ern township of Kalpakkam, a government-owned company began building a 500-megawatts-of-electricity (MWe) fast-breeder reactor that will use fast neutrons to produce U-233. In its core, the reactor will use a "seed" fuel containing uranium and plutonium oxide; this source will send neutrons into a surrounding thorium blanket.

Indian atomic energy officials are confident that this exotic fuel system can be scaled up from a smaller, 40-megawatt Fast Breeder Test Reactor (FBTR) that has been running in Kalpakkam without major problems since 1985. This reactor and other research projects at the Indira Gandhi Center for Atomic Research in Kalpakkam have demonstrated, IGCAR officials say, that India has mastered the new technology. In a "bold step forward," says Anil Kakodkar, chair of the Atomic Energy Commission (AEC) in Mumbai, researchers at IGCAR in May of this year successfully extracted plutonium in high purity from the unique plutonium-rich mixed carbide fuel discharged from FBTR.

AEC anticipates that the fast breeder at Kalpakkam will cost about $700 million and produce 500 MWe. The long-term goal, according to Kakodkar, is to increase nuclear electric output from 3360 MW today to "around 275 gigawatts" by the middle of this century.

Proof of principle. Researchers at Kalpakkam used thorium fuels in a 40-megawatt test reactor.

Construction at Kalpakkam ran into trouble early this year: The 26 December 2004 tsunami flooded the foundations of the reactor building and set the schedule back by 4 months, says Baldev Raj, IGCAR's director. But he says that the work is now on track and predicts that the reactor will go critical as planned in September 2010.

Mujid Kazimi, a nuclear engineer who studies thorium fuels at the Massachusetts Institute of Technology in Cambridge, says India's approach to breeding nuclear fuel from thorium is "slightly more complicated" than fuel breeding planned elsewhere in the world. But he adds, "everything they have reported to date indicates they are on track."

India cannot go it entirely alone, however. It still requires uranium, including for two boiling water reactors it bought from General Electric in the 1960s, and that may be one reason it is interested in opening nuclear trade with other countries. At a meeting last month with Prime Minister Manmohan Singh, President George W. Bush called India "a responsible state" with "advanced nuclear technology." The opening could lead to future exchanges of personnel and technology—and possibly fuel. Singh reassured Parliament, however, that the deal would not undermine India's nuclear self-sufficiency. **–PALLAVA BAGLA**

Despite this, few believe the United States should embark on fuel reprocessing anytime soon because that would open a Pandora's box that the public is just not ready for. An influential 2003 report on the future of nuclear power, co-chaired by former CIA director John Deutch, concluded that for the next 50 years, a once-through fuel cycle was the best option for the United States. "Once-through will dominate for many years," says Regis Matzie, chief technology officer at Westinghouse Electric. "Reprocessing is very costly in comparison, and utilities always take the least-cost route."

CREDITS (TOP TO BOTTOM): PALLAVA BAGLA; WESTINGHOUSE

Gentle giant. Westinghouse's AP1000 design now has passive safety systems using gravity and natural circulation.

Few, however, believe that this situation can continue forever. "I don't see how we can expand nuclear with the way we are doing it today. We have to clean up the fuel cycle, and [reprocessing] may be the only way to do it," says Campbell. "It's a 100-year problem, not a 10-year problem." Farther down the road than the NGNP, 25 or more years from now, a new breed of reactor will be needed that can destroy much of its own waste. DOE has begun looking for such designs through a program called Generation IV and has enlisted a handful of other countries to collaborate. Beginning in 2000, a panel of more than 100 international nuclear experts sifted through many proposed designs and whittled them down to six generic types worthy of further study. Some of these are quite exotic, including one cooled by molten lead and another in which the fuel itself is a circulating mixture of molten salts.

All but one of the six Generation IV designs have the ability to burn up the more long-lived products of the fission reaction. Nevertheless, industry experts seemed underwhelmed by the prospect of such futuristic reactors. "They're too far out, too speculative, and I can't see the advantage," says Matzie. But France's AREVA, which already has experience of building fast neutron reactors for destroying waste, is looking that far ahead. "AREVA must be ready to produce plants with fast neutrons. We know how to do it, but we have 20 or 30 years to develop better, cheaper, safer technology," says Garderet.

U.S. reactor makers appear more focused on the near term, waiting for that spark that will set their industry burning again. "The Bush Administration is clearly supportive of nuclear power. This provides a window of opportunity: If steps are not taken by 2008, the opportunity will be lost," says GE's Wells. Matzie agrees: "A big banner will go up when U.S. utilities start buying again. Once the U.S. starts building and establishes a track record, it will be time for others to do the same."

–DANIEL CLERY

With reporting by Gong Yidong of *China Features* in Beijing.

Science Online

Address: http://www.sciencenow.org

Q **Where can you read breaking science news right now?**

A ***Science*NOW:**
www.sciencenow.org

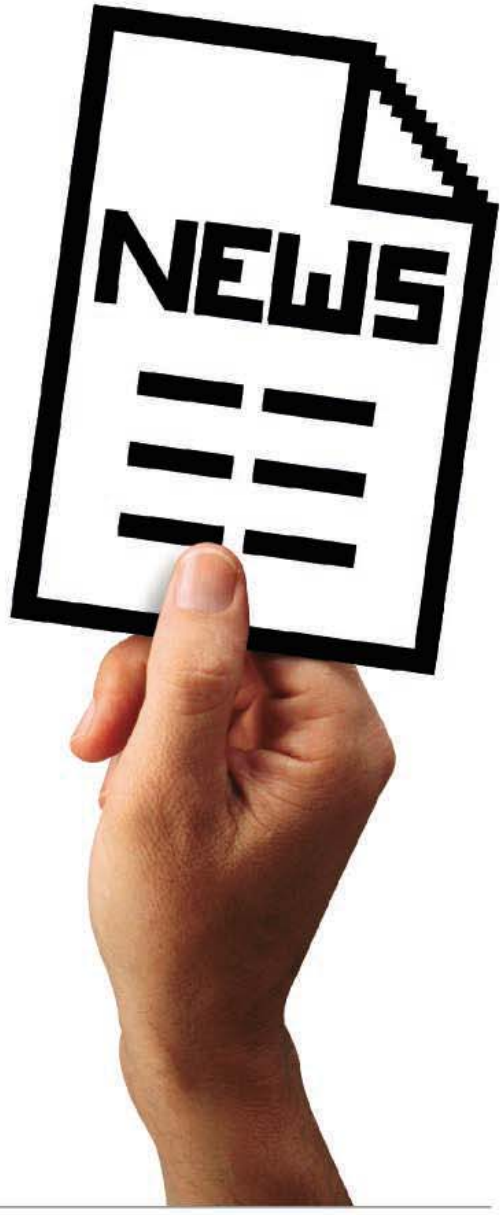

Science's team of tireless reporters works across global time zones to keep you informed—with daily updates of breaking news and current research published in leading science journals. The forefront of exploration and discovery, policy and funding, and science and technology breakthroughs from around the world is at your fingertips. Right now.

As an AAAS member, you have 24/7 access to *Science*NOW. Not a member? Sign up today at www.aaas.org/join

Science, published by AAAS, with over 700,000 readers weekly, is the world's most widely-read general science journal. Scientists around the world submit over 12,000 papers each year for evaluation, with only one in 12 making it into final publication. This rigorous process ensures the quality of material, whether it's research on proteomics, therapeutic cloning, nanotechnology, or dark matter. To find out how to subscribe to *Science*, go to **www.aaas.org/join**

Science
AAAS

Asia's Demand for Electricity Fuels a Regional Nuclear Boom

While Western governments debate the pros and cons of replacing old nuclear power plants, India, China, and Japan are investing rapidly in new systems

Nuclear power may have fallen on hard times in some parts of the world, but not in Asia. Demand for electricity is growing steadily across the region, and a number of countries have seized on nuclear fission as a secure energy source that avoids coal's air-choking carbon and sulfur emissions. And as oil and gas prices rise to record high levels, nuclear energy is starting to look more affordable. The result—on paper at least—is a boom. "Sixteen of the 25 nuclear power plants currently under construction worldwide are in Asia," says Akira Omoto, director of the Division of Nuclear Power of the International Atomic Energy Agency in Vienna, Austria.

China is embarking on a nuclear power plant building spree. Korea and India are both beefing up their nuclear electric grids. And Japan—despite public opposition that has blocked one project—plans an expanded nuclear power network that includes a controversial fast neutron reactor. Other novel designs are being tried in China and India.

Steep climb

China has the most ambitious nuclear plans of any country in the world, although it is starting from a small base. Nine nuclear power plants are operating in China today, accounting for about 2% of the national power output. Two more reactors are under construction in eastern Jiangsu Province; they will come online by the end of this year, raising total nuclear capacity from 6.7 billion watts, or gigawatts, of electric power (GWe) to 8.7 GWe. For comparison, the 104 nuclear power plants in the United States now produce more than 10 times as much power, about 98 GWe. China's target is to have nuclear power supply 6%, or about 40 GWe, of the nation's electrical energy needs by 2020.

Kang Rixin, general manager of China National Nuclear Corp. (CNNC), says meeting this goal will require the construction of about 30 new 1-GWe nuclear power plants over the next 15 years. And many of China's nuclear power boosters believe that will only be the start. Zhang Zuoyi, head of the Tsinghua Institute of Nuclear and New Energy Technology (INET), envisions a bigger leap after that: "Nuclear power generation should reach 300 GWe by 2040, as it is the only solution to meet demand for energy in China." CNNC puts the cost of 30 new plants at roughly $50 billion.

Xu Mi, a nuclear power engineer at the China Institute of Atomic Energy, says China has the technology and talent to handle the ramp-up. He notes that France built more than 40 nuclear power plants in the 1970s and '80s. "Given China's pace of development, constructing 30 nuclear power plants is not unrealistic," Xu says. And China is ready to pay for foreign help. AREVA in France, AtomStroyExport in Russia, and Westinghouse Electric Co., which is based in the United States but owned by British Nuclear Fuels PLC, have submitted bids on four new 1-GWe power plants to be completed by 2010. A decision is expected this November.

China is sticking mainly to proven designs: All 30 nuclear power plants planned through 2020 are likely to be based on pressurized water reactors, which make up the bulk of commercial plants worldwide.

And China is not the only country in Asia ramping up conventional nuclear power. Japan's Ministry of Economy, Trade, and Industry, in its 2004 nuclear power development plan, projected conventional nuclear power increasing from 25.5% of the total generated in 2003 to 40.4% in 2013. Two nuclear power plants are being brought online this year, two more are under construction, and another 12 are in various stages of design. India has eight nuclear power plants currently under construction. And Korea is planning eight plants.

Breeders multiply

Although this growth spurt builds mainly on conventional reactor designs, researchers in Asia are also pushing forward with more unusual approaches. INET is planning to build a prototype pebble bed reactor with a capacity of 200 MWe in east China's Shandong province by around 2011, according to the institute's Zhang (see p. 1172). And a technology that has been all but abandoned in Europe and United States—the fast neutron reactor—will be tested in experimental or prototype reactors in China, Japan, and India.

Fast reactors do away with the moderator—typically water—that's used in current commercial reactors to slow down highly energetic neutrons in the core. Applying the brakes increases collisions between neutrons and the limited amount of uranium-235. Instead, fast reactors use more highly fissile fuels, such as plutonium or a mixture of plutonium and uranium, and they can be used to produce additional plutonium that can in turn be recycled as reactor fuel.

Western governments once saw the "breeder" as a boon because it promised to reduce the amount of raw ore needed at the front and cut down on waste at the back end. The United States, United Kingdom, Germany, France, Russia, and Japan all built experimental or prototype reactors between the 1970s and '90s. France even built a 1200-MWe commercial reactor, the Super-Phenix, in Creys-Malville, in 1985. But the plants were prone to leaks of the molten sodium used as the coolant, and they relied on complex heat-transfer systems.

Commercial interest faded as it became clear that fast reactors would cost several times more than a conventional light-water plant. The critical factor, however, was public opposi-

On the way. China has completed a building and workshop for its experimental fast reactor; the system is scheduled to be commissioned in 2008.

CREDIT: D. NORMILE/*SCIENCE*

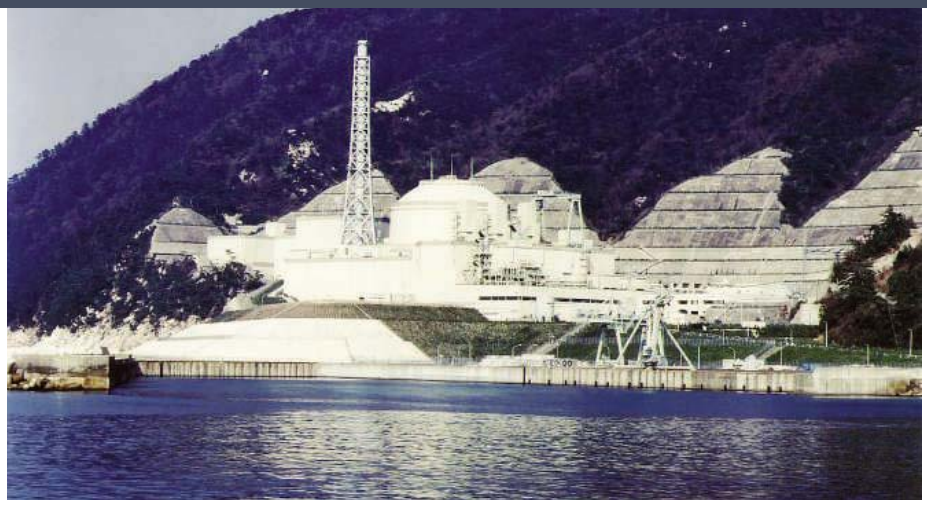

Watching the tides. Japan's troubled prototype fast reactor—Monju—has remained idle on the scenic coast of the Japan Sea for more than 10 years.

tion to creating and guarding stockpiles of plutonium, which could potentially be diverted for use in nuclear weapons. With the exception of France's small experimental Phenix, all the fast reactors in the United States and Western Europe have been shut down, although studies of the technology continue.

Although an international planning effort known as Generation IV envisions the future use of fast reactors, it is not clear who will be the first to build a commercial version, or when. Japan, China, India, South Korea, and Russia are all building or planning new reactors using this concept.

In Asia, Japan's fast reactor program is the oldest and furthest along. The Japan Nuclear Cycle (JNC) Development Institute is now hoping to restart a prototype that's been on prolonged standby. Monju, a 280-MWe unit in Fukui Prefecture on the Japan Sea Coast, has a troubled history. It achieved initial criticality in 1994 but in December 1995 suffered a massive leak of sodium coolant because of a design flaw in the piping. Plant managers tried to hide the magnitude of the accident, making it worse. After nearly 10 years of investigations, redesign, negotiations with different levels of government, and a court case, the local prefecture gave the green light earlier this year to begin modifications. If all goes smoothly, Monju could be operating again in 2008.

"The basic design of this plant is very old," admits Yutaka Sagayama, director of JNC's studies for commercializing fast reactors. But JNC is intent on running Monju to verify its reliability and gain technical expertise. The big challenge will be to lower the price. Sagayama says a Monju-type reactor would cost in the neighborhood of $8000 per KW of capacity, making fast reactors prohibitively expensive.

JNC engineers have been studying more economical fast reactors that would use lead-bismuth and helium gas as potential coolants. They concluded that sodium is still the most promising option. Simplifying the cooling system and using more compact heat exchangers could improve efficiency. But these modifications depend on perfecting a high-chrome-content steel alloy that at present is too brittle. JNC is working with Japan's steel companies to improve it. If the materials research and other modifications pan out, JNC's studies show they could build a new advanced sodium-cooled fast reactor plant about one-sixth the size of Monju but five times as productive, at 1500 MWe. This would cut the cost per kilowatt of capacity to $1600. Sagayama says they hope to start building a demonstration commercial fast reactor in about 2015.

The China Institute of Atomic Energy is a few steps behind with an experimental fast reactor with a power capacity of 20 MWe, due to be commissioned in 2008. China plans to follow up with a 600-MWe prototype by 2020 and commercial-scale fast reactors around 2030. India is hoping to complete a 500-MWe Prototype Fast Breeder Reactor by 2010, and Korean researchers are designing a 600-MWe fast reactor.

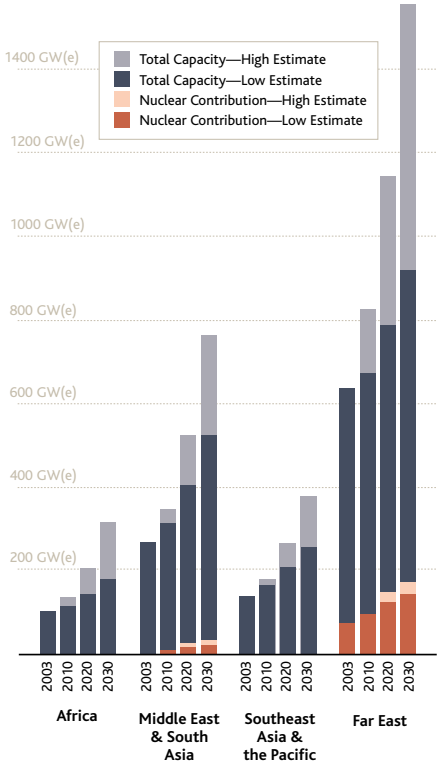

All these countries foresee an important role for fast reactors. Japan's long-term plan, Sagayama says, calls for fast reactors to replace conventional reactors completely, although there is no target date. And Huang Guojun, a CNNC deputy general manager, told a conference earlier this year that fast reactors will be the "main type of nuclear reactor to be used in China" by the middle of this century. Researchers in both countries say they will be needed to recycle scarce nuclear fuels. Xu notes that if nuclear power accounts for 20% of China's power needs in 2050, the country would have to acquire 75% of all known easily accessible uranium deposits.

Japan might still have a problem with public acceptance. Hideyuki Ban, co-director of the Citizens' Nuclear Information Center (CNIC), a Japanese antinuclear group, says the delays and accidents at Monju and other facilities make it clear that "Japan's fast breeder program is in trouble." He says the government's main nuclear advisory commission has been unwilling to "change a policy established 50 years ago," and the program seems to be running on inertia.

Also targeted by critics is Japan's large-scale reprocessing plant at Rokkasho, at the northern tip of Honshu Island, capable of producing 8 tons of plutonium a year. In May 2007, the plant is scheduled to start converting plutonium into so-called mixed-oxide fuel that can be used in conventional reactors, a stopgap until commercial fast reactors come online. Ban's bottom-line worry is that "if more and more countries acquire [reprocessing] technologies, there will be no controlling the proliferation of nuclear weapons." CNIC is calling for a moratorium on all plutonium production.

In China, the public seems less aware of such controversies, says Xue Ye, executive director of Friends of Nature, the country's largest environmental organization. With just nine plants scattered throughout the country, "people have not felt their existence." He thinks that could change, however, as more plants are constructed. "The Chornobyl explosion is still vivid in the memory of most Chinese," he says. Beijing residents have protested the construction of laboratories handling dangerous pathogens near their homes; he thinks similar protests could interrupt China's plans for nuclear electricity. The big question facing Asia's booming nuclear industry is can it stay ahead of this nascent public opposition?

–GONG YIDONG AND DENNIS NORMILE

Gong Yidong is a writer with *China Features*.

CREDITS (TOP TO BOTTOM): JAPAN NUCLEAR CYCLE DEVELOPMENT INSTITUTE; IAEA

Down to Earth: Lingering Nuclear Waste

Few countries have a concrete plan for disposing of long-lived radioactive waste, but those that do are converging on the same idea: Dig a deep mine, store the material in robust containers, and rely on geology to keep it out of the biosphere for tens of thousands of years. The concept seems simple. But the potential flaws are hotly debated, and only a few projects are under way.

First off the blocks were the United States and Finland, which have actually chosen locations. Yucca Mountain, Nevada, in effect became the official U.S. site in 1987 but has been delayed by continuous legal battles and scientific questions. The Department of Energy (DOE) has spent $5 billion on planning and does not have a target opening date.

About 51,000 metric tons of high-level waste have been earmarked for Yucca Mountain; if all U.S. nuclear power plants run to the end of their current licenses, DOE spokesperson Allen Benson says, the country will have about 120,000 metric tons to dispose of—70% more than the site is legally permitted to hold. But "people are just assuming ... the law will be changed, allowing Yucca Mountain to expand," says geologist Steve Frishman of the Nevada Agency for Nuclear Projects, which monitors the project.

DOE's design relies on elevation and waste heat to keep water out of the repository, which would be carved into volcanic tuff. But water is its bugbear. Critics say that the site isn't dry enough, the rock is fractured and leaky, and the oxidizing environment will corrode the waste containers.

Both Finland and Sweden are well along with designs much different from the U.S. approach. Finland is planning a $3 billion repository near the community of Eurajoki on the country's southwestern coast, and Sweden will choose one of two candidate sites in 2008. Their repositories are to be built in granite and maintain a relatively cool, nonoxidizing environment that could work even if damp. The Swedish and Finnish designs "have vastly reduced the uncertainties" about how well they will contain the waste, says geologist Allison Macfarlane of the Massachusetts Institute of Technology (MIT) in Cambridge. Eurajoki's deep-bedrock repository will hold about 5600 tons of waste, 40% more than existing Finnish plants could produce in their lifetimes. Sweden voted in 1980 to phase out nuclear power; if the decision sticks, its $2.5 billion repository will store about 8000 metric tons of waste.

France, Japan, and Russia are exploring possible burial sites but keeping wastes near the surface indefinitely while they decide what to do next. All now reprocess spent fuel to extract usable isotopes, which they argue conserves fuel and reduces waste. But a blue-ribbon review published in 2003 by MIT concluded that, for many decades, reprocessing will cost more than "once-through" use of fuel. And because reprocessing increases the risk that material will be diverted to a dirty bomb or a nuclear weapon, the MIT group argued that it should be stopped.

Many countries hope to reduce waste eventually through "transmutation": bombarding highly radioactive elements with neutrons to convert them to less threatening isotopes. But this method is expensive, and it may not be practical for decades, if ever.

Russia and some countries with small nuclear programs that would have difficulty funding a repository are exploring the possibility of pooling wastes in shared, multinational repositories. The chief advocate of this approach is the International Atomic Energy Agency (IAEA), in part as a way to help keep dangerous waste under lock and key.

But repository plans everywhere face a significant first hurdle in winning public support, IAEA Director Mohammad ElBaradei has said: "Once the first country has succeeded in placing a geological repository in service, ... the road ahead for other countries will be made much easier." So all eyes are on the groundbreaking projects in the United States, Finland, and Sweden.

–MASON INMAN

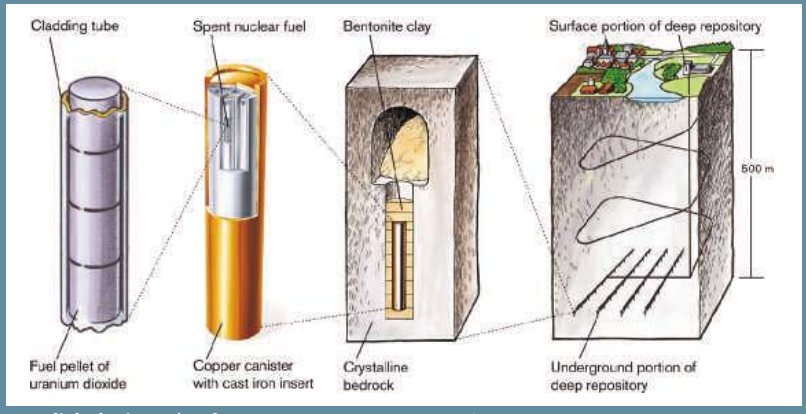

CREDIT: SKB, SWEDISH NUCLEAR FUEL AND WASTE MANAGEMENT COMPANY

Swedish design. Plan for a permanent waste repository.

Planning for Deep Geologic Repositories

UNITED STATES
Reprocesses fuel: No
Status: Chose site at Yucca Mountain. Repository being designed.
Opening date: After 2012
Capacity: 70,000 metric tons of spent fuel
Cost: $5 billion spent so far on planning

SWEDEN
Reprocesses fuel: No
Status: Site to be chosen in 2008. Repository being designed.
Opening date: 2017
Capacity: 8000 metric tons of spent fuel
Cost: $2.5 billion

FINLAND
Reprocesses fuel: No
Status: Chose site at Olkiluoto. Repository being designed.
Capacity: 5600 metric tons of spent fuel
Cost: $3 billion

FRANCE
Reprocesses fuel: Yes
Status: Studying candidate sites. To decide in 2006 between repository or surface storage.
Opening date: After 2025
Capacity and cost: No estimates

RUSSIA
Reprocesses fuel: Yes
Status: Studying candidate sites and designs.
Opening date: After 2025
Capacity and cost: No estimates

JAPAN
Reprocesses fuel: Yes
Status: Seeking candidate sites for a planned repository.
Opening date: Scheduled for 2035
Capacity: Undecided; by 2020 will have 6000 m^3 vitrified waste
Cost: $27 billion for 6000 m^3 waste

CHINA
Reprocesses fuel: Yes
Status: Studying candidate sites for a planned repository.
Opening date: Scheduled for 2050
Capacity and cost: No estimates

UNITED KINGDOM
Reprocesses fuel: Yes
Status: Reconsidering all disposal options for decision in 2007.
Opening date: Undecided
Capacity: Undecided; existing plants will produce 1500 m^3 vitrified waste
Cost: No estimate

Random Samples

Edited by Constance Holden

Starvation and Schizophrenia

Epidemiologists have long suspected that malnourishment in pregnant women can raise the risk of schizophrenia in their offspring. The hypothesis is based in part on a study showing that people conceived in the Netherlands during the winter of 1944–45, when Hitler's army blockaded food supplies, were twice as likely to develop the mental disorder.

Now a new and larger analysis of people born during the Chinese famine of 1959–61 has bolstered the connection. Geneticists David St. Clair of the University of Aberdeen, U.K., and Lin He of Shanghai Jiao Tong University in China analyzed 3 decades of records from the Fourth People's Hospital, the only psychiatric hospital in the Wuhu region of eastern China, which was hit hard by the famine. After adjusting for differing mortality rates before, during, and after the famine, the researchers found that 2% of people conceived in the region in 1960 and 1961 developed schizophrenia, as opposed to 0.9% of those conceived in the 3 years before or after the famine.

The study, which appeared in the 3 August issue of the *Journal of the American Medical Association*, "offers a compelling confirmation" of the theory that prenatal malnutrition raises schizophrenia risk, says epidemiologist Richard Neugebauer of the New York State Psychiatric Institute in New York City. If animal studies can identify the key nutrients, this could yield "an almost utopian opportunity" to reduce schizophrenia risk by ensuring that pregnant women receive adequate nutrition, he says.

A Whiff of Malaria to Whet the Appetite

Offering another example of how shrewdly manipulative parasites can be, researchers have discovered that *Plasmodium falciparum*, which causes malaria, can make its human host more attractive to *Anopheles* mosquitoes, thus boosting its chances of being transferred to another host. The "bite me" signal is sent out only when the parasites are in the gametocyte stage, ready to be picked up by a mosquito.

Researchers had long speculated that parasites might tinker with mosquito attraction. To test the idea, a team led by Jacob Koella of the Université Pierre et Marie Curie in Paris screened schoolchildren in a Kenyan village for the presence of malaria parasites. Then every day for 12 days they selected three different children: one who was uninfected, one who carried the parasite in the nontransmissible stage, and one with parasites in the gametocyte stage.

At sunset, the three lay down in three nylon tents connected to a central chamber, into which 100 uninfected mosquitoes were set loose and given 30 minutes to choose a tent. On average, the children carrying the gametocytes drew about twice as many mosquitoes as the other two, but after the infected subjects were treated with antimalarial drugs, the difference disappeared.

Presumably, the parasite triggers changes in breath or body odors, the researchers report in the September issue of *Public Library of Science: Biology*. The study has a "very, very elegant design," says Andrew Read, an evolutionary biologist at the University of Edinburgh, U.K., and may eventually help scientists in designing so-called olfactory traps to catch the insects.

Chacun à son Goût

"It's fine that someone has it who will enjoy it. If I had that money, I'd probably be buying pictures."

—Art connoisseur James Watson, to *The New York Times*, about his sometime rival J. Craig Venter spending several million dollars to buy a collection of historically important biology papers, including an early draft of Watson's famous account of the discovery of DNA's structure.

Image Doctors

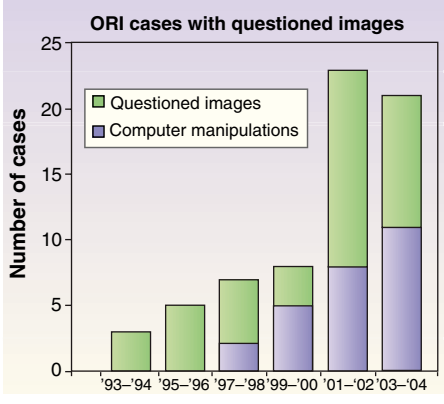

Do two bands on that Southern blot in the paper you're reading look oddly similar? Do the colors on a gene-expression microarray figure appear suspiciously bright? The federal Office of Research Integrity (ORI) reports that, in part thanks to the wonders of computer graphics, over the past decade cases involving questioned images—such as fabricated bands on a gel and cut-and-pasted cells in a micrograph—have grown from 4% of its caseload in 1993–94 to more than 40%.

ORI investigator John Krueger says that whereas the ORI cases reflect possible deliberate fakery, in many other instances, biologists probably are just trying to make data clearer and don't realize they're crossing an ethical line. "We think there should be a broader discussion in the community about this," Krueger says. Some journals are trying to screen for doctored images. To help them and anyone else who wants to play forensic scientist, ORI has posted some computer tools and practice examples from actual ORI cases at ori.hhs.gov/tools/data_imaging.shtml.

CREDITS (TOP TO BOTTOM): BETTMANN/CORBIS; ARS

Edited by Yudhijit Bhattacharjee

AWARDS

Personal connection. Theoretical physicist Samuel Edwards of the University of Cambridge last week won a prize awarded in the name of one of his former teachers. Edwards (top left), who studied quantum mechanics under Nobelist Paul Dirac as a Cambridge undergraduate 60 years ago, received the Dirac Medal from the International Center for Theoretical Physics in Trieste, Italy, for his work on polymers, spin glasses, and granular materials.

Dirac was a mediocre instructor whose lectures consisted of reading aloud from his book *The Principles of Quantum Mechanics*, recalls Edwards, 78. "And sometimes he missed pages," he says.

The other physicist to receive this year's medal—awarded on 8 August, Dirac's birthday—was Patrick Lee (bottom left) of the Massachusetts Institute of Technology in Cambridge, honored for his work on the localization and interactions of electric charges in metals. "I'm pleased to see our field—condensed matter physics—get recognized," says Lee, 58, about an award typically given to research in particle theory and other esoteric fields.

JOBS

Capital's call. Keeping his lab going at Arizona State University was a prerequisite for Jim Collins before agreeing last week to become head of the biology directorate at the National Science Foundation (NSF) in Arlington, Virginia. "My obligations are to the foundation, which I think is a terrific institution," says the 58-year-old ecologist, who has spent 30 years at the Tempe, Arizona, university interrupted by a 1-year sabbatical as an NSF program manager. "But I had to convince myself that I could still interact with students before I decided to take the job." His solution: a 2-year stint as a rotator, "commuting as much as is reasonable" to shepherd his flock of a dozen undergraduates, grad students, and postdocs.

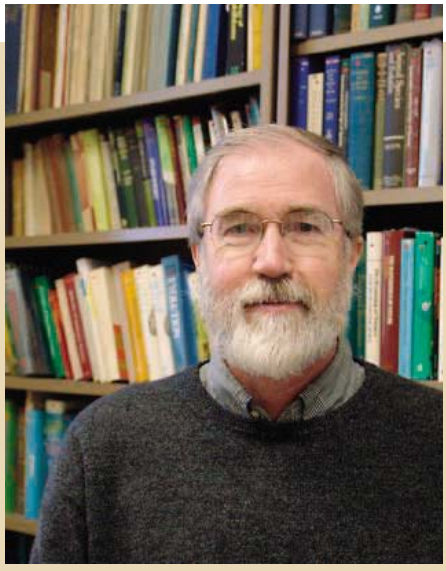

A longtime NSF grantee for his work on morphological variation within species, using salamanders as a model organism, Collins has more recently begun to explore the fledgling field of ecological ethics. He hopes to expand biology's interactions with NSF's seven other directorates and other federal agencies and says he isn't fazed by the dim prospects for significant budget increases. But he's not planning to set down roots in the nation's capital: "I love the Sonoran Desert and my research. I certainly wasn't looking for a change of scenery."

THEY SAID IT

"The trouble with the 'missing link' is that it is still missing! ... The theory of evolution ... has more holes in it than a crocheted bathtub."

—Utah state senator D. Chris Buttars in an op-ed published in the 9 August edition of *USA Today*.

Got any tips for this page? E-mail people@aaas.org

DATA POINT

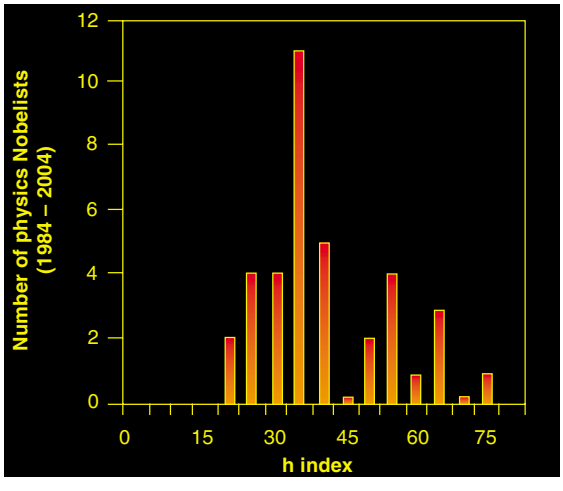

Impact factor. A theoretical physicist has proposed an index to rank the productivity of scientists by a single number. Named "h" by its creator—Jorge Hirsch of the University of California, San Diego—it is the largest number such that the researcher has h papers with at least h citations. For example, Edward Witten, a string theorist at the Institute for Advanced Study in Princeton, New Jersey, has an h of 110 because 110 papers of his papers have received at least 110 citations. The index favors researchers who produce a stream of influential papers over those who publish many quickly forgotten ones or a few blockbusters. "I can't imagine a person with a high h index who hasn't done important work," says Hirsch, whose own h is 49.

Manuel Cardona (h = 86), a physicist at the Max Planck Institute for Solid State Research in Stuttgart, Germany, says "the great advantage of the index is that you can get it in about 30 seconds" using the ISI Web of Knowledge. However, he says, researchers shouldn't use it as the only measure of their colleagues' performance. The index is described in a preprint posted at www.arxiv.org.

CREDITS (TOP TO BOTTOM): C. J. KAZILEK; UNIVERSITY OF CAMBRIDGE; PATRICK LEE

LETTERS

The Problem of Child Sexual Abuse

THE POLICY FORUM "THE SCIENCE OF CHILD sexual abuse" by J. J. Freyd *et al.* (22 Apr., p. 501) provides an extremely important call to action to the scientific community. In 1999, James Mercy, Senior Scientist at the U.S. Centers for Disease Control and Prevention, noted the importance of viewing child sexual abuse with "new eyes" (*1*). The implementation of Freyd *et al.*'s policy recommendations would help us to do this. For too long, the fact that the topic makes us uneasy has caused too many of us to avert our eyes. But what if child sexual abuse were a newly discovered disease—a disease that affects up to 20% of women and 10% of men, a disease that forms a potent risk factor for developing a host of mental and physical problems, a disease that, according to a conservative estimate by the U.S. Department of Justice, costs society over $24 billion each year (*2*)? Imagine what we as concerned scientists would do if we discovered such a disease decimating the lives of our young people?

> "But what if child sexual abuse were a newly discovered disease—a disease that affects up to 20% of women and 10% of men... a disease that... costs society over $24 billion each year?"
>
> –FINK

Our response to child sexual abuse thus far "has been far from the full-court press reserved for traditional diseases or health concerns of equal or even lesser magnitude" [(*2*), p. 317]. We have severely underestimated the effects of this problem on our children's health. It is time to recognize that the problem is not solely a product of the action of a few sick individuals; child sexual abuse is a preventable health problem that has been allowed to spread unabated due to scientific and social neglect.

PAUL FINK

President, The Leadership Council on Child Abuse & Interpersonal Violence, and Past President, American Psychiatric Association, 191 Presidential Boulevard, Suite C-132, Bala Cynwyd, PA 19004, USA. E-mail: Pjayfink@aol.com

References

1. U.S. Department of Health and Human Services (DHHS), Child Maltreatment 2003 (DHHS, Washington, DC, 2005).
2. J. A. Mercy, *Sex. Abuse* **11**, 317 (1999).

IN THE POLICY FORUM "THE SCIENCE OF child sexual abuse" (22 Apr., p. 501), J. J. Freyd and colleagues succinctly summarized an enormous amount of research and rightly highlighted the depressing bias of those researchers who "emphasized false allegations rather than false denials." It is a sad fact of life that after decades of ignoring the issue altogether, research showing the alarming prevalence of child abuse has met with a kind of "backlash."

Mental health professionals have a poor track record in this field. It was only three decades ago (1975) that the leading psychiatric textbook in the United States informed students that the rate of incest was 1 case per million (*1*).

If I have a criticism of the Policy Forum, it is that the list of proven effects of child sexual abuse did not include psychosis and schizophrenia. Recent large-scale studies in the UK (*2*) and the Netherlands (*3*) have confirmed our smaller studies in New Zealand (*4*, *5*) that child sexual abuse is highly predictive of these supposedly biologically based "mental illnesses."

JOHN READ

Psychology Department, University of Auckland, Auckland 1020, New Zealand.

References

1. D. Henderson, in *Comprehensive Textbook of Psychiatry*, A. Freedman, H. Kaplan, B. Saddock, Eds. (Williams & Wilkins, Baltimore, MD, 1975), pp. 1530–1539.
2. P. Bebbington *et al.*, *Br. J. Psychiatry* **185**, 220 (2004).
3. I. Janssen *et al.*, *Acta Psychiatr. Scand.* **109**, 38 (2004).
4. J. Read, K. Agar, N. Argyle, V. Aderhold, *Psychol. Psychotherapy Theory Res. Practice* **76**, 1 (2003).
5. J. Read, L. Goodman, A. Morrison, C. Ross, V. Aderhold, in *Models of Madness: Psychological, Social and Biological Approaches to Schizophrenia*, J. Read, L. Mosher, R. Bentall, Eds. (Brunner-Routledge, Hove, UK, 2004), pp. 223–252.

IN THEIR POLICY FORUM "THE SCIENCE OF child sexual abuse" (22 Apr., p. 501), J. J. Freyd *et al.* assert that "[s]urveys likely underestimate prevalence [of child sexual abuse] because of underreporting and memory failure" There is no way of making that inference.

Consider a 2×2 table in which we assess the relationship between actual abuse and reported abuse. Let a be the joint frequency with which abuse is both actual and reported, b be the joint frequency with which actual abuse is not reported, c be the joint frequency with which there is no actual abuse but a report of it, and d be the joint frequency with which there is no actual abuse and no reported abuse. The finding that there is "underreporting" of abuse simply states that the frequency of $b > 0$. In contrast, the statement that reporting underestimates actual abuse is the statement that $a + c < a + b$, or $c < b$. There is no way of making this inference until there is some way of knowing the joint frequency with which abuse does not occur but is reported (for whatever reason). Moreover, given that abuse (fortunately) is uncommon (according to the authors, well less than 50% of children are abused, i.e., fall in cells a and b), it is plausible to hypothesize that c might be greater than b, despite the value of $b > 0$. Of course, the most accurate way to determine c would be to survey people randomly whom we know have not been abused and then estimate how many nevertheless report having been abused, a daunting task.

		Reported abuse	
		+	–
Actual abuse	+	*a*	*b*
	–	*c*	*d*

ROBYN M. DAWES

Department of Social and Decision Sciences, Carnegie Mellon University, Porter Hall 208, Pittsburgh, PA 15213–3890, USA.

THE POLICY FORUM "THE SCIENCE OF CHILD sexual abuse" by J. J. Freyd *et al.* (22 Apr., p. 501) calls for more and better scientific research on child sexual abuse (CSA). Yet it misleadingly suggests that the "[c]ognitive and neurological mechanisms that may underlie the forgetting of abuse have been identified." This statement implies that the forgetting of CSA is somehow special and cannot be explained by the sorts of principles familiar in the cognitive and neuroscientific study of memory.

The notion that individuals can develop amnesia for seemingly unforgettable traumatic events, followed by "recovery" of these memories months or years later, has been part of the folklore of psychiatry and clinical psychology for more than 100 years and has been described under such headings as "repression," "dissociation," and "traumatic amnesia" (*1*). But, in fact, surveys of trauma victims show that they typically remember their experiences all too well, and any forgetting is easily accounted for by organic factors or by normal memory processes such as ordinary forgetting and infantile or childhood amnesia (*2*).

Genuinely traumatic events—those experienced at the time as overwhelmingly terrifying and life-threatening—are seldom, if ever, truly forgotten. Evidence to the contrary comes from methodologically weak studies that generally fail to obtain corroboration for retrospective self-reports of either trauma, amnesia, or both. Some investigators also confuse forgetting and amnesia with a simple failure to disclose a memory, or the recovery of memory with the reinterpretation of an event always remembered. The study cited by Freyd *et al.* (*3*) concluded that its results "do not support the existence of special memory mechanisms unique to traumatic events, but instead imply that normal cognitive operations underlie long-term memory for CSA" (p. 117).

These facts have long been known (*4*, *5*), although they are often ignored or discounted by professionals—researchers as well as clinical practitioners—and unappreciated by the public at large. So far as the scientific evidence is concerned, traumatic amnesia appears to be a myth. Rather than searching for the cognitive and neurological mechanisms underlying a phenomenon that appears to be nonexistent, scientists and policy-makers might better focus their resources on the very real problems of CSA: its causes, correlates, and all-too-real consequences, and the most effective means by which it can be treated and prevented.

JOHN F. KIHLSTROM,[1] RICHARD J. MCNALLY,[2] ELIZABETH F. LOFTUS,[3] HARRISON G. POPE JR.[4]

[1]Department of Psychology, University of California, Berkeley, Berkeley, CA 94720–1650, USA. [2]Department of Psychology, Harvard University, Cambridge, MA 02138, USA. [3]Department of Psychology and Social Behavior, University of California, Irvine, Irvine, CA 92697–7085, USA. [4]Department of Psychiatry, McLean Hospital, Harvard Medical School, Belmont, MA 02478, USA.

References

1. J. F. Kihlstrom, in *Truth in Memory* (Guilford Press, New York, 1998), pp. 3–31.
2. R. J. McNally, *Remembering Trauma* (Harvard Univ. Press, Cambridge, MA, 2003).
3. G. S. Goodman *et al.*, *Psychol. Sci.* **14** (no. 2), 113 (2003).
4. E. F. Loftus, *Am. Psychol.* **48**, 518 (1993).
5. H. G. Pope Jr., P. S. Oliva, J. I. Hudson, in *Science in the Law: Social and Behavioral Science Issues*, D. L. Faigman, D. H. Kaye, M. J. Saks, J. Sanders, Eds. (West Group, St. Paul, MN, 2002), pp. 487–526.

Response

We concur with the Letter writers that child sexual abuse (CSA) is a serious public health problem. We also agree with Read that links between CSA and adult psychosis (*1*) should not be overlooked.

As Dawes indicates, one must take into account both false allegations and denials in determining the prevalence of sexual abuse. However, evidence indicates that false allegations occur at rates lower than nondisclosure rates. Prevalence is underestimated (in Dawes' notation, $c < b$) whenever the likelihood that reports of abuse are false $[c/(a+c)]$ is less than the likelihood that true abuse is not disclosed $[b/(a+b)]$. Mechanisms of false allegations, such as suggestive therapy or interviewer bias, occur in a small minority of abuse reports: 2% of survey respondents claiming abuse report having recovered their memory with the help of a professional or others (*2*), and approximately 10% report that the abuse was disclosed to authorities, setting an upper bound on adult influences (*3*). On the other hand, most surveys of adults with "well-documented serious abuse or neglect" have found nondisclosure rates over 30% [(*4*), p. 270].

High rates of nondisclosure also speak to Kihlstrom and colleagues' assertion that sexual abuse is "seldom, if ever, truly forgotten." Although underreporting is attributable in part to abuse victims' reluctance to disclose, Williams' (*5*) difficulty in eliciting abuse reports despite extensive questioning of women with documented abuse histories led

Loftus *et al.* (*6*) to acknowledge that "many children can forget about a sexually abusive experience from their past" (p. 1177). What Kihlstrom *et al.* call "folklore" is actually over 100 years of clinical and scientific evidence for the forgetting of trauma (*7*). Although the frequency and mechanisms of forgetting are not completely clear, the basic phenomenon is documented in dozens of empirical studies (*8*) and corroborated case studies (*9*).

> "Claims that traumatic amnesia rarely occurs, as well as legitimate disagreements over the prevalence and accurate recall of CSA, reinforce [our] recommendations."
>
> –FREYD ET AL.

Kihlstrom *et al.* argue that trauma victims typically remember their experiences "all too well." However, both intrusive recall and an "inability to recall an important aspect of the trauma" [(*10*), p. 428] are diagnostic of pathological posttraumatic conditions and may both reflect, in part, some common underlying disregulation of memory processes (*8*). Indeed, traumatized individuals exhibit a range of memory impairments (*11*). Research on executive control over recall of unwanted memories (*12*), and research on children's (*13*) and adults' (*14*) encoding and memory of trauma stimuli has provided preliminary support for models of repression and traumatic amnesia. The relations among the effects of trauma on encoding, retrieval inhibition, and memory functioning are worthy of future study.

In our Policy Forum, we recommended a series of international consensus panels on scientific and clinical practice issues related to CSA, expansion of the National Child Traumatic Stress Network, and the creation of a new Institute of Child Abuse and Interpersonal Violence within the NIH that would foster research on CSA and related conditions. Claims that traumatic amnesia rarely occurs, as well as legitimate disagreements over the prevalence and accurate recall of CSA, reinforce these recommendations. Denial and underestimation of the effects of CSA continue to be serious obstacles to ending a preventable public health problem.

JENNIFER J. FREYD,[1] FRANK W. PUTNAM,[2] THOMAS D. LYON,[3] KATHRYN A. BECKER-BLEASE,[4] ROSS E. CHEIT,[5] NANCY B. SIEGEL,[6] KATHY PEZDEK[7]
[1]Department of Psychology, University of Oregon, Eugene, OR 97403–1227, USA. [2]Department of Pediatrics, Children's Hospital Medical Center, Cincinnati, OH 45229, USA. [3]University of Southern California Law School, Los Angeles, CA 90089, USA. [4]Department of Psychology, Washington State University, Vancouver, WA 98686, USA. [5]Department of Political Science, Brown University, Providence, RI 02912, USA. [6]NBS Associates, Columbia, MD 21046, USA. [7]Department of Psychology, Claremont Graduate University, Claremont, CA 91711, USA.

References

1. I. Janssen *et al.*, *Acta Psychiatr. Scand.* **109**, 38 (2004).
2. S. C. Wilsnack, S. A. Wonderlich, A. F. Kristijanson, N. D. Vogeltanz-Holm, R. W. Wilsnack, *Child Abuse Neglect* **26**, 139 (2002).
3. R. F. Hanson *et al.*, *Child Abuse Neglect* **23**, 559 (1999).
4. J. Hardt, M. Rutter, *J. Child Psychol. Psychiatry* **45**, 260 (2004).
5. L. M. Williams, *J. Consult. Clin. Psychol.* **62**, 1167 (1994).
6. E. F. Loftus *et al.*, *J. Consult. Clin. Psychol.* **62**, 1177 (1994).
7. J. M. Arrigo, K. Pezdek, *Curr. Dir. Psychol. Sci.* **6**, 148 (1997).

8. D. H. Gleaves, S. M. Smith, L. D. Butler, D. Spiegel, *Clin. Psychol. Sci. Practice* **11**, 3 (2004).
9. R. E. Cheit, The Recovered Memory Project, www.brown.edu/PublicPolicy/Recovmem (2005).
10. American Psychiatric Association, *Diagnostic and Statistical Manual of Mental Disorders* (DSM-IV) (American Psychiatric Association, Arlington, VA, ed. 4, 1994).
11. J. D. Bremner, *J. Aggression Maltreatment Trauma* **4**, 165 (2001).
12. M. C. Anderson *et al.*, *Science* **303**, 232 (2004).
13. K. A. Becker-Blease, J. J. Freyd, K. C. Pears, *J. Trauma Dissociation* **5**, 113 (2004).
14. M. L. Moulds, R. A. Bryant, *J. Traumatic Stress* **18**, 233 (2005).

A Celebration of Ignorance

CONGRATULATIONS TO *SCIENCE* FOR SHIFTing paradigms in the 125th Anniversary issue (125 questions: what don't we know?, 1 July), not only by focusing on what leading contemporary scientists "don't know," but also by unabashedly labeling this collection of 125 important unanswered questions as a "survey of scientific ignorance." Back in 1984, based on my mentor Lewis Thomas' whimsical suggestion (*1*), my late husband and I brought ignorance out of the closet by creating the University of Arizona's "Curriculum on Medical Ignorance" (featuring a Summer Institute, distinguished visiting "ignorami," and ignorance logs and exercises) to teach medical and later undergraduate and K-12 students and science teachers how to recognize and deal with ignorance—"what we know we don't know, don't know we don't know, and think we know but don't"—about a wide range of medical and scientific topics (*2*). Our curriculum has resulted in various ignorance-based publications, presentations, media coverage, and products, earning me the dubious title of "Ignorama Mama," mother of the global ignorance movement. Indeed, all learning and discovery do take place in the terrain of ignorance, not knowledge, and it is questions, questioning, and questioners that impel scientific advances. These mysteries and puzzles, not dry facts and pat answers, should also drive science education as well as the research enterprise. A *Wall Street Journal* editorial (*3*) paradoxically hailed our evolution from the Information Age to the "Age of Ignorance," where we can recuse ourselves from excessive information, admit we don't know, and humbly "google" or grope our way through what we need to know. And newly minted Nobel physicist David Gross lauded "ignorance—the most important product of knowledge" as "lucky for science, scientists, and the Nobel Foundation" (*4*).

MARLYS HEARST WITTE
Professor of Surgery and Director of Student Research, University of Arizona College of Medicine, Post Office Box 245200, Tucson, AZ 85724, USA. E-mail: grace@surgery.arizona.edu

References
1. L. Thomas, in *Cecil Textbook of Medicine*, J. B. Wyngaarden, L. H. Smith, Eds. (W.B. Saunders, Philadelphia, PA, ed. 16, 1982), pp. xli–xliii.
2. See www.medicine.arizona.edu/ignorance and www.medicalignorance.org.
3. H. Stein, "The age of ignorance," *Wall Street J.*, 11 June 1993, p. A10.
4. D. Gross, *Science News* **167** (no. 4), 59 (2005).

What Are Our Research Priorities?

The advancement of science depends on what James Clerk Maxwell termed "thoroughly conscious ignorance" ("In praise of hard questions," Special Section on 125 questions: what don't we know, 1 July, p. 76). If deepening the "consciousness" of our ignorance is a prerogative of scientists, then this implies a responsibility to reflect on what to know first or the (type of) knowledge our world needs most urgently. Which hard scientific questions should become research prior-

Q AAAs

Who's helping scientists stay one jump ahead?

"I read my *Science* when I'm at the skatepark with my son. It's great to be out in the fresh air. And an interesting cover picture will often provoke questions and interesting conversations with parents and kids alike."

AAAS member Lorraine J. Kuhn, Ph.D., Stormwater Management Assistant for the Village of Ardsley, New York

Photo: Dr. Martin Levy

Lorraine Kuhn at Ardsley Village Skatepark

AAAS is committed to advancing science and giving a voice to scientists around the world. We work to improve science education, promote a sound science policy, and support human rights.

Helping our members stay abreast of their field is a key priority for AAAS. One way we do this is through *Science*, which features all the latest breakthroughs and groundbreaking research, and keeps scientists connected wherever they happen to be. Members like Lorraine find it essential reading.

To join the international family of science, go to www.aaas.org/join.

AAAS

ADVANCING SCIENCE, SERVING SOCIETY

www.aaas.org/join

ities if we take into consideration Kofi Annan's urgent appeal to the scientific community to improve global human welfare (*1*)?

It would be fascinating to see how much science could contribute to a research agenda that serves mankind by making our ignorance with respect to people, planet, and profit more conscious. Which not, yet, answered scientific questions could produce a genuine breakthrough in mankind's understanding of sustainable development?

AD VAN DOMMELEN AND GEERT R. DE SNOO
Institute of Environmental Sciences (CML), Leiden University, Post Office Box 9518, Leiden, The Netherlands. E-mail: vandommelen@cml.leidenuniv.nl

Reference
1. K. Annan, *Science* **299**, 1485 (2003).

CORRECTIONS AND CLARIFICATIONS

Table of Contents: (22 July, p. 525). The credit for the image of parrots on page 529 was not given. It should be Roland Seitre.

Reports: "Causal protein-signaling networks derived from multiparameter single-cell data" by K. Sachs *et al.* (22 Apr. p. 523). The author names in reference (*26*) were incorrect. The authors are I. M. Ong, J. D. Glasner, D. Page. The URL for the supporting online material was incorrect; it should be www.sciencemag.org/cgi/content/full/308/5721/523/DC1. There was also a reference missing in the last sentence of the last paragraph on page 527 that continues on page 528. The new reference (*29*) is P. O. Krutzik, G. P. Nolan, *Cytometry* **55**, 61 (2003). The acknowledgments will now be reference (*30*).

Technical Comment Abstracts: "Response to Comment on 'Molybdenum isotope evidence for widespread anoxia in mid-Proterozoic oceans' " (12 Aug., p. 1017). The first author should be A. D. Anbar, not D. Anbar. The name appears correctly in the full-text online version.

TECHNICAL COMMENT ABSTRACTS

COMMENT ON "Quantum State Transfer Between Matter and Light"

S. J. van Enk and H. J. Kimble

Matsukevich and Kuzmich (Reports, 22 October 2004, p. 663) claim to have produced several types of nearly maximally entangled states involving photons and atomic ensembles. We show that their experimental evidence is insufficient to support these claims, that their comparisons to a previous experiment are misleading, and that their sweeping assertions related to quantum networks are unjustified.

Full text at
www.sciencemag.org/cgi/content/full/309/5738/1187b

RESPONSE TO COMMENT ON "Quantum State Transfer Between Matter and Light"

D. N. Matsukevich and A. Kuzmich

van Enk and Kimble criticize several aspects of our study but do not challenge our main result, the achievement of quantum state transfer between matter and light. Instead, their critique focuses on the quantitative amount of entanglement present in our experiment and how the vacuum should be accounted for in these measures, both in our experiment and in others. Although a careful discussion of this topic has some value for the field, it does not alter the conclusions of our paper.

Full text at
www.sciencemag.org/cgi/content/full/309/5738/1187c

Letters to the Editor

Letters (~300 words) discuss material published in *Science* in the previous 6 months or issues of general interest. They can be submitted through the Web (www.submit2science.org) or by regular mail (1200 New York Ave., NW, Washington, DC 20005, USA). Letters are not acknowledged upon receipt, nor are authors generally consulted before publication. Whether published in full or in part, letters are subject to editing for clarity and space.

PALEOANTHROPOLOGY

Finding Life in Old Bones

Robert N. Proctor

The Ape in the Tree
An Intellectual and Natural History of *Proconsul*
by Alan Walker and Pat Shipman

Harvard University Press, Cambridge, MA, 2005. 285 pp. $26.95, £17.95, €24.90. ISBN 0-674-01675-0.

We live in a spectacular period for paleoanthropology. Over the past dozen or so years, newly discovered species of fossil hominids have been reported at the rate of about one per year. Although doubts remain as to whether all these finds should be granted status as separate species—having only bones with which to work, we generally can't say for sure who could breed with whom—a picture is emerging of an adaptive radiation typical of other large carnivores.

Time is not equally fair to all paleontologists, however, and there remain some irritating gaps in the fossil record. We have, for example, very few fossil remains of chimpanzees or gorillas, the closest living relatives of modern humans. That paucity must stem from the many obstacles to the fossilization of forest-dwelling animals, although some of the creatures we classify as hominids may actually be more closely related to chimps or gorillas than to humans. Molecular geneticists have not yet been able to sequence remains more than about 50,000 years old, so it is not (yet) possible to add such evidence to our phylogenetic reconstructions.

Perhaps naturally, most attention has been focused on the history of our closest kin. But a glance further back reveals other data-poor intervals that frustrate our decipherment of anthropoid phylogeny. One such gap has been the near-total absence of ape-like fossils from between ~12 and 7 million years ago (Ma), a period during which monkey-like apes (or ape-like monkeys) must have diverged to give rise to the ancestors of today's remnant trident of chimps, humans, and gorillas.

The picture is clearer, however, if we look back further into the Early and Middle Miocene, an interval from about 21 to 14 Ma, when an ape-like creature known as *Proconsul* lived in Africa—along with lots of other "apes." What exactly *Proconsul* was and how we have come to know this are the topics of *The Ape in the Tree*, the latest book by Alan Walker and Pat Shipman (paleoanthropologists now at Pennsylvania State University). The book is, somewhat oddly, written in the first person singular of Walker's voice, so I shall refer to it as his.

Walker is probably best known for having found the Nariokotome Boy, a 1.7-million-year-old specimen of *Homo erectus* (or *H. ergaster*, as the splitters have it). The discovery and significance of that remarkably complete hominid fossil from the western shores of Lake Turkana are beautifully chronicled in the authors' *Wisdom of the Bones* (*1*), which won the Rhone-Poulenc science books prize. *The Ape in the Tree* is a successor volume of sorts, presented with Shipman's well-honed flair for telling a good story. And it offers lots of good stories: from early carnivals with apes (Consul was a famous Parisian performing chimp from 1903), to early fossil hunters attacked by hippos and eaten by crocodiles, to Louis Leakey's push to find very early cultural hominids in Africa (and, less sagely, even in America, whence his endorsement of the bogus Calico Early Man site in California). We read about how the 1947 Pan-African Congress of Prehistory became a turning point in the recognition of Africa as the birthplace of humanity (as Darwin had predicted and most everyone else had later denied); about Leakey *et al.*'s expedition to Rusinga Island in Lake Victoria, where Mary Leakey in 1948 found a nearly complete *Proconsul* skull; about Louis Leakey's misfired efforts to humanize the creature; and about how a "pothole" full of fossils on Rusinga turned out to be a hollowed-out petrified tree.

***Proconsul* skull found by Mary Leakey.**

Early on in the book, we are told that "*Proconsul* is not just a human ancestor but also an ape one, the last common ancestor to whom we—humans and apes alike—all trace our past." But Walker is not particularly interested in either taxonomy or phylogeny; his focus is more on how the creature behaved, especially what it ate and how it moved. A master at using bones to elucidate behavior, Walker shows that *Proconsul* was probably a slow-moving climber rather than an agile brachiator. (In other words, it didn't swing through the trees.) Such inferences sound simple enough, but the techniques he has marshaled to make them are remarkable. With anatomist Fred Spoor, for example, Walker has been looking at the semicircular canals (of the inner ear) of different species. They find that mammals that move quickly through the forest tend to have canals with large radii of curvature, a consequence of their greater need for maintaining balance and orientation, whereas slow-moving species (such as sloths) have canals of much smaller radii. For his *Proconsul* fossils, Walker found that their radii of curvature (yes, these tiny canals sometimes fossilize) were more like those of a slow-moving howler monkey than a tree-swinging gibbon or siamang.

Walker also makes an important point about not getting trapped in the question of whether *Proconsul* was a monkey or an ape, the point being that these present-day categories may not do justice to organisms of the distant past. (How far back can one call the ancestors of today's whales "whales"?) The authors repeatedly caution against this "pull of the present": the tendency to characterize ancient creatures in terms we today find familiar. (Historians are familiar with this danger and call it "presentism.") We talk about "early apes" or "early humans" as if these were animals waiting to become something they weren't yet, when inclusion within some modern taxon may be misleading. It isn't really proper to call *Proconsul* an ape, a monkey, or even a monkey-like ape or an ape-like monkey. *Proconsul* is what it is, and our descriptors are only useful when they don't lead us down a blind path of familiarity when we should be seeing strangeness.

The Ape in the Tree is a fine account of new ways to puzzle out the behaviors of fossilized animals from odd scraps of bones. Reading it, I got the sense that maybe we should fuss a little bit less over genealogy and pay more attention to ancient landscapes, environments, climates, diets, and behaviors. And we really need to find a lot more fossils.

The reviewer is in the History Department, Stanford University, Stanford, CA 94305–2024, USA. E-mail: rproctor@stanford.edu

Reference

1. A. Walker, P. Shipman, *The Wisdom of the Bones: In Search of Human Origins* (Knopf, New York, 1996).

10.1126/science.1112101

BROWSINGS

Divine Wind. The History and Science of Hurricanes. *Kerry Emanuel*. Oxford University Press, New York, 2005. 295 pp. $40, £26.99. ISBN 0-19-514941-6.

Hurricanes and typhoons are among the most destructive of natural phenomena. Emanuel interweaves scientific, historical, and cultural perspectives on these intense tropical cyclones, spiral low-pressure systems that develop heavy rainfall and maximum sustained surface winds of at least 33 m/s. Starting with the physics of the tropical atmosphere, he describes how the cyclones develop and move; the rain, waves, and storm surge they deliver; and how they are tracked, studied, and forecast. In between these chapters, the author offers short accounts of individual hurricanes (from the 1502 blow that Columbus weathered off Hispaniola to Hurricane Andrew of 1992) and sketches of the storms' influence on history (from the disruption of the Mongol invasion of Japan in 1274 through to the possibility that global warming will increase hurricanes' impact on coastal development). Besides photographs and Doppler images, the illustrations include folk art, classic paintings, and recent works such as Suzette Barton Chandler's *Storm II The Hurricane* (right). Many of these images are used effectively to illustrate passages from poems, songs, and other literature.

CREDIT: SUZETTE BARTON CHANDLER

The Evolutionary Biology of Flies. *David K. Yeates and Brian M. Wiegmann, Eds*. Columbia University Press, New York, 2005. 439 pp. $89.50, £58. ISBN 0-231-12700-6.

For the last 250 million years, life in terrestrial environments has been accompanied by the buzz of flies. Today, dipterans comprise about 15% of described animal species and are among the most abundant arthropods. Their broad ecological diversity is supported by a wide range of adult feeding strategies and the flies' holometabolous life cycle (larvae and adults have quite different anatomies, behaviors, and niches). Much has been learned from studies of dipteran model systems (such as the fruit fly, malarial mosquitos, medfly, and housefly). This volume offers researchers and students a broad comparative and evolutionary perspective on dipteran biology. It begins with reviews of the order's phylogenetic position and the relationships among dipteran lineages. A second section covers genomics (especially *Drosophila* and *Anopheles*), evo-devo, and neural development in dipterans along with the evolutionary roles of transposable elements and sex chromosomes. The section on evolutionary ecology and biogeography includes considerations of the fossil record of dipteran-plant associations, sexual selection and mating systems, genetics of host use, molecular approaches to studying invasive species, and a guild analysis of some rainforest faunas.

CAREERS IN SCIENCE

More Women in Science

Jo Handelsman,[1,2]* Nancy Cantor,[3] Molly Carnes,[2,4] Denice Denton,[5] Eve Fine,[2] Barbara Grosz,[6] Virginia Hinshaw,[7] Cora Marrett,[8] Sue Rosser,[9] Donna Shalala,[10] Jennifer Sheridan[2]

It has been 25 years since Congress passed the Women in Science and Technology Equal Opportunity Act, which declares it "the policy of the United States that men and women have equal opportunity in education, training, and employment in scientific and technical fields (*1*)." Although there have been major advances, academic institutions are still not fully utilizing the pool of women scientists they have produced. The difference between the proportions of women who earn Ph.D.'s and those who are in faculty positions at top universities is clear in the biological and physical sciences, as well as in engineering (see table at right).

Enhanced online at www.sciencemag.org/cgi/content/full/309/5738/1190

Recently, much has been made of biological differences between men and women that might affect their representation in science. Although there is a substantive body of evidence indicating that overall intelligence does not differ between men and women, controversy persists as to whether specific aspects of cognitive ability differ (*2*, *3*). A recent debate by experts illuminates the issues and provides a summary of the literature in the field (*4*). We chose not to discuss these possible differences here for a number of reasons. First, there is no ideal constellation of cognitive abilities required to be a scientist. To be successful, scientists need deductive reasoning abilities, verbal skills, quantitative reasoning, intuition, and social skills. Men and women may differ, on average, in some of these abilities, but that is not a basis on which we can predict success because different mixtures lead to diverse, yet successful, approaches and styles in science. Second, there is no convincing evidence that women's representation in science is limited by innate ability. Between 1970 and 2003 (a time too brief for observable changes in innate ability), there was a 30-fold increase in the proportion of Ph.D.'s granted to women in engineering. This was a time in which attitudes and laws pertaining to gender changed dramatically, which provides strong evidence of the cultural and structural impediments to women. In this Policy Forum, we focus on the cultural issues that manifest in the behaviors of individuals and the policies of institutions because these factors make a difference and can be changed.

Moral and legal imperatives to ensure equal opportunity provide sufficient reasons to examine the causes of the disparities and to attempt to rectify them. Equally compelling is the impact that equity will have on the quality of our universities and the competitiveness of our nation. Heterogeneity among students, faculty, and staff strengthens universities in fundamental ways (*5*, *6*). Heterogeneous groups design more innovative solutions to problems than do homogeneous ones (*6*, *7*) and bring a higher level of critical analysis to decisions (*6*, *8*). Furthermore, institutions that welcome women foster more favorable working environments for all community members (*9*).

The National Science Foundation (NSF) founded the ADVANCE Institutional Transformation Program (*10*) to analyze the impact of interventions on advancement of women in science. Many universities have launched initiatives to enhance hiring, promotion, and productivity of women scientists, including Harvard University, which recently committed $50 million to this effort (*11*). Initial results from the NSF ADVANCE sites and other universities suggest several strategies that appear to work (*6*). Detailed documentation can be found in the supporting online material.

Barriers and Strategies to Overcome Them

The pipeline. The low number of women trained in certain fields is partially to blame for the paucity of women on the faculty. Nevertheless, many fields continue to suffer a faculty gender imbalance even though women compose from one-quarter to almost half of their graduating doctoral candidates (see table). Superb women scientists may not pursue academic careers simply because they are not encouraged to do so, question whether they have what it takes to be successful, or lack female role models who would help them envision themselves as faculty. Well-meaning advisers may interpret women's hesitation and concerns as disinclination and may fail to press their women students to consider academic careers. Explicit encouragement of outstanding doctoral candidates to enter the professoriate will help close the gap. Programs designed to prepare students to be faculty, such as those offered by many professional societies, universities, and

WOMEN Ph.D.'s AND FACULTY, TOP 50 DEPARTMENTS IN SELECTED DISCIPLINES*

Discipline	Career level (% women)			
	Ph.D.	Asst. Prof.	Assoc. Prof.	Full Prof.
Biology	45.89	30.20	24.87	14.79
Physical Science	24.68	16.13	14.18	6.36
Astronomy	22.88	20.18	15.69	9.75
Chemistry	33.42	21.47	20.50	7.62
Computer Science	15.27	10.82	14.41	8.33
Math & Statistics	26.90	19.60	13.19	4.56
Physics	14.78	11.15	9.41	5.24
Engineering	15.34	16.94	11.17	3.68
Electrical	12.13	10.86	9.84	3.85
Civil	17.90	22.26	11.50	3.52
Mechanical	10.93	15.65	8.89	3.17
Chemical	24.98	21.38	19.19	4.37

*Data on Ph.D.'s and faculty come from the same "Top 50" departments for each discipline; departments are ranked by NSF according to research expenditures in that discipline. Top 50 departments detailed at (*23*). Ph.D. data (*24*) are from 2001 to 2003; faculty data (*23*) are from 2002 except Astronomy (2004) and Chemistry (2003).

[1]Howard Hughes Medical Institute, professor, Department of Plant Pathology, University of Wisconsin–Madison; [2]Women in Science and Engineering Leadership Institute, University of Wisconsin–Madison; [3]Chancellor and president, Syracuse University; [4]Department of Medicine and Center for Women's Health Research, University of Wisconsin–Madison; [5]Chancellor, University of California, Santa Cruz; [6]Higgins Professor of Natural Sciences, Harvard University; [7]Provost and executive vice chancellor, University of California, Davis; [8]Senior vice president and deputy president, University of Wisconsin System; [9]Dean of the Ivan Allen College of Liberal Arts, Georgia Institute of Technology; [10]President, University of Miami. [For complete addresses, see the supporting online material.]

*Author for correspondence. E-mail: joh@plantpath.wisc.edu

private organizations (*6*), can provide access to role models and may inspire confidence and commitment (*12*).

To keep women moving through the pipeline to the senior ranks, they need sound advice about how best to invest their time as junior faculty. Women, more often than men, are asked to provide campus service on committees, as speakers, and as advisers to students (*13*). To assist junior faculty in managing pretenure activities, Georgia Tech ADVANCE Professor Jane Ammons developed a "speed mentoring" workshop in which junior faculty members consult for 15 to 20 minutes with each of four experienced tenure case reviewers who identify gaps and offer suggestions for strengthening the tenure case.

Climate. Many women attribute their exit from the academy to hostility from colleagues and a chilly campus climate (*14*). This atmosphere is invisible to many men, who typically describe a better climate for women than women report experiencing, as indicated by faculty surveys at MIT, Princeton, the University of Michigan, and the University of Wisconsin (*6*). Campus-wide programs to educate members of the community can identify and help eliminate discrimination in hiring and promotion, sexual harassment, and other illegal behaviors (*6*, *15*). Faculty members can assist by becoming educated about these behaviors and then taking steps to discourage them, including supporting women who voice concerns about illegal behavior.

Far more pervasive are the subtle effects of exclusion from the department community and its decision-making processes and the slights, ridicule, and attention to women's sexuality in professional settings. Although these behaviors may seem innocuous in isolation, the cumulative effect can be devastating (*6*, *16*). University administrators can set a campus standard in fostering inclusivity. Programs to train department chairs to recognize and combat the isolation experienced by women may transform local environments. The University of Michigan's ADVANCE program developed an interactive theater program that portrays typical academic situations and engages academic audiences in discussion that helps them recognize interpersonal behaviors that affect climate (*6*).

Unconscious bias. People who are committed to egalitarian principles and believe that they are not biased may nevertheless unconsciously or inadvertently behave in discriminatory ways (*6*, *17–19)*. When evaluators rated writing skills, resumes, journal articles, and career paths, they gave lower ratings on average if they were told that the subject of evaluation was a woman (*6*). A study of postdoctoral fellowships awarded by the Medical Research Council of Sweden found that women candidates needed substantially more publications to achieve the same competency rating as men (*18*). On the basis of results in other fields, it might be wise for scientists to consider ways to mask applicant gender. For example, introducing a screen to obscure the gender of musicians auditioning for symphony orchestra positions increased the likelihood that a woman was selected by 30 to 60% (*20*).

A number of interventions undertaken through the ADVANCE programs are predicated on the supposition that unconscious bias can be redressed by awareness. The University of Wisconsin–Madison has designed workshops to train search committees in good search methods and to sensitize them to bias (*6*). In these workshops, faculty members are encouraged to recruit women by deliberate action to overcome unconscious biases and to cultivate professional relationships with promising women scholars at professional meetings. Martell (*21*) showed that sex bias emerged when evaluators were under time pressure and distracted. Consequently, the search committee training includes reminding participants of the time required to conduct a thorough review and encouraging them to devote sufficient time to the evaluation of each individual to prevent assumptions from substituting for data. Georgia Tech has developed a Web-based computer instrument, Awareness of Decisions in Evaluating Promotion and Tenure (ADEPT), to aid promotion and tenure committee members, chairs, and deans to understand biases related to gender, race and/or ethnicity, disability, and interdisciplinarity. It consists of a downloadable application that contains case studies and summaries of scholarly research on bias and other materials to provoke discussion (*6*).

Balancing family and work. The responsibilities for family caretaking (for children and aging parents) continue to fall disproportionately on women (*6*). Young women can be encouraged by meeting or reading about prominent women scientists who have families and by learning about academic programs designed to reduce the conflicts between personal and professional life, including dual-career hiring programs, tenure clock extensions for childbirth and adoption, and on-campus lactation rooms and child care facilities. All members of the university community can advocate for such programs and can provide flexibility for colleagues with family responsibilities.

Conclusion

Institutional transformation necessitates collective examination of attitudes and the behaviors they spawn, which can be disquieting, because it requires engagement with issues of life-style, reproduction, hiring, and academic customs. Most uncomfortable is the discovery that we all harbor unconscious biases that can shape our behavior. Essential to the process is individual ownership of the blueprint for change. Strategies for this blueprint exist and are being tested, but systemic change can only be fostered if propelled by a vigilant and widespread campaign launched by tenacious women and men at all levels (*6*), and advocated by prominent leaders of our universities (*22*). Only such a campaign will fulfill the promise of the Science and Technology Equal Opportunities Act and will create a scientific community reflective of the pluralist society that supports it.

References and Notes

1. Bill S. 568 in the 96th Congress (http://thomas.loc.gov/).
2. American Sociological Association Council, 28 February 2005 (www.asanet.org/public/summers.html).
3. E. S. Spelke, "Sex differences in intrinsic aptitude for mathematics and science: A critical review," draft, 20 April 2005 (www.wjh.harvard.edu/~lds/sexsci/).
4. "The science of gender and science: Pinker vs. Spelke, a debate," 10 May 2005 (www.edge.org/documents/archive/edge160.html#d).
5. J. F. Milem, in *Compelling Interest: Examining the Evidence on Racial Dynamics in Colleges and Universities*, M. Chang, D. Witt, J. Jones, K. Hakuta, Eds. (Stanford Univ. Press, Stanford, CA, 2003), pp. 126–169.
6. Related resources, see http://wiseli.engr.wisc.edu/Products/MoreWomen.htm.
7. P. L. McLeod *et al.*, *Small Group Res.* **27**, 248 (1996).
8. C. J. Nemeth, *Adv. Group Process.* **2**, 57 (1985).
9. K. Miner-Rubino, L. M. Cortina, *J. Occup. Health Psychol.* **9**,107 (2004).
10. For information on ADVANCE, see www.nsf.gov/funding/pgm_summ.jsp?pims_id=5383.
11. L. H. Summers, S. E. Hyman, 16 May 2005 (www.president.harvard.edu/speeches/2005/0516_womensci.html).
12. M. F. Fox, in *Equal Rites, Unequal Outcomes: Women in American Research Universities*, L. S. Hornig, Ed. (Kluwer Academic, New York, 2003), pp. 91–109.
13. S. Park, *J. Higher Educ.* **67**, 46 (1996).
14. E. Seymour, N. Hewitt, *Talking About Leaving: Why Undergraduates Leave the Sciences* (Westview Press, Boulder, CO, 1997).
15. S.V. Rosser, *The Science Glass Ceiling: Academic Women Scientists and the Struggle to Succeed* (Routledge, New York, 2004).
16. V. Valian, *Why So Slow: Advancement of Women* (MIT Press, Boston, MA, 1999).
17. J. F. Dovidio, S. L. Gaertner, *Psychol. Sci.* **11**, 315 (2000).
18. C. Wenneras, A. Wold, *Nature* **387**, 341 (1997).
19. F. Trix, C. Psenka, *Discourse Soc.* **14**. 191 (2003).
20. C. Goldin, C. Rouse, *Am. Econ. Rev.* **90**, 715 (2000).
21. R. F. Martell, *J. Appl. Soc. Psychol.* **21**, 23 (1991).
22. J. Handelsman, J. Sheridan, E. Fine, M. Carnes, 4 April 2005 (http://wiseli.engr.wisc.edu/Products/top_10_tips.pdf).
23. D. J. Nelson, "Nelson diversity surveys" (Diversity in Science, Norman, OK, 2004) (http://cheminfo.chem.ou.edu/~djn/diversity/top50.html).
24. NSF survey of earned doctorates/doctorate records file, WebCASPAR (http://webcaspar.nsf.gov).

Supporting Online Material

www.sciencemag.org/cgi/content/full/309/5738/1190/DC1

10.1126/1113252

CHEMISTRY

X-ray Fingerprinting of Chemical Intermediates in Solution

Philip Anfinrud and Friedrich Schotte

In the early 1800s, the English scientist John Dalton postulated that matter is made up of indestructible atoms whose identities are unchanged by chemical reactions. These atoms have a definite size and mass, are countable, and through chemical reactions can combine to produce molecules as simple as diatomic oxygen (O_2), the vital component in the air we breathe, or macromolecules far more complex than myoglobin ($C_{822}H_{1035}FeN_{222}O_{220}S_3$), an oxygen-storage protein found in our muscle tissue. It is the controlled structural rearrangement of atoms and molecules that adds value to industrial chemical feedstock, and gives life to biological organisms. The selectivity of the transformation from reactant to product depends on the reaction mechanism, and the structures of intermediates along the reaction pathway are often hotly debated. Because the atoms are so small (~10^{-10} m), and the time it takes for them to slip past their neighbors is so short (~10^{-13} s), the direct observation of these intermediates has proven quite elusive. Recently, researchers working at the European Synchrotron Radiation Facility (ESRF) rose to this experimental challenge and pursued structural studies of photochemically generated, short-lived (<10^{-6} s), iodo radicals. Davidson *et al*. studied diiodomethane (*1*), whereas Ihee and coworkers studied diiodoethane (as reported on page 1223 in this issue) (*2*). In particular, Ihee *et al*. identified the structure of a radical that purportedly plays a crucial role in certain stereoselective chemical reactions.

The old adage, "seeing is believing," implies that disputes are often settled with a picture, or in the case of chemistry, with a molecular structure. Methods capable of extracting structural details at or near atomic resolution include x-ray diffraction (crystals and solutions), electron diffraction (gas phase, thin films, and surfaces), scanning tunneling microscopy (surfaces), nuclear magnetic resonance spectroscopy (solids and solutions), and microwave spectroscopy (gas phase). The diffraction methods make use of photons or particles that can be produced in pulses shorter than 10^{-12} s, and are therefore uniquely suited for structural determinations with ultrafast time resolution. This feat has generally been accomplished with the pump-probe method, where a "pump" laser triggers a reaction and a delayed "probe" pulse captures a snapshot of the transient species. In recent years, structural changes in protein crystals have been determined with ~5-ns (*3*–*5*) and 150-ps (*6*, *7*) time resolution, the structures of short-lived intermediates in the gas phase have been elucidated with 1-ps time resolution (*8*), and photothermally induced structural changes have been monitored in solid-state materials with ~120- to 600-fs time resolution (*9*, *10*) and on surfaces with 1-ps time resolution (*11*).

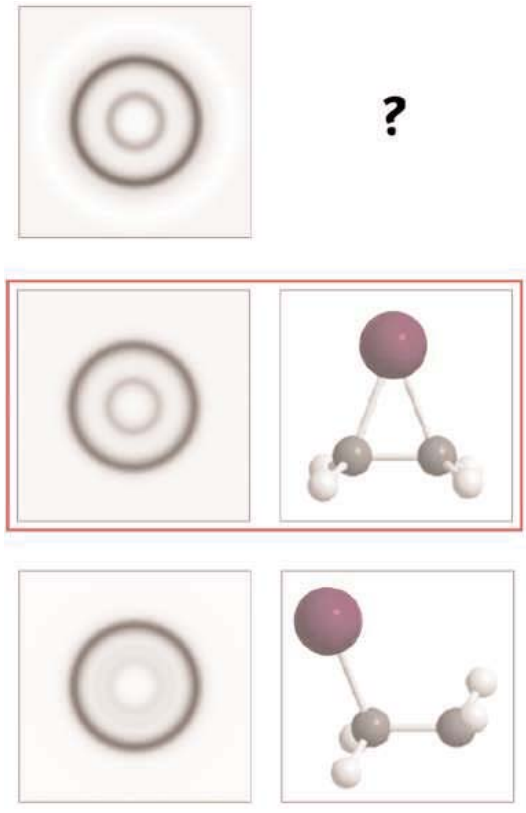

Matching fingerprints. Time-resolved x-ray diffraction can reveal changes in the pair-distribution function (histogram of interatomic distances) during the course of a chemical reaction in solution. Snapshot of $C_2H_4I_2$ in methanol taken 100 ps after photolysis (**top**). The calculated pair distribution function for the bridged C_2H_4I radical (**middle**) is a better match than that for the anti radical (**bottom**).

Notably absent from the recent literature are time-resolved structural determinations of molecules in solutions, the environment most relevant to biology and industrially important chemical synthesis. And for good reason. Reagents are typically dissolved at relatively low concentration in an ocean of solvent whose scattering is orders of magnitude stronger than that from the reagents themselves. The pump pulse deposits energy into the probed volume, and the resulting jump in the solvent temperature and pressure triggers a time-dependent change in the solvent structure and its scattering signature. The pump pulse rarely transforms 100% of the reagent to intermediates of interest, and the photoexcited sample volume contains a time-evolving mixture of several species. The scattering from the solvation shell surrounding each reacting molecule can be as strong as that from the molecule itself, and its scattering signature changes as the solvent shell adapts to the transforming molecule. Consequently, a time-resolved liquid diffraction experiment will produce a small time-dependent signal on a large time-dependent solvent background, and the weak signal of interest will generally arise from a mixture of species with overlapping features. To have any hope for success, it is crucial that the time-dependent scattering signal be recorded with very high precision. Because the signal-to-noise ratio for this type of experiment is limited by photon-counting statistics, high-precision measurements require a very high flux source. The ID09B time-resolved x-ray beamline at the ESRF, developed by Wulff *et al*. (*12*), produces a flux well suited for these experiments.

When x-ray photons pass through a liquid sample that is thin compared to its x-ray absorption depth, less than 1% of the photons are scattered. Photons scattered from atoms whose separation is narrowly defined by chemical bonding or molecular packing can interfere constructively or destructively, with the resulting scattering

The authors are in the Laboratory of Chemical Physics, National Institutes of Health, Bethesda, MD 20892–0520, USA. E-mail: anfinrud@nih.gov

pattern appearing as a set of concentric rings. The pump-induced change of the radial intensity distribution is related, through Fourier transformation, to the pair-distribution function, and provides a "fingerprint" of the characteristic interatomic distances (see the figure). The scattering data are one-dimensional, but a molecule's structure is three-dimensional. Consequently, a structure "determination" from liquid scattering data requires much help from theory. First, the solvent contribution to the scattering pattern must be accurately calculated and subtracted from the data. This procedure is far from trivial. Next, the diffraction patterns from three-dimensional models of putative intermediates must be calculated and compared with the solvent-corrected curves. Finding a match between the experimental and theoretical curves should not be confused with a structure determination in the crystallographic sense; nevertheless, a match that exhibits significantly higher fidelity than other proposed structures makes a compelling case for that structural assignment.

Ihee and co-workers chose their system wisely. When comparing the scattering patterns from bridged and anti iodoethane radicals with their solvent-subtracted scattering curves, the bridged form gave a much better match, thereby providing the most direct and compelling case for the structural assignment of this important radical intermediate. This achievement was aided by the fact that iodine atoms scatter x-rays more than 10 times as strongly as methanol, thereby enhancing the signal arising from iodo radical intermediates. Because diiodoethane ($C_2H_4I_2$) has only four heavy atoms (hydrogen scatters very weakly), scattering from it and its photo-generated intermediates is relatively easy to assign and interpret. Moreover, the iodo radical intermediate is sufficiently long-lived to be easily captured with 100-ps time-resolved snapshots. Finally, the radical is produced with relatively high quantum efficiency, so a sizable population could be generated and characterized. Although it should be possible to study molecules that lack heavy-atom substituents, such systems would require that the signal-to-noise ratio of the scattering data be improved. For example, to recover a signal that is 10 times weaker, the data integration time would have to be increased by at least that factor squared, or 100 times longer. One could envision studying more complex molecules as well; however, diffraction rings from disordered solutions are not sharply defined, so the amount of structural information that can be extracted from the radial intensity distribution is limited. Therefore, there is a molecular size beyond which it would prove increasingly difficult to correctly match the scattering pattern to a specific three-dimensional molecular structure.

When seeking a match to a "fingerprint," the correct structure must be included in the lineup. As more candidates are included, the chance for a false-positive becomes greater. As a result, one must exercise sound chemical intuition when selecting candidate structures for comparison, as was done in the study by Ihee and co-workers.

Although it has a few limitations, the technique of picosecond time-resolved liquid diffraction can provide an unprecedented glimpse into the structures of reactive intermediates involved in solution-phase chemistry. Once efforts to generate high-flux x-ray pulses on the few-picosecond (*13*) and the femtosecond (*14*–*16*) time scales are realized, the time resolution of liquid diffraction studies could be extended to the so-called chemical time scale, where a wealth of new insights into chemical reaction pathways awaits discovery.

References and Notes

1. J. Davidsson *et al.*, *Phys. Rev. Lett.* **94**, 245503 (2005).
2. H. Ihee *et al.*, *Science* **309**, 1223 (2005); published online 14 July 2005 (10.1126/science.1114782).
3. V. Srajer *et al.*, *Science* **274**, 1726 (1996).
4. M. Brunori, D. Bourgeois, B. Vallone, *J. Struct. Biol.* **147**, 223 (2004).
5. H. Ihee *et al.*, *Proc. Natl. Acad. Sci. U.S.A.* **102**, 7145 (2005).
6. F. Schotte *et al.*, *Science* **300**, 1944 (2003).
7. F. Schotte, J. Soman, J. S. Olson, M. Wulff, P. A. Anfinrud, *J. Struct. Biol.* **147**, 235 (2004).
8. H. Ihee *et al.*, *Science* **291**, 458 (2001).
9. A. Rousse *et al.*, *Nature* **410**, 65 (2001).
10. B. J. Siwick, J. R. Dwyer, R. E. Jordan, R. J. Miller, *Science* **302**, 1382 (2003).
11. S. Chen, M. T. Seidel, A. H. Zewail, *Proc. Natl. Acad. Sci. U.S.A.* **102**, 8854 (2005).
12. M. Wulff *et al.*, *Faraday Discuss.* **122**, 13 (2003).
13. K.-J. Kim, D. M. Mills, "Workshop Generation and Use of Short X-ray Pulses at APS" (Advanced Photon Source, Argonne National Laboratory, 2005); www.aps.anl.gov/News/Conferences/2005/Generation_and_Use_of_Short_Xray_Pulses.
14. T. Åberg *et al.*, in *Conceptual Design Report of a 500 GeV e+e- Linear Collider with Integrated X-ray Laser Facility*, G. Materlik, Ed. (DESY, Hamburg, 1997).
15. M. Cornacchia *et al.*, "Linac Coherent Light Source (LCLS) Design Study Report," *Tech. Rep. No. SLAC-R-512* (Stanford Linear Accelerator Center, Stanford University, CA, 1998).
16. A. Cho, *Science* **296**, 1008 (2002).

17. Supported by the Intramural Research Program of the NIH, NIDDK.

10.1126/science.1117325

EVOLUTION

Is Invariance Across Animal Species Just an Illusion?

Gerdien de Jong

There is obvious variation in the way different animals live their lives—in their life span, in their age and size at maturity, and in their size as full-grown adults, to name a few attributes. But are there fundamental similarities in the life history strategies that different animals use? Charnov (*1*) argued that there are: He proposed fundamental similarities—"life history invariants"—to be a major explanatory ingredient of life history evolution. Life history invariants generalize a life history model over species boundaries and over a wide range of animal sizes, leading to an understanding of universal life history strategies. On page 1236 of this issue, Nee *et al.* (*2*) call into question the principal method to detect life history invariants. The authors have determined that the approach is misleading, throwing the very existence of the concept into doubt.

Life history invariants are dimensionless ratios of two life history traits—for instance, age at maturity and average length of life. Such a ratio is used to answer questions such as "At what relative age do animals first reproduce?" Whether we talk about rabbits or whales, we hope the ratio will enable us to forget about differences in life span, size, environment, and taxonomy. Thus, life history invariants point to common properties of organisms not immediately clear from direct observation. As such, they are potentially very useful for understanding and modeling life history evolution: The models are meant to be general, doing away with the need to model each species separately. The existence of life history invariants is a major argument for one general theory of life history evolution, rather than a theory as a set of recipes for how to make species-specific models.

Life history invariants are canonically identified from a log-log plot of two life history traits involved in a dimensionless ratio. In such a plot, the slope is expected to equal 1. Consider two life history traits, a and b, and ask whether their dimensionless ratio a/b is a life history invariant. If their ratio is constant (c), a log-log plot with $\ln(b)$ on the x axis and $\ln(a)$ on the y axis

The author is in the Evolutionary Population Biology Group, Utrecht University, Padualaan 8, NL-3584 CH Utrecht, Netherlands. E-mail: g.dejong@bio.uu.nl

would show points on a line defined by $\ln(a) = \ln(c) + \ln(b)$, with a slope of 1 and intercept $\ln(c)$ (see the top figure). The line is the regression line and the intercept can be used to estimate the life history invariant, c. A log-log plot of two traits involved in a life history invariant leads to a slope of 1 with all variation in the dependent variable on the y axis explained by the variable on the x axis (that is, $R^2 = 1$ for an ideal invariant where R^2 of the regression is the proportion of the variation in the dependent variable a explained by the variation in the independent variable b). An empirically determined slope of 1 at high explained variance R^2 has therefore been taken to indicate a life history invariant. This is common experimental logic, but treacherous, as it disregards the potential existence of other ways to arrive at the predicted slope of 1 and very high R^2. If a life history invariant is the only way to arrive at a slope of 1 and very high R^2, then one can conclude from an empirical slope of 1 and very high R^2 that a life history invariant exists.

Many such log-log plots of traits that indicate potential life history invariants exist. Allsop and West (*3*) presented data on relative body size at sex change for animals ranging from a 2-mm shrimp to a 1.5-m fish. The log-log plot of body size at sex change versus maximum body size showed a slope of 1.05, and all the points were near the regression line, with $R^2 = 0.98$. The life invariant "relative body size at sex change" was perfectly present.

Buston *et al.* (*4*) then threw a spanner in the works. Commenting on Allsop and West's data, Buston *et al.* pointed out that random distributions of both total body size and size at sex change lead to identical properties in a log-log plot as a life history

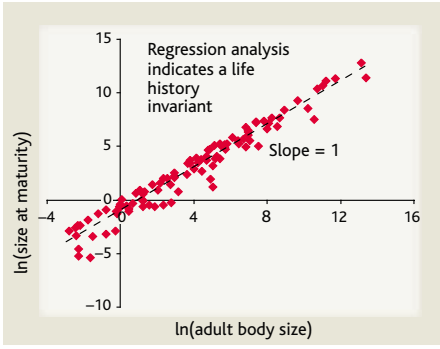

What log-log plots reveal about life histories. The log-log plot shows a life history invariant. Size at maturity seems a constant fraction of adult size for all animals over a body size range from 6×10^{-2} to 6×10^{5}. The slope equals 1.01 and R^2 equals 0.95. The life history invariant estimated would equal 0.34. The plot has been generated from values that were randomly produced according to Nee *et al.* (*2*), indicating the misleading nature of regression analysis.

invariant: a slope of 1 and an R^2 of >0.95. More null models followed (*5*, *6*), using different random distributions of traits. But Nee *et al.* (*2*) describe the general rationale of how slopes of 1 at high R^2 arise in log-log plots, independent of the distributions of the traits. The culprit is a variable on the y axis that is a fraction of the x-variable: The plot is of $y = cx$, with $c < 1$. In a log-log plot of cx versus x, a slope of 1 follows automatically. A wide range on the x axis—from rabbit to whale—guarantees a high R^2. The evidence for life history invariants vanishes as the method of finding them evaporates.

Suppose full-grown body size is plotted on the x axis, and size at maturity of the same individual on the y axis [see the bottom figure; (*4*)]. Size at maturity might be any fraction of full-grown body size, with fractions $c = 0.1, 0.2, \ldots, 0.9$ in nine different groups of animals. Each animal group has its own relative size at maturity. Relative size at maturity is invariant within each group but varies among groups. All possible combinations of full-grown body size and size at maturity can be found over the nine groups. When data from multiple animal groups are plotted directly, the variance among them is quite apparent. The same data can be depicted in a log-log plot for the total range of body sizes, still distinguishing each animal group. Each group now has its own line $\ln(y) = \ln(c) + \ln(x)$, all with a slope of 1 but each with different intercepts $\ln(c)$, again revealing variation between animal groups. However, if the same data are again depicted on a log-log plot, but without differentiation as to which animal group the data points belong, a single regression line can be drawn over all groups together that now seems to indicate a life history invariant ratio of body size at maturity to full-grown body size over all groups. The regression analysis is therefore misleading.

If life history invariants are important in evolution, we expect them to surface in models that use their component variables. That would validate the idea of invariants, especially if a model restricts them to certain values. Kozlowski (*7*) modeled growth in animals and optimal body size. In his model and simulation, many life history variables that partake in life history invariants can be evaluated. The slopes in log-log plots of model values are 1 for the proposed life history invariants. Yet very much variation in the simulated traits and their ratios exists, and direct observation of the values will not give the impression of life history invariants. Kozlowski (*7*) concluded that "Charnov's life history invariants can be

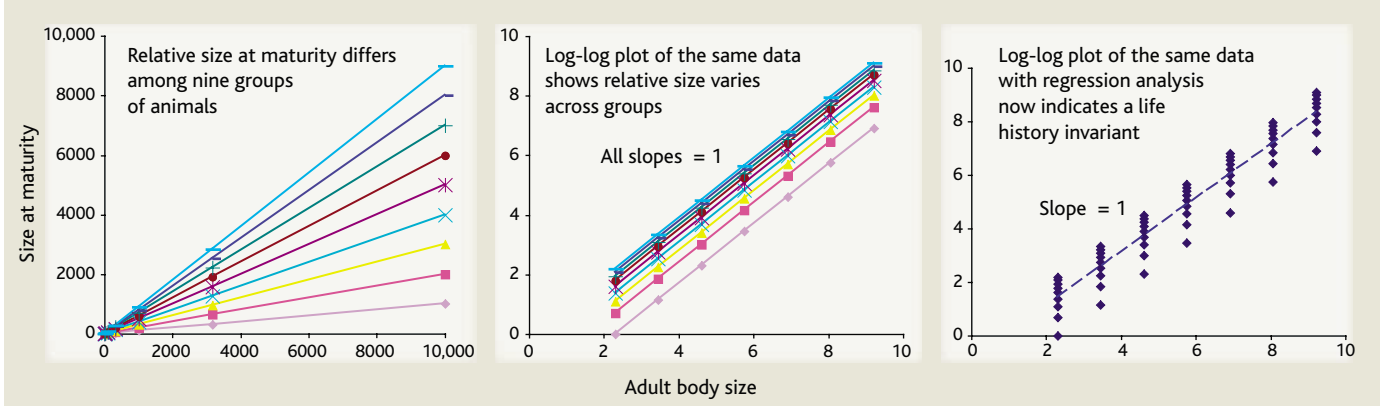

A mirage of invariance. Consider nine groups of animals that differ in whether they mature at large or small size. In group 1, size at maturity equals one-tenth of adult body size; in group 2, size at maturity equals two-tenths of adult body size, and so on. [Adapted from (*4*)] **(Left)** Size at maturity is plotted as a function of body size for the nine groups and for seven body sizes: 10, $10\sqrt{10}$, 100, $100\sqrt{10}$, 1000, $1000\sqrt{10}$, and 10,000. The lines give $y = cx$ for nine values of c ($c = 0.1, 0.2, \ldots, 0.9$). **(Middle)** The same data are plotted on a log-log plot. The lines are now $\ln(y) = \ln(c) + \ln(x)$, and all lines show a slope of 1 but possess different intercepts. Within each group, the relative size at maturity is invariant, but not across groups. **(Right)** A log-log plot of the same data but without assignment to different animal groups reveals a regression line with a slope of 1, an intercept of –0.88, a high R^2 of 0.92, and a life history invariant of 0.42. The estimated "life history invariant" is actually a complicated way of averaging all nine values for c. Any conclusion that a life history invariant exists is spurious.

called invariants only in the sense that the regression lines between their components have slopes close to +1 or –1."

Life history evolution is not the only field where invariants or universal constants are proposed. The Universal Temperature Dependence of metabolism proposal asserts that the metabolism of all organisms can be described by a single equation (*8*). Scaling laws (as, for instance, basic metabolic rate scale as mass to the power $^3/_4$) are called universal over all life (*9*, *10*). This hankering for universal explanations has been criticized not only on technical grounds (*11*) but also for ignoring biology and the variation between organisms (*12*). Interesting biology might not be in life history invariants but in biological variation.

Consider again the issue of relative body size at sex change. Allsop and West (*3*) collected data on this question and interpreted their log-log plot as showing a life history invariant indicating that a fundamental similarity exists among all animals in the fitness components leading to sex change. However, looking at specific cases of sex change does not strengthen that impression. In both the clown fish and the bluebanded goby, an individual's sex is determined by its rank in the social hierarchy. Among clown fish, the largest fish of the group is female, the second largest fish is male, and lower ranking group members are queuing for their turn to reproduce (*13*). Among bluebanded gobies, the fish at the top of the hierarchy is male and below him are several breeding females; the group has no nonbreeding adults (*14*). In both fish species, the second ranking member in the hierarchy changes sex and starts growing in size when the top brass exits (*13*, *14*). The interesting biology is to identify what determines differences such as those between these two fish species.

This brings us back to species-specific life histories and back to looking at biological mechanisms. If a fundamental similarity does exist among all animals in the fitness components leading to sex change, it has to be shown that relative body size at sex change for both the clown fish and the bluebanded goby can be directly described by similar fitness relations. The model of optimal relative body size at sex change (*15*) must be shown to work by direct estimation of its parameters for both fish species, not by log-log plot.

We should be wary of treating an average across species as an explanatory general life history invariant. That's not to say that we might not keep searching for invariants that indicate fundamental similarities in the biology of all living organisms. We just need to know for certain how to identify them.

References

1. E. L. Charnov, *Life History Invariants: Some Explorations of Symmetry in Evolutionary Ecology* (Oxford Univ. Press, Oxford, 1993).
2. S. Nee, N. Colegrave, S. A. West, A. Grafen, *Science* **309**, 1236 (2005).
3. D. J. Allsop, S. A. West, *Nature* **425**, 783 (2003).
4. P. M. Buston, P. L. Munday, R. R. Warner, *Nature* **428**, 10.1038/nature02512 (2004).
5. A. Gardner, D. J. Allsop, E. L. Charnov, S. A. West, *Am. Nat.* **165**, 551 (2005).
6. R. Cipriani, R. Collin, *J. Evol. Biol.*, 10.1111/j.1420-09101.2005.00949.x (2005).
7. J. Kozlowski, *Proc. R. Soc. London Ser. B* **263**, 559 (1996).
8. J. F. Gillooly, J. H. Brown, G. B. West, V. M. Savage, E. L. Charnov, *Science* **293**, 2248 (2001).
9. G. B. West, W. H. Woodruff, J. H. Brown, *Proc. Natl. Acad. Sci. U.S.A.* **99**, 2473 (2002).
10. G. B. West, J. H. Brown, *Phys. Today* **57**, 36 (September 2004).
11. J. Kozlowski, M. Konarzewski, *Funct. Ecol.* **18**, 283 (2004).
12. A. Clarke, *Funct. Ecol.* **18**, 252 (2004).
13. P. Buston, *Nature* **424**, 145 (2003).
14. E. W. Rodgers, S. Drane, M. S. Grober, *Biol. Bull.* **208**, 120 (2005).
15. E. L. Charnov, U. Skuladottir, *Evol. Ecol. Res.* **2**, 1067 (2000).

10.1126/science.1117591

CHEMISTRY

Geometric Phase in Chemical Reactions

David C. Clary

Quantum mechanical effects such as tunneling through a classically impenetrable potential energy barrier have long been known to occur in chemical reactions (*1*). More subtle quantum effects can also arise for reactions in which two different electronic states touch (that is, coincide in energy) to produce a conical intersection (see the figure). An example is the geometric or Berry phase, which refers to a change in sign of an electronic wave function when nuclei of atoms involved in the reaction complete an odd number of loops around the conical intersection (*2*–*4*). The effect of the geometric phase on the energy levels of bound-state molecules is well understood (*5*). However, the conditions under which the geometric phase effect can be detected for chemical reactions are less certain. Studies of this effect have largely been directed at the simplest chemical reaction, $H + H_2 \rightarrow H_2 + H$, which serves as the benchmark for definitive experimental and theoretical studies of reaction dynamics. On page 1227 of this issue, Juanes-Marcos *et al*. (*6*) provide a novel topological argument to show when the geometric phase is likely to be observable in this hydrogen exchange reaction and also clarify the findings of previous calculations.

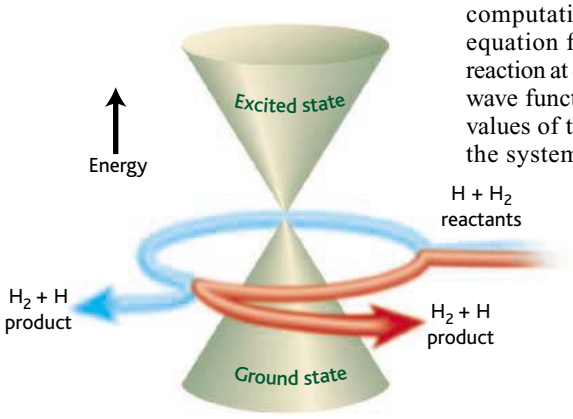

Chemical topology. Conical intersection shown in plot of energy versus two reaction coordinate dimensions with direct (red) and looping (blue) reaction paths. The cones correspond to the upper excited-state and lower ground-state potential energy surfaces.

To understand chemical reactions, theorists solve the Schrödinger equation for the electrons to calculate potential energy surfaces on which the nuclei move. These surfaces are then used in quantum dynamical computations that solve the Schrödinger equation for the nuclei taking part in the reaction at different energies (*7*). The nuclear wave functions are calculated for different values of the total angular momentum J of the system of three hydrogen atoms, and these partial wave functions are summed to produce quantities that can be observed in molecular beam experiments such as the angular distributions of the $H_2 + H$ products. These quantum dynamical calculations can be done with time-independent or time-dependent theory. One set of time-independent quantum dynamical calculations on an accurate potential energy surface suggested that the geometric phase effect might be

The author is in the Department of Physical and Theoretical Chemistry, University of Oxford, South Parks Road, Oxford OX1 3QZ, UK. E-mail: david.clary@chem.ox.ac.uk

observable in molecular beam experiments of angular distributions for this reaction at energies well below that of the conical intersection (*8*). However, other calculations that did not account for the geometric phase gave good agreement with measured angular distributions for this reaction at the same collision energies, which suggests that the effect would not be detectable at these energies (*9*).

More recent time-independent quantum mechanical calculations by Kendrick (*10*) gave an intriguing result: Geometric phase effects did occur for individual J values, but the numerical results for odd and even J canceled out when computing the angular distributions at collisional energies below that of the conical intersection. Therefore, no overall geometric phase effect was predicted in the observable quantities for these energies. The result also held for isotopic substitution of the hydrogen atoms by deuterium atoms in the reaction. These findings were confirmed in calculations that used a time-dependent quantum dynamical theory of Althorpe (*11*). The agreement of these two sets of results is important because they were obtained using two totally different scattering theories.

An explanation was needed, however, as to why the effect of the geometric phase for scattering solutions of odd and even J cancels out at the energies considered. These solutions are obtained from highly complex and computationally time-consuming numerical calculations of the nuclear Schrödinger equation that do not provide a simple physical picture for the even-odd cancellation. The paper by Juanes-Marcos *et al*. provides this explanation.

Juanes-Marcos *et al*. exploit the seemingly abstract mathematical mapping of a pair of connected Möbius strips onto a double cylinder. This topological trick enables them to show that the nuclear wave function around a conical intersection separates into even and odd components with a sign that depends on the geometric phase. As shown in the figure, there are two possible paths to form $H_2 + H$ products. For energies below the conical intersection, most reaction paths pass through just one transition state that corresponds to the even or "direct" component. A very small proportion of reactions paths can also pass through two transition states, and these correspond to the odd or "loop" components. These odd and even components can quantum-mechanically interfere.

To understand why there is a cancellation of even and odd J solutions to the scattering problem, Juanes-Marcos *et al*. examine the direct and loop scattering amplitudes of the angular-dependent components of the scattering wave function at large values of the H_2-H separations. The scattering amplitudes for low J contribute mainly to angular distributions in which the reaction products are scattered backward with respect to the $H + H_2$ direction of approach, and the amplitudes for high J contribute to angular distributions largely in the sideways direction. Classical trajectory calculations show that, for low J, the direct paths scatter mainly in the backward region, whereas the looping paths are concentrated in the forward region. Thus, the direct and looping scattering amplitudes do not interfere in this case. This explains why, for smaller values of J, no geometric phase effect is observed when summing the squares of the scattering amplitudes over even and odd values of J. For larger values of J the analysis is more involved, as the direct and looping components do interfere. However, by making use of a theory of angular distributions developed by Connor and co-workers (*12*), it is possible to explain why the even and odd J solutions cancel in this case also.

One of the findings of Juanes-Marcos *et al*. is that the interference between the direct and looping reaction paths should become more pronounced at collision energies close to the conical intersection, leading to an observable geometric phase effect. This is also found in the quantum dynamical calculations (*11*). The effect of the upper excited electronic surface could also become important at these energies. It would be of interest to compare measurements of the angular distribution in this energy region with the calculations obtained with and without consideration of the geometric phase. The group of Zare has compared their measurements with calculations on this benchmark reaction (*13*), and groups so equipped might be able to perform such experiments at the required collision energies. It is noteworthy that the findings are general and will be applicable to many other chemical reactions beyond $H + H_2$ when conical intersections occur (*14*).

References

1. R. P. Bell, *The Tunnel Effect in Chemistry* (Chapman & Hall, New York, 1980).
2. G. Herzberg, H. C. Longuet-Higgins, *Discuss. Faraday Soc.* **35**, 77 (1963).
3. C. A. Mead, D. G. Truhlar, *J. Chem. Phys.* **70**, 2284 (1979).
4. M. V. Berry, *Proc. R. Soc. London Ser. A* **392**, 45 (1984).
5. B. E. Applegate, T. A. Barckholtz, T. A. Miller, *Chem. Soc. Rev.* **32**, 38 (2003).
6. J. C. Juanes-Marcos, S. C. Althorpe, E. Wrede, *Science* **309**, 1227 (2005).
7. S. C. Althorpe, D. C. Clary, *Annu. Rev. Phys. Chem.* **54**, 493 (2003).
8. B. Lepetit, A. Kuppermann, *Chem. Phys. Lett.* **166**, 581 (1990).
9. E. Wrede *et al.*, *J. Chem. Phys.* **110**, 9971 (1999).
10. B. K. Kendrick, *J. Phys. Chem. A* **107**, 6739 (2003).
11. J. C. Juanes-Marcos, S. C. Althorpe, *J. Chem. Phys.* **122**, 204324 (2005).
12. A. J. Dobbyn, P. McCabe, J. N. L. Connor, J. F. Castillo, *Phys. Chem. Chem. Phys.* **1**, 1115 (1999).
13. S. C. Althorpe *et al.*, *Nature* **416**, 67 (2002).
14. L. J. Butler, *Annu. Rev. Phys. Chem.* **49**, 125 (1998).

10.1126/science.1117201

PHYSIOLOGY

Biological Clocks Coordinately Keep Life on Time

Martha U. Gillette and Terrence J. Sejnowski

Eating, sleeping, seasonal migration, cell proliferation—a few examples of the many behaviors and life processes that are driven by biological clocks. These "chronometers" coordinate the passage of time with orchestrated cycles that extend from molecular through cellular and systems levels. Timekeeping is part of the very fabric of life, and the clocks that regulate life processes do so over a broad range of time scales: from millisecond oscillations of neuronal activity to seasonal changes that mark shifts in the relative amount of daylight over the course of a year. These timekeeping mechanisms have traditionally been studied in isolation. But a new era in chronobiology is emerging as unexpected interactions among these clocks are discovered, raising interesting questions about why life processes are organized in this way *(1)*.

One of the most studied biological clocks at the genetic, cellular, and molecular levels is that which regulates the dynamic process of eukaryotic cell division (mitosis). Cells of different types and/or sizes spend different amounts of time in different parts of the cell cycle. We know that control of cell cycle progression requires that key proteins, the cyclins, undergo post-translational modifications, including phosphorylation, proteolysis, and spatial targeting. The cell assesses successful completion of critical events at "check points," when decisions are made whether to pro-

M. U. Gillette is in the Department of Cell and Developmental Biology and the Neuroscience Program, University of Illinois, Urbana-Champaign, IL 61801, USA. T. J. Sejnowski is in the Howard Hughes Medical Institute, Salk Institute for Biological Studies, La Jolla, CA 92037, USA and Department of Biology, University of California, San Diego, La Jolla, CA 92093, USA. E-mail: terry@salk.edu

ceed. Is this timing mechanism influenced by other cellular timekeepers? For example, yeast cells oscillate between a reductive and oxidative phase of metabolism and interestingly, yeast cell replication is restricted to the reductive phase of this metabolic cycle. Is this just a coincidence or are the cell division and metabolic cycles meaningfully linked? Because similarly linked metabolic and mitotic oscillations have been observed in high-density cultures of human cells, a functionally relevant interface between these two clocks may be a general feature. The cell division cycle has been modeled as a relaxation oscillator of embedded negative-feedback loops involving the cyclins (*2*), based on studies of budding yeast (*3*). Coupling of this model with metabolic models could reveal how these clocks are coordinated.

Interestingly, yeast undergo a genome-wide, high-frequency (~40 min) oscillation in transcription that is synchronized with respiration (*4*). Transcripts encoding proteins that are necessary for reductive versus respiratory (oxidative) functions are made at opposite points in the ensuing metabolic cycles. Dividing cells may have become tuned to metabolic oscillations in ways that permit unwinding of the DNA during cell division to take place during the reductive metabolic phase in order to maximize faithful replication.

Cycles of cell division and metabolism also appear coordinated with the circadian pacemaker, which has been well studied at the cellular and genetic levels (*5*). The circadian clock is an innate timekeeping mechanism that governs a rhythmic activity cycle, based on (roughly) 24-hour intervals, that is exhibited by many organisms. Like the cell cycle, the cell-based circadian clock is governed by a control point (*6*), where a decision is made whether to proceed with the circadian cycle. And, like the cell cycle, the check point appears to involve posttranslational modification of a clock element. The circadian clock in mammals is primarily located in a region of the brain called the suprachiasmatic nucleus (SCN). Many circadian clock genes encode proteins that are transcription factors—for example, BMAL, PERIOD, CRYPTOCHROME, and CLOCK—that regulate their own transcription. Transcriptional-translational and posttranslational regulation of core circadian clock genes forms feedback loops that generate circadian time (*5*).

Null mutation of the mouse circadian *Period* clock genes, m*Per1* and m*Per2* disrupts circadian rhythms of behavior (*7*). Because these animals also displayed abnormal regulation of cell proliferation with increased hyperplasias, a link between the cell cycle and circadian clocks was proposed. Moreover, mice lacking m*Per2* express altered levels of cell cycle regulators such as c-Myc. The BMAL-CLOCK heterodimeric transcriptional complex of the circadian clock also directly controls the expression of WEE1, a regulator of the mammalian cell cycle (*8*). Microarray analysis of m*Per1, 2*-null mice for changes in other clock-controlled genes identified *Alas1*, which encodes a rate-limiting enzyme for mitochondrial heme biosynthesis (*9*). Interestingly, PER2 has a region called the PAS domain that binds to heme. Furthermore, treatment of cultured mammalian cells with heme synchronizes circadian clock gene expression. Hence, key regulators of cell division, circadian timekeeping, and metabolic state appear coupled, suggesting that these three cycles may interact such that the state of one system can alter regulators in another (see the figure).

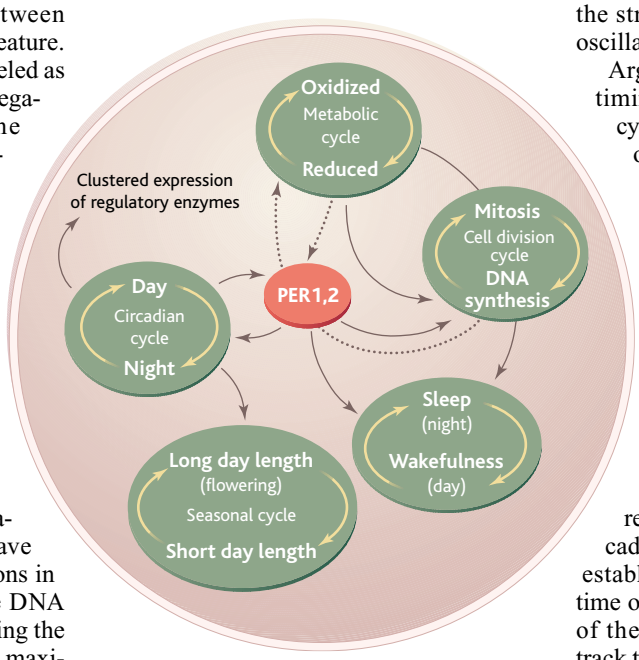

How timekeepers interact with each other. The cell division cycle takes place during the reduced phase of the metabolic cycle (in yeast). The circadian clock regulates cell division cycle, metabolism, and restorative sleep through the transcription factors PER1 and PER2. The length of the day within the circadian cycle controls seasonal changes in plants, such as flowering.

A recent dramatic revelation about the circadian cycle links it directly to the metabolic cycle (*10*). Surprisingly, the transcriptional regulators of the circadian pacemaker control clusters of genes that encode rate-limiting enzymes in intermediary metabolism (*11*). Those clock proteins with PAS domains are regulated, in turn, by metabolites that oscillate over the circadian cycle. Clustered gene expression is observed during the metabolic cycle of yeast, and this regulatory logic can be extended to mammalian metabolic cycles. Metabolic cycles can regulate circadian cycles through sensors such as embedded heme moieties in clock proteins, suggesting that lessons learned regarding temporal clustering of gene expression in yeast may be fundamental and provide insights into the structures of circadian and metabolic oscillatory processes (*10*, *11*).

Arguably the most familiar oscillatory timing system in organisms is the daily cycle of sleep and wakefulness. Studies of human sleep, performance, and quantitative electroencephalograms indicate that the sleep-wake cycle is regulated by dual brain mechanisms (*12*). The "two-process model" of sleep regulation integrates (i) the drive to sleep, called sleep homeostasis, that increases with time awake and is restorative during rest, and (ii) the circadian process that is regulated by the ~24-hour clock in the SCN and organizes sleep and wakefulness with respect to night and day. Whereas circadian clock genes in the SCN have well-established roles in determining internal time of day, in other brain areas expression of these core clock elements appears to track time spent awake and allow for adaptability of sleep when food is restricted (*13*). Sleep homeostasis is linked directly to loss and restoration of the brain's energy stores. These findings raise the possibility that circadian clock genes may play an important, unanticipated role, interfacing with cellular metabolism in neurons that contribute to sleep homeostasis.

The sleep-wake cycle also controls a cascade of oscillatory electrical activity in the brain. These neural oscillations take place on time scales ranging from seconds for slow oscillations and brain rhythms to hours for the regulation of slow wave sleep and rapid eye movement sleep. Traditionally, neuroscientists view sleep oscillations through the lens of electrical recordings, but growing evidence suggests that gene regulation is involved. The low-threshold calcium currents that are activated during sleep oscillations allow a massive influx of calcium ions into the dendrites of cortical neurons of the brain. These calcium fluxes may prepare the way for changes in gene regulation and remodeling of dendrites and synapses during the subsequent phase of slow wave sleep (*14*). The relationship of these calcium fluxes to cellular metabolism and clock gene function is unexplored.

Biological systems must adapt on even longer time scales. Seasonal variations in light and nutritional environments regulate cyclic processes in cells that affect behavioral and developmental change. Cyanobacteria, obligate phototrophs that produce 40% of the oxygen in Earth's atmosphere, exhibit a mitotic rate that depends on light intensity. Organisms in which the period of circadian rhythm matches the period of the environmental light-dark cycle are most nutritionally competitive and less exposed to light stress. Light intensity may determine the state of their redox pool within the metabolic cycle, altering circadian clock elements and global transcription (*15*).

Additional evidence for pleiotropy in circadian clock function and time scale of action is emerging in the responsiveness of the plant *Arabodopsis thaliana* to light signals, leaf movement, and regulation of flowering time. Induction of flowering is a developmental change that does not occur daily, but rather annually, when the photoperiod lengthens (*16*). Transition from producing leaf-after-leaf to stalk-borne flowers occurs within the shoot meristem upon temporal coincidence between duration of day length and the circadian clock. The clock controls timing of the expression and the turnover of a key clock transcription factor called timing of chlorophyll a/b binding protein (TOC), which is a clock-controlled factor. During long days, the circadian pattern of TOC protein expression in the meristem moves into daytime, when it can interact with FT, a flowering transcription factor, to induce homoeotic genes that pattern flower formation (see the figure). Remarkably, these findings at the molecular level support Bünning's 1936 "coincidence model" of photoperiodism for how circadian timing controls photoperiodic timing.

Biological oscillations likely emerged from the earliest cyclic life processes on Earth—those of opposing metabolic states imposed by the presence versus absence of solar energy and light-induced stress. Reciprocal regulation of the circadian clock mechanism and the metabolic cycle would ensure that these cycles, and interfacing cell division, mesh in alignment with the external cycle of light and darkness. As organisms evolved and became more complex, physiological and developmental systems also became organized around the day and night cycle, and may have incorporated elements of the ancestral cycles in new ways for their regulation. A consequence of these insights is that the separate computational models that have been developed for each of these biological clocks will need to be integrated.

It is time to focus on the interrelationships between the many cyclical processes in organisms and how they interact across a wide range of temporal and spatial scales. While keeping watch over life's diverse cyclic processes, nature's clocks are not oscillating in isolation.

References and Notes

1. National Academies Keck Futute Initiatives Workshop on Computational Chronobiology, Irvine, CA, 6 to 8 January 2005; http://www.7.nationalacademies.org/keck/compcronobio.html.
2. J. C. Leloup, A. Goldbeter, *J. Theor. Biol.* **230**, 541 (2004).
3. F. R. Cross, V. Archambault, M. Miller, M. Klovstad, *Mol. Biol. Cell* **13**, 52 (2002).
4. R. R. Klevecz, J. Bolen, G. Forrest, D. B. Murray, *Proc. Natl. Acad. Sci. U.S.A.* **101**, 1200 (2004).
5. P. L. Lowrey, J. S. Takahashi, *Annu. Rev. Genomics Hum. Genet.* **5**, 407 (2004).
6. S. A. Tischkau *et al.*, *Neuron* **43**, 539 (2004).
7. B. Zheng *et al.*, *Cell* **105**, 683 (2001).
8. T. Matsuo *et al. Science* **302**, 255 (2003).
9. K. Kaasik, C. C. Lee, *Nature* **430**, 467 (2004).
10. J. Rutter, M. Reick, S. L. McKnight, *Annu. Rev. Biochem.* **71**, 307 (2002).
11. M. Reick, J. A. Garcia, C. Dudley, S. L. McKnight, *Science* **293**, 506 (2001).
12. D. J. Dijk, W. Larkin, *Aviat. Space Environ. Med.* **75**, A119 (2004).
13. C. A. Dudley *et al.*, *Science* **301**, 379 (2003).
14. A. Destexhe, T. J. Sejnowski, *Physiol. Rev.* **83**, 1401 (2003).
15. N. B. Ivleva, M. R. Bramlett, P. A. Lindahl, S. S. Golden, *EMBO J.* **24**, 1202 (2005).
16. S. Panda, J. B. Hogenesch, S. A. Kay, *Novartis Found. Symp.* **253**, 73 (2003).

10.1126/science.1111420

PHYSICS

Freezing and Melting: Action at Grain Boundaries

Peter N. Pusey

We all have experience with liquids that freeze and melt. Yet the detailed mechanisms underlying this apparently simple phase transition are still not fully understood. Experiments on simple liquids such as argon or water are difficult because the molecules are small and move rapidly. A more successful approach examines the freezing and melting of a colloid, which can be followed directly by video light microscopy (*1*); micrometer-sized Brownian particles suspended in a liquid typically join or leave a colloidal crystal in about 1 second. Furthermore, colloidal particles that interact through a steep repulsive potential mimic the theorists' ideal of an assembly of hard spheres, the simplest system to show a freezing/melting transition. On page 1207 of this issue, Alsayed *et al.* (*2*) describe the melting of colloidal crystals of thermosensitive gel particles that interact almost as if they were hard spheres. Through beautiful video images, they provide what is probably the clearest direct evidence to date that the process of melting starts by "premelting" at defects such as vacancies, dislocations, and particularly grain boundaries.

The freezing transition of hard spheres was discovered by computer simulation in 1957 (*3*) and confirmed some 30 years later by experiments on colloidal suspensions (*4*). The transition is driven by entropy—paradoxically, the apparently ordered crystal has a higher entropy than the metastable fluid from which it grows, for example (*5*, *6*)—and is controlled by just one variable, the concentration by volume, or volume fraction, of the particles in the suspension. As the concentration is increased, spheres in the fluid become increasingly crowded by their neighbors. By crystallizing, they gain more freedom for local motions: While ordered on the large scale, a crystal is locally disordered. Above the melting concentration (volume fraction 0.545) the entropy loss associated with large-scale ordering is more than offset by the entropy gain associated with increased local freedom.

Studying the melting of hard spheres is difficult because the volume fraction of rigid colloidal particles cannot be changed continuously in a single sample: Both the number of particles and their size are fixed. Alsayed *et al.* cleverly overcome this difficulty by using colloidal particles whose size, and therefore volume fraction, changes with temperature. The particles are spherical "droplets" of a temperature-sensitive, cross-linked polymer gel. Suspended in water, these microgel droplets are themselves mostly water, containing only a few percent polymer. On heating, the polymer becomes less soluble, and the particles expel water and shrink. A small increase in temperature, from 25° to 30°C, causes the volume fraction of the suspension to decrease by almost 50%, while the interaction between the particles remains steeply repulsive.

Although a number of researchers have studied the phase behavior and flow properties of suspensions of these temperature-sensitive microgels, for example (*7*) (see the first figure, lower left), Alsayed *et al.* are the first to exploit the temperature dependence of the volume fraction for a detailed study of melting. They monitored the positions of the

The author is in the Scottish Universities Physics Alliance (SUPA), School of Physics, University of Edinburgh, Mayfield Road, Edinburgh EH9 3JZ, UK. E-mail: p.n.pusey@ed.ac.uk

particles by video microscopy and measured the excursions (in Brownian motion) of the particles around their lattice sites, obtaining the "Lindemann parameter" or L, the average amplitude of this excursion, expressed as a fraction of the distance between nearest neighbors. In a crystalline sample at a low temperature of ~ 25°C, the particles were close-packed (volume fraction ~ 0.74) and hardly moving (L ~ 0). As the temperature was increased (and the volume fraction decreased), L also increased, indicating larger particle motions. At 28.0°C, the crystal began to premelt at defects, particularly grain boundaries, with particles jumping from site to site (see the second figure, right). A further small increase in temperature to 28.3°C led to complete melting. At this temperature, the volume fraction of particles, ~ 0.54, was close to the hard-sphere melting value of 0.545. In the interior of a crystal, the Lindemann parameter reached 0.085 just before melting, while its value in the grain boundaries was about 0.180, reflecting the much larger particle motion there. In fact, these two values of L span 0.125, the value found in earlier computer simulations of a perfect, single, hard-sphere crystal at melting (*8*). Melting in a real polycrystalline system is clearly quite spatially heterogeneous, with defects playing a major role in determining the regions of initial melting. It would be interesting to repeat Alsayed's experiment on a perfect single crystal (without defects)—allowing direct comparison with the early computer simulation—although experimentally these are hard to prepare.

These new results on the melting of a three-dimensional crystal can be compared with the classic experiments of Zahn *et al*. (*9*) on two-dimensional melting. These researchers also studied colloidal particles, in this case in a single layer confined by gravity to a flat water/air interface. The particles were paramagnetic, and the dipolar interaction between them was controlled by varying an applied magnetic field. The melting of a perfect two-dimensional crystal closely followed the multistage scenario of Kosterlitz, Thouless, Halperin, Nelson and Young who predicted the creation, then separation, of pairs of dislocations (*10*–*12*). By contrast, Alsayed *et al.* find that melting in three dimensions starts at preexisting defects.

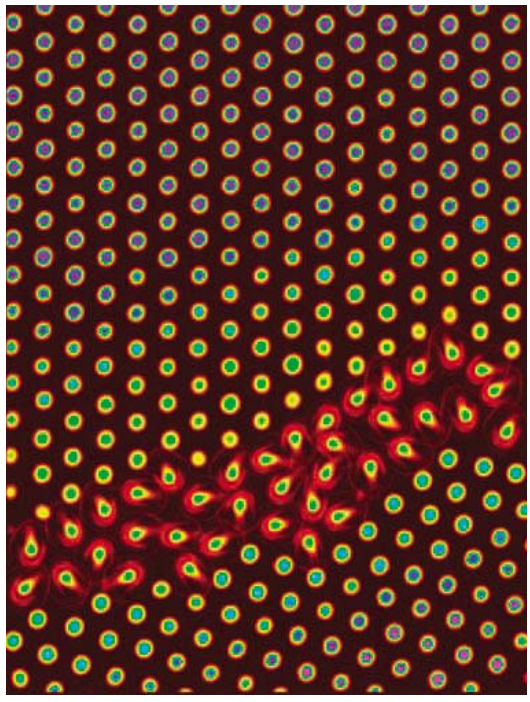

Caught in the act of melting. Before completely melting, crystalline colloids premelt along grain boundaries (diagonal rising from left to right). Near these boundaries, the particles move rapidly and show liquidlike diffusion. Red represents the most movement; violet, the least.

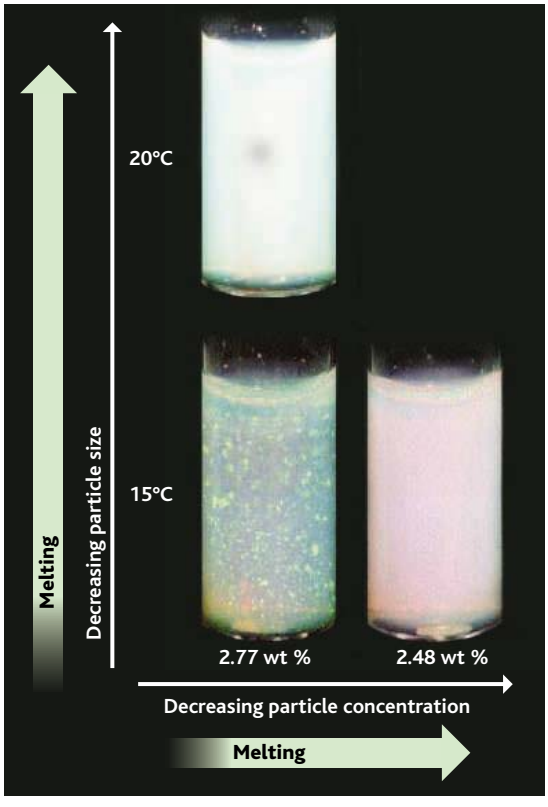

CREDIT: (SECOND FIGURE) A. ALSAYED, F. MACERA A. YODH

Temperature-sensitive colloidal gel particles facilitate studies of melting. Melting induced by decreasing particle concentration is difficult to achieve experimentally (bottom, left to right). But it can be mimicked by a more tractable, heat-induced decrease in the size of polymer gel particles (left, bottom to top). Concentrations by weight of polymer are indicated; effective hard-sphere volume fractions range from < 0.49 in the liquid samples (top and right) to > 0.55 in the crystal (bottom left). Small crystallites appear colored due to Bragg reflection of light (bottom left). These particles are somewhat different from those used in (*2*) and exhibit a soft interaction (*6*). [Adapted from (*6*, *15*)]

Freezing in colloidal systems is easier to study than melting because rigid particles can be used. A crystalline sample is "shear melted" to a metastable fluid by thorough shaking, and the recrystallization process is followed (*1*, *4*). On page 1231 of this issue, de Villeneuve *et al*. (*13*) consider the crystallization of rigid, hard-sphere colloids of diameter 1.5 μm in the presence of large spherical impurities. At a volume fraction of ~0.55 without impurities, crystals were nucleated heterogeneously at the bottom of the sample cell, and a polycrystalline front grew upward. Over the next 12 hours, the system annealed, with grain boundaries disappearing, leaving much larger crystallites with scattered line and point defects. The presence of large impurity particles, ~5 to 20 μm in diameter, in the growing crystal front changed this scenario in several ways. The growth of the crystal was slowed near the impurities, and the smaller ones slowed growth more than the larger ones. The grain boundaries did not anneal out with time, but were pinned by the impurities. Unexpectedly, the first layer of the smaller particles around the impurities remained highly mobile throughout the process.

With video microscopy in its various forms now a mature, though still advancing, technology, we may expect experiments on colloidal systems to continue to illuminate important fundamental phenomena, including freezing, melting, and glass formation (*14*).

References

1. U. Gasser *et al*., *Science* **292**, 258 (2001).
2. A. M. Alsayed, M. F. Islam, J. Zhang, P. J. Collings, A. G. Yodh, *Science* **309**, 1207 (2005); published online 30 June 2005 (10.1126/science.1112399).
3. B. J. Alder, T. E Wainwright, *J. Chem. Phys*. **27**, 1208 (1957).
4. P. N. Pusey, W. van Megen, *Nature* **320**, 340 (1986).
5. B. J. Ackerson, *Nature* **365**, 11 (1993).
6. D. Frenkel, *Phys. World* **6**, 24 (1993).
7. H. Senff, W. Richtering. *J. Chem. Phys*. **111**, 1705 (1999).
8. D. A. Young, B. J. Alder, *J. Chem. Phys.* **60**, 1254 (1974).
9. K. Zahn, R. Lenke, G. Maret, *Phys. Rev. Lett*. **82**, 2721 (1999).
10. J. M. Kosterlitz, D. J. Thouless, *J. Phys. C* **6**, 1181 (1973).
11. D. R. Nelson, B. I. Halperin, *Phys. Rev. B* **19**, 2457 (1979).
12. A. P. Young, *Phys. Rev. B* **19**, 1855 (1979).
13. V. W. A. de Villeneuve *et al*., *Science* **309**, 1231 (2005).
14. E. R. Weeks *et al*., *Science* **287**, 627 (2000).
15. www.ipc.rwth-aachen.de/richtering/

10.1126/science.1116597

The Convergence of Synthetic Organic and Polymer Chemistries

Craig J. Hawker[1]* and Karen L. Wooley[2]*

Several recent conceptual advances, which take advantage of the design criteria and practical techniques of molecular-level control in organic chemistry, allow preparation of well-defined polymers and nanostructured materials. Two trends are clear: the realization that synthesis of complex macromolecules poses major challenges and opportunities and the expectation that such materials will exhibit distinctive properties and functions. Polymer synthesis methods now being developed will yield well-defined synthetic macromolecules that are capable of mimicking many of the features of proteins (for example, three-dimensional folded structure) and other natural materials. These macromolecules have far-reaching potential for the study of molecular-level behavior at interfaces, in thin films, and in solution, while also enabling the development of encapsulation, drug-delivery, and nanoscale-patterning technologies.

By varying the three-dimensional (3D) structure and position of functional groups, synthetic organic chemists have developed the ability to accurately control, and in some cases predict, the physical properties of small molecules or their interactions with biological systems. Classic examples include the design of volatile esters in both nature and the fragrance industry, whose odors are directly related to molecular shape and size, and the discovery of numerous synthetic drugs. This general theme of property control through molecular design has found increasing attention and application in polymer science during recent years. Small changes in structure have been shown to have dramatic effects on the properties of polymers, and one need look no further than poly(ethylene) and poly(propylene) to observe these effects, with poly(propylene) having lower impact strength but superior working temperature and tensile strength compared with poly(ethylene). Increasing the sophistication of molecular design in polymers through the exploitation of organic chemistry concepts and tools is, therefore, a major direction of materials research with considerable potential for cross-fertilization between disciplines.

The most profound recent developments in polymer chemistry are based on this growing synergy between advanced organic chemistry and polymer synthesis. A driving force is the realization that many of the promising applications of nanotechnology rely on extending synthetic organic chemistry into the nanometer-length scale, especially as nanodevices are designed with increasing sophistication. There is also a desire to study fundamental aspects of polymer physics that require an exacting level of control over the structure of a polymer molecule to a degree that is associated traditionally with organic chemistry. Further developments in related fields, such as the synthesis of new catalysts, have also created new tools for making complex molecules. As a result, creative approaches using organic chemistry are required to control every facet of macromolecular structure and to enable functional groups to be introduced at defined locations.

Polymer Synthesis Is Different

Although the promise of accurately controlling chemical structure and functionality at the macromolecular level is considerable, it should be realized that it is not a simple process of transferring synthetic techniques directly from organic chemistry to polymer synthesis. Rather, because of the distinctive features of macromolecules compared with small molecules (e.g., number of functional groups, molecular weight distribution, and purification techniques), the elucidation of polymer synthesis protocols that proceed with structural fidelity and high levels of functional group compatibility is a grand challenge.

In general, polymerization is a multistage process involving an initiation or oligomerization step. Propagation, which follows, involves the successive addition of more monomers/oligomers to these initial activated species. Finally, a termination step halts chain growth to produce a stable polymer. Many traditional polymer syntheses are chaotic processes in which all stages of the polymerization operate concurrently and growing chains can merge with or branch off from one another. Recently, however, several polymerization systems have been developed that offer much better control. In a living radical polymerization (LRP), each molecule of catalyst promotes rapid initiation and then stabilizes the growing chain to prevent branching or termination. Thus, different types of monomer can be added to the reaction consecutively, leading to polymers with well-defined blocks that vary in structure and function.

The discovery of simple and powerful approaches to polymerization reactions, which are not limited by the presence of additional functional groups and provide accurate molecular weights and narrow molecular weight distributions, allows nonspecialists access to well-defined materials, previously the domain of a select few. This issue has been addressed by the development of new chemistry and catalysts for LRPs and ring-opening metathesis polymerization (ROMP) (Fig. 1, Ai and Aii, respectively). Both polymerizations are characterized by a controlled-growth strategy, with LRP involving the addition of vinyl monomers (i.e., styrene) to growing polymers with a very reactive radical chain end. Control is afforded by the reversible capping of this radical chain end with a mediating molecule. In contrast, ROMP involves the ring opening of strained olefins (i.e., norbornene) by organometallic initiators and has benefited greatly by the design of faster, more efficient initiators that are highly selective for the ring-opening reaction and do not undergo unwanted side reactions with functional groups or impurities. These radical and ring-opening systems allow for a substantial degree of control over polymer topology and functional group incorporation through independent synthetic manipulation of the initiating moiety, the terminating unit, and the monomeric repeat units. The conditions for LRP and ROMP are considerably more user friendly (aqueous conditions and no monomer purification) than those employed for anionic polymerization (strictly water-free and oxygen-free with a high level of monomer purification), which is still the "gold standard" in polymer chain growth control. This fidelity allows for their wider adoption and exploitation. Moreover, the increased tolerance of functional groups for these new polymerization

[1]Materials Research Laboratory, Materials Department and Department of Chemistry, University of California, Santa Barbara, CA 93106, USA. [2]Center for Materials Innovation and Department of Chemistry, Washington University, Saint Louis, MO 63130, USA.

*To whom correspondence should be addressed. E-mail: hawker@mrl.ucsb.edu (C.J.H.); klwooley@artsci.wustl.edu (K.L.W.)

processes offers opportunities for combining different chemistries and the construction of macromolecules with a hierarchical arrangement of functional groups and branches.

Architecturally Defined Macromolecules

The basic importance of shape in defining the physical properties of macromolecules has been recognized in recent years, and the study of globular and rodlike materials has evolved in concert with synthetic procedures and advanced architectural designs. A major effort has been directed toward achieving accurate control over each parameter of composition and structure, including the chain ends and backbone segment lengths, as well as the overall macromolecular topology.

Traditionally, structural control could be gained by repetitive coupling reactions to produce macromolecules having accurate molecular sizes, compositions, and functional group placements (*1*). As an example, dendritic macromolecules, derived most often from condensation-based syntheses, have been recognized as adopting a synthetic protein-like structure, based on their monodisperse, globular 3D structures having diameters of a few nanometers. This feature, combined with the large number of chain-end functional groups, has led to their exploitation in a number of novel medicinal applications, for example, as an antiviral HIV drug (VivaGel) (*2*).

Although stepwise, condensation growth strategies and controlled addition chain polymerizations are often limited in the size to which the macromolecules can be constructed or the complexity of the resulting architectures, combinations of these two mechanisms have led to interesting new synthetic routes to distinctive macromolecular architectures. The application of multiple synthetic methods to construct complex macromolecules is most effective when a target structure is identified and then reverse engineered through a retrosynthetic analysis. For example, the tubular, dendronized polymers, important building blocks for nanotechnology, are difficult to prepare using traditional techniques involving the direct polymerization of a monomer carrying the large dendritic unit (*3*). In contrast, divergent and convergent chemistries have been developed to produce such structures by growth of the dendritic side groups or connection of preestablished dendritic units (Bi and Bii) on a prefabricated polymer backbone.

The stepwise, divergent growth of dendritic polyesters on linear poly(*p*-hydroxystyrene) by repetitive, generational coupling of benzylidene acetal- or isopropylidene ketal–protected 2,2-bis(hydroxymethyl)propionyl anhydride and acid-catalyzed cleavage of the protecting groups allowed for the preparation of dendronized polymers (*4*). Starting with poly(*p*-hydroxystyrene) of high molecular weight and narrow molecular weight distribution, the dendronization procedure maintained the narrow molecular weight distribution and chain length; however, the macromolecule underwent an expected but interesting transformation from a random coil (2.1 nm persistence length) to a rigid rod (12.2 nm persistence length) as the dendrimer generation number increased from 0 to 5. These materials represent one of the first examples of synthetic, molecular-based nano-objects that are nonspherical and have well-defined and controllable dimensions. Just as nature makes use of a variety of different building blocks to construct more sophisticated structures, the ability to make synthetic 3D shapes other than simple spheres or to combine different shapes holds enormous potential for understanding and optimizing the properties of <20-nm nano-objects. In addition, the effect of these structures on physical properties, such as increasing the strength or crack resistance of bulk materials, holds considerable promise.

Click Chemistry for Material Synthesis

To be applicable and useful in polymer synthesis, an organic reaction must proceed in high yield with little or no by-product. Both of these criteria are aptly fulfilled by the recent development of the click chemistry concept by Sharpless (*5*). Originally developed for use in organic synthesis and chemical biology, click chemistry encompasses any reaction that proceeds with complete specificity, 100% yield, and almost perfect fidelity in the presence of a wide variety of other functional groups. For example, Tirrell has recently demonstrated a reliable and site-specific method of labeling cell surfaces based on Cu-catalyzed [3+2π] cycloaddition chemistry that takes advantage of the benign reaction conditions and functional group tolerance (*6*).

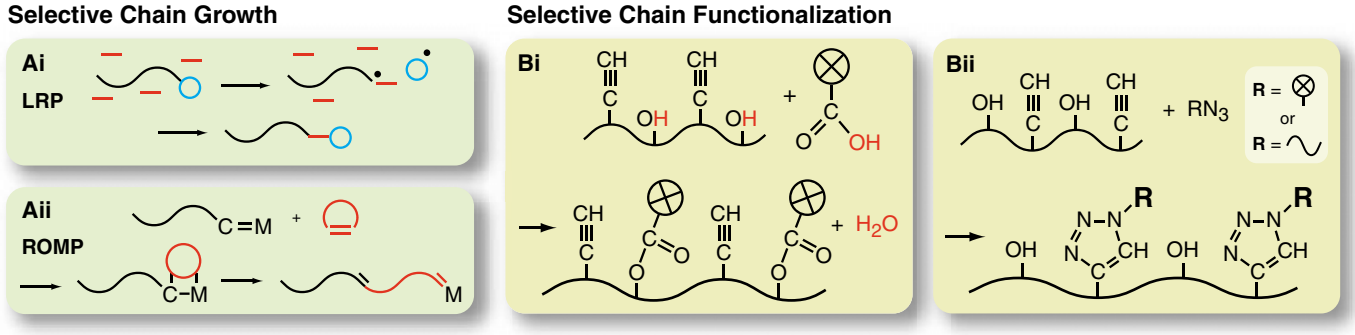

Fig. 1. (**A**) Strategies for selective chain growth. (**i**) In LRP, the growing polymer chain is stabilized by an end group that rapidly associates and dissociates for controlled addition of monomers. Different monomers can be added in batches to produce structurally distinct blocks in the polymer backbone. The end group is either a persistent radical or an atom such as a halogen that shuttles between the chain and a metal complex. (**ii**) In ROMP, a transition metal catalyst breaks open a cyclic alkene at the carbon double bond. The resulting complex then reacts with another cyclic alkene, and the process repeats to yield a chain of opened rings. Current catalysts are tolerant of a huge range of chemical groups adjacent to the double bond, so richly substituted monomers can be prepared and stitched together. (**B**) Strategies for elaborating preformed polymers. (**i**) Esterification is an efficient way to add large substituents to a polymer backbone. The backbone is prepared with pendant hydroxyl (OH) groups, which can be coupled to carbonyl (C=O) groups attached to dendrimers or other macromolecules. (**ii**) Click chemistry, or copper-catalyzed coupling of alkyne and azide groups, is another fast and high-yielding reaction to decorate a polymer backbone or to link two polymer chains together.

The promise of click chemistry toward materials synthesis has been demonstrated also by the complete modification of the side-chain functionalities of a linear polymer by reaction with a sterically bulky dendritic unit (*7*). The Cu(I)-catalyzed Huisgen [3+2π] dipolar cycloaddition reactions between the alkynyl repeat units of poly(vinyl acetylene) and the azido focal point unit of benzyl ether dendrimers were shown to occur with regiochemical control and quantitative conversion for dendrimers of generations 1 and 2 and with >98% conversion for the third-generation dendrimer (Fig. 1Bii). The efficiency of the click reactions, in comparison, for example, to esterification (Fig. 1Bi), allowed for macromolecule-macromolecule couplings to the extent that rigidified nano-objects were obtained.

Click chemistry has also been used as a highly efficient reaction to couple two distinct linear polymers to make block copolymers, a

notoriously difficult synthetic challenge because of the reduced reactivity that occurs between polymeric chain ends (*8*). Linear homopolymers of methyl methacrylate and styrene, for which α-alkynyl or ω-azido functionalities were incorporated from an alkynyl-functionalized initiator or from chain-end modification, were found to undergo high-yielding Cu(I)-catalyzed dipolar cycloaddition reactions to produce block copolymers. This is a particularly elegant example, because it illustrates chemical control over the polymer backbone composition and structure as well as the chain-end functionalities. The approach was also demonstrated for monoalkynyl or monoazido poly(ethylene oxide) and for telechelic azido-terminated polystyrene, offering a general and efficient method by which to conduct chemoselective ligation of well-defined polymers (of any architecture) bearing distinctive terminal or side-chain functionalities (*9*).

The quantitative yields for these click reactions overcame one of the central difficulties in translating organic chemistry to the preparation of polymeric systems, as even high yields (i.e., >95%) can lead to decreased purity and poor molecular level control when large numbers of reactions are performed on a single macromolecule. Hawker and Sharpless have exploited the fidelity of the click chemistry during an accelerated dendrimer synthesis. Their synthetic route avoided numerous time-consuming purification steps as a result of complete chain-end functionalization of the acetylene-terminated dendrimer. For example, reaction with the azidothymidine derivative has no need for protection/deprotection strategies or large excesses of reagents, and represented an ~99.9% yield over 12 to 48 coupling reactions (Fig. 2) (*10*). In a similar vein, Matyjaszewski prepared well-defined homopolymers and copolymers of acrylonitrile by atom transfer radical polymerization, which were further modified using a click reaction with sodium azide and zinc chloride to yield polymeric materials having 5-vinyltetrazole side-chain units (*9*). The widespread use and availability of poly(acrylonitrile)-based materials makes this a simple and attractive route to functionalized materials derived from a commodity polymer.

Discrete Molecular Objects by Diels-Alder Chemistry

In considering highly efficient reactions that can be used to construct polymeric materials, the broad scope and simplicity of operation for Diels-Alder chemistry makes it one of the most powerful synthetic methods and one that is accessible to specialists and nonspecialists. The Diels-Alder reaction consists of the cycloaddition of a conjugated diene to a dienophile, typically an alkene or alkyne, with the driving force of the reaction being the formation of new σ bonds, which are energetically more stable than the π bonds.

This efficiency overcomes one of the key challenges in synthetic organic chemistry—the preparation and isolation of complex molecules with functionalities in specific spatial orientations. Control over the spatial orientation of functional groups becomes increasingly difficult with increasing molecular size, as conformational degrees of freedom and dynamics increase. However, a recent report by Müllen exploits the efficiency of Diels-Alder chemistry to construct poly(phenylene)-based molecular objects of increasing size and sophistication and with distinctive physical properties between regioisomers, which allows for their separation (*11*). This report is also of importance as the first route to the preparation of desymmetrized poly(phenylene) objects by a two-step approach, each involving Diels-Alder cycloaddition reactions and the extrusion of carbon monoxide. In the first step, substoichiometric ratios of reagents were used to generate a monosubstituted desymmetrized core as a mixture of two regioisomers. It was not until subsequent reactions upon the remaining three alkynyl sites with various cyclopentadienones and growth of the full, shape-persistent structure that topological isolation of surface functional groups was achieved. The chain ends then occupied different environments, permitting chromatographic separation of the regioisomers. This discovery has been followed by the selective placement of peptides in specific locations within a 3D macromolecular framework, bringing the spatial refinement of small organic molecules to macromolecular systems (*12*).

Supramolecular Chemistry

The use of noncovalent interactions and supramolecular assembly is a recurring theme in

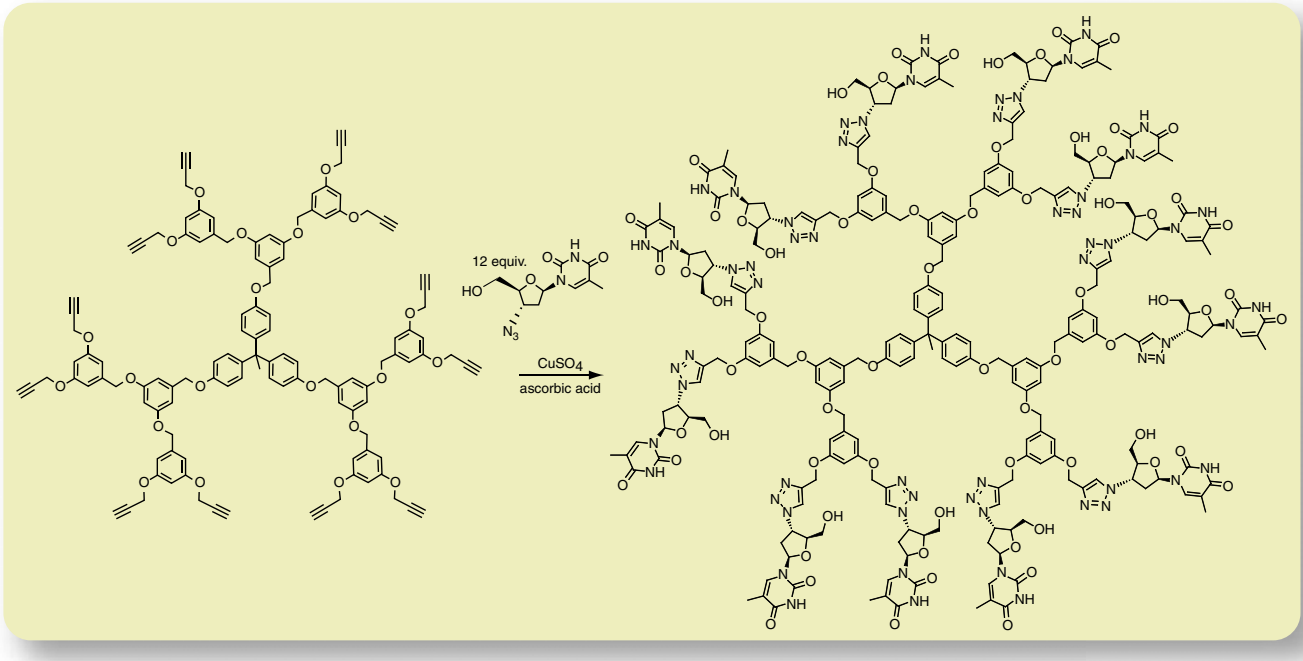

Fig. 2. Preparation of dendritic macromolecules terminated with 3′-azido-3′-deoxythymidine groups using aqueous click chemistry, illustrated with second-generation, dodeca-functionalized derivative.

many natural systems, where its full exploitation is enabled by accurate placements of functional subunits at specific points within macromolecular building blocks such as peptide chains, oligosaccharides, or nucleic acid sequences. Nature exploits both intramolecular and intermolecular assembly in the construction of many functional systems, and this combination of intra/intermolecular assembly has only recently been addressed synthetically. Foldamers have emerged as elegant oligomeric structures that take advantage of the synthetic advances in preparing well-defined materials described above. In particular, synthetic control over the backbone structure and side-group presentation allows for 3D macromolecular designs with defined conformational states of the backbone and side-chain units similar to those found in biological materials such as proteins (*13*). These structural elements guide the intramolecular coiling and intermolecular stacking of the linear segments, through a combination of intramolecular interactions and solvent-directed supramolecular assembly, to afford interesting programmed 3D structures.

Supramolecular assembly of well-defined macromolecular subunits can also lead to the preparation of functional nanoscopic objects based on intermolecular interactions alone. In the simplest forms, for example, fibrillar or core-shell micellar and vesicular assemblies have been related to extracellular matrix materials, lipoproteins, and virus particles (*14*–*16*). Recent work has included the synthesis and use of porphyrin-functionalized initiators for LRP of styrene. The resulting amphiphilic polymers underwent multimolecular supramolecular assembly in tetrahydrofuran/water to afford structures that differed depending on the hydrophilic balance of the porphyrin head group relative to the apolar polystyrene chain segment (*17*). The zinc metalloporphyrin was of particular interest because of the ability to exchange metal ions, altering the physical properties and the energy transfer and catalytic properties. Additionally, polymers having the longest apolar polystyrene chain segment aggregated into nanoscale spherical micelles when water was added to a tetrahydrofuran solution of the amphiphile, whereas the fraction having a polystyrene chain segment of comparable radius of gyration as the porphyrin head group assembled into microscopic hollow spherical vesicles. This ingenious example of functional group incorporation and its effect on self-assembly by Nolte (*17*) also demonstrates the power and enabling capability of new polymerization techniques such as LRP. The ability of LRP to tune the PS chain length while tolerating a wide variety of functional groups, which permits numerous well-defined materials to be easily prepared, provides the foundation for these structure-property studies. Using traditional anionic procedures to prepare a similar range of materials is structurally restrictive and not synthetically practical.

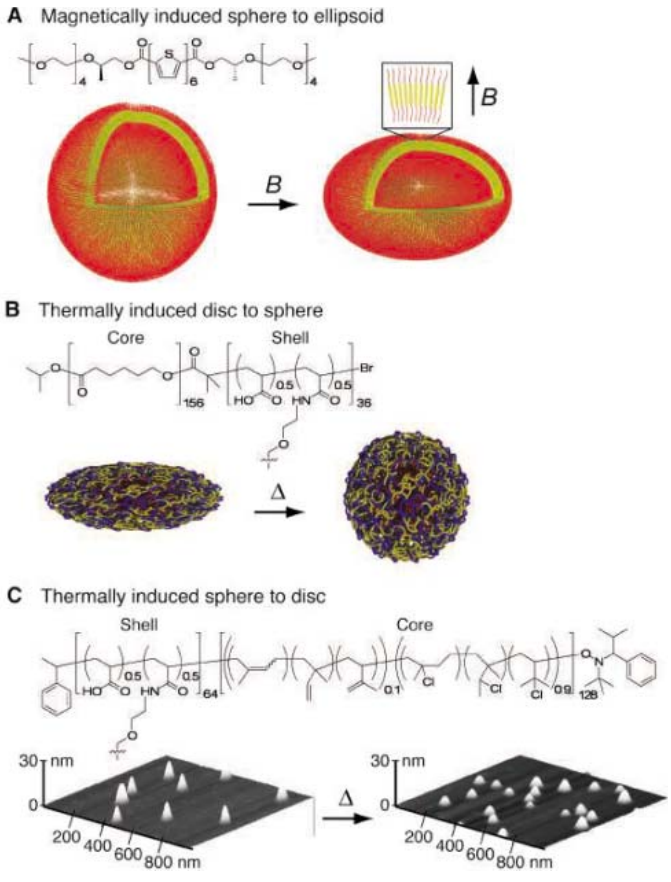

Fig. 3. The physical shaping of nanostructures derived from the supramolecular assembly of amphiphilic linear block copolymers. (**A**) Application of an external magnetic field to assemblies having hexameric thiophene core components. (**B** and **C**) The application of heat to shell cross-linked nanoparticles having (B) crystalline or (C) glassy core domains.

Shapeable Molecular Objects

Shaping of prefabricated polymeric assemblies is a process that is being developed as a new methodology for the preparation of distinctive nanostructures, a similar concept to the foldamers but on a much larger size scale. As described above, the large number of functional groups along a polymeric backbone can lead to difficulties during synthesis; however, their presence can be advantageously used during self-assembly to facilitate and enhance phase separation. By the use of retrosynthetic analysis, traditionally associated with small-molecule syntheses, high levels of control over the structure of monodisperse oligomers and polymer molecules have recently been achieved. This increased level of structural perfection also facilitates the development of an understanding of the rules that govern the assembly of block copolymers and the fundamental polymer physics aspects.

Advances in synthetic organic polymer chemistry have recently allowed a magnetically induced spherical to ellipsoidal transition, predicted theoretically for three decades, to be confirmed experimentally for nanoscale vesicles comprising an ABA bola-amphiphile based on the oligio(thiophene) derivative, 2,5‴″-(*R*-2-methyl-3,6,9,12,15-pentaoxahexadecyl ester)sexithiophene prepared by a multistep organic reaction sequence (*18*). As observed by increasing birefringence, the hollow spheres became increasingly oblate with increasing magnetic field. This shaping process was promoted by the differing degrees of torque exerted by the external magnetic field on each of the molecular subunits within the different regions of the spherical vesicular assemblies (polar versus equatorial regions) due to the large anisotropy in the diamagnetic susceptibility imparted by the six thiophene repeat units (Fig. 3A).

The thermally induced shaping of nanoscale block copolymer micelle assemblies by the chemical transformation of polymer chains within their corona or core domains is also an example of the importance of controlling functional group reactivity and protecting group strategies. The synthesis and reaction of these structures is highly reliant on protection/deprotection strategies borrowed directly from organic chemistry. A multitude of structures can, thereby, be prepared and shaped in solution and upon substrates, mediated by the thermal properties of the core domains. For crystalline core chain segments of poly(ε-caprolactone), the lamellar crystalline phase exerts a disc-shaped morphology to each nanoscale object, which collapses to a sphere upon heating above the melt-transition temperature (*19*) (Fig. 3B). The disc-shaped nanostructure was reestablished upon cooling to induce recrystallization of the core material. Alternatively, a sphere to disc transition was induced thermally upon adsorption from

solution onto a flat substrate (mica or graphite) for core-shell nanoparticles containing polyisoprene core materials (*20*) (Fig. 3C).

The programmed assembly of structurally and compositionally detailed block copolymers has also been studied while in contact with various substrates, which, with subsequent physical and chemical manipulation, has led to important technological developments. The physical adsorption of amphiphilic copolymers upon CdSe/ZnS core-shell quantum dots has been followed by covalent cross-linking to establish robust water-soluble quantum dots, which are of interest for a number of biological and medical applications (*21*, *22*). Remaining carboxylic acid residues allow for conjugation of targeting ligands, for example, whereas the cross-linked polymer shell provides for a stable barrier layer between the quantum dot and the surrounding medium (*23*). Physical isolation of gold nanoparticles has been accomplished similarly, by the physical encapsulation of dodecanethiol-functionalized Au nanoparticles within mixtures of polystyrene-*b*-poly(acrylic acid) and poly(methyl acrylate)-*b*-poly(acrylic acid) (*24*). Dodecanethiol functionalization of the Au nanoparticles allowed for hydrophobic physisorption of the amphiphilic block copolymer to produce the aqueous-phase dispersible encapsulated materials. These studies confirm the need to control the nature of the block copolymer and the interfaces with which contact will be made to achieve the desired nanoscale conformational and directional alignment of the polymer chains as they adsorb onto the substrate. Moreover, these examples illustrate that the reversible intermolecular interactions that drive the assembly process thermodynamically can be supplemented by covalent linkages to capture and stabilize the desired morphologies.

Hybrid Synthetic-Biological Macromolecules

The challenge of combining biopolymers with synthetic macromolecules represents an interesting and powerful opportunity for merging the distinctive properties of each class of material (i.e., programmed assembly of biomolecules and synthetic versatility of synthetic polymers) while at the same time overcoming specific limitations (i.e., decreased stability of biopolymers and poor structural control of synthetic systems) (*25*). In fact, synthetic polymer-protein hybrids (*26*) are already used to increase the circulation time of medicinally relevant proteins, such as Filgrastim, by the covalent attachment of poly(ethylene glycol). Recent work has substantially increased both the complexity of the synthetic polymers and the sophistication of the organic coupling chemistry employed, while at the same time strategies have been developed for the conjugation of these systems to specific points along the backbone of each macromolecule.

This increase in sophistication is perhaps best exemplified by the development of polymer-DNA hybrids by Mirkin and Nguyen (*27*, *28*). In the original studies, hydroxymethyldiphenylacetylene-functionalized poly(norbornene) was prepared by ROMP, followed by phosphoamidite coupling with preformed oligonucleotides. Although synthetically interesting, the promise of these hybrid systems was not realized until the complexity of the synthetic polymer backbone was increased by the incorporation of redox active elements into a multiblock architecture. The living nature of the ROMP process coupled with recent breakthroughs in the design of Ru initiators allowed low polydispersity, controlled molecular weight ferrocenyl- and dibromoferrocenyl-substituted poly(norbornene) blocks to be integrated into the hybrid DNA structure. These triblock systems exhibited high DNA duplex stability and unusually sharp melting transitions with electrochemically distinct signals for the ferrocenyl derivatives, allowing single base-pair mismatches to be detected on the basis of triblock composition.

The development of solid-phase techniques for the synthesis of organic and biological molecules has been instrumental in allowing the coupling between biological and synthetic macromolecules to evolve from random coupling along the polymeric backbone to specific attachment at predetermined sites. Initial work (*29*) demonstrated the efficiency achieved in biosynthetic hybrid syntheses by sequential growth of peptide fragments from a solid-phase support using standard chemistry followed by initiator attachment and growth of the synthetic polymer through LRP techniques (*30–32*). Conversely, the preformed synthetic macromolecule can be attached to (or grown from) the solid support and peptide fragments extended from the appropriate functional groups along the backbone or at the chain terminus of the synthetic system. This approach has been developed for the preparation of amphiphilic diblock and triblock copolymers of hydrophilic peptide sequences and hydrophobic polystyrene chain segments (*33*). By skillfully manipulating the structure of the initial synthetic system, Stupp has recently demonstrated the design of "reverse" peptide amphiphiles, constructed by coupling at the C terminus instead of the traditional and synthetically easier N terminus (*15*). Having free N termini and opposite peptide polarities, these reversed structures permit a wider array of 3D assemblies to be prepared with improved properties by coassembly with the complementary structures having free C termini. For example, nanofibers containing β sheets prepared by mixing traditional and "reverse" hybrids exhibited improved stability when compared with each parent material.

Polysaccharides represent the third main class of biomacromolecular components, and their coupling strategies involve many organic reactions developed for small-molecule oligosaccharides. A particularly interesting development from Haddleton's laboratory used oligosaccharide-functionalized initiators for LRP to place the saccharide moiety at the synthetic polymer-chain terminus (*34*). This was then extended to placement at the terminus of the hydrophilic chain segment of amphiphilic block copolymers to decorate block copolymer micelles (*35*) and cross-linked nanoparticles (*36*) with biologically active sugar residues. Well-defined nanostructures bearing surface accessible and bioavailable ligands are of interest as polyvalent containment devices for carrying imaging labels and therapeutics to selective tissues for development broadly in medical applications (*30*, *37*).

Challenges for Polymer Design

In many cases, specific applications are driving areas of research. For targeted drug delivery and/or diagnostic agents, precisely defined macromolecules and nanoscale objects are needed and will require multiple functional groups for drug payload, cell targeting, delivery, and tracking. Other diverse fields, such as microelectronics, where the drive is to develop <50-nm feature sizes, require polymers with accurate control over their length, dispersity, and functionality not only for traditional photolithography but also for alternative nanopatterning techniques. An excellent example is the enabling influence of functionalized block and random copolymers, prepared by LRP, on self-assembling block copolymer template strategies (*38–41*). This synergy and molecular-level focus will be matched by a closer connection between nanotechnology and organic/polymer chemistry. The controlled manipulation of nanoscale objects and patterns by predictable changes in polymer structure is a potent concept that is only beginning to be exploited.

References and Notes

1. D. A. Tomalia, J. M. J. Fréchet, *J. Polym. Sci. Part A: Polym. Chem.* **40**, 2719 (2002).
2. B. Halford, *Chem. Eng. News* **83** (24), 30 (2005).
3. L. Shu, A. D. Schlüter, C. Ecker, N. Severin, J. P. Rabe, *Angew. Chem. Int. Ed. Engl.* **40**, 4666 (2001).
4. M. Yoshida, Z. M. Fresco, S. Ohnishi, J. M. J. Fréchet, *Macromolecules* **38**, 334 (2005).
5. V. V. Rostovtsev, L. G. Green, V. V. Fokin, K. B. Sharpless, *Angew. Chem. Int. Ed. Engl.* **41**, 2596 (2002).
6. A. J. Link, M. K. S. Vink, D. A. Tirrell, *J. Am. Chem. Soc.* **126**, 10598 (2004).
7. B. Helms, J. L. Mynar, C. J. Hawker, J. M. J. Fréchet, *J. Am. Chem. Soc.* **126**, 15020 (2004).
8. J. A. Opsteen, J. C. M. van Hest, *Chem. Commun.* 57 (2005).
9. N. V. Tsarevsky, K. V. Bernaerts, B. Dufour, F. E. Du Prez, K. Matyjaszewski, *Macromolecules* **37**, 9308 (2004).
10. M. Malkoch *et al.*, *Macromolecules* **38**, 3663 (2005).
11. G. Mihov, I. Scheppelmann, K. Müllen, *J. Org. Chem.* **69**, 8029 (2004).
12. G. Mihov *et al.*, *Bioconjugate Chem.* **16**, 283 (2005).
13. J. C. Nelson, J. G. Saven, J. S. Moore, P. G. Wolynes, *Science* **277**, 1793 (1997).
14. J. A. A. W. Elemans, A. E. Rowan, R. J. M. Nolte, *J. Mater. Chem.* **13**, 2661 (2003).
15. H. A. Behanna, J. J. J. M. Donners, A. C. Gordon, S. I. Stupp, *J. Am. Chem. Soc.* **127**, 1193 (2005).
16. K. L. Wooley, *J. Polym. Sci. Part A: Polym. Chem.* **38**, 1397 (2000).
17. F. de Loos, I. C. Reynhout, J. J. L. M. Cornelissen, A. E. Rowan, R. J. M. Nolte, *Chem. Commun.* 60 (2005).

18. I. O. Shklyarevskiy *et al.*, *J. Am. Chem. Soc.* **127**, 1112 (2005).
19. Q. Zhang, C. G. J. Clark, M. Wang, E. E. Remsen, K. L. Wooley, *Nano Lett.* **2**, 1051 (2002).
20. K. S. Murthy, Q. Ma, E. E. Remsen, T. Kowalewski, K. L. Wooley, *J. Mater. Chem.* **13**, 2785 (2003).
21. D. R. Larson *et al.*, *Science* **300**, 1434 (2003).
22. X. Wu *et al.*, *Nat. Biotechnol.* **21**, 41 (2003).
23. X. Michalet *et al.*, *Science* **307**, 538 (2005).
24. Y. Kang, T. A. Taton, *Angew. Chem. Int. Ed. Engl.* **44**, 409 (2005).
25. H.-A. Klok, *J. Polym. Sci. Part A: Polym. Chem.* **43**, 1 (2005).
26. K. Velonia, A. E. Rowan, R. J. M. Nolte, *J. Am. Chem. Soc.* **124**, 4224 (2002).
27. J. M. Gibbs *et al.*, *J. Am. Chem. Soc.* **127**, 1170 (2005).
28. K. J. Watson, S.-J. Park, J.-H. Im, S. T. Nguyen, C. A. Mirkin, *J. Am. Chem. Soc.* **123**, 5592 (2001).
29. M. L. Becker, J. Liu, K. L. Wooley, *Chem. Commun.* 180 (2003).
30. M. L. Becker, J. Liu, K. L. Wooley, *Biomacromolecules* **6**, 220 (2005).
31. M. L. Becker, E. E. Remsen, D. Pan, K. L. Wooley, *Bioconjugate Chem.* **15**, 699 (2004).
32. Y. Mei, K. L. Beers, H. C. M. Byrd, D. L. VanderHart, N. R. Washburn, *J. Am. Chem. Soc.* **126**, 3472 (2004).
33. I. C. Reynhout, D. W. P. M. Löwik, J. C. M. van Hest, J. J. L. M. Cornelissen, R. J. M. Nolte, *Chem. Commun.* 602 (2005).
34. D. M. Haddleton, K. Ohno, *Biomacromolecules* **1**, 152 (2000).
35. L. Bes, S. Angot, A. Limer, D. M. Haddleton, *Macromolecules* **36**, 2493 (2003).
36. M. J. Joralemon, K. S. Murthy, E. E. Remsen, M. L. Becker, K. L. Wooley, *Biomacromolecules* **5**, 903 (2004).
37. A. Verma, V. M. Rotello, *Chem. Commun.* 303 (2005).
38. K. Temple *et al.*, *Adv. Mater.* **15**, 297 (2003).
39. K. Shin *et al.*, *Nano Lett.* **2**, 933 (2002).
40. J. Y. Cheng, A. M. Mayes, C. A. Ross, *Nat. Mater.* **3**, 823 (2004).
41. D. Y. Ryu, K. Shin, E. Drockenmuller, C. J. Hawker, T. P. Russell, *Science* **308**, 236 (2005).
42. Supported in part by the National Science Foundation (DMR 0080034, DMR 0210247, and DMR 0301833) and the Office of Naval Research (N000140510057).

10.1126/science.1109778

Highly Pathogenic H5N1 Influenza Virus Infection in Migratory Birds

J. Liu,[1*†] H. Xiao,[2,4*] F. Lei,[3*] Q. Zhu,[5] K. Qin,[1] X.-w. Zhang,[6] X.-l. Zhang,[1] D. Zhao,[1] G. Wang,[2,4] Y. Feng,[2,4] J. Ma,[2] W. Liu,[2] J. Wang,[6] G. F. Gao[2†]

Avian influenza virus (AIV) involving at least three subtypes, H5, H7, and H9, has emerged as an important pathogen in the poultry industry and is of major current global health concern (*1*). The first case report of chicken-to-human transmission was in Hong Kong in 1997 (*2*); since 2003, H5N1, a highly pathogenic AIV, has emerged in 10 Asian countries, including Thailand, Vietnam, and China (Fig. 1), and has claimed at least 53 human lives. Until recently, migratory waterfowl seemed to be exempt from widespread infection, although sporadic cases were recorded (*3*). Here we describe an outbreak of highly pathogenic H5N1 infection among waterfowl in Lake Qinghaihu, Gangcha County, Qinghai Province, in western China (Fig. 1).

On 4 May 2005, a few birds were found dead on Bird Island, and by the end of June more than a thousand birds were affected. This lake is one of the most important breeding locations for migratory birds that overwinter in Southeast Asia, Tibet, and India (Fig. 1). Several species were infected, including the bar-headed goose (*Anser indicus*), great black-headed gull (*Larus ichthyaetus*), and brown-headed gull (*Larus brunnicephalus*). Two key symptoms were noticed: abnormal neurological signs (tremor and opisthotonus) and diarrhea. Among the gross lesions, pancreatic necrosis was obvious and was confirmed by tissue section where extensive areas of lytic necrosis were seen, consistent with pathology observed in domestic geese and ducks infected with H5N1 AIV (*3*). Brain sections revealed glial cell infiltration, perivascular cuffing, and congestion in the blood vessels. Serological tests (*4*) from one bar-headed goose and one brown-headed gull confirmed the presence of high-titer antibody against H5N1 AIV.

Several H5N1 viruses were isolated from the viscera, brain, and swabs of the oropharynx and cloaca of sick and dead birds. Four of the isolates from different bird species were completely sequenced (*4*) and appeared to be closely related. None of the GenBank sequence data for known H5N1 AIV genomes completely matched our sequences, implying the viruses are reassortants. Five of the eight genomic segments (M, PA, PB1, PB2, and NS) were closely related to a Hong Kong 2004 isolate (A/peregrine falcon/HK/D0028/04) (*3*). We observed several characteristics in our four isolates: first, the sequence PQGERRRKKR/G, denoting multiple basic amino acids at the cleavage site of the hemagglutinin; second, a virulence island in the PB2 gene, E627K, first seen in Hong Kong in 1997 (*5*); and third, a deletion of 20 amino acids in neuramidase (amino acid positions 49 to 69), also associated with high virulence.

To test virulence, mice and chickens were infected with the BhGoose/QH/1/05 (*4*) isolate. All eight infected chickens died within 20 hours, and seven of eight infected mice died within 72 hours; the last died 96 hours post-infection. Earlier isolates taken from ducks in China were less virulent in mice and chickens (*6*). Hence we speculate that viruses might be emerging from reassortants that originate in birds overwintering in southeast Asia (*7*).

The occurrence of highly pathogenic H5N1 AIV infection in migrant waterfowl indicates that this virus has the potential to be a global threat: Lake Qinghaihu is a breeding center for migrant birds that congregate from southeast Asia, Siberia, Australia, and New Zealand.

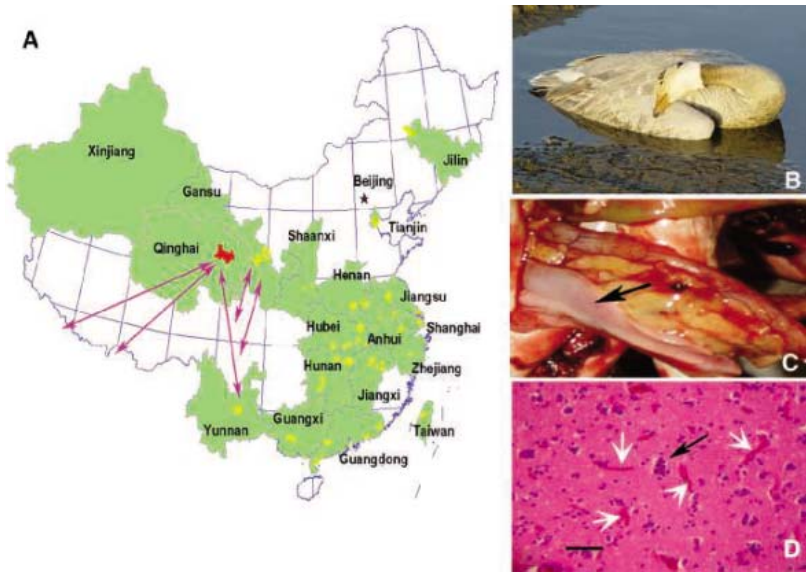

Fig. 1. (**A**) The reported H5N1 AIV prevalence sites during the 2004 outbreak in China are highlighted in yellow (*8*). Arrows indicate the migratory routes of the bar-headed goose (*A. indicus*) to Lake Qinghaihu. (**B**) A sick bar-headed goose showing typical opisthotonus before dying. (**C**) Bar-headed goose pancreas with pin-point necrotic lesions (arrow). (**D**) Microscopic lesions in bar-headed goose brain, showing congestion in the blood vessels (white arrows) and glial cell infiltration (black arrow). Hematoxylin and eosin ×25 (scale bar, 50 μm).

References and Notes

1. R. J. Webby, R. G. Webster, *Science* **302**, 1519 (2003).
2. K. Subbarao *et al.*, *Science* **279**, 393 (1998).
3. K. S. Li *et al.*, *Nature* **430**, 209 (2004).
4. Materials and methods are available as supporting material on *Science* Online.
5. M. Hatta *et al.*, *Science* **293**, 1840 (2001).
6. H. Chen *et al.*, *Proc. Natl. Acad. Sci. USA* **101**, 10452 (2004).
7. T. H. Cheng *et al.*, *Fauna Sinica: Aves* (Science Press, Beijing, 1979), vol. 2.
8. Available at www.china.com.cn/chinese/zhuanti/qlg/483177.htm
9. Supported by the Ministry of Science and Technology, PR China [grant nos. 2004BA519A29, 2004BA519A11, 2004BA519A10, and 2004BA519A50; National Basic Research Program (973) of China 2005CB523000], the Chinese Academy of Sciences (The President Fund and CAS Information Special grant no. INF105-SDB-3-A2), the State Forestry Administration of China, and the National Natural Sciences Foundation of China (grant nos. 30471282 and 30228025). Sequence data derived from this study were deposited in GenBank with accession no. DQ100542-DQ100573.

Supporting Online Material
www.sciencemag.org/cgi/content/full/1115273/DC1
Materials and Methods
Figs. S1 and S2
References and Notes

25 May 2005; accepted 29 June 2005
Published online 6 July 2005;
10.1126/science.1115273
Include this information when citing this paper.

[1]College of Veterinary Medicine, China Agricultural University, Beijing 100094, China. [2]Institute of Microbiology, Chinese Academy of Sciences, Beijing 100080, China. [3]Institute of Zoology, Chinese Academy of Sciences, Beijing 100101, China. [4]Graduate School, Chinese Academy of Sciences, Beijing, China. [5]Institute of Microbiology and Epidemiology, Academy of Military Medical Sciences, Beijing 100071, China. [6]Beijing Genomics Institute, Chinese Academy of Sciences, Beijing 101300, China.

*These authors contributed equally to this work.
†To whom correspondence should be addressed. E-mail: gaof@im.ac.cn (G.F.G); jhl@cau.edu.cn (J.L.)

Premelting at Defects Within Bulk Colloidal Crystals

A. M. Alsayed,[1] M. F. Islam,[1] J. Zhang,[1] P. J. Collings,[1,2] A. G. Yodh[1]*

Premelting is the localized loss of crystalline order at surfaces and defects at temperatures below the bulk melting transition. It can be thought of as the nucleation of the melting process. Premelting has been observed at the surfaces of crystals but not within. We report observations of premelting at grain boundaries and dislocations within bulk colloidal crystals using real-time video microscopy. The crystals are equilibrium close-packed, three-dimensional colloidal structures made from thermally responsive microgel spheres. Particle tracking reveals increased disorder in crystalline regions bordering defects, the amount of which depends on the type of defect, distance from the defect, and particle volume fraction. Our observations suggest that interfacial free energy is the crucial parameter for premelting in colloidal and atomic-scale crystals.

The importance of melting in nature can hardly be overestimated, and yet a detailed understanding of the mechanisms that drive this transformation is still evolving. Scientists have speculated for more than a century about how crystalline solids melt (*1*–*3*). In the process, they have generated microscopic models emphasizing the role of lattice vibrations (*4*, *5*), dislocations (*6*, *7*), grain boundaries (*8*, *9*), surfaces (*10*–*14*), dimensionality (*15*), and combinations thereof. In contrast to the continuous transitions that arise in ferromagnetism and liquid-vapor systems, a first-principle theory of the solid-liquid transition is difficult to derive because of long-range many-body effects, symmetry, and a lack of universality. Furthermore, experimental investigations to test underlying theoretical assumptions are extraordinarily difficult, because they must track motions of individual atoms or defects within crystals. Nevertheless, recent experiments (*16*, *17*) and theory (*18*) have shown that atomic crystal surfaces at equilibrium below the bulk melting point often form melted layers. This premelting lowers the energy barrier for liquid nucleation and effectively prevents superheating of the solid (*16*, *19*).

Many theories have suggested that a similar premelting should occur at defects such as grain boundaries, stacking faults, and dislocations located within the bulk crystal, but these effects have not been observed. Simulations of grain boundaries (*20*, *21*), for example, have found that the free energy of the solid-solid interface can be larger than two solid-liquid interfaces, thereby favoring premelting near the grain boundary. In this work, we imaged the motions of particles in three-dimensional (3D) colloidal crystals during the melting process. The images reveal premelting near grain boundaries and dislocations. Furthermore, particle tracking enabled us to quantify the spatial extent of local particle fluctuations near a variety of defects, as well as within the more ordered parts of the crystal.

Increased disorder was observed in crystalline regions bordering the defects as a function of defect type (e.g., grain boundaries, dislocations, and vacancies), distance from the defect, and particle volume fraction. These observations answer longstanding fundamental questions about melting mechanisms, suggest that grain boundary and dislocation premelting are important effects in the melting process, and introduce new quantitative measures of local disorder. Besides their intrinsic importance for colloid science and technology, all indications suggest that interfacial free energy is the crucial parameter for premelting. Thus, these results are also relevant for atomic-scale materials.

The colloidal crystals used for these studies were equilibrium systems composed of micrometer-sized, nearly hard-sphere particles (*22*). At a high volume fraction, these particles are driven entropically to condense into close-packed crystalline solids (*23*, *24*). A key feature of these measurements is our use of microgel particles (*25*, *26*), whose diameters depend on temperature. Thus, by slightly changing the sample temperature, we precisely vary the volume fraction of particles in the crystal over a significant range, driving the crystal from close packing toward its melting point at a lower volume fraction.

Particle synthesis. The temperature-sensitive colloidal particles required for this investigation were synthesized by free-radical polymerization of *N*-isopropylacrylamide (NIPA) and 2-aminoethyl-methacrylate hydrochloride (AEMA) and cross linked with *N*,*N*′-methylene-bisacrylamide in a buffer solution (pH = 4.0, 50 mM acetic acid) (*27*). The resultant particles were centrifuged down and resuspended in a different buffer solution (pH = 8.3, 0.1 M sodium bicarbonate).

Succinimidyl ester (TAMRA), which is a fluorophore that reacts with the AEMA amine group 5-(6)-carboxytetramethylrhodamine, was added to the preparation solution for fluorescence studies that are not reported here. The microgel particles with TAMRA became slightly smaller in size, but the presence or absence of TAMRA changed the phase behavior of the suspension only slightly.

The particles were then cleaned cyclically, by first concentrating them with centrifugation and then resuspending them in a buffer solution (pH = 4.0, 20 mM acetic acid). Finally, in order to minimize particle aggregates, the suspensions were centrifuged for a few minutes, the supernatant was collected, and the process was repeated (~10 times). For temperatures below 32°C, NIPA solubility increases with decreasing temperature. Consequently, the NIPA-AEMA particle diameter varies in our experimental temperature regime (20° to 28°C) as a result of water moving into and out of the microgel. The particles made from NIPA-AEMA copolymer have higher surface charge and are more stable against aggregation in solution during processing than are particles made from pure NIPA. Counterions in the buffer solution ensure that the charges on the particles are screened. In addition, the polymerization rate in our acidic solutions (pH = 4.0) was slow, resulting in reduced size polydispersity. Dynamic light-scattering measurements at 25°C determined the particle radius to be ~375 nm, with a polydispersity less than 3%.

Microscopy and temperature control. Experimental observations were made with an upright microscope (Leica DMRXA2) equipped with a 12-bit monochrome cooled camera (QImaging RETIGA) and a motorized stage. The dimensions of the sample chamber were 18 mm by 4 mm by 0.1 mm. The temperature of the sample and objective lens (magnification ×100, 1.4 numerical aperture) were controlled to within 0.1°C and were increased in 0.1°C increments. Samples were left to equilibrate at each temperature for 1 hour. In order to track premelted regions and defects, we took bright-field video images for 0.6 s at 100-nm intervals throughout the ~100-μm-thick chamber. Because the microgel particles were ~95% water, their refractive index was very close to that of water, allowing us to obtain high-quality images throughout the sample volume. In order to track individual particle movement, we used a video shutter time of 2 ms. Image fields were chosen to contain ~400 particles, and particle positions were determined at resolutions much smaller than the particle radius or crystal lattice constant

[1]Department of Physics and Astronomy, University of Pennsylvania, 209 South 33rd Street, Philadelphia, PA 19104–6396, USA. [2]Department of Physics and Astronomy, Swarthmore College, Swarthmore, PA 19081–1397, USA.

*To whom correspondence should be addressed. E-mail: yodh@physics.upenn.edu

(*28*). Fifteen minutes of video were recorded at each temperature.

Sample preparation. The particle suspensions were loaded into the chamber using capillary forces at 28°C; i.e., just below the melting temperature. In this process, the suspension was sheared. Initially we found that well-oriented face-centered cubic (fcc) crystals grew from the glass coverslip surfaces and that the middle of the sample was fluid-like. After loading, we annealed the sample at 28°C for 24 hours, during which the samples crystallized. Bragg diffraction (Fig. 1, inset) from various parts of the annealed sample, measured in the microscope with a Bertran lens, exhibited no detectable change in peak positions. The crystal had very few defects close to the glass walls. We never observed premelting near the walls; it is possible the walls stabilized the crystal or that the (111) planes near the wall surfaces were intrinsically stable (*19*). Interior crystalline regions had many more defects. A few defects in the sample interior are shown in Figs. 2 and 3. Most of the defects we observed were stacking faults, which caused the formation of partial dislocations (Fig. 3) (*29*). We also observed vacancies. Typically, the crystals lost their preferential orientation after melting and recrystallization, displaying large crystalline regions with different orientations separated by grain boundaries (Fig. 2).

Premelting from grain boundaries. One of the common melting mechanisms exhibited by our colloidal crystals is illustrated in Fig. 2. The figure shows a small-angle (~13°) grain boundary. The grain boundary is composed of an array of dislocations, one of which is shown in the inset of Fig. 2A. The number of particle nearest neighbors along the grain boundary varies from five to seven (red and blue particles in the inset). These packing mismatches create stress in the crystal near the grain boundary. The dashed line in Fig. 2A shows a Shockley partial dislocation that continues into the grain boundary. The region to the right of the dashed line is out of focus, and the particles in this portion of the image appear darker than average, whereas the region to the left is in focus and the particles appear whiter than average.

Figure 2B shows the same region at higher temperature (lower particle volume fraction). In order to minimize the interfacial free energy caused by stress and surface tension, particles near the grain boundary start to premelt. The inset of Fig. 2B shows these particles jumping rapidly from one site to another. In contrast, melting is not observed near the partial dislocation (dashed line); its interfacial free energy is apparently less than that of the grain boundary. In Fig. 2C, the temperature is slightly higher and melting has erupted along the grain boundary. At this stage, the sample volume fraction is higher than the bulk melting particle volume fraction, and the melted region has engulfed the partial dislocation. The width of the premelted region continues to increase as the temperature is raised from 28.0° to 28.2°C (Fig. 2, B to D).

Premelting from dislocations. In addition to grain boundary premelting, the colloidal crystals display premelting from partial dislocations (Fig. 3). This effect is more apparent when the grain boundaries are relatively far from the partial dislocations. Figure 3, A and B, show images of the 61st layer (green) and the 62nd layer (red and yellow), respectively, of the colloidal crystal at 25.0°C.

Figure 3C shows a superposition of these layers. Both of these layers represent (111) planes in the crystal. The Burger's circuit in the 61st layer (green) yields a zero Burger's vector, indicating no defect in the layer. Because a dislocation is present in the next layer, some of the particles are slightly out of focus. The Burger's circuit for the 62nd layer (yellow) reveals a Shockley partial dislocation with a Burger's vector of $\frac{1}{6}(\bar{1}\bar{1}2)$ (*29*). The inset contains a 3D illustration of the Shockley dislocation, showing the 61st layer and the undisplaced particles in the 62nd to 64th layers in green and the displaced particles in the 62nd to 64th layers in yellow.

In monodisperse nearly hard-sphere colloidal crystals, the difference in the energy between fcc and hexagonal close-packed (hcp) structures is very small (*30*, *31*) and stacking faults are common (*32*). Shockley partial dislocations arise as a result of these stacking faults. Face-centered cubic crystals stack in the pattern ABCABC along the (111) direction, and hcp crystals stack in the pattern ABAB. The green particles in Fig. 3A are in the A positions, whereas the red and yellow particles are in the B and C positions of the next layer, respectively. This stacking fault opens up gaps between the two close-packed structures within the crystal (two gaps are visible in the image and make an

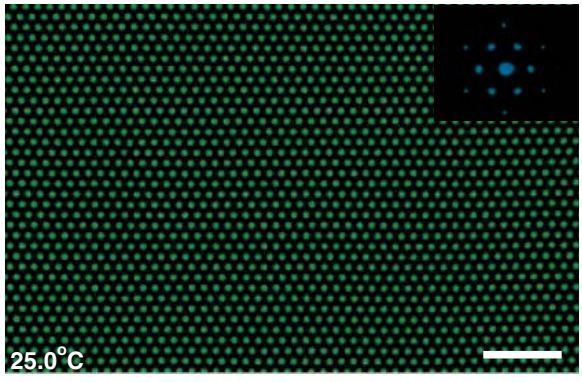

Fig. 1. Bright-field image of the NIPA particle colloidal crystal showing no defects; the slice is of the seventh layer from the coverslip. Each bright spot corresponds to the central region of a 0.75-μm-diameter particle. Because of sample preparation and annealing, the primary defects are partial dislocations that exist in the interior of the crystal. Scale bar, 5 μm. (Inset) Bragg diffraction (wavelength = 405 nm) of the same sample.

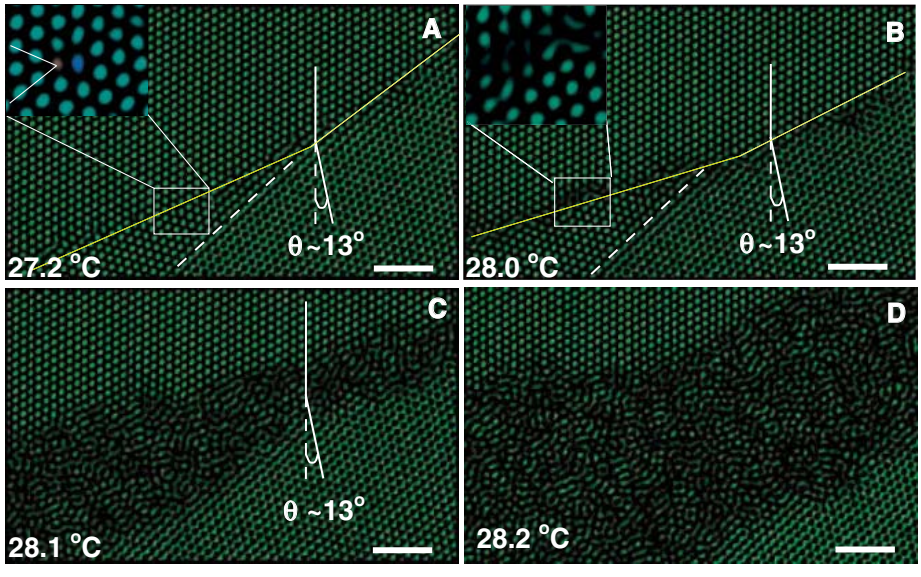

Fig. 2. Premelting of the colloidal crystal at a grain boundary. The figure shows bright-field images at different temperatures (i.e., particle volume fractions) of two crystallites separated by a grain boundary (crystallites tilted at an angle θ ~ 13° with respect to one another). (**A**) Sample at 27.2°C. The solid and dashed lines show the grain boundary and a partial dislocation, respectively. The grain boundary cuts the two crystals along two different planes (the yellow line has two slopes). It is composed of an array of dislocations; the two extra planes are indicated by lines in the inset. (**B**) Sample at 28.0°C. The grain boundary starts to premelt; nearby particles undergo liquid-like diffusion (inset). The partial dislocation, denoted by the dashed line, is not affected. (**C** and **D**) The same sample at 28.1° and 28.2°C, respectively. The width of the premelt region near the grain boundary increases. Scale bars, 5 μm.

angle of 120°C with respect to one another). Nearby particles fluctuate into and out of these gaps. The angle the gaps make with the (111) plane suggests that the gaps cut the crystal along (100) planes, as shown in the 3D illustration. Finally, Fig. 3D shows the 62nd crystal layer at 28.2°C. At this temperature, which is higher than the grain boundary premelting temperature, the crystal has begun to premelt from the partial dislocation.

Positional fluctuations. Using the Lindemann parameter L, which is a measure of the particle mean square fluctuation, we have quantified these observations as a function of sample temperature and volume fraction (Fig. 4). Inset 1 shows the time evolution of mean square displacement (MSD) for particles in the bulk crystal at three different temperatures. On short time scales, the MSD exhibits free particle diffusion; on long time scales, the particles are caged by nearest neighbors and the MSD asymptotically approaches a constant. This asymptotic constant corresponds to twice the variance of the particle's displacement from its equilibrium position (*33*, *34*). We computed the 3D L by using the measured 2D MSD and assuming that particle fluctuations were isotropic. We used the relation $L = \frac{1}{r_{nn}}\sqrt{\frac{3}{4}\langle r^2(\tau \to \infty)\rangle}$, where r_{nn} is the crystal nearest-neighbor distance, and $\langle r^2\ (\tau \to \infty)\rangle$ is the asymptotic value of the 2D particle MSD.

In the main plot of Fig. 4A, L experiences a change in slope at 24.7°C. At this temperature, the hydrodynamic diameter of the particles as measured by dynamic light scattering is ~754 nm (inset 2), and the nearest-neighbor distance derived from pair correlation functions measured by microscopy is ~750 nm. Thus, at this temperature, it is reasonable to assume that the particles are close packed with a volume fraction of ~0.74. Below this temperature, the particle motions are constrained, and L varies less strongly with temperature. With this assumption, we can deduce the particle number density. This number density and the measured hydrodynamic radius (inset 2) determine the particle volume fraction as a function of temperature (upper scale of Fig. 4A). The crystal appears to melt at a particle volume fraction of ~0.54, which is close to the hard-sphere prediction of 0.545 (*24*). The lattice constant in the solid regions, derived from our measurements of the particle pair correlation functions, also decreases sharply near this volume fraction. Although our particles are not perfect hard spheres (*22*), the melting point suggests that they may be approximated reasonably well as such.

The Lindemann melting criterion, which predicts melting for $L \sim 1/8$ (*4*), continues to provide a useful benchmark nearly 100 years after it was originally suggested. The data for L in Fig. 4A are taken from deep within the crystalline regions of the sample, below the melting point. At 28.3°C, the sample begins to melt, and a coexistence of liquid and solid domains is observed. In Fig. 4B, we show local measurements of L near various crystalline defects and near the premelt boundary just before bulk melting (28.3°C). We find that the particle fluctuations in the proximity of these regions are measurably larger than those in the bulk crystal. Furthermore, we find that the magnitude of these fluctuations decreases approximately exponentially as the measurement position is translated away from the premelt region toward the interior of the bulk crystal. Extrapolation of our exponential fits of L to zero distance suggest that $L \sim 0.18$ in the premelt region, twice its interior value of ~0.085 at the same temperature. Evidently, the greater number of vacancies in the premelted region increases the free volume for particle

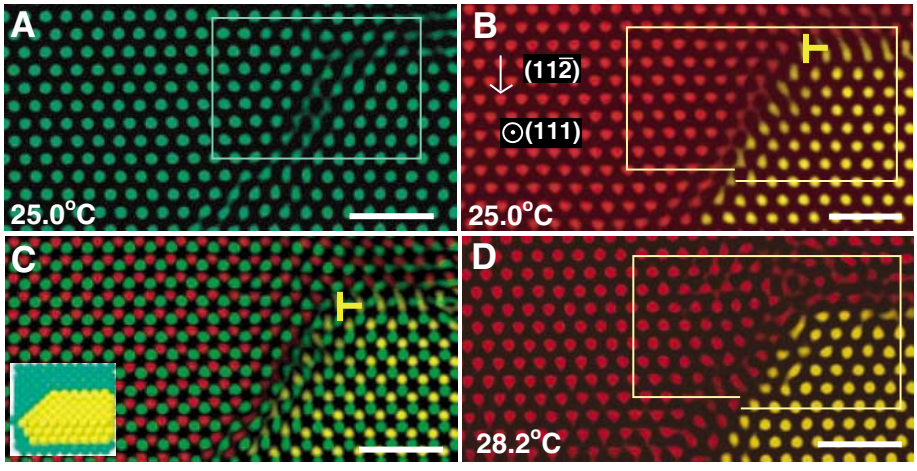

Fig. 3. Melting of a colloidal crystal initiated at a Shockley partial dislocation in the absence of grain boundaries. (**A** and **B**) Bright-field images of the 61st and 62nd layers at 25.0°C, respectively. Colloidal particles fluctuate more in the 62nd layer because of the gap created by the dislocation. (**C**) Superposition of 61st (green) and 62nd (red and yellow) layers. The image shows particles in positions A (green), B (red), and C (yellow). (Inset) 3D illustration of the 61st to 64th layers (bottom to top) showing the displacement of the yellow spheres in the 62nd to 64th layers. (**D**) 62nd layer at 28.2°C, where the crystal starts to premelt at the dislocation. Scale bars, 3 μm.

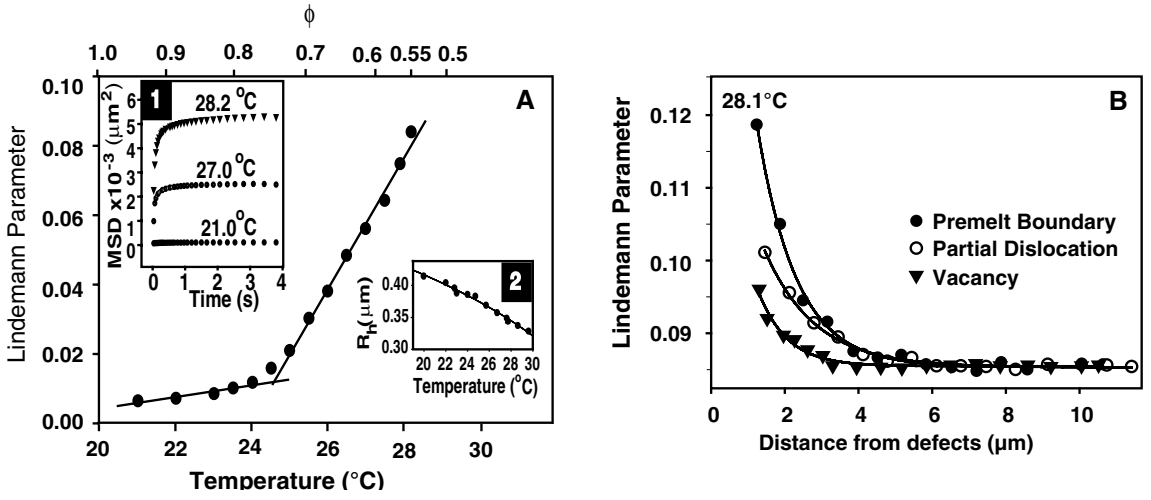

Fig. 4. (**A**) L as a function of colloidal crystal temperature (and computed particle volume fraction ϕ). These data are for regions far from defects. The curve exhibits a change in slope at 24.7°C. The crystal melts at 28.3°C, ϕ ~0.55. (Inset 1) Time evolution of 2D particle MSD; L is derived from the MSD plateau value. The error bars for ϕ, L, and temperature are 0.02, 0.004, and 0.1°C, respectively. (Inset 2) Measured microgel particle hydrodynamic radius R_h as a function of temperature. (**B**) The local L as a function of distance from a vacancy, a partial dislocation, and a melt front. Within 1 μm of the defects, the particle motion was too rapid and calculation of L was unreliable.

movement, so that the nearby particle fluctuations are large. Even the particles near isolated vacancies have large L, but the decay of L to bulk values is fastest from isolated vacancies.

Conclusions. We have demonstrated that premelting occurs at grain boundaries and dislocations located within colloidal crystals. These observations confirm an important mechanism for theories of melting. The amount of premelting depends on the nature of the interfaces and defects. Particle tracking has enabled us to study particle fluctuations both nearby and far from these defects in ways that are inaccessible to experimental probes of atomic crystals, revealing the excess free energy in these regions through higher values of L.

References and Notes

1. H. Lowen, *Phys. Rep.* **237**, 249 (1994).
2. J. G. Dash, *Rev. Mod. Phys.* **71**, 1737 (1999).
3. J. G. Dash, H. Fu, J. S. Wettlaufer, *Rep. Prog. Phys.* **58**, 115 (1995).
4. R. W. Cahn, *Nature* **413**, 582 (2001).
5. F. A. Lindemann, *Z. Phys.* **11**, 609 (1910).
6. S. F. Edwards, M. Warner, *Philos. Mag.* **40**, 257 (1979).
7. L. Burakovsky, D. L. Preston, R. R. Silbar, *Phys. Rev. B* **61**, 15011 (2000).
8. R. Lipowsky, *Phys. Rev. Lett.* **57**, 2876 (1986).
9. G. Ciccotti, M. Guillope, V. Pontikis, *Phys. Rev. B* **27**, 5576 (1983).
10. W. A. Curtin, *Phys. Rev. B* **39**, 6775 (1989).
11. B. Pluis, D. Frenkel, J. F. van der Veen, *Surf. Sci.* **239**, 282 (1990).
12. R. Ohnesorge, H. Lowen, H. Wagner, *Phys. Rev. E* **50**, 4801 (1994).
13. R. Lipowsky, U. Breuer, K. C. Prince, H. P. Bonzel, *Phys. Rev. Lett.* **62**, 913 (1989).
14. R. W. Cahn, *Nature* **323**, 668 (1986).
15. M. S. Pettersen, M. J. Lysek, D. L. Goodstein, *Phys. Rev. B* **40**, 4938 (1989).
16. U. Dahmen, S. Hagege, F. Faudot, T. Radetic, E. Johnson, *Philos. Mag.* **84**, 2651 (2004).
17. J. W. M. Frenken, J. F. van der Veen, *Phys. Rev. Lett.* **54**, 134 (1985).
18. J. F. van der Veen, *Surf. Sci.* **433-435**, 1 (1999).
19. B. Pluis, A. W. D. van der Gon, J. W. M. Frenken, J. F. van der Veen, *Phys. Rev. Lett.* **59**, 2678 (1987).
20. J. Q. Broughton, G. Gilmer, *Phys. Rev. Lett.* **56**, 2692 (1986).
21. S. Phillpot, J. F. Lutsko, D. Wolf, S. Yip, *Phys. Rev. B* **40**, 2831 (1989).
22. M. Stieger, J. S. Pedersen, P. Lindner, W. Richtering, *Langmuir* **20**, 7283 (2004).
23. J. Zhu *et al.*, *Nature* **387**, 883 (1997).
24. P. N. Pusey, W. van Megen, *Nature* **320**, 340 (1986).
25. S. B. Debord, L. A. Lyon, *J. Phys. Chem. B* **107**, 2927 (2003).
26. J. Wu, B. Zhou, Z. Hu, *Phys. Rev. Lett.* **90**, 048304 (2003).
27. A. M. Alsayed, M. F. Islam, A. G. Yodh, data not shown.
28. J. C. Crocker, D. G. Grier, *J. Colloid Interface Sci.* **179**, 298 (1996).
29. J. P. Hirth, J. Lothe, *Theory of Dislocations* (Wiley, New York, ed. 2, 1982).
30. P. Schall, I. Cohen, D. A. Weitz, F. Spaepen, *Science* **305**, 1944 (2004).
31. S. Pronk, D. Frenkel, *J. Chem. Phys.* **110**, 4589 (1999).
32. P. N. Pusey *et al.*, *Phys. Rev. Lett.* **63**, 2753 (1989).
33. J. Bongers, H. Versmold, *J. Chem. Phys.* **104**, 1519 (1996).
34. Y. N. Ohshima, I. Nishio, *J. Chem. Phys.* **114**, 8649 (2001).

35. We thank T. Lubensky, D. Discher, R. Kamien, E. Burstein, C. Crouch, and T. Sinno for useful discussions. This work was supported by NSF through grants DMR-0203378 and DMR-079909 (Materials Research Science and Engineering Center) and by NASA (NAG8-2172). P.J.C. acknowledges the support of the American Chemical Society Petroleum Research Fund.

Supporting Online Material

www.sciencemag.org/cgi/content/full/1112399/DC1
Movies S1 to S3

17 March 2005; accepted 24 May 2005
Published online 30 June 2005;
10.1126/science.1112399
Include this information when citing this paper.

Structure of a Synaptic γδ Resolvase Tetramer Covalently Linked to Two Cleaved DNAs

Weikai Li,[1] Satwik Kamtekar,[1] Yong Xiong,[1,2] Gary J. Sarkis,[1]* Nigel D. F. Grindley,[1] Thomas A. Steitz[1,2,3]†

The structure of a synaptic intermediate of the site-specific recombinase γδ resolvase covalently linked through Ser[10] to two cleaved duplex DNAs has been determined at 3.4 angstrom resolution. This resolvase, activated for recombination by mutations, forms a tetramer whose structure is substantially changed from that of a presynaptic complex between dimeric resolvase and the cleavage site DNA. Because the two cleaved DNA duplexes that are to be recombined lie on opposite sides of the core tetramer, large movements of both protein and DNA are required to achieve strand exchange. The two dimers linked to the DNAs that are to be recombined are held together by a flat interface. This may allow a 180° rotation of one dimer relative to the other in order to reposition the DNA duplexes for strand exchange.

Enzymes that catalyze site-specific recombination rearrange DNA in all three kingdoms to integrate, excise, or invert DNA segments for a variety of biological purposes. Site-specific recombinases are classified into the tyrosine and serine recombinase families, and the detailed mechanisms by which they achieve specific recombination are gradually emerging (*1*).

The γδ resolvase is a 20.5-kD transposon-encoded enzyme that belongs to the resolvase-invertase family of serine recombinases and catalyzes a recombination between two 114–base pair (bp) sites (*res*) that are arranged in the same orientation on negatively supercoiled circular DNA, resulting in the formation of two catenated DNA molecules. Each *res* site contains three different subsites, which are called sites I, II, and III, and each subsite binds a resolvase dimer (Fig. 1A). Six resolvase dimers and two *res* sites assemble into a higher-order structure called the synaptosome. Resolvase dimers bound at sites II and III of the two *res* sites initiate the formation of this assembly and activate the resolvase dimers bound at site I for synapsis, strand cleavage, strand exchange, and religation (*2*). Cleavage is achieved by a transesterification reaction that covalently links the Ser[10] (S10) residue of each subunit to a 5′ phosphate at the center of site I, freeing the 3′ hydroxyl group of the adjacent nucleotide (*3*, *4*). While covalently linked to the protein, the strands are exchanged with a resulting net 180° rotation (*5*–*7*). The four rearranged ends are then joined by an attack of the free 3′ hydroxyl groups on the phosphoserine linkages.

Several crystal structures of wild-type γδ resolvase have been determined, including a domain containing the active site (*8*, *9*), the full-length protein (*10*), and a resolvase dimer complexed with a site I DNA analog (*11*). γδ resolvase has an N-terminal catalytic domain followed by an extended α-helical arm (the E helix) and a C-terminal DNA binding domain. Two states of the molecules have been captured in these structures. First, crystals of the unliganded γδ resolvase identify one interface that promotes the formation of a dimer via the E helices and a second higher-order interdimer interface (termed the 2-3′) that is essential for *res* site synapsis (*8*–*10*, *12*, *13*). Second, the structure of a wild-type γδ-resolvase dimer complexed with a 34-bp analog of site I (*11*) captures a state before synapsis. In this structure, both catalytic S10 residues are distant from the scissile phosphates of the site I DNA, which is consistent with the inability of the wild-type protein to cleave linear DNA containing only a site I sequence.

Two models have been proposed for the structure of the synaptic tetramer bound at site I and the consequent strand-exchange mechanisms (*10*, *11*, *14*). In one model, two site I DNAs are held in close proximity inside a protein scaffold (*10*, *11*), whereas in the other they lie outside of a protein core and are separated by more than 50 Å (*10*, *11*, *14*). The DNA inside model was initially appealing because the DNA strands could be exchanged through subtle movements of the protein and the DNA at the cleavage sites, analogous to those subsequently observed with the tyrosine recombinase Cre (*15*). However, DNA phasing experiments

[1]Department of Molecular Biophysics and Biochemistry, and [2]Department of Chemistry, Yale University, and [3]Howard Hughes Medical Institute, New Haven, CT 06520, USA.

*Present address: 454 Life Sciences, 20 Commercial Street, Branford, CT 06405, USA.
†To whom correspondence should be addressed. E-mail: eatherton@csb.yale.edu

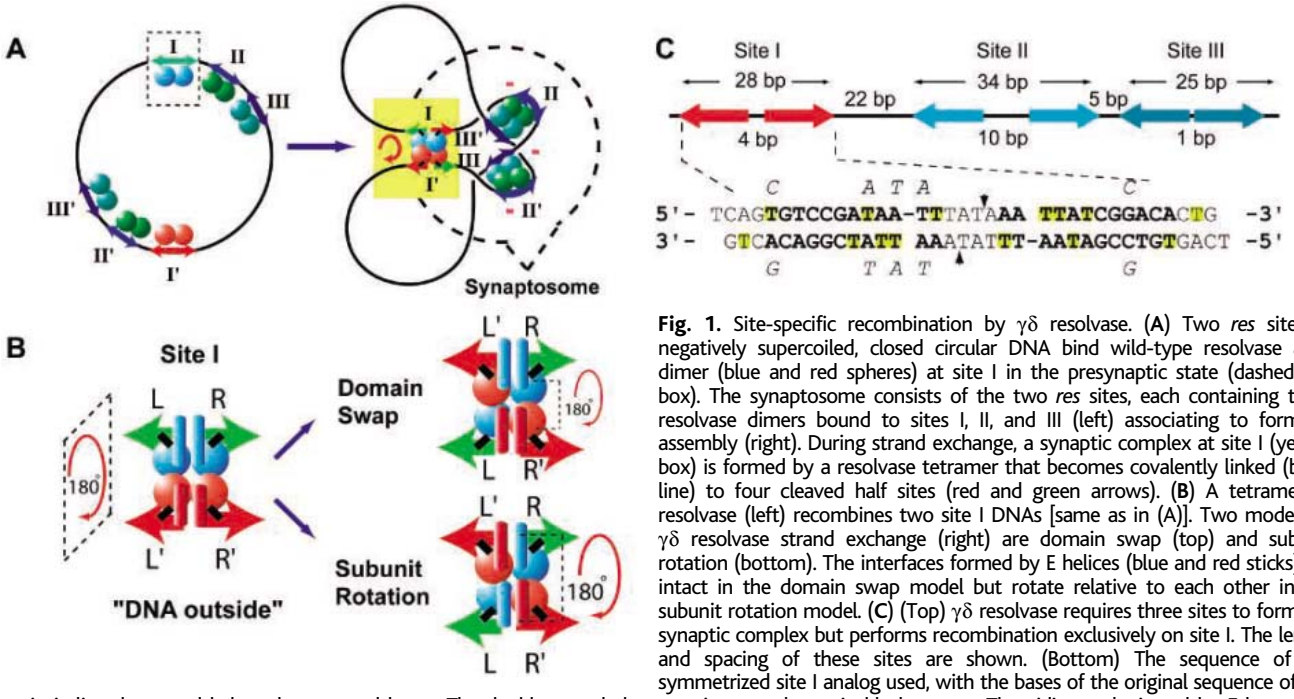

Fig. 1. Site-specific recombination by γδ resolvase. (**A**) Two *res* sites in negatively supercoiled, closed circular DNA bind wild-type resolvase as a dimer (blue and red spheres) at site I in the presynaptic state (dashed-line box). The synaptosome consists of the two *res* sites, each containing three resolvase dimers bound to sites I, II, and III (left) associating to form an assembly (right). During strand exchange, a synaptic complex at site I (yellow box) is formed by a resolvase tetramer that becomes covalently linked (black line) to four cleaved half sites (red and green arrows). (**B**) A tetramer of resolvase (left) recombines two site I DNAs [same as in (A)]. Two models of γδ resolvase strand exchange (right) are domain swap (top) and subunit rotation (bottom). The interfaces formed by E helices (blue and red sticks) are intact in the domain swap model but rotate relative to each other in the subunit rotation model. (**C**) (Top) γδ resolvase requires three sites to form the synaptic complex but performs recombination exclusively on site I. The length and spacing of these sites are shown. (Bottom) The sequence of the symmetrized site I analog used, with the bases of the original sequence of site I shown in italics above and below the mutated bases. The double-strand cleavage sites are shown in black arrows. Thymidines substituted by 5-bromo-2′-deoxyuridine in oligonucleotide derivatives are shown shaded in yellow. Nicks in the crystallographic substrates are opposite the dashes.

(*16*), as well as recent x-ray scattering experiments (*17*), favor the DNA outside model. In order to achieve recombination, substantial movement of the DNA is required if it lies outside of a protein core because of the large separation of the DNA fragments to be religated. This would likely be achieved by substantial movements of the protein that is covalently linked to the DNA during strand exchange (Fig. 1B). A subunit rotation model posits a 180° rotation between protein subunits that would both juxtapose the DNA ends to be recombined and accomplish the required change in DNA topology (*6*, *7*). In contrast, a domain swap model (*2*) proposed that only a pair of catalytic domains plus their associated DNAs move, thus preserving the interface between subunits and avoiding their dissociation. To resolve these debates, we have pursued the structure of an active synaptic complex of a resolvase tetramer bound to two site I DNAs. A synaptic complex can be achieved by using mutant enzymes that, unlike the wild-type enzymes, are capable of recombining linear DNA substrates containing only site I DNA (*14*, *18*).

Structure of the synaptic complex. The structures of two crystal forms of a tetramer of a γδ-resolvase mutant protein bound to two 34-bp symmetrical analogs of *res* site I (Fig. 1C) have been determined (*19*). This mutant of resolvase protein contains the changes $Gly^{101}\rightarrow Ser^{101}$ (G101S), $Glu^{102}\rightarrow Tyr^{102}$ (E102Y), $Met^{103}\rightarrow Ile^{103}$ (M103I), and $Glu^{124}\rightarrow Gln^{124}$ (E124Q) that activate recombination on linear site I DNA (*14*), as well as the mutations $Arg^{2}\rightarrow Ala^{2}$ (R2A) and $Glu^{56}\rightarrow Lys^{56}$ (E56K) that improve its solubility by suppressing the 2, 3′ interaction between dimers. The structure of a $P3_221$ crystal form was determined by a combination of multiple isomorphous replacement and multiwavelength anomalous diffraction methods (Table 1) (*20*). The phasing power for five of the heavy atom derivatives used for phasing the $P3_221$ crystal form ranged between 0.5 and 0.91 for the centric data and between 1.05 and 1.7 for the acentric data, yielding an overall figure of merit of 0.60. Multidomain, cross-crystal averaging with the presynaptic complex and sharpening of the amplitudes dramatically improved phases and electron density maps (Fig. 2) and allowed refinement of the model to an R of 27.1% and an R_{free} of 32.4% at 3.9 Å resolution. The structure of a $P2_12_12_1$ crystal form was subsequently determined by molecular replacement and refined to an R of 26.3% and an R_{free} of 29.4% at 3.4 Å resolution. The tetramer in the $P3_221$ crystal form, which incorporates a crystallographic two fold, has essentially the same conformation as that observed in the asymmetric unit of the $P2_12_12_1$ crystal form, except that the DNA and DNA binding domains adopt somewhat different orientations.

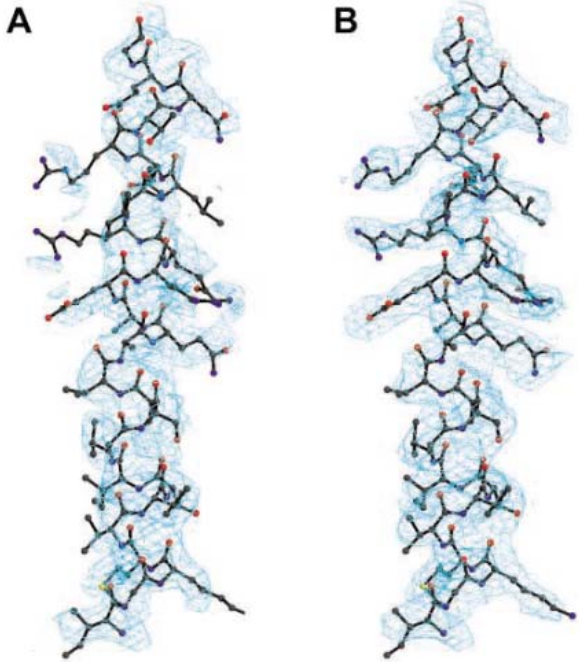

Fig. 2. Map improvement by multidomain cross-crystal averaging of the presynaptic and synaptic complexes. The electron density maps of the E helix region are compared. This region has been excluded from the averaging masks; improvement of the density in this unaveraged region is an unbiased indication of overall phase improvement. (**A**) Before cross-crystal averaging, the phases have been improved by multidomain noncrystallographic symmetry averaging within the $P3_221$ crystal form of the synaptic complex. (**B**) The 3.9 Å resolution experimental map after multidomain cross-crystal averaging of the synaptic complex ($P3_221$) and the presynaptic complex ($P2_12_12_1$). The multidomain averaging was performed on the catalytic domains and the DNA binding domains with the bound DNAs.

The catalytic domains of the activated resolvase form the tetrameric core of a complex having pseudo-222 symmetry, and the site I DNA substrates lie on the outside of the protein core (Fig. 3A and movie S1). Both strands of the two substrate duplexes have been cleaved by resolvase, and each of the four 5′ ends is covalently linked to a resolvase subunit via a phosphoserine linkage (Fig. 3B). These four half sites are well separated, and this complex thus appears to correspond to an intermediate in the strand exchange process. We have labeled the left and right halves of the top and bottom DNA duplexes L and R (green) and L′ and R′ (yellow and orange), respectively, in Fig. 3A. The distances between the free 3′ hydroxyl groups and the phosphoserine bonds are 17 Å, 40.5 Å, and 41 Å for the L-R (and L′-R′), L-L′, and L-R′ DNAs, respectively. Further, of all possible pairs of resolvase subunits, the subunit interaction and relative orientation of the L and R (blue and green) or L′ and R′ (red and magenta) subunits most closely resembles that of the resolvase dimer bound to the uncleaved site I (*11*). These observations imply that the L and R half sites and their attached subunits correspond to one of the initial site I–bound dimers and that the L′ and R′ half sites correspond to the other, trapped at a stage soon after cleavage or slightly before religation. Thus, the L and R as well as the L′ and R′ dimers are referred to as the site I dimers.

The newly formed interface that holds together the two site I dimers in the tetrameric complex, which we call the synaptic interface, is extensive (1780 Å^2 per dimer) and consists primarily of two four-helix bundles of D and E helix pairs joining resolvase subunits bound to L and L′ (or to R and R′) half sites. In these four helix bundles, interactions across the synaptic interface involve a pair of antiparallel E helices that are associated by hydrophobic interactions made by side chains lying between Y102 (*21*) to Q120 (Fig. 3C), and a pair of antiparallel D helices that are associated via residues lying between D72 to K81.

Comparison of presynaptic and synaptic complex structures. The transition from the presynaptic dimer to the synaptic tetramer is accompanied by dramatic changes in the tertiary (and quaternary) structures of the resolvase subunits. The differences in tertiary structure lie primarily in the relative orientations of the catalytic domain, the E helix, and the DNA binding domain (Fig. 4A), which can be seen by superimposing either the DNA molecules or the catalytic domains. The orientations of the DNA binding domains also vary in different crystal forms (*11*). Superimposing the catalytic domains shows that the E helix had bent and rotated by 40° toward the D helix in the transition from the presynaptic to the strand-exchange state (Fig. 4A) by pivoting about a flexible linker that lies between the D and E helices at G101 and E102 (Fig. 4B) (*21*). These changes move the catalytic S10 residue of the activated resolvase 12 Å toward the scissile phosphate, thereby allowing its hydroxyl group to form a covalent link (movie S2). In contrast, S10 and the scissile phosphate are separated by either 14 or 20 Å (*11*) in the inactive presynaptic state.

These changes in the tertiary structure of the subunits are associated with a completely different quaternary structure. The structure of the site I dimer of the tetramer was compared with that of the presynaptic dimer (Fig. 4C) by aligning the dyad axes relating the site I dimers and superimposing the two complexes. Whereas in the presynaptic state, the E helices cross each other at a 45° angle and form the primary interface between dimer subunits, in the synaptic tetramer, these two interacting E helices open up like a scissors to produce a crossing angle of 100°. This scissoring of the E helices, together with the subunit conformational changes, alter and reduce the interactions seen in the presynaptic dimer and create a new intricate synaptic interface between site I dimers.

The changes in tertiary and quaternary structure that occur between these two states result in a dramatically different and flat interface between the subunits of each site I dimer, which may have implications for the mechanism of strand exchange. In the presynaptic state, the interface between the subunits of the dimer is grooved, and the crossed E helices interlock with each other in a manner that appears inconsistent with any rotational motion between the subunits (Fig. 4D). In contrast, in the synaptic complex planarity between the subunits of each site I dimer interface extends across the tetramer (Fig. 4D). Fitting the coordinates of the atoms from one of the surfaces making contact to a plane gives a root mean square deviation of 3.0 Å from this plane for the contacting surface of a subunit in the presynaptic state and 1.3 Å for the interface formed by an antiparallel dimer in the strand-exchange state. This is at the lowest limit for proteins of a similar size in the protein interfaces database (fig. S3).

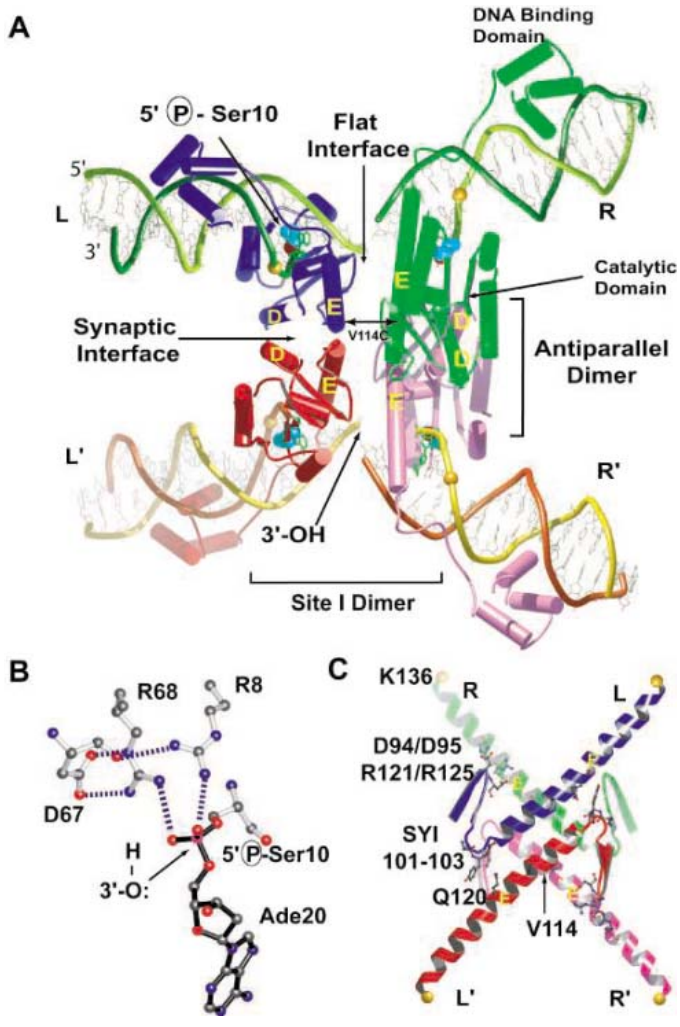

Fig. 3. The structure of the mutant γδ-resolvase tetramer covalently linked to cleaved DNA. (**A**) The two site I DNAs (light and dark green, yellow, and orange coils) are cleaved into half sites labeled L, R, L′, and R′. S10 (blue and red spheres) in each subunit is covalently linked to the 5′ phosphate of adenine 20 (Ade20, green stick). The subunits of the resolvase tetramer (blue, green, red, and magenta) can be divided into two dimers containing antiparallel E helices (L-L′ and R-R′) or two site I dimers bound to L-R DNA or L′-R′ DNA. The D and E helices form a four-helix bundle within the antiparallel dimer. The two antiparallel E helix dimers interact through a flat interface, and the V114→C114 (*21*) mutation in the E helix crosslinks across the flat interface. The position of the missing phosphates resulting from the use of symmetrized oligos is marked by an orange sphere; its absence does not distort the DNA. (**B**) The active site at the covalent, cleaved DNA intermediate. A phosphoserine bond formed between Ade20 and S10. R8, D67, R68, and the two nonbridging oxygens of the phosphoserine form a hydrogen-bonding network (blue dashed lines). In the religation step, the free 3′-hydroxyl attacks of the DNA to be exchanged (black arrow) is presumably in line with the phosphoserine bond. (**C**) A view of the tetramer rotated by 90° from the orientation in (A) shows the packing of four E helices and preceding loops and β strands.

Formation of the synaptic conformation. The transition between the presynaptic dimer and the synaptic tetramer was modeled with use of the program MORPH (*22*), which calculates stereochemically allowed structural intermediates between two known structures. The E helix appears to play a central role in achieving this dramatic repacking. During this transition the E helices, which form the dimer interface in the presynaptic complex, open up like scissors (Fig. 4C) and slide relative to each other, thereby allowing the helices of one site I dimer to interdigitate with those of the other and creating an extensive antiparallel E-helix interaction between dimers (movie S3). Together, these changes create the flat interface between the site I subunits (Fig. 4D).

The mutations that facilitate the formation of the synaptic tetramer in the absence of site II and site III complexes appear to do so by either destabilizing the presynaptic dimer conformation or stabilizing the tetramer. The side chain of Q120 and the mutant side chain of Y102 stabilize the synaptic tetramer conformation through their hydrophobic stacking between the antiparallel E helices (Fig. 4B). Because G101 has backbone ϕ-ψ angles in the dimer that are only allowed for glycine, the serine mutation should destabilize the presynaptic dimer conformation as well as stabilize the tetramer through its interaction with the backbone (Fig. 4B).

The active site and double strand cleavage. A number of residues that are highly conserved among the members of the resolvase-invertase family either contact the substrate at the active site or are indirectly involved in maintaining the structure of the active site and thus presumably play important roles in the catalysis of strand cleavage. These include R8, D67, and R68 (Fig. 3B) (*21*). The guanidinium groups of R8 and R68 interact with the nonbridging phosphate oxygens, whereas D67 helps to position R68. R125 interacts with the nucleotide containing the free 3′ hydroxyl group that is formed by cleavage of the DNA. R71 is another highly conserved residue and is very close to the active site, but it seems to interact with S43 and to not be directly involved in catalysis.

The initial cleavage of both DNA strands and their subsequent religation require that the orientations of both the DNA binding domains and DNA as well as the catalytic domains must differ substantially from both the presynaptic and the synaptic structures. Although the orientation of each half site is correct for cleavage in the synaptic tetramer, the distance of 30 Å between the active site S10 residues of the L and R subunits is much larger than the distance of 14 Å between the two scissile phosphates in B-form DNA (or the 16 Å in the presynaptic complex). This implies that, whether the two cleavage steps occur sequentially or simultaneously, significant alterations in the positions of the DNA, the DNA binding domains, and the catalytic domains from their conformations in either the presynaptic or synaptic structures would be required. Neither simultaneous nor sequential mechanisms can be ruled out by model building.

Strand exchange. The most interesting question raised by this structure is the mechanism by which the strands are exchanged, because the free 3′ OH groups lie about 50 Å from the phosphoserine group they are presumed to attack in the religation step and the space between them is filled with the catalytic domains. This is unlike the situation with the tyrosine recombinases Cre (*15*) and Flp (*23*), where the DNA strands to be recombined form a Holliday junction intermediate that, importantly, is not separated by protein and thus can rearrange by relatively modest changes in the DNA and protein structures. Far larger structural changes in the $\gamma\delta$ protein are necessary to achieve strand exchange.

Analysis of the structure of this synaptic resolvase complex strongly supports the subunit rotation model of strand exchange. Although this structure does not establish with certainty which subunits contain the half sites of DNA that are to be religated after exchange, the expectation in the case of the wild-type enzyme that the two site I DNAs are being

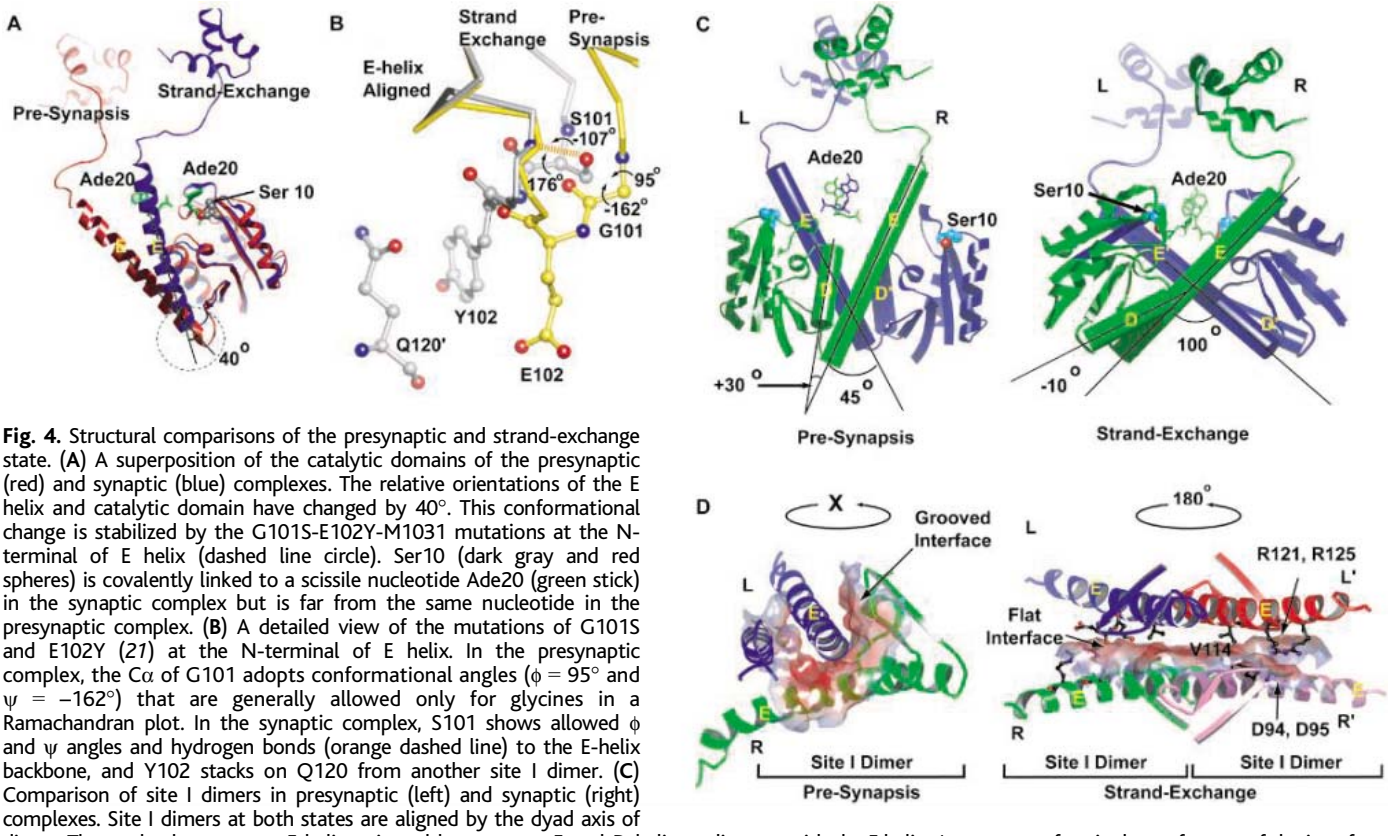

Fig. 4. Structural comparisons of the presynaptic and strand-exchange state. (**A**) A superposition of the catalytic domains of the presynaptic (red) and synaptic (blue) complexes. The relative orientations of the E helix and catalytic domain have changed by 40°. This conformational change is stabilized by the G101S-E102Y-M1031 mutations at the N-terminal of E helix (dashed line circle). Ser10 (dark gray and red spheres) is covalently linked to a scissile nucleotide Ade20 (green stick) in the synaptic complex but is far from the same nucleotide in the presynaptic complex. (**B**) A detailed view of the mutations of G101S and E102Y (*21*) at the N-terminal of E helix. In the presynaptic complex, the Cα of G101 adopts conformational angles (ϕ = 95° and ψ = −162°) that are generally allowed only for glycines in a Ramachandran plot. In the synaptic complex, S101 shows allowed ϕ and ψ angles and hydrogen bonds (orange dashed line) to the E-helix backbone, and Y102 stacks on Q120 from another site I dimer. (**C**) Comparison of site I dimers in presynaptic (left) and synaptic (right) complexes. Site I dimers at both states are aligned by the dyad axis of dimer. The angles between an E-helix pair and between an E and D helix pair have changed between the two states. (**D**) Side views show the dimer interfaces between the left and right subunits that lie within a 4 Å contact distance with the E helix. A contact surface is shown for one of the interface partners. The interface of the site I dimer is grooved in the presynaptic state, and that of the tetramer is flat in the strand-exchange state.

presented to this synaptic tetramer by the rest of the synaptosome bound to sites II and III makes it stereochemically more likely that the two site I DNAs are binding parallel to each other. This orientation would require a recombination between the DNA half sites attached to the diagonal subunits. If this conclusion is correct, then the synaptic structure is entirely compatible with a subunit rotation model, which is particularly attractive because we have shown that the two halves of the complex that must move relative to each other are held together by an unusually flat and largely hydrophobic interface (Fig. 4D). This interface is formed as a consequence of synapsis, consistent with the hypothesis that it is functionally important. Furthermore, because this flat interface is roughly round, rotation of one flat interface about the orthogonal tetramer dyad axis results in a moderate variation in contact surface area from 880 Å^2 to 1200 Å^2 per dimer, consistent with the two dimers remaining hydrophobically attached throughout a rotation. Two complementary electrostatic interactions across the flat interface between the negative patches formed by D94 and D95 (*21*) and the positive patches formed by R125 and R121 that lie outside the hydrophobic patch could re-form after a 180° rotation to provide the recombinants the correct relative subunit orientation that would facilitate religation. Negative superhelicity of the DNA presumably drives the direction of rotation. Lastly, if the intermediate states of a subunit rotation are modeled and an energy minimization refinement carried out by using the program CNS (*24*), the energy is calculated to remain constant throughout the rotation (fig. S5). Only small motions of side chains are required to avoid steric clashes (movie S4).

A subunit rotation model for strand exchange is consistent with experiments on the topological changes associated with strand exchange (*5*–*7*) as well as with several crosslinking experiments. Mutation of V114 (*21*) to cysteine on the E helix results in crosslinking of the E helices across the flat interface when the C114 residues are oxidized (*20*). The crosslinked protein is able to cleave DNA to form the covalent intermediate but is unable to form the recombinant DNA product. Reducing the disulfide crosslinks restores the recombination activity. Because the sulfur atoms of the C114 residues are separated by about 4.0 Å, it seems unlikely that formation of the crosslink substantially distorts the protein conformation. It thus appears that strand exchange requires the movement of one antiparallel pair of subunits relative to the other pair that lies across the flat interface. This is consistent with a subunit rotation model of recombination. Furthermore, a Q-to-C mutation of Hin recombinase at an E helix residue that is homologous to residue 136 in γδ resolvase efficiently crosslinks when oxidized; oxidation stops religation of the cleaved DNA (*25*). Similarly, mutation of K136 to C136 in an activated γδ resolvase also crosslinks (fig. S4). The ability of Q134→C134 Hin or K136→C136 resolvase to be crosslinked can be explained by subunit rotation. Indeed, the two pairs of 136 residues are far apart in the present synaptic structure (Fig. 3C) but could be within crosslinkable distance across the flat interface after a 75° rotation of one antiparallel dimer relative to the other. The inability of crosslinked Hin Q134C to religate the covalently attacked, cleaved DNA is consistent with the crosslink stabilizing a rotated intermediate.

There are two issues that also need to be accommodated by the subunit rotation model. The products of recombination by the wild-type resolvase retain superhelicity, indicating that no dissociation of subunits occurs during strand exchange (*2*). Furthermore, the products are almost exclusively the result of a single 180° rotation (*2*). What prevents dissociation, and what limits the rotation? The total hydrophobic surface area buried upon formation of the flat interface varies from 1760 to 2400 Å^2, which is larger than the 1390 Å^2 buried upon formation of the trypsin-pancreatic trypsin inhibitor complex, whose dissociation constant is 10^{-13} M (*26*), which corresponds to a dissociation rate of about a day. Thus, it is plausible that the recombination rate is far faster than the rate of dissociation. Second, although the negative superhelicity of the DNA explains the direction of a single 180° rotation, subunit rotation does not easily explain why a single rotation dominates in a recombination assay using wild-type protein and *res* sites. Perhaps the protein assembly at sites II and III plays an unexplained role in controlling the change in linking number.

A domain swap model, which posits tetramer contacts are maintained by the E helices while a portion of the catalytic domain and the DNA are exchanged, is hard to reconcile with the current structure. First, the flexible linker (G101 and E102) through which two catalytic domains are to be swapped are 30 Å apart. Substantial unfolding of the E helix or catalytic domain would be required before the swap. Additionally, the DNA

Table 1. Crystallographic data and structure refinement statistics. MAD, multiwavelength anomalous diffraction; SAD, single wavelength anomalous diffraction; SIR, single isomorphous replacement; N/A, not applicable; blank entries, data not collected.

Space group	$P3_221$	$P2_12_12_1$
Unit cell dimension (Å)	125 by 125 by 127	117 by 125 by 138
Solvent content (%)	72	68
Native data		
Resolution (Å)	3.9	3.4
R_{sym} (overall/last shell)	0.094/0.738	0.068/>1.0
I/σ (overall/last shell)	11.9/1.5	25.7/2.0
Completeness (%)	94.9	99.8
Redundancy	2–3X	7–8X
Unique reflections	10,987	33,091
Derivative data		
$Pb(NO_3)_2$	3 wavelength MAD	
Resolution (Å)	4.1, 4.4, 4.6	
Cross *R* (%)	18.8–20.5	
Phasing power (centric/acentric)	0.83/1.21	
K_2PtCl_6	3 wavelength MAD	SIR
Resolution (Å)	3.8, 4.0, 4.2	3.4
Cross *R* (%)	19.9–20.4	24.8
Phasing power (centric/acentric)	0.73/1.42	1.20/2.13
$KAu(CN)_2$	SAD	
Resolution (Å)	4.2	
Cross *R* (%)	21.3	
Phasing power (centric/acentric)	0.73/1.05	
Bromine erivative 1	SAD	
Resolution (Å)	4.5	
Cross R (%)	25.0	
Phasing power (centric/acentric)	0.91/1.44	
Bromine derivative 2	SAD	
Resolution (Å)	4.8	
Cross *R* (%)	20.2	
Phasing power (centric/acentric)	0.50/1.71	
Se-Met derivative	SAD	
Resolution (Å)	5.8	
Cross *R* (%)	24.6	
Phasing power (centric/acentric)	N/A	
Overall figure of merit	0.60	0.42
Refinement statistics		
Resolution range	41–3.9	41–3.4
No. of atoms (protein/DNA)	2837/1428	5673/2847
RMSD bond length	0.009	0.009
RMSD bond angle	1.327	1.454
R	27.1	26.3
R_{free}	32.4	29.4

would have to dissociate from the DNA binding domain. Second, a processive 360° rotation, or multiples thereof, has been observed when using an artificial substrate that has two sites mismatching in the central region of site I (*27*) and is not easily explained by the domain swap model.

The synaptosome. How this synaptic tetramer bound to site I can be accommodated in a model of the complete synaptosome is unclear. The relationship between the synaptic tetramer seen here and the rest of the complex must differ from the model proposed earlier (*14*) for a synaptosome structure. That model was constructed making the assumption, on the basis of extensive genetic data (*12*, *13*), that dimers bound to sites I, II, and III of the same *res* site DNA are making the 2, 3′ interactions. There are, however, no biochemical or structural data to support the proposed interaction between the three resolvase dimers bound to each of the two *res* sites. Our attempts to model the synaptic complex at site I (via the R and R′ subunits) onto the structure of a site II and III complex presumed in earlier models (*10*, *14*) show that, although the dimensions roughly match, an interaction of the 2, 3′ type cannot be made.

We presume that resolvase dimers bound to sites II and III of two *res* sites contained in negatively supercoiled DNA are able to synapse and present two dimers bound to site I DNAs in such a manner that they promote the formation of the synaptic complex structure seen here. Perhaps two resolvase dimers are bound to the two site I DNAs in a presynaptic conformation initially and then form a synaptic tetramer at site I, facilitated by an increase in the local concentration and orientation of site I dimers by the rest of the synaptosome. However, the transition to the tetramer structure by the site I–bound resolvase subunits is likely accompanied by release of their 2,3′ interactions with the rest of the complex. It will doubtless be necessary to determine the structure of the whole synaptosome in order to understand how resolvase dimers bound to sites II and III promote synapsis at site I.

References and Notes

1. N. Craig, R. Craigie, M. Gellert, A. Lambowitz, Eds., *Mobile DNA II* [American Society for Microbiology (ASM), Washington, DC, 2002].
2. N. D. F. Grindley, in (*1*), p. 272.
3. R. R. Reed, N. D. F. Grindley, *Cell* **25**, 721 (1981).
4. G. F. Hatfull, N. D. F. Grindley, *Proc. Natl. Acad. Sci. U.S.A.* **83**, 5429 (1986).
5. S. A. Wasserman, J. M. Dungan, N. R. Cozzarelli, *Science* **229**, 171 (1985).
6. W. M. Stark, D. J. Sherratt, M. R. Boocock, *Cell* **58**, 779 (1989).
7. W. M. Stark, M. R. Boocock, *J. Mol. Biol.* **239**, 25 (1994).
8. M. R. Sanderson *et al.*, *Cell* **63**, 1323 (1990).
9. P. A. Rice, T. A. Steitz, *Structure* **2**, 371 (1994).
10. P. A. Rice, T. A. Steitz, *EMBO J.* **13**, 1514 (1994).
11. W. Yang, T. A. Steitz, *Cell* **82**, 193 (1995).
12. R. E. Hughes, G. F. Hatfull, P. Rice, T. A. Steitz, N. D. F. Grindley, *Cell* **63**, 1331 (1990).
13. L. L. Murley, N. D. F. Grindley, *Cell* **95**, 553 (1998).
14. G. J. Sarkis *et al.*, *Mol. Cell* **8**, 623 (2001).
15. F. Guo, D. N. Gopaul, G. D. van Duyne, *Nature* **389**, 40 (1997).
16. A. E. Leschziner, N. D. F. Grindley, *Mol. Cell* **12**, 775 (2003).
17. M. Nollmann, J. He, O. Byron, W. M. Stark, *Mol Cell.* **16**, 127 (2004).
18. P. H. Arnold, D. G. Blake, N. D. F. Grindley, M. R. Boocock, W. M. Stark, *EMBO J.* **18**, 1407 (1999).
19. Protein Data Bank codes are 1ZR2 and 1ZR4.
20. Materials and methods are available as supporting materials on *Science* Online.
21. Single-letter abbreviations for the amino acid residues are as follows: A, Ala; C, Cys; D, Asp; E, Glu; G, Gly; K, Lys; L, Leu; Q, Gln; R, Arg; S, Ser; V, Val; and Y, Tyr.
22. W. G. Krebs, M. Gerstein, *Nucleic Acids Res.* **28**, 1665 (2000).
23. Y. Chen, P. A. Rice, *Annu. Rev. Biophys. Biomol. Struct.* **32**, 135 (2003).
24. A. T. Brünger *et al.*, *Acta Crystallogr.* **D54**, 905 (1998).
25. G. Dhar, E. R. Sanders, R. C. Johnson, *Cell* **119**, 33 (2004).
26. C. Chothia, J. Janin, *Nature* **256**, 705 (1975).
27. M. J. McIlwraith, M. R. Boocock, W. M. Stark, *J. Mol. Biol.* **266**, 108 (1997).

28. This research was supported by NIH grants GM28470 to N.D.F.G. and GM57510 to T.A.S. The structures and the structure factors have been deposited in the Protein Data Bank under codes 1ZR2 and 1ZR4.

Supporting Online Material
www.sciencemag.org/cgi/content/full/1112064/DC1
SOM Text
Figs. S1 to S4
References and Notes
Movies S1 to S4

9 March 2005; accepted 15 June 2005
Published online 30 June 2005;
10.1126/science.1112064
Include this information when citing this paper.

REPORTS

Strong, Transparent, Multifunctional, Carbon Nanotube Sheets

Mei Zhang,[1] Shaoli Fang,[1] Anvar A. Zakhidov,[1] Sergey B. Lee,[1] Ali E. Aliev,[1] Christopher D. Williams,[1] Ken R. Atkinson,[2] Ray H. Baughman[1]*

Individual carbon nanotubes are like minute bits of string, and many trillions of these invisible strings must be assembled to make useful macroscopic articles. We demonstrated such assembly at rates above 7 meters per minute by cooperatively rotating carbon nanotubes in vertically oriented nanotube arrays (forests) and made 5-centimeter-wide, meter-long transparent sheets. These self-supporting nanotube sheets are initially formed as a highly anisotropic electronically conducting aerogel that can be densified into strong sheets that are as thin as 50 nanometers. The measured gravimetric strength of orthogonally oriented sheet arrays exceeds that of sheets of high-strength steel. These nanotube sheets have been used in laboratory demonstrations for the microwave bonding of plastics and for making transparent, highly elastomeric electrodes; planar sources of polarized broad-band radiation; conducting appliqués; and flexible organic light-emitting diodes.

Carbon nanotube sheets are usually made using techniques from the ancient art of papermaking, typically by a week-long filtration of nanotubes dispersed in water and then peeling the dried nanotubes as a layer from the filter (*1*, *2*). Variations of the filtration route produce ultrathin nanotube sheets that are highly transparent and highly conducting (*3*, *4*). Although filtration-produced sheets are normally isotropic within the sheet plane, sheets having partial nanotube alignment result from the application of high magnetic fields during filtration (*5*) and from mechanical rubbing of nanotubes that are vertically trapped in filter pores (*6*). In other important advances, nanotube sheets have been fabricated from a nanotube aerogel (*7*), by Langmuir-Blodgett deposition (*8*), by casting from oleum (*9*), and by spin coating (*10*).

We produced highly oriented, free-standing nanotube sheets by a solid-state process that appears to be scalable for continuous high-rate production. This development builds on previous advances in the dry-state spinning of nanotube yarns from forests (*11*) and the introduction of twist to increase sheet strength a thousandfold (*12*).

[1]NanoTech Institute, University of Texas at Dallas, Richardson, TX 75083–0688, USA. [2]Commonwealth Scientific and Industrial Research Organization Textile & Fibre Technology, Post Office Box 21, Belmont, Victoria 3216, Australia.

*To whom correspondence should be addressed. E-mail: ray.baughman@utdallas.edu

These transparent nanotube sheets were drawn from a sidewall of multiwalled nanotube (MWNT) forests that were synthesized by catalytic chemical vapor deposition, using acetylene gas as the carbon source (*12*). The MWNTs were ~10 nm in diameter, and the range of investigated forest heights was 70 to 300 μm. Draw was initiated using an adhesive strip, like that on a 3M Post-it Note, to contact MWNTs teased from the forest sidewall. Meter-long sheets, up to 5 cm wide, were then made at 1 m/min by hand drawing (Fig. 1A and movie S1). Despite a measured areal density of only ~2.7 μg/cm^2, these 500-cm^2 sheets were self-supporting during draw. A 1-cm length of 245-μm-high forest converts to about a 3-m-long freestanding MWNT sheet. The sheet production rate was increased to 5 m/min by using an automated linear translation stage to accomplish draw (Fig. 1B) and was increased to up to 10 m/min by winding the sheet on a rotating centimeter-diameter plastic cylinder. The sheet fabrication process is quite robust, and no fundamental limitations on sheet width and length are apparent: The obtained 5-cm sheet width equaled the forest width when the draw rate was about 5 m/min or lower. At constant draw rates above ~7 m/min, the sheets progressively narrowed, and MWNT fibrils began to break at the intersection between the sheet sides and the forest.

This draw process does not work for all MWNT forests, and the maximum allowable draw rate depends on the structure of the forest. Intermittent bundling within the forest seems to be important, in which individual nanotubes migrate from one bundle of a few nanotubes to another. Bundled nanotubes are simultaneously pulled from different elevations in the forest sidewall, so that they join with bundled nanotubes that have reached the top and bottom of the forest, thereby minimizing breaks in the resulting fibrils (Fig. 1, B and C). Disordered regions exist at the top and bottom of the forests, where a fraction of the nanotubes form loops, which might help maintain continuity. For forests having similar topology, the highest forests were easiest to draw into sheets, probably because increasing the nanotube length increases interfibril mechanical coupling within the sheets.

Nanotube orientation is evident in the micrograph of Fig. 1B and in ultraviolet (UV)–visible absorption and Raman scattering measurements for as-drawn single MWNT sheets and sheet stacks. Depending on the sample, the ratio of Raman intensity (632.8-nm excitation) of the G band for polarization parallel and perpendicular to the draw direction is between 5.5 and 7.0 for the VV configuration (parallel polarization for incident light and Raman signal), which corresponds to polarization degrees of 0.69 and 0.75, respectively, for the investigated four-sheet stacks (fig. S1). Ignoring the effect of light scattering, the ratio of absorption coefficients for parallel and perpendicular polarizations for the as-drawn single sheet was 4.1 at 633 nm and monotonically increased to 6.0 at 2.2 μm.

The thickness of the as-produced MWNT sheet increased with increasing forest height and was ~18 μm in scanning electron microscopy (SEM) images of a sheet drawn from a 245-μm-high forest. From this thickness and the measured areal sheet density of ~2.7 μg/cm^2, the volumetric density was 0.0015 g/cm^3. Hence, the as-produced sheets are an electronically conducting, highly anisotropic aerogel. These sheets, which can easily be stacked (Fig. 1D), can support millimeter-sized liquid droplets that are 50,000 times more massive than the supporting sheet region in contact with the droplet (Fig. 1E).

We can easily densify these highly anisotropic aerogel sheets into highly oriented sheets having a thickness of 50 nm (*13*) and a density of ~0.5 g/cm^3. We obtain this 360-fold density increase simply by causing the as-produced sheet to adhere to a planar substrate (such as glass, many plastics, silicon, gold, copper, aluminum, or steel) by contact, vertically immersing the substrate with the attached MWNT sheet in a liquid (such as ethanol) along the nanotube alignment direction, and then retracting the substrate from the liquid. Surface tension effects during ethanol evaporation shrink the aerogel sheet thickness to ~50 nm. SEM micrographs taken normal to the sheet plane suggest a decrease in nanotube orientation as a result of densification. This observation is deceptive: The collapse of ~20-μm sheets to ~50-nm sheets without changes in lateral sheet dimensions means that out-of-plane deviations in nanotube orientation become in-plane deviations that are noticeable in the SEM micrographs. The aerogel sheets can be effectively glued to a substrate by contacting selected regions with ethanol and allowing evaporation to densify the aerogel sheet. Adhesion increases because the collapse of aerogel thickness increases the contact area between the nanotubes and the substrate.

The sheet resistance in the draw direction changes by <10% upon sheet densification by a factor of ~360, which increases sheet transparency (Fig. 2, A and B). Although the

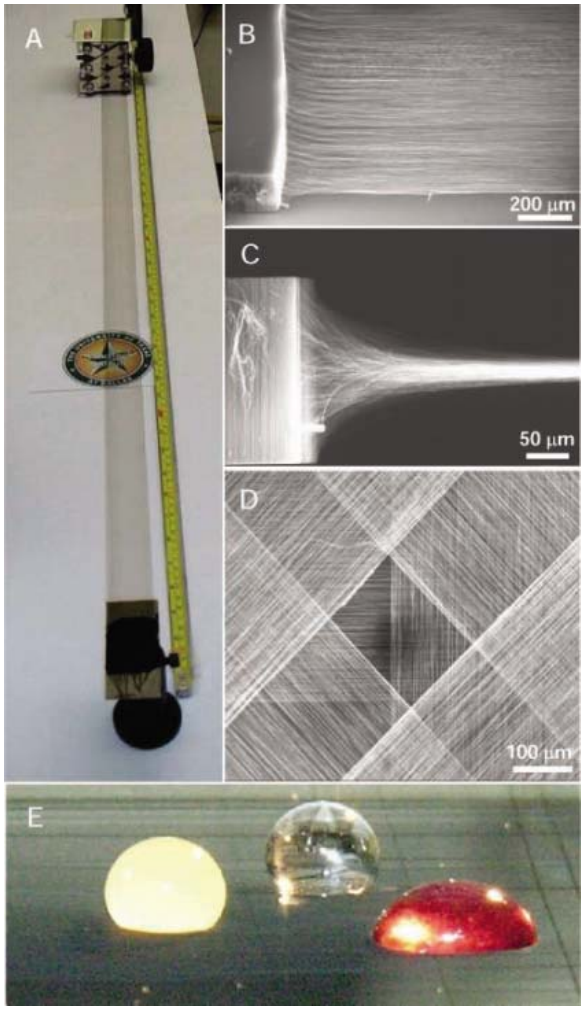

Fig. 1. MWNT forest conversion into sheets and assemblies of those sheets. (**A**) Photograph of a self-supporting 3.4-cm-wide, meter-long MWNT sheet that has been hand drawn from a nanotube forest at an average rate of 1 m/min. Its transparency is illustrated by the visibility of the NanoTech Institute logo that is behind the MWNT sheet. (**B**) SEM image, at a 35° angle with respect to the forest plane, capturing a MWNT forest being drawn into a sheet. (**C**) SEM micrograph showing the cooperative 90° rotation of MWNTs in a forest to form a sheet. (**D**) SEM micrograph of a two-dimensionally re-reinforced structure fabricated by overlaying four nanotube sheets with a 45° shift in orientation between successive sheets. The dark circle is the shadow of the in-lens detector. (**E**) Photograph showing two orthogonal as-drawn nanotube sheets supporting droplets of water (~2.5 mm in diameter), orange juice, and grape juice, where the mass of the droplet is up to 50,000 times that of the contacting nanotube sheets. The aerogel sheet regions under the aqueous droplets are densified during water evaporation.

anisotropy ratio for sheet resistance decreases from 50 to 70 for the undensified sheets to 10 to 20 for the densified sheets, this anisotropy ratio for the densified sheets is nearly temperature-invariant. In fact, the temperature dependence of sheet resistivity is nearly the same for the forest-drawn densified nanotube sheets and for sheets made by the filtration route using the same forest-grown MWNTs, and is much smaller than for single-walled nanotube (SWNT) sheets fabricated by filtration (*14*) (Fig. 2A). In addition, the low-frequency (f) noise power density in the draw direction for a densified forest-drawn sheet is 10^4 and is 10 times lower than for ordinary filtration-produced sheets of SWNTs and MWNTs, respectively (Fig. 2C). The literature reports high $1/f$ noise for individual SWNTs and SWNT mats (*15*) and low noise having either a $1/f$ (*16*) or a $1/f^2$ dependence (*17*) for individual MWNTs. In contrast with the latter single-MWNT results, the noise power density for our densified MWNT sheets has a $1/f$ frequency dependence.

A possible explanation for these electronic properties is found in SEM micrographs (fig. S2), which indicate that up to ~50-nm-wide fibrils (containing many bundled MWNTs) laterally fork and then eventually recombine with the forked legs of other fibrils to form a laterally extended network. High resistance of interfibril contacts formed during densification, as compared with those within the original fibril network, might explain why sheet resistance changes little as a result of over 300-fold sheet densification. Because low-frequency noise inversely depends on the number of atoms at resistive contacts (*15*), the low $1/f$ noise of the solid-state fabricated MWNT sheets could result from the long path length where MWNTs overlap within the fibril network. Whatever the explanation for these properties, the low electrical noise and low temperature coefficient of resistivity for the forest-drawn sheets could be important for electronic applications such as chemical sensors.

The densified nanotube sheets showed high transparency in combination with usable electrical conductivity, a combination needed for such applications as displays, video recorders, solar cells, and solid-state lighting (*3*). The sheet resistivity was ~700 ohms per square in the draw direction before and after densification for the forest-drawn sheets, and 10 to 20 times higher in the orthogonal in-plane direction for the densified sheet. The transmittance for the densified MWNT sheet was >85% for perpendicular polarization, >65% for parallel polarization between 400 nm and 2 μm, and >85% for unpolarized radiation between 1.5 and 10 μm (Fig. 2B). These MWNT sheets will adhere to transparencies made of poly(ethylene terephthalate) and to silicone rubber sheets, thereby providing transparent bilayer composites that can be bent in any direction without causing a substantial decrease in electrical conductivity (movie S2). This ability to bend without degradation of electronic conductivity is important for flexible electronic circuits and is not found in conventional transparent conductors such as indium tin oxide (ITO).

After an initial conditioning strain cycle, in which conductivity decreased ~6% with increasing strain, the nanotube/elastomer sheet was repeatably deformable over 100% strain (fig. S3) without causing a substantial change in conductance (*18*). Ordinary conductors cannot undergo nearly such large strains without losing electrical contact with the actuating material. Although conducting greases are used to maintain electrical contact to electrostrictive actuator materials that generate 100% or higher strains (*19*), these greases are not suitable for use as electrodes for stacks of electrostrictive sheets that can generate large forces and high strains without requiring several-thousand-volt applied potentials.

Although no alternative solid-state conductors combine elastic deformability to 100% strain and essentially constant electronic conductivity, transparent doped SWNT sheets having ~20 times higher electrical conductivity are known (*3*). The transparency of those SWNT sheets (either doped or undoped) strongly depends on wavelength in the visible and near-infrared. Thus, the monotonic increase in transmittance with increasing wavelength (Fig. 2B) of our MWNT sheets provides an advantage for broadband applications. Also, the electrical conductivity of those SWNT sheets decreases 10 times upon dedoping. Extension of the present solid-state sheet fabrication technology to doped MWNTs and doped SWNTs is desirable in order to increase electrical conductivity for transparent conductor applications, and even the latter appears feasible because of the recent development of 2.5-mm-high nanotube forests comprising SWNTs (*20*).

The forest-drawn MWNT sheets can be conveniently assembled into biaxially reinforced sheet arrays (Fig. 1D) and as conducting layers on nonplanar surfaces, such as by helically wrapping a sheet strip on a millimeter- or larger-diameter cylinder (fig. S4). Chiral structures, which will likely be optically active for long infrared and microwave wavelengths, can be made by stacking parallel sheets so that the orientation direction varies helically along the stack thickness and then densifying the stacked array so that the individual sheet thickness is ~50 nm.

Especially considering the absence of polymer binder, the mechanical properties of the

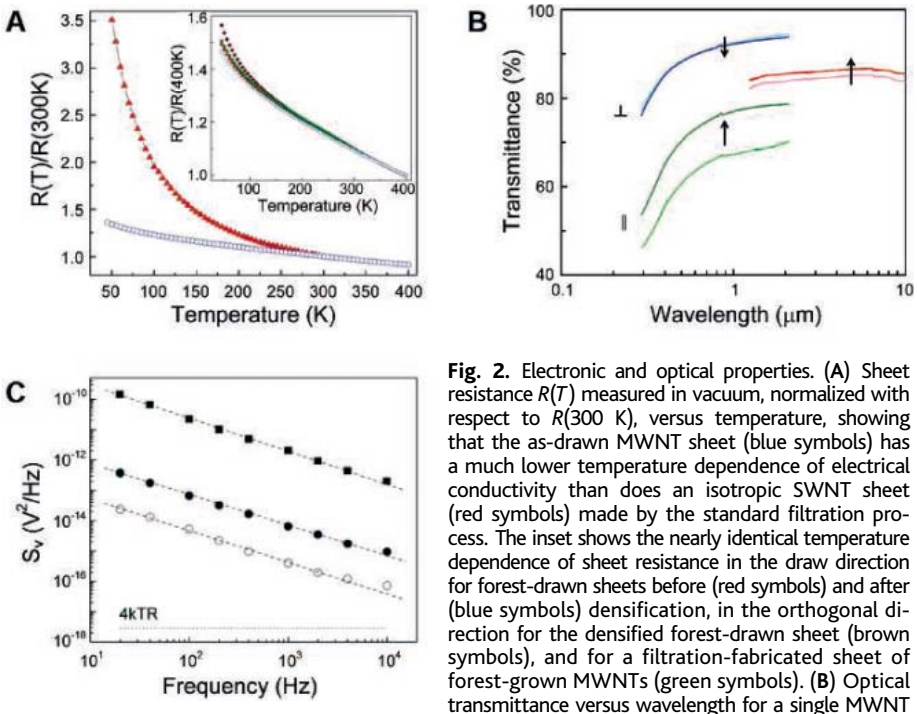

Fig. 2. Electronic and optical properties. (**A**) Sheet resistance $R(T)$ measured in vacuum, normalized with respect to R(300 K), versus temperature, showing that the as-drawn MWNT sheet (blue symbols) has a much lower temperature dependence of electrical conductivity than does an isotropic SWNT sheet (red symbols) made by the standard filtration process. The inset shows the nearly identical temperature dependence of sheet resistance in the draw direction for forest-drawn sheets before (red symbols) and after (blue symbols) densification, in the orthogonal direction for the densified forest-drawn sheet (brown symbols), and for a filtration-fabricated sheet of forest-grown MWNTs (green symbols). (**B**) Optical transmittance versus wavelength for a single MWNT sheet, before and after densification, for light polarized perpendicular to (⊥) and parallel to (∥) the draw direction and for unpolarized light (the two curves on the right), where the arrow points from the data for the undensified sample to those for the densified sample. (**C**) Noise power density (S_V, measured in air for 10-mA biasing) versus frequency (f) for a densified forest-drawn MWNT sheet (open circles), compared with that for ordinary filtration-produced MWNT sheets (solid circles) and SWNT sheets (solid rectangles) having the same 40-ohm resistance. The dashed lines are data fits for a $1/f^{\alpha}$ dependence, where α is 0.98 ± 0.04, 0.97 ± 0.02, and 1.20 ± 0.02 for the lower, middle, and upper data sets, respectively. The lower-limit noise power at temperature T (the product of 4 kT and the sample resistance R, where k is Boltzmann's constant) is indicated by the horizontal dotted line.

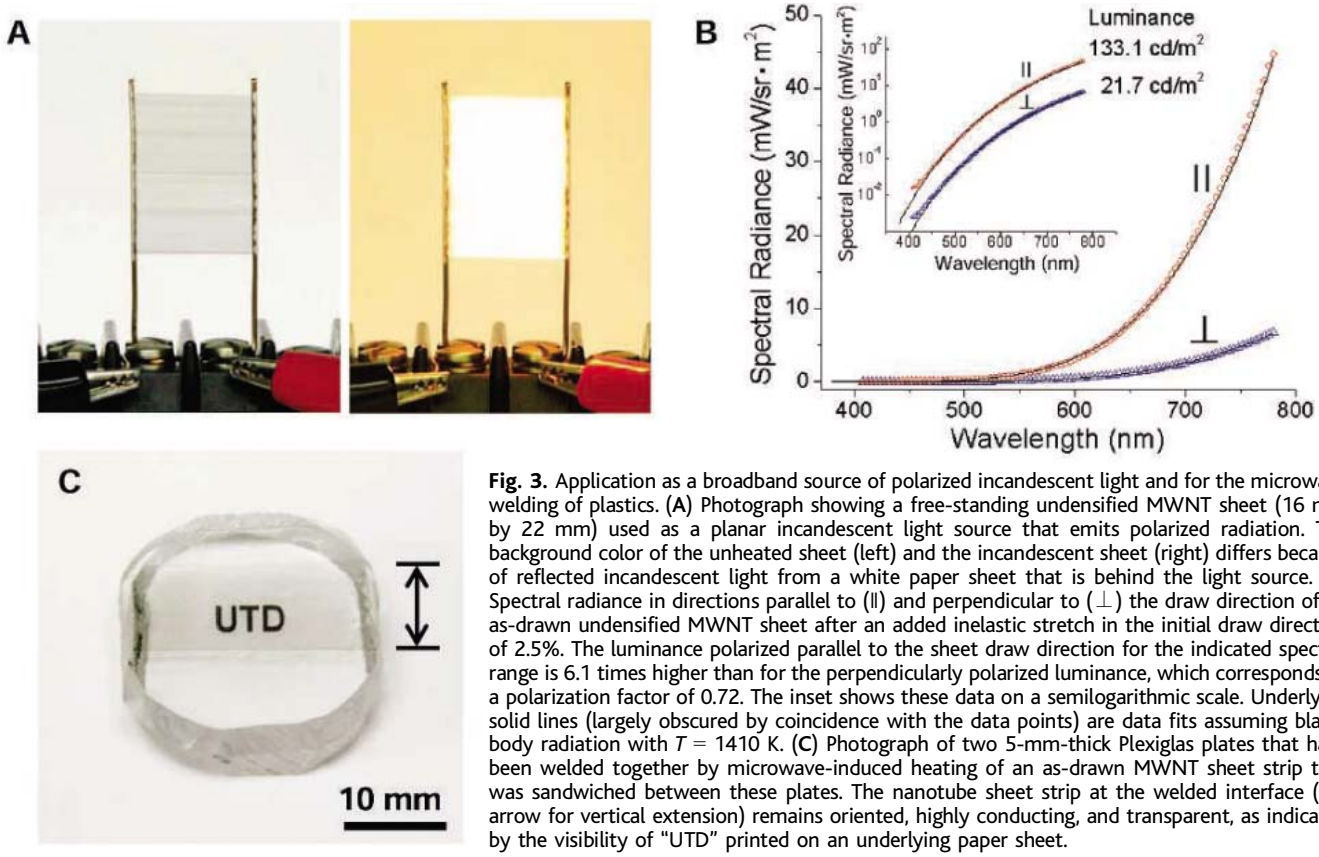

Fig. 3. Application as a broadband source of polarized incandescent light and for the microwave welding of plastics. (**A**) Photograph showing a free-standing undensified MWNT sheet (16 mm by 22 mm) used as a planar incandescent light source that emits polarized radiation. The background color of the unheated sheet (left) and the incandescent sheet (right) differs because of reflected incandescent light from a white paper sheet that is behind the light source. (**B**) Spectral radiance in directions parallel to (∥) and perpendicular to (⊥) the draw direction of an as-drawn undensified MWNT sheet after an added inelastic stretch in the initial draw direction of 2.5%. The luminance polarized parallel to the sheet draw direction for the indicated spectral range is 6.1 times higher than for the perpendicularly polarized luminance, which corresponds to a polarization factor of 0.72. The inset shows these data on a semilogarithmic scale. Underlying solid lines (largely obscured by coincidence with the data points) are data fits assuming black-body radiation with T = 1410 K. (**C**) Photograph of two 5-mm-thick Plexiglas plates that have been welded together by microwave-induced heating of an as-drawn MWNT sheet strip that was sandwiched between these plates. The nanotube sheet strip at the welded interface (see arrow for vertical extension) remains oriented, highly conducting, and transparent, as indicated by the visibility of "UTD" printed on an underlying paper sheet.

aerogel-like and densified MWNT sheets are unexpectedly high, which is probably a consequence of the interconnected fibril network (fig. S2). The density-normalized mechanical strength is much more accurately determined than mechanical strength, because the sheet thickness is less reliably measured than the ratio of maximum force to mass-per-length in the stretch direction. Stacks of undensified sheets have an observed tensile strength of between 120 and 144 MPa/(g/cm^3) (fig. S5, A and B). A densified stack containing 18 identically oriented sheets had a strength of 465 MPa/(g/cm^3), which decreased to 175 MPa/(g/cm^3) when neighboring sheets in the stack were orthogonally oriented to make a densified biaxial structure. These density-normalized strengths are already comparable to or greater than the ~160 MPa/(g/cm^3) strength of the Mylar and Kapton films used for ultralight air vehicles and proposed for use in solar sails for space applications (*21*) and those for ultra–high-strength steel [~125 MPa/(g/cm^3)] and aluminum alloy [~250 MPa/(g/cm^3)] sheets.

Sheets generally have much lower limiting strengths than do fibers of the same material. However, at a value of 465 MPa/(g/cm^3), the tensile strength of the densified MWNT sheet is comparable to or exceeds reported values for nanotube fibers and yarns that do not include a binding agent: 575 MPa/(g/cm^3) for forest-spun twisted MWNT yarns (*12*), 500 MPa/(g/cm^3) for aerogel-spun yarns (*7*), 105 MPa/(g/cm^3) for SWNT yarns spun from superacids (*22*), and 65 MPa/(g/cm^3) for SWNT yarns spun using an acidic coagulation bath (*23*). Order-of-magnitude or greater increases in mechanical strength have been observed when internanotube coupling is enhanced by polymer incorporation into nanotube sheets and yarns (*23*–*26*), and similar strength increases might be achievable by infiltration of suitable polymers into the present MWNT sheets.

Initial results suggest additional promising applications. One is as a stable planar source of polarized UV, visible, and infrared incandescent light (Fig. 3, A and B) for use in sensors, infrared beacons, infrared imaging, and reference signals for device calibration. The degree of polarization of emitted radiation for 2.5% stretched as-drawn sheets increases from 0.71 at 500 nm to 0.74 at 780 nm (Fig. 3B), which is substantially higher than the degree of polarization (0.33 for 500 to 900 nm) previously reported for a 600-μm-long MWNT bundle with an emitting length of ~80 μm (*27*). The wavelength dependence of light intensity for both polarizations fits the functional form expected for black-body radiation, and the degree of polarization does not significantly depend on sheet temperature for the observed temperature range between 1000 and 1600 K. Cost and efficiency benefits result from decreasing or eliminating the need for a polarizer, and the MWNT sheet provides spatially uniform emission over a broad spectral range that is otherwise hard to achieve. The low heat capacity of these very-low-mass incandescent emitters means that they can turn on and off within the observed 0.1 ms or less in vacuum and provide current modulated light output on a shorter time scale.

By simply contacting the as-drawn MWNT sheets to ordinary adhesive tape, we have made optically transparent adhesive appliqués that could be used for electrical heating and for providing microwave absorption (*14*). Because of MWNT sheet porosity, the peel strength is largely maintained when an undensified MWNT sheet is laminated between an adhesive tape and a contacted plastic or metal surface (*14*) (fig. S6). We have used the known microwave absorption capability of MWNTs (*28*, *29*) to demonstrate another possible application: polymer welding through heating of a transparent MWNT sheet that is sandwiched between plastic parts (*14*). Figure 3C shows two 5-mm-thick Plexiglas (polymethyl methacrylate) plates that were welded together using microwave heating of a sandwiched undensified MWNT sheet to provide a strong, uniform, and transparent interface in which nanotube orientation and sheet electrical conductivity are little changed. The combination of high transparency and ultrahigh thermal stability provides advantages

for microwave-based welding not found in the conducting polymers (*30*). This microwave heating process could be used to make polymer composites from stacks of polymer sheets that are separated by nanotube sheets, car windows that are electrically heated, or antennas in car windows that have high transparency.

The work function of these transparent MWNT sheets (~5.2 eV) is slightly higher than that of the ITO typically used as the transparent hole-injecting electrode in organic light-emitting diodes (OLEDs), and these sheets have the additional benefits of being porous and flexible. MWNT sheets made with previous techniques have not been successfully used for optically transmissive, hole-injecting layers in OLEDs: The sheet thickness and surface roughness dwarf the typical 100-nm layer thickness of emissive layers needed for OLEDs (*31*), thereby causing interelectrode shorts; and in thicker devices, the unbalanced hole and electron currents prevent light emission. However, black sheets of solution-spun MWNTs have been used as nontransmissive hole-collecting electrodes in solar cells (*10*), and transparent p-type SWNT sheets have been used as hole-injection electrodes in inorganic LEDs based on gallium nitride (*32*).

We have taken advantage of the nanometer-scale thickness, transparency, flexibility, porosity, and high work function of our densified MWNT sheets to demonstrate polymer-based OLEDs on both flexible plastic and rigid glass substrates (*14*). Hole injection occurs over the high-surface-area interior of the nanoporous nanotube electrode, as opposed to at a planar interface in the previous inorganic LEDs (*32*). The onset voltage for emission is quite low (2.4 V, about the same as for the highest-performance ITO in similar devices), and rather bright electroluminescence was obtained (up to 500 cd/m^2) (fig. S7). The emitted light is slightly polarized, but in an orthogonal direction from that for the above incandescent light source, because the MWNT sheet acts as a polarizer. If a polymeric light-emitting layer were aligned using known methods (*33*) to provide emission in the same polarization direction, absorption due to the MWNT hole injector could be minimized, which is not possible for conventional ITO hole-injecting electrodes.

Although solution- or melt-based processing becomes increasingly difficult as nanofiber length increases, the opposite is true for the present solid-state sheet fabrication process: 300-μm-long nanotubes are easier to convert into sheets than are 70-μm-long nanotubes. Also, ultrasonication used for nanotube dispersion in solution-based processing decreases nanotube length, and this degradative step is absent from the present sheet fabrication process. These are important advantages of the present technology, because long, high-perfection nanotubes are needed for maximizing electrical and thermal conductivities and mechanical properties.

References and Notes

1. A. G. Rinzler *et al.*, *Appl. Phys. A* **67**, 29 (1998).
2. M. Endo *et al.*, *Nature* **433**, 476 (2005).
3. Z. Wu *et al.*, *Science* **305**, 1273 (2004).
4. L. Hu, D. S. Hecht, G. Grüner, *Nano Lett.* **4**, 2513 (2004).
5. J. E. Fischer *et al.*, *J. Appl. Phys.* **93**, 2157 (2003).
6. W. A. De Heer *et al.*, *Science* **268**, 845 (1995).
7. Y. Li, I. A. Kinloch, A. H. Windle, *Science* **304**, 276 (2004).
8. Y. Kim *et al.*, *Jpn. J. Appl. Phys.* **42**, 7629 (2003).
9. T. V. Sreekumar *et al.*, *Chem. Mater.* **15**, 175 (2003).
10. H. Ago, K. Petritsch, M. S. P. Shaffer, A. H. Windle, R. H. Friend, *Adv. Mater.* **11**, 1281 (1999).
11. K. Jiang, Q. Li, S. Fan, *Nature* **419**, 801 (2002).
12. M. Zhang, K. R. Atkinson, R. H. Baughman, *Science* **306**, 1358 (2004).
13. The per-sheet thickness measured by stylus profilometer varied from ~50 to ~150 nm, depending on forest height and draw and densification conditions. Atomic force microscopy provides a sheet thickness of down to 30 to 50 nm, which is close to the maximum width of fibrils in the sheet, which can be far from cylindrical.
14. See supporting data on *Science* Online.
15. P. G. Collins, M. S. Fuhrer, A. Zettl, *Appl. Phys. Lett.* **76**, 894 (2000).
16. H. Ouacha *et al.*, *Appl. Phys. Lett.* **80**, 1055 (2002).
17. L. Roschier, R. Tarkiainen, M. Ahlskog, M. Paalanen, P. Hakonen, *Appl. Phys. Lett.* **78**, 3295 (2001).
18. A 1-mm-thick sheet of silicone rubber (ECOFLEX 0040 from Smooth-On) was stretched to 105% strain, and then a single as-drawn MWNT sheet was laid over it to provide self-generated adhesive contact before strain relaxation. The initial sheet resistance of the obtained unloaded silicone rubber/MWNT sheet composite was 755 ohms per square. However, after an initial increase in resistance by ~6%, the resistance changed less than 3% during the subsequent four strain cycles to 100% strain.
19. R. Pelrine, R. Kornbluh, Q. Pei, J. Joseph, *Science* **287**, 836 (2000).
20. K. Hata *et al.*, *Science* **306**, 1362 (2004).
21. D. E. Edwards *et al.*, *High Perf. Polymers* **16**, 277 (2004).
22. L. M. Ericson *et al.*, *Science* **305**, 1447 (2004).
23. M. E. Kozlov *et al.*, *Adv. Mater.* **17**, 614 (2005).
24. J. N. Coleman *et al.*, *Appl. Phys. Lett.* **82**, 1682 (2003).
25. B. Vigolo, P. Poulin, M. Lucas, P. Launois, P. Bernier, *Appl. Phys. Lett.* **81**, 1210 (2002).
26. A. B. Dalton *et al.*, *Nature* **423**, 703 (2003).
27. P. Li *et al.*, *Appl. Phys. Lett.* **82**, 1763 (2003).
28. P. C. P. Watts, W.-K. Hsu, A. Barnes, B. Chambers, *Adv. Mater.* **15**, 600 (2003).
29. J. Wu, L. Kong, *Appl. Phys. Lett.* **84**, 4956 (2004).
30. A. J. Epstein, A. G. MacDiarmid, *Synth. Metals* **69**, 179 (1995).
31. D. B. Romero, M. Carrard, W. De Heer, L. Zuppiroli, *Adv. Mater.* **8**, 899 (1996).
32. K. Lee, Z. Wu, Z. Chen, F. Ren, S. J. Pearton, A. G. Rinzler, *Nano Lett.* **4**, 911 (2004).
33. K. S. Whitehead, M. Grell, D. D. C. Bradley, M. Jandke, P. Strohriegl, *Appl. Phys. Lett.* **76**, 2946 (2000).

34. Supported by Defense Advanced Research Projects Agency/U.S. Army Research Office grant W911NF-04-1-0174, the Texas Advanced Technology Program grant 009741-0130-2003, the Air Force STTR program on topic AF04-TO20, Air Force grant F49620-03-1-0164, Robert A. Welch Foundation grant AT-0029, and the Strategic Partnership for Research in Nanotechnology consortium in Texas. The authors thank J. P. Ferraris and M. Zhou for the synthesis of the emissive polymer used for the OLEDs, A. Kuznetsov for assistance with OLED preparation, and V. H. Ebron for assistance with the microwave welding.

Supporting Online Material

www.sciencemag.org/cgi/content/full/309/5738/1215/DC1
Materials and Methods
Figs. S1 to S7
References
Movies S1 and S2

25 May 2005; accepted 13 July 2005
10.1126/science.1115311

Understanding the Infrared Spectrum of Bare CH_5^+

Oskar Asvany,[1]* Padma Kumar P,[2]* Britta Redlich,[3] Ilka Hegemann,[2] Stephan Schlemmer,[1,4] Dominik Marx[2]†

Protonated methane, CH_5^+, continues to elude definitive structural assignment, as large-amplitude vibrations and hydrogen scrambling challenge both theory and experiment. Here, the infrared spectrum of bare CH_5^+ is presented, as detected by reaction with carbon dioxide gas after resonant excitation by the free electron laser at the FELIX facility in the Netherlands. Comparison of the experimental spectrum at ~110 kelvin to finite-temperature infrared spectra, calculated by ab initio molecular dynamics, supports fluxionality of bare CH_5^+ under experimental conditions and provides a dynamical mechanism for exchange of hydrogens between CH_3 tripod positions and the three-center bonded H_2 moiety, which eventually leads to full hydrogen scrambling. The possibility of artificially freezing out scrambling and internal rotation in the simulations allowed assignment of the infrared spectrum despite this pronounced fluxionality.

Protonated methane, CH_5^+, is of great interest in vibrational spectroscopy (*1–4*) as the prototype of hypercoordinated carbon and three-center two-electron bonding (*5*, *6*). The equilibrium structure—that is, the global minimum of its potential energy surface (PES)—can be viewed as a CH_3 tripod with a H_2 moiety attached to the carbon in an eclipsed C_s configuration, e-C_s, via a three-center bond (*7*). However, rapid hydrogen scrambling has called into question the notion of assigning it such a traditional molecular structure (*8–11*), despite the stability of CH_5^+ once it is formed (*12*). This fluxionality has been traced back

to an unusually shallow PES (*13*–*15*). A staggered structure, s-C_s, only ~0.1 kcal/mol higher in energy (*15*) than e-C_s, is reached by internal rotation of the H_2 moiety about the quasi-C_3 axis while keeping the three-center bonding pattern. Most important, a structure where the H_2 moiety is broken apart—a C_{2v} first-order saddle point characterized by four-center four-electron bonding (*7*)—is only ~0.8 kcal/mol (corresponding to ~300 cm^{-1} or 0.03 eV) above the e-C_s ground state (*15*). This allows for large-amplitude motion upon quantum mechanical and/or thermal rotational-vibrational excitation (*16*–*23*).

Without direct access to real-space structure and dynamics (*24*), the only link between experiment and theory to date has been spectroscopy. After considerable experimental effort (*1*, *2*), including a pioneering infrared (IR) study (*3*) of the microsolvated cation $CH_5^+ \cdot (H_2)_{n\geq 1}$, the high-frequency wing of the C-H stretching band of bare CH_5^+ was recently published (*4*). However, no assignment or even qualitative understanding could be offered (*4*); hence, clear evidence of fluxionality, challenged by mass spectrometric data (*25*, *26*), is still lacking. On the other hand, given a molecule that continuously changes not only its shape and the symmetry of its instantaneous structure but also its chemical bonding topology through rapid intramolecular dynamics, it is unclear how the IR spectrum would look or how such a spectrum could be assigned once known.

Here, the IR spectrum of bare, cold CH_5^+ could be studied by combining a low-temperature 22-pole ion trap with the large tuning range of the free electron laser (FEL) at the FELIX facility (*27*, *28*) and the laser-induced reaction (LIR) technique. In LIR, infrared excitation induces a bimolecular reaction of the parent molecule, CH_5^+, and the amount of product formed is a measure of the absorption intensity as a function of the excitation wavelength. The major benefits of LIR are the storage of mass-selected ions at variable temperatures, 10 to 300 K, in conjunction with mass analysis of product ions that are detected with close to perfect efficiency. Thus, LIR can be much more sensitive than traditional absorption detection techniques. The experimental spectra are complemented by the calculation of anharmonic IR spectra via ab initio molecular dynamics (*29*–*31*). Dissecting the trajectories obtained in full dimensionality elucidates the scrambling mechanism and its effect on the spectrum. Furthermore, comparison of the computed and the measured stretching and bending modes strongly supports fluxionality of bare CH_5^+ under experimental conditions. Most notably, the computational strategy of artificially freezing out scrambling and internal rotation paves the way for assigning the IR spectrum.

In the experiment, mass-selected ions are stored in a variable-temperature 22-pole ion trap (Fig. 1). In the trap they interact with reactant gas of constant number density and with the radiation field of an IR laser held at a constant wavelength. After a trapping time of several seconds, reactant and product ions are extracted, mass-analyzed, and detected with near-100% collection efficiency. An action spectrum of the parent ion is obtained by recording the number of mass-selected product ions as a function of the IR wavelength. In previous LIR benchmarks (*32*–*34*), a small endothermicity hindered the reaction of interest but was overcome by the resonant excitation of the parent ion. For the spectroscopy of CH_5^+, the endothermic proton transfer reaction $CH_5^+ + CO_2 \xrightarrow{h\nu} CH_4 + OCOH^+$ was chosen (*35*). The difference in proton affinities of CO_2 and CH_4 amounts to an endothermicity of ~0.7 kcal/mol ≈ 250 cm^{-1}, implying that the reaction proceeds very slowly at the trap temperature of 110 (±5) K. With each filling of the 22-pole trap, an ensemble of about 3000 CH_5^+ ions was stored for 4 s in the cold CO_2 gas environment and exposed to the tunable IR light of the FELIX FEL (*27*, *28*). After this storage period, the number of $OCOH^+$ ions produced by LIR was recorded, the laser was tuned to the next frequency, and the trap was filled again. The FEL was operated at its maximum repetition rate of 10 Hz with pulses having a typical length of 7 μs and an energy content varying from 10 to 30 mJ (at user station) depending on the wavelength region. The bandwidth of the FELIX FEL is adjustable but always transform-limited; here, the resolution was set to ~0.5% full width at half maximum of the central frequency at a given wavelength.

The product ion counts were background-corrected and divided by the spectral energy density $\rho = P/(A \cdot c \cdot \Delta\nu)$, where P, A, and $\Delta\nu$ are the power, area, and bandwidth of the laser beam, respectively, and c is speed of light. The resulting normalized action spectrum corresponds to the product of the Einstein $B(\nu)$ coefficient, the population g of the accessible rotational states, and the reaction probability of the excited CH_5^+ with neutral CO_2 gas (*35*). To a first approximation, this reaction probability is proportional to the rate coefficient $k^*(\nu)$ of the excited ion, which, unfortunately, is unknown. Because of the limited resolution of the laser, $\Delta\nu \propto \nu$, an increasing number of rotational states is excited simultaneously with increasing photon energy, $h\nu$. Assuming a linear relationship between g and the laser bandwidth, $g \sim \Delta\nu \sim \nu$, the LIR signal should be proportional to the product of the absorption cross section $\alpha(\nu)$ and $k^*(\nu)$.

The resulting experimental spectrum (Fig. 2A) consists of a very broad high-frequency band extending from about 2200 cm^{-1} beyond 3200 cm^{-1}; only the dominant peak close to 3000 cm^{-1} was observed earlier (*3*, *4*). The frequency range probed here reveals important additional features: Substructures extending down to about 2200 cm^{-1} are discernible at the low-frequency wing of the dominant C-H stretching peak. Furthermore, a broad and featureless unimodal bending band is found near 1250 cm^{-1}. Note that the reaction probability

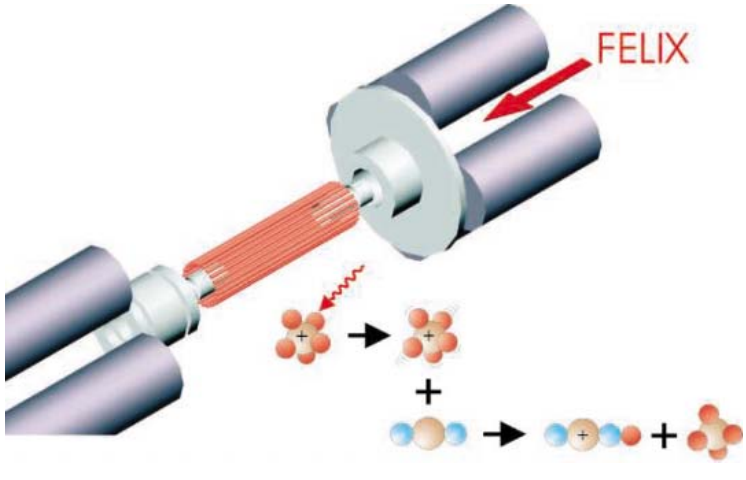

Fig. 1. Schematic of the 22-pole ion trap as used for LIR. The mass-selected ensemble of ions is injected into the trap from the left and kept there for several seconds. Once captured, the ions are cooled down to the trap temperature (110 K) by a short, intense helium pulse. In the trap, the ions are exposed to reactant gas molecules and tunable laser light (coming from the right through the axially transparent setup). The result of this interaction is detected by extracting the stored ion cloud to the right into a mass filter and counting the number of product ions. An action spectrum of the stored parent ions is recorded by repeating this process while scanning the IR laser. Color code: orange, carbon; red, hydrogen; blue, oxygen.

[1]Leiden Observatory, 2300 RA Leiden, Netherlands. [2]Lehrstuhl für Theoretische Chemie, Ruhr-Universität Bochum, 44780 Bochum, Germany. [3]FELIX Facility, Foundation for Fundamental Research on Matter (FOM) Institute for Plasma Physics "Rijnhuizen," 3430 BE Nieuwegein, Netherlands. [4]I. Physikalisches Institut, Universität zu Köln, Zülpicher Strasse 77, 50937 Köln, Germany.

*These authors contributed equally to this work.
†To whom correspondence should be addressed. E-mail: dominik.marx@theochem.rub.de

(and thus the a priori sensitivity of the experiment) decreases with decreasing frequency, approaching the small thermal rate coefficient k observed without laser excitation [$k^*(\nu) \xrightarrow{\nu \to 0} k$; see dashed line in Fig. 2A]; thus, features at much lower frequencies are difficult to detect.

To link these experimental data to a molecular picture, we computed the IR spectrum of bare CH_5^+ at finite temperatures from the Fourier transform of the classical time-autocorrelation function of the total dipole moment, subject to a quantum correction most suitable for vibrational spectra including anharmonic floppy modes (*36*). The underlying trajectories were generated by ab initio molecular dynamics (*29*–*31*) relying on a density functional approach (*17*, *18*) well-tested for comparable benchmark structures and energies (*14*, *15*). The absorption cross sections $\alpha(\nu)$ shown in Fig. 2, B and C, denoted "high"- and "low"-temperature spectra, were obtained as a canonical average based on independent microcanonical trajectories sampled from Nosé-Hoover chain (*30*) constant-temperature runs at 300 and 50 K, respectively. The high-temperature simulations at 300 K lead to a behavior known to emulate closely the true ground-state quantum behavior (*17*, *18*), whereas at ~50 K hydrogen scrambling is frozen and the internal rotation of the H_2 moiety is partly frozen.

This freezing restriction clearly is an artifact, because it is known that the molecule scrambles even in the ground state once nuclear quantum effects are accounted for (*9*, *17*, *18*). However, at the same time, it is an extremely useful computational trick for separating the impact of hydrogen scrambling and internal rotation from trivial effects due to small-amplitude motion. Thus, the "low-temperature" spectrum is not the expected experimental one for bare CH_5^+ at that temperature, but rather is a simplification for understanding the spectral features of the computed "high-temperature" spectrum, which in turn should approximate the measured one. In addition, standard power spectra or vibrational densities of states (VDOS), based on suitably defined velocity autocorrelation functions of (quasi-) local modes, are of great help in assigning the spectrum.

Overall, the computed spectrum depicted (Fig. 2B) compares favorably with experiment (Fig. 2A). In particular, there are three subpeaks contributing to the broad band extending from about 2200 to 3400 cm^{-1} in addition to a rather symmetric peak close to 1200 cm^{-1}; note that the usual frequency scaling (*14*, *37*) by an empirical correction factor of typically 0.91 to 0.95 would yield quantitative agreement. Generally, the corresponding VDOS above and below 2000 cm^{-1} can by approximation be decoupled upon projection onto C-H stretching and H-C-H bending coordinates, respectively; the broad feature near 1200 cm^{-1}, which comprises five modes in the harmonic approximation (*14*, *19*), is close to the highly degenerate bending mode of CH_4. Further decomposition of the high-temperature spectrum (Fig. 2B) is hampered by the fact that the instantaneous arrangement of atoms (i.e., the molecular structure) is constantly changing as a result of hydrogen scrambling (*23*).

Fortunately, the artificial cooling of the molecule to a sufficiently low temperature results in freezing of the scrambling dynamics. In this nonscrambling regime (Fig. 2C), the most prominent peak splits into a triplet centered near 3220 cm^{-1}, which is close to both the experimental and calculated (≈ 3210 cm^{-1}) C-H stretching frequency of CH_4; we also note the good agreement of the low-temperature IR peak positions in Fig. 2C with the resonances of the low-energy power spectrum (*19*) obtained from a PES at the MP2/cc-pVTZ level of theory. Most interesting, however, is the qualitative agreement of the triplet structure (due to tripod stretching modes; see below) observed only in the nonscrambling regime with the emergence of a three-peak characteristic in the measured IR spectrum (*3*) under progressive microsolvation of bare CH_5^+ by H_2, which has been interpreted as being caused by a slowing down of the scrambling dynamics.

Extended time intervals exist in the nonscrambling regime where the internal rotation of the H_2 moiety about the pseudo-C_3 axis is either free or hindered. In the latter so-called librational regime, only librational motion in the e-C_s minimum is possible, whereas in the former (rotational) regime, full rotation is activated, thus interconverting the e-C_s and s-C_s structures (Fig. 3). Decomposition of the VDOS reveals that the central peak of the triplet gains intensity in the rotational regime, where all three tripod hydrogens are statistically equivalent. This dynamical degeneracy, however, is lifted in the librational regime, which favors the eclipsed equilibrium structure, e-C_s, and results in red- and blue-shifted satellites. The central peak and its blue-shifted satellite are respectively assigned to symmetric and antisymmetric stretches of the tripod hydrogens that are instantaneously non-eclipsed by the H_2 moiety, whereas the red-shifted satellite is due to stretching of the eclipsed tripod hydrogen (*14*). Despite the observed pronounced mixing of stretching and bending modes due to anharmonicity, the peak doublet around 2425 and 2700 cm^{-1}, which is a well-separated feature only in the nonscrambling regime, can approximately be assigned to those antisymmetric and symmetric stretching modes that involve only the H_2 moiety in agreement with the harmonic analysis (*14*).

Thus, the protons forming the H_2 moiety and those engaged in the CH_3 tripod lead to three well-separated stretching peaks in the low-temperature regime, the prominent one of highest frequency (tripod modes) having a triplet substructure. In the high-temperature regime where the computed spectrum matches closely the experimental one, the lifetime of the H_2 moiety is ~55 fs, allowing for several C-H stretching vibrational periods in C_s-like structures. In comparison, the time spent close to the transition state for scrambling (see below), corresponding to the lifetime of C_{2v}-like structures, is considerably shorter: ~10 fs. Thus, the three-center two-electron bonding pattern, characterizing the C_s-like ground-state structure and the resulting correlated motion of the five protons around the central carbon

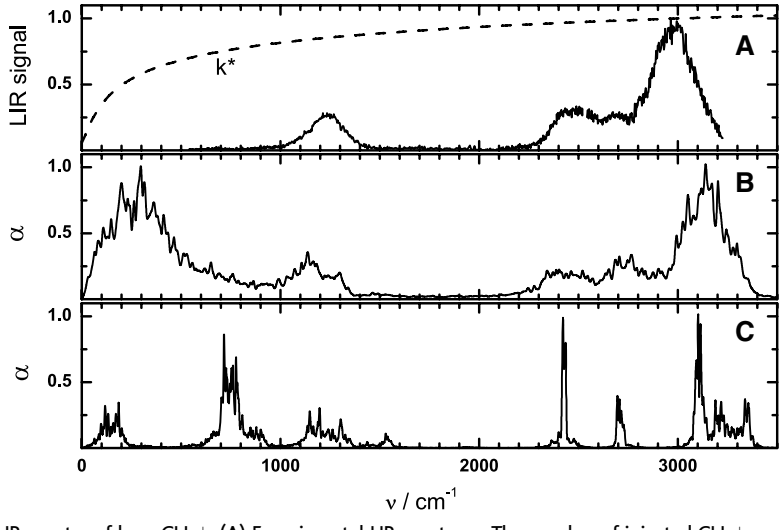

Fig. 2. IR spectra of bare CH_5^+. (**A**) Experimental LIR spectrum. The number of injected CH_5^+ parent ions is >3000, the $OCOH^+$ signal ion count had a maximum of ~500 at the C-H bend frequency (1250 cm^{-1}), and the data were normalized as described in the text. The LIR rate coefficient $k^*(\nu)/k^*$(3000 cm^{-1}), shown by dashed line, was calculated on the basis of the heat capacity of CH_5^+, the temperature of the experiment (110 K), and the endothermicity of the LIR reaction (*35*). (**B** and **C**) Absorption cross sections from high-temperature (B) and low-temperature (C) ab initio simulations; see text for details.

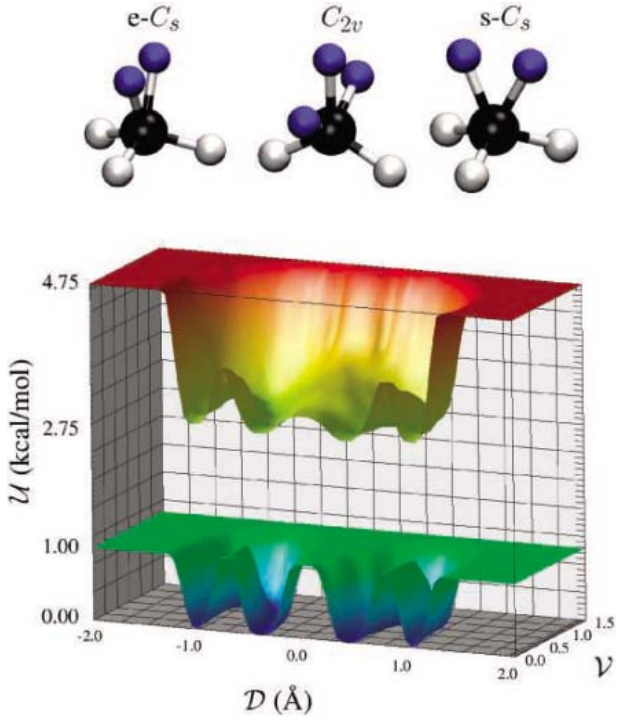

Fig. 3. Top: Eclipsed (e-C_s) and staggered (s-C_s) structures with CH_3 tripod (black and gray) and H_2 moiety (blue); saddle point structure (C_{2v}) with three coplanar hydrogen atoms (blue). Bottom: Effective PES $\mathcal{U}$ as a function of the generalized coordinates $\mathcal{D}$ and $\mathcal{V}$ (see text), shown at high (upper graph) and low (lower graph) temperature, corresponding to the scrambling (*23*) and nonscrambling regime, respectively. For the purpose of presentation, $\mathcal{U}(\mathcal{D},\mathcal{V})$ is smoothed and set to a constant value above 4.75 kcal/mol in the upper graph and 1.00 kcal/mol in the lower graph.

nucleus, is the key to understanding the IR spectrum, despite the underlying scrambling dynamics.

Having identified hydrogen scrambling as the dominant dynamical process, the underlying rearrangement path can be analyzed with the help of Fig. 3. An effective PES, $\mathcal{U}$, as explored by the two sets of simulations, is shown in a subspace spanned by $\mathcal{D} = \pm|d_{12} - d_{23}|$ (where d_{ij} is the distance between $H^{(i)}$ and $H^{(j)}$) and $\mathcal{V} = \hat{\mathbf{n}}_{1,2}\cdot\hat{\mathbf{r}}_3$ (where $\hat{\mathbf{n}}_{1,2}$ is the unit normal to the plane containing $\hat{\mathbf{r}}_1$ and $\hat{\mathbf{r}}_2$, and $\hat{\mathbf{r}}_i$ denote the unit vectors along the C-$H^{(i)}$ bonds) averaged over the fluctuations in all remaining degrees of freedom. The three protons $H^{(1)}$, $H^{(2)}$, and $H^{(3)}$ are those that are instantaneously involved in hydrogen scrambling events, as identified before and after every such event by analyzing the configurational trajectories. Briefly, $\mathcal{V}$ measures deviations of the three scrambling protons from coplanarity (where $\mathcal{V} = 0$), whereas $\mathcal{D}$ is sensitive to their deviations from the C_{2v} saddle point arrangement (where $\mathcal{D} = 0$). In the low-temperature limit of artificially frozen hydrogen scrambling (lower graph in Fig. 3), only internal rotational motion of the H_2 moiety is possible, interconverting the e-C_s and s-C_s structures without breaking up the H_2 moiety. This restriction leads to two steep, fully disconnected, horseshoe-like valleys, implying that the molecule never explores the PES close to $(\mathcal{D},\mathcal{V}) = (0,0)$.

Upon activating scrambling (*23*) by increasing the temperature (upper graph), the two valleys broaden and become connected by an extremely flat ridge, thus yielding an unusually shallow PES in the scrambling coordinates. In particular, the most probable connecting path passes through $(\mathcal{D},\mathcal{V}) \approx (0,0)$, which characterizes the C_{2v} first-order saddle point. Thus, this analysis of the PES topology strongly supports the idea that the C_{2v} structure can serve as a meaningful approximation to the transition complex structure for the scrambling motion in CH_5^+, although deviations very large in amplitude (i.e., $\mathcal{V} \gg 0$) are observed in view of the flatness of the ridge. In the scrambling regime, the effective barrier for this process is ~0.3 kcal/mol, versus ~0.6 kcal/mol obtained along the minimum-energy path from the static e-C_s and C_{2v} structures. This low value implies that fluctuations of the remaining degrees of freedom suppress the effective barrier to hydrogen scrambling considerably, calling into question reduced-dimensionality theories.

Together, these experiments and simulations clearly indicate full hydrogen scrambling of bare CH_5^+ at experimental conditions. In addition to describing the scrambling mechanism in atomic detail, the presented methods offer an understanding of the measured IR spectrum despite the underlying rapid proton motion that dynamically interconverts structures of different symmetry and chemical bonding pattern. In particular, the fact that the C-H stretching modes of the H_2 moiety and CH_3 tripod resolve into distinct peaks is arguably an experimental support for three-center two-electron bonding being operative in bare CH_5^+ under experimental conditions. The current approach to IR spectra could guide future studies on cold molecular ions in general, exploiting the use of deuterated species, overtone spectroscopy, microsolvation, and double-resonance techniques.

References and Notes

1. R. J. Saykally, *Science* **239**, 157 (1988).
2. T. Oka, *Philos. Trans. R. Soc. London Ser. A* **324**, 81 (1988).
3. D. W. Boo, Z. F. Liu, A. G. Suits, J. S. Tse, Y. T. Lee, *Science* **269**, 57 (1995).
4. E. T. White, J. Tang, T. Oka, *Science* **284**, 135 (1999).
5. G. A. Olah, *Angew. Chem. Int. Ed. Engl.* **34**, 1393 (1995).
6. G. A. Olah, G. Rasul, *Acc. Chem. Res.* **30**, 245 (1997).
7. D. Marx, A. Savin, *Angew. Chem. Int. Ed. Engl.* **36**, 2077 (1997).
8. G. A. Scuseria, *Nature* **366**, 512 (1993).
9. D. Marx, M. Parrinello, *Science* **284**, 59 (1999).
10. P. R. Schreiner, *Angew. Chem. Int. Ed. Engl.* **39**, 3239 (2000).
11. D. Gerlich, *Phys. Chem. Chem. Phys.* **7**, 1583 (2005).
12. D. Talbi, R. P. Saxon, *Astron. Astrophys.* **261**, 671 (1992).
13. V. Dyczmons, W. Kutzelnigg, *Theor. Chim. Acta (Berlin)* **33**, 239 (1974).
14. P. R. Schreiner, S.-J. Kim, H. F. Schaefer III, P. von Ragué Schleyer, *J. Chem. Phys.* **99**, 3716 (1993).
15. H. Müller, W. Kutzelnigg, J. Noga, W. Klopper, *J. Chem. Phys.* **106**, 1863 (1997).
16. J. S. Tse, D. D. Klug, K. Laasonen, *Phys. Rev. Lett.* **74**, 876 (1995).
17. D. Marx, M. Parrinello, *Nature* **375**, 216 (1995).
18. D. Marx, M. Parrinello, *Z. Phys. D* **41**, 253 (1997).
19. A. Brown, B. J. Braams, K. Christoffel, Z. Jin, J. M. Bowman, *J. Chem. Phys.* **119**, 8790 (2003).
20. A. B. McCoy *et al.*, *J. Phys. Chem. A* **108**, 4991 (2004).
21. A. Brown, A. B. McCoy, B. J. Braams, Z. Jin, J. M. Bowman, *J. Chem. Phys.* **121**, 4105 (2004).
22. K. C. Thompson, D. L. Crittenden, M. J. T. Jordan, *J. Am. Chem. Soc.* **127**, 4954 (2005).
23. For an animation of the scrambling dynamics, see www.theochem.rub.de/go/ch5p.html.
24. D. Marx, M. Parrinello, *Science* **271**, 179 (1996).
25. A. J. R. Heck, L. J. de Koning, N. M. M. Nibbering, *J. Am. Soc. Mass Spectrom.* **2**, 453 (1991).
26. G. M. Kramer, T. Oka, E. T. White, D. Marx, M. Parrinello, *Science* **286**, 1051a (1999).
27. D. Oepts, A. F. G. van der Meer, P. W. van Amersfoort, *Infrared Phys. Technol.* **36**, 297 (1995).
28. FELIX users' page (www.rijnh.nl/felix).
29. R. Car, M. Parrinello, *Phys. Rev. Lett.* **55**, 2471 (1985).
30. D. Marx, J. Hutter, in *Modern Methods and Algorithms of Quantum Chemistry*, J. Grotendorst, Ed. [John von Neumann-Institut für Computing (NIC), Forschungszentrum Jülich, Jülich, Germany, 2000], pp. 301–449 (available at www.theochem.rub.de/go/cprev.html).
31. J. Hutter *et al.*, CPMD Software Package, Max-Planck-Institut für Festkörperforschung and IBM Zürich (1995–1999).
32. S. Schlemmer, T. Kuhn, E. Lescop, D. Gerlich, *Int. J. Mass Spectrom.* **185**, 589 (1999).
33. S. Schlemmer, E. Lescop, J. von Richthofen, D. Gerlich, M. A. Smith, *J. Chem. Phys.* **117**, 2068 (2002).
34. O. Asvany, T. Giesen, B. Redlich, S. Schlemmer, *Phys. Rev. Lett.* **94**, 073001 (2005).
35. S. Schlemmer, O. Asvany, *J. Phys. Conf. Ser.* **4**, 134 (2005).
36. R. Ramírez, T. López-Ciudad, P. Kumar P, D. Marx, *J. Chem. Phys.* **121**, 3973 (2004).
37. A. P. Scott, L. Radom, *J. Phys. Chem.* **100**, 16502 (1996).

38. Supported by Deutsche Forschungsgemeinschaft (DFG) Forschergruppe FOR 388 ("Laboratory Astrophysics") and DFG grant MA 1547/4-1, the Netherlands Research School for Astronomy (NOVA), Fonds der Chemischen Industrie, and a Netherlands Organization for Scientific Research (NWO) Spinoza grant (O.A.). The Bochum group thanks A. Chandra, H. Forbert, A. Kohlmeyer, and H. Langer for useful discussions and technical help; the simulations were carried out at BOVILAB@RUB (Bochum). The Leiden/Köln group thanks FOM for beam time and highly appreciates the skillful assistance by the FELIX staff and by the workshops of Leiden University. S.S. thanks D. Gerlich for the opportunity to transfer the 22-pole ion trap machine to Leiden/Köln in order to continue the work on LIR.

18 April 2005; accepted 22 June 2005
Published online 30 June 2005;
10.1126/science.1113729
Include this information when citing this paper.

Ultrafast X-ray Diffraction of Transient Molecular Structures in Solution

H. Ihee,[1]* M. Lorenc,[2] T. K. Kim,[1] Q. Y. Kong,[2] M. Cammarata,[2,3] J. H. Lee,[1] S. Bratos,[4] M. Wulff[2]

We report direct structural evidence of the bridged radical (CH_2ICH_2•) in a polar solution, obtained using time-resolved liquid-phase x-ray diffraction. This transient intermediate has long been hypothesized to explain stereochemical control in many association and/or dissociation reactions involving haloalkanes. Ultrashort optical pulses were used to dissociate an iodine atom from the haloethane molecule ($C_2H_4I_2$) dissolved in methanol, and the diffraction of picosecond x-ray pulses from a synchrotron supports the following structural dynamics, with ~0.01 angstrom spatial resolution and ~100 picosecond time resolution: The loss of one iodine atom from $C_2H_4I_2$ leads to the C-I-C triangular geometry of CH_2ICH_2•. This transient C_2H_4I then binds to an iodine atom to form a new species, the C_2H_4I-I isomer, which eventually decays into $C_2H_4 + I_2$. Solvent dynamics were also extracted from the data, revealing a change in the solvent cage geometry, heating, and thermal expansion.

The prediction of molecular structures during a chemical reaction has progressed substantially because of advances in computational chemistry and molecular dynamics simulations (*1*). In contrast, direct structural characterization of short-lived reaction intermediates has only recently become accessible, with the advent of picosecond electron (*2–5*) and x-ray (*6–11*) diffraction techniques. These experiments are conducted using the pump and probe method: An ultrashort laser pulse initiates a reaction, and as it progresses, the diffraction signal from a delayed electron or x-ray pulse probes the change in the spatial correlations between atoms and molecules. Because the scattering cross section of electrons is high, electron diffraction is particularly useful for atoms and molecules in the gas phase (*4*, *5*), thin films (*3*), and surfaces (*2*). However, the high cross section translates into shallow sample penetration, which makes it difficult for electrons to probe condensed samples such as liquids.

The scattering cross section of hard x-rays is six orders of magnitude lower than for electrons. Thus, x-rays can probe bulk samples, provided that the pulse intensity is sufficiently high, as is the case in our study using synchrotron radiation (5×10^8 photons per pulse at 18 keV). The main difference between gas-phase and solution-phase diffraction is the relative concentration of excited molecules. In solution studies, scattering from the laser-excited solutes is typically well below 1% of the diffraction signal from the solvent. With a typical pump-pulse excitation efficiency of 10%, only about 1 in 1000 molecules is excited. The laser-induced signal is thus embedded in a strong background from non-excited molecules, which limits the signal-to-noise ratio of the diffraction data. In addition, structural rearrangements in the solvation shell complicate deconvolution of the solute and solvent signals.

Most reactions relevant to biology and industrial applications occur in the solution phase, and the chemistry of reactions in solution is extremely rich because of the complex solvent interactions with the solute. Although ultrafast optical spectroscopy (*12*, *13*) has provided a wealth of information regarding the time scale for these processes, x-ray diffraction offers direct insight into the three-dimensional (3D) structures of transient intermediates, as well as solvent shell rearrangements.

We have applied time-resolved liquid-phase x-ray diffraction to the elimination reaction of 1,2-diiodoethane ($C_2H_4I_2$), which gives an iodine atom and a short-lived iodoethyl radical (CH_2ICH_2•) intermediate in solution (*14*). Haloethyl radicals such as CH_2ICH_2• play a crucial role in the stereoselectivity of certain chemical processes (*15–19*). Skell and co-workers proposed a bridged structure for the radical, which is distinct from the classical anti structure, in order to explain the stereochemistry of free-radical addition reactions (*20*). However, despite numerous theoretical (*21–23*) and experimental investigations (*14*, *24–26*), direct structural evidence for the bridged structure has been lacking. Here, time-resolved x-ray diffraction data provide such evidence, together with the associated solvent dynamics.

To follow the structural dynamics during the course of the reaction, we collected time-resolved diffraction data for time delays of –3 ns, –100 ps, 100 ps, 300 ps, 1 ns, 3 ns, 10 ns, 30 ns, 50 ns, 70 ns, 100 ns, 300 ns, 1 μs, and 3 μs. The data point at –3 ns served as a (nonexcited) reference point, and another point at negative time delay (–100 ps) was collected to check the timing at high resolution. To recover the changes from the laser excitation only, difference signals were generated by subtracting the reference data at –3 ns from the data at any other time delay (*27*).

The image at –100 ps shows no difference intensity, as expected (Fig. 1). At positive times, difference features emerge and progress with time. After radial integration of the 2D difference images to 1D difference curves, $\Delta S(q)$, these curves were multiplied by q to magnify the intensity at high scattering angles [$q = (4\pi/\lambda)\sin(2\theta/2)$, where λ is the x-ray wavelength and 2θ the scattering angle]. The $q\Delta S(q)$ curves contain direct q-space information on the structural changes in the solute and in the solvent. It is more intuitively helpful to examine the sine-Fourier transforms, $r\Delta S(r)$, of the $q\Delta S(q)$ curves, where r is the interatomic distance. This representation corresponds to the change in the atom-atom pair distribution functions during the course of the reaction (*28*) and is a measure, biased by the x-ray form factor, of the change in the electron density around an (average) excited atom, as a function of r. There are three contributions to the measured signal (Fig. 2, A and B): the structural change in the solute, the change in the solvation cage caused by solute/solvent interaction, and the bulk solvent response to heating and thermal expansion.

To explain the experimental data theoretically and fit the measured signal, we included all known components to the signal. Specifically, we included not only the contributions from the solutes, but also the contribution to the signal from the heating of the surrounding solvent by calculating the temperature and density of the bulk solvent as a function of time (*27*). For the solute, we considered all possible reaction pathways. Upon photoexcitation, the parent solute molecule $C_2H_4I_2$ can dissociate through three possible channels: (i) a new transient species C_2H_4I and an I atom, (ii) $C_2H_4 + 2I$, and (iii) $C_2H_4 + I_2$. Because C_2H_4I is not stable, it can further dissociate into $C_2H_4 + I$, or it can bind to a free I atom to form a C_2H_4I-I isomer. In summary, we can have the following solute species: $C_2H_4I_2$, C_2H_4I, C_2H_4, C_2H_4I-I, I, and I_2.

[1]Department of Chemistry and School of Molecular Science (BK21), Korea Advanced Institute of Science and Technology (KAIST), Daejeon, 305-701, Republic of Korea. [2]European Synchrotron Radiation Facility, Grenoble Cedex 38043, Boîte Postal 220, France. [3]National Institute for the Physics of Matter and Department of Physical and Astronomical Sciences, via Archirafi 36, 90123, Palermo, Italy. [4]Laboratoire de Physique Théorique des Liquides, Université Pierre et Marie Curie, Case courrier 121, 4, Place Jussieu, Paris Cedex 75252, France.

*To whom correspondence should be addressed. E-mail: hyotcherl.ihee@kaist.ac.kr

Theoretical scattering curves from these species, which include the change in solute and solvent cage structure, were obtained from molecular dynamics (MD) simulations (*11*), in which the system was set up to be in quasi–thermodynamic equilibrium at all times. Perturbation of the solvation cage can be expressed as a change in the atom-atom distance distribution between solute/solvent pairs. The changes in solute structure account for only part of the total signal, because of the presence of the solvent. In addition, the energy released from the photon-absorbing solute molecules causes a change in the temperature, pressure, and density of the solvent as a function of time. The shifts in intermolecular positions in the solvent are very small, on the milliangstrom length scale, but given the huge excess of solvent molecules over solutes, the integrated solvent signal can be comparable to or larger than the solute signal. A quantitative description of these solvent effects was also obtained from MD simulations (*11*).

Once all the components were obtained from MD simulations, the experimental data were fit to a sum of these components, with constraints to ensure conservation of total energy in the x-ray–probed volume (*27*). The hydrodynamics of the solvent, expressed through the time-dependent solvent temperature and density, were mathematically related to the solute dynamics through time-dependent solute concentrations, which lead to release of energy into the solvent during the solute reactions. Instead of fitting the data at each time point separately, data at all time delays were linked and fitted globally. Global fitting parameters included the rate coefficients. In Fig. 1, the fitting results for all time points are shown; more detailed depictions are given for the 100-ps time delay in Fig. 2, A and B. More detailed decompositions for other time points are given in (*27*). The fit yields, as a function of time, the change in concentration of putative solutes and the change in temperature and density of the bulk solvent (Fig. 2, E and F).

Figure 2, C and D, shows the major components in the fits. The first two curves from the top represent the change in the bulk solvent $\{q[\partial S(q)/\partial T]_V$ and $q[\partial S(q)/\partial \rho]_T\}$, where T is temperature, ρ is density, and V is volume. The other three curves represent the change related to the reaction channels: ($C_2H_4I_2 \rightarrow C_2H_4I + I$), ($C_2H_4I_2 \rightarrow C_2H_4I\text{-}I$), and ($C_2H_4I_2 \rightarrow C_2H_4 + I_2$). These curves bear imprints of the change in both solute and cage structure. According to the result of the least-square fit, C_2H_4I and I are the dominant solute species at 100 ps, and the formation of C_2H_4 or I_2 is not observed. This new transient C_2H_4I does not decay through the formation of C_2H_4 + I; rather, it reacts with an iodine atom to form a new species, the C_2H_4I-I isomer, with a bimolecular rate constant of 2.1 (±0.3) × 10^{12} $M^{-1}s^{-1}$, which is larger by two orders of magnitude than the rate constant for nongeminate formation of molecular iodine (*29*). The nascent isomer becomes the dominant solute species after a few nanoseconds. Eventually, this isomer also decays into C_2H_4 + I_2 in microseconds, with the rate constant of 4.8 (±0.9) × 10^5 s^{-1}.

The characteristic (Gaussian-like) time constant of the solvent density change was 33 ± 5 ns and depends on the size of the laser beam and the speed of sound in the solvent (*27*); the fit gives 83 ± 10 μm (full width at half maximum) for the size of the laser beam, which is in agreement with the value measured by scanning the laser profile.

Initially (<10 ns), the temperature and pressure of the solvent build up at fixed volume and density, a process expressed in the first component, $q[\partial S(q)/\partial T]_V$, in Fig. 2, C and D. The peaks and valleys in r space are mainly ascribed to a broadening of the atom-atom distributions O···O and O···C (where ··· indicates an interatomic pair) at constant volume between adjacent methanol molecules. Then the thermal expansion progresses with the observed time constant, and the solvent eventually returns to ambient pressure at a slightly expanded volume (and therefore decreased density) after about 100 ns {the second curve, $q[\partial S(q)/\partial \rho]_T$, in Fig. 2, C and D}. The peaks and valleys are caused by shifts in the interatomic distributions of O···O and O···C in the solvent.

After the thermal expansion, the solvent density has decreased by 2.1 kg m^{-3} (0.26%), which corresponds to a temperature rise of 1.8 K. Because we have determined the concentration of the end product C_2H_4 + I_2 to be 3.3 mM, and given that each decay $C_2H_4I_2^* \rightarrow C_2H_4$ + I_2 (where * indicates an excited state) releases 4.30 eV of energy, these transitions account for a temperature rise of 0.68 K in the solvent rather than the observed 1.8 K. We assign this difference to an invisible component in this experiment at 100-ps resolution: fast geminate recombination of $C_2H_4I_2^*$, which loses energy to the solvent through collisions in a few picoseconds (vibrational cooling). Consequent-

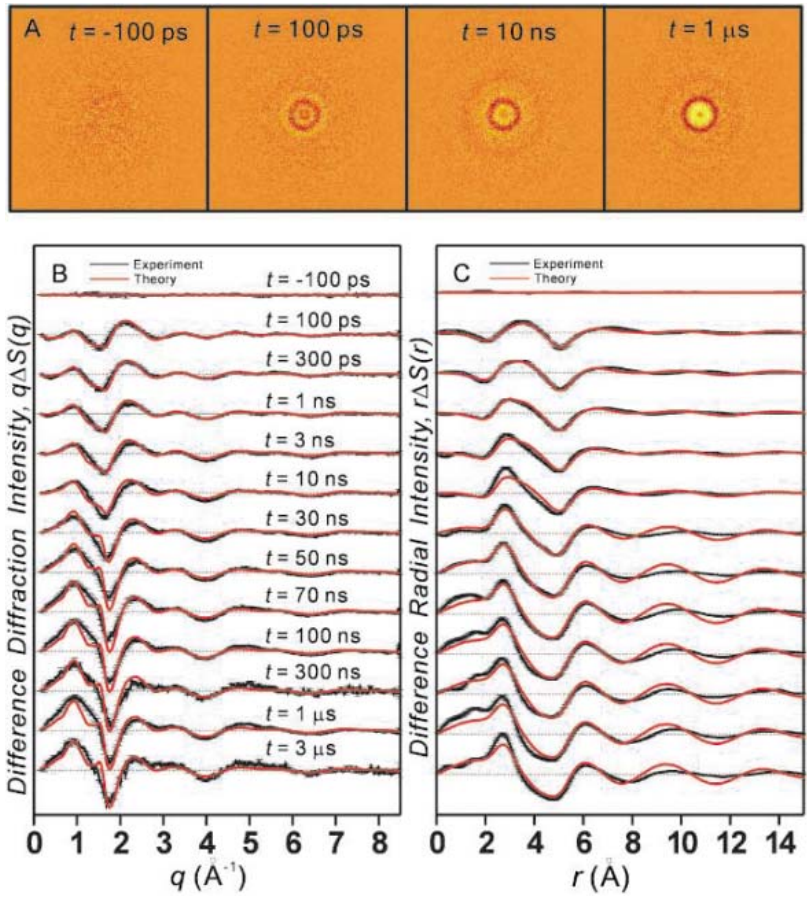

Fig. 1. Time-resolved diffraction signal as a function of time delay for $C_2H_4I_2$ in methanol. (**A**) Raw difference images for selected time delays (time t = –100 ps, 100 ps, 10 ns, and 1 μs). (**B**) Difference diffraction intensities, $q\Delta S(q)$, excited minus nonexcited. These are radial averages of the 2D images from (A). Least-square fits to a theoretical model are also shown. Error bars represent the experimental error associated with each scattering angle. (**C**) Difference radial density functions, $r\Delta S(r)$. These are sine-Fourier transforms of the difference intensities in (B). Error bars are also given to indicate the error in the real space representation.

ly, 60% of the initially excited $C_2H_4I_2$* molecules decay directly to the ground state [see (*27*) for details on the analysis of this contribution].

After the major thermal expansion has started, the change in bulk density dominates the signal. However, at early times, the structural change in the bulk is relatively smaller than at later times, and the solute and cage dynamics dominate because of the heavy iodine atoms in the solute. The data can therefore be decomposed into the change in the solute only, the change in the solvation cage, and the solvent response (Fig. 2, A and B). This decomposition helps the assignment of the peaks and valleys in Fig. 2B. The negative peak around 5 Å is mainly due to the change in the solute only, and the positive peak around 7 Å is mainly due to the change in the solvation cage. The positive peak near 4 Å is due to the change in the solvent. One cage splits into two smaller cages, with the overall effect of increasing the solute/solvent coordination number and shifting the distance distribution between the solute and solvent. As a consequence, the relative population of $I\cdots O_{solvent}$ and $I\cdots C_{solvent}$ distances increases around 4, 7, and 11 Å and decreases around 9 and 13 Å (Fig. 2B). The data offer a direct visualization of the change in the solvent cage; i.e., the change in solvent packing around the excited solutes.

In view of the complex interplay of factors contributing to these data, we could not refine molecular structures comparably to a single-crystal study. Instead, we compared our data to the calculated (ab initio and density functional theory) lowest-energy bridged and anti geometries. Figure 3 shows the ratio of the statistical significance, χ^2, for the fit using the bridged model and that using the anti model for all investigated time delays. As the concentration of C_2H_4I decreases, the ratio expectedly approaches 1. However, below 1 ns, where C_2H_4I is the major component, the ratio is significantly less than 1. To be sure that the experimental setup did not bias the result, we collected, in a separate experiment with a modified setup, the time delays ranging from –100 ps to 1 ns in steps of 25 ps, and the results are shown in the inset of Fig. 3. All time points below 1 ns have the ratio well below 1, thus confirming that the bridged structure reproduces the experimental curves with higher fidelity than does the anti structure. The apparent falling edge between –50 and 50 ps is due to the temporal profile of the x-ray pulse.

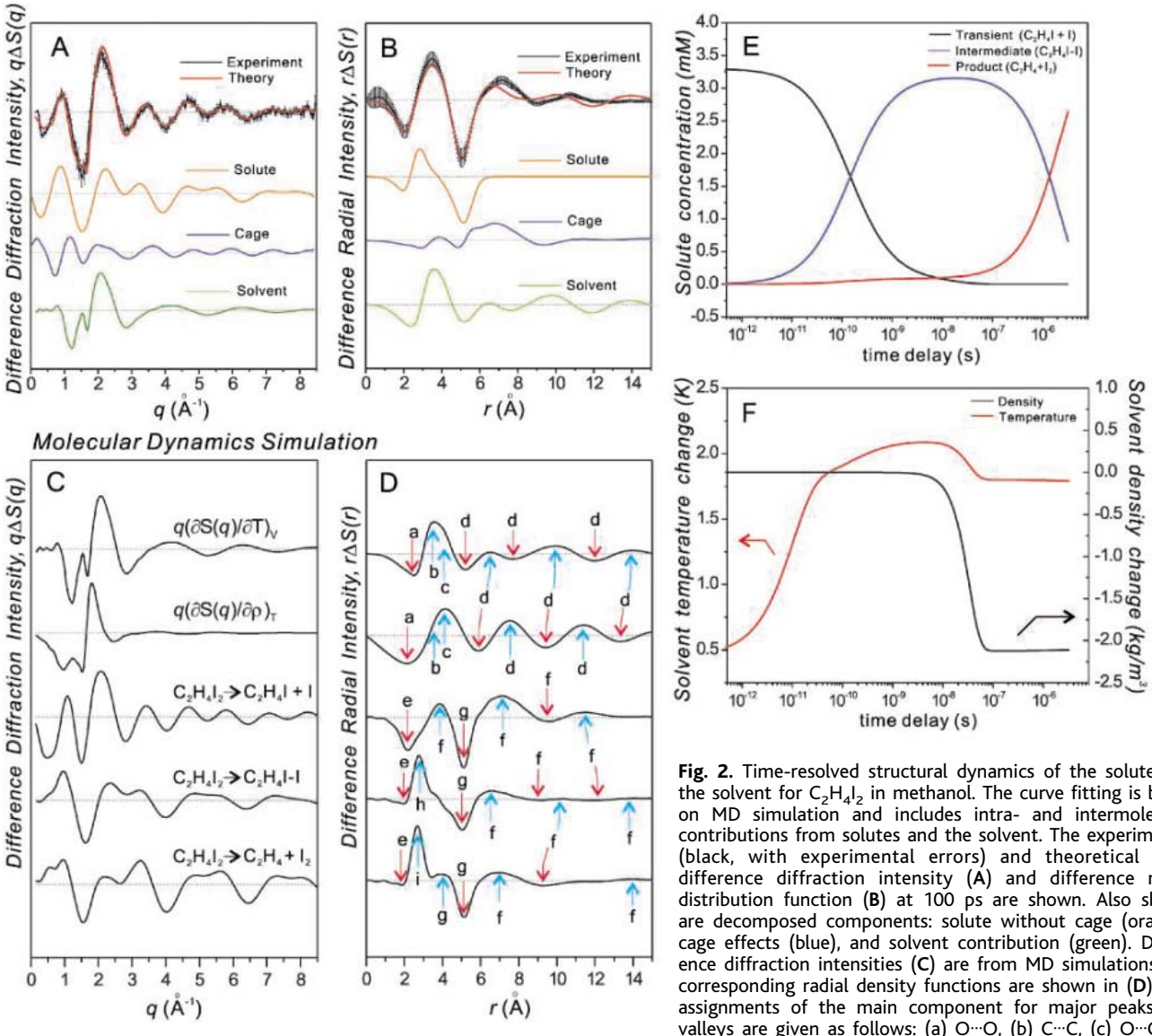

Fig. 2. Time-resolved structural dynamics of the solute and the solvent for $C_2H_4I_2$ in methanol. The curve fitting is based on MD simulation and includes intra- and intermolecular contributions from solutes and the solvent. The experimental (black, with experimental errors) and theoretical (red) difference diffraction intensity (**A**) and difference radial distribution function (**B**) at 100 ps are shown. Also shown are decomposed components: solute without cage (orange), cage effects (blue), and solvent contribution (green). Difference diffraction intensities (**C**) are from MD simulations and corresponding radial density functions are shown in (**D**). The assignments of the main component for major peaks and valleys are given as follows: (a) O···O, (b) C···C, (c) O···C, (d) O···O and O···C, (e) C···I of $C_2H_4I_2$, (f) $I\cdots O_{solvent}$ and $I\cdots C_{solvent}$, (g) I···I of $C_2H_4I_2$, (h) I···I of C_2H_4I-I, and (i) I···I of I_2. (**E**) The population change of the transient C_2H_4I (black), the intermediate isomer C_2H_4I-I (blue), and the final product, I_2 (red), as a function of time delay. (**F**) The change in the solvent density (black) and the solvent temperature (red). This time behavior is well described by an exponential function with a time constant of 33 ± 5 ns, which is typical of thermal expansion. Arrows point to the corresponding axis of each curve.

If we include a mixture of the anti and bridged forms in the fit, the fraction of the anti form converges to zero.

The distinction between fits to the bridged and anti forms is emphasized when the contribution of C_2H_4I alone is carefully extracted, by subtracting from the original data other contributions of solvent, cage, and other nascent solutes, and the high q range is used to deduce the transient-only structural changes. This approach allows the transient C_2H_4I to be modeled as a naked gas-phase structure (*11*). For the data at 100 ps, the experimental and theoretical curves for the putative reaction channels (Fig. 4) visually demonstrate the validity of the bridged structure against the classical anti structure. The negative peak near 5 Å corresponds to the depletion of the I···I internuclear distance in the parent molecule. This feature is common for all reaction channels, and both models agree with the data in this region. The peaks between 1 and 3 Å—the fingerprint region—are sensitive to the position of the I atom relative to the two carbon centers. The bridged structure gives only a single peak in the fingerprint region, and our data reproduce the feature with high accuracy, whereas the anti structure gives two overlapping peaks, which is in stark contrast to the experiment. We consider the formation of $C_2H_4I^+$ ions, rather than neutral radicals, unlikely, because the C-I distance for the ion (~2.25 Å) is much smaller than that determined for the radical (~3.06 Å) from our data (*30*).

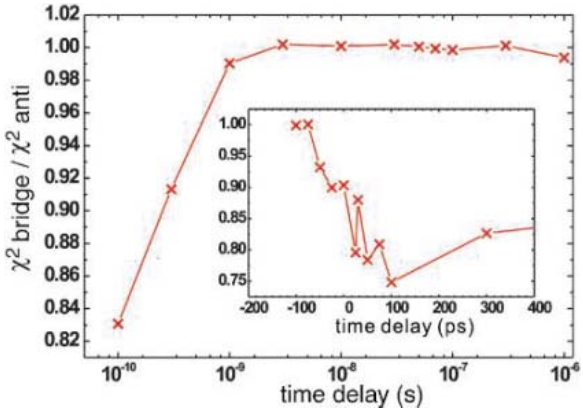

Fig. 3. The bridged model versus the anti model. The data were fit to both models and the final figures of merit (χ^2) were compared as a ratio. Below 1 ns, where the concentration of C_2H_4I is high, the ratio is significantly below 1, confirming that the bridged model fits the data better than the anti model. The inset shows the results from a separate experiment including more time points below 1 ns, which supports the above conclusion.

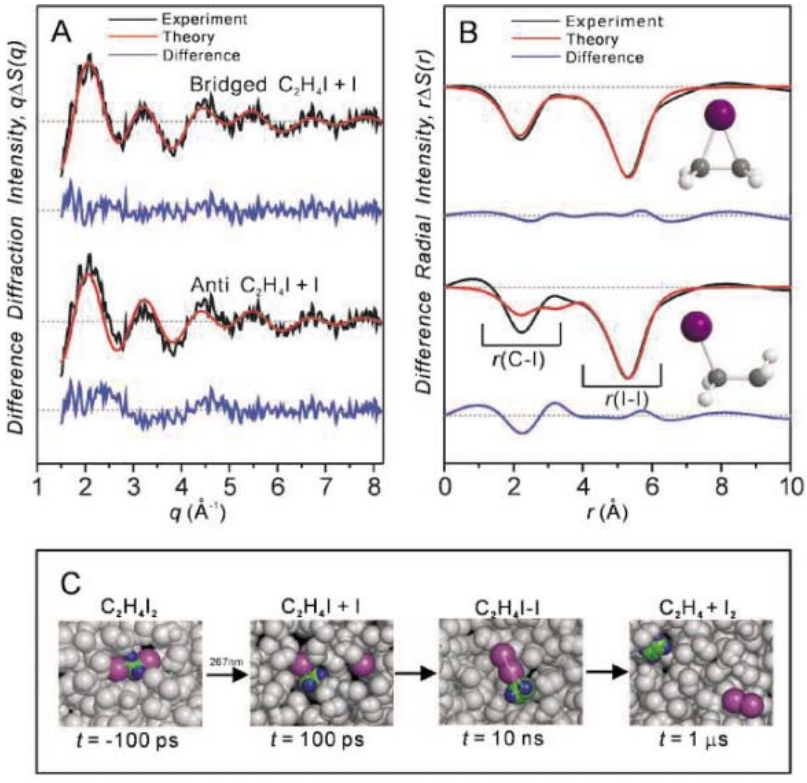

Fig. 4. (**A** and **B**) Structure determination of the C_2H_4I radical in methanol at t = 100 ps. The contribution from C_2H_4I alone is isolated by subtracting other contributions from the raw data, allowing comparison with the gas-phase model of the anti and bridged structures. (A) Theoretical (red) and experimental (black) difference intensities for two possible reaction channels. The differences between the theory and experiment are also shown in blue. The upper curves are for the formation of the bridged C_2H_4I radical and the lower ones are for the classical anti structure. (B) Corresponding radial density functions for the two possible reaction channels, and molecular structures (iodine, purple; carbon, gray). (**C**) A schematic reaction mechanism based on time-resolved x-ray diffraction in solution.

References and Notes

1. P. Allen, D. J. Tildesley, *Computer Simulation of Liquids* (Clarendon Press, Oxford, 1989).
2. C.-Y. Ruan, V. A. Lobastov, F. Vigliotti, S. Chen, A. H. Zewail, *Science* **304**, 80 (2004).
3. B. J. Siwick, J. R. Dwyer, R. E. Jordan, R. J. D. Miller, *Science* **302**, 1382 (2003).
4. H. Ihee *et al.*, *Science* **291**, 458 (2001).
5. R. C. Dudek, P. M. Weber, *J. Phys. Chem. A* **105**, 4167 (2001).
6. C. Rischel *et al.*, *Nature* **390**, 490 (1997).
7. F. Schotte *et al.*, *Science* **300**, 1944 (2003).
8. I. V. Tomov, D. A. Qulianov, P. Chen, P. M. Rentzepis, *J. Phys. Chem. B* **103**, 7081 (1999).
9. C. Rose-Petruck *et al.*, *Nature* **398**, 310 (1999).
10. C. W. Siders *et al.*, *Science* **286**, 1340 (1999).
11. A. Plech *et al.*, *Phys. Rev. Lett.* **92**, 125505 (2004).
12. S. Gnanakaran, R. M. Hochstrasser, *J. Am. Chem. Soc.* **123**, 12886 (2001).
13. A. B. Vakhtin, J. E. Murphy, S. R. Leone, *J. Phys. Chem. A* **107**, 10055 (2003).
14. M. Rasmusson, A. N. Tarnovsky, T. Pascher, V. Sundstrom, E. Akesson, *J. Phys. Chem. A* **106**, 7090 (2002).
15. J. K. Kochi, Ed., *Free Radicals* (Wiley, New York, 1973), vol. II.
16. A. L. J. Beckwith, K. U. Ingold, in *Rearrangements in Ground and Excited States*, P. d. Mayo, Ed. (Academic Press, New York, 1980), vol. 1, pp. 273–275.
17. J. Fossey, D. Lefort, J. Sorba, Eds., *Free Radicals in Organic Chemistry* (Wiley, New York, 1995).
18. H. L. Goering, P. I. Abell, B. F. Aycock, *J. Am. Chem. Soc.* **74**, 3588 (1952).
19. W. Thaler, *J. Am. Chem. Soc.* **85**, 2607 (1963).
20. P. S. Skell, D. L. Tuleen, P. D. Readio, *J. Am. Chem. Soc.* **85**, 2849 (1963).
21. B. Engels, S. D. Peyerimhoff, *J. Mol. Struct.* **138**, 59 (1986).
22. F. Bernardi, J. Fossey, *J. Mol. Struct.* **180**, 79 (1988).
23. H. Ihee, A. H. Zewail, W. A. Goddard III, *J. Phys. Chem. A* **103**, 6638 (1999).
24. A. J. Bowles, A. Hudson, R. A. Jackson, *Chem. Phys. Lett.* **5**, 552 (1970).
25. D. J. Edge, J. K. Kochi, *J. Am. Chem. Soc.* **94**, 6485 (1972).
26. S. Paul Maj, M. C. R. Symons, P. M. R. Trousson, *Chem. Commun.* 561 (1984).
27. Materials and methods are available as supporting material on *Science* Online.
28. S. Bratos, F. Mirloup, R. Vuilleumier, M. Wulff, A. Plech, *Chem. Phys.* **304**, 245 (2004).
29. S. Aditya, J. E. Willard, *J. Am. Chem. Soc.* **79**, 2680 (1957).
30. The least-squares fit gives a C-I bond length of 3.06 ± 0.02 Å in the bridged structure, as compared with a theoretical value of 3.11 Å. The CCI angle is 77.2 ± 0.1°. The errors are 1 SD in the fit, and they do not account for systematic errors. The C-I bond distance in the parent molecule, 2.17 ± 0.01 Å, is also slightly smaller than the theoretical value of 2.20 Å. The complete dissociation to C_2H_4 + 2I does not fit our experimental data. Moreover, the inclusion of a gauche component in the population of the parent molecules ($C_2H_4I_2$) makes the fit worse, indicating that the majority of the parent molecules adopt the anti rather than the gauche form, in agreement with the calculated energy difference of 13 kJ/mol.
31. We thank R. Vuilleumier and F. Mirloup for invaluable help in developing the theoretical

framework for time-resolved x-ray diffraction from liquids, including MD simulations, and P. Anfinrud, F. Schotte, A. Plech, and A. Cupane for discussions and assistance. This work was supported by the Korea Research Foundation Grant funded by Korean Government (Ministry of Education and Human Resources Development) grant no. R08-2004-000-10076-0 to H.I. and by the European Union grant nos. HPRI-CT-1999-50004 and HPRN-CT-00160. H.I. also acknowledges support from the Korea Advanced Institute of Science and Technology (KAIST) and from fellow faculty members in the KAIST chemistry department.

Supporting Online Material
www.sciencemag.org/cgi/content/full/1114782/DC1
Materials and Methods
Figs. S1 to S11
References and Notes

12 May 2005; accepted 30 June 2005
Published online 14 July 2005;
10.1126/science.1114782
Include this information when citing this paper.

Theoretical Study of Geometric Phase Effects in the Hydrogen-Exchange Reaction

Juan Carlos Juanes-Marcos,[1] Stuart C. Althorpe,[1]* Eckart Wrede[2]

The crossing of two electronic potential surfaces (a conical intersection) should result in geometric phase effects even for molecular processes confined to the lower surface. However, recent quantum simulations of the hydrogen exchange reaction ($H + H_2 \rightarrow H_2 + H$) have predicted a cancellation in such effects when product distributions are integrated over all scattering angles. We used a simple topological argument to extract reaction paths with different senses from a nuclear wave function that encircles a conical intersection. In the hydrogen-exchange reaction, these senses correspond to paths that cross one or two transition states. These two sets of paths scatter their products into different regions of space, which causes the cancellation in geometric phase effects. The analysis should generalize to other direct reactions.

Recent work (*1*) has established that conical intersections (CIs) play a central role in the dynamics of many chemical reactions and photoprocesses. At a CI, two electronic states touch, so that the Born-Oppenheimer approximation (that electronic and nuclear motion are separable) breaks down. A system with a CI can therefore convert rapidly between electronic states by passing through the intersection. Such rapid switching is exploited in many light-harvesting and charge-transfer processes. Another consequence of the Born-Oppenheimer breakdown is the geometric (*2*–*6*) [or Berry (*7*)] phase (GP), which occurs even if the system is confined to the lower electronic surface and avoids the neighborhood of the conical intersection. The GP is the sign change (or π phase shift) acquired by the electronic wave function Φ, when the nuclei complete an odd number of loops around the CI. The GP produces a corresponding sign change in the boundary condition of the nuclear wave function Ψ (*4*–*6*), in order to make the total wave function ($\Phi\Psi$) single-valued (i.e., uniquely specified at each nuclear geometry). As a result, even without electronic excitation, the vibrational and rotational motions on the lower electronic state are changed by the proximity of a CI. The implications of such changes for chemical reactivity are poorly understood.

In isolated molecules, the effects of the GP are reasonably well understood, thanks mainly to detailed experiments and theoretical predictions on Jahn-Teller systems (*6*, *8*). In the simplest "particle on a ring" system, the effect of the GP is to switch the allowed quantum numbers of the nuclear wave function from integer to half-integer values. Comparable shifts

[1]School of Chemistry, University of Nottingham, University Park, Nottingham, NG7 2RD, UK. [2]Department of Chemistry, University of Durham, South Road, Durham, DH1 3LE, UK.

*To whom correspondence should be addressed. E-mail: stuart.althorpe@gmail.com

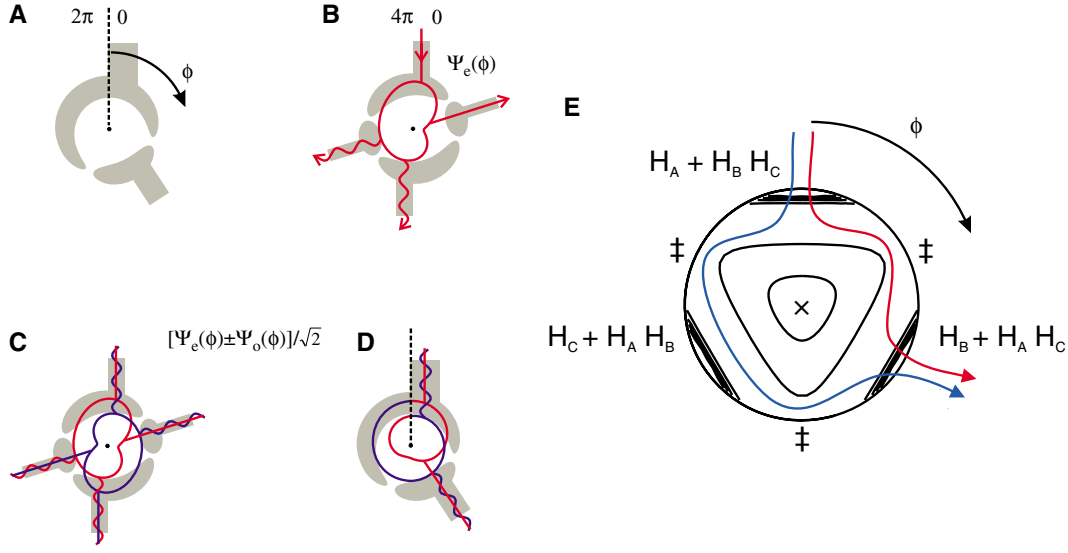

Fig. 1. (**A** to **D**) Schematic representation of a generic chemical reaction with a CI. The shaded areas represent the accessible region of the potential energy surface, which permits the nuclear function to encircle the CI (the dot at the center). (**A**) The reagent entrance channel is at the top, and the product exit channel is on the bottom right. The angle ϕ represents the path around the CI (such that $\phi = 0 \rightarrow 2\pi$ is one complete revolution). (**B**) The potential is extended to the artificial $\phi = 0 \rightarrow 4\pi$ double-cover space. The red line is a schematic representation of the (artificial) nuclear wave function $\Psi_e(\phi)$. Scattering boundary conditions are applied at the entrance channel (top) and at each of the three exit channels. Wavy lines are used to distinguish exit paths in the $2\pi \rightarrow 4\pi$ sector from those in the $0 \rightarrow 2\pi$ sector. (**C**) The symmetrized combinations $1/\sqrt{2}[\Psi_e(\phi) \pm \Psi_o(\phi)]$ of $\Psi_e(\phi)$ (red) and $\Psi_o(\phi)$ (blue), with the arrows removed for clarity. (**D**) The same functions in the $0 \rightarrow 2\pi$ space, showing that they are the solutions $\Psi_N(\phi)$ (no GP) and $\Psi_G(\phi)$ (GP) of Eq. 1. (**E**) A cut through the H_3 reactive potential energy surface, showing the position of the three $H + H_2$ arrangements, transition states (‡), and the CI (×). Representative direct (red) and looping (blue) reaction paths are also shown. The cut was obtained using the hyperspherical coordinate system of Kuppermann, which represents all different geometries of the three H nuclei, at a given overall separation ρ [defined by Kuppermann (*28*)], which is here set to 3.9 bohr. The center of the circle is the equilateral triangle geometry, and the geometries become flatter as they move outwards to the perimeter, which represents linear arrangements of the three nuclei.

in the allowed energy levels occur in more realistic systems. However, the effect of the GP on chemical reactions is less well understood (*5*, *9*–*16*). It is known (*4*) that the GP will only affect observables if the nuclear wave function encircles the intersection and that including the effect of the GP is equivalent to including a vector potential in the nuclear hamiltonian. If the encirclement is produced by a symmetry transformation, then one can predict the effects of the GP using symmetry arguments (*17*). However, in general, it is not known how the GP affects the wave functions of encircling reaction paths.

Recent calculations by Kendrick (*11*, *12*) explored the hydrogen-exchange reaction, the simplest reaction whose ground state potential energy surface has a CI (*2*). The results of theory agree very closely with detailed experimental data (*15*, *18*–*21*) for the state-to-state reaction $H + H_2(v,j,k_j) \rightarrow H_2(v',j',k_j') + H$, where v, j, and k_j are the vibrational and rotational quantum numbers of the H_2 molecules. Kendrick's calculations, which two of us later reproduced (*22*), reported small GP effects in the state-to-state reaction probabilities expressed as a function of the total angular momentum quantum number J. However, when these probabilities were summed over J to give the state-to-state integral cross section (ICS) (the amount of product integrated over all scattering angles), the GP effects cancelled. The cancellation occurred for all tested initial and final states, collision energies, and isotopic substitutions of the nuclei. This consistency suggested that the cancellation was caused by a general aspect of the GP in reactive systems that was not understood. We now demonstrate that the cancellation occurs because of a general topological effect of the GP on the nuclear wave function of a reactive system. To explain the effect, we make a simple application of the familiar mapping of two connected Möbius strips onto a double cylinder (*23*).

Figure 1A shows the potential energy surface for a general reactive system with a CI. The reagents enter at the top ($\phi = 0$, where ϕ is the encirclement angle) and can leave either at the bottom right (to form products) or at the top again (to give inelastically scattered reagents). The aim is to predict how the nuclear wave function Ψ_G, computed with the GP boundary condition of inverted phase [$\Psi_G(\phi) = -\Psi_G(\phi + 2\pi)$], differs from the nuclear wave function Ψ_N, computed with the normal boundary condition of conserved phase [$\Psi_N(\phi) = \Psi_N(\phi + 2\pi)$]. To accomplish this task, we consider an artificial system (Fig. 1B) in what is known topologically as a "double-cover" space (*23*), obtained by "unwinding" the potential surface, so that two complete revolutions (i.e., $\phi = 0 \rightarrow 4\pi$) are represented as one revolution on the page. We then consider the nuclear wave function $\Psi_e(\phi)$ (this notation will become clear shortly), computed in this double space, using the boundary condition $\Psi_e(\phi) = \Psi_e(\phi + 4\pi)$. This condition differs from both the $\Psi_G(\phi)$ and the $\Psi_N(\phi)$ boundary conditions, and in fact $\Psi_e(\phi)$ is a completely artificial nuclear wave function, which describes a system in which the $\phi = 0 \rightarrow 2\pi$ section is physically distinct from the $\phi = 2\pi \rightarrow 4\pi$ section.

However, it is easy to construct Ψ_G from Ψ_e. The potential surface in Fig. 1B has a twofold axis of rotational symmetry, passing through the CI. We may therefore construct linear combinations $1/\sqrt{2}[\Psi_e(\phi) \pm \Psi_o(\phi)]$, where $\Psi_o(\phi) = \Psi_e(\phi + 2\pi)$; these linear combinations are symmetric and antisymmetric, respectively, under $\phi \rightarrow \phi + 2\pi$ (Fig. 1C). It is then clear that these functions satisfy $\Psi(\phi) = \pm\Psi(\phi + 2\pi)$, and therefore it follows that

$$\Psi_N = \frac{1}{\sqrt{2}}[\Psi_e + \Psi_o]$$
$$\Psi_G = \frac{1}{\sqrt{2}}[\Psi_e - \Psi_o] \quad (1)$$

and that we can represent these expressions in the original $0 \rightarrow 2\pi$ space (Fig. 1D). Thus,

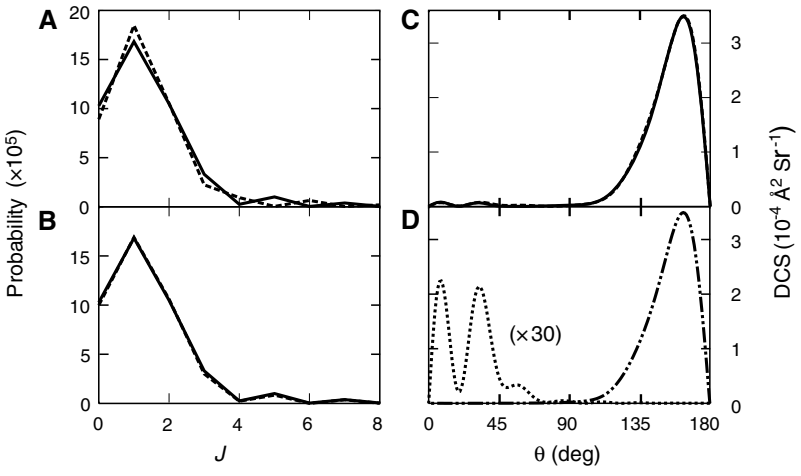

Fig. 2. Effect of the GP on the low-impact parameter state-to-state angular distributions for the hydrogen-exchange reaction. The results shown are for the $H_2(v = 1, j = 0) \rightarrow H_2(v' = 2, j' = 5, k_j' = 0)$ transition, at a total energy of 2.3 eV above the potential minimum, and are representative of the GP effects found in other state-to-state distributions at this energy. (**A**) The fixed-J reaction probabilities, obtained by projecting $f_N(\theta)$ (dashed line) and $f_G(\theta)$ (solid line) onto the angular momentum wave functions. (**B**) The fixed-J probabilities obtained from $f_G(\theta)$ (solid line) and from $f_N(\theta)$ (dashed line), when the latter is multiplied by -1 over the range of $0 \leq \theta \leq 60°$. (**C** and **D**) The angular distributions [differential cross sections (DCS)] obtained from the scattering amplitudes (C) $f_N(\theta)$ (dashed line) and $f_G(\theta)$ (solid line) and (D) $f_{dir}(\theta)$ (direct paths, dashed-dotted line) and $f_{loop}(\theta)$ (looping paths, dotted line). For clarity, the $f_{loop}(\theta)$ distributions are shown multiplied by a factor of 30. Sr, steradian (unit of solid angle).

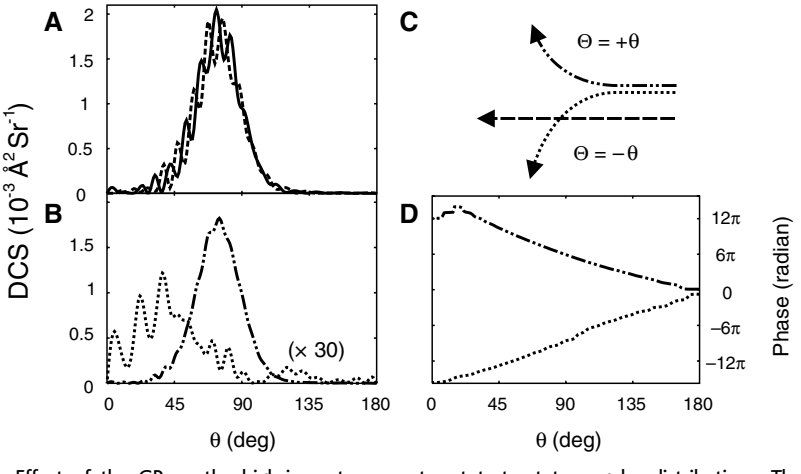

Fig. 3. Effect of the GP on the high-impact parameter state-to-state angular distributions. The total energy (2.3 eV) and initial and final states [$(v = 1, j = 0) \rightarrow (v' = 2, j' = 5, k_j' = 0)$] are the same as in Fig. 2. (**A** and **B**) The angular distributions obtained from the scattering amplitudes $f_N(\theta)$ (dashed line), $f_G(\theta)$ (solid line), $f_{dir}(\theta)$ (dashed-dotted line), and $f_{loop}(\theta)$ (dotted line). (**C** and **D**) The phases of $f_{dir}(\theta)$ (dashed-dotted line) and $f_{loop}(\theta)$ (dotted line) as a function of the scattering angle θ. The slopes in (D) indicate that the direct products scatter with positive deflection Θ, and the looping products scatter with negative Θ, as shown schematically in (C).

we have demonstrated that the nuclear wave function around a CI splits into two components, Ψ_e and Ψ_o, and that the sole effect of the GP is to change their relative sign.

A related argument is given in the Feynman path integral literature (*24*–*26*), where it has been applied to a model system in which an electron encircles a magnetic solenoid and acquires a geometric phase. When the final result of the latter argument is compared with Eq. 1 and Fig. 1, it yields the simple interpretation that Ψ_e (Ψ_o) contains all the Feynman paths that complete an even (odd) number of clockwise loops about the CI and an odd (even) number of counterclockwise loops. In the language of topology, Ψ_e and Ψ_o contain paths from different sets of homotopy classes (*23*) (meaning that paths in Ψ_e cannot be continuously deformed into paths in Ψ_o).

This simple result accounts for the cancellation of GP effects in the $H + H_2$ reaction. In the H_3 potential energy surface (*27*, *28*) (Fig. 1E), the CI is at the center (which is a cut through the line that links all the equilateral triangle geometries), and the three different exit channels lie near the perimeter, at $\phi = 0, 2\pi/3, 4\pi/3$. If the reagents enter the $H_A + H_BH_C$ channel (*29*) (at the top) and if we detect the $H_B + H_AH_C$ products, then most of the reaction paths will pass over just one transition state (Fig. 1E, red line). These are the Ψ_e paths; we will also call these the "direct" paths Ψ_{dir}. When the total energy is greater than ~2 eV above the potential minimum, a tiny proportion of paths [less than 1% (*9*, *30*)] will pass over two transition states (Fig. 1E, blue line). These are the Ψ_o paths, which we will also call the "looping" paths Ψ_{loop}. It is the interference of the direct and looping paths that gives an encircling nuclear wave function, which must manifest the GP effects predicted by Kendrick (*11*, *12*).

To understand what causes the cancellation in GP effects, we need to extract the direct and looping paths from the wave function and follow them as they scatter their products into space. In general, extracting different reaction paths from a scattering wave function is difficult, if not impossible, because the two sets of paths become inextricably mixed together. However, from Eq. 1, we have simply to compute the scattering amplitudes $f_G(\theta)$ and $f_N(\theta)$. These functions are the long-range parts of Ψ_G and Ψ_N, whose square moduli yield the angular distributions of the scattered products [as a function of θ, the angle between the product and reagent velocity vectors, in the center-of-mass frame (*31*)]. Using Eq. 1, we then evaluate

$$f_{dir}(\theta) = \frac{1}{\sqrt{2}}[f_N(\theta) + f_G(\theta)]$$
$$f_{loop}(\theta) = \frac{1}{\sqrt{2}}[f_N(\theta) - f_G(\theta)] \quad (2)$$

where $f_{dir}(\theta)$ and $f_{loop}(\theta)$ are the scattering amplitudes of, respectively, the direct and looping paths; their square moduli yield the corresponding angular distributions.

We decided to split the scattering amplitudes into low-impact ($0 \le J < 10$) and high-impact ($10 \le J < 40$) parameter contributions,

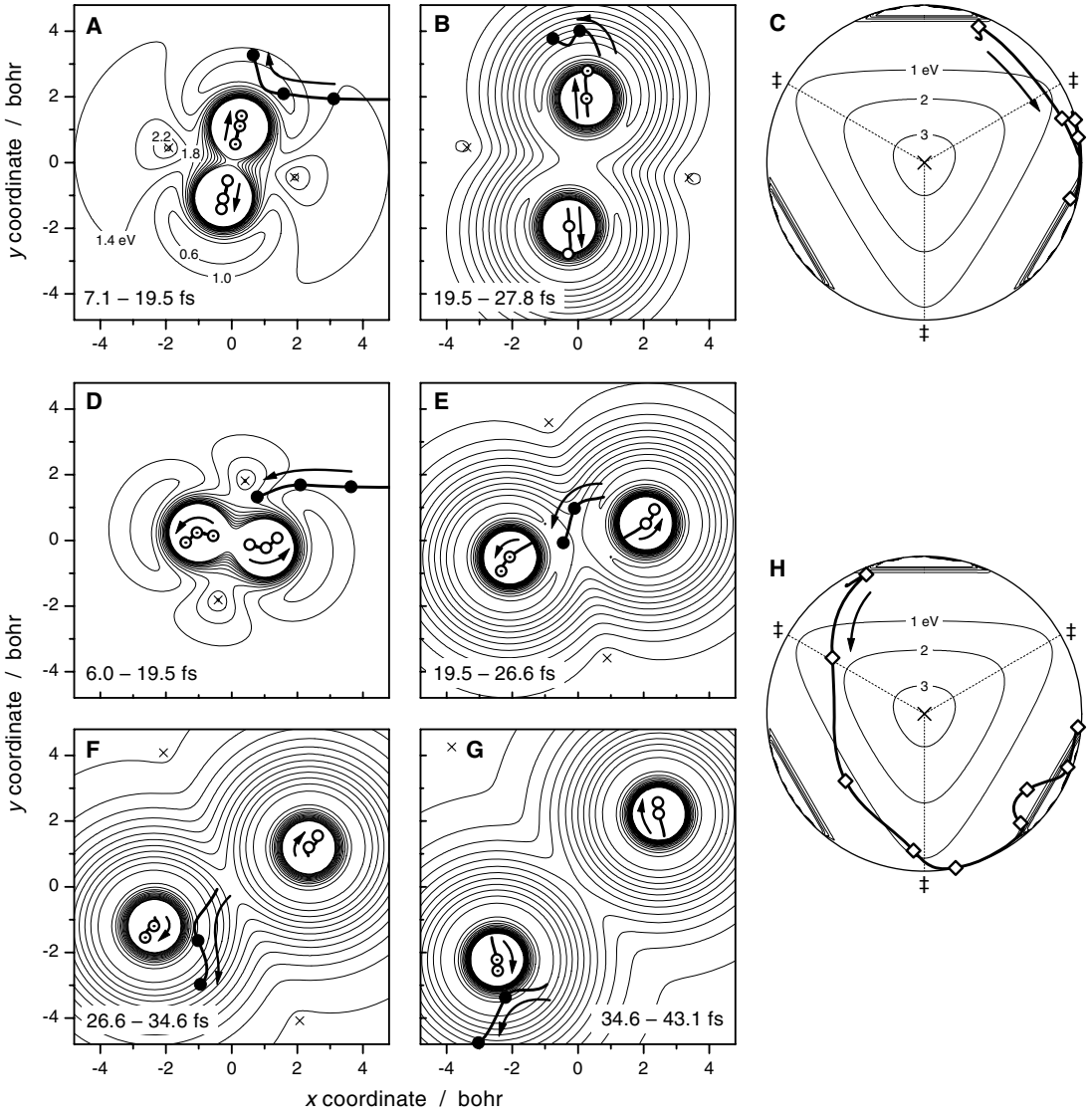

Fig. 4. Representative classical trajectories for the $H + H_2(v = 1, j = 0)$ reaction, illustrating why the direct and looping reaction paths scatter their products in opposite directions. Both trajectories lead to $H_2(v' = 2, j' = 6)$ products and a scattering angle of 72°. (**A** and **B**) A direct trajectory. The positions of the atoms (H_A, solid circles, H_B, open circles, H_C, dotted circles) are plotted at constant time intervals of 4.1 fs on top of the potential energy surface in a space-fixed frame centered at the reactant H_BH_C molecule. The locations of the CI are indicated by crosses (×). (**C**) Direct trajectory in hyperspherical coordinates (cf. Fig. 1E), showing the different $H + H_2$ arrangements (open diamonds) at the same time intervals as (A) and (B); the potential energy contours correspond to an overall separation of $\rho = 3.9$ bohr (an average value for the trajectory). The CI is located at the center with the transition states (‡) indicated by dotted lines. (**D** to **H**) As above, for the looping trajectory.

which correspond to, respectively, head-on and glancing collisions (*31*). The low-impact amplitudes give angular distributions concentrated mainly in the backward ($\theta = 180°$) direction (with respect to the initial $H_2 \leftarrow H$ approach velocity vector), and the high-impact amplitudes give angular distributions concentrated mainly in the sideways ($\theta = 90°$) direction (*11*, *12*, *15*, *16*, *20*–*22*). One reason for splitting the calculation is that the GP effects cancel in the low-impact parameter angular distribution (*11*, *12*, *22*) but not in the high-impact parameter angular distribution (*22*). In both cases, the GP effects cancel completely on integrating over θ, as integration yields the ICS.

In the low-impact regime, it is clear immediately from Fig. 2 why GP effects appear in the reaction probabilities for individual J states (Fig. 2A) but cancel in the angular distributions (Fig. 2C): The direct paths scatter their products mainly in the backward ($\theta = 180°$) hemisphere, whereas the looping paths scatter mainly in the forward hemisphere ($\theta = 0$) (Fig. 2D). Thus, the amplitudes $f_{dir}(\theta)$ and $f_{loop}(\theta)$ cannot interfere, and so the angular distributions produced by $f_G(\theta)$ and $f_N(\theta)$ are identical (Fig. 2C). When the J states are not superposed, however, the Ψ_{dir} and Ψ_{loop} contributions do interfere, because they then have the same angular distribution, determined by J; this interference gives rise to the differences between the GP and non-GP probabilities (Fig. 2A). As a check, these differences are seen to disappear when the forward part of $f_N(\theta)$ is multiplied by -1 and projected back onto the angular momentum wave functions (Fig. 2B). The differences alternate with J, because $f_{dir}(\theta)$ and $f_{loop}(\theta)$ have opposite signs in the forward hemisphere and the same sign in the backward hemisphere, and the angular momentum functions are even functions of θ for even J and odd for odd J.

In the high-impact regime, there are evidently GP effects in the angular distributions (Fig. 3A), which could potentially be observed in a scattering experiment (with sufficient angular resolution). These effects are produced by the overlap and interference of $f_{dir}(\theta)$ and $f_{loop}(\theta)$ (Fig. 3B). To explain why these effects cancel out upon integration over θ to give the ICS, we plotted the phases of $f_{dir}(\theta)$ and $f_{loop}(\theta)$ (Fig. 3D). The slopes of these phases depend in opposite senses on θ. As a result, the interference term $f_{dir}(\theta)^* f_{loop}(\theta)$ is highly oscillatory (with a period of $\sim 10°$) and cancels out upon integration over θ. Analysis of Fig. 3D, using well-known scattering theory (*31*, *32*), indicates that the direct and looping paths scatter in opposite directions (positive and negative deflection angles Θ, respectively). Hence, if the collision were initiated with a plane wave confined to the upper hemisphere, then the direct and looping paths would avoid each other, and there would be no GP effects in the resulting scattering amplitudes (Fig. 3C). In the full collision, however, the initial plane wave covers both hemispheres, so that each scattering angle θ contains contributions from both positive and negative deflection angles ($\theta = |\Theta|$). Interference from these deflection angles produces the GP effects. Thus, just as in the low-impact collisions, the direct and looping paths scatter their products into opposite hemispheres, cancelling the GP effects on integration over all scattering directions.

To investigate why the direct and looping paths scatter their products in opposite directions, we ran classical trajectories on the same potential surface (*27*) used to calculate the scattering wave functions in our earlier work (*22*). Although these simulations cannot predict a quantum effect such as the GP, they are expected to describe correctly the underlying dynamics (which are essentially semiclassical). Of a total of almost 1.1 million reactive trajectories with a total energy of 2.3 eV, ~99.6% reacted through one transition state (the direct paths of Fig. 1E) and only 4065 (~0.37%) through two transition states (the looping paths of Fig. 1E). As in the quantum calculations, the direct and looping paths scattered their products in opposite directions, with the low-impact products going into the backward and forward hemispheres and the high-impact products being scattered sideways.

Figure 4 shows a comparison between typical direct and looping trajectories. Both trajectories lead to the same product quantum state, ($v' = 2, j' = 6$), and the same scattering angle, $\theta = 72°$, and would thus give $f_{dir}{}^* f_{loop}$ interference in the quantum picture (cf. Fig. 3C). The minimum energy of the CI is 2.75 eV. At a total energy of 2.3 eV, the system lacks sufficient energy to reach the CI, which in the context of these trajectories is just a large mountain on the potential energy surface. The direct trajectory passes very near to the linear transition state (Fig. 4A), and the product is scattered directly into the positive (upper) hemisphere (Fig. 4B). In the looping trajectory, the atom H_A (Fig. 4D, solid circles) approaches the CI and first forms a temporary bond with atom H_B (Fig. 4D, open circles). As the H_B–H_C bond stretches, the gap between the molecule and the CI widens, and H_A inserts between H_B and H_C (Fig. 4E) to form the final bond with H_C (Fig. 4F). This insertion path deflects the H_A atom toward the center of the reactant H_BH_C molecule, which leads to scattering into the negative (lower) hemisphere (Fig. 4G). This insertion path is common to the majority (~90%) of looping trajectories at this energy. A second mechanism, in which the H_A atom first migrates around one end of the H_2 molecule before insertion, also leads to scattering into the negative hemisphere. The direct and looping nature of the reaction paths, which is not apparent in the scattering plots, becomes obvious if the trajectories are plotted in hyperspherical coordinates (Fig. 4, C and H).

The above topological analysis should prove useful when investigating GP effects in other reactive systems. In particular, there should be similar reductions or cancellations of GP effects in other significantly direct reactions, such as $H + O_2$ (*33*) and triplet $(H + H_2)^+$ (*34*), which do not scatter their products over the full sphere.

References and Notes

1. W. Domcke, D. R. Yarkony, H. Köppel, Eds., *Conical Intersections: Electronic Structure, Dynamics and Spectroscopy* (World Scientific, River Edge, NJ, 2003).
2. G. Herzberg, H. C. Longuet-Higgins, *Discuss. Faraday Soc.* **35**, 77 (1963).
3. H. C. Longuet-Higgins, *Proc. R. Soc. London Ser. A* **344**, 147 (1975).
4. C. A. Mead, D. G. Truhlar, *J. Chem. Phys.* **70**, 2284 (1979).
5. C. A. Mead, *Rev. Mod. Phys.* **64**, 51 (1992).
6. M. S. Child, *Adv. Chem. Phys.* **124**, 1 (2002).
7. M. V. Berry, *Proc. R. Soc. London Ser. A* **392**, 45 (1984).
8. B. E. Applegate, T. A. Barckholtz, T. A. Miller, *Chem. Soc. Rev.* **32**, 38 (2003).
9. B. Lepetit, A. Kuppermann, *Chem. Phys. Lett.* **166**, 581 (1990).
10. A. Kuppermann, Y.-S. M. Wu, *Chem. Phys. Lett.* **349**, 537 (2001).
11. B. K. Kendrick, *J. Chem. Phys.* **112**, 5679 (2000).
12. B. K. Kendrick, *J. Phys. Chem. A* **107**, 6739 (2003).
13. A. J. C. Varandas, L. P. Viegas, *Chem. Phys. Lett.* **367**, 625 (2003).
14. S. Mahapatra, H. Köppel, L. S. Cederbaum, *J. Phys. Chem. A* **105**, 2321 (2001).
15. F. Fernández-Alonso, R. N. Zare, *Annu. Rev. Phys. Chem.* **53**, 67 (2002).
16. A. Kuppermann, in *Dynamics of Molecules and Chemical Reactions*, R. E. Wyatt, J. Z. H. Zhang, Eds. (Marcel Dekker, New York, 1996), pp. 411–472.
17. C. A. Mead, *J. Chem. Phys.* **72**, 3839 (1980).
18. E. Wrede *et al.*, *J. Chem. Phys.* **110**, 9971 (1999).
19. E. Wrede, L. Schnieder, *J. Chem. Phys.* **107**, 786 (1997).
20. S. C. Althorpe *et al.*, *Nature* **416**, 67 (2002).
21. S. A. Harich *et al.*, *Nature* **419**, 281 (2002).
22. J. C. Juanes-Marcos, S. C. Althorpe, *J. Chem. Phys.* **122**, 204324 (2005).
23. J. Stillwell, *Classical Topology and Combinatorial Group Theory* (Springer, New York, 1993).
24. R. P. Feynman, A. R. Hibbs, *Quantum Mechanics and Path Integrals* (McGraw-Hill, New York, 1965).
25. L. S. Schulman, *Techniques and Applications of Path Integration* (Wiley, New York, 1981).
26. G. Morandi, E. Menossi, *Eur. J. Phys.* **5**, 49 (1984).
27. A. I. Boothroyd, W. J. Keogh, P. G. Martin, M. R. Peterson, *J. Chem. Phys.* **104**, 7139 (1996).
28. A. Kuppermann, *Chem. Phys. Lett.* **32**, 374 (1975).
29. From here onward, we are treating the H nuclei as three distinguishable particles. This model gives the physically correct results for (j = even) → (j' = odd) transitions and vice versa. If necessary, the wave function could be symmetrized, which would give the correct even-even and odd-odd results by producing interference between the reactive and inelastic scattering amplitudes. The GP would change the sign of this interference for the direct paths [consistent with an earlier prediction by Mead (*17*)], and leave it unchanged for the looping paths.
30. J. C. Juanes-Marcos, S. C. Althorpe, *Chem. Phys. Lett.* **381**, 743 (2003).
31. M. S. Child, *Molecular Collision Theory* (Dover, New York, 1996).
32. A. J. Dobbyn, P. McCabe, J. N. L. Connor, J. F. Castillo, *Phys. Chem. Chem. Phys.* **1**, 1115 (1999).
33. B. Kendrick, R. T Pack, *J. Chem. Phys.* **106**, 3519 (1997).
34. O. Friedrich, A. Alijah, Z. Xu, A. J. C. Varandas, *Phys. Rev. Lett.* **86**, 1183 (2001).

35. We thank D. Manolopoulos for reading through the manuscript. S.C.A. acknowledges the award of a Royal Society University Research Fellowship. J.C.J.-M. was funded by grant no. GR/S13972 from the UK Engineering and Physical Sciences Research Council.

16 May 2005; accepted 11 July 2005
10.1126/science.1114890

Colloidal Hard-Sphere Crystal Growth Frustrated by Large Spherical Impurities

Volkert W. A. de Villeneuve, Roel P. A. Dullens, Dirk G. A. L. Aarts, Esther Groeneveld, Johannes H. Scherff, Willem K. Kegel, Henk N. W. Lekkerkerker*

Impurities affect the nucleation, growth, and structure of crystals. Here we report the effect of large, spherical, polymethylmethacrylate impurities on the crystal growth of monodisperse, hard, polymethylmethacrylate colloids in a density- and optically matching apolar solvent mixture. Crystal growth, initiated at the bottom of the sample, was studied by imaging sequences of two-dimensional *xy* slices in the plane of the impurity's center with a laser scanning confocal microscope. Impurities form the center of grain boundaries, and a single fluid particle layer around the impurity persists in all cases. The growth rate sensitively depends on the impurity's size. Crystal growth is inhibited to a greater extent near smaller impurities, pointing to local crystal frustration induced by the curvature of the impurity.

Impurities substantially affect crystal nucleation and growth, whether present as an unavoidable nuisance or intentionally added to modify a product or process. Depending on the nature of both the impurity and the main component(s), nucleation and crystal growth are either inhibited, suppressed, or promoted (*1*–*5*). Great effort has been put into understanding many of these altered processes, which are crucial to areas as diverse as the pharmaceutical industry (*6*), mineralogy (*7*), semiconductors (*8*), single-crystal production (*1*, *2*), polymer processing (*9*), and protein crystals (*10*).

We consider the introduction of a large hard sphere, which is the simplest conceivable impurity, into a growing crystal of hard spherical particles. The particle sizes and time scales in colloidal systems enable real-time studies down to the particle level and are therefore excellent model systems for such studies. The impurity (i)/particle (p) diameter ratio $\alpha \equiv (\sigma_i/\sigma_p)$ is a critical factor for such systems: In two-dimensional (2D) binary arrays, translational order is substantially reduced (*11*) and crystal nucleation can be inhibited in polydisperse 3D systems (*12*). In contrast, a single impurity in a metastable fluid phase may induce crystallization by heterogeneous nucleation (*3*). A sphere with infinite diameter (that is, a flat wall) can induce a pre-freezing transition (*13*, *14*). We studied the influence of impurity curvature on a crystal growing around impurities with ratios of α = 5 to 21, which is a different scenario than a crystal nucleating on a curved surface (*3*).

We obtained very large, polydisperse, fluorescently labeled polymethylmethacrylate spheres (PMMA) with diameters ranging from 100 nm to 100 μm from a synthesis following the method of (*15*). A small amount (<0.1 weight %) of these particles, size-fractionated by sedimentation, was mixed with 6% polydisperse 1.5-μm-diameter PMMA particles in an apolar solvent mixture of tetraline, cis-decaline, and tetrachloromethane (solvent volume fractions = 0.35/0.30/0.35; density difference $\Delta\rho \approx$ 0.01 g/ml; and refractive index mismatch $\Delta n_D \approx$ 0.005) (*16*), with a 5-mm sample height. At a 0.55 volume fraction, the high viscosity minimizes impurity diffusion. The crystal nucleates heterogeneously at the glass sample bottom and grows upward, as shown by a control experiment without impurities (Fig. 1A and supporting online material). Homogeneous nucleation occurs only far from the wall. The impurity locks into its current position and moves less than the colloidal particle diameter over several hours. In a sense, this is the reverse scenario from (*17*), where a crystal is disturbed by an external pressure after it has formed. Sequences of 2D *xy* slices were imaged in the plane of the impurity's center; near impurities with α = 5, 10, ~13, and ~ 21 (referred to as I_5, I_{10}, I_{13}, and I_{21}, respectively); 15 to 25 μm above the glass sample bottom; at a rate of three to six slices per minute; up to 2 hours after homogenization. Imaging was performed with a Nikon Eclipse TE2000U confocal microscope with a Nikon C1 scanning head.

Representative confocal slices of crystal growth near impurities are shown in Fig. 1, B to E. Around impurity I_5, crystal growth is initially observed only far from the impurity (Fig. 1B1). The crystal front subsequently grows toward the impurity but is clearly frustrated (Fig. 1B). Frustration is characterized both by limited growth near the impurity (dynamic frustration) and by persistant grain boundaries directed toward the impurity (static frustration). In Fig. 1, C and D, frustration near I_{10} and I_{13} is reduced: A crystal front is present, but crystal growth is observed near the impurity's shell as well (Fig. 1, C2 and D1). Particles in the first layer around the impurity do not crystallize at all; particles in the second layer crystallize only very slowly (Fig. 1, C2 and D2). Here, a relatively low degree of crystallinity during late stages of crystal growth is observed (Fig. 1, C3 and D3). Finally, crystal growth near I_{21} occurs all through the field of view (Fig. 1E). Particles neighboring the impurity are far more dynamic than bulk particles and appear fluidlike (Fig. 1E). Other impurities appear in the field of view through diffusion and sedimentation for this particular sequence. These clearly affect crystal growth, as observed from the grain boundaries connecting impurities. This is not apparent in all cases, because some impurities lie outside the field of view. Grain size seems to scale with impurity size, but the limited data set prohibits statistical analysis. The control experiment also reveals that samples with and without impurities initially have a comparable number of grain boundaries (Fig. 1, A to E, and fig. S1). At low impurity concentrations, the impurities therefore pin the grain boundaries but do not increase their quantity. The grain boundaries gradually anneal in a sample without impurities (Fig. 2C and fig. S3), but persist in between impurities (Fig. 2A).

Several trends are obtained from mere visual comparison of the slice sequences for different values of α. Crystal growth in the first few layers around the impurity seems to proceed faster as α increases. In all sequences, the grain boundaries are directed toward the impurities. The grain boundaries are a consequence of both simultaneous crystal growth at different locations and structural frustration caused by the impurity (Fig. 2, A and B). The first layer around the impurity fails to crystallize: 18 hours after homogenization the fluidlike character of the first layer is still observed (Fig. 2D). At different volume fractions, the same scenario occurs; although at lower volume fractions, sedimentation of the impurity makes experiments difficult. At higher volume fractions, a transition to a glassy state occurs.

To quantify the impurity's effect on local crystal growth, we use the local orientational bond order parameter ψ_6 (*18*)

$$\psi_6(\vec{r}) = \frac{1}{N}\sum_j^N e^{6i\theta(\vec{r_j})} \qquad (1)$$

where $\psi_6 = 1$ for a perfect 2D hexagonal crystal. The summation j runs over all N next neighbors of a given particle. The angle between the bond vector connecting the particle with next neighbor j and an arbitrary fixed reference axis is defined as $\theta(\vec{r_j})$. Particle coordinates are obtained by methods such as those in (*19*). The minimal translation and rotation of the impu-

Van't Hoff Laboratory, Debye Research Institute, University of Utrecht, Padualaan 8, 3584 CH Utrecht, Netherlands.

*To whom correspondence should be addressed. E-mail: h.n.w.lekkerkerker@chem.uu.nl

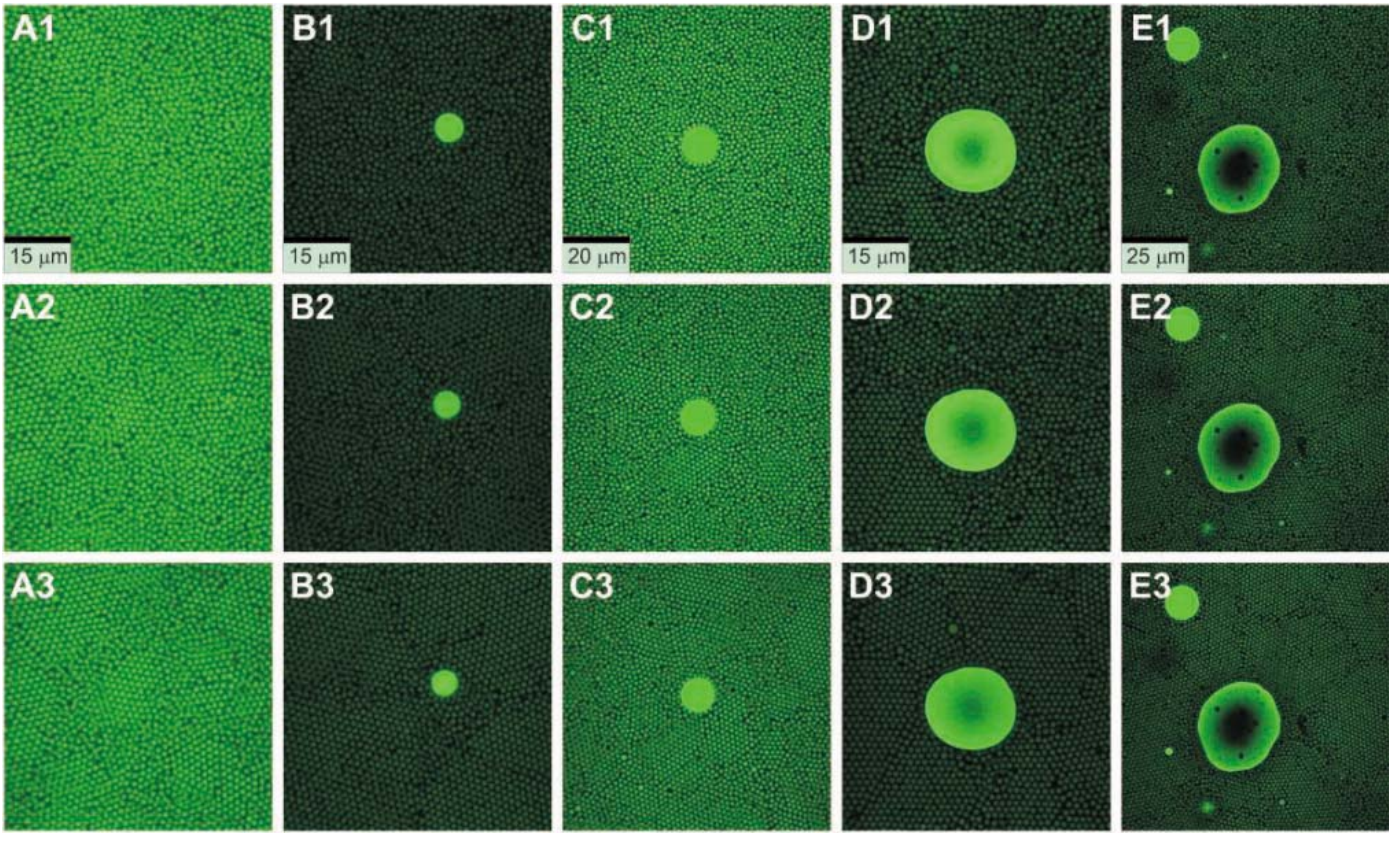

Fig. 1. Confocal images of crystal growth in a sample without impurities (**A**) and near spherical impurities (**B** to **E**). (A) 22 μm above the sample bottom at (A1) 40 min, (A2) 48 min, and (A3) 55 min. (B) I_5 at (B1) 31 min, (B2) 50 min, and (B3) 90 min. (C) I_{10} at (C1) 68 min, (C2) 86 min, and (C3) 103 min. (D) I_{13} at (D1) 41 min, (D2) 57 min, and (D3) 82 min. (E) I_{21} at (E1) 74 min, (E2) 82 min, and (E3) 94 min. Times are the times after sample homogenization.

rity are tracked as well. Particles are divided in shells around the impurity, based on the distance to its shell. Averaging over all particles of shell s, its hexagonal order parameter $\langle|\psi_6|\rangle_s$ is obtained, which is used to obtain a time-dependent crystal growth profile per shell. The presence of other impurities in the I_{21} sequence was "filtered out" (Fig. 3A).

Typical crystal growth profiles of shells 5.0 μm thick around I_{10} are shown in Fig. 3B. All shells start crystallizing simultaneously. The shells evolve from a fluid $\langle|\psi_6|\rangle_s \approx 0.4$ into a more crystalline $\langle|\psi_6|\rangle_s \approx 0.8$, where $\langle|\psi_6|\rangle_s$ reaches a plateau. A constant $\langle|\psi_6|\rangle_s$ value is not reached for the first shell during the image sequence. Crystal growth clearly takes place more rapidly further away from the impurity. An inner shell will have a larger proportion of its shell made up of grain boundaries than will an outer shell. This contributes to the lower observed growth rate close to the impurity. Similar initial and final $\langle|\psi_6|\rangle_s$ values are observed for all α. The degree of crystallinity rises faster with distance to the impurity as α increases, however. This is nicely illustrated in Fig. 3C for the 15- to 20-μm shell, where t_0 indicates the time at which $\langle|\psi_6|\rangle_s$ starts steadily increasing. Crystal growth sets in before I_5 has been locked at its position at depths above ~10 layers. The impurity slowly moves downward because of gravity, which limits the sequences to relatively short intervals, and these are therefore not shown.

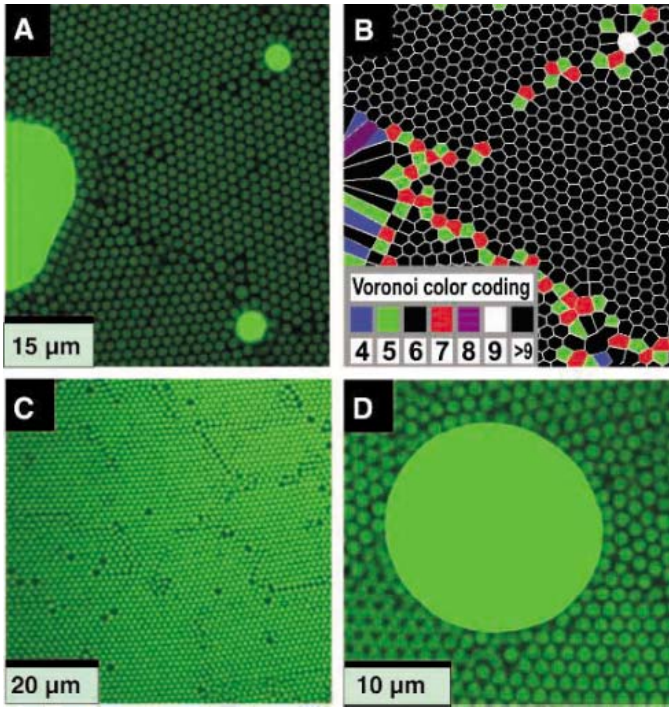

Fig. 2. Grain boundaries and the persisting fluid layer. (**A**) Grain boundaries connect impurities [height, 10 μm; time (*t*), 17 hours]. (**B**) Voronoi representation of (A). Voronoi polygon centers are particle positions. The number of vertices equals the number of next neighbors graphically represented by the color coding in the image. The defects nicely depict the grain boundary. (**C**) In a sample without impurities, grain boundaries have annealed (height, 20 μm; *t*, 13.5 hours). (**D**) The mobile layer of single-particle thickness around an impurity with diameter ratio $\alpha = 13$ appears fluidlike (height, 38 μm; *t*, 18 hours). Heights are distances to the sample bottom. Times are the times after sample homogenization.

The increase in $\langle|\psi_6|\rangle_s$ is approximately linear right after the initial rise. We use this to define the 2D growth rate r_C of shell s

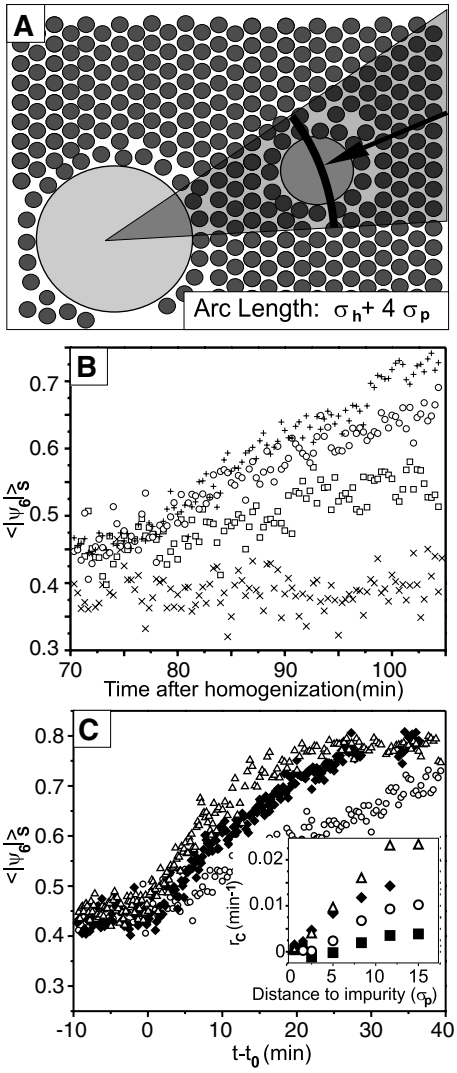

Fig. 3. Quantitative analysis of crystal growth. (**A**) Filtering: Areas affected by other impurities (with a diamenter σ_h) are not taken into account by excluding the shaded area for analysis. (**B**) Crystal growth profiles of shells around I_{10}: 0 to 5 μm (crosses), 5 to 10 μm (squares), 10 to 15 μm (circles), and 15 to 20 μm (plus signs). (**C**) Crystal growth profile of the 15- to 20-μm shell for I_5 (squares, inset only), I_{10} (circles), I_{13} (diamonds), and I_{20} (triangles). (Inset) Frustration of crystal growth increases both as the impurity is approached and as α is decreased. r_C close to I_5 is ~0, because no local increase of order occurs during the recorded image sequence. Rates at 0.5, 1.5, and 2.5 σ_p are based on shells of σ_p thickness. Other r_C values are obtained from shells 5 μm thick: r_C at 5 σ_p corresponds to the 5- to 10-μm shell.

(during linear rise) as $r_C = \Delta\langle|\psi_6|\rangle_s/\Delta t$. The effect of an impurity's size on the local growth rate can now be compared quantitatively (Fig. 3C, inset). Several general trends can be observed. First, a larger α results in a higher rate close to the impurity. Second, the rate rises faster per shell as α increases. Finally, the rates for different α apparently approach a different maximum rate at less than ~17 particle diameters instead of converging to a bulk growth rate of ~0.02 min^{-1} [measured at 5 to 25 μm above the sample bottom in the control sample (fig. S2) and at sample locations far (>40 μm) from impurities]. Relatively far from the impurity (>8 σ_p), a trend is observed between the growth rate and α. We argue that grain boundaries are pinned by impurities (Fig. 2, A and B): If nearby impurities are present, more boundaries appear. To approximate the ideal case of no nearby impurities, the image is filtered (Fig. 3A); grain boundaries leading to impurities further away are not included. The obtained increase of r_C by a factor of 1.6 for the filtered I_{21} sequence therefore is too high, whereas not filtering leads to values that are too low. We therefore expect the rates to converge at sufficient distance, which might very well be beyond ~17 particle diameters. Furthermore, the growth rate in the first layer is about zero for all α—a confirmation of the observed fluid layer (Fig. 2D).

Using laser confocal scanning microscopy, we have shown that the bulk crystal growth rate is substantially reduced near impurities. The extent to which the growth rate is reduced decreases with distance to the impurity. The size ratio α is a critical factor; the (local) curvature of an impurity is therefore crucial for real hard-sphere–like systems such as metals. Grain boundaries are pinned by the impurities, and the first particle layer around the impurity remains fluid. Impurities locally substantially frustrate the crystal growth and structure of hard-sphere systems, the very same impurities that, in a different scenario, can induce heterogeneous crystal nucleation (*3*).

References and Notes

1. N. Kubota, *Cryst. Res. Technol.* **36**, 749 (2001).
2. T. A. Land, T. L. Martin, S. Potapenko, G. T. Palmore, J. J. De Yoreo, *Nature* **399**, 442 (1999).
3. A. Cacciuto, S. Auer, D. Frenkel, *Nature* **428**, 404 (2004).
4. T. A. Eremina *et al.*, *J. Cryst. Growth* **273**, 586 (2005).
5. M. Rak *et al.*, *J. Cryst. Growth* **273**, 577 (2005).
6. A. J. Malkin, Y. G. Kuznetsov, T. A. Land, J. J. Deyoreo, A. McPherson, *Nat. Struct. Biol.* **2**, 956 (1995).
7. K. J. Davis, P. M. Dove, J. J. De Yoreo, *Science* **290**, 1134 (2000).
8. D. T. J. Hurle, P. Rudolph, *J. Cryst. Growth* **264**, 550 (2004).
9. R. Kern, R. Dassonville, *J. Cryst. Growth* **116**, 191 (1992).
10. S. D. Durbin, G. Feher, *Annu. Rev. Phys. Chem.* **47**, 171 (1996).
11. D. Nelson, M. Rubinstein, F. Spaepen, *Philos. Mag. A* **46**, 105 (1982).
12. S. Auer, D. Frenkel, *Nature* **413**, 711 (2001).
13. M. Dijkstra, *Phys. Rev. Lett.* **93**, 103303 (2004).
14. S. Auer, D. Frenkel, *Phys. Rev. Lett.* **91**, 015703 (2003).
15. G. Bosma *et al.*, *J. Colloid Interface Sci.* **245**, 292 (2002).
16. E. H. A. de Hoog, thesis, University of Utrecht, Utrecht, the Netherlands (2001).
17. P. Schall, I. Cohen, D. A. Weitz, F. Spaepen, *Science* **305**, 1944 (2004).
18. D. Nelson, *Defects and Geometry in Condensed Matter Physics* (Cambridge Univ. Press, Cambridge, 2002), pp. 68–91.
19. J. C. Crocker, D. G. Grier, *J. Colloid Interface Sci.* **179**, 298 (1996).
20. G. Bosma is acknowledged for particle synthesis. This work is part of the research program of the Stichting voor Fundamenteel Onderzoek der Materie (FOM), which is financially supported by the Nederlandse Organisatie voor Wetenschappelijk Onderzoek (NWO). Support through the Transregio Sonderforschungsbereich 6 (SFB-TR6) through the Deutsche Forschungsgemeinschaft (DFG) is acknowledged.

Supporting Online Material
www.sciencemag.org/cgi/content/full/309/5738/1231/DC1
SOM Text
Figs. S1 to S3

5 April 2005; accepted 20 July 2005
10.1126/science.1113207

Osmium Isotope Evidence for an *s*-Process Carrier in Primitive Chondrites

A. D. Brandon,[1]*† M. Humayun,[2]† I. S. Puchtel,[3] I. Leya,[4] M. Zolensky[5]

Osmium extracted from unequilibrated bulk chondrites has isotope anomalies consistent with an insoluble *s*-process carrier, termed Os(i) here. Osmium from metamorphosed bulk chondrites does not have isotope anomalies, implying that the Os(i) carrier was destroyed by metamorphism. The isotopic homogeneity of metamorphosed bulk chondrites is consistent with extremely effective mixing of presolar grains from varied sources in the nebula. Osmium in the Os(i) carrier is likely from nucleosynthetic sites with a neutron density about two to four times as high as that of the average solar *s*-process Os.

Presolar grains (such as SiC and nanodiamonds) are prevalent in unequilibrated chondrites and preserve material from nucleosynthetic processes occurring in the stars from which these grains formed (*1*, *2*). The degree to which these grains and solar material were mixed in the solar nebula is uncertain but important for discerning solar system processes. Isotopic anomalies have been identified in presolar grains and Ca-Al–rich inclusions (CAIs) in chondrites (*1*–*4*). We measured Os isotopes to assess heterogeneities in bulk chondrite meteorites: ^{184}Os is produced by the *p* process only; ^{186}Os [*p*-process contribution 1.1% relative (*5*)] and ^{187}Os are produced by the *s* process and radiogenic decay from

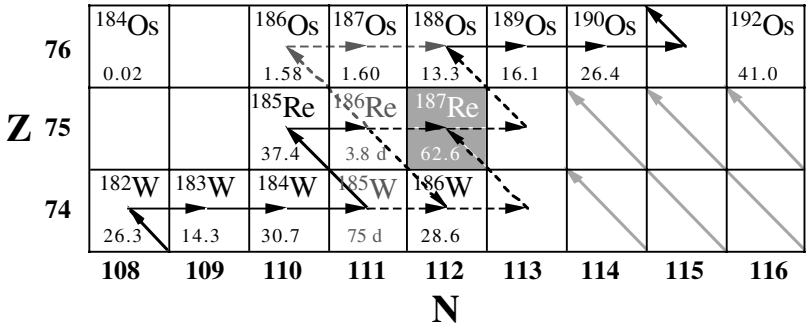

Fig. 1. The *s*-process pathway in the W-Os region. Stable isotopes are indicated in black letters with their isotopic abundances given below the nuclide symbol. Long-lived radioactive elements are indicated in white letters on gray background, and short-lived radioactive elements are indicated in gray letters with their half-lives shown below the nuclide symbol; radionuclides that are not part of this discussion are left blank. The *s*-process pathway comes through monoisotopic ^{181}Ta, branches first at ^{185}W, and then again at ^{186}Re. Both branches combine at ^{188}Os. Three processes occur at ^{186}Re: β^- decay to ^{186}Os (92%), electron capture to ^{186}W (8%, lower at stellar temperatures), and neutron capture to ^{187}Re. The *r* process is shown as oblique long arrows emerging from the lower right corner of the field and terminating at the first stable nuclide. Isotopes shielded from the *r* process include ^{186}Os and ^{187}Os; ^{184}Os is a *p*-only isotope; ^{192}Os is an *r*-only isotope (*s*-process contribution $\ll$1% relative). Z, atomic number; N, neutron number.

^{190}Pt and ^{187}Re, respectively; ^{188}Os, ^{189}Os, ^{190}Os, and ^{192}Os are produced partly by the *s* process but are dominanted by the *r*-process Pt peak (*6*–*8*) (Fig. 1). Stellar nucleosynthetic processes release their products to the interstellar medium as both gas and grains. Osmium condenses as an ultrarefractory metal alloy with Re and W, and behaves as one of the most refractory elements during condensation of stellar outflows. Ultrarefractory grains are more likely to survive nebular thermal processing. We studied seven ordinary chondrites: Chainpur LL3.4, Parnellee LL3.6, Sharps H3.4, St. Marguerite H4, Forest Vale H4, Allegan H5, and Weston H5; three enstatite chondrites: Daniels Kuil EL6, Yilmia EL6, and Indarch EH4; and three carbonaceous chondrites: Tagish Lake C2, Ornans CO3, and Allende CV3. Together, these chondrites span a wide range of compositional groups and metamorphic grades.

The measured Os isotope data (*9*) are displayed in epsilon units (Fig. 2), where ε_{Os} is 10^4 parts deviation from the mean of H-group ordinary chondrites measured in this study. This is because of the overlap of the H-group Os isotope ratios with those of the terrestrial materials, which are interpreted as bulk solar values (Fig. 2). The ε_{186} values are corrected for ^{190}Pt decay over 4.558 billion years to initial values (ε_{186i}; Fig. 2 and table S1). This results in a systematic ~1.1-epsilon correction for all chondrite samples. Because ^{189}Os and ^{192}Os are used for correcting for instrumental mass fractionation, all data have ε_{189} and ε_{192} of zero. The ^{189}Os and ^{192}Os isotopes were chosen for normalization because in solar system Os, these isotopes contain the smallest contribution of *s*-process nucleosynthesis [4.8% and 0.4%, respectively (*6*–*8*)]. This normalization best illustrates variations in the *s*-process components relative to those in *r*-process components (*10*).

Tagish Lake (C2), and to a lesser extent Ornans (CO3), display deficiencies in the *s*-process isotopes relative to most of the ordinary and enstatite chondrites measured, with anomalies in the order: ^{186}Os > ^{188}Os > ^{190}Os (Fig. 2). These deficiencies correlate with the *s*-process abundances of each isotope. Also, Parnellee (LL3.6) and Indarch (EH4) exhibit small negative ε_{186i} (98.9% *s*-process isotope) anomalies.

The variations observed in ε_{Os} could result from cosmic-ray exposure effects, incomplete digestion of insoluble Os carrying phases, or inhomogeneous distribution of the *s*- and *r*-process isotopes in the solar nebula. The effects on Os isotopes from cosmic-ray exposure can be estimated (*11*). For an exposure age of 100 million years, the effect should be from 0.2 to 1 epsilon units for burnout and production of the different Os isotopes. The exposure age for Tagish Lake calculated from ^{21}Ne is 7.8 million years (*12*), and hence, the effects for cosmic-ray exposure should be negligible.

Osmium is hosted in Fe-Ni alloy, refractory metal nuggets, and possibly in presolar SiC or graphite, similar to Ru (*13*–*15*). To determine whether incomplete digestion of an Os carrier was responsible for the effect, we performed a digestion of Tagish Lake using sealed metal jackets with CO_2 overpressure, at temperatures of 325°C for 1 week (*9*, *16*), compared with no overpressure, 240° to 270°C, and 48 to 72 hours for the other digestions. The Os isotopic data for this digestion retains the Os isotopic anomalies (Fig. 2) but not to the same extent as the other digestions for this rock. In addition, the four separate digestions of different clasts from the Tagish Lake meteorite show variable anomalies with systematic depletions, where ^{186}Os > ^{188}Os > ^{190}Os. These observations imply that there is an *s*-process deficit in

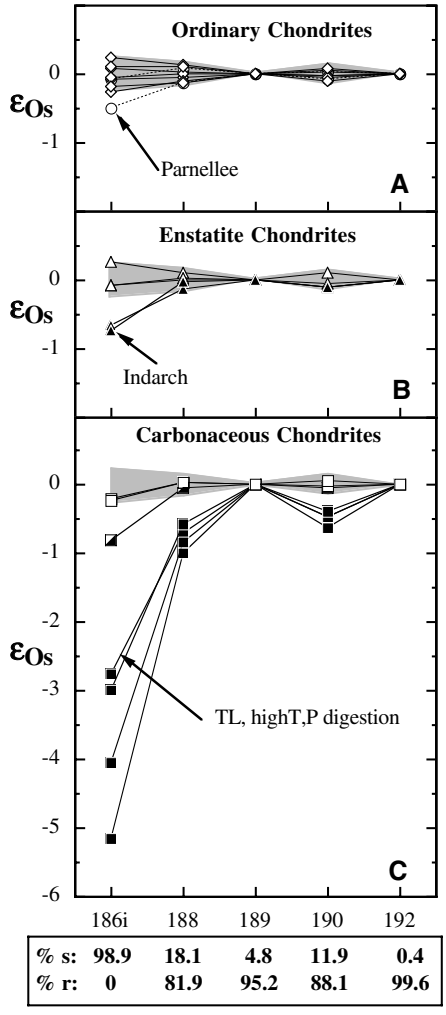

Fig. 2. (**A**) Normalized Os isotopic compositions of H-group (diamonds) and LL-group (circles) ordinary chondrites. (**B**) Normalized Os isotopic compositions of enstatite chondrites. Open triangles, EL6; solid triangles, Indarch EH4. (**C**) Normalized Os isotopic compositions of the carbonaceous chondrites Allende (open squares), Ornans (half-solid squares), and Tagish Lake (TL) (solid squares). The ^{187}Os data are not shown because of large variable contributions from radioactive decay (*9*). The shaded regions are the ±2σ error envelope on 39 runs of the terrestrial standard (external precision). Terrestrial mantle samples (table S1) all plot within these envelopes. Individual data points for each sample have ±0.25 ε_{Os} (2σ) or better uncertainties. The calculated atomic percentage of *s* and *r* processes for each isotope listed are based on models from Beer *et al*. (*8*).

[1]NASA Johnson Space Center, Mail Stop KR, Houston, TX 77058, USA. [2]National High Magnetic Field Laboratory and Department of Geological Sciences, Florida State University, 1800 East Paul Dirac Drive, Tallahassee, FL 32310, USA. [3]Department of Geology, University of Maryland, College Park, MD 20742, USA. [4]Physikalisches Institut, Universität Bern, Sidlerstrasse 5, CH-3012 Bern, Switzerland. [5]NASA JSC, Mail Stop KT, Houston, TX 77058, USA.

*To whom correspondence should be addressed. E-mail: alan.d.brandon1@jsc.nasa.gov

†These authors contributed equally to this work.

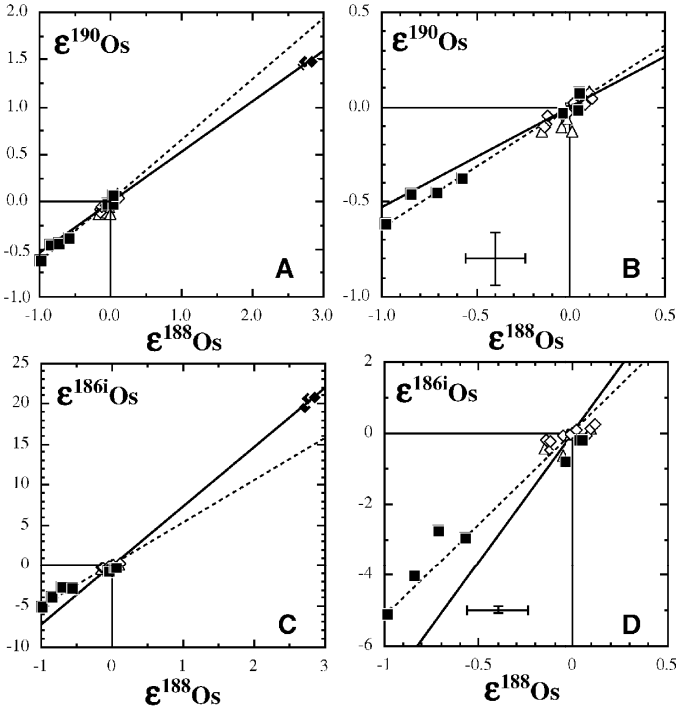

Fig. 3. (**A** and **B**) ε_{190} versus ε_{188} and (**C** and **D**) ε_{186i} versus ε_{188} for carbonaceous chondrites (solid squares), ordinary chondrites (open diamonds), and enstatite chondrites (open triangles). Solar values are at zero. The solid lines are for a regression between solar values at zero and three model solar *s*-process (*7*, *8*) values, which are solid diamonds plotted at times 10^{-4} of their respective values. In (B) and (D) the $\pm 2\sigma$ error bars are shown based on replicate measurements of the terrestrial standard (external precision). The dashed lines are regressions between the Tagish Lake data and solar values at zero. Any component not accessed in the Tagish Lake digestions should lie along these lines at positive values. The Tagish Lake regression line agrees within error of the solar *s*-process regression line for ε_{188} versus ε_{190}. However, the Tagish Lake regression line for ε_{188} versus ε_{186i} is resolvable from the solar *s*-process regression line and trends toward positive values with a depletion in ε_{186i} at a given ε_{188}, relative to the solar regression line.

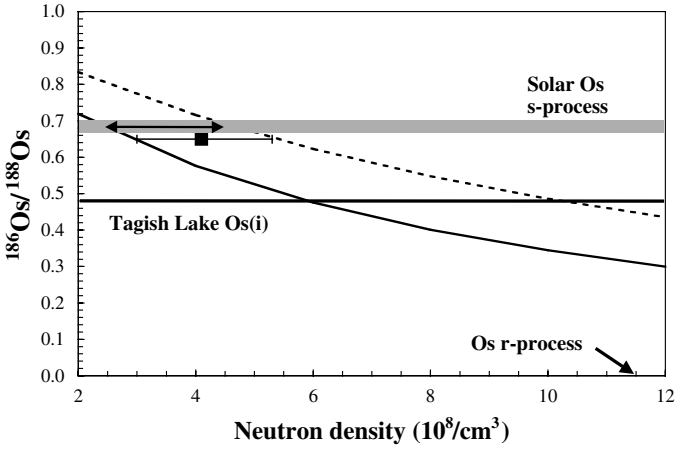

Fig. 4. The *s*-process $^{186}Os/^{188}Os$ ratio depicted as a function of stellar neutron density. The input data, including decay constants and *n*-capture cross-sections, were adjusted for stellar temperature and the curves are shown for $T = 1 \times 10^8$ K (solid black curve) and for $T = 3 \times 10^8$ K (dashed curve). The average solar *s*-process $^{186}Os/^{188}Os$ (*7*, *8*) is shown as the gray shaded band, the *r*-process $^{186}Os/^{188}Os \sim 0$, and the Tagish Lake Os(i) component has $^{186}Os/^{188}Os \sim 0.48$. The range of neutron density implied by the model for the average solar *s* process is shown by the double-arrow compared with the result from Käppeler *et al*. (*21*), which is shown as an error bar. The range of neutron density required to explain the missing component in Tagish Lake is about 2 to 4 times as high as the solar value.

Os extracted from Tagish Lake and suggest that whatever phase is carrying the *s*-process Os, it is either heterogeneously distributed or variably accessed by the digestions. From the *s*-process anomalies observed in Tagish Lake, it can be estimated that 30 to 50 parts per million (ppm) of the total Os (14 to 24 pg/g out of 476 ng/g) are located in the *s*-process carrier. If the carrier phase is presolar SiC, present at ~5 to 8 ppm by weight of Tagish Lake (*17*), then the *s*-process Os concentration is ~1 to 5 ppm. The actual Os concentration could be higher because isotopically normal Os is incorporated from the stellar atmosphere. Elemental abundances in presolar SiC by synchotron x-ray fluorescence for Ru (2 to 57 ppm) and Mo (1 to 54 ppm) (*15*) are of the same order of magnitude as the mean Os abundance (5 to 8 ppm, if SiC is assumed as the carrier phase) in the *s*-process carrier inferred here. The chemical similarity of Os to Ru indicates that some Os may occur in SiC, even though neither element is known to form carbides. Osmium occurs as refractory metal inclusions within presolar graphite grains (*14*), raising the prospect that SiC acts as a protective coating (against acid attack) for ultrarefractory metal condensates. Graphite is soluble in nitric acid, and Os alloys are expected to dissolve in aqua regia, so these grains are not the likely carriers of the observed anomaly given that such grains would have been consumed in the digestions carried out here, unless shielded in a resistant phase such as SiC.

Chondrite metamorphism has been documented to destroy presolar graphite and SiC (*18*). SiC typically has not survived to higher metamorphic grades of >3.8 for ordinary chondrites, and ~5 for enstatite chondrites (*19*, *20*) consistent with such samples showing no Os isotope anomalies (Fig. 2). Thus, the likely interpretation is that an undigested carrier phase, probably SiC, retains the presolar *s*-process Os required to yield the solar *s*/*r* ratio for Os exhibited by H-group ordinary chondrites and terrestrial samples (Fig. 2). This is supported by the observation that two chondrites that underwent less metamorphism—Parnellee (LL3.6) and Indarch (EH4)—show *s*-process anomalies in their Os isotope profiles, but less so than Tagish Lake (C2) and Ornans (CO3). Presolar SiC is present in Indarch and some unequilibrated ordinary chondrites (*19*, *20*). Sharps (H3.4) and Chainpur (LL3.6) do not exhibit Os isotope anomalies but instead plot within the range of epsilon values exhibited by the other H-group ordinary chondrites in Fig. 2.

Although most of Os originates in the *r* process (90%), about 10% of the solar system Os is produced by the *s* process (*6*–*8*). Correlated trends between ε_{186i}, ε_{188}, and ε_{190} can be used to evaluate the nature of the anomalous Os isotopic component (Fig. 3). Mixing lines between average *s*-process Os isotopic composition (*8*) and average solar Os (i.e., ε_{186i}, ε_{188}, and $\varepsilon_{190} = 0$) are resolvable from the correlations of the chondrite data for ε_{188} to ε_{186i} and ε_{190} to ε_{186i} but match the ε_{188} to ε_{190} correlation within error of the measurements (Fig. 3). This implies that the $^{186}Os/^{188}Os$ ratio of the anomalous *s*-process component was lower relative to average solar system *s*-process Os. Here, we term this insoluble Os component Os(i). There are two branches in the *s*-process pathway at ^{185}W and ^{186}Re that allow the *s* process to flow to ^{186}W, ^{187}Re, and then to ^{188}Os (Fig. 1). Neutron capture on ^{185}Re forms ^{186}Re that decays 92% of the time by β^- (half-life of 3.8 days) to ^{186}Os. The two branch points are relatively insensitive to stellar temperature but sensitive to stellar neutron density. These branch points have been used to estimate that the neutron density for average solar *s* process is 4×10^8 n/cm^3 (*5*, *21*). The Os(i) fraction of the solar *s* process requires a stellar source with higher

neutron density. The neutron density (n_n) of the source was modeled by solving the simultaneous linear equations describing *s*-process flow with β^- decay branching to yield

$$\frac{(\langle\sigma\rangle N_s)_{186_{Os}}}{(\langle\sigma\rangle N_s)_{188_{Os}}} = \left(\frac{\lambda_{\beta^-}}{\lambda_{\beta^-} + v_T n_n \langle\sigma\rangle}\right)_{185_W} \times \left(\frac{\lambda_{\beta^-}}{\lambda_{\beta^-} + v_T n_n \langle\sigma\rangle}\right)_{186_{Re}} \times \prod_{A=185}^{A=188} \left[1 + \frac{1}{\tau_0 \langle\sigma\rangle_{A_i}}\right] \quad (1)$$

where v_T is the thermal neutron velocity, λ is the decay constant, N_s is the *s*-process abundance, $\langle\sigma\rangle$ is the maxwellian-averaged neutron capture cross-section, and τ_0 is the average neutron exposure (*21*). The branching decay of ^{186}Re to ^{186}W by electron capture was neglected for this calculation, because electron capture is diminished at the higher degree of ionization prevailing in stellar interiors (*22*). Using cross-sections, decay constants, and τ_0 typical of the *s* process (*5*, *21*, *22*), we calculated ^{186}Os/^{188}Os ratios as a function of stellar neutron density and temperature (Fig. 4). The calculated neutron density for solar *s* process is similar to that obtained in (*21*). The ^{186}Os/^{188}Os ~ 0.48 in Tagish Lake Os(i) is matched at stellar neutron densities of 6×10^8 to 10×10^8 n/cm^3.

There are two major neutron sources for the *s* process produced by helium-burning stellar reactions (α capture): ^{13}C(α,*n*)^{16}O and ^{22}Ne(α,*n*)^{25}Mg. The ^{13}C-source operates at $T \sim 1 \times 10^8$ K and the ^{22}Ne source operates at $T \sim 3 \times 10^8$ K (*8*, *23*). Coupled models of stellar evolution and nucleosynthesis in low-mass asymptotic giant branch stars indicate that during a double neutron pulse the ^{22}Ne source contributes importantly to the abundances of nuclides produced at high neutron densities (up to 10^{10} n/cm^3) (*23*). This has been identified with the meteoritic Ne-E(H) component (*23*) and may also contribute the Os(i) component in Tagish Lake. Likely, the main component of *s*-process Os (and other heavy elements) may be resolved to be a mixture of varied neutron density sources operating in multiple low-mass stars with variable metallicity. Our technique resolved solar *s*-process Os in primitive chondrites into two components: Os(i) that is likely trapped in SiC grains, and aqua regia–soluble Os that is hosted by other phases (magnetite or Fe sulfides), which provide insights into the galactic chemical evolution of Os. The extractable Os either condensed into acid-soluble minerals from stellar outflows with C/O < 1, or it initially condensed in SiC grains which were then selectively destroyed in the interstellar medium (possibly older grains).

This interpretation—that the anomalous Os isotopic composition in unequilibrated chondrites results from incomplete access of up to 50 ppm of the total Os present during digestion—has important ramifications to understanding the presence or absence of isotopic anomalies in bulk meteorites for other elements, including Zr, Mo, and Ru (*4*, *24–29*). Because the Os abundance in bulk meteorites is small (≤1 ppm) and because Os is one of the first elements to condense, mixing within the solar nebula before condensation into planetesimals must have been extremely efficient in order to result in a homogeneous Os isotopic composition of ±0.25 epsilon units (i.e., ±25 ppm) observed in chondrites with greater metamorphic equilibration.

References and Notes

1. E. Zinner, *Annu. Rev. Earth Planet Sci.* **26**, 147 (1998).
2. L. R. Nittler, *Earth Planet. Sci. Lett.* **209**, 259 (2003).
3. M. T. McCulloch, G. J. Wasserburg, *Astrophys. J.* **220**, L15 (1978).
4. Q. Yin, S. Jacobsen, K. Yamashita, *Nature* **415**, 881 (2002).
5. F. Käppeler, R. Gallino, M. Busso, G. Picchio, C. M. Raiteri, *Astrophys. J.* **354**, 630 (1990).
6. E. Anders, N. Grevesse, *Geochim. Cosmochim. Acta* **53**, 197 (1989).
7. H. Palme, H. Beer, *Landolt-Bornstein New Series VI/3a* (Springer-Verlag, Berlin, 1993), pp. 196–221.
8. H. Beer, F. Corvi, P. Mutti, *Astrophys. J.* **474**, 843 (1997).
9. Materials and methods are available as supporting material on *Science* Online.
10. The traditional normalization to ^{188}Os results in the same systematic differences between the chondrites, but the patterns are shifted and *s*-process anomalies are obscured because of the relative deficiency of ^{188}Os due to *s* process.
11. I. Leya, R. Wieler, A. N. Halliday, *Geochim. Cosmochim. Acta* **67**, 529 (2003).
12. T. Nakamura, T. Noguchi, M. E. Zolensky, N. Takaoka, *Lunar Planet. Sci.* **XXXII**, 1621 (abstr.) (2001).
13. R. J. Walker *et al.*, *Geochim. Cosmochim. Acta* **66**, 4187 (2002).
14. T. K. Croat, F. J. Stadermann, T. J. Bernatowicz, *Lunar Planet. Sci.* **XXXVI**, 1507 (abstr.) (2005).
15. Y. Kashiv, Z. Cai, B. Lai, S. R. Sutton, R. S. Lewis, A. M. Davis, R. N. Clayton, M. J. Pellin, *Lunar Planet. Sci.* **XXXII**, 2192 (abstr.) (2001).
16. H. Becker *et al.*, *Lunar Planet. Sci.* **XXXV**, 1310 (abstr.) (2004).
17. M. M. Grady, A. B. Verchovsky, I. A. Franchi, I. P. Wright, C. T. Pillinger, *Meteorit. Planet. Sci.* **37**, 713 (2002).
18. G. R. Huss, *Nature* **347**, 159 (1990).
19. G. R. Huss, R. S. Lewis, *Geochim. Cosmochim. Acta* **59**, 115 (1995).
20. G. R. Huss, in *Astrophysical Implications of the Laboratory Study of Presolar Materials*, T. J. Bernatowicz, E. Zinner, Eds. (Proceedings of the American Institute of Physics, New York, 1997), vol. 402, pp. 721–748.
21. F. Käppeler, S. Jaag, Z. Y. Bao, G. Reffo, *Astrophys. J.* **366**, 605 (1991).
22. K. Takahashi, K. Yokoi, *Atomic Data Nucl. Data Tables* **36**, 375 (1987).
23. R. Gallino *et al.*, *Astrophys. J.* **497**, 388 (1998).
24. N. Dauphas, B. Marty, L. Reisberg, *Astrophys. J.* **565**, 640 (2002).
25. J. H. Chen, D. A. Papanastassiou, G. J. Wasserburg, H. H. Ngo, *Lunar Planet. Sci.* **XXXV**, 1431 (abstr.) (2004).
26. D. A. Papanastassiou, J. H. Chen, G. J. Wasserburg, *Lunar Planet. Sci.* **XXXV**, 1828 (abstr.) (2004).
27. H. Becker, R. J. Walker, *Nature* **425**, 152 (2003).
28. H. Becker, R. J. Walker, *Chem. Geol.* **196**, 43 (2003).
29. M. Schönbächler *et al.*, *Earth Planet. Sci. Lett.* **216**, 467 (2003).

30. We thank the NASA Cosmochemistry program for funding NAG5-13133 (M.H.), NNG05GB81G (M.H.), and RTOP 344-31-72-06 (A.B.). Samples were obtained from the Field Museum of Natural History, American Museum of Natural History, Museum National d'Histoire Naturelle, Natural History Museum of London, and the Smithsonian Institution. We thank H. Becker and an anonymous reviewer for journal reviews.

Supporting Online Material

www.sciencemag.org/cgi/content/full/309/5738/1233/DC1
Materials and Methods
Figs. S1 and S2
Tables S1 to S4
References

19 May 2005; accepted 20 July 2005
10.1126/science.1115053

The Illusion of Invariant Quantities in Life Histories

Sean Nee,[1]* Nick Colegrave,[1] Stuart A. West,[1] Alan Grafen[2]

Life-history theory attempts to provide evolutionary explanations for variations in the ways in which animal species live their lives. Recent analyses have suggested that the dimensionless ratios of several key life-history parameters are the same for different species, even across distant taxa. However, we show here that previous analyses may have given a false picture and created an illusion of invariants, which do not necessarily exist; essentially, this is because life-history variables have been regressed against themselves. The following question arises from our analysis: How do we identify an invariant?

Key parameters that determine how species live their lives are the size at which weaning and sexual maturity occur, the number of offspring produced per year, and life span, among others (*1–3*). A recent approach to understanding the evolution of such life-history parameters has been to show how these analyses can be simplified by examining dimensionless ratios of these parameters, such as the ratio of offspring weaning weight to maternal weight (*1*). This approach has been stimulated by analyses that suggest that these dimensionless ratios can be the same for different species, within and even across taxa (Table 1) (*1*, *4–13*). These life-history invariants can be extremely striking, with the regression analyses used to test for them usually explaining 70 to 97% of the variation

in the data. Such strong correlations are exceptional for evolutionary or ecological studies, where the average study explains approximately 5% of the variation in the data (*14*).

It has been argued that the existence of these invariants implies "symmetry at a deeper level of causal factors" molding life-history evolution (*1*). Potentially, such invariants, along with other dimensionless ratios that can be derived from them, could underpin the form and shape of the tradeoffs that constrain life-history evolution. Consequently, invariants provide the basis of a unified approach to the study of the evolution of life histories, rather than a mixed basket of species-specific models. This potential importance has led not only to a considerable effort being devoted to measuring these invariants empirically (Table 1) (*1*, *4*–*13*) but also to a substantial body of theory that attempts to explain their existence and consequences (*1*, *6*, *7*, *15*–*29*).

However, we show here that previous analyses may have given a false picture and created an illusion of invariants that do not necessarily exist. We start by considering the clearest case, where one of the variables being examined is necessarily a fraction of the other variable. For example, consider offspring-weaning weight, w, and maternal weight, m, measured for a number of species, with the dimensionless ratio w/m postulated to be an invariant (*24*, *25*, *30*). The standard methodology used to test for life-history invariants is to test whether the regression slope of the relationship between $\ln(w)$ and $\ln(m)$ equals 1.0. This is because if the ratio w/m is invariant and equal to some constant c, then a regression of $\ln(w)$ versus $\ln(m)$ would have a slope of 1.0, and an intercept of $\ln(c)$. Although this is true, the converse is not; i.e., a slope of 1.0 does not imply invariance.

Consider the extreme case where the ratio w/m is not invariant and is actually a random variable drawn from a uniform distribution between 0 and 1, which we represent by the variable c. The model is $\ln(w) = \ln(m) + \ln(c)$, which is in the form of a simple linear regression with slope 1.0, $y = x + \varepsilon$, where $\ln(c)$ is the non-normally distributed error term ε. A regression analysis of data simulated according to this model would return a slope not significantly different from 1.0. Suppose, for the sake of simplicity, that a regression analysis returns a slope of exactly 1.0. Then the R^2 of the regression, which is the proportion of the variation (var) in the dependent variable y, explained by the variation in the independent variable x, is given by

$$R^2 = \frac{\mathrm{var}[\ln(w)] - \mathrm{var}[\ln(c)]}{\mathrm{var}[\ln(w)]} = \frac{\mathrm{var}[\ln(m)]}{\mathrm{var}[\ln(m)] + \mathrm{var}[\ln(c)]} \quad (1)$$

An example of an analysis performed on simulated data is given in Fig. 1A. This analysis returns a regression slope of 1.0 and an R^2 of 0.94. Figure 1B makes clear that the ratio w/m is far from invariant. Hence, this approach to identifying invariants is invalid.

For this class of so-called invariants, the slope of 1.0 arises because we are, in effect, regressing a variable, X, on X. What accounts for the high R^2? When c is drawn from a uniform distribution between 0 and 1, $\ln(c)$ has a variance of 1.0. What accounts for the fact that $\mathrm{var}[\ln(m)] \gg 1.0$? The short answer is that we assumed it does; we simulated data with a variance of 9 (Fig. 1). In real studies, a large variance arises when the data vary over several orders of magnitude; loosely speaking, when the ratio of the largest to the smallest is high. The relationship between orders of magnitude and the variance of a log-normal distribution is as follows. For reasons of familiarity, we will discuss this in terms of $\log_{10}$ transformations. If two data values differ by a factor of 10, an order of magnitude, this is their ratio and it is dimensionless. The value of $\mathrm{var}[\ln(m)]$ is also independent of the scale of measurement. If we plot the logarithmically transformed data, each unit increment on the $\log_{10}$ scale corresponds to a factor of 10. 95% of the data lie between ±2 SD (σ) of the mean. If on the arithmetic scale, the bulk of the data span M orders of magnitude, then the variance of the data $\sigma^2 \approx (M/4)^2$.

Hence, if m varies over many orders of magnitude, then $\mathrm{var}[\ln(m)] \gg 1.0$, and our R^2 is guaranteed to be high. The most notable invariants are typically taken to be those that hold over several orders of magnitude of variation in the value of the biological characters; we now see that it is this wide variability of the characters that inevitably makes the invariants notable. (The converse also holds: Data that do not span several orders of magnitude may be highly likely to display a slope numerically different from 1.0 and may have a low R^2.) The R^2 in this particular example would be even higher if we chose values of c from more realistic uniform distributions, such as from the range 0.3 to 1.

The above argument applies to a number of other proposed life-history invariants, where one variable is a simple fraction of the other; for example, size at sex change divided by the maximum body size, or the body size at maturity divided by the maximum asymptotic body size (Table 1).

However, this argument can be readily generalized to other biological variables that involve somewhat more complicated relationships. Consider, for example, the relationship between age at maturity, α, and average adult life span, A, the ratio of which has been argued to be invariant within several taxa (Table 1). Let T be the average total life span of members of a species. Let p be a uniform random number between 0 and 1, so that $\alpha = pT$ and $A = (1 - p)T$, giving

$$\frac{\alpha}{A} = \frac{p}{1 - p} \quad (2)$$

Clearly the ratio α/A is not an invariant. However, our model is again of the form $\ln(\alpha) = \ln(A) + \ln(p) - \ln(1 - p)$, so we expect

Table 1. Life-history invariants. Shown are some of the dimensionless ratios that have been shown to be life-history invariants, with the use of the regression analysis described in the text.

Dimensionless ratio	Taxa within which invariance has been demonstrated	References
Weaning weight (w)/maternal weight (m)	Mammals	(*1*, *8*, *9*)
Average adult life span (A)/age at maturity (α)	Mammals, angiosperms, snakes, lizards, shrimps, nematodes	(*1*, *6*, *10*, *11*)
Mortality rate (M)/growth coefficient (K)	Fish, shrimps, snakes, lizards, sea urchins, turtles	(*1*)
Length at maturity (l_α)/ maximum asymptotic length (l_∞)	Fish, lizards, snakes	(*1*, *35*)
Yearly fecundity (b) × age at maturity (α)	Mammals	(*1*)
Yearly fecundity (b)/mortality rate (M)	Birds, bats	(*1*, *9*, *13*)
Maximum asymptotic length (l_∞)/ growth coefficient (K)	Fish genera	(*1*)
Size at sex change (L_{50})/maximum size (L_{max})	Animals (fish, crustaceans, mollusks, echinoderms)	(*4*, *7*)
Age at sex change (τ)/age at maturity (α)	Fish	(*5*)
Fraction of body mass to reproduction per unit time (C)/average adult life span (A)	Fish, birds, mammals	(*29*)

[1]Institute of Evolutionary Biology, School of Biological Sciences, University of Edinburgh, West Mains Road, Edinburgh, EH9 3JT, UK. [2]Department of Zoology, University of Oxford, South Parks Road, Oxford, OX1 3PS, UK.

*To whom correspondence should be addressed. E-mail: sean.nee@ed.ac.uk

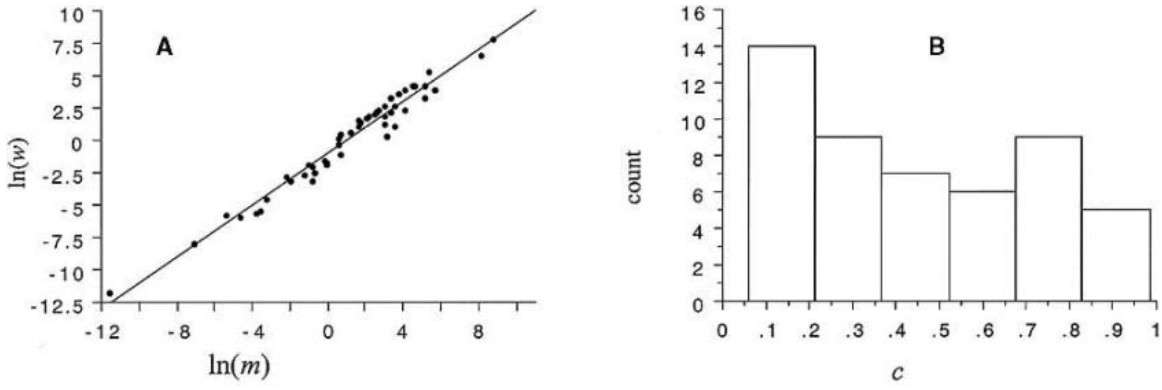

Fig. 1. (**A**) We randomly generated 50 log-normally distributed maternal weights, m, such that $\ln(m)$ was normally distributed with mean = 2 and SD = 3. This generated a range of weights between 0.001 and just under 7000 units. Because weaning weight, w, must obviously be some fraction of adult body weight, we generated the ratios, c, by drawing 50 random numbers from a uniform distribution between 0 and 1. The figure shows weaning weight plotted against maternal weight on a log-log scale [$\ln(w)$ versus $\ln(m)$]. Regression analysis gives a slope not significantly different from 1, and $R^2 = 0.94$. According to current convention (Table 1), this means that the ratio, c, is invariant. If we repeat this process 1000 times we get an average R^2 of 0.900 ± 0.001 (SE) with 95% of the runs giving values between 0.799 and 0.957. (**B**) The ratio of weaning weight divided by maternal weight ($c = m/w$) plotted as a histogram. Other random simulations on bounded variables provide similar results (*24*, *25*, *30*).

a regression slope of 1.0, because we are regressing X on X, and we expect an R^2 of

$$R^2 = \frac{\mathrm{var}[\ln(A)]}{\mathrm{var}[\ln(A)] + \mathrm{var}[\ln\left(\frac{p}{1-p}\right)]} \quad (3)$$

Once again, R^2 will be high if A is highly variable.

Some invariants require a moment's reflection before it is seen how they fit into this framework. Consider, for example, the relation between a bird's yearly clutch size, b, and adult mortality rate, M. Suppose that a bird species has E eggs in total over its adult lifetime of Y years; then its yearly clutch size b is E/Y and its annual mortality rate M is $1/Y$. Therefore, $b = ME$, a regression of $\ln(b)$ against $\ln(M)$ is expected to have a slope of 1.0, and

$$R^2 = \frac{\mathrm{var}[\ln(M)]}{\mathrm{var}[\ln(M)] + \mathrm{var}[\ln(E)]} \quad (4)$$

Charnov [table 1.1 and fig. 1.2 in (*1*)] carries out this regression analysis on data on b and M and finds a slope not significantly different from 1.0. When we compute $E = b/M$ from his tabulated data, we can use the above formula to calculate that the R^2 should be 0.84, which is what Charnov found it to be. More generally, it can be shown that all of the other so-called invariants listed in Table 1 are amenable to the same treatment we have illustrated here.

The studies in Table 1 all explicitly use the regression analysis we have described to demonstrate that a ratio is invariant. From the time of the introduction of invariants, many other studies and discussions have accepted their existence on the basis of these sorts of demonstrations and attempted to explain them theoretically or infer their consequences (*6*, *15*–*23*, *26*, *27*). For example, in his review of the canonical monograph on life-history invariants (*1*), Maynard Smith refers to the M/b data we have just discussed and says "M/b is approximately constant (≈0.2) for species as different as the tree sparrow and wandering albatross" (*31*). This is in spite of the fact that the data to which he is referring show the ratio varying between 0.1 and 0.5. Maynard Smith was not the only reviewer to accept that this ratio is constant (*32*), and the status of these life-history invariants is such that they have now found their way into the popular physics literature (*33*). In fact, in a population of constant size, the ratio M/b is, essentially, the probability of surviving from egg to breeding age and therefore is constrained to be between 0 and 1.

Given the clear invalidity of using the regression analysis described, a major unresolved problem is how we should search for invariants. One approach that has been suggested is to continue using such analyses, but to compare the R^2 generated by an explicit null model, similar to that used to produce Fig. 1, with that generated by the actual data. Invariance is then accepted if the real data produce an unusually high R^2 (*24*, *25*, *30*). However, there is an obvious difficulty with this approach. How does one choose the null model for comparison (*25*)? In Fig. 1, we used a uniform distribution between 0 and 1, but we could have equally argued for a uniform distribution between, say, 0.5 and 0.9. In addition, the uniformity of the data is not relevant to the question of invariance, because non-uniform distributions can be highly variable, whereas a uniform distribution may have tight bounds. An alternative approach is to examine the covariation between the proposed invariant and other traits considered to be of general importance to life history, such as body size. If covariance is found, the candidate invariant can be rejected (*34*). However, the lack of any systematic variation in a trait, although it is potentially interesting, is very different from a lack of any variation.

We believe that the best way forward in addressing the existence and importance of invariants is to develop procedures to compare the relative variation in the proposed invariant across species to variation in other scale-free, but not necessarily invariant, measures. If proposed invariants can be expressed in terms of other scale-free measurements, randomization procedures can be used to determine whether the observed values of the invariant are a particularly constrained subset of those that are obtained when the scale-free measurements are allowed to vary independently. Furthermore, this emphasizes that although life-history invariants are often seen as the flagship of the dimensionless approach, the two are in fact separate, and there is no doubt that the dimensionless approach is useful for organizing life histories and looking for general differences across taxa (*1*, *6*, *29*). There may even be a benefit to generalizing the study of dimensionless quantities beyond simple ratios to other homogenous functions of degree zero. Although the dimensionless numbers being examined may not be invariant, the mean values may still differ in interesting ways across taxa. For example, the relationship between the age at maturity, α, and the average adult life span, A, groups taxa into poikilothermic indeterminate growers (fish, nematodes, and shrimp), mammals, and birds (*1*, *10*). Such analyses suggest differences that are likely to reflect major differences in the forms of the underlying tradeoffs and open up an array of questions that are more specific (*6*).

References and Notes

1. E. L. Charnov, *Life History Invariants* (Oxford Univ. Press, Oxford, 1993).
2. S. C. Stearns, *The Evolution of Life Histories* (Oxford Univ. Press, Oxford, 1992).
3. D. A. Roff, *Life History Evolution* (Sinaue, Sunderland, MA, 2002).
4. D. J. Allsop, S. A. West, *J. Evol. Biol.* **16**, 921 (2003).
5. D. J. Allsop, S. A. West, *Nature* **425**, 783 (2003).
6. E. L. Charnov, *Evol. Ecol. Res.* **4**, 749 (2002).

7. E. L. Charnov, U. Skuladottir, *Evol. Ecol. Res.* **2**, 1067 (2000).
8. A. Purvis, P. H. Harvey, *J. Zool.* **237**, 259 (1995).
9. K. E. Jones, A. MacLarnon, *Evol. Ecol. Res.* **3**, 465 (2001).
10. A. W. Gemmill, A. Skorping, A. F. Read, *J. Evol. Biol.* **12**, 1148 (1999).
11. S. Morand, *Funct. Ecol.* **10**, 210 (1996).
12. R. E. Willemsen, *J. Zool.* **248**, 379 (1999).
13. R. E. Ricklefs, *Condor* **102**, 9 (2000).
14. A. P. Moller, M. D. Jennions, *Oecologia* **132**, 492 (2002).
15. M. Heino, V. Kaitala, *J. Evol. Biol.* **12**, 423 (1999).
16. N. P. Lester, B. J. Shuter, P. A. Abrams, *Proc. R. Soc. London Ser. B* **271**, 1625 (2004).
17. K. Hawkes, *Nature* **428**, 128 (2004).
18. E. P. Economo, A. J. Kerkhoff, B. J. Enquist, *Ecol. Lett.* **8**, 353 (2005).
19. J. X. He, *Ecology* **82**, 784 (2001).
20. J. Kozlowski, J. Weiner, *Am. Nat.* **149**, 352 (1997).
21. M. Mangel, *Evol. Ecol.* **10**, 249 (1996).
22. A. L. Jensen, *Can. J. Fish. Aquat. Sci.* **53**, 820 (1996).
23. J. R. Beddington, G. P. Kirkwood, *Philos. Trans. R. Soc. London Ser. B* **360**, 163 (2005).
24. P. M. Buston, P. L. Munday, R. R. Warner, *Nature* **428**, 783 (2004).
25. A. Gardner, D. J. Allsop, E. L. Charnov, S. A. West, *Am. Nat.* **165**, 551 (2005).
26. E. H. Williams, K. W. Shertzer, *Can. J. Fish. Aquat. Sci.* **60**, 710 (2003).
27. J. Kozlowski, *Proc. R. Soc. London Ser. B* **263**, 556 (1996).
28. E. L. Charnov, *Nature* **387**, 393 (1997).
29. E. L. Charnov, T. F. Turner, K. O. Winemiller, *Proc. Natl. Acad. Sci. U.S.A.* **98**, 9460 (2001).
30. R. Cipriani, R. Collin, *J. Evol. Biol.* 10.1111/j.1420-9101.2005.00949.x (2005).
31. J. Maynard Smith, *Q. Rev. Biol.* **68**, 557 (1993).
32. D. B. Miles, *Ecology* **75**, 2143 (1994).
33. G. B. West, J. H. Brown, *Phys. Today* **57**, 36 (2004).
34. J. Clobert, T. Garland, R. Barbaut, *J. Evol. Biol.* **11**, 329 (1998).
35. R. E. Willemsen, A. Hailey, *J. Zool.* **248**, 379 (1999).
36. S.W. is funded by The Royal Society. We are grateful to three anonymous referees, one of whom pointed out the constraint on the *M/b* ratio referred to in the text.

5 May 2005; accepted 4 July 2005
10.1126/science.1114488

Multiple Causes of High Extinction Risk in Large Mammal Species

Marcel Cardillo,[1,2]* Georgina M. Mace,[2] Kate E. Jones,[4]† Jon Bielby,[2] Olaf R. P. Bininda-Emonds,[5] Wes Sechrest,[4]‡ C. David L. Orme,[1] Andy Purvis[1,3]

Many large animal species have a high risk of extinction. This is usually thought to result simply from the way that species traits associated with vulnerability, such as low reproductive rates, scale with body size. In a broad-scale analysis of extinction risk in mammals, we find two additional patterns in the size selectivity of extinction risk. First, impacts of both intrinsic and environmental factors increase sharply above a threshold body mass around 3 kilograms. Second, whereas extinction risk in smaller species is driven by environmental factors, in larger species it is driven by a combination of environmental factors and intrinsic traits. Thus, the disadvantages of large size are greater than generally recognized, and future loss of large mammal biodiversity could be far more rapid than expected.

A major challenge for conservation biology is to explain why some species are more likely to be threatened with extinction than others (*1*). One of the traits associated most often with high extinction risk among animal species is large body size (*2*). In mammals, for example, declining species considered threatened with extinction are an order of magnitude heavier (1374 ± 1.43 g), on average, than nonthreatened species (139 ± 1.13 g) (*3*). Futhermore, the size selectivity of the current extinction crisis echoes past extinction events such as that of the late Pleistocene, which disproportionately affected larger species (*4*, *5*). However, it is not clear which mechanisms are primarily responsible for the association between body size and extinction risk (*5*–*9*), and a thorough investigation requires large comparative data sets for sizable groups of species spanning a wide range of body sizes. Here, we investigate the association between size and risk with the use of a data set including nearly 4000 species of nonmarine mammals, a group spanning eight orders of magnitude in body mass, from the 2-g least woolly bat to the 4000-kg African elephant.

We used multiple linear regression on phylogenetically independent contrasts (*10*) to test associations between extinction risk and a range of predictor variables. As our measure of extinction risk, we followed previous studies in the use of classifications based on criterion A of the IUCN Red List (*3*), converted to a numerical index from 0 to 5 (*11*–*13*). This corresponds to a coarse but quantitative measure of the rate of recent and ongoing decline and excludes those threatened species listed simply on the basis of small geographic distribution or population size (*3*). Potential predictors of extinction risk can be grouped into three broad types: (i) environmental factors, where the size and location of a species' geographic range determines the environmental features and human impact to which it is exposed; (ii) species' ecological traits, such as population density; and (iii) species' life-history traits, such as gestation length. To represent each of these types, we selected six key predictors [geographic range size, human population density, an index of external threat level, population density, gestation length, and weaning age; see (*10*) for justification].

Extinction risk shows a positive association with adult body mass [t = 3.86, degrees of freedom (d.f.) = 1530, P = 0.0001, controlling for geographic range size]. In separate regression models, each key predictor except weaning age is also significantly associated with extinction risk (Table 1). When a term describing the interaction between body mass and the key predictor is added to each model, a significant interaction is found in every case except in the model for geographic range size (Table 1). In every model, the sign of the interaction term indicates that the slope of extinction risk against the key predictor becomes steeper with increasing body mass. The effects of risk-promoting factors on extinction risk, therefore, become stronger as body mass increases.

To visualize the effects of these interactions between body mass and the key predictors on extinction risk, we fitted models within a sliding window with a width of 2 units on the scale of ln(body mass) and moved the window along the body-mass axis at increments of 0.5 units (Fig. 1). For all predictors, slopes of extinction risk varied substantially along the body-mass axis, confirming the significant body-mass interactions in the regression models. In all cases, there was a sharp increase in slope toward the upper end of the body-mass scale, with steepest slopes found in or near the largest body-mass interval. For weaning age, population density, and external threat, this sharp increase in slope occurs at around 3 kg; for gestation length and geographic range size, it occurs above 20 kg. The slope of extinction risk against human population density increases steadily at smaller body sizes, then drops sharply at around 3 kg, although the steepest positive slope is nevertheless found in the largest body-mass interval (Fig. 1).

[1]Division of Biology, Imperial College London, Silwood Park, Ascot SL5 7PY, UK. [2]Institute of Zoology, Zoological Society of London, Regent's Park NW1 4RY, UK. [3]Natural Environmental Research Council (NERC) Centre for Population Biology, Imperial College London, Silwood Park, Ascot SL5 7PY, UK. [4]Department of Biology, University of Virginia, Charlottesville, VA 22904–4328, USA. [5]Lehrstuhl für Tierzucht, Technical University of Munich, Alte Akademie 12, 85354 Freising-Weihenstephan, Germany.

*To whom correspondence should be addressed. E-mail: m.cardillo@imperial.ac.uk

†Present address: Earth Institute, Center for Environmental Research and Conservation, Columbia University, 1200 Amsterdam Avenue, MC5556, New York, NY 10027, USA.

‡Present address: World Conservation Union (IUCN) Global Mammal Assessment, c/o Center for Applied Biodiversity, Conservation International, 1919 M Street N.W., Suite 600, Washington, DC 20036, USA.

Dividing mammal species into small-bodied and large-bodied subgroups at a cutoff of 3 kg, we used multiple regression with model simplification to find the sets of predictors, selected from a wide range of variables (table S1), that independently contribute to extinction risk in each subgroup (Table 2). For species smaller than the cutoff body mass, the minimum adequate regression model includes no intrinsic biological traits, only environmental factors determined by the size and the location of species' geographic ranges (size and median latitude of geographic range and human population density and external threat level within the geographic range). For species larger than the cutoff body mass, intrinsic biological traits (population density, neonatal mass, and litters per year), in addition to environmental factors, are independent, significant predictors of extinction risk. This basic result is robust to bracketing the small-large cutoff below and above 3 kg; the sets of significant predictors vary only slightly in each case (*10*).

Large size has often been linked to elevated extinction risk in mammals because larger species tend to exist at lower average population densities (*14*), the intrinsic rate of population increase declines with body mass (*15*), and larger species are disproportionately exploited by humans (*16*, *17*). However, our models reveal further complexity in the association between size and extinction risk and provide a compelling explanation for the strong size selectivity of the current extinction crisis that goes beyond a simple scaling of risk-promoting factors with body size. Intrinsic factors predict extinction risk only in species weighing more than 3 kg; above this size, susceptibility to both intrinsic and external threats increases sharply. This may represent the approximate body mass above which extinction risk begins to be compounded by the cumulative effects of multiple threatening factors. For example, forest fragmentation elevates the sensitivity to hunting pressure of populations of medium- and large-sized vertebrates (*18*), and larger body sizes demand larger home ranges, bringing individuals into increasing contact with people in fragmented habitats (*19*). Above certain critical body sizes, species become targets for increased hunting pressure: in neotropical forests, subsistence hunter preference increases abruptly for mammal species above about 6.5 kg (*16*). Those species with low population densities or slow life histories, which tend to be of larger size, are the most vulnerable to population declines caused by hunting (*17*).

The reason for the sharp dip in the slope of extinction risk against human population density around the same body mass that the slopes of other predictors increase is less intuitive. It could represent the effects of an extinction filter, whereby the most susceptible species have long since disappeared from regions of highest human population density, leaving behind a fauna consisting of species more robust to extinction (*20*). This scenario is supported by evidence for widespread disappearance of mammal populations from regions of high human population density (*21*).

Our results also suggest that, as human impacts on natural environments continue to increase, declines toward extinction will be more rapid, on average, in large species compared with small species with similar biological characteristics or that are exposed to similar amounts of human impact. This can be illustrated with the use of our model predicting extinction risk from the level of external threat (Table 1 and table S2). We predicted extinction risk for two hypothetical species that vary in body mass but are identical in other respects (we assigned both species the median values for all mammals of geographic range size and degree of exposure to external threat). From this model we obtained a predicted extinction risk index value of 1.00 for a species of 300 kg compared with only 0.38 for a species of 300 g. The difference in predicted risk stems solely from the difference in body size and the interaction between body size and external threat. This, together with the interactions between other risk-promoting factors and body

Table 1. Separate regressions of key predictors against extinction risk. Each test includes geographic range size as a covariate; tests for weaning age, gestation length, and population density also include adult body mass as a covariate. For clarity, only results for key predictors and interaction terms are shown here; quadratic and cubic terms are shown where significant. Full model results are in table S2. HPD, mean human population density; ETI, external threat index (*10*). Dagger indicates $P \leq 0.1$; single asterisk, $P \leq 0.05$; double asterisks, $P \leq 0.01$; triple asterisks, $P \leq 0.001$. Blank entries indicate terms that were not measured or not significant in a particular model.

Predictors	Predictors tested without body-mass interaction			Predictors tested with body-mass interaction		
	d.f.	slope	*t*	d.f.	slope	*t*
Weaning age	674	0.034	0.5	673	–0.344	–2.87**
Weaning age:body mass					0.074	3.8***
Gestation length	748	–5.754	–3.34***	747	–1.447	–2.96**
(Gestation length)^2		0.666	3.5***			
Gestation length:body mass					0.183	4.19***
Population density	570	–0.058	–3.35***	569	0.064	1.73†
Population density:body mass					–0.015	–3.73***
Geographic range size	1625	0.311	1.61	1623	0.305	1.52
(Geographic range size)^2		–0.043	–2.47*		–0.042	–2.36*
(Geographic range size)^3		0.001	2.37*		0.001	2.26*
Geographic range size:body mass					0.0004	0.12
HPD	1595	–0.154	–2.95**	1594	–0.075	–0.63
HPD^2		0.024	3.14**		–0.053	–1.34
HPD^3					0.008	2.06*
HPD:body mass					0.018	3.51***
ETI	1592	–0.562	–1.32	1589	–5.783	–4.45***
ETI^2		1.02	3.6***		6.256	3.48***
ETI^3					–1.941	–2.71**
ETI:body mass					0.366	5.73***

Table 2. Minimum adequate regression models of extinction risk. Results shown are models where each predictor is significant at $P \leq 0.05$ after model simplification (*10*). Dagger, $P \leq 0.1$; single asterisk, $P \leq 0.05$; double asterisks, $P \leq 0.01$; triple asterisks, $P \leq 0.001$. Blank entries indicate terms that were not measured or not significant in a particular model.

Predictors	Small species (<3 kg) (d.f. = 1207)		Large species (≥3 kg) (d.f. = 131)		All species (d.f. = 404)	
	slope	*t*	slope	*t*	slope	*t*
Geographic range size	–0.142	–14.03***	–0.165	–3.9***	–0.516	–2.52*
(Geographic range size)^2					0.016	2.13*
Latitude	0.01	5.49***				
HPD	–0.084	–2.1*			1.65	5.36***
HPD^2	0.03	3.48***			–0.081	–3.81***
ETI	0.629	3.71***	1.82	2.99**		
Weaning age					0.3	3.46***
Neonatal mass			0.401	2.09*		
Litters per year			–0.618	–2.04*		
Population density			–0.111	–0.27**	–0.148	–0.45***
(Population density)^2					0.013	2.91**
Geographic range size:HPD					–0.087	–4.62***
Geographic range size:population density					–0.045	–3.03**

size, suggests that the ongoing loss of the world's large mammal biodiversity could be far more rapid than currently predicted [for example, by extrapolating from current extinction risk levels (*22*, *23*)]. The likelihood of this loss being highly selective and clustered in large-bodied groups, such as ungulates and primates, means the concomitant loss of mammalian evolutionary history and ecological diversity could also be greater and more rapid than currently expected (*24*, *25*).

A recurring question in the study of extinctions, both recent and prehistoric, has been whether species that have declined or gone extinct have been the victims of bad genes or simply bad luck (*26*, *27*). Our results suggest the answer to this question may be different for small and large mammals. Smaller species are more likely to become threatened simply through environmental disadvantage: that is, the size and location of their geographic ranges and the levels of human impact to which they are exposed. For larger species, intrinsic biological traits become a significant determinant of extinction risk in addition to environmental factors: Large species are thus more likely to be evolutionarily predisposed to decline. One implication this has for conservation is that it provides a possible means of reconciling opposing views over whether area-based or species-based approaches to conservation are most effective (*28*). Smaller species should, in general, benefit more from the conservation of important threatened areas, whereas larger species will tend to benefit most from a conservation approach that also singles out individual species for particular attention. We do not suggest that detailed ecological studies of small mammal species are unimportant; in conservation planning, there is no substitute for a thorough knowledge of each species' unique circumstances. However, analyses of global patterns of extinction risk from large-scale comparative studies such as ours can lead to a better general understanding of the underlying causes of decline and, importantly, of the selectivity of decline among different species. This may help to identify those species likely to be most susceptible to future decline, providing the basis for a more preemptive approach to conservation planning.

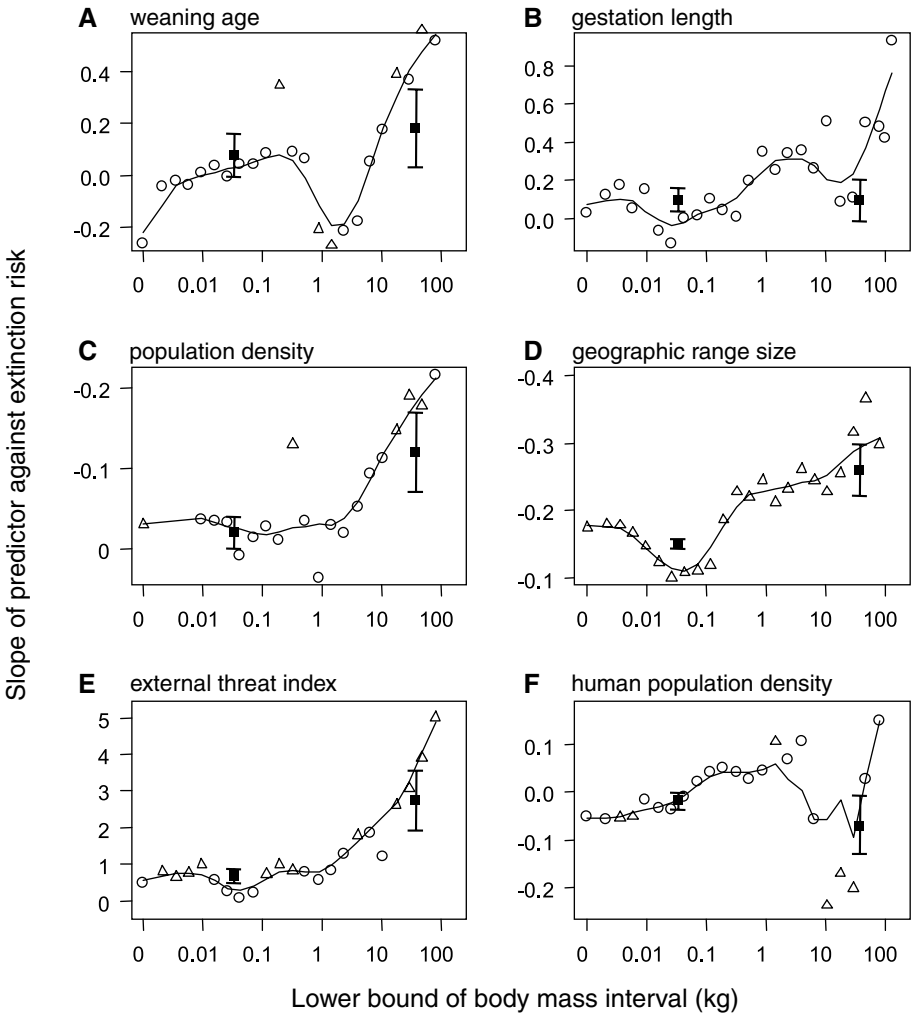

Fig. 1. (**A** to **F**) Slopes of key predictors against extinction risk at different body masses. Each point is located at the lower bound of a body-mass interval of width 2ln(g). Triangles indicate slopes significantly greater or less than zero ($P \leq 0.05$); circles, slopes not significantly different from zero. Lines are Lowess smoothers fitted through the points with span of 0.3. Solid squares indicate slopes (±1 SE) of the predictor against extinction risk for small (<3 kg) and large (≥3 kg) species, respectively. Dashed horizontal lines indicate slopes of zero. Note that the y axes in (C) and (D) have been inverted to improve the visual clarity of the pattern.

References and Notes

1. M. L. McKinney, *Annu. Rev. Ecol. Syst.* **28**, 495 (1997).
2. D. O. Fisher, I. P. F. Owens, *Trends Ecol. Evol.* **19**, 391 (2004).
3. IUCN, *2003 IUCN Red List of Threatened Species* (IUCN, Gland, Switzerland, 2003).
4. P. S. Martin, in *Pleistocene Extinctions: The Search for a Cause*, P. S. Martin, H. E. Wright, Eds. (Yale Univ. Press, New Haven, CT, 1967), pp. 75–120.
5. C. N. Johnson, *Proc. R. Soc. Lond. Ser. B* **269**, 2221 (2002).
6. M. Cardillo, L. Bromham, *Conserv. Biol.* **15**, 1435 (2001).
7. J. H. Lawton, in *Extinction Rates*, J. H. Lawton, R. M. May, Eds. (Oxford Univ. Press, Oxford, 1995), pp. 147–163.
8. S. L. Pimm, *The Balance of Nature?* (Univ. of Chicago Press, Chicago, 1991).
9. S. L. Pimm, H. L. Jones, J. Diamond, *Am. Nat.* **132**, 757 (1988).
10. Materials and methods are available as supporting material on *Science* Online.
11. M. Cardillo *et al.*, *PLoS Biol.* **2**, 909 (2004).
12. K. E. Jones, A. Purvis, J. L. Gittleman, *Am. Nat.* **161**, 601 (2003).
13. A. Purvis, J. L. Gittleman, G. Cowlishaw, G. M. Mace, *Proc. R. Soc. Lond. Ser. B* **267**, 1947 (2000).
14. J. Damuth, *Nature* **290**, 699 (1981).
15. T. Fenschel, *Oecologia* **14**, 317 (1974).
16. A. Jerozolimski, C. A. Peres, *Biol. Conserv.* **111**, 415 (2003).
17. R. E. Bodmer, J. F. Eisenberg, K. H. Redford, *Conserv. Biol.* **11**, 460 (1997).
18. C. A. Peres, *Conserv. Biol.* **15**, 1490 (2001).
19. R. Woodroffe, J. R. Ginsberg, *Science* **280**, 2126 (1998).
20. A. Balmford, *Trends Ecol. Evol.* **11**, 193 (1996).
21. G. Ceballos, P. R. Ehrlich, *Science* **296**, 904 (2002).
22. M. L. McKinney, *Anim. Conserv.* **1**, 159 (1998).
23. G. J. Russell, T. M. Brooks, M. L. McKinney, C. G. Anderson, *Conserv. Biol.* **12**, 1365 (1998).
24. J. Jernvall, P. C. Wright, *Proc. Natl. Acad. Sci. U.S.A.* **95**, 11279 (1998).
25. A. Purvis, P.-M. Agapow, J. L. Gittleman, G. M. Mace, *Science* **288**, 328 (2000).
26. D. M. Raup, *Extinction: Bad Genes or Bad Luck?* (Oxford Univ. Press, Oxford, 1993).
27. P. M. Bennett, I. P. F. Owens, *Proc. R. Soc. Lond. Ser. B Biol. Sci.* **264**, 401 (1997).
28. G. M. Mace, J. L. Gittleman, A. Purvis, *Science* **300**, 1707 (2003).

29. We thank S. Adamowicz, L. Bromham, B. Collen, T. Coulson, J. Gittleman, C. Godfray, M. Hassell, E. J. Milner-Gulland, and I. Owens for comments and discussions and R. Beck, E. Boakes, C. Carbone, T. Clary, C. Connolly, M. Cutts, J. Davies, J. Foster, R. Grenyer, M. Habib, V. Kanchaite, R. Liu, M. Miyamoto, J. O'Dell, C. Plaster, S. Price, E. Rigby, J. Rist, M. Tambutti, A. Teacher, and R. Vos for contributing to the construction of the databases. This work was funded by grants from NERC (U.K.) to G.M.M. and A.P. (NER/A/S/2001/00581 and NE/B503492/1), from NSF to J.L.G. (DEB/0129009), from Bundesministerium für Bildung und Forschung (Germany) to O.R.P.B. (031U212E), and by an Earth Institute Fellowship to K.J.

Supporting Online Material

www.sciencemag.org/cgi/content/full/1116030/DC1
Materials and Methods
Figs. S1 to S3
Tables S1 to S3
References and Notes

13 June 2005; accepted 8 July 2005
Published online 25 July 2005;
10.1126/science.1116030
Include this information when citing this paper.

Genome Streamlining in a Cosmopolitan Oceanic Bacterium

Stephen J. Giovannoni,[1]* H. James Tripp,[1] Scott Givan,[2] Mircea Podar,[3] Kevin L. Vergin,[1] Damon Baptista,[3] Lisa Bibbs,[3] Jonathan Eads,[3] Toby H. Richardson,[3] Michiel Noordewier,[3] Michael S. Rappé,[4] Jay M. Short,[3] James C. Carrington,[2] Eric J. Mathur[3]

The SAR11 clade consists of very small, heterotrophic marine α-proteobacteria that are found throughout the oceans, where they account for about 25% of all microbial cells. *Pelagibacter ubique*, the first cultured member of this clade, has the smallest genome and encodes the smallest number of predicted open reading frames known for a free-living microorganism. In contrast to parasitic bacteria and archaea with small genomes, *P. ubique* has complete biosynthetic pathways for all 20 amino acids and all but a few cofactors. *P. ubique* has no pseudogenes, introns, transposons, extrachromosomal elements, or inteins; few paralogs; and the shortest intergenic spacers yet observed for any cell.

Pelagibacter ubique, strain HTCC1062, belongs to one of the most successful clades of organisms on the planet (*1*), but it has the smallest genome (1,308,759 base pairs) of any cell known to replicate independently in nature (Fig. 1). In situ hybridization studies show that these organisms occur as unattached cells suspended in the water column (*1*). They grow by assimilating organic compounds from the ocean's dissolved organic carbon (DOC) reservoir, and can generate metabolic energy either by a light-driven proteorhodopsin proton pump (*2*) or by respiration (*3*). The marine planktonic environment is poor in nutrients, and the availability of N, P, and organic carbon typically limits the productivity of microbial communities. *P. ubique* is arguably the smallest free-living cell that has been studied in a laboratory, and even its small genome occupies a substantial fraction (~30%) of the cell volume. The small size of the SAR11 clade cells fits a model proposed by Button (*4*) for natural selection acting to optimize surface-to-volume ratios in oligotrophic cells, such that the capacity of the cytoplasm to process substrates will be matched to steady-state membrane transport rates.

Surprisingly, this genome appears to encode nearly all of the basic functions of α-proteobacterial cells (Table 1). The small genome size is attributable to the nearly complete absence of nonfunctional or redundant DNA and the paring down of all but the most fundamental metabolic and regulatory functions. For example, *P. ubique* falls at the extreme end of the range for intergenic DNA regions, with a median spacer size of only three bases (Fig. 2). Intergenic DNA regions vary considerably among bacteria and archaea, even including parasites that have small genomes (*5*). No pseudogenes, phage genes, or recent gene duplications were found in *P. ubique*.

To further explore this trend, we investigated paralogous gene families by means of BLAST clustering with variable threshold limits. The genome had the smallest number of paralogous genes observed in any free-living cell (Fig. 1) (fig. S1). A steep slope in

[1]Department of Microbiology, [2]Center for Gene Research and Biotechnology, Oregon State University, Corvallis, OR 97331, USA. [3]Diversa Corporation, 4955 Directors Place, San Diego, CA 92121, USA. [4]Hawaii Institute of Marine Biology, School of Ocean and Earth Science and Technology, University of Hawaii, Post Office Box 1346, Kaneohe, HI 96744, USA.

*To whom correspondence should be addressed. E-mail: steve.giovannoni@oregonstate.edu

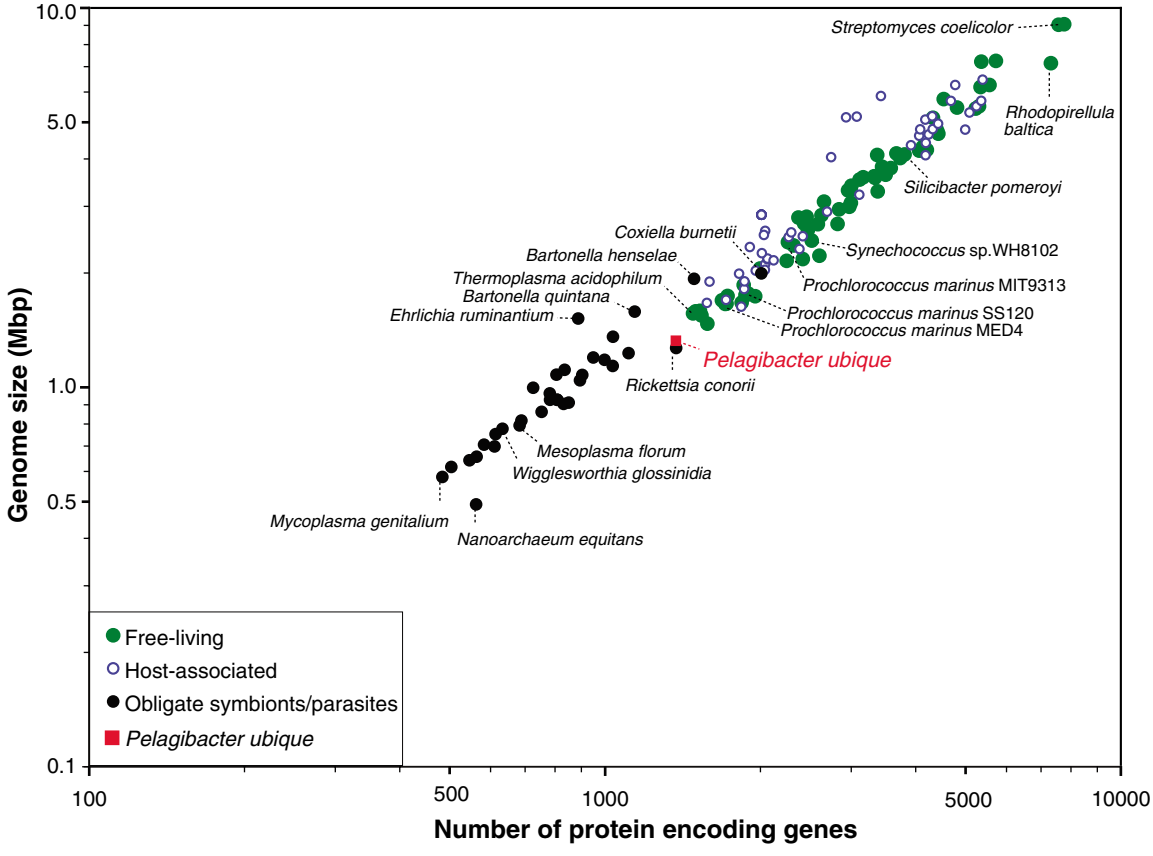

Fig. 1. Number of predicted protein-encoding genes versus genome size for 244 complete published genomes from bacteria and archaea. *P. ubique* has the smallest number of genes (1354 open reading frames) for any free-living organism.

the decline of potential paralogs with increasing gene pairwise similarity threshold, relative to other organisms, suggested that the few paralogs present in *P. ubique* are descended from relatively old duplication events, and that steady evolutionary pressure has constrained the expansion of gene families in this organism (fig. S2). Furthermore, there was no evidence of DNA originating from recent horizontal gene transfer events. The presence of DNA uptake and competence genes (*PilC*, *PilD*, *PilE*, *PilF*, *PilG*, *PilQ*, *comL*, and *cinA*) in the genome suggests that *P. ubique* has the ability to acquire foreign DNA. These data are consistent with the hypothesis that cells in some ecosystems are subject to powerful selection to minimize the material costs of cellular replication; this concept is known as streamlining (*5*).

Several hypotheses have been used to explain genome reduction in prokaryotes, particularly in parasites, which have the smallest cellular genomes known. The relaxation of positive selection for genes used in the biosynthesis of compounds that can be imported from the host, together with a bias favoring deletions over insertions in most or all bacteria, appear to account for genome reduction in many parasites and organelles (*5*). The streamlining hypothesis assumes that selection acts to reduce genome size because of the metabolic burden of replicating DNA with no adaptive value. Under this hypothesis, it is presumed that repetitive DNA arises when mechanisms that add DNA to genomes—for example, recombination and the propagation of self-replicating DNA (e.g., introns, inteins, and transposons)—overwhelm the simple economics of metabolic costs. However, evolutionary theory predicts that the probability that selection will act to eliminate DNA merely because of the metabolic cost of its synthesis will be greatest in very large populations of cells that do not experience drastic periodic declines (*6*).

The streamlining hypothesis has been used to explain genome reduction in *Prochlorococcus*, a photoautotroph that reaches population sizes in the oceans that are similar to those of *Pelagibacter* (*7*–*9*). *Prochlorococcus* genomes range from 1.66 to 2.41 million base pairs (Mbp). Many organisms with reduced genomes, including some pathogens, also have very low G:C to A:T ratios (*10*) (fig. S3), which can be attributed to biases in mutational frequencies, but alternatively might convey a selective advantage by lowering the nitrogen requirement for DNA synthesis, thereby reducing the cellular requirement for fixed forms of nitrogen (*7*). N and P are both proportionately important constituents of DNA that are frequently limiting in seawater. The *P. ubique* genome is 29.7% G+C. Of four complete *Prochlorococcus* genome sequences, the two that lack the DNA repair enzyme 6-0-methylguanine-DNA methyltransferase also have very low G:C to A:T ratios. In the absence of this enzyme, the extent of accepted G:C to A:T mutations increases; however, the *P. ubique* genome encodes this enzyme, which suggests that other factors are the cause of its low G:C to A:T ratio.

Annotation revealed a spare metabolic network encoding a variant of the Entner-Duodoroff pathway, a tricarboxylic acid (TCA) cycle, a glyoxylate bypass, and a typical electron transport chain (Table 1). Anapleurotic pathways for cellular constituents, other than five vitamins, appeared to be complete, but genes that would confer alternate metabolic lifestyles, motility, or other complexities of structure and function were nearly absent. Conspicuous exceptions were genes for carotenoid synthesis, retinal synthesis, and proteorhodopsin. *P. ubique* constitutively expresses a light-dependent retinylidine proton pump and is the first cultured bacterium to exhibit the gene that encodes it (*2*). The genome also contained genes for type II secretion (including adhesion) and type IV pilin biogenesis. Examination of gene distributions among metabolic categories (fig. S4) supported the conclusion that genome reduction in *P. ubique* has spared genes for core proteobacterial functions while reducing the proportion of the genome devoted to noncoding DNA. Relative to other α-proteobacterial genomes, the proportions of *P. ubique* genes encoding transport functions, biosynthesis of amino acids, and energy metabolism were high (table S3).

The sheer size of *Pelagibacter* populations indicates that they consume a large proportion of the labile DOC in the oceans. The global DOC pool is estimated to be 6.85×10^{17} g C (*11*), roughly equaling the mass of inorganic C in the atmosphere (*12*). Examination of the *P. ubique* genome revealed that about half of all transporters, and nearly all nutrient-uptake transporters, are members of the ATP-binding cassette (ABC) family (table S1). ABC transporters typically have high substrate affinities and therefore provide an advantage at the cost of ATP hydrolysis. Inferred transport functions included the uptake of a variety of nitrogenous compounds: ammonia, urea, basic amino acids, spermidine, and putrescine. Broad-specificity transporters for sugars, branched amino acids, dicarboxylic and tricarboxylic acids, and a number of common osmolytes (including glycine betaine, proline, mannitol, and 3-dimethylsulfoniopropionate) were found in the genome. Autoradiography with native populations of SAR11 has demonstrated high uptake activity for amino acids and 3-dimethylsulfoniopropionate (*13*). Hence, efficiency is achieved in a low-nutrient system by reliance on transporters with broad substrate ranges (*14*) and a number of specialized substrate targets, in particular, nitrogenous compounds and osmolytes.

Table 1. Metabolic pathways in *Pelagibacter*.

Pathway	Prediction
Glycolysis	Uncertain
TCA cycle	Present
Glyoxylate shunt	Present
Respiration	Present
Pentose phosphate cycle	Present
Fatty acid biosynthesis	Present
Cell wall biosynthesis	Present
Biosynthesis of all 20 amino acids	Present
Heme biosynthesis	Present
Ubiquinone	Present
Nicotinate and nicotinamide	Present
Folate	Present
Riboflavin	Present
Pantothenate	Absent
B_6	Absent
Thiamine	Absent
Biotin	Absent
B_{12}	Absent
Retinal	Present

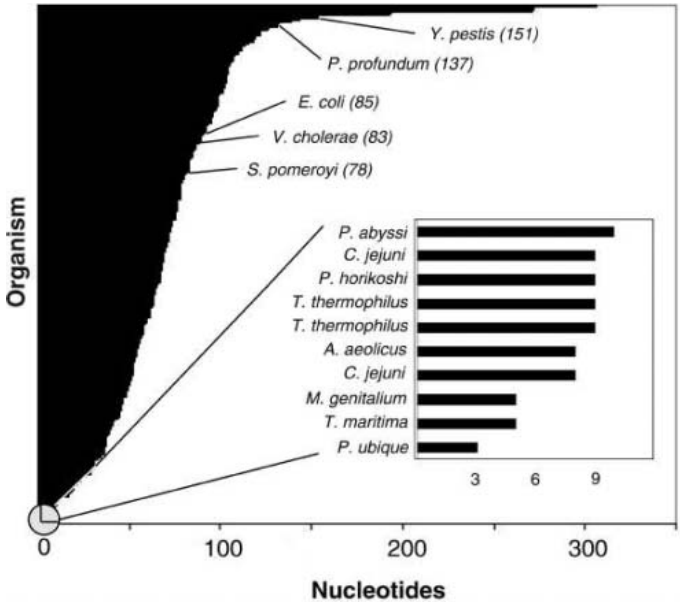

Fig. 2. Median size of intergenic spacers for bacterial and archaeal genomes. Inset shows expanded view of range for organisms with the smallest intergenic spacers.

The genome encoded two sigma factors, the heat shock factor σ^{32} and a σ^{70} (*rpo*D), but no homolog of *rpo*N, the gene for the nitrogen starvation factor σ^{54} (table S2). Only four two-component regulatory systems were identified, three of which match the only two-component regulatory systems in *Rickettsia* (*15*). The presence of homologs to *PhoR*/*PhoB*/*PhoC*, *NtrY*/*NtrX*, and *envZ*/*OmpR* suggested regulated responses to phosphate limitation, N limitation, and osmotic stress. The only additional two-component system, *RegB*/*RegA*, has been implicated in the regulation of cellular oxidation/reduction processes in phototrophic α-proteobacteria (*16*). A gene encoding a ferric iron uptake regulator was also present.

In its simplicity the *P. ubique* genome is unique among other heterotrophic marine bacteria, such as *Vibrio* sp. (*17*), *Pseudoalteromonas* (*18*), *Shewanella* (*19*), and *Silicibacter* (*20*), which have considerably larger genomes (4.0 to 5.3 Mbp) and global regulatory systems that enable them to implement a variety of metabolic strategies in response to environmental variation. We hypothesize that *P. ubique* makes use of the ambient DOC field (*21*), whereas heterotrophic bacterioplankton with larger genomes are poised to rapidly exploit pulses of nutrients (*22*) at the expense of replication efficiency during the intervening periods (*23*). This hypothesis is consistent with the observation that *P. ubique* has a single ribosomal RNA (rRNA) operon and a low growth rate (0.40 to 0.58 cell divisions per day) that does not vary in response to nutrient addition. In contrast, heterotrophic marine bacteria with large genomes have some of the highest recorded growth rates and are very responsive to nutrient concentration.

Like some other α-proteobacteria and especially archaea, HTCC1062 has an alternate thymidylate synthase for thymine synthesis,

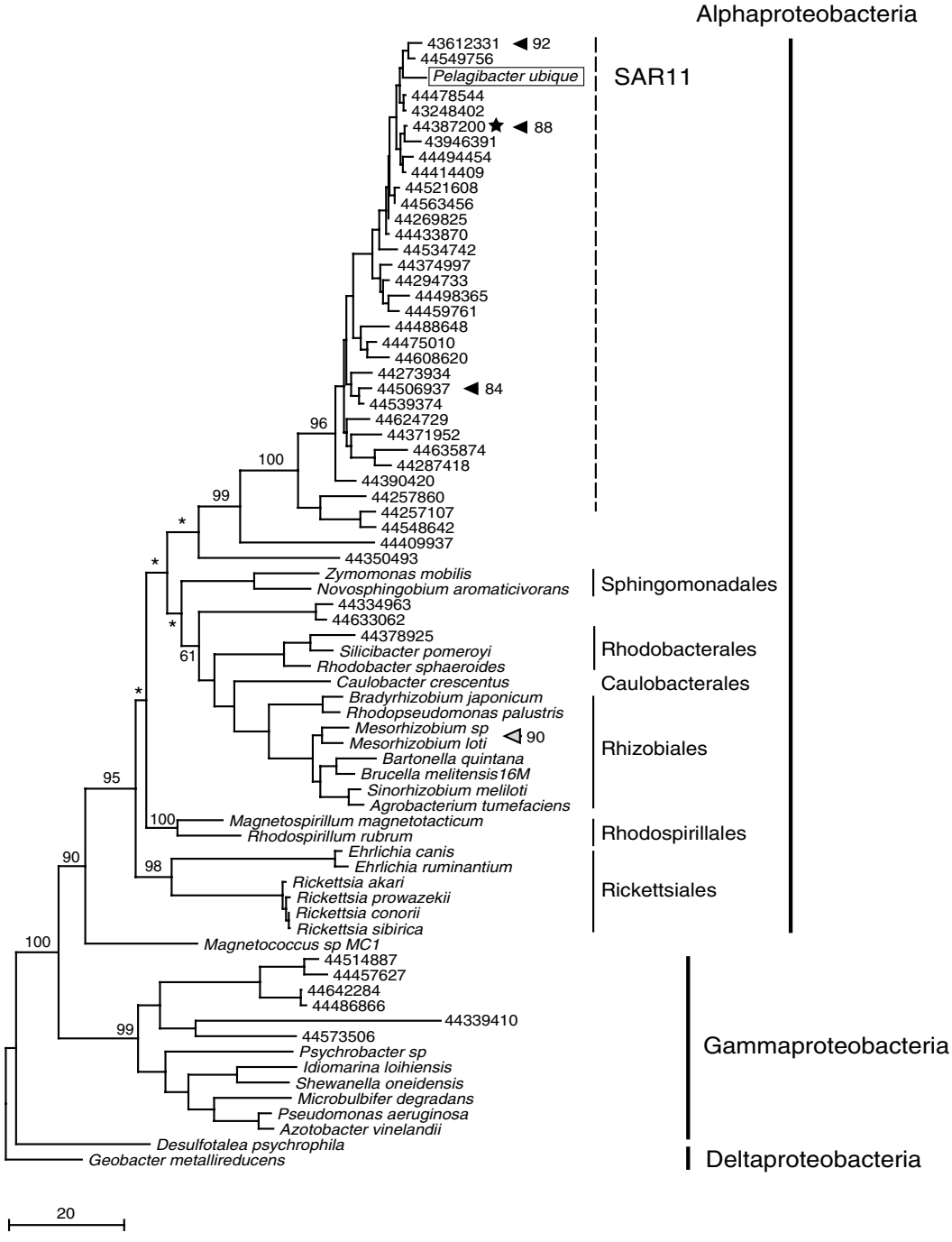

Fig. 3. Maximum likelihood phylogenetic tree for the gene encoding RNA polymerase subunit B. Sequences represented by accession numbers are environmental sequences from the Sargasso Sea (*19*). The sequence indicated by a star is part of the 5.7-kb contig IBEA_CTG_2159647 that is part of a conserved gene cluster also present in *Pelagibacter ubique*. Numbers indicated by solid arrowheads represent amino acid percentage identity to the *Pelagibacter* gene. For comparison, the identity between two species of *Mesorhizobium* is also indicated (open arrowhead). Bootstrap support (100 maximum-likelihood replicates) is indicated for the major clades (* if less than 50).

thyX (*24*). As in other strains that lack the most common thymidylate synthase (thyA) but have thyX, HTCC1062 also lacks the dihydrofolate reductase folA (*25*). Evidence suggests that the gene encoding thyX can substitute for folA (*24*). A full glycolytic pathway was not reconstructed because of the confounding diversity of glycolytic pathways (*26*). Five enzymes in the canonical glycolytic pathway were not seen, including two key enzymes involved in allosteric control: phosphofructokinase and pyruvate kinase. An enzyme thought to substitute for pyruvate kinase (*27*), known as PPDK (pyruvate-phosphate dikinase), was found. Some but not all of the enzymes for the nonphosphorylated Entner-Duodoroff pathway, considered more ancient than canonical glycolysis (*26*, *28*), were detected, as well as a complete pathway for gluconeogenesis, also considered more ancient than canonical glycolysis (*29*). Sugar transporters with best BLAST hits to maltose/trehalose transport were found, so presumably a complete glycolytic pathway does function in this cell.

Whole-genome shotgun (WGS) sequence data from the Sargasso Sea segregated at high similarity values, relative to other α-proteobacteria and proteobacteria, in a BLASTN analysis of the *P. ubique* genome (fig. S4). Sequence diversity prevented Venter *et al.* (*19*) from reconstructing SAR11 genomes from the Sargasso Sea WGS data set, although SAR11 rRNA genes accounted for 380 of 1412 16*S* rRNA genes and gene fragments they recovered (26.9%), and the library was estimated to encode the equivalent of about 775 SAR11 genomes. Three Sargasso Sea contiguous sequences (contigs) that were long (5.6 to 22.5 kb) and highly similar to the *P. ubique* genome were analyzed in detail. Genes on these contigs were syntenous with genes from the *P. ubique* genome, with amino acid sequence identities ranging from 68 to 96% (fig. S5). Phylogenetic analysis of four conserved genes from these contigs (those encoding RNA polymerase subunit B, Fig. 3; elongation factor G, fig. S6; DNA gyrase subunit B, fig. S7; and ribosomal protein S12, fig. S8) showed them to be associated with large, diverse environmental clades that branched within the α-proteobacteria. We hypothesize that evolutionary divergence within the SAR11 clade and the accumulation of neutral variation are the most likely explanations for the natural heterogeneity in SAR11 genome sequences.

Metabolic reconstruction failed to resolve why *P. ubique* will not grow on artificial media. When cultured in seawater, it attains cell densities similar to populations in nature, typically 10^5 to 10^6 ml^{-1} depending on the water sample (*3*). No evidence of quorum-sensing systems was found in the genome, and experimental additions of nutrients supported the results from metabolic reconstruction, which suggests that an unusual growth factor may play a role in the ecology of this organism.

P. ubique has taken a tack in evolution that is distinctly different from that of all other heterotrophic marine bacteria for which genome sequences are available. Evolution has divested it of all but the most fundamental cellular systems such that it replicates under limiting nutrient resources as efficiently as possible, with the outcome that it has become the dominant clade in the ocean.

References and Notes

1. R. M. Morris *et al.*, *Nature* **420**, 806 (2002).
2. S. J. Giovannoni *et al.*, *Nature*, in press.
3. M. S. Rappé, S. A. Connon, K. L. Vergin, S. J. Giovannoni, *Nature* **418**, 630 (2002).
4. D. K. Button, *Appl. Environ. Microbiol.* **57**, 2033 (1991).
5. A. Mira, H. Ochman, N. A. Moran, *Trends Genet.* **17**, 589 (2001).
6. M. Kimura, *The Neutral Theory of Molecular Evolution* (Cambridge Univ. Press, Cambridge, 1983).
7. A. Dufresne, L. Garczarek, F. Partensky, *Genome Biol.* **6**, R14 (2005).
8. B. Strehl, J. Holtzendorff, F. Partensky, W. R. Hess, *FEMS Microbiol. Lett.* **181**, 261 (1999).
9. G. Rocap *et al.*, *Nature* **424**, 1042 (2003).
10. D. W. Ussery, P. F. Hallin, *Microbiology* **150**, 749 (2004).
11. D. A. Hansell, C. A. Carlson, *Global Biogeochem. Cycles* **12**, 443 (1998).
12. D. A. Hansell, C. A. Carlson, *Deep Sea Res.* **48**, 1649 (2001).
13. R. R. Malmstrom, R. P. Kiene, M. T. Cottrell, D. L. Kirchman, *Appl. Environ. Microbiol.* **70**, 4129 (2004).
14. D. K. Button, B. Robertson, E. Gustafson, X. Zhao, *Appl. Environ. Microbiol.* **70**, 5511 (2004).
15. S. G. Andersson *et al.*, *Nature* **396**, 133 (1998).
16. S. Elsen, L. R. Swem, D. L. Swem, C. E. Bauer, *Microbiol. Mol. Biol. Rev.* **68**, 263 (2004).
17. E. G. Ruby *et al.*, *Proc. Natl. Acad. Sci. U.S.A.* **102**, 3004 (2005).
18. B. D. Lanoil, L. M. Ciufettii, S. J. Giovannoni, *Genome Res.* **6**, 1160 (1996).
19. J. C. Venter *et al.*, *Science* **304**, 66 (2004); published online 4 March 2004 (10.1126/science.1093857).
20. M. A. Moran *et al.*, *Nature* **432**, 910 (2004).
21. C. A. Carlson, H. W. Ducklow, A. F. Michaels, *Nature* **371**, 405 (1994).
22. F. Azam, *Science* **280**, 694 (1998).
23. J. A. Klappenbach, J. M. Dunbar, T. M. Schmidt, *Appl. Environ. Microbiol.* **66**, 1328 (2000).
24. H. Myllykallio *et al.*, *Science* **297**, 105 (2002); published online 23 May 2002 (10.1126/science.1072113).
25. H. Myllykallio, D. Leduc, J. Filee, U. Liebl, *Trends Microbiol.* **11**, 220 (2003).
26. T. Dandekar, S. Schuster, B. Snel, M. Huynen, P. Bork, *Biochem. J.* **343**, 115 (1999).
27. R. E. Reeves, R. A. Menzies, D. S. Hsu, *J. Biol. Chem.* **243**, 5486 (1968).
28. E. Melendez-Hevia, T. G. Waddell, R. Heinrich, F. Montero, *Eur. J. Biochem.* **244**, 527 (1997).
29. R. S. Ronimus, H. W. Morgan, *Archaea* **1**, 199 (2003).

30. Supported by NSF grant EF0307223, Diversa Corporation, the Gordon and Betty Moore Foundation, and the Oregon State University Center for Gene Research and Biotechnology. We thank S. Wells, M. Hudson, D. Barofsky, M. Staples, J. Garcia, B. Buchner, P. Sammon, K. Li, and J. Ritter for technical assistance and J. Heidelberg for advice about genome assembly. We also acknowledge the crew of the R/V Elakha for assistance with sample and seawater collections, the staff of the Central Services Laboratory at Oregon State University for supplementary sequence analyses, and the staff of the Mass Spectrometry Laboratory at Oregon State University for proteomic analyses. The sequence reported in this study has been deposited in GenBank under accession number CP000084.

Supporting Online Material

www.sciencemag.org/cgi/content/full/309/5738/1242/DC1
Materials and Methods
Tables S1 to S3
Figs. S1 to S9
References

26 April 2005; accepted 11 July 2005
10.1126/science.1114057

Contact-Dependent Inhibition of Growth in *Escherichia coli*

Stephanie K. Aoki, Rupinderjit Pamma, Aaron D. Hernday, Jessica E. Bickham, Bruce A. Braaten, David A. Low*

Bacteria have developed mechanisms to communicate and compete with each other for limited environmental resources. We found that certain *Escherichia coli*, including uropathogenic strains, contained a bacterial growth-inhibition system that uses direct cell-to-cell contact. Inhibition was conditional, dependent upon the growth state of the inhibitory cell and the pili expression state of the target cell. Both a large cell-surface protein designated Contact-*d*ependent *i*nhibitor A (CdiA) and two-partner secretion family member CdiB were required for growth inhibition. The CdiAB system may function to regulate the growth of specific cells within a differentiated bacterial population.

Bacteria communicate with each other in multiple ways, including the secretion of signaling molecules that enable a cell population to determine when it has reached a certain density or that a potential partner is present for conjugation (*1*, *2*). Cellular communication can also occur through contact between cells, as has been shown for *Myxococcus xanthus*, which undergoes a complex developmental pathway (*3*, *4*). Here we describe a different type of intercellular interaction in which bacterial growth is regulated by direct cell-to-cell contact.

Wild-type *Escherichia coli* isolate EC93 inhibited the growth of laboratory *E. coli* K-12

Molecular, Cellular, and Developmental Biology, University of California–Santa Barbara (UCSB), Santa Barbara, CA 93106, USA.

*To whom correspondence should be addressed. E-mail: low@lifesci.ucsb.edu

strains, such as MG1655, when the bacteria were mixed together in shaking liquid culture (Fig. 1A). In contrast, *E. coli* K-12 strains in general (e.g., EPI100) did not express growth-inhibitory activity (Fig. 1A). We isolated genes from strain EC93, *cdiA* and *cdiB*, that when expressed in *E. coli* K-12 conferred a growth-inhibitory phenotype (Fig. 1A). Growth inhibition was dependent upon the growth state of the inhibitory cells, occurring in logarithmic but not stationary phase. Target cells, however, were inhibited regardless of their growth phase (fig. S1). Protein synthesis also appeared to be required for inhibition, because $cdiA^+B^+$ *E. coli* inhibitor cells pretreated for 2 hours with chloramphenicol did not have measurable inhibitory activity (fig. S2). Experiments measuring the inhibitor-to-target ratio over time (fig. S3) indicate that one $cdiA^+B^+$ *E. coli* cell inhibited the growth of multiple target cells. Starting at an initial ratio of 1 inhibitor to 10 target cells, after 1 hour this ratio increased more than a thousandfold (fig. S3). In contrast, a control experiment with *cdiAB*-negative cells in place of $cdiA^+B^+$ inhibitory cells showed that the control-to-target ratio was not altered over the 3-hour time course (fig. S3).

The growth-inhibitory activity did not appear to be a colicin, which is a secreted antimicrobial peptide, because supernatant solutions from logarithmic phase EC93 cultures lacked inhibitory activity even when a known inducer of colicin synthesis, mitomycin C, was present (*5*, *6*). To test the possibility that induction of inhibitory activity might occur only when target cells are present, we prepared conditioned medium from a mixed culture of $cdiA^+B^+$ inhibitor cells and *E. coli* K-12 target cells (with a 10:1 inhibitor-to-

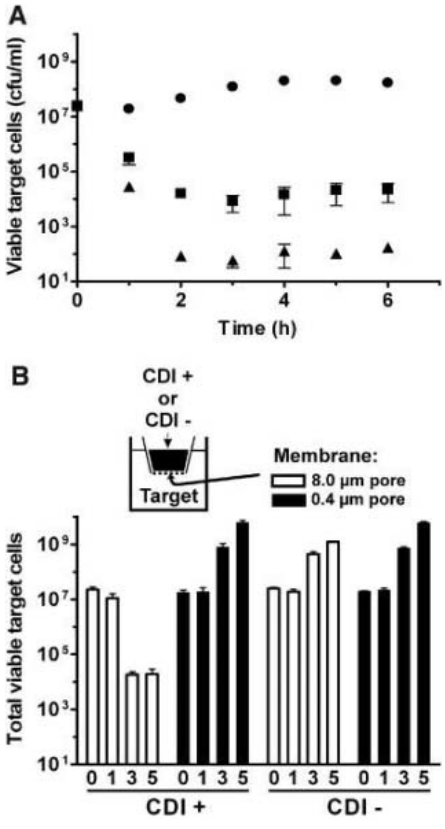

Fig. 1. Contact-dependent inhibition of bacterial growth. (**A**) Target *E. coli* MG1655 tet^R cells were mixed with the following test strains: *E. coli* EC93 inhibitory cells (squares); *E. coli* K-12 EPI100 str^R containing pDAL660Δ1-39 ($cdiA^+B^+$, triangles); and control *E. coli* K-12 EPI100 str^R (circles). The inhibitor-to-target ratio for these experiments was 10:1. At the times indicated, viable target cell counts were obtained. CFU, colony-forming units. (**B**) *E. coli* CDI^+ K-12 (DL4577) or CDI^- *E. coli* K-12 (DL4527) were grown to logarithmic phase and added to the top chamber of a six-well plate containing either a 0.4-μm (solid bars) or an 8-μm (open bars) PET membrane. Target *E. coli* MG1655 tet^R cells were added to the bottom well (in a 20:1 inhibitor-to-target ratio). Viable counts for the top and bottom chambers were measured after incubation (hours). Data are means ± SEM; $n = 2$.

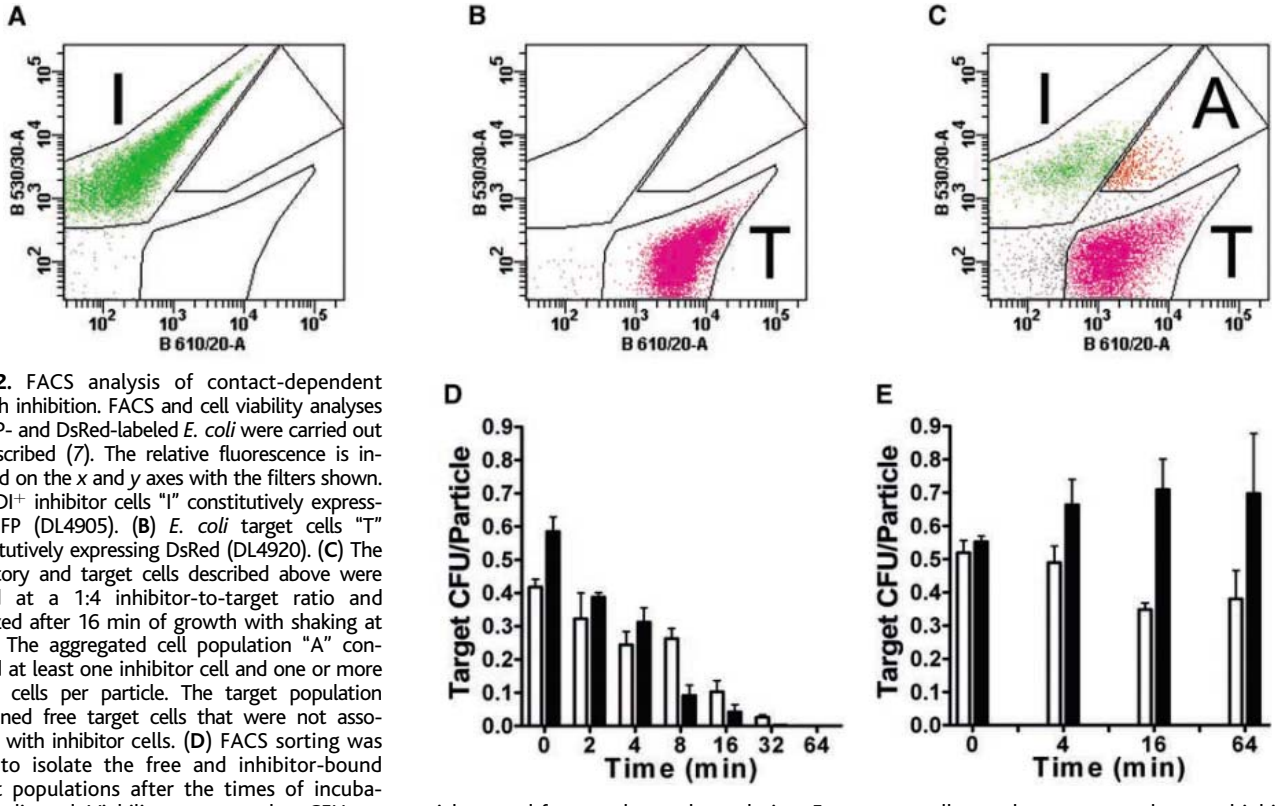

Fig. 2. FACS analysis of contact-dependent growth inhibition. FACS and cell viability analyses of GFP- and DsRed-labeled *E. coli* were carried out as described (*7*). The relative fluorescence is indicated on the *x* and *y* axes with the filters shown. (**A**) CDI^+ inhibitor cells "I" constitutively expressing GFP (DL4905). (**B**) *E. coli* target cells "T" constitutively expressing DsRed (DL4920). (**C**) The inhibitory and target cells described above were mixed at a 1:4 inhibitor-to-target ratio and analyzed after 16 min of growth with shaking at 37°C. The aggregated cell population "A" contained at least one inhibitor cell and one or more target cells per particle. The target population contained free target cells that were not associated with inhibitor cells. (**D**) FACS sorting was used to isolate the free and inhibitor-bound target populations after the times of incubation indicated. Viability was scored as CFUs per particle sorted from each gated population. Free target cells are shown as open bars, and inhibitor-bound target cells are shown as solid bars. (**E**) As in (D), except that CDI^- *E. coli* containing *cdiA-FLAG1* (DL4955) was mixed with target cells (DL4920).

target ratio). Target cell viability was reduced more than a thousandfold after 1 hour of incubation (fig. S4A), indicating substantial growth inhibitory activity. Conditioned medium from this 1-hour mixture, when added to fresh K-12 target cells, did not affect cell growth compared to conditioned medium from control *cdiA*$^-$*B*$^-$ cell mixtures (fig. S4B).

We tested the possibility that growth inhibition might occur through cell-to-cell contact by separating *cdiA*$^+$*B*$^+$ inhibitory cells from target cells, using polyethylene terephthalate (PET) porous membranes in a six-well plate (Fig. 1B). Growth inhibition was not observed when contact between inhibitory cells and target cells was blocked by 0.4-μm pores; however, growth inhibition (~1000-fold) was observed when 8-μm pores were used, allowing inhibitor and target cell mixing. Addition of *cdiAB*-negative control *E. coli* did not affect growth of target cells, regardless of pore size (Fig. 1B). We obtained similar results using EC93, from which the *cdiAB* genes were isolated for cloning into *E. coli* K-12 (*5*). A potential caveat is that a secreted inhibitory molecule might bind to the PET membrane and be sequestered or inactivated. However, addition of excess PET membranes did not affect the ability of *cdiA*$^+$*B*$^+$ *E. coli* K-12 to inhibit cell growth (fig. S5). Similar results were obtained with polycarbonate membranes (*5*). These results support the hypothesis that growth inhibition mediated by *cdiAB* requires cell-to-cell contact, designated as contact-dependent inhibition (CDI).

It is possible that the inhibitory factor could be an unstable secreted molecule that is only effectively delivered to target cells in close proximity. To address this possibility, we mixed fluorescently labeled *cdiA*$^+$*B*$^+$ inhibitory cells [green fluorescent protein (GFP)–labeled] with *E. coli* K-12 target cells [Discosoma red (DsRed)–labeled], and after incubation with shaking, the cell mixtures were sorted by fluorescence-activated cell sorting (FACS). We observed three cell populations, corresponding to green inhibitory cells, red target cells, and cell aggregates containing at least one inhibitory and one target cell per aggregate particle (Fig. 2, A to C). The appearance of the aggregated particles was dependent upon *cdiAB,* indicating that CdiAB mediates intercellular binding (*5*). If cell-to-cell contact were required for growth inhibition, then the viability of target cells bound to inhibitory cells should decrease more rapidly than the viability of free target cells (Fig. 2D). The viability of aggregated targets compared with free targets decreased at time points of 8 min and longer, indicating that observable growth inhibition occurred after 4 to 8 min of contact. Although the viability of free targets was only marginally reduced at times up to 8 min, at later times viability was significantly reduced, albeit at a lesser rate than for aggregated targets (Fig. 2D). It is likely that the observed reduction in viability of "free" target cells was primarily the result of prior contact with *cdiA*$^+$*B*$^+$ inhibitory cells and release from cell aggregates.

The rapid decrease in viability of the aggregated targets might be due to a nonspecific effect of intercellular binding. FACS analysis was carried out using a *cdiA* mutant (Fig. 3A, *cdiA-FLAG1*) that no longer conferred CDI but retained intercellular adhesion. Under these conditions, the viability of aggregated target cells was not reduced compared to free target cells over the same time course (Fig. 2E), showing that the rapid decrease in viability of target cells bound to inhibitory cells required CDI activity. These results strongly indicate that CdiAB mediates growth inhibition through cell-to-cell contact.

We cloned a DNA region from *E. coli* EC93 that conferred a CDI$^+$ phenotype to *E. coli* K-12 and generated 15 base-pair (bp) insertions within the region (*7*). Stop codon insertions within open reading frames (ORFs) designated *cdiA* and *cdiB* (GenBank accession no. DQ100454) abolished CDI activity (Fig. 3A), showing that the *cdiA* and *cdiB* ORFs were necessary for CDI. In addition, we identified a small ORF (Fig. 3A, *cdiI*) adjacent to *cdiA* that conferred full immunity to CDI (fig. S6), explaining why cells expressing *cdiAB* do not inhibit their own growth. The translated *cdiA* and *cdiB* ORFs showed significant amino acid sequence identity with two-partner secretion proteins (fig. S7) that are proteolytically processed during export to the cell surface (*8*). Using FLAG epitope tagging (Fig. 3A), we found that CdiA was expressed as a 303-kD protein on the cell surface (*5*), which was then processed to 284-kD and 195-kD proteins (Fig. 3B). A FLAG insertion in the *cdiB* ORF yielded a 56-kD protein, consistent with the predicted

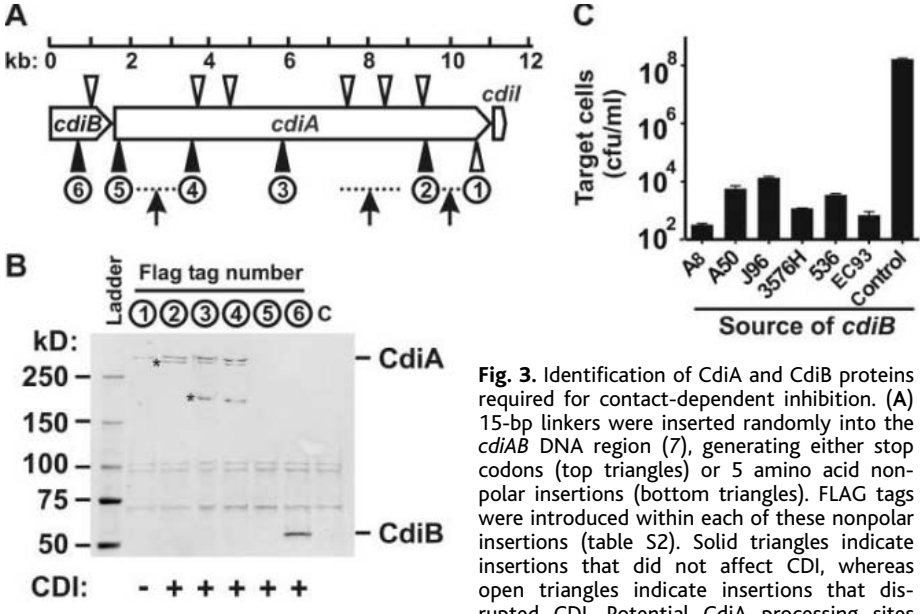

Fig. 3. Identification of CdiA and CdiB proteins required for contact-dependent inhibition. (**A**) 15-bp linkers were inserted randomly into the *cdiAB* DNA region (*7*), generating either stop codons (top triangles) or 5 amino acid nonpolar insertions (bottom triangles). FLAG tags were introduced within each of these nonpolar insertions (table S2). Solid triangles indicate insertions that did not affect CDI, whereas open triangles indicate insertions that disrupted CDI. Potential CdiA processing sites (arrows) were predicted from the estimated protein sizes obtained in (B). (**B**) *E. coli* containing CdiA and B proteins labeled with FLAG tags (lanes 1 to 6) or no FLAG tag control (lane C) were analyzed by SDS–polyacrylamide gel electrophoresis and immunoblotting with monoclonal antiserum to FLAG. A molecular weight ladder and CdiA and CdiB protein positions are shown. Asterisks indicate CdiA fragments, and CDI phenotypes are shown at the bottom. (**C**) *cdiB* homologs from five UPEC isolates and *cdiB* from EC93 were cloned in plasmid pCC1 and tested for CDI complementation in *cdiA*$^+$*B*$^-$ *E. coli* (DL4958). Vector control plasmid pCC1 is shown (control).

Fig. 4. Effect of Pap pili expression on CDI. *E. coli* HB101 rif^R target cells lacking pili (*18*) were transformed with plasmids expressing P pili, S pili, type 1 pili, or plasmid vector alone (pili minus) as indicated at the bottom. Target cells were incubated with CDI$^+$ inhibitory *E. coli* DL4577. Viable target cell counts at 0 and 3 hours are depicted by open and solid bars, respectively.

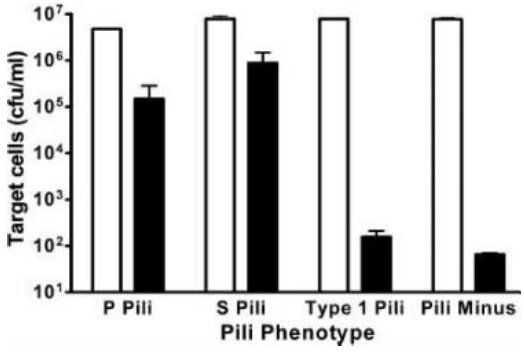

size of CdiB. Proteolytic fragments of CdiA were detected in the growth medium (*5*) but were not growth-inhibitory (fig. S4), indicating that the secreted forms of CdiA are inactive.

High amino acid sequence identity was found between CdiA/CdiB and predicted proteins from uropathogenic *E. coli* (UPEC), including strain 536 (*9*). Complementation analysis indicated that UPEC 536 and four additional UPEC strains contain genes that are functional homologs of *cdiB* (Fig. 3C) and *cdiA* (fig. S8). Bioinformatic analysis showed that *Yersinia pestis* (plague) and *Burkholderia pseudomallei* (melioidosis) also encode possible CdiAB homologs (fig. S7). Filamentous hemagglutinin from *Bordetella pertussis* (whooping cough) appeared more distantly related, sharing sequence identity to CdiA primarily in the N-terminal portion of the protein (fig. S7).

The *cdiAB* homologs in UPEC 536 are present within pathogenicity island II (*10*), but a *cdiI* homolog is not present, nor is it found in the sequenced genome of UPEC CFT073, which also contains a *cdiAB* homolog (*11*). This observation suggests that *cdiAB* expression in UPEC strains would inhibit their growth. Pathogenicity island II in UPEC 536 also contains a pyelonephritis-associated pili (*pap*) operon closely linked to *cdiAB*. Because Pap pili are expressed at the cell surface, we tested the possibility that pili expression might affect CDI because contact between CdiA and the target cell surface could be blocked. *E. coli* K-12 constitutively expressing P pili (*12*) or S pili (*13*) showed resistance to CDI, whereas cells expressing type 1 pili were 1000- to 10,000-fold more sensitive to growth inhibition (Fig. 4). Thus, resistance to CDI conferred by P and S pili involves specific interaction(s) and is not likely to be the result of nonspecific steric hindrance that blocks cell-to-cell contact.

Many UPEC strains contain *fim* (type 1 pili), *pap* (P pili), and *sfa* (S pili) operons (*10*, *11*). The expression of these pili types is normally subject to reversible off/on switching, generating diversity within bacterial populations by a differentiation mechanism (*14*, *15*). Such a mechanism might play a role in the temporal control of the differentiation observed for UPEC strains inside bladder cells, during which the bacteria progress through distinct developmental stages, including a quiescent growth state (*16*). *E. coli* K-12 cells inhibited by CDI appear to be nonviable because of their lack of growth on agar medium. However, CDI-inhibited cells appeared to be viable because they excluded propidium iodide (*5*), a standard criterion for distinguishing viable cells from nonviable cells (*17*). The identification of this sophisticated mechanism in *E. coli,* with possible homologs in a broad range of species, opens the door for exploration of the potential roles of CDI in controlling bacterial development and pathogenesis.

References and Notes

1. J. M. Henke, B. L. Bassler, *Trends Cell Biol.* **14**, 648 (2004).
2. G. J. Lyon, R. P. Novick, *Peptides* **25**, 1389 (2004).
3. R. Welch, D. Kaiser, *Proc. Natl. Acad. Sci. U.S.A.* **98**, 14907 (2001).
4. L. Jelsbak, L. Sogaard-Andersen, *Curr. Opin. Microbiol.* **3**, 637 (2000).
5. S. K. Aoki, A. D. Hernday, R. Pamma, B. A. Braaten, D. A. Low, unpublished data.
6. R. Spangler, S. P. Zhang, J. Krueger, G. Zubay, *J. Bacteriol.* **163**, 167 (1985).
7. Materials and methods are available as supporting material on *Science* Online.
8. G. Renauld-Mongenie, J. Cornette, N. Mielcarek, F. D. Menozzi, C. Locht, *J. Bacteriol.* **178**, 1053 (1996).
9. S. Knapp, J. Hacker, T. Jarchau, W. Goebel, *J. Bacteriol.* **168**, 22 (1986).
10. U. Dobrindt *et al.*, *Infect. Immun.* **70**, 6365 (2002).
11. R. A. Welch *et al.*, *Proc. Natl. Acad. Sci. U.S.A.* **99**, 17020 (2002).
12. D. Low, E. N. Robinson Jr., Z. A. McGee, S. Falkow, *Mol. Microbiol.* **1**, 335 (1987).
13. T. Schmoll *et al.*, *Microb. Pathog.* **9**, 331 (1990).
14. I. C. Blomfield, *Adv. Microb. Physiol.* **45**, 1 (2001).
15. A. D. Hernday, B. A. Braaten, D. A. Low, *Mol. Cell* **12**, 947 (2003).
16. S. S. Justice *et al.*, *Proc. Natl. Acad. Sci. U.S.A.* **101**, 1333 (2004).
17. L. Boulos, M. Prevost, B. Barbeau, J. Coallier, R. Desjardins, *J. Microbiol. Methods* **37**, 77 (1999).
18. I. Johanson, R. Lindstedt, C. Svanborg, *Infect. Immun.* **60**, 3416 (1992).

19. We thank P. Cotter and S. Poole for helpful discussion, J. Hacker for *E. coli* UPEC 536, M. Mulvey for antisera to Type 1 pili, and K. Dane and P. Daugherty (UCSB) for FACS technical assistance. Supported by a Cottage Hospital Research Grant (UCSB), a University of California Biotechnology grant (no. 2002-14), and NIH grant no. AI23348 (D.A.L.).

Supporting Online Material

www.sciencemag.org/cgi/content/full/309/5738/1245/DC1
Materials and Methods
Figs. S1 to S8
Tables S1 and S2

20 May 2005; accepted 11 July 2005
10.1126/science.1115109

Genome-Wide RNAi Screen for Host Factors Required for Intracellular Bacterial Infection

Hervé Agaisse,[1,2]*†‡ Laura S. Burrack,[1]* Jennifer A. Philips,[2] Eric J. Rubin,[3] Norbert Perrimon,[2] Darren E. Higgins[1]‡

Most studies of host-pathogen interactions have focused on pathogen-specific virulence determinants. Here, we report a genome-wide RNA interference screen to identify host factors required for intracellular bacterial pathogenesis. Using *Drosophila* cells and the cytosolic pathogen *Listeria monocytogenes*, we identified 305 double-stranded RNAs targeting a wide range of cellular functions that altered *L. monocytogenes* infection. Comparison to a similar screen with *Mycobacterium fortuitum*, a vacuolar pathogen, identified host factors that may play a general role in intracellular pathogenesis and factors that specifically affect access to the cytosol by *L. monocytogenes*.

During bacterial infections, macrophages play a critical role in eliminating engulfed pathogens. However, intracellular bacterial pathogens have evolved varying strategies to avoid elimination by host macrophages (*1*). One strategy used by pathogens, such as *Mycobacterium tuberculosis*, is to modify the phagosomal compartment to allow for vacuolar replication (*2*). Other bacterial pathogens, such as *Listeria monocytogenes*, escape the phagocytic vacuole to enter the host cell cytosol where replication occurs (*3*). Whereas numerous bacterial determinants that facilitate intracellular infection have been characterized from diverse bacterial species (*4*), less is known about the host factors that are exploited or subverted by intracellular bacterial pathogens. Here, we report the results of a genome-wide RNA interference (RNAi) screen conducted in *Drosophila* SL2 cells to identify host factors required for infection by *L. monocytogenes*, a cytosolic pathogen. In addition, we present the results of a comparison to a similar RNAi screen conducted with *Mycobacterium fortuitum*, a vacuolar pathogen (*5*).

Both *Drosophila* and cultured *Drosophila* cells are tractable models for analysis of *L. monocytogenes* pathogenesis (*6*, *7*). We tested the ability of macrophage-like *Drosophila* SL2 cells to support intracellular infection by *L. monocytogenes*. DH-L1039, a green fluorescent protein (GFP)–expressing *L. monocytogenes* strain derived from wild-type 10403S, replicated within *Drosophila* SL2 cells (fig. S1, A and B). In contrast, GFP fluorescence of DH-L1137, a variant lacking the pore-forming cytolysin listeriolysin O (LLO), was punctate in appearance and growth was inefficient in SL2 cells (fig. S1, A and B), consistent with LLO-negative bacteria that remained trapped within phagocytic vacuoles (*3*, *8*). Next, we developed a microscopy-based, high-throughput RNAi screen to identify host factors required for intracellular infection by *L. monocytogenes* (Fig.

1A) (*9*). We confirmed the feasibility of the approach by analyzing the impact of β-COPI double-stranded RNA (dsRNA) treatment on *L. monocytogenes* infection. Interfering with β-COPI expression by RNAi results in a strong defect in *Escherichia coli* phagocytosis (*10*). The impact of blocking *L. monocytogenes* entry by β-COPI dsRNA treatment was clearly detectable by fluorescence microscopy (fig. S1C). For the screen, we used a library of ~21,300 dsRNAs (*11*) that target >95% of annotated genes in the *Drosophila* genome (*12*), and we identified several phenotypes (Fig. 1, B to F): (i) Decreased GFP fluorescence ("down" phenotype). In some instances only a few host cells were infected, but in those cells the infection was as robust as observed in control wells, consistent with a defect in entry (Fig. 1C). In other cases, the percentage of host cells displaying GFP fluorescence appeared to be similar to control wells, yet the intensity of GFP fluorescence per cell was decreased, consistent with a defect in intracellular replication (Fig. 1D). Combinations of these two phenotypes were also observed. (ii) Punctate GFP fluorescence ("spots" phenotype). This phenotype was similar to the phenotype observed during infection by DH-L1137 (fig. S1A) and is consistent with a defect in vacuole escape. However, bacteria in dsRNA-treated wells appeared to be capable of increased replication within the localized clusters (Fig. 1E). (iii) Increased GFP fluorescence ("up" phenotype). The intensity of GFP fluorescence per infected SL2 cell was more robust, consistent with an increase in intracellular replication rate or increased bacterial uptake (Fig. 1F).

From the primary RNAi screen, we identified 358 *Drosophila* genes that potentially affect *L. monocytogenes* infection, including genes coding for ribosome components (61 genes) and proteasome components (25 genes). With the exception of the dsRNAs targeting ribosome and proteasome components [supporting online material (SOM) text], the candidate dsRNAs identified in the primary RNAi screen were retested at least six times and ~70% were confirmed as affecting *L. monocytogenes* infection. Of these dsRNAs, less than 13% were shown to have effects on host cell viability in a previous screen with the use of the same dsRNA library (*11*), suggesting a specific effect on intracellular bacterial infection rather than nonspecific effects on the host cells. The putative host factors required for *L. monocytogenes* infection spanned a wide range of cellular functions (tables S1 and S2). Many of the identified targets resulting in a down phenotype are predicted to be involved in vesicular trafficking (19%), signal transduction (10%), and cytoskeletal organization (10%). Knockdown of many of these targets resulted in a phenotype consistent with an entry defect, including Syx5 (vesicular trafficking) (Fig. 1C), Cdc42 (signal transduction), and Arp2/3 complex members (cytoskeleton). Other targets in these categories had phenotypes consistent with defects in steps beyond entry, such as Tor (target of rapamycin) (signal transduction) (Fig. 1D) and Rab2 (vesicular trafficking) (SOM text). Furthermore, dsRNAs targeting 48 *Drosophila* genes caused an up phenotype (Fig. 2A and table S1). The gene products of these targets are predominantly predicted to be involved in cell cycle (40%) and RNA processing (13%).

To determine whether the identified host factors were specific to *L. monocytogenes* infection or more generally required for intracellular pathogenesis, we compared the results with a similar RNAi-based screen that tested *M. fortuitum* (*5*, *9*). We focused our comparative analysis on candidates that caused decreased infection (Fig. 2, B and C). The majority of dsRNAs that decreased infection by both pathogens target factors that are predicted to be involved in vesicular trafficking or cytoskeleton components (table S3 and Fig. 2C). Many of these may be required for nonspecific uptake of both pathogens, because they were also found to affect phagocytosis of *E. coli* (*5*). However, some host factors appeared to be specific for entry. For example, a knockdown of CG7228 (Pes), a member of the CD36 family of scavenger receptors, reduced entry of both *L. monocytogenes* (fig. S2) and *M. fortuitum*, but had no effect on uptake of *E. coli* or *Staphylococcus aureus* (*5*). In addition, several candidates affecting both pathogens appeared to have roles other than entry (SOM text).

We also identified dsRNAs that decreased infection by one pathogen but not the other. For example, dsRNA targeting CG6121 decreased intracellular infection by *M. fortuitum*, but did not interfere with *L. monocytogenes* infection (Fig. 3). CG6121 (dTip60) is a member of a complex with histone acetyltransfer-

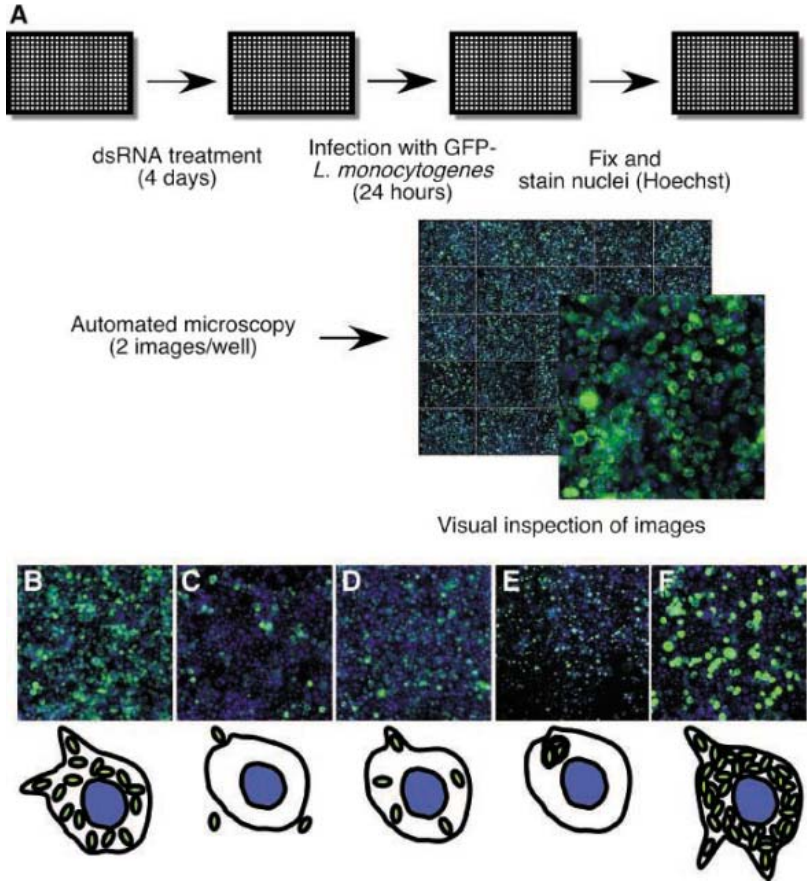

Fig. 1. RNAi screening procedure and phenotypes observed. (**A**) Screen design. [(B) to (F)] Candidates representative of the observed phenotypes. (**B**) No dsRNA (control). (**C**) Syx5: down phenotype in which a decreased percentage of cells expressed GFP. (**D**) Tor: down phenotype in which each cell displayed decreased GFP expression. (**E**) CG5691: spots phenotype, in which GFP expression was clustered within the cell. (**F**) CG3605: up phenotype, in which each cell displayed increased GFP expression. Below each image is a schematic depiction of the corresponding phenotype.

[1]Department of Microbiology and Molecular Genetics, [2]Department of Genetics, Harvard Medical School, Boston, MA 02115, USA. [3]Department of Immunology and Infectious Diseases, Harvard School of Public Health, Boston, MA 02115, USA.

*These authors contributed equally to this work.
†Present address: Section of Microbial Pathogenesis, Yale University School of Medicine, New Haven, CT 06519, USA.
‡To whom correspondence should be addressed. E-mail: herve.agaisse@yale.edu (H.A.); dhiggins@hms.harvard.edu (D.E.H.)

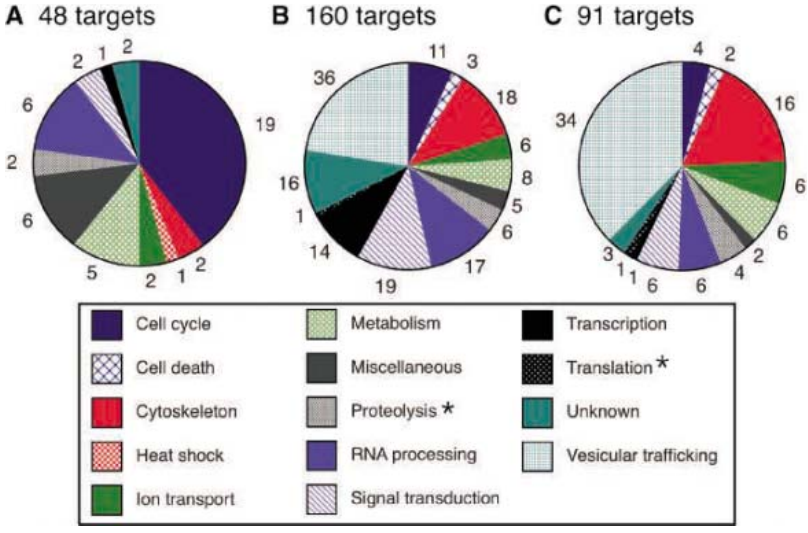

Fig. 2. Functional categories of dsRNA targets identified in *L. monocytogenes* and *M. fortuitum* RNAi screens. [(A) to (C)] Functional categories identified. The numbers surrounding the charts indicate the number of target genes within each functional category. Stars (*) indicate targets other than proteasome or ribosome subunits that are categorized as proteolysis or translation. (**A**) dsRNAs resulting in an up phenotype for *L. monocytogenes*. (**B**) dsRNAs resulting in a down phenotype for *L. monocytogenes*. (**C**) dsRNAs resulting in a down phenotype for both *L. monocytogenes* and *M. fortuitum*.

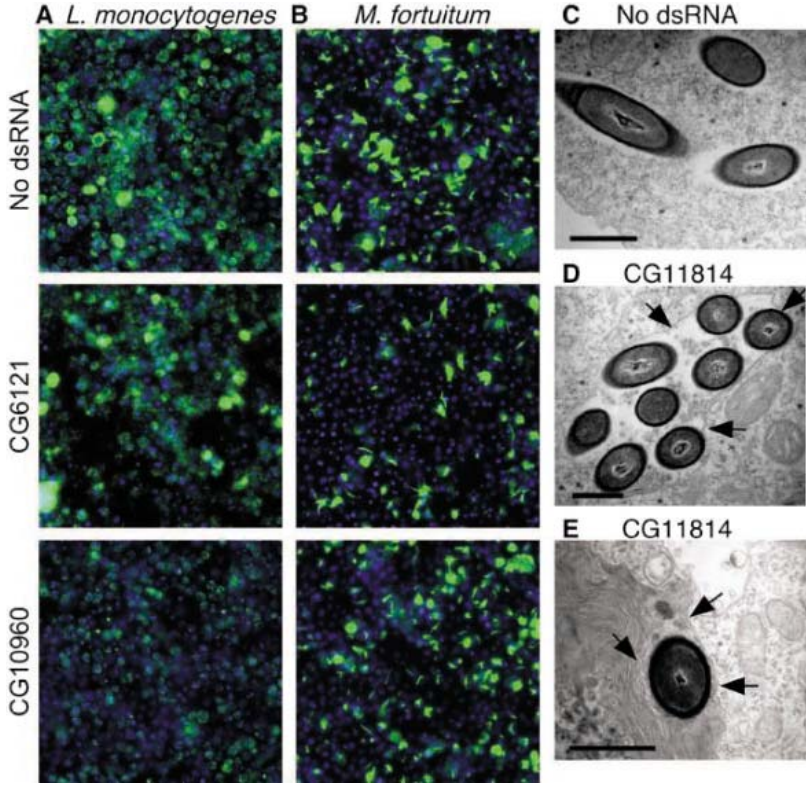

Fig. 3. Representative phenotypes for dsRNAs that uniquely affect *L. monocytogenes* or *M. fortuitum* infection. (**A** and **B**) SL2 cells were untreated (top), treated with CG6121 dsRNA (middle), or treated with CG10960 dsRNA (bottom) and infected with *L. monocytogenes* (A) or *M. fortuitum* (B) expressing GFP (green) (*5*). At 24 hours postinfection (*L. monocytogenes*) or 48 hours postinfection (*M. fortuitum*) cells were fixed and stained with Hoechst dye (blue). Fluorescent images (20×) are representative of infections performed at least six times for each pathogen. (**C** to **E**) Electron micrographs of (C) untreated or [(D) and (E)] CG11814 dsRNA-treated SL2 cells infected with wild-type *L. monocytogenes*. Arrows indicate membranes surrounding bacteria in the CG11814 dsRNA-treated cells. Scale bars, 0.5 μm.

ase activity (*13*). Two other members of the *Drosophila* Tip60 complex, dom and E(Pc), were also identified as affecting *M. fortuitum* infection. Human immunodeficiency virus Tat protein interaction with Tip60 in mammalian cells alters expression of host cell genes (*14*). Thus, it is possible that *M. fortuitum* similarly targets the Tip60 complex to modify the expression of specific host factors. In all, 17 dsRNAs that decreased infection by *M. fortuitum* did not affect *L. monocytogenes* infection. Six dsRNAs that decreased infection by *M. fortuitum* caused an up phenotype for *L. monocytogenes* (table S3). A total of 59 dsRNAs, including those targeting a putative glucose transporter, CG10960, decreased infection by *L. monocytogenes* but did not affect *M. fortuitum* (table S3 and Fig. 3). Ten dsRNAs that caused a down phenotype for *L. monocytogenes* appeared to increase *M. fortuitum* intracellular growth (table S3). Furthermore, all 11 dsRNAs resulting in the spots phenotype for *L. monocytogenes* (table S1) did not detectably affect *M. fortuitum* infection. As confirmed by electron microscopy, the spots phenotype corresponded to a vacuolar escape defect. In untreated SL2 cells, *L. monocytogenes* were found free in the cytosol (Fig. 3C), whereas treatment with CG11814 dsRNA, which caused a spots phenotype, resulted in membrane-bound compartments harboring multiple bacteria (Fig. 3D). CG11814 is predicted to have roles in lysosomal transport. Spots vacuoles appeared to be more permissive for growth of *L. monocytogenes*. Indeed, LLO-negative bacteria replicated two times more in SL2 cells treated with CG11814 dsRNA than in untreated SL2 cells (fig. S3). Of membrane-bound compartments containing one or more bacteria in CG11814 dsRNA-treated cells, 52% were surrounded by multilamellar structures (Fig. 3E) compared with 8% in untreated control cells. Similar structures surround mutants of another cytosolic pathogen, *Shigella flexneri* (*15*). These multilamellar structures result from an attempt of the host cell to control intracellular infection by a process related to autophagy (*15*). Thus, autophagy may represent a defense mechanism that limits *L. monocytogenes* infection (SOM text). Because infection of *Drosophila* cells by intracellular bacterial pathogens is similar to infection of mammalian host cells, it is likely that many homologous mammalian host factors will be conserved in their requirement for intracellular infection.

References and Notes

1. A. Aderem, D. M. Underhill, *Annu. Rev. Immunol.* **17**, 593 (1999).
2. I. Vergne, J. Chua, S. B. Singh, V. Deretic, *Annu. Rev. Cell Dev. Biol.* **20**, 367 (2004).
3. J. A. Vazquez-Boland *et al.*, *Clin. Microbiol. Rev.* **14**, 584 (2001).
4. B. B. Finlay, S. Falkow, *Microbiol. Mol. Biol. Rev.* **61**, 136 (1997).
5. J. A. Philips, E. J. Rubin, N. Perrimon, *Science* **309**, 1251 (2005).

6. L. W. Cheng, D. A. Portnoy, *Cell. Microbiol.* **5**, 875 (2003).
7. B. E. Mansfield, M. S. Dionne, D. S. Schneider, N. E. Freitag, *Cell. Microbiol.* **5**, 901 (2003).
8. K. E. Beauregard, K. D. Lee, R. J. Collier, J. A. Swanson, *J. Exp. Med.* **186**, 1159 (1997).
9. Materials and methods are available as supporting material on *Science* Online.
10. M. Ramet, P. Manfruelli, A. Pearson, B. Mathey-Prevot, R. A. Ezekowitz, *Nature* **416**, 644 (2002).
11. M. Boutros *et al.*, *Science* **303**, 832 (2004).
12. M. Hild *et al.*, *Genome Biol.* **5**, R3 (2003).
13. T. Kusch *et al.*, *Science* **306**, 2084 (2004).
14. M. Creaven *et al.*, *Biochemistry* **38**, 8826 (1999).
15. M. Ogawa *et al.*, *Science* **307**, 727 (2005).
16. We are grateful to the *Drosophila* RNAi Screening Center for providing access to the dsRNA library and screening facilities. We thank members of the Perrimon lab and Higgins lab for assistance and support, especially A. Shen for construction of strain DH-L1039. This work was supported by grant AI053669 (D.E.H.) and AI048704 (E.J.R.) from the NIH. N.P. is an Investigator of the Howard Hughes Medical Institute (HHMI). Work in the Perrimon lab was supported by HHMI and the NIH. L.S.B. is a HHMI Predoctoral Fellow.

Supporting Online Material
www.sciencemag.org/cgi/content/full/1116008/DC1
Materials and Methods
SOM Text
Figs. S1 to S4
Tables S1 to S4
References

13 June 2005; accepted 5 July 2005
Published online 14 July 2005;
10.1126/science.1116008
Include this information when citing this paper.

Drosophila RNAi Screen Reveals CD36 Family Member Required for Mycobacterial Infection

Jennifer A. Philips,[1]* Eric J. Rubin,[3] Norbert Perrimon[1,2]*

Certain pathogens, such as *Mycobacterium tuberculosis*, survive within the hostile intracellular environment of a macrophage. To identify host factors required for mycobacterial entry and survival within macrophages, we performed a genome-wide RNA interference screen in *Drosophila* macrophage-like cells, using *Mycobacterium fortuitum*. We identified factors required for general phagocytosis, as well as those needed specifically for mycobacterial infection. One specific factor, Peste (Pes), is a CD36 family member required for uptake of mycobacteria, but not *Escherichia coli* or *Staphylococcus aureus*. Moreover, mammalian class B scavenger receptors (SRs) conferred uptake of bacteria into nonphagocytic cells, with SR-BI and SR-BII uniquely mediating uptake of *M. fortuitum*, which suggests a conserved role for class B SRs in pattern recognition and innate immunity.

About one-third of the world's population is infected by *M. tuberculosis*, which is responsible for more deaths yearly than any other bacterial pathogen. In addition, other pathogenic mycobacteria, including *M. fortuitum*, are capable of causing infection in humans (*1*). Although macrophages play a central role in host defense, recognizing and destroying pathogens, pathogenic mycobacteria are able to survive within this hostile environment. Mycobacteria can escape phagosome-lysosome fusion (*2*) and grow in a variety of evolutionarily divergent phagocytic cells, including mammalian macrophages, fish monocytes (*3*), fly hemocytes (*4*), and amoeba (*5*). Thus, mycobacteria appear to target evolutionarily conserved molecules for intracellular survival and growth. Although several factors involved in phagosome maturation arrest have been studied (*6*), there has been no systematic, genetic approach for identifying host factors required for mycobacterial survival. Here we describe a model of infection using *Drosophila* S2 cells, a macrophage-like cell line (*7*–*9*) that is readily amenable to RNA interference (RNAi). This allowed us to conduct a systematic functional genomic screen to identify host factors required for uptake and growth of mycobacteria.

M. fortuitum has several properties that make it a useful model mycobacterium. Like *M. tuberculosis*, it restricts interferon-γ (IFN-γ)–induced nitric oxide production and limits phagosome fusion with lysosomes (*10*), suggesting it has virulence properties in common with other mycobacteria. In addition, *M. fortuitum* infects *Diptera* in nature (*11*), so flies may have innate mechanisms to combat infection. Practically, *M. fortuitum* grows relatively rapidly at 25°C, the temperature at which S2 cells grow, thus facilitating development of a robust assay of intracellular growth. To detect intracellular growth, we tested constructs in which green fluorescent protein (GFP) expression is under control of the *map24* and *map49* promoters that are induced when the fish pathogen *Mycobacterium marinum* infects macrophages (*12*). We found that these promoters could also be used to efficiently detect intracellular growth of *M. fortuitum* (fig. S1). By 24 hours after infection of S2 cells, expression of *map24* and *map49* was induced (figs. S1 and S2; Fig. 1A).

In mammalian cells, recruitment of the Arp2/3 complex is required for phagocytosis (*13*), whereas expression of a dominant-negative version of Rab5 causes internalized *Mycobacterium avium* to be delivered to the lysosome (*14*). Thus, we reasoned that double-stranded RNAs (dsRNAs) targeting

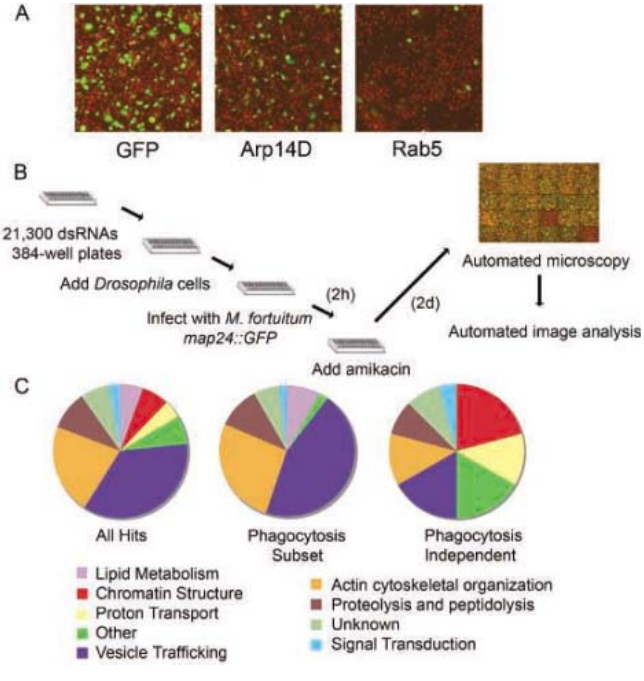

Fig. 1. Host factors required for *M. fortuitum* infection identified by RNAi. After treatment with dsRNAs, S2 cells were infected with *M. fortuitum map24::GFP*. (**A**) dsRNA targeting Arp14D or Rab5 decreased infection as compared to controls treated with dsRNA targeting GFP. (**B**) This assay was used as the basis of a genomewide screen (*15*). A composite image of 35 wells is shown. (**C**) Pie charts based upon GeneOntology (GO) index biological function show the categories of host factors that reproducibly decreased infection after 3 days of dsRNA treatment, as well as the subsets that are required for phagocytosis and those that are apparently phagocytosis independent.

[1]Department of Genetics, [2]Howard Hughes Medical Institute, Harvard Medical School, 77 Louis Pasteur Avenue, Boston, MA 02115, USA. [3]Department of Immunology and Infectious Disease, Harvard School of Public Health, 665 Huntington Avenue, Boston, MA 02115, USA.

*To whom correspondence should be addressed. E-mail: jphilips@partners.org (J.A.P.), perrimon@receptor.med.harvard.edu (N.P.)

Arp14D and Rab5 would decrease infection in *Drosophila* cells. Indeed, we found that these dsRNAs blocked intracellular growth of *M. fortuitum* (Fig. 1A). Using this assay, we performed a genomewide RNAi screen in which each unique dsRNA was tested for its ability to disrupt infection on the basis of visual inspection and automated image analysis (*15*) (Fig. 1B). We found six out of seven Arp2/3 components, five out of seven COPI components, and all six alleles of actin, suggesting a false-negative rate of less than 20%. Upon repeat testing of the candidates identified in the primary screen, 86 dsRNAs decreased infection by 2 SDs ($P < 0.05$; tables S1 and S3). These dsRNAs target genes involved in basic cellular processes, the largest categories of which are predicted to have a role in vesicle trafficking and actin cytoskeletal organization (Fig. 1C).

Because GFP expression requires internalization of bacteria, we expected to find dsRNAs that block general phagocytosis. Indeed, 54 dsRNAs caused a significant decrease in phagocytosis, as measured by the uptake of fluorescent *Escherichia coli* ($P < 0.01$; table S2 and fig. S3). About two-thirds of these dsRNAs target factors involved in the actin cytoskeleton and vesicle trafficking (Fig. 1C). Nearly all of the actin cytoskeletal components that affected *M. fortuitum* infection appeared to be generally required for phagocytosis, including Cdc42, the Arp2/3 complex, actin capping proteins, and cofilin, all molecules previously implicated in phagocytosis (*13*). Most vesicle trafficking genes also affected phagocytosis, with exceptions such as CG1515 (predicted to have SNAP receptor activity) and Rab2.

However, the requirement for many genes for infection could not be explained by their role in phagocytosis. For example, dsRNA that targets *chickadee* (*chic*), which encodes a Profilin, caused a small increase in phagocytosis (118% of GFP-treated well; $P < 0.05$), similar to what has been reported in hemocytes heterozygous for *chic* ($chic^{01320}/+$) (*9*). Hence, Chic is unlikely to act at the level of uptake and may play a unique role in mycobacterial infection. Some dsRNAs, such as those that target Rab5 and Rac2, caused a mild defect in phagocytosis relative to their severe defect in the *M. fortuitum* infection, indicating that they may have additional roles later in infection. Finally, some categories of host factors were not required for bacterial uptake in general but were nonetheless needed for infection with *M. fortuitum*. These include components of the vacuolar adenosine triphosphatase and chromatin factors, along with many that do not fit into distinct categories (Fig. 1C).

We further characterized one host factor that appeared to be specifically required for mycobacterial uptake. The dsRNA that targeted CG7228, a member of the CD36 family of scavenger receptors (SRs), blocked infection by *M. fortuitum* (Fig. 2A), but appeared to be dispensable for phagocytosis in general. dSR-CI, a class C scavenger receptor, makes a small contribution toward the uptake of *E. coli* and *Staphylococcus aureus* in S2 cells (*8*), but we could not detect a similar contribution from CG7228 (Fig. 2B). However, CG7228 was required for uptake of *Mycobacterium smegmatis*, as were more general phagocytosis factors (Fig. 2C). In addition, CG7228 is required for uptake of *Listeria monocytogenes* (*16*). That CG7228 is required for infection with *M. fortuitum* and for uptake of *M. smegmatis* and *L. monocytogenes*, but makes no contribution toward the uptake of *E. coli* or *S. aureus*, suggests that it functions in pattern recognition, detecting some component of *Mycobacteria* and *Listeria*. On the basis of its role in bacterial infection, we have named it *peste* (*pes*).

To determine whether Pes was sufficient to confer uptake of mycobacteria, we expressed it in human embryonic kidney 293 (HEK293) cells that are refractory to infection with *M. fortuitum*. HEK293 cells transfected with Pes could be infected with *M. fortuitum* (Fig. 3A), showing that the *Drosophila* SR can mediate uptake of mycobacteria in human cells. Pes also caused a small increase in the uptake of *E. coli* and *S. aureus* when transfected in HEK293 cells (Fig. 3, B and C), although it did not seem to be required for their uptake in S2 cells. This apparent discrepancy may be explained by genetic redundancy provided by PGRP-Lc (*7*), dSR-CI (*8*), and potentially other SRs that mediate uptake of *E. coli* and *S. aureus* in S2 cells.

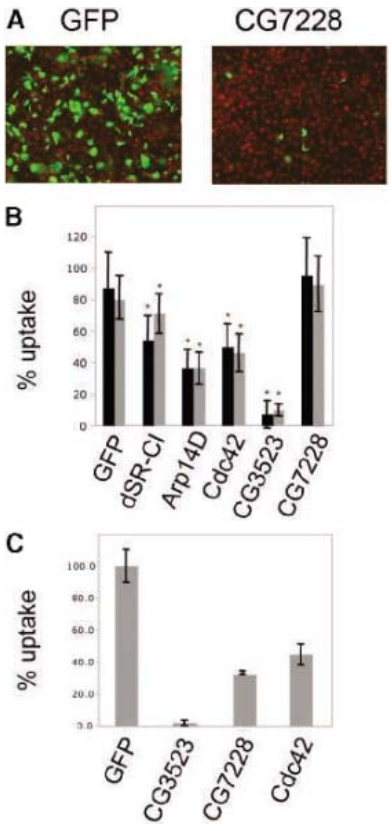

Fig. 2. CG7228 is required in S2 cells for infection by *M. fortuitum* and uptake of *M. smegmatis* but not *E. coli* or *S. aureus*. (**A**) dsRNA against CG7228 blocked infection by *M. fortuitum* as compared to controls treated with dsRNA against GFP. (**B**) Uptake of fluorescein isothiocyanate (FITC)–conjugated *E. coli* (black bars) and *S. aureus* (gray bars) is blocked by dsRNA toward dSR-CI, Arp14D, Cdc42, and CG3523, but not CG7228. Data show the percent uptake as compared to that in untreated cells (fig. S3). The mean ± SD of six experiments is shown in which each dsRNA was tested in triplicate (*$P < 0.05$ compared to GFP-treated wells, Students *t* test.) (**C**) Antibiotic protection experiments demonstrate the role of CG7228, CG3523, and Cdc42 in the uptake of *M. smegmatis*. Data are normalized to GFP; the mean ± SD is shown from a representative experiment performed in triplicate.

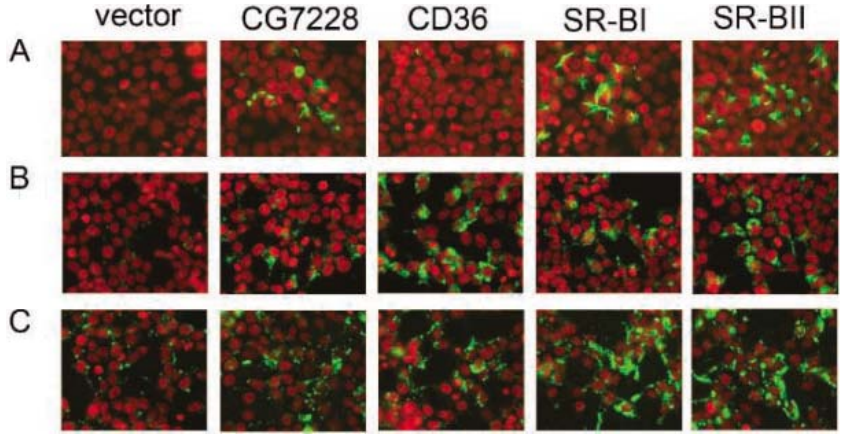

Fig. 3. Class B SRs mediate uptake of *M. fortuitum*, *E. coli*, and *S. aureus*. HEK293 cells transfected with vector (pcDNA3.1) or expression constructs for CG7228 (Pes), CD36, SR-BI, or SR-BII were (**A**) infected with *M. fortuitum map24::GFP* or (**B**) incubated with FITC–*E. coli* or (**C**) FITC–*S. aureus*. In (A) green represents GFP expression from the *map24* promoter, whereas in (B) and (C) green shows the FITC signal from internalized bacteria. Nuclei are stained red. Magnification, ×40.

Whereas in *Drosophila* there are more than 10 class B SRs, in humans and mice there are four—CD36, SR-BI, its splice isoform SR-BII, and LIMP-II. We tested the ability of these molecules to mediate infection with *M. fortuitum* and found that human SR-BI and SR-BII (*17*) resulted in an even greater level of infection than Pes when transfected in HEK293 cells. In contrast, expression of murine CD36 caused little, if any, increase in infection with *M. fortuitum* (Fig. 3A). However, cells transfected with CD36 were capable of taking up *E. coli*, and to a lesser extent *S. aureus*. SR-BI and SR-BII seemed more indiscriminate in terms of their bacterial recognition, as they were able to mediate uptake of all bacteria tested (Fig. 3, B and C). Whereas SR-BI and SR-BII have been extensively studied for their role in cholesterol transport in liver and steroidogenic tissue, their role in macrophages is less clear (*18*). We suggest that these receptors may be important in host defense against a broad range of bacteria, including *M. fortuitum*, *E. coli*, and *S. aureus*, and could play a role in the nonopsonic uptake of *M. tuberculosis*. Consistent with this idea, fucoidin, a nonspecific inhibitor that blocks both class A SRs and SR-BI (*19*), interferes with binding and uptake of *M. tuberculosis* in monocyte-derived macrophages (*20*). CD36 may play a partially overlapping role in recognizing bacteria, but is unable to mediate uptake of *M. fortuitum*. Because CD36 augments Toll-like receptor 2 (TLR2) signaling in response to a subset of TLR2 ligands (*21*), we speculate that CD36, SR-BI, and SR-BII serve partially overlapping roles in both bacterial uptake and TLR signaling, which may represent an evolutionarily conserved strategy in host defense, linking phagocytosis to antimicrobial signaling.

References and Notes

1. D. E. Griffith, R. J. Wallace Jr., *Semin. Respir. Infect.* **11**, 301 (1996).
2. D. G. Russell, *Nat. Rev. Mol. Cell Biol.* **2**, 569 (2001).
3. S. H. El-Etr, L. Yan, J. D. Cirillo, *Infect. Immun.* **69**, 7310 (2001).
4. M. S. Dionne, N. Ghori, D. S. Schneider, *Infect. Immun.* **71**, 3540 (2003).
5. J. D. Cirillo, S. Falkow, L. S. Tompkins, L. E. Bermudez, *Infect. Immun.* **65**, 3759 (1997).
6. I. Vergne, J. Chua, S. B. Singh, V. Deretic, *Annu. Rev. Cell Dev. Biol.* **20**, 367 (2004).
7. M. Ramet, P. Manfruelli, A. Pearson, B. Mathey-Prevot, R. A. Ezekowitz, *Nature* **416**, 644 (2002).
8. M. Ramet *et al.*, *Immunity* **15**, 1027 (2001).
9. A. M. Pearson *et al.*, *Microbes Infect.* **5**, 815 (2003).
10. T. R. Da Silva *et al.*, *Infect. Immun.* **70**, 5628 (2002).
11. O. Fischer *et al.*, *Med. Vet. Entomol.* **15**, 208 (2001).
12. L. Ramakrishnan, N. A. Federspiel, S. Falkow, *Science* **288**, 1436 (2000).
13. S. Greenberg, S. Grinstein, *Curr. Opin. Immunol.* **14**, 136 (2002).
14. V. A. Kelley, J. S. Schorey, *Mol. Biol. Cell* **14**, 3366 (2003).
15. Materials and methods are available as supporting material on *Science* Online.
16. H. Agaisse *et al.*, *Science* **309**, 1248 (2005).
17. J. V. Mulcahy, D. R. Riddell, J. S. Owen, *Biochem. J.* **377**, 741 (2004).
18. D. Rhainds, L. Brissette, *Int. J. Biochem. Cell Biol.* **36**, 39 (2004).
19. J. Husemann, J. D. Loike, T. Kodama, S. C. Silverstein, *J. Neuroimmunol.* **114**, 142 (2001).
20. S. Zimmerli, S. Edwards, J. D. Ernst, *Am. J. Respir. Cell Mol. Biol.* **15**, 760 (1996).
21. K. Hoebe *et al.*, *Nature* **433**, 523 (2005).

22. We thank C. Cosma and L. Ramikrishnan (University of Washington) for providing *map24* and *map49* plasmids. Expression constructs for CD36, SR-BI and SR-BII, and LIMP-II were provided by K. Moore (Massachusetts General Hospital), J. Owen (University College London), and K. Akasaki (Fukuyama University), respectively. S. De Bruin and N. Gliksman (Universal Imaging) provided MetaMorph software training. E. Troy, L. Burrack, and D. Higgins assisted with bone marrow–derived macrophages experiments. We are indebted to the *Drosophila* RNAi Screening Center for providing expertise and the facilities for screening, and to the Perrimon and Rubin laboratory members for assistance, in particular S. Cherry. D. Higgins, B. Mathey-Prevot, L. Burrack, and M. Gibson provided useful comments on the manuscript. This work was supported by the NIH. N.P. is an Investigator of the Howard Hughes Medical Institute.

Supporting Online Material

www.sciencemag/org/cgi/content/full/1116006/DC1
Materials and Methods
Figs. S1 to S3
Tables S1 to S3
References and Notes

13 June 2005; accepted 5 July 2005
Published online 14 July 2005;
10.1126/science.1116006
Include this information when citing this paper.

Effects of Telomerase and Telomere Length on Epidermal Stem Cell Behavior

Ignacio Flores, María L. Cayuela, María A. Blasco*

A key process in organ homeostasis is the mobilization of stem cells out of their niches. We show through analysis of mouse models that telomere length, as well as the catalytic component of telomerase, Tert, are critical determinants in the mobilization of epidermal stem cells. Telomere shortening inhibited mobilization of stem cells out of their niche, impaired hair growth, and resulted in suppression of stem cell proliferative capacity in vitro. In contrast, Tert overexpression in the absence of changes in telomere length promoted stem cell mobilization, hair growth, and stem cell proliferation in vitro. The effects of telomeres and telomerase on stem cell biology anticipate their role in cancer and aging.

Tumor formation and aging are associated with alterations in the number or functional competence of tissue stem cells (*1*–*3*). Both processes have also been linked to alterations at the telomere (*4*–*7*), the nucleoprotein structure that caps chromosome ends (*8*, *9*), and to changes in the activity of telomerase, the reverse transcriptase that elongates telomeres (*10*, *11*). The catalytic subunit of telomerase (Tert) is expressed in the stem cell compartment of several adult tissues (*12*), although telomerase levels in these tissues are not sufficient to prevent progressive telomere shortening with age (*10*). Reduced telomerase activity due to mutations in telomerase components in the human diseases dyskeratosis congenita and aplastic anemia (*10*) leads to accelerated telomere shortening and premature loss of tissue regeneration, which suggests that telomerase levels in the adult organism are rate limiting and influence organ homeostasis. Further evidence for a role of telomerase and telomere length in organ homeostasis comes from the study of telomerase-deficient mice (*Terc*$^{-/-}$ mice), which show premature aging and a decreased proliferative potential of adult stem cell populations (*13*–*15*).

To investigate the role of telomerase and telomere length on stem cell biology, we used mouse models with altered telomerase activity (*16*). We compared epidermal stem cell number in different generations of telomerase-deficient mice, which have telomeres ranging from slightly reduced in length (first generation, G1 *Terc*$^{-/-}$ mice) to critically short (third generation, G3 *Terc*$^{-/-}$ mice) (*17*, *18*). Because telomerase activity per se is not required for cell proliferation when telomeres are long, the study of G1 and G3 *Terc*$^{-/-}$ mice allowed us to assess independently the impact of telomerase deficiency and telomere length on epidermal stem cells. To visualize epidermal stem cells, we used a labeling technique previously shown to mark self-renewing and multipotent epidermal cells, the so-called "label-retaining cells" (LRCs) (*16*, *19*) (Fig. 1A). Confocal microscopy revealed that LRCs are enriched at the bulge area of the hair follicle in *Terc*$^{+/+}$ (wild-type) mice, which corresponds to the niche of epithelial stem cells (Fig. 1B, fig. S1A, and

Telomeres and Telomerase Group, Molecular Oncology Program, Spanish National Cancer Centre (CNIO), Melchor Fernández Almagro 3, Madrid E-28029, Spain.

*To whom correspondence should be addressed. E-mail: mblasco@cnio.es

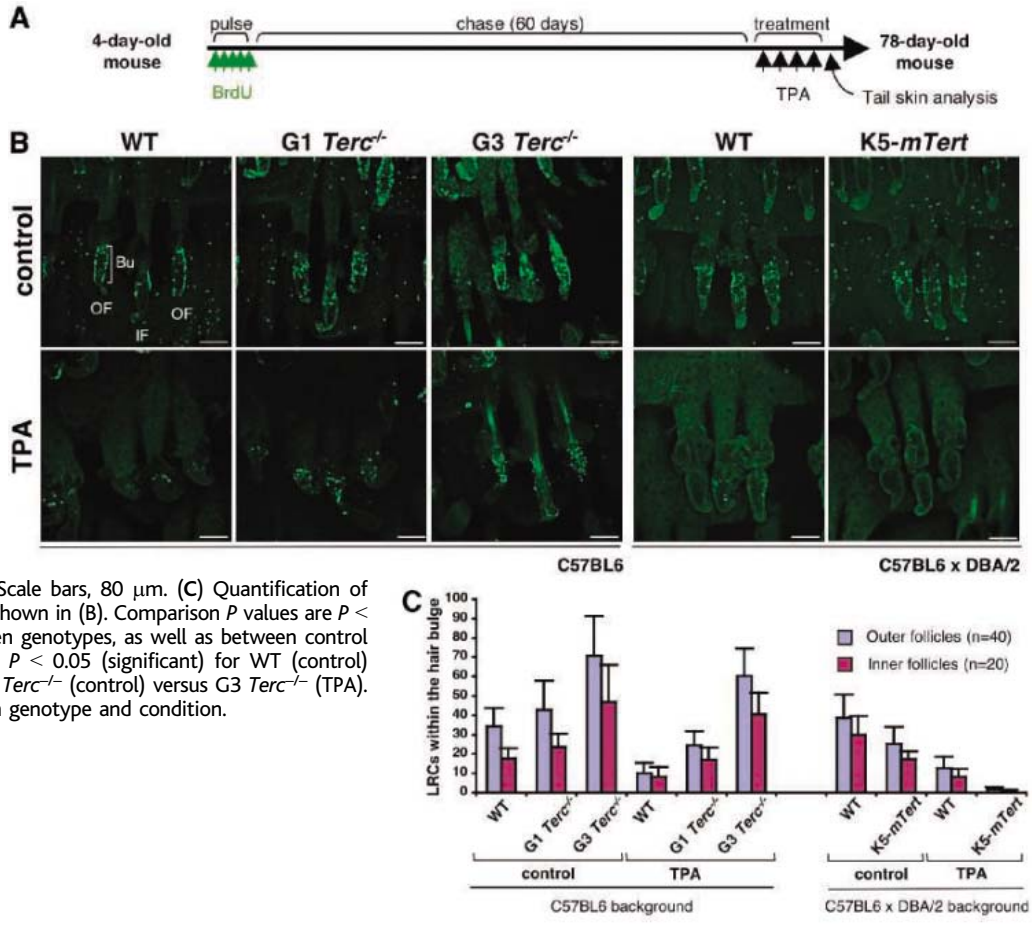

Fig. 1. Telomere attrition and Tert overexpression are independent determinants of LRC mobilization upon TPA treatment. (**A**) Strategy to assay mobilization of LRCs (*16*). Mice were injected with bromodeoxyuridine (BrdU) and, 69 days later, whole mounts of tail epidermis were collected from untreated and TPA-treated mice and stained with an antibody to BrdU. (**B**) Representative confocal micrographs of tail follicles from wild-type (WT), G1 $Terc^{-/-}$, and G3 $Terc^{-/-}$ mice in a C57BL6 background (left) and from WT and K5-*mTert* mice in a C57BL6 x DBA/2 background (right), stained for BrdU (green) after LRC labeling and treatment (*16*). The tail-hair follicles are grouped in sets of three (triplets), two outer follicles (OF) and one inner follicle (IF), which generally contains fewer LRCs (*23*). LRCs of all genotypes accumulate in the bulge (Bu) region of the hair follicle. Scale bars, 80 μm. (**C**) Quantification of LRCs in the conditions and genotypes shown in (B). Comparison *P* values are $P < 0.0001$ (significant) in all cases between genotypes, as well as between control treatment and TPA treatment, except $P < 0.05$ (significant) for WT (control) versus G1 $Terc^{-/-}$ (control) and for G3 $Terc^{-/-}$ (control) versus G3 $Terc^{-/-}$ (TPA). SD is represented on each bar for each genotype and condition.

SOM Text) (*19*). Interestingly, G1 $Terc^{-/-}$ hair follicles contained significantly more LRCs than did $Terc^{+/+}$ follicles (Fig. 1, B and C). Even greater numbers were present in the G3 $Terc^{-/-}$ follicles (Fig. 1, B and C). As with $Terc^{+/+}$ mice, LRCs in $Terc^{-/-}$ mice accumulated in the niche/stem cell compartment (Fig. 1B and fig. S1A). The increased number of LRCs in mice with short telomeres was an unexpected finding, because $Terc^{-/-}$ mice are resistant to tumor-inducing protocols (*20*, *21*) and enlarged numbers of cells with stem characteristics have been associated with increased tumor formation (*2*).

To investigate whether LRCs in $Terc^{-/-}$ mice mobilize (exit their quiescent state and migrate) out of the niche, we studied the response of wild-type, G1 $Terc^{-/-}$, and G3 $Terc^{-/-}$ LRCs to treatment with 12-*O*-tetradecanoylphorbol 13-acetate (TPA), a potent tumor promoter (*22*) that activates LRCs to give numerous progeny (*16*). TPA treatment results in rapid disappearance of LRCs (*23*), skin hyperplasia (*24*), and entry of hair follicles (HF) in their anagen (growing) phase (*25*). After TPA treatment, wild-type epidermis showed ~70% reduction in the number of LRCs localized within the stem cell niche (Fig. 1C). In contrast, TPA-treated G1 $Terc^{-/-}$ mice showed ~43% reduction, which suggests a defect in their mobilization (Fig. 1C). This defect was even more pronounced in G3 $Terc^{-/-}$ mice, which showed only ~14% reduction after TPA treatment (Fig. 1C). Coincidentally, the proliferation index in different compartments of the G3 $Terc^{-/-}$ follicle was lower than that of wild-type follicles (fig. S2, A and B, and SOM Text). Furthermore, in contrast to wild-type mice, interfollicular skin thickness (IFE) and HF length were not significantly increased in G3 $Terc^{-/-}$ mice (Fig. 2, A to C), reflecting defective hyperplasia and anagen responses in these mice after TPA treatment. An alternative explanation for the differences in the number of LRCs between genotypes, such as different apoptotic rates (*16*) (fig. S3 and SOM Text) or migration of stem cells out of the niche without division, were ruled out (fig. S1A and SOM Text). All $Terc^{-/-}$ mice used had a histopathologically normal skin at the time of analysis (*16*) (fig. S4), which suggests that stem cell mobilization defects anticipate the aging and cancer-resistant phenotypes of these mice (*18*, *20*).

Next, we performed clonogenic assays to compare the proliferation potential of $Terc^{+/+}$ and $Terc^{-/-}$ epidermal stem cells (*16*). Individual colonies in this assay have been proposed to derive from single stem cells (*26*). In agreement with the in vivo results, keratinocytes from G1 and G3 $Terc^{-/-}$ mice formed fewer and smaller colonies than those from $Terc^{+/+}$ controls (Fig. 3, A and B), reflecting the defective capacity of G3 $Terc^{-/-}$ cells to proliferate. Interestingly, colony formation was particularly impaired in those G3 $Terc^{-/-}$ mice showing a small-size phenotype (Fig. 3, A and C), which in turn is associated with shorter telomeres (*18*). Finally, G1 and G3 $Terc^{-/-}$ colonies were able to fully differentiate upon high calcium treatment (*16*) (fig. S5 and SOM Text), which suggests that decreased colony number in these mice is not due to defects in stem cell multipotency.

To study the impact of telomerase upregulation on the stem cell compartment and cancer, we used K5-*mTert* transgenic mice, which have increased telomerase activity and increased *Tert* expression in skin, including the stem cell niche (*24*, *27*). K5-*mTert* mice have an increased susceptibility to tumorigenesis in the absence of changes in telomere length (*16*, *24*, *28*, *29*) (fig. S6 and SOM Text). To determine whether increased *mTert* expression affected the number and mobilization of epidermal stem cells, we compared LRC number and functionality in wild-type mice versus K5-*mTert* mice (*16*). In K5-*mTert* mice, the basal number of LRCs in the absence of TPA treatment was ~65% lower than in wild-type mice (Fig. 1, B and C). After TPA treatment, ~94% of the LRCs mobilized in K5-*mTert* mice, compared with ~67% in wild-type mice (Fig.

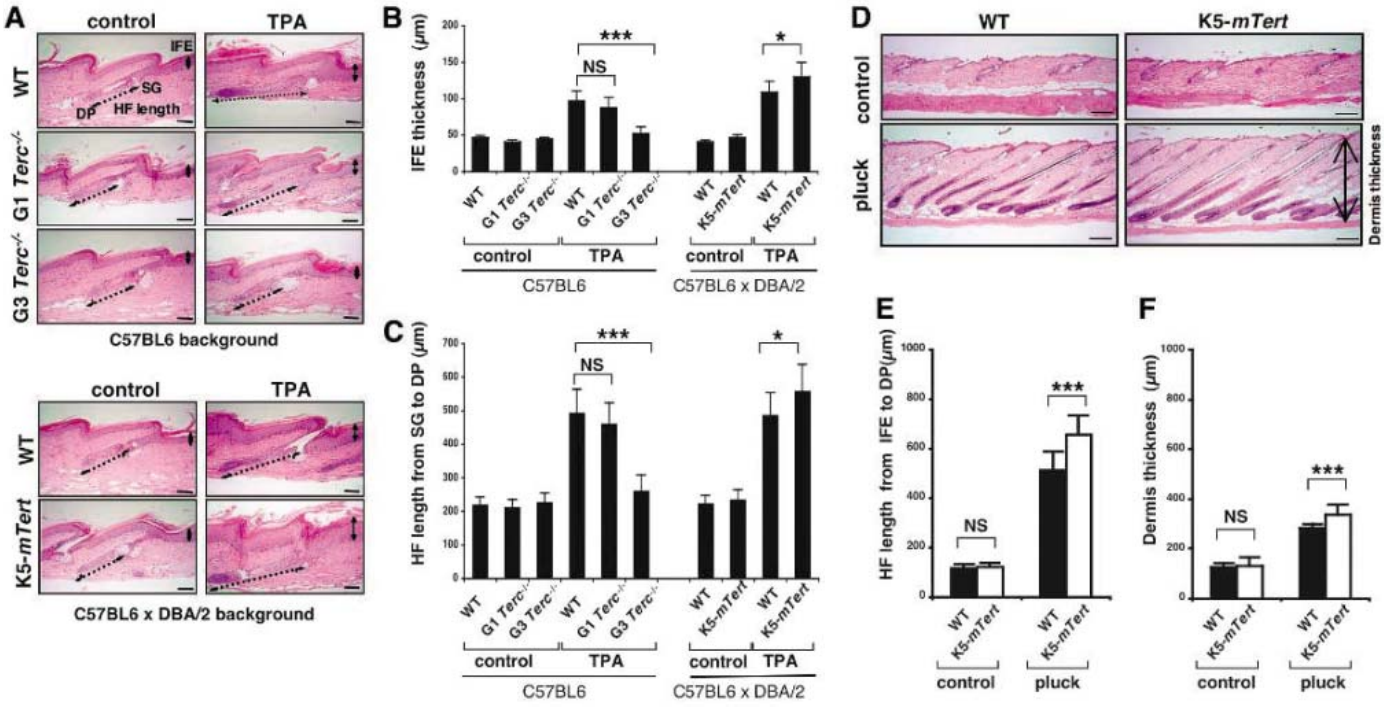

Fig. 2. Telomere attrition and Tert overexpression influence both TPA-induced hyperplasia and anagen. (**A**) Representative tail-skin sections from mice of the indicated genotypes before and after TPA treatment. Continuous black double-pointed arrows mark interfollicular (IFE) thickness. Black dashed double-pointed arrows mark hair-follicle (HF) length from sebaceous glands (SG) to dermal papilla (DP). Quantification of IFE thickness (**B**) and of HF length from SG to DP (**C**) in tail skin from mice of the indicated genotype. Histomorphometry was performed in three mice of each genotype before and after TPA treatment, quantifying a total of 30 follicles in the control group and 90 follicles in the TPA-treated group. (**D**) Representative back skin sections from 8-week-old male mice before and 10 days after plucking. Double-pointed arrows mark dermis thickness. Quantification of HF length from IFE to DP (**E**) and dermis thickness (**F**) in 30 different sections per genotype before and after plucking. NS, not significant, $P > 0.05$; *, significant, $P < 0.05$; ***, significant, $P < 0.001$. SD is represented on each bar for each genotype and condition. Scale bars, μm.

1, B and C). In fact, at the end of the experiment, only 1 to 2 cells were labeled in K5-*mTert* outer follicles, compared with an average of 12.7 cells in wild-type mice (Fig. 1, B and C). Thus, *mTert* overexpression in epidermal stem cells appears to promote LRC mobilization. Again, this occurred in the absence of changes in apoptotic rates (fig. S3) or LCR accumulation out of the stem cell niche (fig. S1B). This Tert-dependent effect is consistent with an increased number of proliferative keratinocytes (fig. S2, A and B), an increased skin hyperplasia (IFE thickness), and increased anagen response (increased HF length) after TPA stimulation (Fig. 2, A to C) or after plucking (*16*) (Fig. 2, D to F, and SOM Text), and it is further supported by a high colony-forming efficiency of isolated K5-*mTert* keratinocytes compared with the wild-type controls (Fig. 3A) in the absence of differences in multipotency (fig. S5).

To address whether Terc is required for the high clonogenicity effect of Tert overexpression, we generated K5-*mTert* mice in a *Terc*$^{-/-}$ genetic background, K5-*mTert*/*Terc*$^{-/-}$ mice. The absence of Terc abolished the effect of Tert overexpression on colony formation (Fig. 3A), which suggests that the formation of Tert/Terc complexes is required for the enhanced clonogenicity of K5-*mTert* cells. Again, no differences in the ability of K5-*mTert* or K5-*mTert*/*Terc*$^{-/-}$ colonies to differentiate upon high calcium conditions were observed (fig. S5).

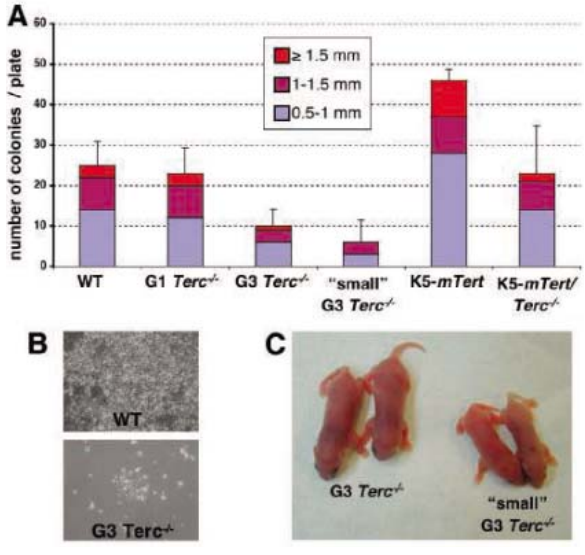

Fig. 3. Telomere attrition and Tert overexpression influence the proliferative potential of stem cells ex vivo. (**A**) Quantification of size and number of macroscopic colonies obtained from isolated keratinocytes of the indicated genotype purified from 2-day-old mice and cultured for 1 week on J2-3T3 mitomycin-C-treated feeder fibroblasts. Comparison *P* values are $P < 0.0001$ (significant) in all cases except $P = 0.041$ (significant) for WT versus G1 Terc$^{-/-}$ and $P = 0.087$ (not significant) for WT versus K5-*mTert*/*Terc*$^{-/-}$. (**B**) Note that a high proportion of G3 *Terc*$^{-/-}$ colonies comprise less than 50 cells. (**C**) G3 *Terc*$^{-/-}$ newborn mice with a smaller size than littermates present an exacerbated deficiency in colony formation. SD is represented on each bar for each genotype and condition.

Telomere length and telomerase activity are independent determinants of the mobilization efficiency and proliferative capacity of epidermal stem cells (fig. S7). On the one hand, critically short telomeres inhibit the mobilization of epidermal stem cells, resulting in the persistence of LRCs in the hair follicle niche. This in turn results in a reduced proliferative potential and reduced anagen response after TPA treatment, as well as in a low in vitro clonogenicity. On the other hand, Tert overexpression promotes

mobilization of epidermal stem cells and decreases the number of LRCs in the stem cell niche after TPA treatment, coincidental with increased numbers of proliferating cells, increased skin thickness and anagen response, and a high efficiency for colony formation. These effects of Tert anticipate the increased susceptibility of K5-*mTert* mice to develop skin tumors (*24*).

References and Notes

1. D. R. Bell, G. Van Zant, *Oncogene* **23**, 7290 (2004).
2. M. Al-Hajj, M. F. Clarke, *Oncogene* **23**, 7274 (2004).
3. G. Van Zant, Y. Liang, *Exp. Hematol.* **31**, 659 (2003).
4. M. A. Blasco, *Cancer Lett.* **194**, 183 (2003).
5. M. A. Blasco, *Eur. J. Cell Biol.* **82**, 441 (2003).
6. N. E. Sharpless, R. A. DePinho, *J. Clin. Invest.* **113**, 160 (2004).
7. J. W. Shay, W. E. Wright, *Carcinogenesis* **26**, 867 (2005).
8. E. H. Blackburn, *Cell* **106**, 661 (2001).
9. T. de Lange, *Oncogene* **21**, 532 (2002).
10. K. Collins, J. R. Mitchell, *Oncogene* **21**, 564 (2002).
11. L. Harrington, *Cancer Lett.* **194**, 139 (2003).
12. L. Harrington, *Oncogene* **23**, 7283 (2004).
13. H. W. Lee *et al.*, *Nature* **392**, 569 (1998).
14. E. Samper *et al.*, *Blood* **99**, 2767 (2002).
15. S. Ferron *et al.*, *Development* **131**, 4059 (2004).
16. Materials and methods are available as supporting material on *Science* Online.
17. M. A. Blasco *et al.*, *Cell* **91**, 25 (1997).
18. E. Herrera *et al.*, *EMBO J.* **18**, 2950 (1999).
19. C. Blanpain, W. E. Lowry, A. Geoghegan, L. Polak, E. Fuchs, *Cell* **118**, 635 (2004).
20. E. Gonzalez-Suarez, E. Samper, J. M. Flores, M. A. Blasco, *Nat. Genet.* **26**, 114 (2000).
21. E. Gonzalez-Suarez, F. A. Goytisolo, J. M. Flores, M. A. Blasco, *Cancer Res.* **63**, 7047 (2003).
22. J. Perez-Losada, A. Balmain, *Nat. Rev. Cancer* **3**, 434 (2003).
23. K. M. Braun *et al.*, *Development* **130**, 5241 (2003).
24. E. Gonzalez-Suarez *et al.*, *EMBO J.* **20**, 2619 (2001).
25. C. Wilson *et al.*, *Differentiation* **55**, 127 (1994).
26. Y. Barrandon, H. Green, *Proc. Natl. Acad. Sci. U.S.A.* **84**, 2302 (1987).
27. T. Tumbar *et al.*, *Science* **303**, 359 (2004).
28. E. Gonzalez-Suarez, J. M. Flores, M. A. Blasco, *Mol. Cell. Biol.* **22**, 7291 (2002).
29. M. A. Blasco, *Nat. Rev. Cancer* **2**, 627 (2002).

30. We thank R. Serrano and E. Santos for mouse care and genotyping, D. Megías and M. Montoya for help with confocal images, V. Coca and P. Gonzalez for help with immunohistochemistry, and M. Arrasate, T. Aragón, and members of the Blasco laboratory for critical reading of the manuscript. Funded by the Ministerio de Ciencia y Tecnología (MCyT) (SAF2001-1869, GEN2001-4856-C13-08), the Regional Government of Madrid (08.1/0054/01), the European Union (TELOSENS FIGH-CT-2002-00217, INTACT LSHC-CT-2003-506803, ZINCAGE FOOD-CT-2003-506850, and RISC-RAD FI6R-CT-2003-508842), and the Josef Steiner Award 2003. I.F. is supported by the Franco-Peral Contract from the Spanish Association Against Cancer.

Supporting Online Material
www.sciencemag.org/cgi/content/full/1115025/DC1
SOM Text
Materials and Methods
Figs. S1 to S7
References

19 May 2005; accepted 8 July 2005
Published online 21 July 2005;
10.1126/science.1115025
Include this information when citing this paper.

Mitogenic Influence of Human R-Spondin1 on the Intestinal Epithelium

Kyung-Ah Kim,[1]* Makoto Kakitani,[2] Jingsong Zhao,[1] Takeshi Oshima,[2] Tom Tang,[1] Minke Binnerts,[1] Yi Liu,[1] Bryan Boyle,[1] Emily Park,[1] Peter Emtage,[1] Walter D. Funk,[1]† Kazuma Tomizuka[2]*†

Several described growth factors influence the proliferation and regeneration of the intestinal epithelium. Using a transgenic mouse model, we identified a human gene, *R-spondin1*, with potent and specific proliferative effects on intestinal crypt cells. Human R-spondin1 (hRSpo1) is a thrombospondin domain-containing protein expressed in enteroendocrine cells as well as in epithelial cells in various tissues. Upon injection into mice, the protein induced rapid onset of crypt cell proliferation involving β-catenin stabilization, possibly by a process that is distinct from the canonical Wnt-mediated signaling pathway. The protein also displayed efficacy in a model of chemotherapy-induced intestinal mucositis and may have therapeutic application in gastrointestinal diseases.

The intestinal epithelium undergoes rapid and continuous self-renewal along the crypt-villus axis, and the β-catenin/T cell factor (TCF) signal transduction pathway plays a pivotal role in the proliferation, differentiation, and oncogenesis of the intestine (*1*–*3*). The Wnt proteins provide a prototype for the ligand-mediated activation of this signaling pathway, and their activities are considered central to the maintenance of the undifferentiated state of intestinal crypt progenitor cells (*4*–*6*). The R-spondin protein family includes four human paralogs (*R-spondin*1–4), each of which contains a leading signal peptide, two cystein-rich, furin-like domains, and one thrombospondin type 1 domain (*7*, *8*). Studies of the *Xenopus R-Spondin* ortholog have shown that this protein class acts as secreted activators of Wnt/β-catenin signaling and Wnt-dependent myogenesis in *Xenopus* (*7*).

We have undertaken an investigation of secreted protein biology by using a transgenic mouse knock-in (KI) approach that allows B cell restricted–transgene expression under control of an immunoglobulin κ promoter (*9*) (figs. S1 and S2). Among the proteins tested, we observed that expression of a cDNA encoding human R-spondin1 (hRSpo1) in KI chimeras led to a dramatic abdominal distention by 8 weeks of age. Examination of hRSpo1-KI chimeras at necropsy revealed a substantial increase in the diameter, length, and weight of the small intestine (Table 1, Fig. 1A, and fig. S3). We also observed an increase in the length of the colon of hRSpo1-KI chimeras (Table 1). Histological analysis and immunohistochemistry of the small intestine of hRSpo1-KI chimeras revealed a marked, diffuse thickening of the mucosa, crypt epithelial hyperplasia, and a greatly expanded zone of proliferating cells as evidenced by the expression of a proliferation marker, Ki-67 (Table 1 and fig. S3).

To further investigate the activity of hRSpo1, we expressed recombinant hRSpo1 protein (*10*) and injected the purified protein into normal mice. Histological evaluation of gastrointestinal sections after 3 days of treatment with hRSpo1 showed significant proliferation of the intestinal crypt epithelial cells in the small intestine and colon, consistent with the results obtained in the hRSpo1-KI chimeras (Table 1 and Fig. 1B). A more detailed examination of the crypts in the small intestine after a single bolus injection of hRSpo1 showed increased proliferation within 3 hours and a peak proliferative effect at approximately 24 hours after injection (Fig. 1C). Immunohistochemistical analysis of the small intestine demonstrated no significant changes in the number of goblet cells and Paneth cells in the small intestine of hRSpo1-treated mice (Fig. 1, D and E), indicating that the transient exposure to hRSpo1 does not affect the maturation and migration of differentiated cells along the crypt-villus axis.

Wnt-mediated activation of epithelial cells results in the stabilization of cytosolic β-catenin, which subsequently translocates to the nucleus and transactivates TCF target genes (*11*, *12*). Isolated colonic crypt cells from mice treated with hRSpo1 displayed stabilization of

[1]Nuvelo, Inc., 675 Almanor Avenue, Sunnyvale, CA 94085, USA. [2]Pharmaceutical Research Laboratories, Pharmaceutical Division, Kirin Brewery Co., Ltd., 3 Miyahara-cho, Takasaki-shi, Gunma 370-1295, Japan.

*These authors contributed equally to this work.
†To whom correspondence should be addressed. E-mail: wfunk@nuvelo.com (W.D.F.); ktomizuka@kirin.co.jp (K.T.)

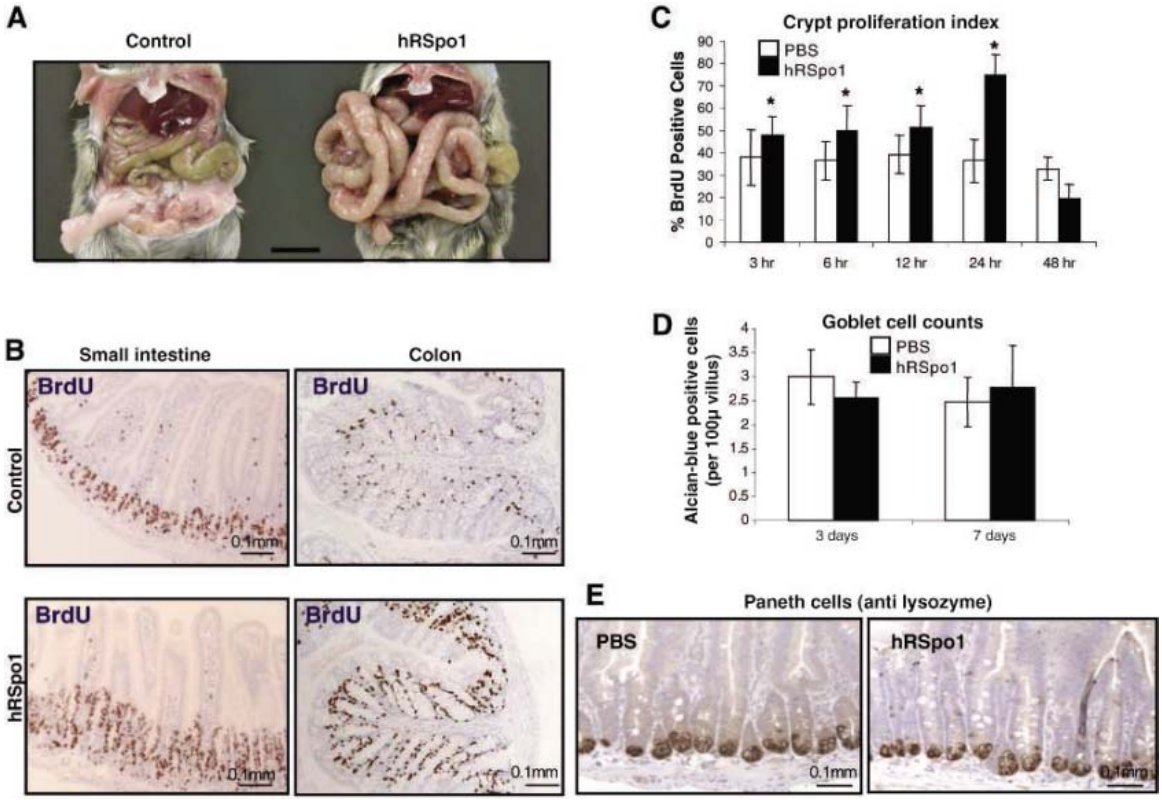

Fig. 1. Expression of hRSpo1 stimulates growth of the intestinal epithelium. (**A**) Gross abdominal anatomy from 8-week-old control (left) and hRSpo1-KI (right) chimeras. Scale bar, 1 cm. (**B**) Recombinant hRSpo1 protein increases the proliferation of intestinal crypt epithelial cells. BALB/c mice were injected daily intravenously (iv) with hRSpo1 (100 μg per injection) or the same volume of phosphate-buffered saline (PBS) as a vehicle control for 3 days. Bromodeoxyuridine (BrdU) immunohistochemistry assays on mid-jejunum and transverse colon sections are shown. (**C**) Crypt proliferative index. BrdU immunohistochemistry assays were performed on mid-jejunal sections after a single injection of hRSpo1 (100 μg per mouse). A total of 40 crypts from two mice were analyzed for BrdU incorporation and are represented as the mean ± SD. *, $P < 0.01$, analysis of variance (ANOVA). (**D**) hRSpo1 treatment does not change the number of goblet cells in small intestine as detected by Alcian blue staining. Animals were injected daily with hRSpo1 (100 μg) or with PBS as a control for 3 or 7 days, and mid-jejunal sections were analyzed ($n = 3$). Error bars, mean ± SD. (**E**) Immunohistochemistry of mid-jejunal sections using antibody to lysozyme. Animals were treated with hRSpo1 for 3 days. Paneth cells are confined to the bottom of crypts, and hRSpo1 treatment did not alter their numbers.

Table 1. Phenotypic data of hRSpo1-KI chimeras and recombinant protein–injected mice. All data are presented as the mean ± SD. Recombinant protein injection: BALB/c mice received a daily injection of 100 μg of hRSpo1 protein for 3 days ($n = 3$).

	KI		Recombinant protein injection	
	Control	hRSpo1	Control	hRSpo1
Small intestine				
Diameter (mid jejunum, mm)†	2.1 ± 0.2	4.0 ± 0.8*	2.3 ± 0.2	3.64 ± 0.1*
Wet weight (KI: including cecum, g)†	3.8 ± 0.4	8.5 ± 2.6*	0.9 ± 0.04	1.34 ± 0.1*
Crypt number/circumference (KI: 4 weeks of age)‡	144 ± 9.3	246 ± 33.9**	125 ± 7.4	154 ± 6.0*
Ki67-positive cell number/crypt unit§	11.5 ± 3.3	60.3 ± 21.1**	ND	ND
Colon length (mm)†	99 ± 9	125 ± 18*	67 ± 3	85 ± 5*

†$n = 4$ to 6 animals per group, 7 to 8 weeks of age. ‡For each animal, two mid-ileal circumferences were analyzed ($n = 2$ animals per group). §Total 30 longitudinally, well-oriented crypt units were counted for mid-ileal sections from hRSpo1-KI and control animals ($n = 2$ animals per group, 4 weeks of age). *$P < 0.05$; **$P < 0.01$ (control versus hRSpo1). ND, not determined.

cytosolic β-catenin (Fig. 2A), and this correlated with an increase in the nuclear localization of β-catenin in the crypts of hRSpo1-KI chimeras (Fig. 2B), indicating functional activation of β-catenin. This phenotype is reminiscent of the increased crypt proliferation and nuclear accumulation of β-catenin by the conditional deletion of adenomatosis polyposis coli (*APC*) in mice (*13*). However, crypt proliferation induced by administration of hRSpo1 protein was completely resolved within 4 days after withdrawal of hRSpo1 (fig. S4), indicating that the action of hRSpo1 protein is transient and reversible, in contrast to the effect of *APC* deletion. Consistent with the activation of β-catenin by hRSpo1, the expression of β-catenin target genes, including *Axin2*, *EphB3*, *CD44*, and *Pla2g2a* (*13*), was increased in hRSpo1-KI chimeras (Fig. 2C) and corresponded to the elevated levels of hRSpo1 mRNA.

To further evaluate the molecular mechanism of RSpo1-induced β-catenin activation, we treated various cell lines with recombinant protein. hRSpo1 induced the stabilization of β-catenin in human embryonic kidney (HEK) 293 cells in a dose-dependent manner, with detectable activity at 10 ng/ml (~300 pM) (Fig. 2D). Similar effects were seen upon treatment with Wnt-3A (Fig. 2F). Peak stabilization of β-catenin occurred ~6 hours after application of hRSpo1 (Fig. 2E), which correlates with the hRSpo1-induced increase in crypt proliferation (Fig. 1C). Simultaneous treatment of HEK 293 cells with hRSpo1 and Wnt3A protein indicated an additive, or mildly synergistic, effect (Fig. 2F). Interestingly, we found that Dickkopf-1 (Dkk-1), a potent Wnt pathway antagonist that interacts with the Wnt coreceptor LRP5/6 (*14*), only partially inhibited hRSpo1-induced β-catenin stabilization, whereas it completely inhibited Wnt3A-mediated β-catenin stabilization in these cells (Fig. 2G). Furthermore, in the mouse fibroblast L cell line, Wnt3A induced β-catenin stabilization, whereas hRSpo1 had no effect (Fig. 2H). These results suggest that

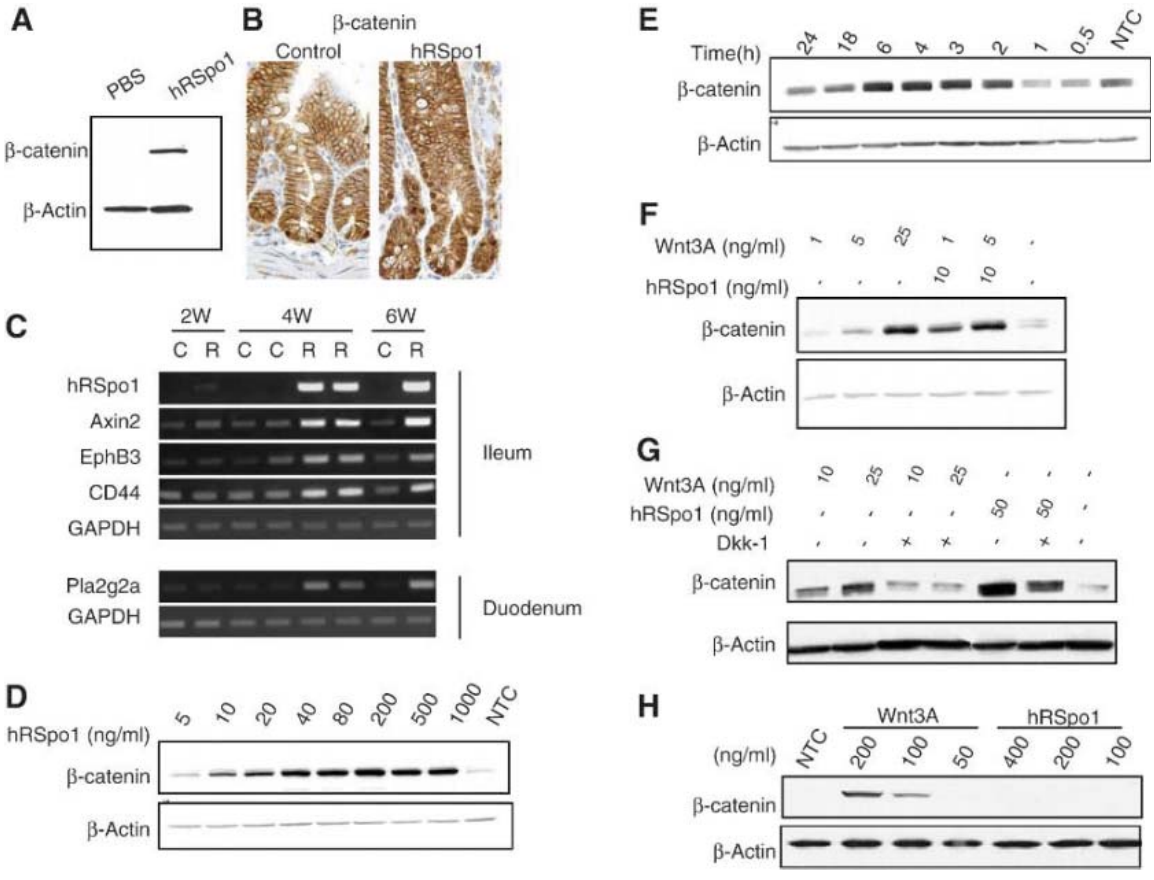

Fig. 2. Modulation of β-catenin signaling by hRSpo1. (**A**) hRSpo1 causes an increase in cytosolic β-catenin in isolated colonic crypts. Colonic crypts were isolated from mice injected with hRSpo1 (100 μg iv) or PBS control 6 hours after injection, and cytosolic fractions were analyzed by Western blotting with antibody to β-catenin. (**B**) hRSpo1 increases nuclear β-catenin in KI mice. β-catenin immunostaining in representative crypts from control (left) and hRSpo1-KI (right) chimeras (4 weeks of age) are shown. Cells with strong nuclear β-catenin staining can be observed in the bottom of the crypts from control chimeras. In hRSpo1-KI chimeras, cells with nuclear β-catenin staining are also found in the upper crypt region corresponding to the extended morphology of the crypt compartment. Magnification, 400x. (**C**) Increased expression of β-catenin target genes in small intestine of hRSpo1-KI chimeras correlates with hRSpo1 expression. Reverse transcription polymerase chain reaction was performed to evaluate time-dependent intestinal expression of transcripts as described (*10*). C, control chimeras; R, hRSpo1-KI chimeras. (**D**) Western analysis of cytosolic β-catenin. HEK 293 cells were treated with recombinant hRSpo1 protein at indicated concentrations for 3 hours, and cytosolic fractions were analyzed by Western blot using antibodies to β-catenin or β-Actin (loading control). NTC, not treated control. (**E**) Time course of β-catenin stabilization. HEK293 cells were treated with 40 ng/ml of hRSpo1, and cytosolic fractions were analyzed. (**F**) hRSpo1 enhances Wnt3A-induced β-catenin stabilization in HEK293 cells. The HEK293 cells were incubated with various concentrations of Wnt3A in the presence or absence of hRSpo1(10 ng/ml). (**G**) Dkk-1 effects on β-catenin stabilization; HEK293 cells were preincubated with 125 ng/ml Dkk-1 for 2 hours, followed by treatment with hRSpo1 or Wnt3A at indicated concentrations. hRSpo1-induced β-catenin stabilization is only slightly inhibited by Dkk-1 protein, whereas Wnt3A-induced β-catenin stabilization is completely inhibited. (**H**) β-catenin stabilization in mouse L cells. Cells were incubated with hRSpo1 or Wnt3A at indicated concentrations for 3 hours, and cytosolic fractions were resolved in SDS–polyacrylamide gel electrophoresis. Whereas Wnt3A causes a dose-dependent increase of cytosolic β-catenin, hRSpo1 fails to stabilize β-catenin in these cells.

hRSpo1 is capable of stabilizing β-catenin by a pathway that does not entirely overlap with the canonical Wnt/β-catenin pathway.

Mucosal damage (mucositis) is frequently encountered as a result of anticancer therapies, and mitogenic agents, including fibroblast growth factor (FGF) family members and glucagon-like peptide-2 (GLP2), have shown efficacy in disease model studies and in clinical applications (*15*–*18*). When tested in mice, FGF-7 and GLP2 also stimulated intestinal crypt proliferation, and isolated colonic crypts from FGF-7- or GLP2-treated mice displayed increased levels of β-catenin (fig. S5, A and B), which suggests that β-catenin is a common mediator of crypt proliferation in vivo. We tested hRSpo1 in a mouse xenograft model that included treatment with the chemotherapeutic agent 5-fluorouracil (5-FU) (*19*, *20*) and evaluated both the extent of mucositis and the effects of hRSpo1 on tumor growth in vivo. The murine colon carcinoma cell line CT26 was inoculated into mice, and tumors were allowed to develop (*20*). hRSpo1 treatment substantially reduced 5-FU-induced diarrhea and weight loss (Fig. 3A), whereas no effect on tumor volume was observed (Fig. 3B). The CT26 line showed an increase in β-catenin levels in response to Wnt3A treatment, indicating that these cells do not have a constitutively activated phenotype, whereas hRspo1 treatment was minimally effective in activating β-catenin (fig. S6). hRSpo1 appeared to exhibit its protective effect by preserving the architecture of both the small intestine and the colon in the presence of 5-FU (Fig. 3C and fig. S7), as well as preventing 5-FU–induced loss of tongue epithelium proliferation (Fig. 3D).

Although the intrinsic function of hRSpo1 in the development and maintenance of normal intestinal epithelium is not yet defined, the expression of hRSpo1 in human intestinal enteroendocrine cells (fig. S8) is consistent with the proposed role of the protein as a crypt cell mitogen and is reminiscent of the expression of the intestinotrophic factor GLP2 (*21*–*23*). Expression was also observed in the epithelium of kidney (renal tubules) and prostate (seminal vesicles), whereas in the adrenal gland and pancreas, expression appeared to be confined to neuroendocrine-type cells (fig. S8).

Ascribing biological function for orphan secreted proteins remains a major challenge in the postgenomic era, and the application of an unbiased in vivo screen, as represented by our transgenic mouse system (*9*), can identify unexpected activities for orphan ligands. Systemic administration of hRSpo1 potently affects proliferation of the intestinal epithelium through activation of β-catenin, and the activation of this pathway by hRSpo1 in vitro would indicate that this effect may result directly from receptor-mediated binding. An epistatic analysis of R-spondin2 has suggested that this protein acts upstream of *dishevelled*, most likely at the receptor level, which suggests that the protein

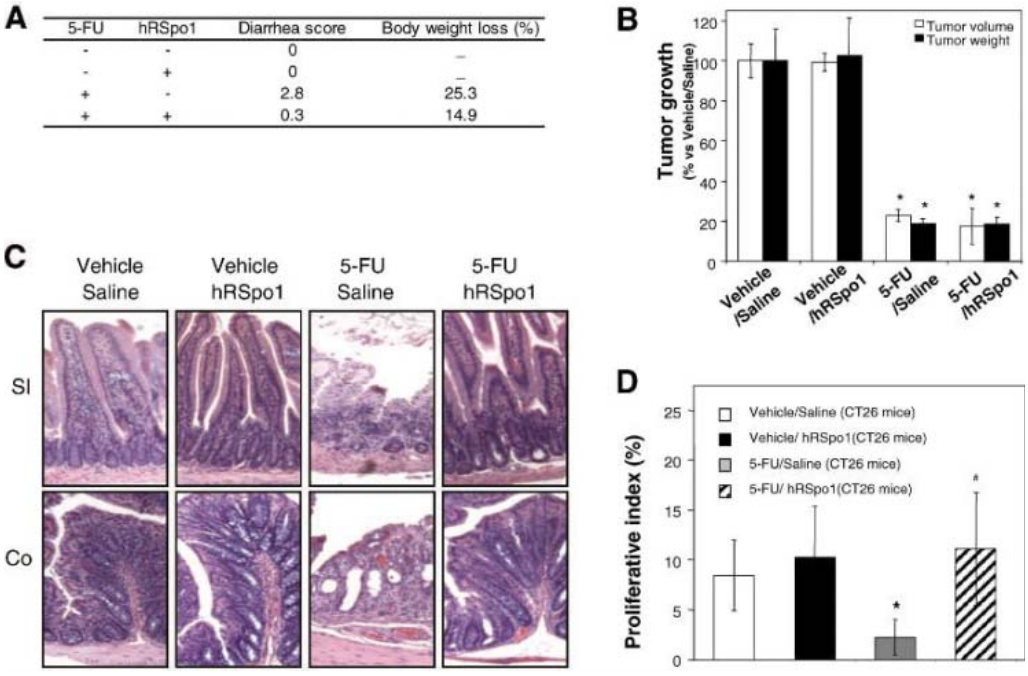

Fig. 3. hRSpo1 reduces 5-FU–induced mucositis in mice without compromising chemotherapy effectiveness. CT26 murine carcinoma cells (1×10^6 cells in Hanks' balanced salt solution buffer) were injected subcutaneously into the left flank of each mouse on Day -5, and solid tumors were allowed to form. Starting on Day 1, 5-FU was injected daily (30 mg per kg of body weight) for 5 days, followed by a 3-day recovery period and sacrifice (Day 8). hRSpo1 was delivered 50 μg/day iv, Day 0 through Day 8. (**A**) Diarrhea score and animal body weight loss were measured on Day 8 of the study ($n = 3$). (**B**) Tumor volume and extirpated tumor weight were measured on Day 8. Error bars, mean ± SD. *, $P < 0.05$ (ANOVA). (**C**) Hematoxylin/eosin stained sections (Day 8) include small intestine (SI) and colon (Co). (**D**) hRSpo1 protects mouse tongue from 5-FU–induced damage. BrdU immunohistochemistry was performed on tongue sections to evaluate proliferation of basal epithelial cells. hRSpo1 prevents 5-FU–induced loss of proliferation in the tongue epithelium. BrdU index was measured in the ventral tongue of mice from each treatment ($n = 3$). Error bars, mean ± SD. *, $P < 0.05$ (ANOVA, 5-FU/saline versus vehicle/saline); #, $P < 0.05$ (ANOVA, 5-FU/saline versus 5-FU/hRSpo1).

works within the context of the canonical Wnt/frizzled pathway (*7*). In contrast, our experiments show that induced accumulation of β-catenin by hRspo1 is relatively insensitive to inhibition by Dkk-1, and we have identified a cell line that responds to Wnt3A but not to hRSpo1. These results suggest that hRSpo1-mediated signaling is not completely dependent on the canonical Wnt/frizzled pathway, although it is possible that hRSpo1 may require a distinct frizzled receptor complex. Clearly it will be very important to identify receptors for R-spondins to fully understand the biology of this important class of activating ligands.

References and Notes

1. D. Pinto, A. Gregorieff, H. Begthel, H. Clevers, *Genes Dev.* **17**, 1709 (2003).
2. E. Batlle *et al.*, *Cell* **111**, 251 (2002).
3. M. van de Wetering *et al.*, *Cell* **111**, 241 (2002).
4. C. Y. Logan, R. Nusse, *Annu. Rev. Cell Dev. Biol.* (2004).
5. M. Bienz, H. Clevers, *Cell* **103**, 311 (2000).
6. R. H. Giles, J. H. van Es, H. Clevers, *Biochim. Biophys. Acta* **1653**, 1 (2003).
7. O. Kazanskaya *et al.*, *Dev. Cell* **7**, 525 (2004).
8. T. Kamata *et al.*, *Biochim. Biophys. Acta* **1676**, 51 (2004).
9. M. Kakitani *et al.*, *Nucleic Acids Res.* **33**, e85 (2005).
10. Materials and methods are available as supporting material on *Science* Online.
11. E. H. Jho *et al.*, *Mol. Cell. Biol.* **22**, 1172 (2002).
12. V. Korinek *et al.*, *Nat. Genet.* **19**, 379 (1998).
13. O. J. Sansom *et al.*, *Genes Dev.* **18**, 1385 (2004).
14. F. Kuhnert *et al.*, *Proc. Natl. Acad. Sci. U.S.A.* **101**, 266 (2004).
15. W. J. Sandborn, S. R. Targan, *Gastroenterology* **122**, 1592 (2002).
16. P. L. Beck *et al.*, *Am. J. Pathol.* **162**, 597 (2003).
17. C. S. Potten *et al.*, *Gut* **36**, 864 (1995).
18. R. M. Housley *et al.*, *J. Clin. Invest.* **94**, 1764 (1994).
19. C. L. Farrell *et al.*, *Cancer Res.* **58**, 933 (1998).
20. R. P. Boushey, B. Yusta, D. J. Drucker, *Cancer Res.* **61**, 687 (2001).
21. M. Bjerknes, H. Cheng, *Proc. Natl. Acad. Sci. U.S.A.* **98**, 12497 (2001).
22. D. G. Munroe *et al.*, *Proc. Natl. Acad. Sci. U.S.A.* **96**, 1569 (1999).
23. N. A. Walsh *et al.*, *Endocrinology* **144**, 4385 (2003).

24. The authors thank M. Yagi, E. Beck, and S. Palencia for supervising animal studies; K. Horikoshi, T. Yoshitome, A. Ueda, M. Kajikawa, Y. Iba, Y. Ozone, Y. Ijima, M. Itoh, S. Seki, A. Aoki, T. Ishihara, C. Lomas, J. Bright, K. Thai, W. Nie, K. Tran, and S. Patel for technical assistance; P. Shinkawa for protein purification; Y. Ide and J. Kawahara for histological analysis; and J. Koumegawa, T. Mikayama, H. Ohashi, K. Ohgami, M. Kakeda, M. Nishikawa, and S. Liu for valuable discussions.

Supporting Online Material

www.sciencemag.org/cgi/content/full/309/5738/1256/DC1
Materials and Methods
Figs. S1 to S8

21 March 2005; accepted 11 July 2005
10.1126/science.1112521

IBC's 12th Annual
International Conference & Exhibition

CHIPS TO HITS® 2005

September 12-15, 2005
Boston Convention and Expo Center
Boston, Massachusetts

Don't forget to
Register Today!
www.chipstohits.com

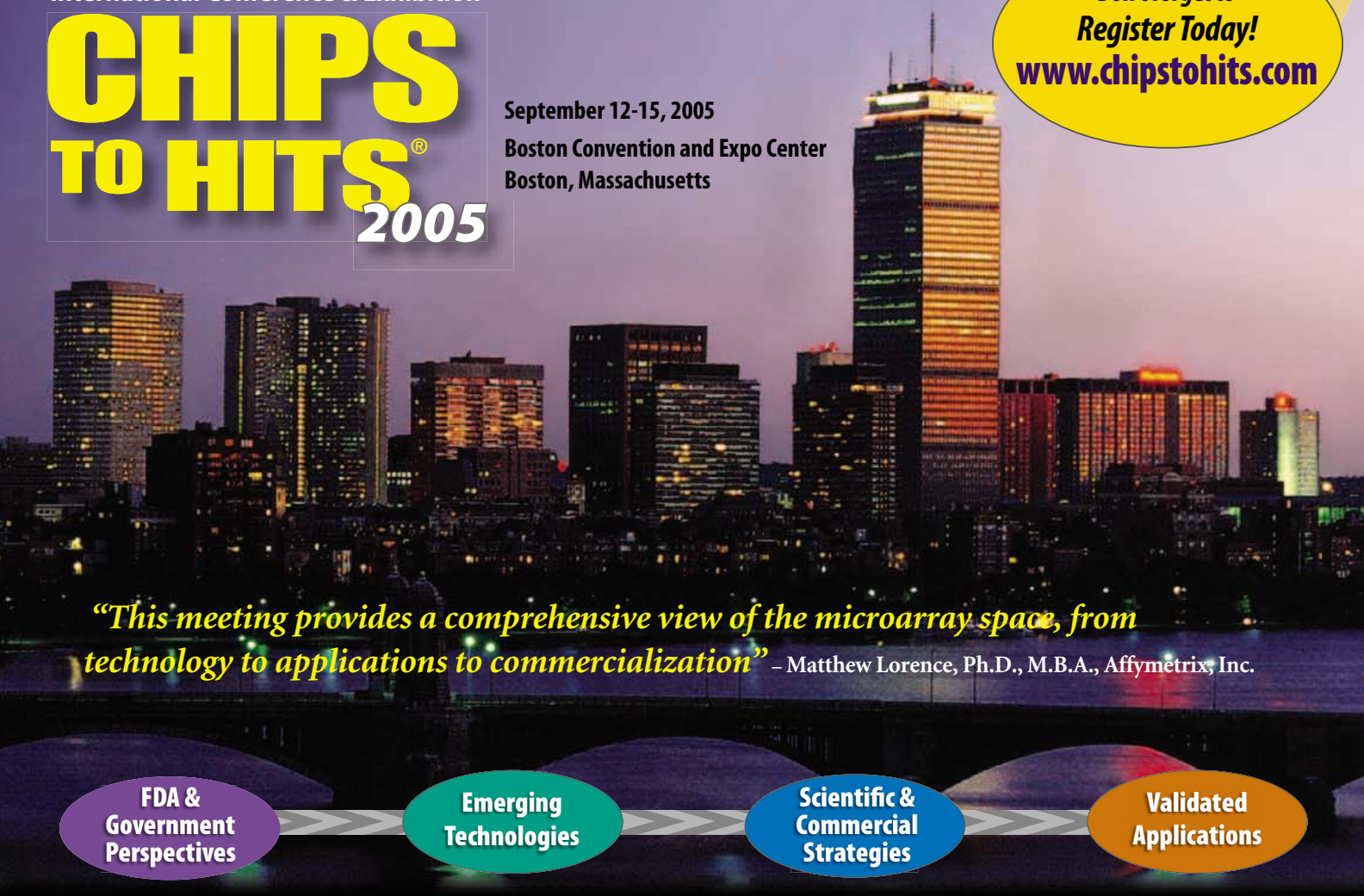

"This meeting provides a comprehensive view of the microarray space, from technology to applications to commercialization" – Matthew Lorence, Ph.D., M.B.A., Affymetrix, Inc.

FDA & Government Perspectives → Emerging Technologies → Scientific & Commercial Strategies → Validated Applications

- **Over 20 Sessions Providing Unbiased, Practical and Novel Information on Developments, Challenges and Opportunities in:**
  - Utilizing new and existing technology to improve drug discovery and development
  - Learning how to succeed from validated applications and case studies
  - Gaining a competitive edge from proven commercial and scientific strategies
- **Unparalleled Formal Networking Opportunities with Over 1,400 Attendees from Industry, Academia and Government**
- **New Product Launches and Scientific Breakthroughs Presented across the Exhibition Hall Featuring over 100 Exhibit Booths and more than 75 Scientific Posters**
- **Free access to two sessions from IBC's co-located Molecular Diagnostics and Personalized Medicine**

Keynote Addresses

Yoshinobu Baba, Ph.D.,
Nagoya University

Klaus Lindpaintner, M.D.,
F. Hoffmann-La Roche AG,
Switzerland

Alan Sachs, Ph.D.,
Merck Research Laboratories
Rosetta Inpharmatic

Michael Snyder, Ph.D.,
Yale University

www.chipstohits.com

Keycode 3050SCI

» advances in:

Biochips

Good Things Come in Small Volumes

After a slow start, microfluidic technologies are now making their mark in the laboratory and even beyond it. Life scientists apply them to tasks as diverse as gene expression and diagnostics. BY PETER GWYNNE AND GARY HEEBNER

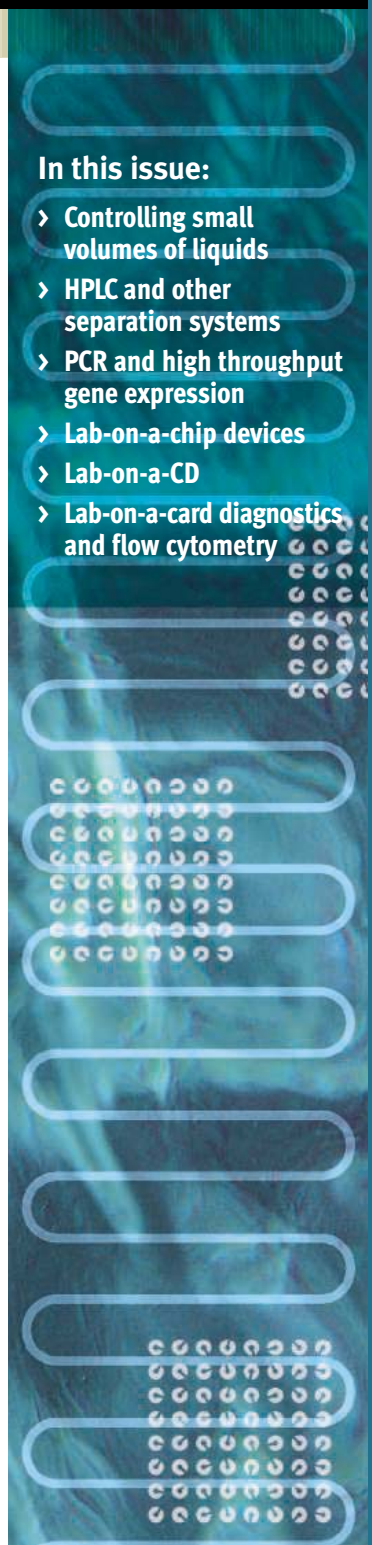

In this issue:

- Controlling small volumes of liquids
- HPLC and other separation systems
- PCR and high throughput gene expression
- Lab-on-a-chip devices
- Lab-on-a-CD
- Lab-on-a-card diagnostics, and flow cytometry

Until recently, microfluidics offered the world of life science more promise than production. The family of technologies gives researchers the opportunity to speed up their experimentation while using smaller amounts of samples and reagents. But scientists have largely ignored those possibilities. "It's still in an early phase," says Per Andersson, senior scientist for microfluidics at Swedish firm **Gyros**. "My impression is that microfluidics is still a trend to follow," agrees Philip Rouhier, international sales and marketing director for **Gilson**. "It could be interesting for big pharmaceutical firms and biotechnology companies to save money. But the fruit is not yet ready to be picked."

Triple Digit Growth

Surekha Vajjhala, director of marketing at **Nanostream**, takes a more optimistic view. "Microfluidics is still in the early stages," she says. "But as the products find more footing in early discovery applications, you'll see more examples of its use." Chris Walworth, marketing manager for gene expression at **Applied Biosystems**, has numerical evidence that researchers have begun to accept the technology. "In some applications we've seen triple digit growth this year," she says. Carsten Buhlmann, product manager for lab-on-a-chip assays and life sciences and chemical analysis at **Agilent Technologies**, agrees. "Some key applications like on-chip electrophoresis with lab-on-a-chip instrumentation can already be considered as established methods in the scientific community, as demonstrated by an exponential growth of reference publications," he says.

Microfluidics clearly offers advantages. "Scientists are most interested in integrating several experiments on a chip or other microfluidic device, thereby speeding up their workflow," Buhlmann explains. "It enables lower consumption of biological samples. Another major impact for customers is the standardization of analysis; it's independent of the user and the chip." Microfluidic methodology is also user-friendly. "It's so simple to use that it can be addictive," says Kathleen Shelton, Applied Biosystems' senior product manager of gene expression.

That compulsion has gradually spread to life scientists in multiple subdisciplines. "Initially microfluidics offered benefits in screening," Vajjhala says. "Next came lead optimization and ADME studies. Now there's more and more traction for these products downstream as miniaturization and other benefits move along the pipeline." Rouhier points out other benefits of the technology. "It has advantages in 'massive research' that deals with many, many samples," he says. "Working on a small volume would be a good advantage for, say, Coca-Cola in its quality control. A company that makes vaccines could test a few nanoliters rather than a few microliters." MORE ›››

Inclusion of companies in this article does not indicate endorsement by either AAAS or Science*, nor is it meant to imply that their products or services are superior to those of other companies.*

This is the third of four special supplements this year on Advances in Biochips. The first two appeared in the 4 March and 6 May issues of Science*; the final one will appear in the 2 September issue.*

» advances in: Biochips

Karen Hedine, president and CEO of **Micronics**, considers the advantages of microfluidics in a different light. "It will always have an important role in drug discovery," she says. "But for us the sweet spot is in diagnostics, where the ability to incorporate reagents on a plastic, disposable, credit card–sized device that can then process complex biological samples in seconds to minutes has immediate impact on patients, doctors, and others with a medical need to know."

Three Basic Technologies

Vendors have developed three basic technologies for applying microfluidics to life science. **Caliper Life Sciences** and its collaborators rely on electro-osmotic flow. Gyros and **Tecan** use centrifugal flow. And technology developed by the **University of Washington** and licensed exclusively by Micronics involves laminar flow diffusion with nonturbulent mixing. The common factor is that the liquids course through channels no larger than several microns in diameter.

Dealing with small volumes of liquids is not new in itself. Such companies as **Eppendorf,** Gilson, and **Matrix Technologies** have provided the means to do so for several years. Initial steps toward miniaturizing laboratory research involved the development of microwell plates and micropipetters. "We have manual pipettes and will soon introduce a motorized new pipette that will allow users to manipulate liquids down to 0.1 to 0.2 microliters," Rouhier says.

Scientists can separate large biological molecules according to properties such as size, shape, charge, hydrophobicity, and affinity for other molecules. They commonly use high performance liquid chromatography (HPLC), which separates molecules under high pressure in a stainless steel column filled with a solid matrix. Now, Agilent, Caliper, **Cepheid**, and Micronics have developed microfluidic separation systems. Some involve integrated processes for sample preparation on the disposable device itself, while others use automated sample preparation in addition to separation capabilities that use electrophoresis or chromatography methods.

Agilent, for example, offers an HPLC-Chip/MS microfluidics-based liquid chromatography/mass spectrometry system based on a reusable microfluidic polymer chip. "Scientists need quality control without sacrificing volume of samples," Buhlmann says. "Ours is a killer application for this."

Nanostream, meanwhile, has introduced micro parallel liquid chromatography (μPLC), which allows chromatographic analysis of a large number of compounds simultaneously. The company's Veloce System enables 24 simultaneous separations and real-time ultraviolet absorbance and fluorescence detection, allowing faster analysis of more samples. This parallel analysis permits scientists to use an increased number of replicates or conditions in their studies while reducing solvent consumption. "Parallel columns allow you to do analytical measurements in areas traditionally underserved by conventional chromatography," Vajjhala explains. "We've repeatedly heard that our batch analysis software is extremely user-friendly."

Bioprocess International Returns

This year's BioProcess International World Conference and Exhibition will take place at the Boston Convention and Exhibition Center from September 19 to September 22. Organized by **IBC Life Sciences**, the event will repeat last year's inaugural conference in offering a four-module format. Visitors can attend segments on production and economics; scaling up from bench to clinic; cell culture and upstream processing; and recovery and purification. Keynote speakers will include Ronald Branning, vice president of commercial quality at Genentech, H. Michael Koplove, vice president of Wyeth BioPharma Operations Network, Michael Glacken, process development head of Millennium Pharmaceuticals, Duncan Low, scientific director of process development at Amgen, and Karl Dane Wittrup, professor of chemical engineering and biological engineering at MIT. The event will run concurrently with the BioProcess International Seminar Series, intended as a rapid introduction to the basic principles of the industry, and IBC's 5th annual Formulation Strategies for Protein Therapeutics meeting, which will target formulation scientists. For compete information, please visit:

» http://www.IBCLifeSciences.com/BPI/US

Influencing PCR

Microfluidics also influences real-time, or quantitative, PCR systems that eliminate the difficulties caused by manual procedures in conventional PCR. The first instrument for real-time PCR was the ABI 7700 (or TaqMan), now offered by Applied Biosystems. Other companies, including **Roche Applied Science**, **Stratagene**, and **Thermo Electron**, offer traditional thermal cyclers and PCR systems.

More recently microfluidics specialists such as Applied Biosystems, **BioTrove**, Cepheid, and **MicroFluidic Systems** have developed lab-on-a-chip devices for PCR. Applied Biosystems bases its 7900HT Fast Real-Time PCR System for high throughput gene expression studies on a microfluidic cartridge design that it developed in partnership with **3M**. The system allows users to load the cartridge or other sample-containing device and run the system without any user involvement. "It's both fast and reliable," says Chris Grimley, line manager for real-time PCR at Applied Biosystems. "It allows larger scale projects to be done in a more cost-effective way than before."

Aclara Biosciences, Agilent, and **MetriGenix** are among vendors that have developed lab-on-a-chip devices for genomic and proteomic research. "The automation, integration, and speed are the main advantages of those devices," says Agilent's Buhlmann. "They also yield a high level of reproducibility in their results. Standardization is very important, especially in drug development."

Agilent's automated 2100 Bioanalyzer System, based on Caliper's LabChip devices, enables analysis of proteins, nucleic acids, and even whole cells. The microfluidic device includes a network of microchannels

that contain a non-cross-linked polymer network for molecular sieving. The Bioanalyzer's optics monitor the channels in which the separations are carried out, and the system uses laser-induced fluorescence to detect and measure the DNA fragments in real time.

Agilent's 5100 Automated Lab-on-a-Chip Platform, introduced last November, allows high throughput gel electrophoresis of DNA and proteins, permitting unattended analysis of samples in up to 12 microwell plates with 96- or 384-well capacity. "It is designed for high throughput customers who need to size and quantitate thousands of biological molecules each day," Buhlmann says.

The CD Alternative

As an alternative to the lab-on-a-chip or lab-on-a-card, several companies have chosen a compact disk for their microfluidics development platform. The CD format uses centrifugal force to move samples from one chamber to another. The advantage: "Gravity never fails," says Gyros's Andersson. "You can use much simpler instruments when you can do your work on the disks. And we get parallel processing, which gets us higher throughput."

Gyros's CD microlaboratory, the Gyrolab MALDI IMAC, permits researchers to identify proteins, especially those with low abundance. It offers a unique solution for detecting phosphorylated peptides with MALDI mass spectrometry. "It is fully automated and faster than manual methods," Andersson says. "The sensitivity comes from the miniature column and the miniaturized target area." A Gyros workstation controls each run through a specific software method, transferring samples and reagents into the microlaboratory and spinning the CD to drive up to 96 samples in parallel through each preparation step.

Another system based on a compact disc, Tecan's LabCD, combines microscale fluid paths, reaction chambers, and passive valves on a disposable compact disc that operates on a single user-friendly platform. Scientists can use the LabCD for several assays, including cytochrome P450 inhibition to measure drug-drug interactions and serum protein-binding assays for measuring the binding characteristics of drug compounds at different serum protein-binding sites.

Besides impacting life science research, microfluidics plays an increasingly prominent role in healthcare. "Japanese firm Fujirebio is interested in our system as a technology for the point-of-care market in terms of diagnostics outside the core facility lab," Andersson says.

Point-of-Use Systems

In fact several suppliers are developing point-of-use systems to allow physicians to conduct diagnostic tests in small offices or in the field with simpler technologies and more dependable formats. Systems include handheld units with integrated laboratory tests on a card or a CD. These platforms will provide rapid, cost-effective methods of diagnostic testing for infectious diseases, testing nucleic acids, analyzing blood type, and checking for cancer. Micronics is among the firms developing diagnostic test systems.

Micronics was recently named the lab card developer for a consortium awarded the first Grand Challenge in Global Health for a point-of-care diagnostic platform based on microfluidics. The Grand Challenges, funded in large part by the Bill and Melinda Gates Foundation, the Wellcome Trust, and the Canadian Institutes of Health Research, aim to develop a portable instrument and low-cost disposable cards for use in analyzing disease in the field.

Early this year, Micronics granted a nonexclusive license for its microfluidics-based flow cytometry to **Honeywell International**. Micronics' microcytometry technology has been compared to commercial "macro sized" instruments in tests that resulted in significantly reduced turnaround time and volume requirements for reagents and samples, and a much tighter coefficient of variation. "This is in keeping with our method of card and instrument design," Hedine says, "in that the lab card can perform more of the functions that typically required numerous user steps."

Despite its slow start, microfluidic technologies will plainly continue to advance in coming years. In doing so, they will add to our body of knowledge about laboratory automation and miniaturization, and will produce more practical solutions for applications inside and beyond the lab.

Peter Gwynne (pgwynne767@aol.com) is a freelance science writer based on Cape Cod, Massachusetts, U.S.A. Gary Heebner (gheebner@cell-associates.com) is a marketing consultant with Cell Associates in St. Louis, Missouri, U.S.A.

Biological Pathway Analysis Software

PathwayStudio Central is client-server software for visualization and analysis of biological pathways and gene regulation networks for biomedical research labs, biotechnology companies, and pharmaceutical companies. PathwayStudio Central builds pathways from microarray data, identifies biomarkers, and models drug responses. The software comes with the ResNet database of more than 500,000 functional relationships and the MedScan tool for automatic extraction of information from the scientific literature. MedScan leverages hand-crafted dictionaries of protein and chemical names, and precise text parsing and pattern matching algorithms specifically developed for biological text analysis. PathwayStudio Central helps scientists keep current with the literature by using the embedded MedScan information extraction tool that can "read" scientific text and extract functional relationships.

Ariadne Genomics For information 847-644-1557 www.ariadnegenomics.com

Protein Stain

Imperial Protein Stain is a ready-to-use Coomassie R-250 dye for protein staining in polyacrylamide gels. This sensitive (≤ 3 ng) dye produces an intense purple stain that photographs well. The reagent stains only protein and allows bands to be viewed directly in the gel during the staining process. For fast results, a five-min stain combined with a 15-min wash detects 6 ng of protein bands. Greater levels of sensitivity and a clear background can be achieved by extending staining and washing times.

Pierce For information 800-874-3723 www.piercenet.com

Biomarker Research

The BIOiTRAQ Systems are mass spectrometry-based solutions for key phases of biomarker research. They can accomplish discovery, identification, and quantitation within a single experiment, with systems available suited to varying research needs and budgets. They incorporate iTRAQ and ICAT reagents; sensitive, versatile instrument platforms; and straightforward software to maximize productivity.

Applied Biosystems
For information 800-327-3002
www.appliedbiosystems.com

Microarray Scanner

The GeneChip Scanner (GCS) 3000 7G supports the latest high-density GeneChip microarrays for tiling, all-exon, and single nucleotide polymorphism genotyping research. It offers the ability to scan smaller features, ranging in size from 2.5 μm to 0.51 μm. The GCS 3000 7G is designed to provide peak scanning performance for all applications, including RNA expression and DNA analysis. The instrument combines advanced design improvements with high-resolution scanning to dramatically improve efficiency in gene expression and DNA analysis applications.

Affymetrix For information 408-731-5791 www.affymetrix.com

Single-Cell Analysis

The Guava EasyCyte system has a new side-scatter option that makes single-cell analysis with accurate cell enumeration more versatile and easier. The side-scatter feature allows researchers to analyze whole blood for different types of white blood cells without having to stain or fix the cells. The granular structures in the cytoplasm of granulocytes cause more scattering of incident light than the more uniform cytoplasm of lymphocytes. This makes it easier to perform a three-part differential on whole blood: assessing the percentage and number of granulocytes, monocytes, and lymphocytes in a given sample. The EasyCyte is a five-parameter system that is flexible, affordable, and compact. It requires only a few microliters, so it saves precious cells, reagents, and compounds. The system enables easy, fast measurements of cell counting/viability, green-fluorescent protein expression and viability, apoptosis, cell cycle analysis, antigen detection, cell tracking, and more.

Guava Technologies For information 510-576-1427 www.guavatechnologies.com

Field Emission Scanning Electron Microscopes

The Supra 40 Series of ultra high-resolution field emission scanning electron microscopes (FESEM) replace the Supra 35 and Supra 50 FESEM models. The new line features a new nano-tool based on the latest version of the Zeiss Gemini FESEM column, which delivers nanoscale high resolution imaging over the entire voltage range without the need for adjustments. It has been developed as a versatile workhorse capable of delivering high-quality imaging solutions for the many demanding applications in the field of nanotechnology. The series includes three models: Supra 40 for standard ultra-high resolution applications; Supra 40VP variable pressure for real topography imaging of nonconducting specimens, and the Supra 40WDS nano-analytical tool with a dedicated specimen chamber to accommodate both fully focusing wavelength dispersive and energy dispersive spectrometers. The instruments offer a 20% increase in resolution for both high and low voltage applications.

Zeiss For information 800-356-1090 www.smt.zeiss.com

Literature

Alexis Biochemicals' 2005 General Catalog features innovative life science reagents in product groups including apoptosis; cell cycle and DNA transactions; signal transduction, immunology, and cancer research; neurochemicals; and nitric acid pathway and oxidative stress. It includes product details, technical information, and literature references for a broad range of research grade biochemicals and antibodies, including more than 400 new products.

Alexis Biochemicals For information 800-900-0065 www.alexis-biochemicals.com

For more information visit GetInfo, *Science*'s new online product index at *http://science.labvelocity.com*

From the pages of GetInfo, you can:
- Quickly find and request free information on products and services found in the pages of *Science*.
- Ask vendors to contact you with more information.
- Link directly to vendors' Web sites.

Newly offered instrumentation, apparatus, and laboratory materials of interest to researchers in all disciplines in academic, industrial, and government organizations are featured in this space. Emphasis is given to purpose, chief characteristics, and availability of products and materials. Endorsement by *Science* or AAAS of any products or materials mentioned is not implied. Additional information may be obtained from the manufacturer or supplier by visiting www.science.labvelocity.com on the Web, where you can request that the information be sent to you by e-mail, fax, mail, or telephone.

ScienceCareers.org

Classified Advertising

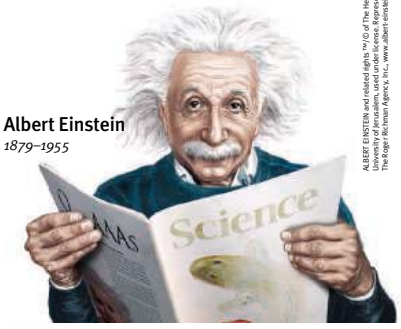

Albert Einstein
1879–1955

For full advertising details, go to **www.sciencecareers.org** and click on **How to Advertise,** or call one of our representatives.

United States & Canada

E-mail: advertise@sciencecareers.org
Fax: 202-289-6742

JILL DOWNING
(CT, DE, DC, FL, GA, MD, ME, MA, NH, NJ, NY, NC, PA, RI, SC, VT, VA)
Phone: 631-580-2445

KRISTINE VON ZEDLITZ
(AK, AZ, CA, CO, HI, ID, IA, KS, MT, NE, NV, NM, ND, OR, SD, TX, UT, WA, WY)
Phone: 415-956-2531

KATHLEEN CLARK
Employment: AR, IL, LA, MN, MO, OK, WI, Canada; Graduate Programs; Meetings & Announcements (U.S., Canada, Caribbean, Central and South America)
Phone: 510-271-8349

EMNET TESFAYE
(Display Ads: AL, IN, KY, MI, MS, OH, TN, WV; Line Ads)
Phone: 202-326-6740

BETH DWYER
(Internet Sales Manager)
Phone: 202-326-6534

Europe & International

E-mail: ads@science-int.co.uk
Fax: +44 (0) 1223-326-532

TRACY HOLMES
Phone: +44 (0) 1223-326-525

HELEN MORONEY
Phone: +44 (0) 1223-326-528

CHRISTINA HARRISON
Phone: +44 (0) 1223-326-510

SVITLANA BARNES
Phone: +44 (0) 1223-326-527

JASON HANNAFORD
Phone: +81 (0) 52-789-1860

To subscribe to *Science*:
In U.S./Canada call 202-326-6417 or 1-800-731-4939
In the rest of the world call +44 (0) 1223-326-515

Science makes every effort to screen its ads for offensive and/or discriminatory language in accordance with U.S. and non-U.S. law. Since we are an international journal, you may see ads from non-U.S. countries that request applications from specific demographic groups. Since U.S. law does not apply to other countries we try to accommodate recruiting practices of other countries. However, we encourage our readers to alert us to any ads that they feel are discriminatory or offensive.

POSITIONS OPEN

FACULTY POSITIONS IN BIOPSYCHOLOGY
The University of Chicago

The University of Chicago is seeking to fill **SENIOR** or **JUNIOR POSITIONS** in biopsychology. Our primary goal is to understand behavior and the mind in relation to biological mechanisms. We construe biological mechanisms to include the interactions among the nervous, endocrine, and immune systems, and we are particularly interested in those who study effects of mental and behavioral processes on biological mechanisms. The Institute for Mind and Biology, housed in a new biopsychological sciences research facility, is dedicated to behavioral studies in animals and humans, with fully accredited animal care facilities and communal research equipment.

Ideal candidates are those whose research interests bridge to other strengths in the Department of Psychology, and are enthusiastic about engaging in collaborative transdisciplinary research within a highly interactive research community both inside and outside the Department of Psychology. We invite applications from individuals who primarily study animals and employ an integrative approach incorporating multiple biological mechanisms (e.g., genetic, molecular, neurochemical, hormonal, immune, electrophysiological) that complement their behavioral research. Of particular interest is research in the developmental, emotional, social, and cognitive aspects of psychological processes.

Evaluation of applicants will begin November 1, 2005. Applicants should submit curriculum vitae, a conceptual summary of research, a statement of teaching interests/philosophy, representative publications, and three letters of reference. Please send all materials to: **Biopsychology Search Committee, 5730 Woodlawn Avenue, Room 101, Chicago, IL 60637.** *The University of Chicago is an Affirmative Action/Equal Opportunity Employer.*

FACULTY POSITIONS
Columbia University Medical Center

The Department of Pathology seeks highly qualified individuals for faculty positions in surgical pathology, anatomic pathology, and research. Appointments can be at the **ASSISTANT, ASSOCIATE,** or **FULL PROFESSOR** level, depending on experience and qualifications. Clinical positions require board certification and a NYS license prior to the start of service. Research positions require record of publication in leading journals and a statement of research directions.

Applicants should submit curriculum vitae and three letters of reference to: **C. Kitzinger, Department of Pathology, Columbia University Medical Center; 630 West 168th Street, New York, NY 10032.** *Columbia University takes Affirmative Action toward Equal Employment Opportunity. Women and minorities are encouraged to apply.*

UNIVERSITY OF ROCHESTER

The Department of Chemistry invites applications for a position at the **ASSISTANT PROFESSOR** level in all areas of experimental chemistry, with special emphasis in biological, physical, and materials chemistry. Exceptional candidates at the senior level may also be considered. Candidates are expected to establish an outstanding program of original research and to be effective teachers at the graduate and undergraduate levels. Applicants should send curriculum vitae and statement of research plans (in PDF or Microsoft Word format) to: **Ms. Karen Dean** at **e-mail: dean@chem.rochester.edu.** Applicants should also arrange for three letters of recommendation to be sent. Review of applications will begin on October 14, 2005. *The University of Rochester is an Equal Opportunity Employer. Women and minority candidates are strongly encouraged to apply.*

POSITIONS OPEN

TEMPORARY FACULTY POSITION
Dartmouth College

Applications are invited for a temporary faculty position in the Dartmouth College Department of Chemistry. We seek an experienced teacher for a spring term (March 28, 2006, through June 6, 2006) physical chemistry course that centers on quantum chemistry and molecular spectroscopy. The course has an associated laboratory as well and is anticipated to have fewer than ten students, all of whom will be highly motivated junior chemistry majors. Preference will be given to individuals who have an established record of outstanding teaching in this area. Applicants should submit curriculum vitae, a statement of their teaching background, and the names and addresses of three references who are willing to send letters on their behalf. All inquiries and applications will be treated confidentially. Application materials should be sent to: **Chair, Physical Chemistry Teaching Search Committee, Department of Chemistry, 6128 Burke Laboratory, Dartmouth College, Hanover, NH 03755-3564.** The Committee will begin to consider completed applications as they are received and will continue to review applications until the position is filled. *With an even distribution of male and female students and over a quarter of the undergraduate student population members of minority groups, Dartmouth is committed to diversity and encourages applications from women and minorities. Dartmouth College is an Equal Opportunity/Affirmative Action Employer.*

JUNIOR FACULTY POSITION, PROSTATE CANCER METASTASIS RESEARCH
University of Michigan Medical School

We are seeking a colleague to join us in a tenure-track position as an **ASSISTANT PROFESSOR** of medicine in the Division of Hematology/Oncology. The successful applicant will join a core group of research investigators from multiple disciplines studying mechanisms underlying prostate cancer metastasis/bone microenvironment interactions. We are seeking an investigator with expertise in the area of signal transduction and prostate cancer metastasis. Applicants are expected to have a Ph.D. (or equivalent) and at least two years of postdoctoral experience in the field of prostate cancer metastasis. Applicants should have a demonstrated ability to communicate and have a record of publications in the field. A history of funding at the postdoctoral level is preferred. To be considered, please submit curriculum vitae, publication list, and a statement of research accomplishments. Completed applications must be received by September 1, 2005. Applications should be submitted to: **Kenneth J. Pienta, M.D., 7308 CCGC, 1500 E. Medical Center Drive, Ann Arbor, MI 48109.** *The University of Michigan is an Equal Opportunity/Affirmative Action Employer.*

In response to the University of Minnesota's Presidential Initiative on Biocatalysis, the Department of Biochemistry, Molecular Biology, and Biophysics and the Biotechnology Institute seek to hire an outstanding faculty member studying fundamental biochemical aspects of biotechnology, biocatalysis, or bioenergy. The position is expected to be at the **TENURE-TRACK ASSISTANT PROFESSOR** level, but outstanding candidates at any level will be considered. Review of applications will begin November 1, 2005, and continue until the position is filled. All candidates must have a Ph.D. degree and a strong publication record. Postdoctoral or equivalent experience is desired. To apply please send curriculum vitae, statements of research and teaching interests, and arrange to have sent three letters of recommendation that consider both teaching and research potential to: **BMBB Search Committee Chair, c/o Kristi Iskierka, Department of Biochemistry, Molecular Biology and Biophysics, 1479 Gortner Avenue, Saint Paul, MN 55108, U.S.A.** An application sent by **e-mail: bmbb-search@cbs.umn.edu** should be followed by a hard copy sent to the address above. *The University of Minnesota is an Equal Opportunity Educator and Employer.*

Positions @ NIH
THE NATIONAL INSTITUTES OF HEALTH

SCIENTIFIC REVIEW ADMINISTRATOR
National Cancer Institute
Division of Extramural Activities

The National Cancer Institute (NCI), the largest research component of the National Institutes of Health (NIH), Department of Health and Human Services (DHHS), is seeking one or more exceptional scientists to serve as Scientific Review Administrators in the Office of Review, Referral and Program Coordination, Division of Extramural Activities. The Scientific Review Administrator(s) selected will organize and manage the comprehensive scientific and technical merit review of applications for multidisciplinary research programs through interaction with established scientists in a variety of fields. Scientific Review Administrators are responsible for assuring the fairness and consistency of the scientific peer review process, and for providing technical guidance on peer review policies and procedures and review criteria to applicants, reviewers, and Institute staff.

Qualifications: Individuals with a Ph.D., M.D., or equivalent degree, and research training and experience in disciplines relevant to basic or translational research in cancer pathogenesis, diagnosis, treatment, prevention or control are encouraged to apply. Individuals with experience in the application of nanotechnology approaches to cancer research are especially invited to apply. Strong oral and written communication skills and knowledge of the Federal grant application process are required. Applicants must be U.S. citizens.

Salary: The current salary range is $74,782 - $114,882. Position requirements and detailed application procedures are provided in vacancy announcement **NCI-05-86536**, which can be obtained by accessing **http://www.usajobs.opm.gov**

How to Apply: Submit a Standard Form 171, Application for Federal Employment or OF-612, Optional Application for Federal Employment; current curriculum vitae/bibliography, or other format that documents your qualifications to: **Mr. Eugene McDougal, National Institutes of Health, NCI Human Resources Office, 6120 Executive Boulevard, Executive Plaza South/room 519, Rockville, MD 20852-7211.** You may also apply online through **http://www.usajobs.opm.gov**. All applications must be postmarked by **September 9, 2005.** For additional information, contact **Mr. Eugene McDougal at (301) 402-2812.**

Proteomics Manager

The Office of the Director of the National Cancer Institute (NCI), National Institutes of Health (NIH), Department of Health and Human Services (DHHS), invites applications for a Proteomics Manager (GS-401-14) in the Center for Bioinformatics (NCICB), located in Rockville, Maryland. NCICB provides biomedical informatics support and integration capabilities to the cancer research community.

The incumbent leads the coordination and execution of large scale biomedical informatics projects in proteomics and structural biology, serves as staff specialist for contracts in the area of informatics for proteomics, and advises NCICB management on the status of proteomics standards and technologies and their implication for current and future NCICB projects. The individual selected for this position must have knowledge of current methods in proteomics, experience in managing the development of software projects, and excellent communication skills.

Salary is at the GS-14 level ($88,369 -$114,883) and a full Civil Service package of benefits (including retirement, health, life and long-term care insurance, Thrift Savings Plan participation, etc.) is available.

The NCI vacancy announcement for this position contains complete application procedures and lists all mandatory information which you must submit with your application. To obtain the vacancy announcement for this position, see announcement number **NCI-05-90464** at **http://usajobs.opm.gov/**. Applications must be received by **September 9, 2005.**

Tenured Investigator Position
Molecular Pathogenesis and Epidemiology of Influenza Virus

The Respiratory Viruses Section of the Laboratory of Infectious Diseases seeks an M.D. scientist to establish a research program on Molecular Pathogenesis and Epidemiology of influenza virus. This is a broad mandate that will include studies of molecular archeology of the influenza viruses, pathogenesis of influenza A virus for diverse host species, and viral evolution and adaptation in human and animal hosts. The person will interact with and likely provide some guidance to the recently established influenza genomics project. The scientist will translate epidemiological observations and insights into the study of the molecular biology of the virus using reverse genetic systems to investigate molecular determinants of host range and of pathogenesis. This work will be multi-dimensional involving molecular epidemiological studies, analysis of viral genomes, molecular virology, and pathogenesis in a variety of animals. Trials of influenza viruses in human volunteers and epidemiological studies in humans will be possible.

The scientist will head a research team group that will consist of up to eight members including professional and technical staff. The group will be located in Building 33, a building under construction that contains BSL2 and BSL3 laboratory and animal space. The BSL2 research laboratory space will be located adjacent to space occupied by a Principal Investigator engaged in pandemic influenza virus research, and it will therefore be possible for both groups to collaborate and to share equipment. Space, technical and postdoctoral Fellow support, supply budget, and salary are committed.

To be considered for this position, you will need to submit curriculum vitae, bibliography, a detailed statement of research interests, and selected publications preferably via email to Felicia Braunstein at braunsteinf@niaid.nih.gov. In addition, three letters of recommendation must be sent to **Alan Sher, Ph.D., Chairperson, NIAID Search Committee, c/o Ms. Felicia Braunstein, DIR Committee Manager, 10 Center Drive MSC 1349, Building 10, Rm. 4A-30, Bethesda, Maryland 20892-1349**. Completed applications MUST be received by **September 16, 2005**. For additional information on this position, and for instructions on submitting your application, please see our website at: **www.niaid.nih.gov.**

WWW.NIH.GOV

ASSOCIATE DIRECTOR FOR RESEARCH INFORMATICS AND INFORMATION TECHNOLOGY

Immediate Office of the Director
National Heart, Lung and Blood Institute

The National Heart, Lung, and Blood Institute (NHLBI) is seeking a strategic-minded scientist with expertise in research informatics and information technology who will bring significant experience in a research environment to operate in an intellectually challenging Federal biomedical research institution engaged in a national research program to understand, treat, and prevent heart, lung and blood diseases and sleep disorders throughout the world.

This position offers a unique and challenging opportunity for the right individual to work directly with the NHLBI Director to develop a program in research informatics, incorporating information technology. Applicants should possess an advanced science degree and research experience related to bioinformatics or research informatics. Specifically, the successful candidate should have experience in providing bioinformatics support in the areas of biology, molecular biology and genetics, including the terminology of basic, translational, and clinical research. In addition, applicants should have sufficient education and experience that will ensure success in managing a professional and technical staff engaged in providing complex and computationally intense modeling and analytics in the areas of bioinformatics, genomics, proteomics and imaging. It is highly desirable for the successful applicant to also have extensive experience in information technology management, encompassing strategic planning, complex organizational structures, technical project management and process transformation. The successful candidate will serve as the Chief Information Officer for the NHLBI, and will oversee NHLBI science support and administration of NHLBI science in areas such as enterprise operations systems, data warehouse and management reporting and information security and the day to day operations of staff providing IT infrastructure development and support. Strong leadership qualities, negotiation skills and exceptional interpersonal skills are imperative.

Application Process: Salary is commensurate with experience and a full package of Civil Service benefits is available including retirement, health and life insurance, long term care insurance, leave and savings plan (401K equivalent). CV, bibliography and two letters of recommendation must be received by **October 15, 2005**. **Application package should be sent to the National Institutes of Health, attn: Mr. Barry Rubinstein, Building 31, Room 5A-28, 31 Center Drive, MSC 2490, Bethesda, MD 20892-2490. For further information, please contact Mr. Rubinstein by email: Rubinstb@nhlbi.nih.gov or telephone (301) 496-2411**. All information provided by applicants will remain confidential and will only be reviewed by authorized officials of the NHLBI.

The NIH encourages the application and nomination of qualified women, minorities, and individuals with disabilities.

Postdoctoral Position
HIV Replication and APOBEC3G

National Institute of Child Health and Human Development

A postdoctoral position is available in the Section on Viral Gene Regulation, Laboratory of Molecular Genetics, NICHD, NIH, for molecular studies on the replication of HIV. Recently, APOBEC3G, a cellular cytidine deaminase, has been identified as a potent inhibitor of HIV-1 infectivity in the absence of the viral Vif protein. We have expressed enzymatically active APOBEC3G in a baculovirus system and, for the first time, have performed detailed molecular analysis of the purified protein, using a combined biochemical, genetic, and cell assay approach. Future studies will include an investigation of the mechanism of APOBEC3G inhibition of specific steps in HIV-1 reverse transcription and its relation to antiviral activity. Further details about our research program can be found at **http://jlevinlab.nichd.nih.gov/**

Candidates must possess a Ph.D. degree and have less than 5 years postdoctoral experience. A strong background in molecular biology and virology is required. Interested applicants should submit a cover letter, curriculum vitae, bibliography, and contact information for three references to:

Dr. Judith G. Levin
Fax: (301) 496-0243
Email: levinju@mail.nih.gov

NIMH
National Institute of Mental Health

Postdoctoral Position in Psychology or Psychiatry
Mood and Anxiety Disorders Research Program

The Section of Developmental Genetic Epidemiology in the Mood and Anxiety Disorders Program at the National Institute of Mental Health is recruiting a postdoctoral fellow in experimental psychology, biological psychology/psychiatry, clinical psychology, neuro-psychology/psychiatry, or related field. The focus of the section is genetic epidemiologic and community studies, particularly family and high-risk studies of the correlates and risk factors for the development of mood and anxiety disorders. The candidate must have a Ph.D. in psychology or an M.D. with psychiatry residency, and some research experience is preferred. Preference will be given to candidates with a background and interest in the fundamentals of stress, the autonomic nervous system, and/or reproductive endocrinology/hormones. Applicants should send a curriculum vitae, statement of research interests, and three letters of reference to **Dr. Kathleen R. Merikangas, Chair Search Committee, National Institute of Mental Health, 35 Convent Drive, Bldg 35 Room 1A201, MSC-2370, Bethesda, MD 20892-3720.**

United States
National Institute of Diabetes & Digestive & Kidney Diseases
of the National Institutes of Health

Research Opportunity at the NIH, DHHS
DIRECTOR, OBESITY CLINICAL RESEARCH CENTER AND CHIEF, DIABETES BRANCH, NIDDK

The Intramural Research Program (IRP) of NIDDK invites applications for the combined position of Chief of the Diabetes Branch and Director of a newly established, NIH-wide initiative in patient-oriented research in obesity ("Obesity Clinical Research Center" – OCRC). The Diabetes Branch, NIDDK conducts basic, translational and clinical research in the areas of diabetes mellitus and obesity. The Chief is responsible for all activities of the Branch, in particular, for integrating the research programs of the several senior investigators and the career development of junior investigators. The goal of the OCRC, which will involve researchers from all Institutes and Centers within the NIH IRP, is to generate knowledge of the pathophysiology, prevention and treatment of obesity and its multisystem co-morbidities, especially type 2 diabetes mellitus. The approach is: 1) to create a center in which to conduct state-of-the-art, patient-oriented obesity research, including metabolic analysis and imaging capabilities, that would support IRP scientists and serve as a magnet facility to foster collaborations with extramural researchers; and 2) to foster multidisciplinary approaches to obesity research, including metabolism, endocrinology, nutrition, gastroenterology, hepatology, imaging, genetics and behavioral sciences.

Priority will be given to applicants at the Professor or Associate Professor level in clinical departments of traditional academic medical centers, or in equivalent positions. The applicant must have a proven record of accomplishments, including evidence of significant, competitively obtained funding for extramural investigators. The appointment will be as a tenured Principal Investigator within NIDDK. The successful candidate will be expected to coordinate the multidisciplinary research proposed for the OCRC and the Diabetes Branch. The position offers unparalleled opportunity to lead a state of the art program in diabetes/obesity research. Salary and benefits are commensurate with the experience of the applicant.

The Diabetes Branch laboratories are in the Warren G. Magnuson Clinical Center and the OCRC Patient Care Unit is a self-contained, metabolic unit located in the new Mark O. Hatfield Clinical Research Center, which are contiguous on the main intramural campus of the NIH in Bethesda, Maryland, a suburb of Washington, D.C.

Interested applicants should send a Curriculum Vitae and list of publications, copies of three major publications, a summary of research accomplishments, a plan for future research and three letters of recommendation to **Dr. James E. Balow, Chair, Search Committee, c/o Ms. Giulia Verzariu, Office of the Scientific Director, NIDDK, Building 10, Room 9N222, NIH, Bethesda, MD 20892.**

Closing Date: October 1, 2005

Department of Health and Human Services
National Institutes of Health
National Institute of Diabetes and Digestive and Kidney Diseases
Equal Opportunity Employers

TRANSFORM
pharmaceuticals

TransForm Your Career!

TransForm Pharmaceuticals is building a culture of excellence and innovation leading to the development of important new medicines for the patients we serve. We work hard but, most importantly, have fun accomplishing what's never been done before. New ideas and new ways of thinking are not only encouraged—they're required. The integration of diverse backgrounds, training, and thinking brings strength to our organization and our products.

We currently have openings in the following areas:

Biology • Chemistry • Chemical Engineering • Computer Science • Material Science

TransForm Pharmaceuticals, Inc., located in Lexington, Massachusetts, is a member of the Johnson & Johnson Family of Companies. We are revolutionizing the pharmaceutical industry by optimizing drug form and formulation to increase the clinical and commercial value of products. We are using scientific expertise and novel platform technology to develop new and improved pharmaceuticals, convergent products, and vaccines to fuel our proprietary product portfolio.

To learn more about our company and available positions, please visit

www.TransFormPharma.com

TransForm Pharmaceuticals has been recognized among the "Best Places to Work in Industry" by The Scientist for the third consecutive year.

TransForm Pharmaceuticals, Inc. is a member of the Johnson & Johnson Family of Companies.

Johnson & Johnson
Family of Companies

small-company environment
big-company impact®

Bauer Center for Genomics Research

Bauer Center for Genomics Research
Harvard University
Fellow Positions in Genomics or Systems Biology

Harvard University's Bauer Center for Genomics Research seeks outstanding applicants to become Fellows in the center.

The Bauer Center is an intensively collaborative, interdisciplinary center, where scientists from a wide variety of backgrounds study cellular pathways and networks, with the goal of finding general principles underlying the structure, behavior and evolution of cells and organisms. The Bauer Fellows are independent researchers who receive funding for a group of up to three people. Fellows are appointed for a three-year term, with the expectation that it will be extended to five years.

For more information about the Bauer Center and the Fellows program, visit our website at **http://cgr.harvard.edu**. For application procedures, see **http://cgr.harvard.edu/fellows/fellows_program.html**.

Applications are welcome at any time, but only those received by **15 October 2005** are guaranteed full consideration.

Harvard University is an Affirmative Action, Equal Opportunity Employer.

Bauer Center for Genomics Research

Bauer Center for Genomics Research
Harvard University
Head of Bioinformatics

Harvard University's Bauer Center for Genomics Research (**http://cgr.harvard.edu**) seeks outstanding applicants for its Head of Bioinformatics position.

This is an exciting opportunity for someone who wants to be in a high-level position in an academic setting, but not pursue a completely independent research agenda. You will manage a group of 7–9 people who provide training, consultation and collaboration to Harvard life scientists, and support the cutting-edge research of the Bauer Fellows. The group develops tools to support the center's goals, and there are opportunities for collaborative research with Fellows and faculty.

The position would suit someone who has run a group in industry, or someone from an academic background who doesn't want to develop her/his own research group, but would enjoy the benefits and flexibility of the academic environment, surrounded by stimulating colleagues.

To apply, go to **http://jobs.harvard.edu/jobs/search_req** and search for requisition number **23903**.

Harvard University is an Affirmative Action, Equal Opportunity Employer.

UNIVERSITY of VIRGINIA

CLINICAL TRIALS SCIENTIST

The University of Virginia Cancer Center is seeking a Clinical Trials Scientist to serve as a critical interface between laboratory and clinical investigators, assisting in the development of innovative cancer clinical trials. Clinical trials include those evaluating diverse investigational agents/devices/methods (e.g. new chemotherapy, radiation therapy, antibody therapy, and targeted drug treatment approaches) for use in a variety of settings (e.g. diagnostic, prognostic, preventive, treatment, and supportive care settings). The Clinical Trials Scientist communicates with the principal investigator(s) of trials, biostatisticians and staff in the Clinical Trials Office and drafts clinical trial protocols in collaboration with study investigators, including basic science researchers conducting pre-clinical studies and translational researchers performing correlative studies on patient samples. Other responsibilities include working with investigators to revise protocols as required for approval from internal and external protocol review committees and to seek external support for investigator-initiated clinical trials, which may include drafting proposals requesting funding and/or investigational agents from pharmaceutical companies or government agencies.

A graduate degree in the field of pharmacology, biochemistry, nursing or related health sciences discipline is desired. A background in laboratory and/or clinical investigation is highly desirable. The ideal candidate possesses knowledge of clinical trials with experience in cancer trials preferred and must show evidence of exceptional writing and interpersonal skills. Experience in science and/or technical writing is preferred. An understanding of federal regulations related to IRB and FDA policies regarding investigational drugs is desired but not required.

Candidates may be eligible for a research faculty appointment in the School of Medicine. Rank will be commensurate with previous experience and qualifications.

Send application materials including CV and letter of interest to: **Search Committee, Attn: Linda Shank, University of Virginia Cancer Center, Box 800334, Charlottesville, VA 22908-0334, E-mail: lfs@virginia.edu**

The University of Virginia is an equal opportunity/affirmative action employer.

MAYO CLINIC
Cancer Center

Director, Mayo Clinic Comprehensive Cancer Center

Mayo Clinic is seeking applications from nationally recognized leaders in cancer research holding the MD, PhD, MD/PhD degree with demonstrated abilities in both administration and research for the position of Director of the Mayo Clinic Cancer Center. The Director will provide leadership and vision for the Cancer Center. He or she will oversee and manage all cancer center programs and activities across Mayo's three campuses.

Mayo Clinic is an internationally renowned academic medical center with comprehensive programs in medical education and research. With campuses in Minnesota, Florida and Arizona, Mayo Clinic sees more than 500,000 patients per year. Mayo has a vibrant research enterprise in clinical, basic and population sciences. In 2004, the institution received more than $250 million in extramural research awards.

The Mayo Clinic Cancer Center is an NCI-designated comprehensive cancer center, now in its 31st year of funding. The Center includes 350 members and is among the top 10 institutions in NCI funding. Total annual extramural support for research exceeds $95 million. The Center supports 17 shared facilities and its research is organized around 12 programs. Additional information about the Mayo Clinic Cancer Center can be found at: cancercenter.mayo.edu.

Applications should include curriculum vitae and bibliography. Submit by mail or e-mail.
John Noseworthy, M.D.
Chair, Department of Neurology • Professor of Neurology, Mayo Clinic College of Medicine • Mayo Clinic • 200 First Street SW • Rochester, Minnesota 55905 • Attn: Penny Griggs • griggs.penny@mayo.edu

Mayo Clinic is an affirmative action/equal opportunity employer.

WASHINGTON STATE UNIVERSITY

ASSISTANT/ASSOCIATE/FULL PROFESSOR
Biopharmaceutics/Drug Delivery

The Department of Pharmaceutical Sciences at Washington State University (**www.pharmacy.wsu.edu/PharmSci/**) invites applications for a tenure-track position to begin 7/1/06 or earlier. This is an entry-level position at the rank of Assistant Professor, although a senior rank may be considered for applicants with recognized stature in the field.

Qualifications: Applicants must have an earned doctorate in pharmaceutical sciences or a related discipline.

Responsibilities: Candidates will be expected to: (a) teach pharmaceutics, biopharmaceutics, and pharmacokinetics at both the professional and graduate levels; (b) develop and maintain a productive research program; and (c) share in service to the department, college and university. The successful candidate will receive a competitive start-up package and will be expected to establish an outstanding research program that will attract continued extramural funding. Preference will be shown to those with post-doctoral research experience and whose research with respect to advanced drug delivery systems for peptide- or nucleic acid-based drugs - including their absorption, metabolism, and stability - complements existing department strengths in the pharmacology and toxicology of cancer and its treatment, developmental immunotoxicology, pain, inflammation, and novel approaches to enzyme engineering. The successful candidate should have excellent communication and interpersonal skills and collegiality and should demonstrate that they will be able to contribute effectively to the department's teaching missions at both the professional and graduate levels.

Screening of applicants will begin **October 15, 2005**. The application must include a letter of interest, curriculum vitae, statements of research and teaching interests and goals, and the names, email addresses, and contact information for three references. Indicate the rank sought. Send applications to: **Paula Marley, Department of Pharmaceutical Sciences, College of Pharmacy, Washington State University, Pullman, WA 99164 6534; marley@mail.wsu.edu**. Applications should be mailed or emailed as PDF documents.

EO/AA/ADA.

RESEARCH FACULTY POSITIONS
Biological Oceanographer
Marine Ecosystems Modeler

The School of Marine Sciences (SMS) at the University of Maine seeks to fill two Research Faculty positions to be located in the newly formed Gulf of Maine Research Institute (GMRI) in Portland, Maine. The broad target areas for **biological oceanography** are secondary production and fisheries oceanography, with wider interests in marine ecosystems; **ecosystems modeling** broad areas are zooplankton dynamics and larval recruitment dynamics, with wider interests in ecosystem trophic processes. The successful candidates will be appointed to 12 month non-tenure track positions in SMS. These soft-money positions carry a substantial University match. Rank (Assistant, Associate, or Research Professor) is open. Salary level will be commensurate with experience.

With some 50 faculty, the University of Maine's School of Marine Sciences is one of the largest research and educational institutions in the Northeast. SMS offers both undergraduate and graduate degrees.

The Gulf of Maine Research Institute was founded to develop knowledge and public understanding of the Gulf of Maine ecosystem through a fusion of scientific research and public education. These two positions complement six Research Scientists expected to be recruited to the GMRI during 2005.

The Research Faculty members will have a unique opportunity to help link ocean processes to fisheries processes, contributing to the vision of GMRI and to graduate education at SMS. Candidates must have a Ph.D. in an appropriate discipline, an established research record, and graduate teaching interests and research in common with SMS and GMRI faculty.

Applications should comprise a cover letter, full CV, a selection of (p)reprints, a list of four references, and statement of research goals. Materials should be sent to: **Research Faculty Search Committee, School of Marine Sciences, 360 Aubert Hall, University of Maine, Orono ME 04469-5741**. For further information visit **http://www.marine.maine.edu** and **www.gmri.org**. Review will begin on **September 15, 2005** and continue until positions are filled.

The University of Maine and the Gulf of Maine Research Institute are EO/AA Employers and encourage women and minorities to apply.

The Jackson Laboratory

FACULTY RECRUITING

The Jackson Laboratory, an independent, mammalian genetics research institution, and an NCI-designated Cancer Center, is engaged in a major research expansion. New faculty will be recruited in the following areas:

- **Neurobiology**
- **Cancer Biology**
- **Reproductive/Developmental Biology**
- **Immunology/Hematology**
- **Metabolic Disease Research**
- **Computational Biology/Bioinformatics**

We are recruiting scientists at all levels who hold a Ph.D., M.D. or D.V.M., completed postdoctoral training, have a record of research excellence and have the ability to develop a competitive, independently funded research program, taking full advantage of the mouse as a research tool.

The Jackson Laboratory offers a unique scientific research opportunity, including excellent collaborative opportunities with our staff of 35 Principal Investigators, unparalleled mouse and genetic resources, outstanding scientific support services, highly successful Postdoctoral and Predoctoral training programs, and a major meeting center, featuring courses and conferences centered around the mouse as a model for human development and disease.

For more information, please visit our web site: www.jax.org.

Applicants for faculty positions should send a curriculum vitae, 2-3 page statement of research interests and plans, and arrange to have three letters of reference sent to facultyjobs@jax.org. Applications should be mailed to Director's Office, The Jackson Laboratory, 600 Main Street, Bar Harbor, Maine 04609, or email (preferred method): facultyjobs@jax.org Application deadline is October 15, 2005.

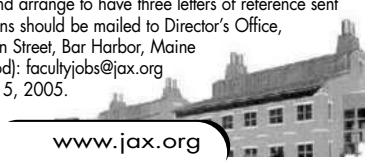

The Jackson Laboratory is an EOE/AA Employer

www.jax.org

PIONEER®
A DUPONT COMPANY

Pioneer Openings

Pioneer Hi-Bred International, Inc, is the world leader in the discovery, development and delivery of elite crop genetics. We have two openings within our Research division in Johnston, IA.

Research Scientist (TP339): This position, in the Insect Control and Herbicide Resistance group, will have responsibility for characterizing transgenic trait and target-pest interactions for early-stage product development in crop plants. The Scientist will design and execute experiments in laboratory, greenhouse and field settings. He or she will evaluate lead traits using artificial diet and plant bioassays. This person will participate on a team responsible for advancing transgenic traits for insect control and herbicide resistance from discovery towards commercialization. PhD in entomology or related field with 3+ years of relevant professional experience or M.S. degree with 4 or more years of equivalent experience in a research environment. Competency in statistics and general business software also is required.

Research Coordinator (TP319): Provide leadership to the advancement, characterization and product knowledge activities of the Grain and Nutritional Sciences group. Provide critical input to multiple teams involved in the development, characterization and commercialization of products containing value added grain, forage and silage quality traits. Develop and implement product knowledge delivery processes for quality traits to ensure business can effectively communicate and promote product attributes and value to internal and external stakeholders. Will ensure understanding of final market needs to create products with right input and output traits to meet end user and grower demands. Ph.D. in plant or biological science and 6-8 yrs research experience beyond Ph.D is required.

For a complete job description and to apply, go to **www.pioneer.com/employment**.

EOE

FACULTY POSITIONS AT THE ROCKEFELLER UNIVERSITY

The Rockefeller University seeks a new generation of exceptional scientists to join its faculty. We invite applications from outstanding candidates working in the biological and biomedical sciences and in other areas relevant to these sciences.

The focus of the search will be on tenure-track Assistant Professors. Applicants should submit either electronically or by CD-ROM the following: Curriculum Vitae, a two page summary of significant research achievements, a two page summary of future research plans and relevant reprints. Please also arrange for at least three letters of reference to be sent directly to the University, and indicate which of the following areas best matches your research program:

- Immunology, Virology & Microbiology
- Biochemistry & Biophysics
- Chemistry & Structural Biology
- Medical Sciences & Human Genetics
- Neurosciences
- Molecular, Cell & Developmental Biology
- Mathematical Biology, Evolutionary Biology & Ecology

Rockefeller University provides strong financial support for the research work of its faculty. It is presently seeking to significantly increase the number of tenure track Assistant Professors and to expand its research interests. Highly motivated, creative and innovative scientists working in the above areas are encouraged to apply.

Applications should be sent by **November 15, 2005** to: **Faculty Search, Office of Academic Affairs, Box 246, The Rockefeller University, 1230 York Avenue, New York, NY 10021 USA; facultysearch@rockefeller.edu**

More specific information regarding the required application material can be found at **http://www.rockefeller.edu/facultysearch/.**

The Rockefeller University is an Affirmative Action/Equal Opportunity Employer. Further information about the research and educational programs at The Rockefeller University can be found at **http://www.rockefeller.edu/.**

CHAIR
Department of Biochemistry and Molecular Medicine

The University of California, Davis, School of Medicine seeks an academic leader to chair the Department of Biochemistry and Molecular Medicine. We seek candidates with a Ph.D. and/or M.D. degree and training in biochemistry, molecular-based medical research, or a related field. The successful candidate is expected to have a distinguished record in research, teaching, and administration, excellent interpersonal skills as well as a vision to further the development of the department and to implement initiatives to meet the challenges of academic medicine.

The Department of Biochemistry and Molecular Medicine has full-time Ph.D. and M.D./Ph.D. faculty in a variety of research areas, including eukaryotic gene expression, signal transduction, cancer biology, membrane biology, neurobiology, muscle physiology, and human genetics. In addition, several new recruitments in the above or additional areas are anticipated.

Interested candidates should send their curriculum vitae, a statement of interests, teaching and administrative responsibilities, and the names of five references to: **Biochemistry and Molecular Medicine Chair Search Committee,** via e-mail at **janice.weir@ucdmc.ucdavis.edu,** or via regular mail to **Janice Weir, c/o Office of Academic Affairs, School of Medicine, University of California, Davis, Medical Center, PSSB Suite 2500, 4150 V Street, Sacramento, CA 95817**.

For full consideration, applications must be received by **October 30, 2005**. The position will remain open until filled.

The University of California is an Affirmative Action/ Equal Opportunity Employer.

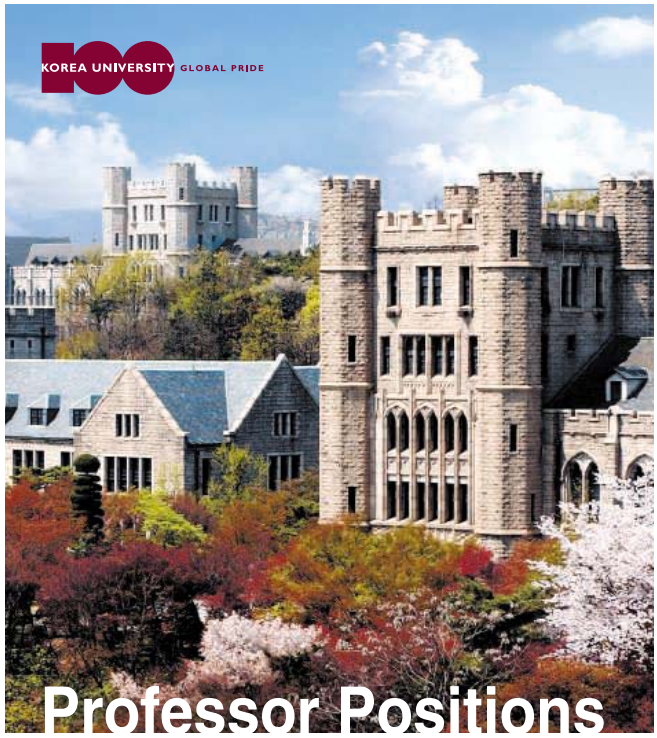

Korea University invites applicants for tenure-track positions at the rank of Assistant Professor to begin in Spring 2006 or Fall 2006. (Responsibilities include teaching two courses per semester (in English), conducting/publishing research, and assuming various administrative duties to support academic functions). Candidates must possess near-native/native fluency in English and have a Ph.D. in hand at time of application. Candidates should also have experience in teaching at the college level, a strong commitment to excellence in scholarship, and dedication to undergraduate and graduate teaching in the applicant's research area. Salary for the entry level Assistant Professor is US$53,000. Send an application form (which can be downloaded from www.korea.ac.kr/~faculty), a cover letter explaining your qualifications and teaching philosophy, CV, transcripts from graduate studies, selected publications or writing samples, proof of highest academic degree, three letters of reference and, if possible, sample syllabi or teaching portfolio to: Department of Academic Affairs, Korea University, Anamdong, Sungbukgu, Seoul, Korea. Enquires: Phone: +82-2-32901071~3; Fax: +82-2-929-9164; Email: faculty@korea.ac.kr.
Application deadline: August 29, 2005.

Korea University is an Equal Opportunity /Affirmative Employer and is committed to a diverse faculty, staff, and student body. Korea University, which is celebrating its centennial this year, is one of the most prestigious universities in Korea, serving more than 30,000 students. The university is a dynamic and innovative doctoral/research-intensive institution recognized for strong undergraduate education and a range of focused graduate programs and research. For more information about the university, visit our home page at www.korea.ac.kr.

KOREA UNIVERSITY
www.korea.ac.kr

POSITIONS OPEN

EVOLUTIONARY BIOLOGY FACULTY POSITION
UCLA Department of Ecology and Evolutionary Biology

The Department of Ecology and Evolutionary Biology at UCLA invites applications for an **OPEN RANK, TENURE-TRACK FACULTY POSITION** in evolutionary biology, broadly defined. The expected start date is September 2006. Candidate must have a Ph.D.; postdoctoral experience is desired. Salary is commensurate with education and experience. Successful candidates are expected to maintain a rigorous research program, and to contribute to undergraduate and graduate teaching. UCLA has outstanding academic support for faculty, including access to the University of California Natural Reserve System, a campus-wide Institute of Pure and Applied Mathematics, several departments with computational and evolutionary biology interests, and attractive startup packages. Submit curriculum vitae, statements of research and teaching interests, and names and addresses of three references online to **website: http://www.eeb.ucla.edu/Evolutionist.** Please contact: **Charles Taylor (e-mail: taylor@biology.ucla.edu)** for additional information. Reviews of applications will begin September 30, 2005.

The University of California is an Equal Opportunity Employer committed to excellence through diversity.

ORGANIC CHEMISTRY
Dartmouth College

Applications are invited for a faculty position at the **ASSISTANT PROFESSOR** level starting July 2006. The Chemistry Department seeks an individual who will establish a nationally recognized research program in organic chemistry at Dartmouth, and who will excel at teaching in our undergraduate and Ph.D. curriculum. Candidates will be expected to be able to teach introductory and advanced courses in organic chemistry, as well as graduate courses in their area of research. Applicants should submit curriculum vitae, a description of their research plans, and a brief statement about their teaching interests. Applicants should also arrange to have three letters of recommendation sent on their behalf. All inquiries and applications will be treated confidentially. Application materials should be sent to: **Chair, Organic Chemist Search Committee, Department of Chemistry, 6128 Burke Laboratory, Dartmouth College, Hanover, NH 03755-3564.** The Committee will begin to consider completed applications on October 15, 2005. *With an even distribution of male and female students and over a quarter of the undergraduate student population members of minority groups, Dartmouth is committed to diversity and encourages applications from women and minorities. Dartmouth College is an Equal Opportunity/Affirmative Action Employer.*

X-RAY CRYSTALLOGRAPHER

The Department of Biochemistry and Biophysics at the University of Rochester Medical Center invites applications for a tenure-track position at the **ASSISTANT PROFESSOR** or higher level from individuals who use X-ray crystallography to study biological macromolecules. The Medical Center features an interactive and expanding biomedical research community, including over 400 Ph.D. students, with close ties to basic science departments at the adjacent Arts and Sciences campus. A state-of-the-art X-ray facility is housed in the Department (see **website: http://dbb.urmc.rochester.edu**). To apply, please submit electronic versions of your curriculum vitae, three publications, and a statement of research interests to **e-mail: gail_marriott@urmc.rochester.edu** and arrange for at least three letters of recommendation to be sent to: **Gail Marriott, Crystallography Search, Department of Biochemistry and Biophysics, Box 712, University of Rochester Medical Center, 601 Elmwood Avenue, Rochester, NY 14642.** Consideration of applications will begin on October 1, 2005, and continue until the position is filled. *Equal Opportunity Employer.*

POSITIONS OPEN

CASE WESTERN RESERVE UNIVERSITY

CHAIR
Department of Physiology and Biophysics
Case Western Reserve University
School of Medicine

Nominations or applications are invited from established, dynamic scientists with a creative vision for the position of Chair of the Department of Physiology at the Case Western Reserve University School of Medicine.

The Department has a fine tradition, excellent faculty, facilities, space, and a vigorous graduate program. The new leadership at the School of Medicine seeks a chairperson who will lead this strong department to greater national prominence and will provide resources to build on existing strengths or to develop a new area. New development and expansion of many programs at the School of Medicine provide exciting opportunities for interdisciplinary collaboration. The successful candidate will have an outstanding record of scholarly achievements with proven leadership, mentoring, and administrative abilities.

In addition to curriculum vitae and a list of publications, applicants should submit a letter describing their research, teaching, service, administrative experience, previous mentoring, and their legacy or vision in building interdisciplinary programs and resources.

Nominations and/or applications should be e-mailed to **e-mail: chairphysiol@case.edu.**

For additional information, visit **website: http://physiology.case.edu.**

For questions or additional information you may call **Lynn Landmesser** at **telephone: 216-368-3996.**

Case Western Reserve University is an Equal Opportunity/Affirmative Action Employer.

DIRECTOR, MCW CANCER CENTER

The Medical College of Wisconsin (MCW) is recruiting a visionary physician-scientist or scientist with a strong history of accomplishment in cancer-related research to serve as Director of the Cancer Center.

Individuals must possess excellent leadership skills and should be outstanding scientists with active NIH-funded research programs. A desire to encourage collaboration among scientists and physicians and to identify promising new areas for basic and translational research applications are important. The Director must also be committed to the goal of achieving National Cancer Institute designation for the Center.

The MCW Cancer Center is organized under an interdepartmental matrix structure and is committed to fostering the translation of basic research efforts into patient care, with acknowledged areas of excellence in breast cancer diagnosis and treatment, pediatric cancers, and blood and bone marrow transplants.

MCW is part of a large regional academic health center which also includes Froedtert Hospital and Children's Hospital of Wisconsin. Construction of a major new research facility with significant emphasis on cancer research is underway, and a new clinical cancer center is also under construction on the campus, with both facilities anticipated to open in 2007.

Prospective applicants are invited to forward a current curriculum vitae and letter of interest to:

Michael J. Dunn, M.D.
Dean and Executive Vice President
Medical College of Wisconsin
8701 Watertown Plank Road
P.O. Box 26509
Milwaukee, WI 53226-0509
Telephone: 414-456-8213
E-mail: mdunn@mcw.edu

An Equal Opportunity/Affirmative Action Employer, Minorities/Females/Persons with Disabilities/Veterans.

POSITIONS OPEN

BIOPHYSICAL CHEMISTRY
Dartmouth College

Applications are invited for a faculty position at the **ASSISTANT PROFESSOR** level starting July 2006. The Chemistry Department seeks an individual who will establish a nationally recognized research program in experimental biophysical chemistry at Dartmouth, and who will excel at teaching in our undergraduate and Ph.D. curriculum. Preference will be given to individuals who investigate structure-function relationships of biological macromolecules using physical techniques complementing existing strength in X-ray crystallography. Candidates will be expected to contribute to the teaching of courses in our biophysical chemistry major, graduate courses in their area of research, and introductory chemistry. Applicants should submit curriculum vitae, a description of their research plans, and a brief statement about their teaching interests. Applicants should also arrange to have three letters of recommendation sent on their behalf. All inquiries and applications will be treated confidentially. Application materials should be sent to: **Chair, Biophysical Chemist Search Committee, Department of Chemistry, 6128 Burke Laboratory, Dartmouth College, Hanover, NH 03755-3564.** The Committee will begin to consider completed applications on October 15, 2005. *With an even distribution of male and female students and over a quarter of the undergraduate student population members of minority groups, Dartmouth is committed to diversity and encourages applications from women and minorities. Dartmouth College is an Equal Opportunity/Affirmative Action Employer.*

FACULTY POSITIONS

The Department of Dermatology of the University of Illinois at Chicago in conjunction with the Department of Pharmacology is recruiting two tenure-track researchers to join the faculty at the level of **ASSISTANT PROFESSOR** or **ASSOCIATE PROFESSOR.** We are seeking outstanding individuals with NIH funding and vibrant research programs and with a potential for growth. The candidates should have the M.D., M.D./Ph.D. or Ph.D. degree with demonstrated research productivity. The successful candidates are expected to establish robust independent research programs with extramural funding and develop interactions within the institution. Recruitment emphasis is on areas of immunology, particularly in inflammation, inflammation-mediated angiogenesis, adhesion molecules, viral immunology or autoimmunity, but significant research accomplishments in other areas of immunology will also be considered.

For fullest consideration, interested individuals should send curriculum vitae, a summary of research goals, along with names and addresses of three references by October 15, 2005, to:

Lawrence S. Chan, M.D., Professor and Head
Department of Dermatology
808 S. Wood Street, M/C 624
Chicago, IL 60612

MONTEREY BAY AQUARIUM
POSTDOCTORAL RESEARCH SCIENTIST.

The Monterey Bay Aquarium is seeking a Postdoctoral Researcher to conduct electronic tagging studies on white sharks along the California coast. Applicants must have a Ph.D. and demonstrated expertise in marine science. Visit **website: http://www.montereybayaquarium.org/aa/aa_jobs/jobs_staf_opening.asp** for a detailed job description. Initial appointment is one year, renewable for a second year. To apply, send curriculum vitae, description of research experience, and names, addresses, telephone numbers, and e-mails of three references to:

Monterey Bay Aquarium
Attn: Human Resources
886 Cannery Row
Monterey, CA 93940
E-mail: jobs@mbayaq.org (no attachments)

Equal Opportunity Employer/Committed to Diversity.

POSITIONS OPEN

TENURE-TRACK POSITIONS
Biochemistry, Immunology, and Organismal/Evolutionary Biology
Macalester College

Applications are invited for three tenure-track positions in immunology and organismal/evolutionary biology in the Department of Biology and Biochemistry in the Department of Chemistry at the level of **ASSISTANT PROFESSOR** beginning fall 2006. We seek applicants who are committed to excellence in teaching at the undergraduate level and who are dedicated to developing an active research program that engages students in research. Full ad and details are available at **website: http://www.macalester.edu/provost/positions/index.html.** To apply for the openings in biology, send a letter, curriculum vitae, statements of teaching philosophy and research plans, and three letters of reference to: **Professor Lin Aanonsen, Chair, Department of Biology, Macalester College, St. Paul, MN 55105.** To apply for the position in chemistry, send all of the above plus undergraduate and graduate transcripts to: **Professor Thomas D. Varberg, Chair, Department of Chemistry, Macalester College, St. Paul, MN 55105.** Applications should be received by October 15, 2005. Macalester College is a selective, private liberal arts college in the Minneapolis-St. Paul metropolitan area. The College prides itself on providing support for excellence in teaching and in faculty scholarship. *Macalester is an Equal Opportunity/Affirmative Action Employer and is committed to diversity. We are especially interested in candidates committed to working with students of diverse backgrounds.*

FACULTY POSITION IN GENOME STABILITY, DNA REPAIR, AND CANCER EPIGENETICS
University of Rochester Medical Center

The Department of Biochemistry and Biophysics and the Wilmot Cancer Center invite applications for a tenure-track position in chromatin regulation or genome injury related to cancer at the **ASSISTANT PROFESSOR** level or higher. The Medical Center offers an interactive environment with strong programs in biochemistry of DNA repair and chromatin and integrative cancer cell biology. Applicants employing genetic approaches in mammalian systems are preferred, but those in areas complementing existing strengths are also invited. Submit curriculum vitae, statement of research accomplishments, and plans to **e-mail: gail_marriott@urmc.rochester.edu,** and three letters of recommendation to: **Robert Bambara, Repair Search, Box 712, University of Rochester Medical Center, 601 Elmwood Avenue, Rochester, NY 14642.** See **websites: http://dbb.urmc.rochester.edu** and **http://www.stronghealth.com/services/cancer.** *Equal Opportunity Employer.*

PLANT VIROLOGY FACULTY POSITION: The Department of Plant Pathology, Kansas State University invites applicants for a virologist to work in the area of arthropod-vectored plant viruses and their ecological and molecular interactions with their plant hosts. The successful candidate will teach a graduate course in plant virology and another graduate course in their area of specialty in alternate years. Applicants must have a Ph.D. in plant pathology, entomology, or related discipline along with postdoctoral research experience. Please submit a letter of application including professional goals and research/teaching interests, detailed curriculum vitae, reprints of up to five relevant publications, transcripts of all college course work, and three current/relevant letters of reference to: **Scot Hulbert, Department Plant Pathology, Kansas State University, Manhattan, KS 66506. E-mail: shulbrt@ksu.edu.** Review of applications will begin November 1, 2005, and continue until the position is filled. For more information concerning the position and the Department, see **website: http://www.oznet.k-state.edu/plantpath/.** *Paid for by Kansas State University, an Equal Opportunity/Affirmative Action Employer.*

RESEARCH INSTRUCTOR/ RESEARCH ASSISTANT PROFESSOR

A nontenure-track position is available in the Center for Stem Cell Biology at Vanderbilt University to perform research related to pancreatic beta cell development and function. Applicants must hold a Ph.D. and have at least three years of postdoctoral training in molecular and/or cell biology. Rank of the appointment will depend on the candidate's prior accomplishments. Experience with gene targeting in embryonic stem cells and phenotypic characterization of germline-altered mice is highly desirable. Effective communication and organizational skills, as well as the ability to work as part of a larger team, must be readily evident. The successful applicant will assist in the mentoring and/or supervision of graduate students, postdoctoral scientists, and other professional staff. Please submit complete curriculum vitae, a brief description of current research interests, and the names of three references to:

Mark A. Magnuson, M.D.
Director, Center for Stem Cell Biology
802 Light Hall
Vanderbilt University
Nashville, TN 37232-0225
E-mail: mark.magnuson@vanderbilt.edu

Vanderbilt University is an Equal Opportunity/Affirmative Action Employer with a strong institutional commitment to diversity.

ASSISTANT PROFESSORSHIP, CHEMISTRY
Department of Chemistry and Chemical Biology
Harvard University

Applicants are invited to apply for a tenure-track Assistant Professorship in the fields of physical chemistry (experimental and theoretical), organic chemistry, or chemical biology. Applicants should arrange to have three letters of recommendation sent independently and should provide curriculum vitae, a list of publications, and an outline of their future research plans. Applications and supporting materials should be sent to:

Chair, c/o Ms. Carol Gonzaga
Department of Chemistry and Chemical Biology
Harvard University
12 Oxford Street
Cambridge, MA 02138-2902

Reference Position: JFCCB133S. The deadline date for receipt of applications and supporting materials is October 15, 2005. *Harvard University is an Affirmative Action/Equal Opportunity Employer. Applications from, and nominations of, women and minority candidates are strongly encouraged.*

RESEARCH ASSISTANT PROFESSOR

Cummings School of Veterinary Medicine at Tufts University invites applications for a Research Assistant Professor position in the Department of Biomedical Sciences. Candidates must have Ph.D. and/or D.V.M. degree with at least three years of postdoctoral research experience, and are expected to supervise laboratory personnel and conduct independent research in hepatobiliary transport mechanisms. The incumbent will be joining a well-established NIH-funded research program. The successful candidate will have the opportunity to participate in graduate teaching programs. Review of applications will begin immediately. Interested applicants should submit a letter of application with a statement of career goals, curriculum vitae, and the names of three or more references to: **Dr. Sawkat Anwer, Distinguished Professor, Department of Biomedical Sciences, Tufts Cummings School of Veterinary Medicine, 200 Westboro Road, North Grafton, MA 01536. E-mail: sawkat.anwer@tufts.edu.** *Tufts University in an Affirmative Action/Equal Opportunity Employer.*

ASSISTANT PROFESSOR
Cornell University

The Psychology Department (in conjunction with the New Life Sciences Initiative and Program in Neuroscience) expects to fill a tenure-track position at the **ASSISTANT PROFESSOR** level for the 2006–2007 academic year. We seek applicants with research interests in integrative approaches to central nervous system function. Research interests could include, but are not limited to: the organization of sensory or motor systems; social communication, social cognition, and social behavior; emotion; or any other aspect of cognition such as learning and memory, spatial navigation, or decision-making. A variety of current recording or imaging techniques are welcome, which could be combined with genomic approaches or reduced preparations. The appointment will begin July 1, 2006. Review of applications will begin November 15, 2005, although later applications will be considered until the position is filled.

Interested applicants should submit a letter of application indicating specific research interests, curriculum vitae, reprints or preprints of completed research, and three letters of recommendation sent directly from three references to: **Secretary, Psychology Search Committee, Department of Psychology, 278D Uris Hall, Cornell University, Ithaca, NY 14853-7601, U.S.A.** *Applications from women and minority candidates are especially welcome. Cornell University is an Equal Opportunity/Affirmative Action Employer.*

Texas A&M University. The Department of Chemistry at Texas A&M University invites applications for multiple tenure-track faculty positions in all areas of chemistry, including biological chemistry, and other interdisciplinary areas, for an anticipated starting date of September 2006. Applications at the **ASSISTANT PROFESSOR** level are particularly sought, but appointments to senior ranks will also be considered for qualified candidates. Successful candidates will be expected to establish and maintain vigorous independent research programs and to teach at both the undergraduate and graduate levels.

Candidates should submit curriculum vitae, a brief description of research plans, and arrange for three letters of recommendation to be sent to:

Dr. Emile A. Schweikert
Head, Department of Chemistry
Texas A & M University
P.O. Box 30012
College Station, TX 77843-3012

Review of applications will begin on October 15, 2005, and will continue until the positions are filled.

Texas A & M University is an Equal Opportunity/Affirmative Action Employer that is dedicated to the goal of building a culturally diverse and pluralistic faculty and staff who are committed to teaching and working in a multicultural environment. We strongly encourage applications from women, minorities, veterans, and individuals with disabilities. In addition, an aggressive faculty-hiring program during the next several years will enable the University to be particularly responsive to the needs of dual career couples.

CURATOR: U.S. National Tick Collection. Georgia. Southern University; 12-month, tenure-track appointment at the **ASSOCIATE** or **FULL PROFESSOR** rank. Ph.D. or equivalent in an area relevant to acarology, entomology, or parasitology required. Experience or demonstrable knowledge of systematics; research experience with ticks; computer skills; sustained research productivity; command of written and spoken English; and grantsmanship required. Full text advertisement, including complete position announcement with all qualifications and application instructions, is available at **website: http://www.bio.georgiasouthern.edu/iap/index.htm.** Screening of applications begins November 15, 2005, and continues until the position is filled. Georgia is an open records state. Individuals who need reasonable accommodations under the ADA should contact the search chair. *Georgia Southern is an Affirmative Action/Equal Opportunity Institution.*

POSITIONS OPEN

DIRECTOR OF GRADUATE DIVERSITY RECRUITMENT INITIATIVES

The University of Washington (UW) seeks a trained professional (scientist or engineer; Ph.D. preferred) to spearhead the development of collegial networks and innovative programs that will enhance diversity throughout the respective graduate science, technology, engineering, mathematics programs on campus. This individual will oversee and initiate collaborative recruitment and retention efforts; establish long-term relationships with target institutions; engage UW faculty; coordinate activities with various minority affairs programs; and shepherd student candidates through and beyond the recruitment process. Candidates must have outstanding communication and interpersonal skills to interact with tact and diplomacy with students, families, and faculty, as well as demonstrated knowledge of cultural, economic, and political impediments and incentives to promoting diversity in higher education. Ability to travel 25 percent to 35 percent. To apply, log on to the UW employment **website: http://www.washington.edu/jobs** and search by Requisition #11475. *Affirmative Action/Equal Opportunity Employer.*

A **POSTDOCTORAL FELLOWSHIP** position is available immediately in a well-funded laboratory in the Department of Pathology at the University of New Mexico. The laboratory is associated with the Center for Infectious Disease and has a primary focus on pulmonary immune regulation with a specific interest in dendritic cells. The project the successful applicant will pursue relates to studying the pathogenesis of pulmonary anthrax in two different animal species as part of a newly funded program project on Category A bioweapons. The minimum requirement: Ph.D. in microbiology, immunology, or closely related field. Must be able to meet Federal requirements to work in a high security biocontainment area and have no physical conditions that would put them at risk for working with animals or with infectious organisms. Preference will be given to applicants with experience working with infection models in experimental animals and whose background qualifies them for NIH training grants. For best consideration, apply before October 30, 2005. Applications should be submitted to: **Dr. Mary F. Lipscomb, c/o Ms. LeeAnn Martinez, University of New Mexico, 915 Camino de Salud, MSC 08-4640, Department of Pathology, Albuquerque, NM 87131. Fax: 505-272-8084; e-mail: lemartinez@salud.unm.edu.**

The Georgia Southern University Chemistry Department invites applications for an **ASSISTANT PROFESSOR** position in biochemistry. The position requires a Ph.D. in biochemistry or chemistry with expertise in biochemistry or related field by the date of appointment; the ability to establish an active and productive research program involving undergraduate students; a demonstrated command of written and spoken English; and evidence of teaching and research abilities. Postdoctoral experience in teaching and/or research; the potential for collaborative research, both within and outside the Department; and the ability to work with diverse populations are preferred. Full text advertisement, including information about the Department, faculty, and the complete position announcement with all qualifications and application instructions, is available at **website: http://cost.georgiasouthern.edu/chemistry/.** Screening of applications begins September 19, 2005, and continues until the position is filled. Georgia is an open records state. Individuals who need reasonable accommodations under the ADA should contact the search chair. *Georgia Southern is an Affirmative Action/Equal Opportunity Institution.*

JOINT ASSISTANT PROFESSOR POSITION, ANTHROPOLOGY AND PATHOBIOLOGY
Anthropology and Ecology of Infectious Diseases
The University of Illinois, Urbana-Champaign

The Department of Anthropology, College of Liberal Arts and Sciences and the Department of Pathobiology, College of Veterinary Medicine at the University of Illinois, Urbana-Champaign invite applications for a joint tenure-track Assistant Professor position in anthropology and ecology of infectious diseases with concurrent appointment as Director of the Earth and Society Initiative in Disease Emergence and Ecosystem Health, effective August 16, 2006.

Applicants must have a doctoral degree, a record of scientific accomplishments related to the ecology of emerging infectious disease, and exceptional leadership abilities. Preference will be given to scholars who study the effects of anthropogenic disturbance on parasite-host interactions and disease dynamics. The successful applicant will be expected to teach courses and lead seminars in anthropology and the College of Veterinary Medicine, develop an extramurally funded research program, and develop and promote the Earth and Society Initiative in Disease Emergence and Ecosystem Health.

Please send a letter of application, curriculum vitae, a statement detailing research and teaching interests, along with names and addresses of three references to: **Paul Garber, Head, Department of Anthropology, 109 Davenport Hall, University of Illinois, 607 S. Mathews Avenue, Urbana, IL 61801.**

Salary is commensurate with experience. For full consideration, applications must be received by October 1, 2005. Postal mail applications or hard copies only, no electronic applications will be accepted. Position #10008. *The University of Illinois is an Affirmative Action/Equal Opportunity Employer.*

ASSISTANT PROFESSOR, CHEMISTRY

The Department of Chemistry of the University of Wisconsin-Madison anticipates an opening for a faculty position to begin in August 2006. We seek outstanding candidates at the Assistant Professor level (tenure track) in all areas of chemistry including chemical education. Candidates must have a Ph.D. in chemistry or a related field; postdoctoral experience is desirable. The position requires development of an internationally recognized program of scholarly research as well as excellent teaching at both the undergraduate and graduate levels. Please submit curriculum vitae and concise description of research plans online at **website: http://www.chem.wisc.edu.** Three letters of recommendation will also be required through the online service directed to: **Chair, Faculty Search Committee, Department of Chemistry, University of Wisconsin-Madison, 1101 University Avenue, Madison WI 53706-1322.** To guarantee full consideration, all materials must arrive before October 1, 2005.

The University of Wisconsin is an Equal Opportunity/Affirmative Action Employer; applications from qualified women and minority candidates are encouraged. Unless confidentiality is requested in writing, information regarding the identity of the applicant must be released on request. Finalists cannot be guaranteed confidentiality.

NIH-funded **POSTDOCTORAL POSITIONS** to study Nrf2/transcription; signaling; mouse genetic tumor models and chemoprevention (*TIPS* **26:**318, 2005; *J. Biol. Chem.* 2005; *J. Biol. Chem.* **279:**23052, 2004; *FRBM* **36:**1505, 2004; *Cancer Res.* **63:**7520, 2003; *J. Biol. Chem.* **277:**48745, 2002; *J. Biol. Chem.* **274:**27545, 1999; *J. Biol. Chem.* **275:**2322, 2000; *J. Biol. Chem.* **275:**9612, 2000; *J. Biol. Chem.* **275:**39907, 2000; *Cancer Res.* **60:**5995, 2000). Applicants must have Ph.D. plus expertise in protein biochemistry, transcription complex, molecular/cell biology, and IHC. Send resume to: **Ah-Ng Tony Kong, Glaxo Professor of Pharmaceutics/Director, Graduate Program in Pharmaceutical Science, Ernest Mario School of Pharmacy, Rutgers University, Piscataway, NJ 08854. E-mail: kongt@rci.rutgers.edu.**

POSTDOCTORAL POSITION in enzyme structure, function, and inhibitor-binding. A Postdoctoral position is available immediately to study the structure and function of several bacterial acetyltransferases and how these enzymes bind small molecule inhibitors identified by high throughput screening techniques. These inhibitors may find use as leads in the search for clinically useful antibiotics. An X-ray crystallographic approach will be used and crystals corresponding to most of these targets are now available. The candidate should have demonstrated experience in protein crystallography and an interest in addressing structural questions concerning chemical mechanism and inhibitor-binding. To apply, send curriculum vitae, summary of research experience, and the names and contact information for three references to:

Dr. Steven L. Roderick
Professor of Biochemistry
Albert Einstein College of Medicine
Jack and Pearl Resnick Campus
1300 Morris Park Avenue
Bronx, NY 10461
E-mail: roderick@aecom.yu.edu

The Albert Einstein College of Medicine is an Equal Opportunity Employer.

The Collaborative Research Center SFB 610 "Variation in Protein Conformation: Cellbiological and Pathological Relevance" at the University of Leipzig invites applications for an: **INDEPENDENT JUNIOR RESEARCH GROUP LEADER** (salary scale BAT 1a).

The candidate, a highly qualified junior scientist with a strong research interest in protein-nuclear magnetic resonance (NMR)-spectroscopy, will hold a Ph.D., obtained no longer than six years ago. We expect relevant postdoctoral research experience, an excellent scientific record, and the ability to lead a research group independently. The junior research group will be integrated into the SFB 610 (see **website: http://www.sfb610.de**), and hosted at the Institute for Analytical Chemistry, where it will be provided with the necessary space and resources (including a 600 and 700 MHz NMR spectrometer).

The evaluation process includes a personal presentation of the project and a panel assessment.

Applications should include a research plan, curriculum vitae, and list of publications and be submitted by September 30, 2005, to: **Professor Dr. A. Beck-Sickinger, Institut of Biochemistry, der University of Leipzig, Brüderstrasse 34, D-04103 Leipzig, Germany.**

EUKARYOTIC GENETICIST. The Department of Biological Sciences, California State University, East Bay, is seeking a Eukaryotic Geneticist for appointment to a tenure-track position at the level of **ASSISTANT PROFESSOR** beginning fall 2006. First consideration will be given to individuals who use cell and molecular approaches in their research. We encourage applications from individuals who are committed to teaching excellence and maintenance of an innovative, externally funded research program at an institution that is intent on fostering a culturally diverse intellectual community. The position will require one to teach genetics and lower- and upper-division cell and molecular biology lectures and laboratories. In addition, applicants who possess an ability to teach courses on proteomics and bioinformatics will be looked upon more favorably. A Ph.D. and postdoctoral experience are required. Send curriculum vitae, research and teaching plans, selected reprints, and three letters of recommendation to: **Eukaryotic Geneticist Search Committee, Department of Biological Sciences, California State University, East Bay, 25800 Carlos Bee Boulevard, Hayward, CA 94542.** Review of applications begins October 1, 2005. *Equal Opportunity Employer.*

Post-Doctoral Positions
The Structural Genomics Consortium
Toronto

CIHR IRSC Canadian Institutes of Health Research / Instituts de recherche en santé du Canada

SGC Structural Genomics Consortium

The Structural Genomics Consortium (SGC) is a charitable enterprise, with a mandate to substantially increase the rate at which three-dimensional structures of medically relevant proteins are deposited in the public domain. Over the past year, the SGC has determined over 80 structures of human proteins implicated in cancer, diabetes and metabolic disease, osteoporosis, and drug metabolism, as well as a number of proteins from malaria parasites. See **www.TheSGC.com** for details of this premier effort in human protein structural genomics.

The Toronto site of the SGC seeks Post-Doctoral Fellows to work on human and malaria protein families with strong medical and/or pharmaceutical relevance. A Ph.D. is required with experience in one or more of the following areas; X-ray crystallography, enzymology, protein expression and purification, protein biophysical characterization, computational chemistry and comparative protein structure analysis, and structural biology of gene families.

Interested candidates should submit their CVs and a brief statement of research interests to **HR.sgc@utoronto.ca**.

VELUT ARBOR ÆVO

The University of Toronto is strongly committed to diversity within its community and especially welcomes applications from visible minority group members, women, Aboriginal persons, persons with disabilities, members of sexual minority groups, and others who may contribute to the further diversification of ideas. All qualified candidates are encouraged to apply; however, Canadians and permanent residents will be given priority.

INCAPS
Indiana Centers for Applied Protein Sciences

Immediate Openings
in
Protein Analysis and Proteomics

INCAPS, based in Indianapolis, is a contract-research organization with expertise in protein analysis, proteomics, technology validation and biomarker collaborations. INCAPS is providing its expertise and technologies to help both commercial and academic institutions solve challenging scientific problems. INCAPS has the following immediate openings:

Research Scientist

Ph.D. degree in Biochemistry or related field. 2-5 years of academic and/or industrial experience. Strong experience in protein biochemistry, protein separation, and mass spectrometric technologies. Excellent interpersonal and communication skills.

Research Associate

MS degree in Biochemistry, Biology or related field. Expertise with protein separation techniques including protein chromatography and electrophoresis. Familiarity with mass spectrometric technologies is desirable.

For detailed responsibilities and requirements of the above positions, please check out our web site **www.indianacaps.com**.

Please send CV to: **jobs@indianacaps.com**

INCAPS is an Equal Opportunity Employer.

Top Employers
in Biotechnology & Pharmaceuticals
A *Science* Advertising Supplement

Who will be #1?

Make sure your ad is in this supplement.

Issue date ..... 30 Sept. 2005
Reserve space by .... 13 Sept. 2005

To advertise, contact:

U.S. Daryl Anderson
Phone: (202) 326-6543
E-mail: advertise@sciencecareers.org

Europe and International
Tracy Holmes
Phone: +44 (0) 1223 326 500
E-mail: ads@science-int.co.uk

Japan Jason Hannaford
Phone: +81 (0) 52 789-1860
E-mail: jhannaford@sciencemag.jp

ScienceCareers.org
We know science AAAS

Duke University Medical Center

FACULTY POSITIONS IN IMMUNOLOGY

The Department of Immunology invites applications for **TENURE-TRACK** faculty positions at all levels.

Candidates working in host defense, models of human disease, molecular and cellular immunology, cancer immunobiology, and lymphocyte signal transduction and development are encouraged to apply.

Interested individuals should send a curriculum vitae, a statement of research interest, and the names of three references to:

Dr. Thomas F. Tedder
Department of Immunology
P.O. Box 3010
Duke University Medical Center
Durham, NC 27710

Website:
http://immunology.mc.duke.edu

Duke University Medical Center is an Equal Opportunity/Affirmative Action Employer.

Division of Hematology/Oncology
Texas Tech University Health Sciences Center, Amarillo, Texas

Faculty Positions

The Division of Hematology/Oncology at Texas Tech University Health Sciences Center, Amarillo has rapidly expanding hematology and oncology clinical and research programs. The Division has openings for several **Research Scientists at the rank of tenure track Assistant/Associate/Full Professor**. These are unique appointments and enjoy the academic and research support of a highly committed university. These positions attract an excellent salary, benefits and start-up package. Candidates will be expected to have established research programs and extramural funding. The successful candidates will play major roles in the development and expansion of the cancer research programs in Amarillo.

Amarillo is one of the most liveable small and cozy cities in the country. It offers the amenities and high standard of living of large cities but at a very affordable cost. It has good public schools and is within easy driving distance from Oklahoma City, Dallas, Santa Fe and Denver.

For further information, send email to **slim@harringtoncc.org**, or send CV to: **Seah H Lim, MD, PhD, Professor and Chief, Director of Biotherapy and Stem Cell Transplant Program, Division of Hematology and Oncology, Don and Sybil Harrington Cancer Center, 1500 Wallace Boulevard, Amarillo, Texas 79106**.

An Equal Opportunity Affirmative Action Employer.

POSITIONS OPEN

POSTDOCTORAL RESEARCH POSITION

A Postdoctoral Research position is available immediately to study combined effects of neurotoxicants and environmental stress at the Environmental and Occupational Health Sciences Institute (EOHSI), a joint institute of the Robert Wood Johnson Medical School, University of Medicine and Dentistry of New Jersey, and of Rutgers, the State University of New Jersey. The research takes place in a collaborative group setting with multiple technologies operative. Experience in psychology, operant behavior, and neurochemistry is highly desirable. Salary will be commensurate with experience. Send curriculum vitae along with names and telephone numbers of three references to:

Dr. Deborah Cory-Slechta
Environmental and Occupational
Health Sciences Institute
170 Frelinghuysen Road
Piscataway, NJ 08854
E-mail: dcs@eohsi.rutgers.edu

The Environmental and Occupational Health Sciences Institute is an Equal Opportunity/Affirmative Action Employer and actively encourages interest from women and minorities.

RESEARCH INSTRUCTOR POSITION, Cancer Center and Division of Hematology/Oncology, University of Alabama at Birmingham (UAB). Scientists of in vivo magnetic resonance imaging and spectroscopy (MRI/MRS) are encouraged to apply. Applicants must have Ph.D. with adequate training in synthesizing ultrasmall iron oxides conjugates with receptors or proteins for imaging. Successful applicant will work with existing team on molecular imaging projects and manage a newly established facility equipped with a new Bruker BiospecAvance 9.4 T/21 and a fully upgraded Bruker 4.7 T/40 MRI/MRS system for small animals. Individuals are encouraged to develop independent, extramurally funded projects.

Please send curriculum vitae and names of three references to: **Dr. Thian C. Ng** at **e-mail: mezzell@uab.edu.** *UAB is an Affirmative Action/Equal Opportunity Employer committed to excellence through diversity.*

STAFF SCIENTIST

Seeking a full-time scientist to supervise and work on research projects related to osteonecrosis and bone repair. Excellent salary based on qualifications with full benefits. A Ph.D. and postdoctoral experience in area of bone and molecular biology is required. Send curriculum vitae and two references to:

Shriners Hospitals for Children-Tampa
Human Resources
12502 Pine Drive
Tampa, FL 33612

Equal Opportunity Employer/Alcohol/Drug-Free/Smoke-Free Workplace.

POSTDOCTORAL RESEARCH FELLOW OR ASSOCIATE RESEARCH SCIENTIST

Positions available immediately for M.D. or Ph.D. scientists in the Division of Molecular Medicine to conduct research on molecular regulation of cellular cholesterol efflux and the role of insulin resistance in macrophage foam cell formation, apoptosis, and atherosclerosis. See **website: http://www.alantall.org** for more information. Send curriculum vitae to: **Dr. Alan Tall, Division of Molecular Medicine, Columbia University, 630 West 168th Street (P&S 8-401), New York, NY 10032.** *We take Affirmative Action toward Equal Employment Opportunity.*

POSTDOCTORALS, SABBATICALS, AND WORKSHOPS AT THE NATIONAL EVOLUTIONARY SYNTHESIS CENTER

NESCent announces a call for proposals for Postdoctorals, Sabbaticals, and two kinds of workshops (Catalysis Meetings and Working Groups). Proposals are welcome from scientists of all nationalities. Deadline is October 15, 2005, for positions and groups beginning in 2006. For instructions, please visit **website: http://www.nescent.org.** *Duke University is an Equal Opportunity Employer.*

POSTDOCTORAL FELLOWSHIPS
Cardiopulmonary Genomics Program
University of Maryland
School of Medicine

The newly formed Cardiopulmonary Genomics Program is seeking Postdoctoral Fellows for research in the genomics, molecular biology, signaling, and pharmacology of G-protein coupled receptors. The ideal candidate (Ph.D., M.D., D.V.M., or equivalent) will have published experience in DNA manipulation and related techniques, human polymorphism discovery, receptor signaling, promoter analysis, and production of transgenic mice. An interest in heart and lung disease is helpful but not required. For examples of research and publications perform National Library of Medicine search on Liggett SB. The program is located in new, well-equipped, state-of-the-art laboratory space at the medical campus in Baltimore, Maryland.

Individuals interested should send their curriculum vitae to: **Stephen B. Liggett, M.D., University of Maryland-Baltimore,** via **e-mail: sbliggett@gmail.com.**

The University of Maryland-Baltimore encourages women and members of minority programs to apply and is an Affirmative Action/Equal Employment Opportunity/ADA Employer.

POSTDOCTORAL POSITIONS: Available for studies in various aspects of cancer research and toxicology in the Center in Molecular Toxicology through the Departments of Biochemistry, Chemistry, Medicine, Pathology, Pediatrics, and Pharmacology. Areas of investigation relating to toxicology and carcinogenesis include enzymatic oxidation and conjugation, oxidative damage, DNA damage and mutagenesis, neurotoxicology, and mechanisms of cell signaling, among others. Center faculty include **Drs. Richard N. Armstrong, Michael Aschner, Raymond F. Burk, Richard M. Caprioli, Walter J. Chazin, David K. Cortez, Martin Egli, F. Peter Guengerich, Diane S. Keeney, Daniel C. Liebler, Lawrence J. Marnett, Jason D. Morrow, Jennifer A. Pietenpol, Ned A. Porter, Carmelo J. Rizzo, Michael P. Stone, William M. Valentine,** and **Michael R. Waterman.** Salaries are negotiable. Applicants should submit curriculum vitae and three letters of recommendation to: **Dr. F. Peter Guengerich, Director, Center in Molecular Toxicology, Vanderbilt University, School of Medicine, Nashville, TN 37232-0146.** *An Affirmative Action/Equal Opportunity Employer.*

ASSISTANT PROFESSOR: Michigan State University (MSU) invites applications for a tenure-track Assistant Professor of biology (organismal focus preferred) in the Lyman Briggs School of Science. The candidate will have a strong record of teaching and research accomplishment and be committed to participation by undergraduate students. Requirements include a Ph.D. in biology and one year of postdoctoral experience. Review of applications will begin on September 22, 2005. Full details at **website: http://www.lymanbriggs.msu.edu/faculty-positions.htm.** *MSU is an Affirmative Action/Equal Opportunity Institution. Women and minorities are strongly encouraged to apply.*

POSTDOCTORAL POSITION is available to study folding, quality control, and sorting of membrane proteins, including Cystic Fibrosis Transmembrane Conductance Regulator. Candidates must hold a Ph.D. and have a strong background in molecular-cell biology. Additional experience in biochemistry and electrophysiology is an asset. Please send a one-page description of research interests, curriculum vitae, and the names of three references to: **Dr. Gergely L. Lukacs, Sick Kids Research Institute, Cell Biology, 555 University Avenue, Toronto, Ontario, M5G 1X8, Canada.**

BIOINFORMATICS
Vassar College

The Department of Biology at Vassar College invites applications for a tenure-track faculty position at the level of **ASSISTANT PROFESSOR** beginning fall 2006. We seek a Biologist whose research and teaching interests include bioinformatic approaches. Areas of expertise may include but are not limited to the following: evolution, functional or comparative genomics, microbiology, cellular and molecular biology, physiological systems, and protein biochemistry/proteomics. The successful candidate should expect to develop an upper-level course on bioinformatics as well as teach at the introductory and intermediate levels. Development of a research program with student participation is expected and startup funding is provided. A Ph.D. in biological science is required and postdoctoral experience is preferred. This position is funded in part by a grant from the Howard Hughes Medical Institute to Vassar College. Consideration of applications will begin on 3 October 2005. Applicants should submit curriculum vitae, representative reprints, a statement of research interests and goals, a statement on teaching interests, and three letters of reference to: **Robert Fritz, Chair, Department of Biology, Box 731, Vassar College, Poughkeepsie, NY 12604-0731. E-mail: fritz@vassar.edu. Website: http://biology.vassar.edu/.** *An Affirmative Action/Equal Opportunity Employer.*

Two **POSTDOCTORAL SCIENTIST POSITIONS.** Molecular Biologist/Protein Biochemist are sought to study basic mechanisms of radiation-induced carcinogenesis. Recent graduates in DNA ds repair mechanisms, protein kinase structure/function relationships, molecular cytogenetics, and/or mouse molecular genetics are encouraged to apply. Colorado State University (CSU) radiobiology faculty are internationally recognized as leaders in the field of radiation carcinogenesis. Research facilities/collaborations are virtually limitless. These positions are funded through a longstanding training grant with the NIH/National Cancer Institute and are *limited to U.S. citizens and permanent residents.* Please e-mail current curriculum vitae and three references to:

Ms. Mary Pridgen
Radiological Sciences Cancer Research Program
Colorado State University
Fort Collins, CO
E-mail: mary.pridgen@colostate.edu

CSU is an Equal Opportunity Employer.

POSTDOCTORAL POSITION
Biological Mass Spectrometry

NIH-funded project to study antagonist and agonist interactions with HIV co-receptors CCR5 and CXCR4. Experience with peptide electrospray ionization/liquid chromatography/mass spectrometry/mass spectrometry required. Exceptionally qualified candidates will be considered for **RESEARCH ASSISTANT PROFESSOR** rank. **Dr. Ed Dratz, Department of Chemistry and Biochemistry, Montana State University, Bozeman, Montana; e-mail: dratz@chemistry.montana.edu.** Complete job announcement and application procedures at **website: http://www.montana.edu/level2/jobs.html.** *ADA/Equal Opportunity/Affirmative Action/Veterans Preference.*

JUNIOR RESEARCHER #88618T University of Hawaii Manoa, Pacific Biomedical Research Center, temporary, to begin approximately April 2006. Responsible for designing and conducting experiments, obtaining and interpreting data, and the preparation of the work for publication. For complete job announcement and how to apply visit **website: http://workatuh.hawaii.edu** or contact: **Dr. G. Bryant-Greenwood** at **telephone: 808-956-3388** or **e-mail: gbg@pbrc.hawaii.edu.** Closes September 15, 2005. *An Equal Employment Opportunity/Affirmative Action Employer.*

Faculty Careers 2

Advertising Supplement

Issue date 16 September 2005
Reserve ad space by 30 August 2005

***Science*'s qualified circulation of 126,954** [1] plus our pass-along readers brings total global weekly readership to over 708,000.[2]

- 81% of subscribers are Ph.D. level
- 51% work in academia

1 *Science* December 2004 BPA Publisher's Statement. 2 *Science* December 2004 circulation as applied to 14 January 2000 Harvey Readership Survey and 2002 Harvey Cumulative Report, publisher's own data.

For more information, contact:
Daryl Anderson – 202-326-6543
advertise@sciencecareers.org

ScienceCareers.org
We know science AAAS

POSTDOCTORAL POSITION

The Genomics Institute
Wadsworth Center/University at Albany

Postdoctoral Position available immediately at The Genomics Institute, Wadsworth Center/University at Albany to investigate genes, especially quantitative trait loci (QTL), that influence complex mouse behaviors such as learning and memory. Microarray gene expression assays will be developed to determine pathways of action. Transgenic and knockout mice will be developed. Excellent state-of-the-art molecular genetic core facilities are available at the Institute.

Send curriculum vitae and three letters of reference to: **Dr. Lorraine Flaherty, Director, Genomics Institute, Wadsworth Center, 465 Jordan Road, Troy, NY 12180; E-mail: valenti@wadsworth.org**.

See **www.wadsworth.org/genomics** for more information.

EOE/AA

Faculty Position in Igneous Geochemistry

The Scripps Institution of Oceanography (**http://sio.ucsd.edu/**) is inviting applications for a tenure-track or tenured Professor position in the broad field of igneous geochemistry. We are seeking a candidate with expertise in analytical, experimental or theoretical approaches to igneous processes. Possible areas of interest include, but are not limited to, geochemical evolution of the Earth and other planetary bodies, petrogenesis of crustal rocks, mineral physics/properties of the deep Earth, and volcanology. We are seeking researchers who are interdisciplinary, possessing a clear vision for the most exciting future research directions, and who can collaborate with the broad spectrum of research that is currently taking place at SIO. The candidate would be expected to teach graduate and undergraduate courses in the general areas of petrology, mineralogy and courses in the candidate's specialty. We would like to hire at the Assistant/Associate level but will entertain applications at the senior level. The level and salary will depend on the experience of the successful applicant and will be based on the University of California pay scale.

Review of applications will begin on October 15, 2005. Applicants should send a letter including descriptions of their teaching and research interests, a list of publications, and names and contact information for three to five potential referees to: **Chair, SIO Graduate Department, Scripps Institution of Oceanography, University of California at San Diego, La Jolla, CA 92093-0208**.

UCSD is an Equal Opportunity/Affirmative Action Employer with a strong institutional commitment to excellence through diversity.

Postdoctoral Positions Pharmacological Sciences

Stony Brook University's Department of Pharmacology has postdoctoral positions available in cell signaling mediating the atheroprotective effects ApoE using KO/transgenic mice. Analysis of signaling cascades operating in atherosclerotic lesions and in suppression by very low expression of ApoE.

Required: Ph.D., DSc, M.D., or equivalent.

Supported by NIH-funded postdoctoral training award, restricted to PR and US citizens only.

To apply, please send C.V. and three letters of reference to:
Dr. Craig C. Malbon, Department of Pharmacology, Stony Brook University SUNY, Stony Brook, NY 11794-8651

E-mail: *craig@pharm.stonybrook.edu*

AA/EOE. Visit *www.stonybrook.edu/cjo* for employment information.

STONY BROOK

Theoretical Chemist/ Physicist Divisional Fellow

The Materials Science Division at the Lawrence Berkeley National Laboratory is seeking a scientist with outstanding promise and creative ability to develop a new theory program in the prediction of the behaviors of novel materials, the growth and dynamics of complex systems or nanostructures, and methods for creating these materials. This is a five-year term appointment that, after review, may culminate in a Senior Scientist position. Learn more about the Materials Science Division at http://www.lbl.gov/msd/.

Please submit CV and publication list online at http://jobs.lbl.gov. Click on Search and enter job # 017994 in the keywords search field, then Search Jobs. Reference source code from the drop down menus. Your statement of research interests and four reference letters will be requested at a later time.

LBNL is an AA/EEO employer dedicated to developing a diverse workforce.

BERKELEY LAB

MARKETPLACE

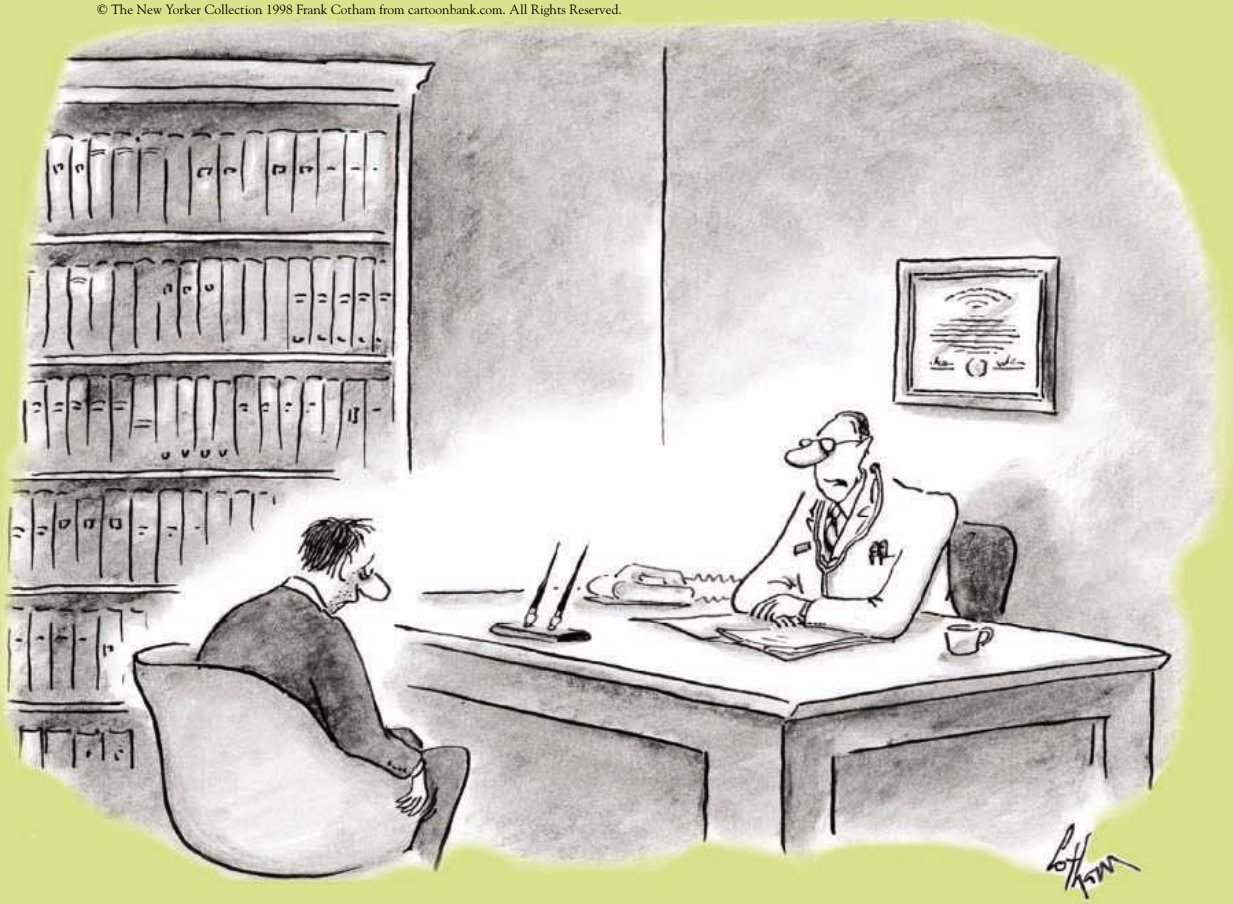

"Unfortunately, there's no cure – there's not even a race for a cure."

There is now.

It's a new day in genetics. For the first time, both pharmaceutical and academic investigators are initiating whole genome case-control studies that analyze millions of unique SNPs in hundreds of patients. And, by partnering with Perlegen, they are finding answers to questions that were previously out of reach.

If you have access to DNA samples for a well-characterized phenotype, we would like to meet with you. Our scientists and analysts collaborate with you to perform, analyze and publish whole genome association studies in months, not years.

Patients are waiting. Join the race.

To partner, contact:
Partnerships11@perlegen.com
www.perlegen.com

Targeting today's drugs. Discovering tomorrow's.™

PERLEGEN SCIENCES®